Study of Schnyder Woods and Intersection Graphs

Daniel Gonçalves

Habilitation à diriger des recherches

présentée à

L'UNIVERSITÉ DE MONTPELLIER

Ecole Doctorale I2S

STUDY OF SCHNYDER WOODS AND INTERSECTION GRAPHS

Daniel GONÇALVES

Jury :

Therese Biedl - University of Waterloo (rapportrice)

Victor Chepoi - Aix-Marseille Université (examinateur)

Éric Colin de Verdière - CNRS, Université Paris-Est Marne-la-Vallée (rapporteur)

Stefan Felsner - Technische Universität Berlin (rapporteur)

Christophe Fiorio - Université de Montpellier (examinateur)

Dieter Rautenbach - Universität Ulm (examinateur)

24 Septembre 2018

Foreword

This document is a long abstract of my research work on graph theory. This is an overview of my research in the last 10 years (posterior to my PhD), and summarizes seven selected papers (included in the appendix) which have been published or are submitted to international journals. It summarizes some results, gives ideas of the proof for some of them, and presents the context of the different topics together with some interesting open questions connected to them. This document is organized as follow. The first two chapters respectively deal with Schnyder woods (and their extension on higher genus surfaces), and with intersection representations of planar graphs. The third chapter is a research project for the 5-10 years to come. Finally in the appendix one can find the full length papers which include all the proofs [1].

To conclude, I would like to mention that these papers are the result of different collaborations and each result is then a collective work. I would like to thank all my co-authors as well as many more colleagues for many nice and exciting moments doing research (or doing other things). I also warmly thank the members of the jury (and in particular the reviewers) for kindly accepting to be a part of it, and for all the time spent on this.

1. As we uniformized notations from different publications, some notations differ between the manuscript and the papers.

Table des matières

Prerequisite

We assume that the reader has basic notions in graph theory, but one should also have a few notion of topology to read this manuscrpt. Let us give a few definitions to ensure that our terminology is clear. A graph embedded on a surface $\mathbb{S}$ is called a *map* of this surface if all its faces are homeomorphic to open disks. A map is a *triangulation* (resp. a *quadrangulation*) if all its faces are bordered by three edges (resp. four edges). A closed curve on a surface is *contractible* if it can be continuously transformed into a single point. In this manuscript, we only consider maps that do not have contractible cycles of size 1 or 2 (i.e. no contractible loops and no contractible double edges). Note that this is a weaker assumption than the graph being *simple*, i.e. not having *any* cycles of size 1 or 2 (i.e. no loops and no multiple edges).

We have a particular attention to plane graphs (i.e. graphs embedded on the plane). Such graphs have an unbounded face called the *outer face*, while the other faces are called *inner faces*. Vertices and edges lying on the outer face are *outer vertices* and *outer edges*. The other ones are *inner vertices* and *inner edges*. A *near-triangulation* is a 2-connected plane graph such that every inner face is triangular. A *separating triangle* is a cycle of length three such that both regions delimited by this cycle (the inner and the outer region) contain some vertices. It is well known that a triangulation is 4-connected if and only if it contains no separating triangle.

If needed, the following textbooks on graph theory [16], embedded graphs [82], Schnyder woods [47], topology [76], and homology [65] contain all the notions needed (and much more) to follow this manuscript.

Chapitre 1

Schnyder Woods

Schnyder woods are nowadays one of the main tools in the area of planar graph representations. Among their most prominent applications are the following : They provide a machinery to construct space-efficient straight-line drawings [89, 35, 44, 79] ; they allow a characterization of planar graphs via the dimension of their vertex-edge incidence poset [88, 44, 79] ; and they are used to encode triangulations [85, 10]. Further applications lie in enumeration [19], representation by geometric objects [57, J13], or graph spanners [18].

The richness of these applications has stimulated research towards generalizing Schnyder woods to non-planar graphs. For higher genus triangulated surfaces, a generalization of Schnyder woods has been proposed by Castelli Aleardi et al. [21], with applications to encoding. In this definition, the simplicity and the symmetry of the original definition of Schnyder woods are lost. This motivated us (with various co-authors) to find another generalization of Schnyder woods.

After introducing basic definitions in Section 1.1, we extend Schnyder woods to toroidal maps (i.e. graphs embedded on the torus) in Section 1.2. We then use these in Section 1.3 to design a drawing algorithm and a bijection leading to a compact encoding of toroidal triangulations. In Section 1.4 we define generalizations of Schnyder woods for (orientable) maps with higher genus, and we make some conjectures on their existence. Towards one of these conjectures we study particular orientations of genus g triangulations in Section 1.5.

1.1 Introduction

Schnyder [88] introduced Schnyder woods for planar triangulations with the following local property :

Definition 1.1 (Schnyder property)**.** Given a map G, a vertex v and an orientation and coloring [1] of the edges incident to v with the colors 0, 1, 2, we say that v satisfies the *Schnyder property*, (see Figure 1.1.(a)) if v satisfies the following local property :

— Vertex v has out-degree one in each color.
— The edges $e_0(v)$, $e_1(v)$, $e_2(v)$ leaving v in colors 0, 1, 2, respectively, occur in counterclockwise order.
— Each edge entering v in color i enters v in the counterclockwise sector from $e_{i+1}(v)$ to $e_{i-1}(v)$.

Definition 1.2 (Schnyder wood)**.** Given a planar triangulation G, a *Schnyder wood* is an orientation and coloring of the inner edges of G with the colors 0, 1, 2, where each inner vertex v satisfies the *Schnyder property*.

See Figure 1.1.(b) for an example of a Schnyder wood. Several authors [35, 44, 79] independently generalized Schnyder woods by allowing edges to be oriented in one direction or in two opposite directions. The formal definition is the following :

1. Throughout the manuscript colors and some of the indices are given modulo 3.

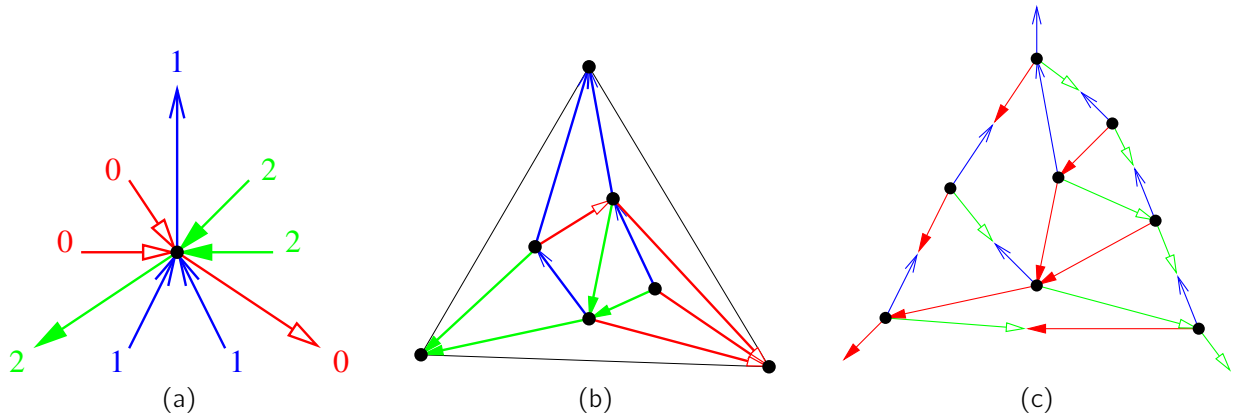

Figure 1.1 – (a) The Schnyder property (b) A Schnyder wood of a planar triangulation (c) A Schnyder wood of a planar map.

Definition 1.3 (Schnyder woods for planar maps)**.** Given a planar map G. Let x_0, x_1, x_2 be three distinct vertices occurring in counterclockwise order on the outer face of G. The *suspension* G^σ is obtained by attaching a half-edge that reaches into the outer face to each of these special vertices. A *Schnyder wood* rooted at x_0, x_1, x_2 is an orientation of the edges of G^σ, where every edge e is oriented in one direction or in two opposite directions, and a coloring of these arcs (with colors 0, 1, 2) satisfying the following (see example of Figure 1.1.(c)) :

(P1) Every vertex satisfies Schnyder's property [2] and the half-edge at x_i is directed outwards and colored i.

(P2) There is no interior face the boundary of which is a monochromatic cycle.

A planar map G is *internally 3-connected* if there exists three vertices on the outer face such that the graph obtained from G by adding a vertex adjacent to the three vertices is 3-connected. The maps admiting a Schnyder wood are characterized as follows.

Theorem 1.4 (Felsner [44], and Miller [79])**.** *A planar map admits a Schnyder wood if and only if it is internally 3-connected.*

Schnyder woods have an auto-dual nature in the sense that a Schnyder wood of a planar map G (almost) defines a Schnyder wood of its dual G^*, but actually this auto-dual nature is better expressed in the following toroidal case.

1.2 Toroidal Schnyder Woods

This section mainly relies on [J18] and it is dedicated to an extension of Schnyder woods for toroidal maps. We consider maps on the torus with no contractible loop and no homotopic multiple edges (i.e. contractible cycles have length at least three). The torus is represented by a parallelogram in the plane whose opposite sides are pairwise identified. This representation is called the *flat torus*. Given a graph G, let n denote the number of vertices and m the number of edges. By Euler's formula, a planar triangulation satisfies $m = 3n-6$. Thus there is not enough edges in a planar triangulation to allow an orientation such that all vertices have out-degree three. This explains why just some vertices (the inner ones) are required to verify Schnyder's property in Definition 1.2. The three outer vertices of the triangulation have a special role. For a toroidal triangulation, Euler's formula gives exactly $m = 3n$ so we looked for a generalization of Schnyder woods satisfying the Schnyder property for every vertex. In the following we will see that such definition exists and that these objects have many similarities with "plane" Schnyder woods.

2. The intervals in Definition 1.1 are closed : If an edge is oriented in two directions, the arcs get different colors.

Definition 1.5 (Schnyder woods for toroidal maps)**.** Given a toroidal map G, a *Schnyder wood* of G is an orientation and coloring of the edges of G with the colors 0, 1, 2, where every edge e is oriented in one direction or in two opposite directions, satisfying the following (see example of Figure 1.2.(a)) :

(T1) Every vertex v satisfies the Schnyder property.

(T2) Every monochromatic cycle of color i intersects at least one monochromatic cycle of color $i-1$ and at least one monochromatic cycle of color $i+1$.

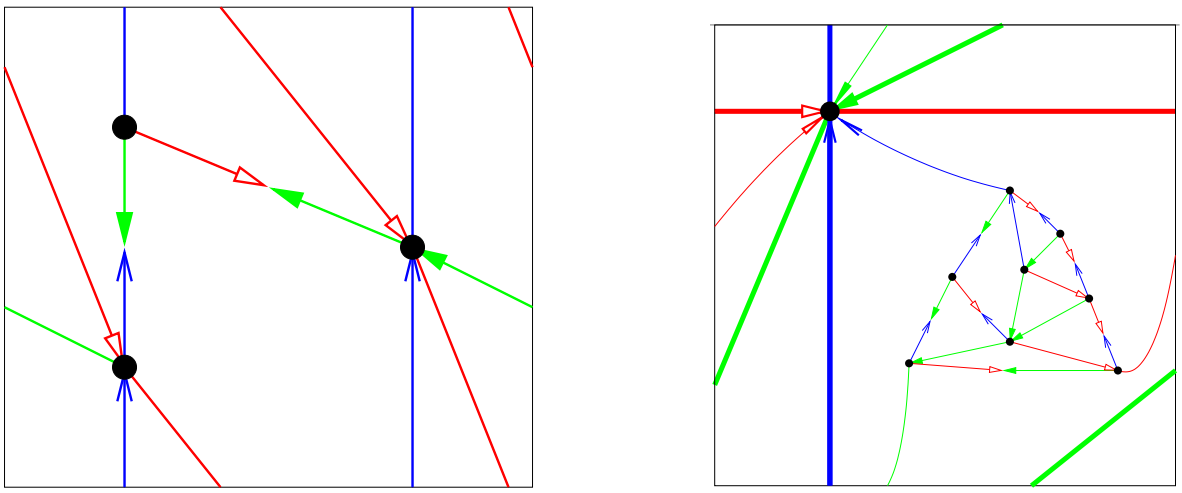

(a) (b)

Figure 1.2 – (a) Example of a Schnyder wood of a toroidal map (b) The toroidal Schnyder wood corresponding to the planar Schnyder wood of Figure 1.1.(c)

Our definition of Schnyder wood on toroidal maps generalizes the planar case. Let G be a planar map and x_0, x_1, x_2 be three distinct vertices occurring in counterclockwise order on the outer face of G. One can transform G^σ into the following toroidal map G^+ (see Figure 1.2.(b)) : Add a vertex v in the outer face of G. Add three non-parallel and non-contractible loops on v. Connect the three half edges leaving x_i to v such that there is no two such edge entering v consecutively. Then we have the following.

Proposition 1.6. *Schnyder woods of the planar map G rooted at x_0, x_1, x_2 are in bijection with Schnyder woods of the toroidal map G^+.*

The *universal cover* G^∞ of a toroidal map G is the infinite planar graph obtained by replicating a flat torus representation of G to tile the plane. Extending the notion of *essentially 2-connectedness* defined in [81], we say that a toroidal map G is *essentially 3-connected* if its universal cover is 3-connected. We have the following.

Proposition 1.7. *A planar map G is internally 3-connected if and only if there exist three vertices on the outer face of G such that G^+ is essentially 3-connected.*

The following theorem thus generalizes Theorem 1.4.

Theorem 1.8. *A toroidal map admits a Schnyder wood if and only if it is an essentially 3-connected toroidal map.*

We proved the existence of Schnyder woods by contracting edges until we obtain a graph with just one vertex. Then the graph can be decontracted step by step to obtain a Schnyder wood of the original graph. The two essentially 3-connected toroidal maps on one vertex are depicted in Figure 1.3 with a toroidal Schnyder wood.

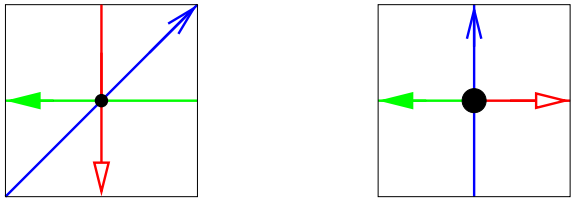

(a) (b)

Figure 1.3 – Schnyder woods of the two essentially 3-connected toroidal maps on one vertex.

As the dual of an essentially 3-connected map is also essentially 3-connected, the auto-dual nature of these Schnyder woods is clearer than in the plane.

Theorem 1.9. *For any toroidal map G, the Schnyder woods of G are in bijection with the Schnyder woods of G^*, and one can be constructed from the other by following the rules suggested in Figure 1.14 (in the middle and in the right).*

Let G be a plane or a toroidal map given with a Schnyder wood. Let G_i be the directed graph induced by the edges of color i (including edges that are half-colored i). If G is plane each vertex, except x_i, has exactly one outgoing arc in G_i. Thus each G_i has exactly $n-1$ edges, and actually each G_i is a spanning tree oriented towards x_i. In other words, for any vertex v, G_i contains a (unique) directed path colored i from v to x_i. The toroidal case is a bit different. If G is a toroidal map, every vertex has exactly one outgoing arc in G_i. Thus each graph G_i has exactly n edges, so it does not induce a rooted tree like for planar maps. Note also that G_i is not necessarily connected (e.g. the blue graph in Figure 1.2.(a)). But each components of G_i has exactly one outgoing arc for each of its vertices, thus each connected component of G_i has exactly one cycle that is a *monochromatic cycle of color i*. Starting from any vertex v one can perform an infinite walk in G_i by following the outgoing arcs. In the universal cover of G such walk corresponds to an infinite path $P_i(v)$ colored i (See the left of Figure 1.4). These paths are used in Section 1.3.1.

Felsner [45] proved that (for planar maps) Schnyder woods are in bijection with Schnyder angle labellings. For toroidal maps, a Schnyder wood defines an angle labeling with the following property : the angles at each vertex and at each face form, in counterclockwise order, nonempty intervals of 0's, 1's, and 2's. This is similar to the planar case, but we did not found an elegant definition of Schnyder labeling that would be equivalent to our definition of Schnyder woods (c.f. Definition 1.5). It seems that property (T2) is truly global unlike (P2). Weaker definitions of Schnyder woods, based on angle labelings, are discussed in Section 1.4.

1.3 Applications of Toroidal Schnyder Woods

1.3.1 Drawing Algorithm

Let G be a toroidal map given with a Schnyder wood and consider the universal cover G^∞ with the corresponding orientation and coloring of the edges. This defines a sort of Schnyder wood in the infinite plane graph G^∞, and these Schnyder woods have several features of plane Schnyder woods. One of those is that for every vertex v and color i, the two paths $P_{i-1}(v)$ and $P_{i+1}(v)$ have v as only common vertex. This implies that for every vertex v, the three paths $P_0(v)$, $P_1(v)$, $P_2(v)$ divide G^∞ into three unbounded regions $R_0(v)$, $R_1(v)$ and $R_2(v)$, where $R_i(v)$ denotes the region delimited by the two paths $P_{i-1}(v)$ and $P_{i+1}(v)$ (See the left of Figure 1.4). This observation motivated us for trying to adapt Schnyder's drawing algorithm (that is based on the existence of similar regions in plane Schnyder woods) to design the first algorithm for straight-line drawing of toroidal triangulations in a flat torus of polynomial size[3] (see [80] for an exponential size and [25, 36] for embedings

3. The size is understood as follows. Vertices are embedded on integer coordinates and the size of the flat torus (that is a parallelogram) is given by its surface.

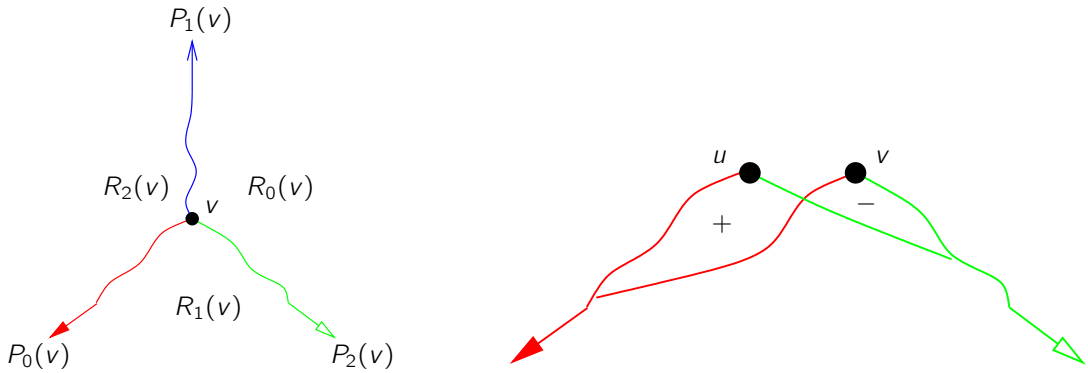

Figure 1.4 – Regions corresponding to a vertex, and the differences between $R_1(u)$ and $R_1(v)$ when $P_0(u)$ meets $P_0(v)$, and $P_2(u)$ meets $P_2(v)$.

that are partially straight-line). Actually we will describe a periodic drawing for the whole universal cover, but a portion of it is sufficient to describe the drawing in a flat torus. Let us now recall Schnyder's algorithm [88] that was initially designed for triangulations and that was generalized to 3-connected planar maps independently by Di Battista et al. [35], Felsner [44], and Miller [79].

Schnyder's Barycentric Drawing Algorithm : In planar Schnyder woods, the paths $P_i(v)$ and the regions $R_i(v)$ also exist, but they are finite. Paths $P_i(v)$ end at x_i, while regions $R_i(v)$ are closed by the edge $x_{i-1}x_{i+1}$. For each such region $R_i(v)$, let us denote by $r_i(v)$ the number of faces in $R_i(v)$. Each vertex v is embedded in $\mathbb{R}^3$ at $(r_1(v), r_2(v), r_3(v))$. Note that as the regions $R_1(v), R_2(v), R_3(v)$ partition the set of inner faces, we have that all the vertices are embedded in the plane $\{x \in \mathbb{R}^3 \mid x_1 + x_2 + x_3 = f\}$, where f is the number of inner faces. Schnyder shows that drawing segments between adjacent vertices one obtains a planar drawing of our map. The (orthogonal) projection of this drawing on the plane $\{x \in \mathbb{R}^3 \mid x_3 = 0\}$ is also a planar drawing of T, and here a vertex v has coordinates $(r_1(v), r_2(v), 0)$.

The first problem for generalizing this algorithm is that in the toroidal case one has to consider the universal cover in order to define regions $R_i(v)$, but these regions have an infinite number of faces, so we cannot deduce the coordinates as in the planar case. We thus have to define the coordinates of vertices relatively to the other vertices. For example, if for two vertices u, v the set of faces in $R_i(u) \triangle R_i(v)$ is finite (see the right of Figure 1.4), then $u_i - v_i$ is equal to the number of faces in $R_i(u) \setminus R_i(v)$ minus the number of faces in $R_i(v) \setminus R_i(u)$. Note that $R_i(u) \triangle R_i(v)$ is finite if and only if $P_{i-1}(u)$ meets $P_{i-1}(v)$, and $P_{i+1}(u)$ meets $P_{i+1}(v)$. If two vertices have their three paths that meet, they lie on the same plane $\mathcal{P}_c = \{x \in \mathbb{R}^3 \mid x_1 + x_2 + x_3 = c\}$. Dealing with infinite $R_i(u) \triangle R_i(v)$ is not too complicated, but afterwards the vertices lie on distinct planes $\mathcal{P}_c$. The issue is that this greatly increases the size of the flat torus we are working on. Another issue is that we could not prove that this algorithm works for any (non-triangular) toroidal map equipped with a Schnyder wood. In the planar case such drawings (of planar maps) are shown to be convex (i.e. every face forms a convex polygon) and this is what we could not prove for toroidal maps. We do not explain how to prove that the algorithm works because it is a rather tedious task. See Figure 1.5 for an illustration of the algorithm.

For a simple toroidal triangulation with n vertices, our algorithm leads to an embedding in a flat torus with surface $O(n^4)$. The same problem was independently considered by Castelli Aleardi et al. [22], and their method achieves a better size for the flat torus, $O(n^{5/2})$. However, we believe that our approach could be improved to reach a smaller flat torus (at least smaller than $O(n^4)$) by considering Schnyder woods where some graphs G_i are connected, or by restraining to embeddings in $\mathbb{R}^3$ which can be projected through vector $\overrightarrow{v} = (1, 1, 1)$ but maybe not through any vector $\overrightarrow{v} = (x, y, z)$ with $x, y, z \geq 0$ (as our approach allows).

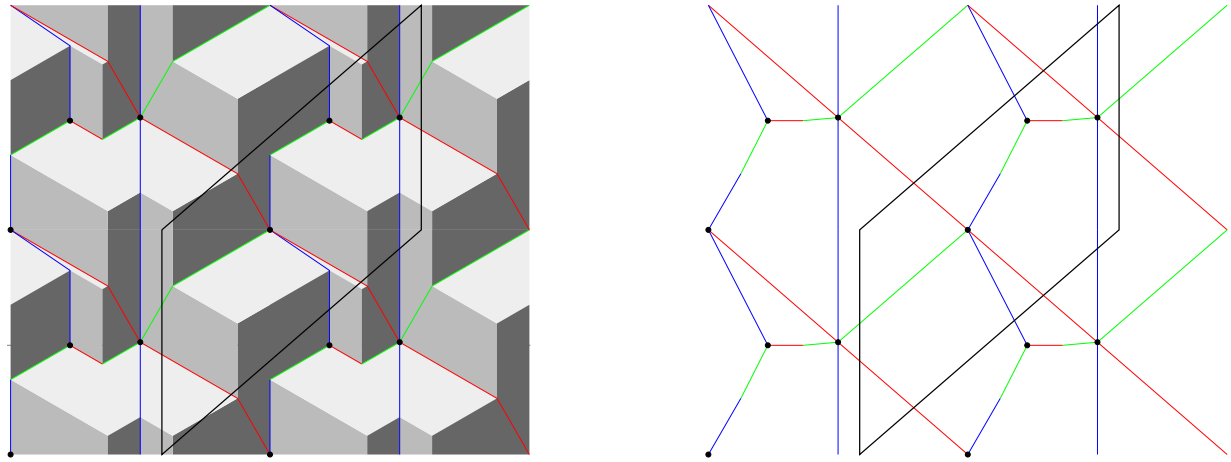

(a) (b)

Figure 1.5 – (a) Embedding of a toroidal map in $\mathbb{R}^3$ (We do not discuss the way edges are embedded in this drawing. This is related to the so-called orthogonal surface and geodesic embeddings.) (b) Its projection on some plane (with straigh-line edges).

1.3.2 Bijection & Encoding

The content of this section mainly relies on [J24] where we adapt an approach developped by Poulalhon et al. [85] to obtain a bijection between planar triangulation and blossoming trees (embedded trees with "stems"). This led to a bijection (c.f. Theorem 1.16) between toroidal quasi-triangulations (all the faces are triangular except one which has size four), and toroidal blossoming unicellular maps (i.e. maps with stems and with a unique face). Let us first discuss some properties of toroidal Schnyder woods.

It is shown in [S2] that similarly to the planar case [46], the set of Schnyder woods of a toroidal map has a lattice structure [4]. Similarly to the plane, one can get from any Schnyder wood to any other one by reversing a succession of contractible directed cycles [5]. The orientation of this lattice depends on the choice of a root face f. Consider a contractible cycles C bounding a pseudo-disk $\mathcal{D}$, such that C is oriented clockwisely around $\mathcal{D}$. If $f \in \mathcal{D}$ reversing the orientation of C we go higher in the lattice, lower if $f \notin \mathcal{D}$. Another important feature of this lattice is that actually, some elements of this lattice are not Schnyder woods in the sense of Definition 1.5 as (T2) is not always fulfilled. On the other hand, note that satisfying (T1) is not a sufficient condition to be an element of this lattice. We call this lattice the *HTC-lattice* [6]

Let us focus on the case of toroidal triangulations. In that case the elements of the lattices can be seen as 3-orientations, that is orientations such that every vertex has outdegree 3. Indeed, once an edge is colored, by satisfying (T1) this coloring propagates to the whole triangulation in a unique way.

Definition 1.10 (γ_0 property)**.** An orientation of a toroidal map has the γ_0 *property* if for any non-contractible cycle C the number of arcs leaving C (i.e. arcs uv such that $u \in C$) on one side equals the number of arcs leaving C on the other side.

In a Schnyder wood of a toroidal triangulation, monochromatic cycles verify this property : for each vertex there is one arc leaving on each side. This property characterizes the 3-orientations of the HTC lattice [S2].

Proposition 1.11. *A 3-orientation of a toroidal triangulation T is an element of its HTC lattice if and only if it has the γ_0 property.*

4. Actually both results can be deduced from [86].
5. Actually we are interested by null-homologous cycles but in the torus these correspond to contractible cycles. This will be discussed a little more in Section 1.4.
6. HTC means "Homological To Crossing" as Schnyder woods have a crossing property (T2).

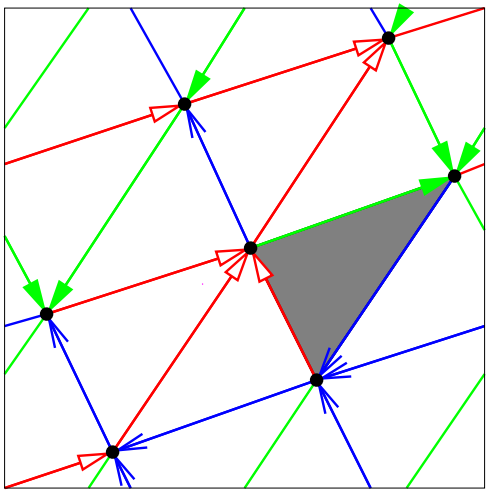

Figure 1.6 – The minimal 3-orientation of the HTC-lattice of K_7 w.r.t. the shaded face. Every oriented contractible cycle is counter-clockwise w.r.t. the shaded face.

Poulalhon et al.'s algorithm on oriented surfaces

Here we introduce a reformulation of Poulalhon et al.'s original algorithm [85]. In an embedded graph G, a *stem* is an embedded arc whose origin is a vertex of G while its other end is not considered as a vertex.

Algorithm PS

Input : An oriented map G on an oriented surface $\mathbb{S}$, a root vertex v_0 and a root edge e_0 incident to v_0.
Output : A graph U with stems, embedded on $\mathbb{S}$.
The algorithm explores some of the edges of the map, marking one edge at each iteration.

1. Let $v := v_0$, $e := e_0$, $U := \emptyset$, Let all the edges being unmarked.
2. Let v' be the extremity of e different from v.
   Case 1 : *e is non-marked and entering v.* Add e to U and let $v := v'$.
   Case 2 : *e is non-marked and leaving v.* Add a stem to U incident to v and corresponding to e.
   Case 3 : *e is already marked and entering v.* Do nothing.
   Case 4 : *e is already marked and leaving v.* Let $v := v'$.
3. Mark e.
4. Let e be the next edge around v in counterclockwise order after the current e.
5. While $(v, e) \neq (v_0, e_0)$ go back to 2.
6. Return U.

Let us stress the fact that the output of Algorithm PS is a graph embedded on the same surface as the input map but that this embedded graph is not necessarily a map (i.e some faces may not be homeomorphic to open disks). However, we showed that in a specific case the output U is an unicellular map, which is not the case for any input.

We associate each couple (v, e) where e is incident to v, to the angle at v that is just before e in counterclockwise order. We thus call *angle* such couple. The particular choice of v_0 and e_0 thus defines a root face f_0 : the face containing the angle (v_0, e_0), that is the face just before e_0 going around v_0 counter-clockwisely. Figure 1.7 illustrates an execution of Algorithm PS . The condition in the while loop ensures that when the algorithm terminates, if it does, the algorithm is back to the root angle. The following proposition shows that the algorithm actually always terminates :

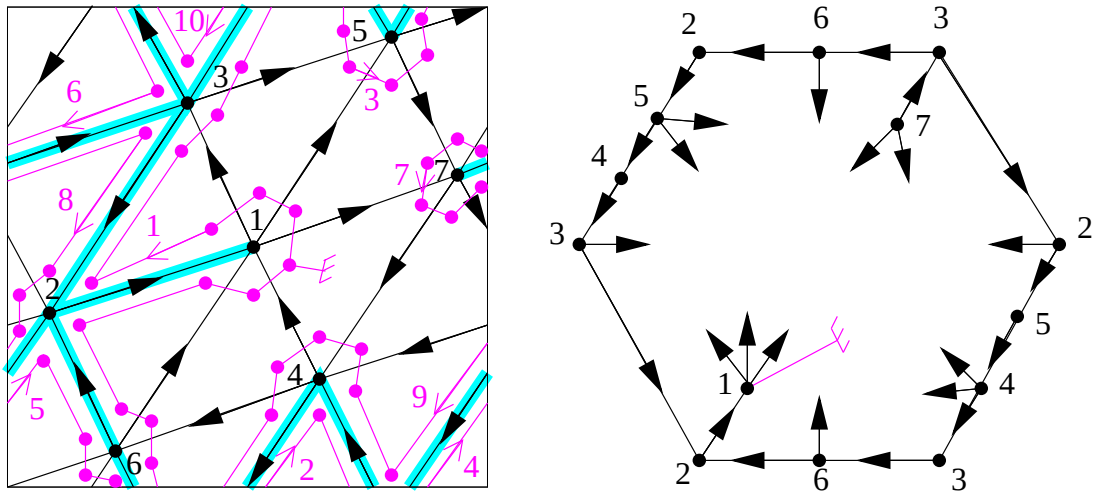

Figure 1.7 – An execution of Algorithm PS on K_7 given with the orientation corresponding to the minimal HTC 3-orientation of Figure 1.6. Vertices are numbered in black. The root angle, $(1, 17)$, is identified by a root symbol and chosen in the face for which the orientation is minimal (i.e. the shaded face of Figure 1.6). The magenta points correspond to the angles considered at each iteration of Algorithm PS and the magenta arrows show the order in which those are considered. The output U is a toroidal unicellular map, represented here in an hexagon where the opposite sides are identified.

Proposition 1.12. *For every oriented map G on any oriented surface $\mathbb{S}$ and for any root angle (v_0, e_0), the execution of* Algorithm PS *on $(G, (v_0, e_0))$ terminates.*

From toroidal triangulations to unicellular maps

In the case of toroidal triangulations we know more on the behavior of Algorithm PS (See Figure 1.7).

Theorem 1.13. *Consider a toroidal triangulation T, a root angle (v_0, e_0) such that v_0 is not inside any separating triangle*[7]*, and the orientation of the edges of T corresponding to the minimal HTC 3-orientation w.r.t. the root face f_0. In this case, the output U of* Algorithm PS *is a toroidal spanning unicellular map, with the following properties :*

- *Vertex v_0 has three stems and the other vertices have two stems, but these values decrease by two for a vertex v if it is contained in two edge-disjoint cycles of U, or by one for a vertex v if it is contained in three (not necessarily edge-disjoint) cycles of U.*
- *While walking along the unique face of U counter-clockwisely (according to this face) and starting at the root angle, at any moment, we have been along more edge sides (each edge of U has two sides on this boundary) than the number of stems we have met.*
- *The orientation of U induced by the minimal HTC 3-orientation of T verifies the γ_0 property (considering the edges and the stems of U).*

Note that every toroidal triangulation T has vertices that are not inside any separating triangles. Let us explain why this condition is necessary. In a 3-orientation of a toroidal triangulation, by Euler's formula, all the edges that are incident to a separating triangle Δ and in its interior are oriented towards the triangle. Thus if one applies Algorithm PS from a vertex inside Δ, the algorithm will remain in the interior of Δ, that is it will only consider angles (v, e) such that v is inside Δ. In this case the output cannot be spanning.

7. In other words, v_0 does not belong to an open pseudo-disk of the torus whose boundary is a cycle of length three.

Recovering the original triangulation

Let us now show how to recover the original triangulation from the output of Algorithm PS. The method is very similar to [85] since like in the plane the output has only one face that is homeomorphic to an open disk.

Theorem 1.14. *Consider a toroidal triangulation T, a root angle (v_0, e_0) such that v_0 is not inside any separating triangle and the orientation of the edges of T corresponding to the minimal HTC 3-orientation w.r.t. the root face f_0. From the output U of* Algorithm PS *applied on $(T, (v_0, e_0))$ one can reattach all the stems to obtain T by starting at the root angle and walking along the face of U in counterclockwise order (according to this face) : each time a stem is met, it is reattached in order to create a triangular face on its left side.*

Figure 1.8 illustrates Theorem 1.14 on the example of Figure 1.7.

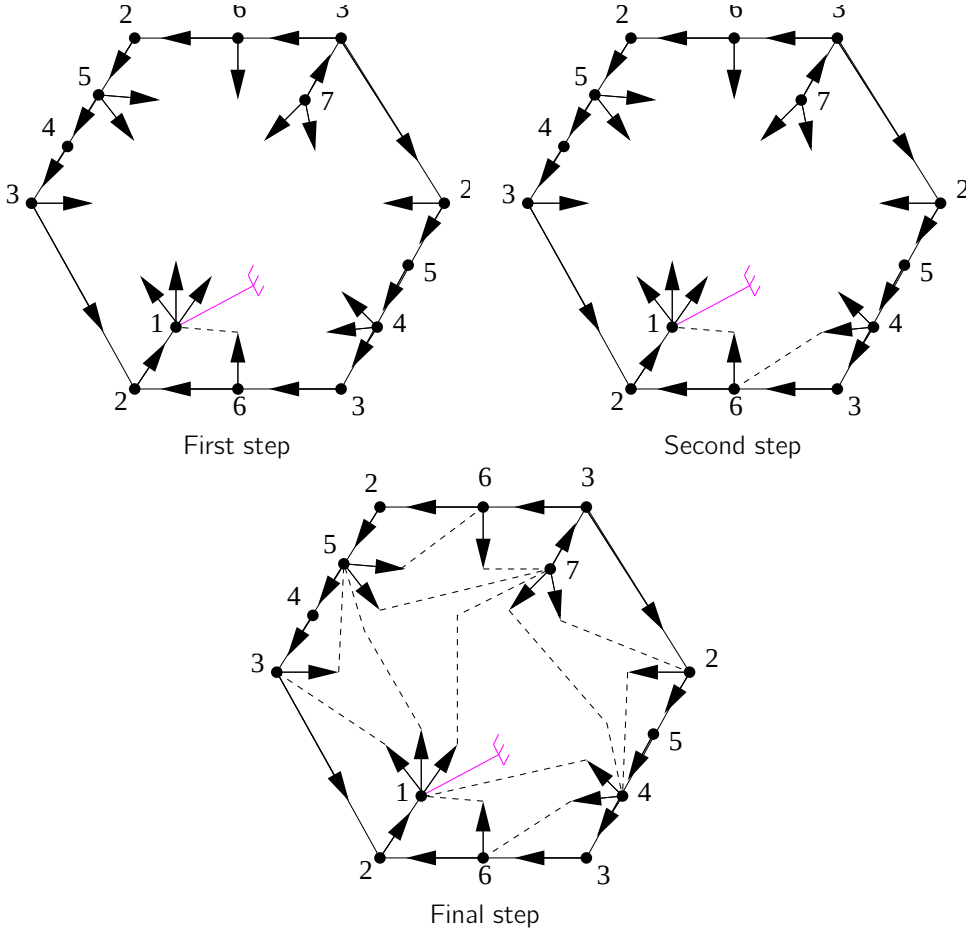

Figure 1.8 – How to recover the original toroidal triangulation from the output of Algorithm PS .

Bijections

Actually the properties of U in Theorem 1.13 almost describe the outputs of Algorithm PS .

Theorem 1.15. *There is a bijection between n-vertex toroidal triangulations rooted at an angle (v_0, e_0) such that v_0 and e_0 are not inside any separating triangle, and n-vertex unicellular maps verifying the properties of Theorem 1.13 and such that their root edge e_0 is a stem*[8]*.*

8. This comes from the fact that e_0 is always outgoing v_0 in the minimal HTC 3-orientation.

Surprisingly, taking the outputs of Algorithm PS , removing their root stem and forgetting the orientation of their edges one obtains an interesting familly of unrooted unicellular maps. We obtained the following bijection on unrooted toroidal maps.

Theorem 1.16. *There is a bijection between the set of n-vertex toroidal maps, where all the faces have length three, except one that has length four and which is not inside a separating triangle, and the set of n-vertex toroidal unicellular maps, with the following properties :*

- *Every vertex has two stems, but this value decreases by two for a vertex v if it is contained in two edge-disjoint cycles, or by one for a vertex v if it is contained in three (not necessarily edge-disjoint) cycles.*
- *Considering only the stems, the map verifies the γ_0 property.*

These unicellular maps are rather simple, and Theorem 1.16 can thus be used to compute the number of such n-vertex quasi-triangulations [9], and maybe also to sample them. The only difficulty comparing to the planar case is the γ_0 property.

Conclusion

Note that Algorithm PS has been studied by other researchers [5, 11], in particular for maps embedded on genus $g \geq 1$ surfaces. Contrarily to [11] our maps T and U have the same genus. This is interesting as fixed genus unicellular maps are getting better understood [29]. The key property that makes U and T have same genus is that there is no non-contractible curve $\mathcal{C}$ of the torus such that all the arcs of T crossing $\mathcal{C}$ cross it in the same direction. We proved [J22] that any simple triangulation of a genus $g \geq 1$ orientable surface admits an orientation of its edges such that every vertex has outdegree at least 3, and divisible by 3. The following would ensure use that Algorithm PS behaves well (i.e. produces a spanning unicellular map).

Conjecture 1.17. A triangulation on a genus $g \geq 1$ orientable surface admits an orientation of its edges such that every vertex has outdegree at least 3, divisible by 3, and such that there is no non-contractible curve $\mathcal{C}$ of the torus such that all the arcs crossing $\mathcal{C}$ cross it in the same direction.

If Conjecture 1.17 is true, one can consider a minimal orientation satisfying its conclusion [10] and apply Algorithm PS to obtain a unicellular map of the same genus. Note that more efforts should be made to obtain a bijection since there might be several minimal orientations [11] satisfying the conjecture and a particular one has to be identified (as the minimal HTC 3-orientation in our case).

1.4 Extensions to (oriented) Surfaces with higher Genus

For higher genus triangulated surfaces, a generalization of Schnyder woods has been proposed by Castelli Aleardi et al. [21], with applications to encoding. In this definition, the simplicity and the symmetry of the original definition of Schnyder woods are lost. Here we propose an alternative generalization of Schnyder woods for higher genus that generalizes the one proposed in [J18] for the toroidal case.

We consider finite maps. Denote by n, m and f the number of vertices, the number of edges, and the number of faces of a map. Euler's formula says that any map on an orientable surface of genus g satisfies $n - m + f = 2 - 2g$. This implies that a triangulation of genus g has exactly $3n + 6(g - 1)$ edges. So to generalize Schnyder woods for all $g \geq 2$ there are too many edges to force all vertices to have outdegree exactly three. This problem can be overcome by allowing vertices to fulfill the Schnyder property (cf Definition 1.1) "several times", i.e. such vertices have outdegree 6, 9, etc. with the color property of Figure 1.1.(a) repeated several times (see Figure 1.9).

9. This was not included in [J24] but should appear in a paper by É. Fusy and B. Lévêque.
10. Note that reversing contractible directed cycles preserves the properties of Conjecture 1.17.
11. Each of these orientations being the unique minimal element in their lattice.

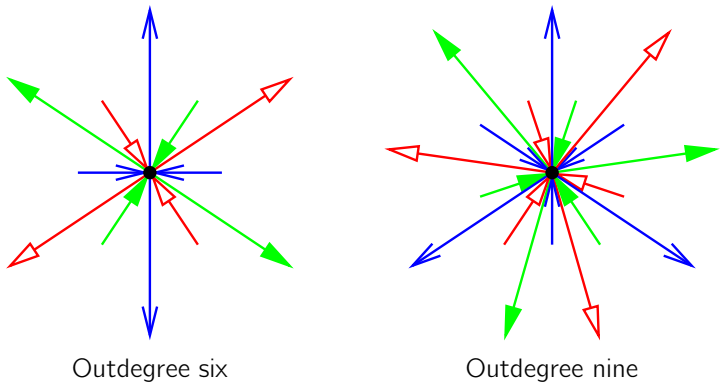

Figure 1.9 – The Schnyder property repeated several times around a vertex.

Figure 1.10 is an example of such a Schnyder wood on a triangulation of the double torus. The double torus is represented by in an octagon whose sides are pairwisely identified as indicated. All the vertices of the triangulation have outdegree three except two vertices, the circled ones, that have outdegree six. Each of the latter appear twice in the representation.

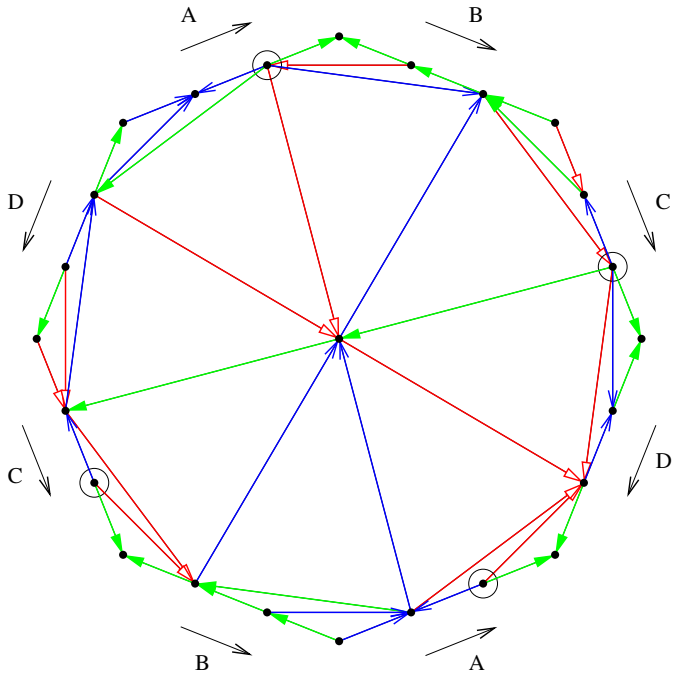

Figure 1.10 – A Schnyder wood of a triangulation of the double torus.

We formalized in [S2] a concept of weak Schnyder woods [12] for general maps (not only triangulations) on arbitrary orientable surfaces. These are defined via angle labelings in Section 1.4.1. Then in Section 1.4.2, we characterize the orientations that correspond to these weak Schnyder woods. While every map admits a "trivial" Schnyder wood, the existence of a non-trivial one remains open but leads to interesting conjectures.

12. We call them weak Schnyder woods in this manuscript because for the torus the definition will be weaker than Definition 1.5.

1.4.1 Angle labelings

Consider a map G on an orientable surface. An *angle* is a face corner at a vertex, and an *angle labeling* of G is a labeling of its angles with colors 0, 1, 2. More formally, we denote an angle labeling by a function $\ell : \mathcal{A} \to \mathbb{Z}_3$, where $\mathcal{A}$ is the set of angles of G. Given an angle labeling, we define several properties of vertices, faces and edges that generalize the notion of Schnyder angle labeling in the planar case [47].

Consider an angle labeling ℓ of G. A vertex or a face v is of *type* k, for $k \geq 1$, if the labels of the angles around v form, in counterclockwise order, $3k$ nonempty intervals such that in the j-th interval all the angles have color ($j \mod 3$). A vertex or a face v is of *type* 0, if the labels of the angles around v are all of color i for some i in $\{0, 1, 2\}$.

An edge e is of *type* 1 or 2 if the labels of the four angles incident to this edge are, in clockwise order, $i-1$, i, i, $i+1$ for some i in $\{0, 1, 2\}$. The edge e is of *type* 1 if the two angles with the same color are incident to the same extremity of e and of *type* 2 if the two angles are incident to the same side of e. An edge e is of *type* 0 if the labels of the four angles incident to e are all i for some i in $\{0, 1, 2\}$ (See Figure 1.11).

If every vertex (resp. edge, or face) x of G is of type $f(x)$, for some function $f : X \to \mathbb{N}$, we say that ℓ is VERTEX (resp. EDGE, or FACE). If every vertex (resp. edge, or face) x of G is of type 1, we say that ℓ is 1-VERTEX (resp. 1-EDGE, or 1-FACE). If every vertex (resp. face) x of G is of type $f(x)$, for some function $f : X \to \mathbb{N}^* = \mathbb{N} \setminus \{0\}$, we say that ℓ is $\mathbb{N}^*$-VERTEX (resp. $\mathbb{N}^*$-FACE). The following lemma expresses that property EDGE is the central notion here.

Lemma 1.18. *Any EDGE angle labeling is VERTEX and FACE.*

Thus we define weak Schnyder labeling and weak Schnyder woods as follows :

Definition 1.19 (weak Schnyder labeling)**.** Given a map G on an orientable surface, a *weak Schnyder labeling* of G is an EDGE angle labeling of G. A *weak Schnyder wood* is an orientation and coloring of the edges of G with edges oriented in one direction or in two opposite directions if it is obtained by applying the rules of Figure 1.11 from a weak Schnyder labeling of G.

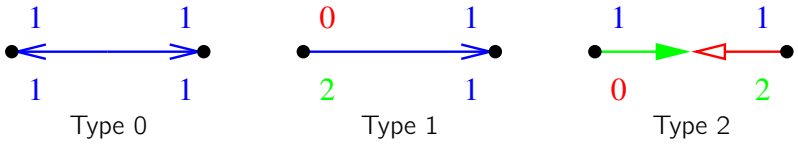

Figure 1.11 – Correspondence between EDGE angle labelings and some bi-orientations and colorings of the edges.

Any map (on any orientable surface) admits a trivial EDGE angle labeling : the one with all angles labeled i (and thus all edges, vertices, and faces are of type 0). A natural non-trivial case, that is also symmetric for the duality, is to consider EDGE, $\mathbb{N}^*$-VERTEX, $\mathbb{N}^*$-FACE angle labelings of general maps. In planar Schnyder woods only type 1 and type 2 edges are used. Here we allow type 0 edges because they seem unavoidable for some maps (see discussion below). Figure 1.10 is an example of a weak Schnyder wood obtained from an EDGE, $\mathbb{N}^*$-VERTEX, $\mathbb{N}^*$-FACE angle labelings.

For every $g \geq 2$, there are genus g maps, with vertex degrees and face degrees at most five. Figure 1.12 depicts how to construct such maps, for all $g \geq 2$. For these maps, type 0 edges are unavoidable. Indeed, take such a map with an angle labeling that has only type 1 and type 2 edges. Around a type 1 or type 2 edge there are exactly three changes of labels, so in total there are exactly $3m$ such changes. As vertices and faces have degree at most five, they are either of type 0 or 1, hence the number of label changes should be at most $3n+3f$. Thus, $3m \leq 3n + 3f$, which contradicts Euler's formula for $g \geq 2$. Furthermore, note that the maps described in Figure 1.12, as well as their dual maps, are 3-connected. Actually they can be modified to be 4-connected

and of arbitrary large face-width [13]. Note that these maps admit EDGE, $\mathbb{N}^*$-VERTEX, $\mathbb{N}^*$-FACE angle labelings (using type 0 edges), but those are not described in this manuscript.

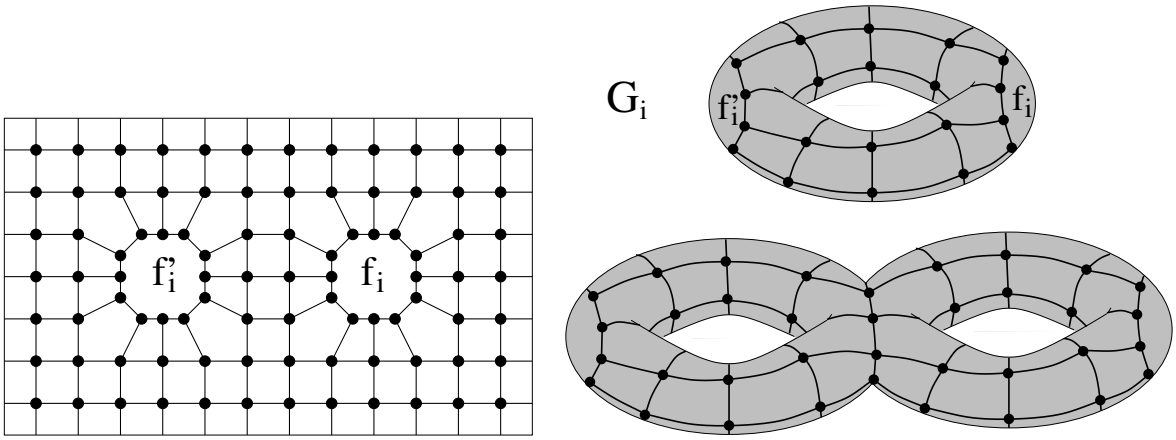

Figure 1.12 – A toroidal map G_i with two distinguished faces, f_i and f_i'. Take g copies G_i with $1 \leq i \leq g$ and glue them by identifying f_i and f'_{i+1} for all $1 \leq i < g$. Faces f_1 and f'_g are filled to have only vertices and faces of degree at most five.

The planar maps that admit a planar Schnyder wood ar exactly the internally 3-connected ones (c.f. Theorem 1.4). We similarly showed that a toroidal map admits a Schnyder wood, if and only if it is essentially 3-connected (c.f. Theorem 1.8). We showed the following for weak Schnyder labelings.

Theorem 1.20. *If a map G on a genus $g \geq 1$ orientable surface admits an EDGE, $\mathbb{N}^*$-VERTEX, $\mathbb{N}^*$-FACE angle labeling, then G is essentially 3-connected.*

We conjecture that this characterizes the maps that admit such angle labelings.

Conjecture 1.21. A map on a genus $g \geq 1$ orientable surface admits an EDGE, $\mathbb{N}^*$-VERTEX, $\mathbb{N}^*$-FACE angle labeling if and only if it is essentially 3-connected.

As we will see in Section 1.5, and as already mentioned, every simple triangulation on a genus $g \geq 1$ orientable surface admits an orientation of its edges such that every vertex has outdegree at least three, and divisible by three. This suggests the existence of 1-EDGE angle labelings with no sinks, i.e. 1-EDGE, $\mathbb{N}^*$-VERTEX angle labelings. One can easily check that in a triangulation, a 1-EDGE angle labeling is also 1-FACE. Thus we can hope that a triangulation on a genus $g \geq 1$ orientable surface admits a 1-EDGE, $\mathbb{N}^*$-VERTEX, 1-FACE angle labeling. Note that a 1-EDGE, 1-FACE angle labeling of a map implies that faces have size three. So we propose the following conjecture, whose "only if" part follows from the previous sentence :

Conjecture 1.22. A map on a genus $g \geq 1$ orientable surface admits a 1-EDGE, $\mathbb{N}^*$-VERTEX, 1-FACE angle labeling if and only if it is a triangulation.

Conjecture 1.21 implies Conjecture 1.22 since for a triangulation every face would be of type 1, and thus every edge would be of type 1. Conjecture 1.21 is proved for $g = 1$ [J18] whereas both conjectures are open for $g \geq 2$.

13. For many problems, maps with high face-width are easier to handle. The *face-width* of a map G is the smallest number k such that there is a non-contractible closed curve that intersects G in k points.

1.4.2 Orientations of weak Schnyder woods

It was shown by de Fraysseix et al. [58], that for any planar triangulation every orientation of its inner edges where every inner vertex has outdegree three corresponds to a Schnyder wood. Thus, any orientation with the proper outdegree corresponds to a Schnyder wood and there is a unique way, up to symmetry of the colors, to assign colors to the oriented edges in order to fulfill the Schnyder property at every inner vertex. This is not true in higher genus as already in the torus, there exist orientations that do not correspond to any Schnyder wood (see Figure 1.13), not even to a weak Schnyder wood.

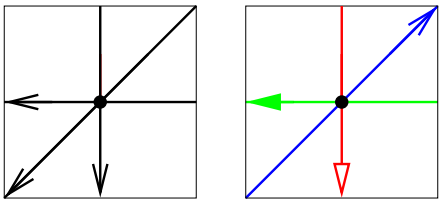

Figure 1.13 – Two different orientations of a toroidal triangulation. Only the one on the right corresponds to a (weak) Schnyder wood.

Consider a map G on an orientable surface of genus g. The orientation of G defined by a weak Schnyder woods can be defined more naturally in the primal-dual-completion of G, as there is no more edges oriented in two directions. The *primal-dual-completion* $\hat{G}$ is the map obtained from simultaneously embedding G and G^* such that vertices of G^* are embedded inside faces of G and vice-versa. Moreover, each edge crosses its dual edge in exactly one point in its interior, which also becomes a vertex of $\hat{G}$. Hence, $\hat{G}$ is a bipartite graph with one part consisting of *primal-vertices* and *dual-vertices* and the other part consisting of *edge-vertices* (of degree four). Each face of $\hat{G}$ is a quadrangle incident to one primal-vertex, one dual-vertex and two edge-vertices. Actually, the faces of $\hat{G}$ are in correspondance with the angles of G. This means that angle labelings of G correspond to face labelings of $\hat{G}$.

Given $\alpha : V \to \mathbb{N}$, an orientation of G is an *α-orientation* [46] if for every vertex $v \in V$ its outdegree $d^+(v)$ equals $\alpha(v)$. We call an orientation of $\hat{G}$ a *$\mod 3$-orientation* if it is an α-orientation for a function α satisfying :

$$\alpha(v) \equiv \begin{cases} 0 \ (\mathrm{mod}3) & \text{if } v \text{ is a primal- or dual-vertex,} \\ 1 \ (\mathrm{mod}3) & \text{if } v \text{ is an edge-vertex.} \end{cases}$$

Note that an EDGE angle labeling (i.e. a weak Schnyder wood) of G corresponds to a mod_3-orientation of $\hat{G}$, by the mapping of Figure 1.14, where the three types of edges are represented. Type 0 corresponds to an edge-vertex of outdegree four. Type 1 and type 2 both correspond to an edge-vertex of outdegree 1 ; in type 1 (resp. type 2) the outgoing edge goes to a primal-vertex (resp. dual-vertex). In all cases we have $d^+(v) \equiv 1 \ (\mathrm{mod}3)$ if v is an edge-vertex. By Lemma 1.18, the labeling is also VERTEX and FACE. Thus, $d^+(v) \equiv 0 \ (\mathrm{mod}3)$ if v is a primal- or dual-vertex.

As mentioned earlier, de Fraysseix et al. [58] showed for planar triangulations, that every internal 3-orientations corresponds to a Schnyder wood. Felsner [46] generalized this result for planar Schnyder woods and orientations of the primal-dual completion having prescribed out-degrees. The situation is more complicated in higher genus (see Figure 1.13). It is not enough to prescribe outdegrees in order to characterize orientations corresponding to weak Schnyder woods. We call an orientation of $\hat{G}$ corresponding to a weak Schnyder wood of G a *weak Schnyder orientation*. In the following we show how to characterize these orientations.

Consider a (not necessarily directed) cycle C of G together with a direction of traversal. We associate to C its corresponding cycle in $\hat{G}$ denoted by $\hat{C}$. We define $\gamma(C)$ by :

$$\gamma(C) = \#\text{ edges of } \hat{G} \text{ leaving } \hat{C} \text{ on its right} - \#\text{ edges of } \hat{G} \text{ leaving } \hat{C} \text{ on its left}$$

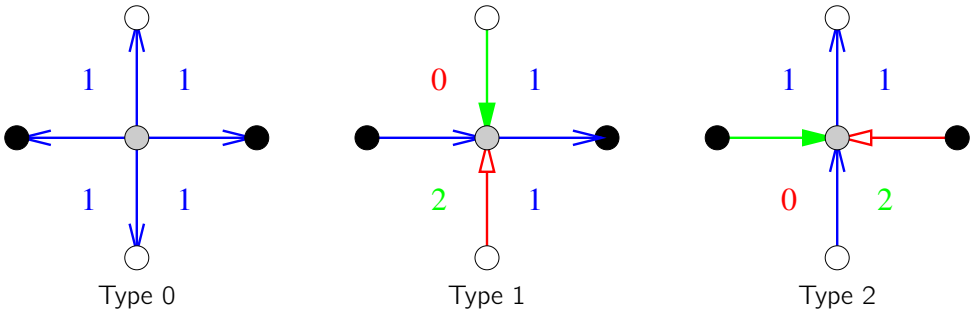

Figure 1.14 – How to map a weak Schnyder labeling to a mod_3-orientation of the primal-dual completion. Primal-vertices are black, dual-vertices are white and edge-vertices are gray.

Theorem 1.23. *Consider a map G on an orientable surface of genus g. Let $\{B_1, \ldots, B_{2g}\}$ be a set of cycles of G that forms a basis for the homology. An orientation of $\hat{G}$ is a weak Schnyder orientation if and only if it is a* mod_3*-orientation such that $\gamma(B_i) \equiv 0 \pmod 3$, for all $1 \leq i \leq 2g$.*

For a given map G, the set of weak Schnyder orientations of $\hat{G}$ with same values $\gamma(B_1), \ldots, \gamma(B_{2g})$ has a lattice structure. The elements (orientations of $\hat{G}$) are linked if they differ only on a directed closed walk W that is null-homologous. If W is a directed separating cycle (which is thus null-homologous), it crosses B_i from left to right as many times as it crosses it from right to left. It is thus clear (in this case) that reversing the edges of W does not change $\gamma(B_i)$. In Section 1.3.2 we used the fact that for toroidal triangulations, all the orientations of $\hat{G}$ corresponding to (non-weak) Schnyder woods belong to the same lattice. This lattice is the one for which $\gamma(B_i) = 0$, for all $1 \leq i \leq 2g$. Note that this does not depend on the choice of the basis $\{B_1, \ldots, B_{2g}\}$ as in this case $\gamma(C) = 0$ for every non-contractible cycle C.

1.5 $(0 \mod 3)$-Orientations

This section is devoted to the following theorem [J22] that was conjectured by Barát et al. [9].

Theorem 1.24. *Every simple triangulation T of a surface of Euler genus*[14] *$k \geq 2$ has an orientation such that each outdegree is at least* 3*, and divisible by* 3*.*

Barát et al.'s proved it for small Euler genus, and for any Euler genus, they proved a weaker version where sinks (i.e. outdegree zero vertices) are allowed. Their conjecture was originally motivated in the context of claw-decompositions of graphs, since given an orientation with the claimed properties the outgoing edges of each vertex can be divided into claws, such that every vertex is the center of at least one claw. Our motivation was more related to Conjecture 1.22, as Theorem 1.24 may be a step towards proving this conjecture. Similarly, answering to the following conjecture would be a step towards Conjecture 1.21 .

Conjecture 1.25. Given an essentially 3-connected map G, its primal-dual-completion $\hat{G}$ has an orientation where primal- and dual-vertices have non-zero outdegrees divisible by three, and where edge-vertices have indegrees divisible by three, that is indegree 0 or 3 (i.e. outdegree 4 or 1).

Recall also that Conjecture 1.17 asks for an improvement of Theorem 1.24 towards obtaining orientations of triangulations that behave well with respect to Algorithm PS . Before going into the proof of Theorem 1.24 let us define induced submaps. Given a triangulation T and a set of vertices $X \subseteq V(T)$, the *induced submap* $T[X]$ is simply the maximal submap with vertex set X. In other words this submap has edge set $\{uv \in E(T) \mid u \in X \text{ and } v \in X\}$, and face set $\{uvw \in F(T) \mid u \in X, v \in X, \text{ and } w \in X\}$. Note that submaps are thus embedded graphs with (a few) faces, that are a subset of the embedded graph's faces.

14. The *Euler genus* of a map is $2 - n + m - f$, where n, m and f stand for the number of vertices, edges, and faces.

1.5.1 Proof of Theorem 1.24

We consider a triangulation T that is a minimal counter example. Then there are several stages. We first prove that one can partition the edges of the triangulation T into the following graphs :

— The *initial graph* I, which is an induced submap containing a non-contractible cycle. Furthermore, I contains an edge uv such that the map $I \setminus uv$ is a maximal outerplanar graph with only two degree two vertices, u and v. See Figure 1.15 for an illustration.

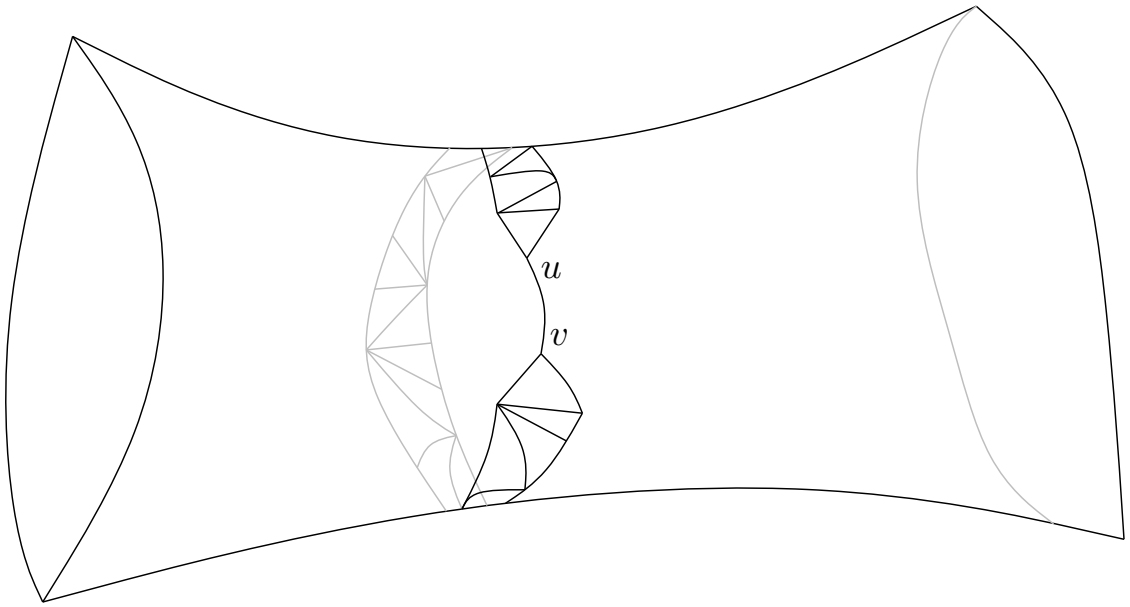

Figure 1.15 – Example of a submap I.

— The *correction graph* B (with blue edges), which is oriented acyclically in such a way that each vertex of $V(T) \setminus V(I)$ has outdegree 2, while the other vertices have outdegree 0,

— The *last correction path* G (with green edges), which is a $\{u, v\}$-path.

— The *non-zero graph* R (with red edges), which is oriented in such a way that all vertices in $(V(T) \setminus V(G)) \cup \{u, v\}$ have out-degree at least 1.

Finding the submap I

We do not explain this not very interesting part of the proof.

Constructing B, G, and R

Starting from I we incrementally explore the whole triangulation T by stacking the vertices one by one (this procedure is inspired by [21]). At each step, we will assign the newly explored edges to B, G or R, and we will orient those assigned to B or R. At each step the *explored region* is a submap of T induced by some vertex set X. Such explored region is denoted by $T[X]$ and its boundary $\partial T[X]$ (See Figure 1.16 for an illustration).

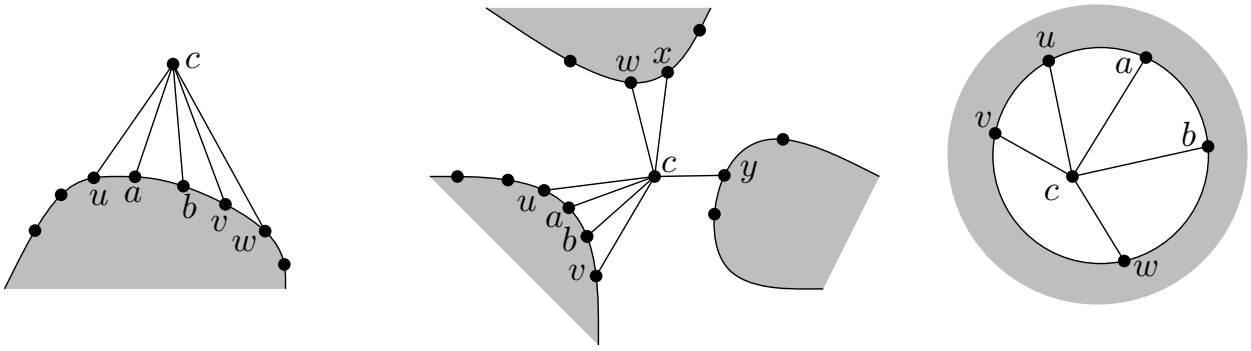

Figure 1.16 – Different types of stacking a vertex c on an induced submap M (grey region). Left : one neighboring path $P_1 = (u, a, b, v, w)$. Middle : three neighboring paths $P_1 = (u, a, b, v)$, $P_2 = (w, x)$, $P_3 = (y)$. Right : A boundary cycle $C = (u, v, w, b, a)$.

During the exploration we maintain the following invariants :

(I) The graphs I, B, G, and R partition the edges of $T[X]$.

(II) All interior vertices of $T[X]$ (i.e. in $X \setminus V(\partial T[X])$) have at least one outgoing R-arc, or two incident G-edges. Furthermore G either is an $\{u, v\}$-path, or is the union of two vertex disjoint paths G_u and G_v, going from u to u_*, and from v to v_*, respectively, for some vertices u_* and v_* on $\partial T[X]$.

Here the vertices u_* and v_* may coincide with vertices u and v, respectively, if G_u or G_v is trivial.

(III) The graph B is acyclically oriented in such a way that the vertices of I have outdegree 0, while the other vertices of $T[X]$ have outdegree 2.

Furthermore, to help us in properly finishing the construction of the graphs B, G and R in the further steps, we introduce the notion of *requests* on the angles[15] of $\partial T[X]$. There are two types of requests, G-requests and R-request. An angle is allowed to have at most one request, and an angle having no request is called *free*. Informally, a G-request (resp. an R-request) for an angle $\widehat{a}$ means that in a further step an edge inside this angle will be added in G (resp. in R and oriented from a to the other end).

(IV) Every vertex of $(\partial T[X] \setminus \{u_*, v_*\}) \cup \{u, v\}$ having (still) no outgoing R-arc, has an incident angle with an R-request.

(V) If G is not a $\{u, v\}$-path (yet), the vertices u_* and v_* (at the end of G_u and G_v, respectively), have one incident angle each, say $\widehat{u_*}$ and $\widehat{v_*}$, that are consecutive on $\partial T[X]$, and that have a G-request. Furthermore, there are no other G-requests.

(VI) If there is an unexplored disk D[16] , then there are at least three free angles (of $\partial T[X]$) around D.

One can observe that if these invariants are maintained until the end of the exploration, we obtain the desired partition of the edges.

15. Here an angle is a triplet (e, v, e') of consecutive elements of $\partial T[X]$.
16. An *unexplored disk* D is an open pseudo disk that does not intersect $T[X]$ but whose border is contained in $T[X]$.

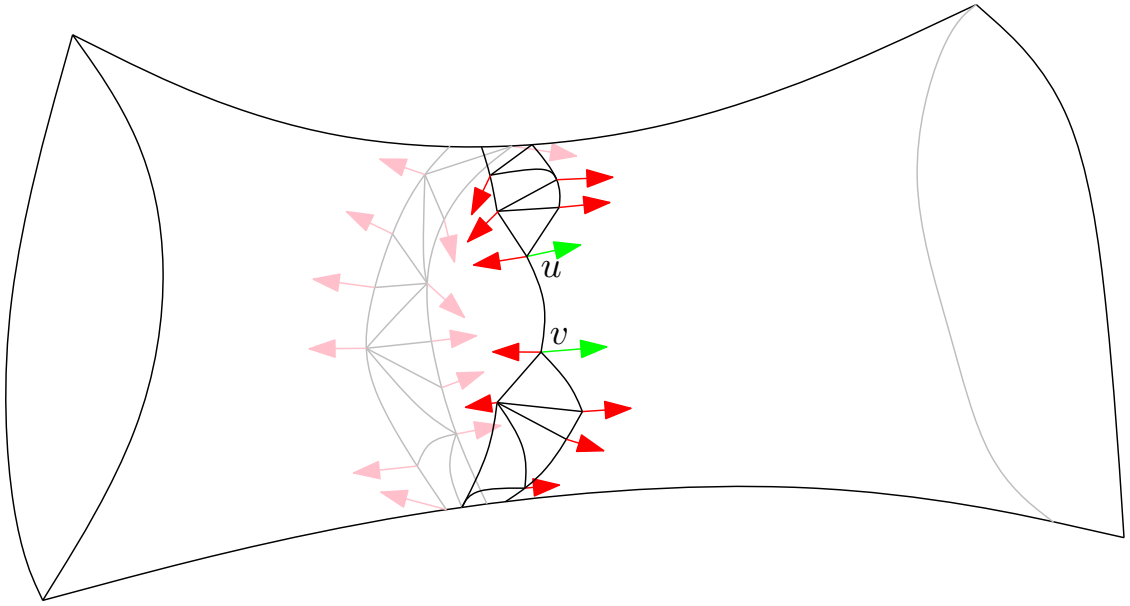

Figure 1.17 – Assigning requests to I in order to satisfy the invariants. G-requests are green, R-requests are red.

The exploration starts with $T[X] = I$ with the following setting of requests on the angles (see Figure 1.17). Set the angles of consecutive appearance of u, v as G-requests, while all the other angles are assigned R-requests. Then one can check that (I)-(VI) are satisfied. We do not explain here how to choose the next vertex to stack, how to partition and color the new edges, nor how to assign requests to the new angles.

Reorienting B

Here we use the same approach as in the proof of Theorem 4.5 in [9]. Given a partial orientation O of T we define the *demand* of a vertex v as $\mathrm{dem}_O(v) := -\delta^+_{|O}(v) \mod 3$, where $\delta^+_{|O}(v)$ denotes the outdegree of v with respect to O. We want to find an orientation of T with all demands 0.

We do not modify the orientation on R, and this guarantees that all vertices in $(V(T) \setminus V(G)) \cup \{u, v\}$ have non-zero outdegrees. Furthermore, as G will be oriented either entirely forward or backwards (this will be chosen later), all its interior vertices will have non-zero outdegrees. Hence every vertex of $T[X]$ has non-zero outdegree. Suppose that G is entirely oriented forward.

Now we linearly order vertices in $V(T) \setminus V(I) = (v_1, \ldots, v_\ell)$ such that with respect to B every vertex has its two outgoing B-neighbors among its predecessors and I (this corresponds to the order the stacking was performed). Denote by B_i the subgraph of B induced by the arcs leaving $v_i, \ldots, v_\ell$ (before the reorienting). We process $V(T) \setminus V(I)$ from the last to the first element. At a given vertex v_i we look at $\mathrm{dem}_{G \cup R \cup B_i}(v_i)$ and reorient the two originally outgoing B-arcs of v_i in such a way that afterwards $\mathrm{dem}_{G \cup R \cup B_i}(v_i) = 0$ (i.e. $\delta^+_{|G \cup R \cup B_i}(v_i) \equiv 0 \mod 3$). As these B-arcs were heading at I or at a predecessor, the demand on the vertices v_j, with $j > i$, is not modified and hence remains 0. Denote by O the obtained partial orientation of T.

Orienting G and I

Now pick an orientation of G (either all forward or all backward) and of uv such that for the resulting partial orientation O' we have $\mathrm{dem}_{O'}(v) = 1$. Let Δ be the triangle of I containing v. Since $I \setminus uv$ is a maximal outerplanar graph it can be peeled by removing degree two vertices until reaching Δ. When a vertex x is removed orient its two incident edges so that $\mathrm{dem}_{O'}(x) = 0$ (as for B-arcs). We obtain a partial orientation O'', such that

all vertices have non-zero outdegree, and such that all vertices except the ones of Δ have outdegree divisible by 3. Since the number of edges of T, and the number of edges of Δ are divisible by 3, the number of edges of $T \setminus \Delta$ is divisible by 3. As this number equals the sum of the outdegrees in O'', and as every vertex out of Δ has outdegree divisible by 3, then the outdegree of Δ's vertices sum up to a multiple of 3. Hence their demands sum up to 0, 3 or 6. As $\mathrm{dem}_{O''}(v) = \mathrm{dem}_{O'}(v) = 1$, the demands of the other two vertices of Δ are either both 1, or 0 and 2. It is easy to see that in either case Δ can be oriented to satisfy all three demands.

Chapitre 2

Intersection Representations for Planar Graphs

2.1 Introduction

Intersection graphs form a large part of nowadays studied classes of graphs. This chapter will only cover a small part of this broad research area. We will only consider intersection graphs of connected shapes in the plane. Research on representations of (planar) graphs by contact or intersection of predefined shapes in the plane started with the work of Koebe in 1936 [71].

Given a shape [1] X, an *X-intersection representation* is a collection of X-shaped geometrical objects in the plane. The *X-intersection graph* described by such a representation has one vertex per geometrical object, and two vertices are adjacent if and only if the corresponding objects intersect. An *intersection representation of a graph* $G = (V, E)$ is thus an intersection representation $\mathcal{C} = \{c(v) : v \in V\}$, such that two geometrical objects, $c(u)$ and $c(v)$, intersect if and only if their corresponding vertices are adjacent, i.e. $uv \in E$. The shapes that are homeomorphic to a segment or to a disk are respectively referred to as *pseudo-segments* or as *pseudo-disks*. If the shape X is a pseudo-segment (resp. a pseudo-disk), an *X-contact representation* is an X-intersection representation such that if an intersection occurs between two objects, then it occurs at a single point that is the endpoint of one of them (resp. it occurs on their boundary). We say that a graph G is an *X-contact graph* if it is the X-intersection graph of an X-contact representation.

2.1.1 Pseudo-disks

The case of shapes homeomorphic to discs has been widely studied ; see for example the literature for disks [71, 6, 33], triangles [57, J13], homothetic triangles [69, 92], rectangles [97, 54], squares [91, 74], hexagons [63], convex bodies [90], or (non-convex) axis aligned polygons [4]. Most of these works actually deal with contact representations.

A *contact point* of a contact representation is a point that is in the intersection of (at least) two shapes. A contact representation is said *simple* if for any two intersecting shapes there is a contact point contained by these two shapes only. Observe that a simple contact representation by pseudo-disks $\mathcal{C} = \{c(v) : v \in V\}$ necessarily represents a plane graph. Indeed, one can draw the represented graph by choosing any point p_v inside $c(v)$, for representing each vertex v, and by drawing curves from p_v to the "private" contact points around $c(v)$ to represent the edges incident to v.

The circle packing theorem of Koebe [71] states that every planar graph admits a contact representation by circles. Here, vertices are represented by homothetic objects, circles. Another case has been explored, the case

1. We do not provide a formal definition of *shape*, but a shape characterizes a family of connected geometric objects in the plane.

of squares, using different tools [91, 74]. Both papers show that 5-connected planar triangulations minus one edge are contact graphs of axis parallel squares.

Several works considered contact representations by shapes that are not necessarily homothetic. Koebe's theorem implies that every planar graph has a contact representation by convex polygons, and de Fraysseix et al. [57] strengthened this by showing that every planar graph admits a contact representation by triangles.

Thomassen [97] considered the contact graphs of axis parallel rectangles. One can observe that such contact representation provides (following the procedure described above) a plane graph where each triangle bounds an inner face. Thomassen proved that this property characterizes these contact graphs. In other words these contact graphs are exactly the proper subgraphs (i.e. strict subgraphs) of 4-connected planar triangulations. The subgraphs being proper one can draw them so that the outerface has length at least four, and the 4-connectedness ensures that every triangle bounds an inner face. Fusy [61, 62] then studied the structures (named *transversal structures*) defined by such contact representations, and used those to design new bijections (linking triangulations and loopless maps) and a drawing algorithm.

Gansner et al. [63] proved that every planar graph has a contact representation with convex hexagons which sides use only 3 slopes (i.e. hexagons with two horizontal sides and which angles are all $\frac{2}{3}\pi$) and where the intersection between two shapes is a segment (not a single point).

Using non-combinatorial arguments Schramm proved a powerfull and very general result, sometimes referred to as the *monster packing theorem*. This theorem deals with any kind of convex shapes [90].

Theorem 2.1 (monster packing theorem [90])**.** *Let T be a planar triangulation with outerface abc. Let $\mathcal{C}$ be a simple closed curve in the plane, and let $c(a)$, $c(b)$, $c(c)$ be three arcs composing $\mathcal{C}$, which are determined by three distinct points of $\mathcal{C}$. For each vertex $v \in V(T) \setminus \{a, b, c\}$, let there be a prototype $\mathcal{P}_v$, which is a convex shape in the plane containing more than one point. Then there is a contact representation in the plane $\mathcal{C} = \{c(v) : v \in V(T)\}$, where each $c(v)$ for $v \in V(T) \setminus \{a, b, c\}$ is either degenerated to a point or (positively) homothetic to $\mathcal{P}_v$, and such that T is a subgraph of the contact graph induced by $\mathcal{C}$.*

We will see in Section 2.2 how this led us to prove the following theorem that was conjectured by Kratochvíl [73] (see also [8]).

Theorem 2.2. *Every 4-connected planar triangulation admits a contact representation by homothetic triangles.*

Then we will use this result as a building block for proving the following result.

Theorem 2.3. *A graph is planar if and only if it is the intersection graph of homothetic triangles, where the intersection of any three triangles is empty.*

This answers a conjecture of Lehmann that planar graphs are max-tolerance graphs (as max-tolerance graphs have shown to be exactly the intersection graphs of homothetic triangles [69]).

There are also many works dealing with contact representations by non-convex shapes such as axis aligned polygons. In order to bypass the limitations of *rectangular cartograms* [96], researcher studied *cartograms* for visualization purposes (e.g. for geographical data) [4]. These cartograms are actually contact representations by polygons which sides are axis parallel. From Thomassen's characterization of contact representations by rectangles, it follows that every 4-connected triangulation admits a contact representation by L-shaped hexagons. We improved this a bit by restraining ourselves to L-shaped hexagons drawn on the integer grid so that the branches of each L are one unit thick (i.e. the topmost and rightmost sides have length one), and so that two touching L's touch on a segment [2]. We call such a representation a *thick L contact representation*.

Theorem 2.4. *Every 4-connected triangulation admits a thick L contact representation.*

We will sketch the proof of this result in Section 2.5.2.

2. This deviate's a little from the original result in [C25] where L's can intersect on a single point.

A *primal-dual contact representation* $(\mathcal{V}, \mathcal{F})$ of a planar map G is a pair of contact representations $\mathcal{V} = \{c(v) : v \in V(G)\}$ and $\mathcal{F} = \{c(f) : f \in V(G^*)\}$, such that $\mathcal{V}$ is a contact representation of G, and $\mathcal{F}$ is a contact representation of G^*, the dual of G, and for every edge uv, bordering faces f and g, the intersection between $c(u)$ and $c(v)$ equals the intersection between $c(f)$ and $c(g)$. Andre'ev [6] strengthened Koebe's theorem as follows :

Theorem 2.5 (Andre'ev [6])**.** *Every 3-connected planar map admits a primal-dual contact representation by circles.*

We proved an analogous result concerning contact representations by triangles. We say that a primal-dual contact representation by triangles is *tiling* if the triangles corresponding to vertices and those corresponding to inner faces form a tiling of the triangle corresponding to the outer face (see Figure 2.1).

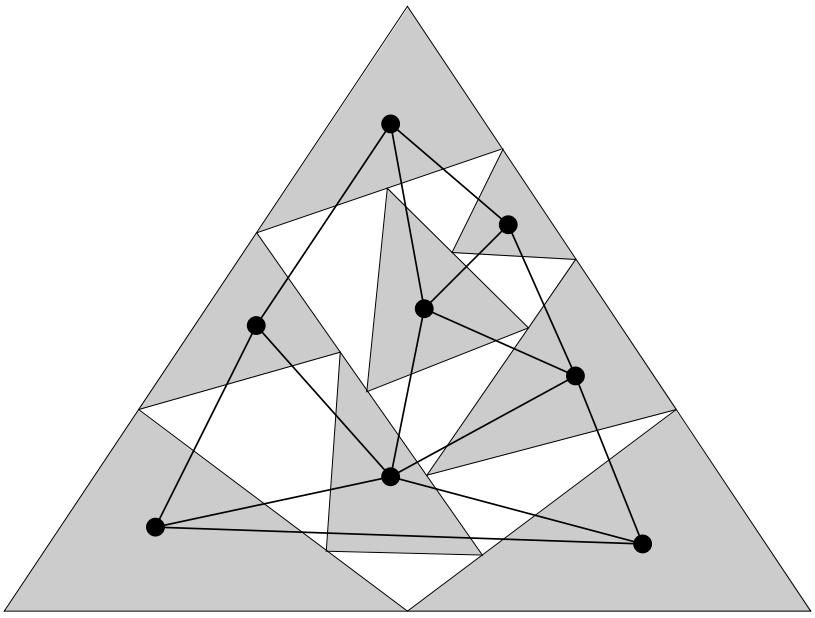

Figure 2.1 – A tiling primal-dual contact representation by triangles

Theorem 2.6. *Every internally 3-connected planar map admits a tiling primal-dual contact representation by triangles.*

In [64], Gansner et al. study representation of graphs by triangles where two vertices are adjacent if and only if their corresponding triangles are intersecting on a segment (they call them *touching representation by triangles*). Theorem 2.6 shows that for 3-connected planar graphs, the incidence graph between vertices and faces admits a touching representation by triangles. We will sketch the proof of Theorem 2.6 in Section 2.3.

2.1.2 Pseudo-segments

In his PhD thesis [87], Scheinerman conjectured that every planar graph has an intersection representation by segments. Several results partially confirmed this conjecture. Hartman et al. [66], de Fraysseix et al. [41], and Czyzowicz et al. [34] proved it for bipartite planar graphs. The case of triangle-free planar graphs was proved by de Castro et al. [23] and more recently de Fraysseix et al. [43] proved it for every planar graph that has a 4-coloring in which every induced cycle of length 4 uses at most 3 colors. We provided two proofs of this conjecture [C12, C25], the most recent one being much simpler that the former one. In this manuscript we will

sketch both proofs (in Section 2.4.3 and in Section 2.5), and we will explain intermediate results that led us to these proofs. To explain these intermediate results, we need a few definitions.

Here, we focus on intersection and contact representations of planar graphs with different types of pseudo-segments. The more general representations of this type are the intersection or contact representations with pseudo-segments (also known as *strings* in this context). It is known that every planar graph has an intersection representation by strings [38]. Indeed, one just has to take a contact representation by circles, and cut the circles to turn them into strings. If one wants to avoid tangent points it suffices to inflate the circles a little. In this case, a pair of strings can cross each other at most twice.

Definition 2.7. A *1-string representation* of a graph is an intersection representation by strings where (1) strings cannot intersect tangentially, and where (2) every two strings intersect at most once.

Seeking a proof of Scheinerman's conjecture, it was suggested [42, 72] to first prove it for slack segments, with the idea in a second time to stretch them and obtain a segment representation. Thus condition (1) and (2) of Definition 2.7 are necessary. This approach of Scheinerman's conjecture was decisive since we first proved that every planar graph has a 1-string representation [J9], and then we manage to improve this proof to obtain the first proof of Scheinerman's conjecture [C12].

Theorem 2.8. *Every planar graph has a 1-string representation.*

Theorem 2.9. *Every planar graph has a segment intersection representation.*

However, note that the latter construction is not a stretching of the former one. One difficulty in these constructions is that the obtained representations somehow violate the original embedding of the planar graph. Actually, Biedl et al. [15] showed that some planar graphs, like planar 3-trees, do not have an order-preserving 1-string representation (that is a representation where the order of the crossings allong a string follow the order of the edges around the corresponding vertex).

In order to introduce the second proof of Scheinerman's conjecture we need to define the following graph classes. A graph is said to be a *VPG-graph* (Vertex-Path-Grid) if it has a contact or intersection representation in which each vertex is assigned to a path of vertical and horizontal segments (see [2, 32]). Asinowski et al. [7] showed that the class of VPG-graphs is equivalent to the class of graphs admitting a string representation. They also defined the class B_k-*VPG*, which contains all VPG-graphs for which each vertex is represented by a path with at most k bends (see [55] for the determination of the value of k for some classes of graphs). It is known that B_k-VPG $\subsetneq$ B_{k+1}-VPG, and that the recognition of graphs of B_k-VPG is an NP-complete problem [26]. These classes have interesting algorithmic properties (see [77] for approximation algorithms for independence and domination problems in B_1-VPG graphs), but most of the literature studies their combinatorial properties.

Chaplick et al. [28] proved that planar graphs are B_2-VPG graphs. This result was recently improved by Biedl et al. [13], as they showed that planar graphs have a 1-string B_2-VPG representation.

Various classes of graphs have been shown to have 1-string B_1-VPG representations, such as planar partial 3-trees [12] and Halin graphs [40]. In these representations, each vertex is assigned to a path formed by at most one horizontal and one vertical segment. There are different types of such paths. For example, the $\llcorner$ shape defines paths where the vertical segment is above and to the left of the horizontal one. Interestingly, it has been shown that the class of simple segment contact graphs is equivalent to the one of B_1-VPG contact graphs [70]. This implies in particular that triangle-free planar graphs are B_1-VPG contact graphs. This has been improved by Chaplick et al. [28] as they showed that triangle-free planar graphs are in fact $\{\llcorner, \ulcorner, |, -\}$-contact graphs (that is without using the shapes $\lrcorner$ and $\urcorner$). In the following, we will always precise when $|$ or $-$ shapes are allowed. This is particularly important as for example some $\{\llcorner, |, -\}$-contact graphs, like the triangular prism, are not $\llcorner$-contact graphs.

The restriction of B_1-VPG to $\llcorner$-intersection or $\llcorner$-contact graphs has been much studied (see for example [55]) and it has been shown that they are in relation with other structures such as Schnyder realizers, canonical orders or edge labelings [27]. The same authors also proved that the recognition of $\llcorner$-contact graphs can be done

in quadratic time, and that this class is equivalent to the one restricted to equilateral $\llcorner$ shapes. The $\llcorner$-contact graphs where the corners lie on a straight line are called *monotone* or *linear* $\llcorner$-contact graphs. Those graphs have been recently studied further, in particular in relation with MPT (Max-Point Tolerance) graphs [24, 3].

In section 2.5 we will prove the following theorems that were both conjectured by Chaplick et al. [28] [3].

Theorem 2.10. *Every triangle-free planar graph has a (simple) $\{\llcorner, |, -\}$-contact representation.*

Theorem 2.11. *Every planar graph has an $\llcorner$-intersection representation.*

In both cases, one cannot restrict the representation to | and − shaped paths. Indeed, any $\{|, -\}$-intersection representation of a triangle-free planar graph defines a vertex partition of the graph into two forests of paths (one induced by the vertical paths and the other induced by the horizontal ones), but such partition is not always possible [93].

As a contact graph of a simple string representation with n vertices has at most $2n$ edges and as a triangle-free planar graph may have up to $2n-4$ edges, Theorem 2.10 cannot be extended to much denser graphs. However, for planar Laman graphs (a large family of planar graphs with at most $2n-3$ edges and which are B_1-VPG intersection graphs [55]), the question of whether these graphs have a $\{\llcorner, |, -\}$-contact representation is open, up to our knowledge. The question whether triangle-free planar graphs are $\{\llcorner, |\}$-contact graphs is also open. Theorem 2.11 implies that planar graphs are 1-string B_1-VPG, improving the results of Biedl and Derka [13] stating that planar graphs are 1-string B_2-VPG. Since an $\{\llcorner, \ulcorner, |, -\}$-intersection representation can be turned into a segment intersection representation [78], Theorem 2.11 provides a rather simple proof of Scheinerman's conjecture.

2.2 Representations by Homothetic Triangles

Theorem 2.1 is the building block for the results presented in this section. As already observed, simple contact representations produce planar graphs, so by ensuring that the representation $\mathcal{C}$ produced by Theorem 2.1, from a triangulation T, is (almost) simple we obtain that the contact graph of $\mathcal{C}$ is actually T itself (by maximality of planar triangulations). We ensure this "almost simplicity" of $\mathcal{C}$ by adding a natural condition on the prototypes :

In a contact representation by pseudo-disks, one can draw the induced graph by choosing an arbitrary point in each set and drawing the edges uv between the corresponding points, inside the region $c(u) \cup c(v)$ and hence passing through a contact point of $c(u)$ and $c(v)$. With such a drawing one can see that the graph induced by the contact representation is a planar graph where some faces are turned into complete graphs (such a complete graph on $k \geq 4$ vertices corresponds to k shapes intersecting at a given point). With such a complete graph on $k \geq 4$ vertices, the contact graph is generally non-planar. We are hence going to forbid k intersecting shapes for $k \geq 4$, and even for $k = 3$ in some cases.

Theorem 2.12. *Consider a k-connected triangulation T, for $k \in \{3, 4, 5\}$, and a set of prototypes $\{\mathcal{P}_v : v \in V(T)\}$, that are convex and with more than one point. If every non-facial cycle $(v_1, \ldots, v_l)$, with $l \geq k$ is such that homothets of $\mathcal{P}_{v_1}, \ldots, \mathcal{P}_{v_l}$ cannot intersect at a single point, then T has a planar contact representation $\mathcal{C} = \{c(v) : v \in V(T)\}$, where each $c(v)$ is a positive homothet of $\mathcal{P}_v$.*

Note that one cannot drop the 4-connectedness (to 3-connectedness) from Theorem 2.2. Indeed, in every contact representation of $K_{2,2,2}$ by homothetic triangles, there are three triangles intersecting in a point (see the left of Figure 2.2). This implies that the triangulation (not 4-connected) obtained from $K_{2,2,2}$ by adding a degree three vertex in every face does not admit a contact representation by homothetic triangles.

Theorem 2.2 immediately follows from Theorem 2.12, with $k = 4$, by setting the prototype to the same triangle. Indeed, we cannot have four interior disjoint homothetic triangles intersecting at a single point. Note that Theorem 2.12 also implies other results like the already known existence of contact representations by

3. In fact, Theorem 2.10 has been proven in the master thesis (written in german) of B. Kappelle in 2015 [68] but never published.

squares for 5-connected planar graphs [91, 74], or the existence of contact representations by homothetic regular pentagons for all planar graphs. The latter, such as Theorem 2.2, is considered by Felsner et al. [51, 56] as they seek a combinatorial proof of these results, and a polynomial algorithm constructing these representations. Recently Schrezenmaier [92] found a more combinatorial proof of Theorem 2.2, while not fully combinatorial yet. This proof uses the link between contact representations by triangles and Schnyder woods.

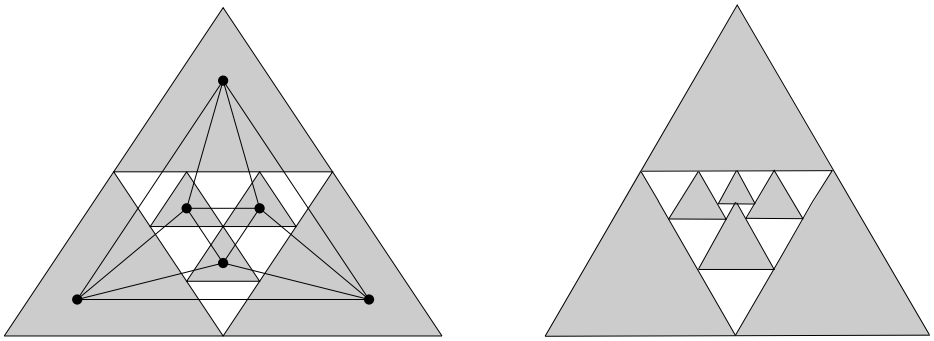

Figure 2.2 – A 4-connected planar triangulation, $K_{2,2,2}$, with a contact representation by homothetic triangles, and a contact representation which contact graph has non-following Schnyder woods.

Given a triangulation T and a contact representation by triangles $\mathcal{T} = \{t(v) : v \in V(T)\}$ of T, we say that a Schnyder wood (see Definition 1.2 in Chapter 1) *follows* $\mathcal{T}$ if each time $t(u) \cap t(v)$ is not a corner of $t(v)$ we have that the edge uv is oriented from u to v in the Schnyder wood. If $\mathcal{T}$ is simple (i.e. at most two triangles intersect at a point), then the orientation of every (inner) edge is specified, and there is at most one Schnyder wood following $\mathcal{T}$, and actually such Schnyder wood always exists [57]. When the triangles of $\mathcal{T}$ are homothetic, the intersections are either simple, and the orientation of the corresponding edge is specified, or it is the intersection of three triangle corners (as in Figure 2.2), and in this case one can choose any of the cyclic orientation for the corresponding triangle of T (clockwise or counter-clockwise), the resulting orientation corresponds to a Schnyder wood. Note that there exist examples of Schnyder woods not following a contact representation by homothetic triangles. This is the case with the representation on the right of Figure 2.2. Looking at this example it seems likely, but it is an open question to know whether contact representations by homothetic triangles are unique or not.

The use of Theorem 2.1 makes the proof of Theorem 2.2 non-constructive. Felsner [51] has proved that given a Schnyder wood, one can define a system of linear equation that has a positive solution if and only if this Schnyder wood follows a contact representation by homothetic triangles. From a positive solution of that system, it is easy to construct the representation. So by enumerating all Schnyder woods of a given 4-connected triangulation, one can compute a representation. However the number of Schnyder woods of a triangulation may be exponential so this approach is not very efficient. Felsner [51] suggested to use cycle flips (i.e. reversal of oriented cycles) in Schnyder woods to change the considered Schnyder wood and eventually end up with a convenient one. The correctness of this method is still open.

Felsner et al. [50] showed that any Schnyder wood following a contact representation by homothetic triangles, can be embedded on an orthogonal surface where edge-points are coplanar, if one allows degenerate patterns (for each point that is the intersection of three triangles). This point of view allowed Felsner et al. [53] to prove that Theorem 2.2 implies that every planar graph has a contact representation by cubes in $\mathbb{R}^3$.

For any two triangles Δ and Δ' there exists a linear mapping of the plane that maps any triangle homothetic to Δ into a triangle homothetic to Δ'. This implies that any intersection representation by triangles homothetic to Δ can be turned into an intersection representation by triangles homothetic to Δ'. From now on we consider a Cartesian coordinate system, and we let the triangle Δ be the triangle with corners at coordinates $(0, 0)$, $(0, 1)$ and $(1, 0)$. Thus the homothets of Δ have corners of the form (x, y), $(x, y + h)$ and $(x + h, y)$ with $h > 0$, and we call (x, y) their *right corner* and h their *height* (See Figure 2.3.(a)).

It is clear that the intersection graph of a set of triangles where no three of them intersect is a planar graph (Put vertex v in $t(v) \setminus \cup_{u \in V(T) \setminus \{v\}} t(u)$ and then draw a curve from v towards $t(v) \cap t(u)$ for each $u \in N(v)$). For proving Theorem 2.3 it thus suffices to construct an intersection representation by homothets of Δ for any planar graph G. In fact we restrict ourselves to triangulations because any such G is an induced subgraph of a triangulation T (an intersection representation of T thus contains a representation of G). The following proposition thus implies Theorem 2.3.

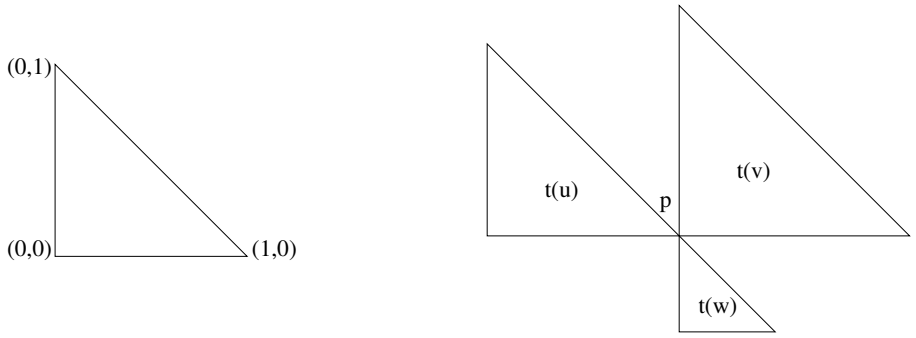

Figure 2.3 – (a) The triangle Δ (b) The triangles $t(u)$, $t(v)$ and $t(w)$.

Proposition 2.13. *For any triangulation T with outer vertices a, b and c, for any three triangles $t(a)$, $t(b)$, and $t(c)$ homothetic to Δ, that pairewise intersect but do not intersect (i.e. $t(a) \cap t(b) \cap t(c) = \emptyset$), and for any $\epsilon > 0$, there exists an intersection representation $\mathcal{T} = \{t(v) : v \in V(T)\}$ of T by homothets of Δ such that :*

(a) No three triangles intersect.

(b) The representation is bounded by $t(a)$, $t(b)$, and $t(c)$ and the inner triangles intersecting those outer triangles intersect them on a point or on a triangle of height less than ϵ.

As we did not published this proof previously, we provide it in full length here.

Proof. Let us first prove the proposition for 4-connected triangulations. Theorem 2.2 tells us that 4-connected triangulations have such a representation if we relax condition (a) by allowing 3 triangles $t(u)$, $t(v)$ and $t(w)$ to intersect if they pairewise intersect in the same single point p ($t(u) \cap t(v) = t(u) \cap t(w) = t(v) \cap t(w) = p$). We call (a') this relaxation of condition (a), and we call "bad points", the points at the intersection of 3 triangles. Let us now reduce their number (to zero) as follows (and thus fulfill condition (a)).

Note that the corners of the outer triangles do not intersect inner triangles. This property will be preserved along the construction below.

Let $p = (x_p, y_p)$ be the highest (i.e. maximizing y_p) bad point. If there are several bad points at the same height, take among those the leftmost one (i.e. minimizing x_p). Then let $t(u)$, $t(v)$ and $t(w)$ be the three triangles pairewise intersecting at p. Let us denote the coordinates of their right corners by (x_u, y_u), (x_v, y_v) and (x_w, y_w), and their height by h_u, h_v and h_w. Without loss of generality we let $p = (x_u + h_u, y_u) = (x_v, y_v) = (x_w, y_w + h_w)$ (see Figure 2.3.(b)). By definition of p it is clear that p is the only bad point around $t(u)$. Note also that none of $t(u)$, $t(v)$ and $t(w)$ is an outer triangle.

Step 1 : By definition of p and $t(u)$, the corner $q = (x_u, y_u + h_u)$ of $t(u)$ is not a bad point. Now inflate $t(u)$ in order to have its right angle in $(x_u - \epsilon', y_u)$ and height $h_u + \epsilon'$, for a sufficiently small $\epsilon' > 0$ (see Figure 2.4.(a)). Here ϵ' is sufficiently small to avoid new pairs of intersecting triangles, new triples of intersecting triangles, or an intersection between $t(u)$ and an outer triangle on a too big triangle (with height $\geq \epsilon$). Since the new $t(u)$ contains the old one, the triangles originally intersected by $t(u)$ are still intersected. Hence, $t(u)$ intersects the same set of triangles, and the new representation is still a representation of T. Since there was no bad point

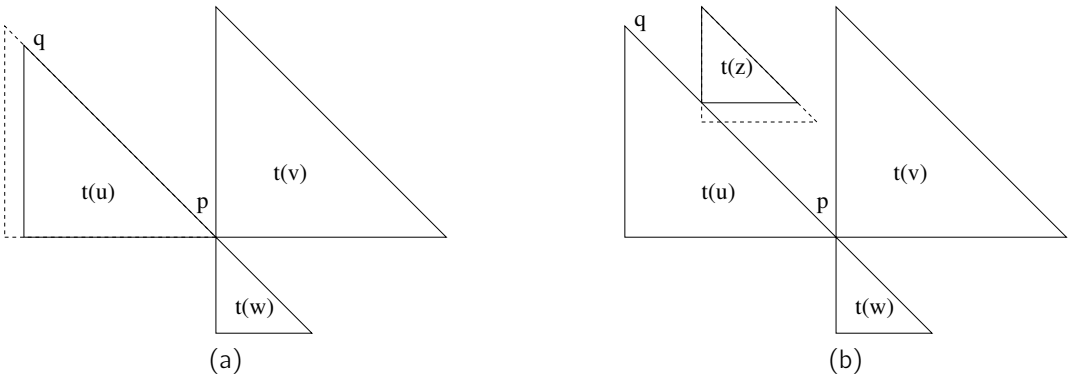

Figure 2.4 – (a) Step 1 (b) Step 2

distinct from p around $t(u)$, it is clear by the choice of $\epsilon' > 0$ that the new representation still fulfills (a') and (b). After this step we have the following.

Claim 2.14. *The top corner of $t(u)$ is not a contact point.*

Step 2 : For every triangle $t(z)$ that intersects $t(u)$ on a single point of the open segment $]p, q[$ do the following. Denote (x_z, y_z) the right corner of $t(z)$, and h_z its height. Note that $t(z)$ is an inner triangle of the representation and that by definition of p there is no bad point involving $t(z)$. Now inflate $t(z)$ in order to have its right corner at $(x_z, y_z - \epsilon')$, and height $h_z + \epsilon'$, for a sufficiently small $\epsilon' > 0$ (See Figure 2.4.(b)). Here ϵ' is again sufficiently small to avoid new pairs or new triples of intersecting triangles, and to preserve (b). Since $t(z)$ was not involved in a bad point, the new representation still fulfills (a'). Since the new $t(z)$ contains the old one, the triangles originally intersected by $t(z)$ are still intersected. Hence, $t(z)$ intersects the same set of triangles, and the new representation is still a representation of T. After doing this to every $t(z)$ we have the following.

Claim 2.15. *There is no contact point on $]p, q]$.*

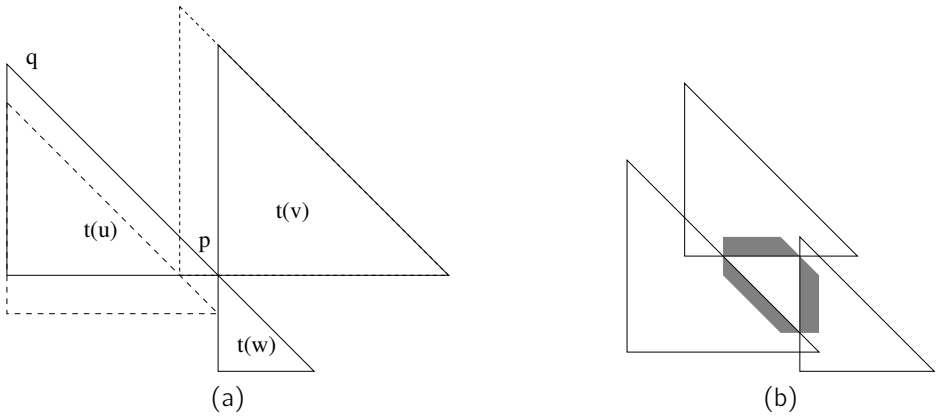

Figure 2.5 – (a) Step 3 (b) Condition (c)

Step 3 : Now translate $t(u)$ downwards in order to have its right corner in $(x_u - \epsilon', y_u)$, and inflate $t(v)$ in order to have its right angle in $(x_v - \epsilon', y_v)$, and height $h_v + \epsilon'$, for a sufficiently small $\epsilon' > 0$ (See Figure 2.5.(a)).

Here ϵ' is again sufficiently small to avoid new pairs or triples of intersecting triangles, and to preserve (b) but it is also sufficiently small to preserve the existing pairs of intersecting triangles. This last requirement can be fulfilled because the only intersections that $t(u)$ could loose would be contact points on $]p, q]$, which do not exist.

After these three steps, it is clear that the new representation has one bad point less and induces the same graph. This proves the proposition for 4-connected triangulations. The conditions (a) and (b) imply the following property.

(c) For every inner face xyz of T, there exists a triangle $t(xyz)$, negatively homothetic to Δ, which interior is disjoint to any triangle $t(v)$ but which 3 sides are respectively contained in the sides of $t(x)$, $t(y)$ and $t(z)$. Furthermore, there exists an $\epsilon' > 0$ such that any triangle t homothetic to Δ of height ϵ' with a side in $t(x) \cap t(xyz)$ does not intersect any triangle $t(v)$ with $v \neq x$, and similarly for y and z (see Figure 2.5.(b)).

We are now ready to prove the proposition for any triangulation T. We prove this by induction on the number of separating triangles. We just proved the initial case of that induction, when T has no separating triangle (i.e. when T is 4-connected). For the inductive step we consider a separating triangle (u, v, w) and we call T_{in} (resp. T_{out}) the triangulation induced by the edges on or inside (resp. on or outside) the cycle (u, v, w). By induction hypothesis T_{out} has a representation fulfilling (a), (b), and (c). Here we choose arbitrarily the outer triangles and ϵ. Since uvw is an inner face of T_{out} there exists a triangle $t(uvw)$ and an $\epsilon' > 0$ (with respect to the inner face uvw) as described in (c). Then it suffices to apply the induction hypothesis for T_{in} (which outer vertices are u, v and w), with the already existing triangles $t(u)$, $t(v)$, and $t(w)$, and for $\epsilon'' = \min(\epsilon, \epsilon')$. Then one can easily check that the obtained representation fulfills (a), (b), and (c). This completes the proof of the proposition. □

Müller et al. [83] considered intersection representations of homothetic triangles which corners have integer coordinates. They proved that for some planar graphs, the representation needs a grid of size $2^{\Omega(n)} \times 2^{\Omega(n)}$ to contain them (where n is the number of vertices).

2.3 Primal-Dual representations with Triangles

This section is devoted to the proof of Theorem 2.6 [J13]. To prove it we construct a contact representation by strings, based on a Schnyder wood, and show that this representation by strings is stretchable. When the strings are stretched into segments, this representation gives the seeked primal-dual contact representation by triangles.

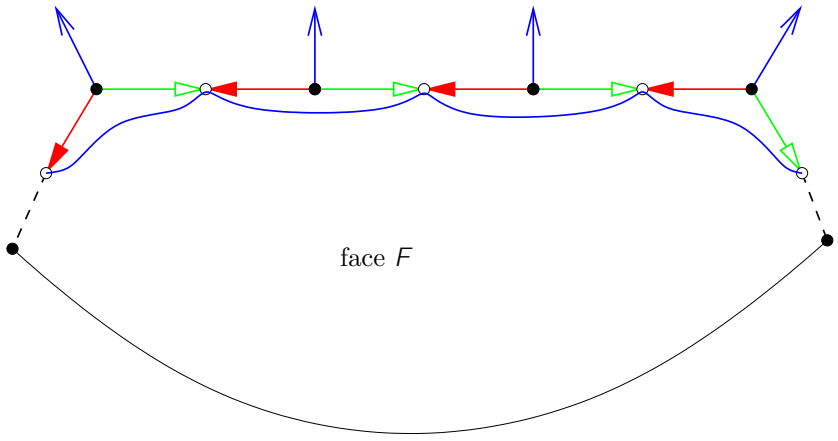

Figure 2.6 – Blue string in face F

Given a planar map equipped with a Schnyder wood we draw a contact representation as follows. For any face F of the map, draw three colored strings (a blue, a green, and a red one) inside F as shown in Figure 2.6. Then we merge any two touching strings with the same color (coming from different faces). Figure 2.7 illustrates the procedure that leads to the primal-dual representation of Figure 2.1. This representation is obtained by stretching [4] the contact representation by strings previously constructed. To prove that this is always possible, we use a characterization of stretchable contact representation by strings [59] (See also [1] for sufficient conditions that make this contact representation stretchable).

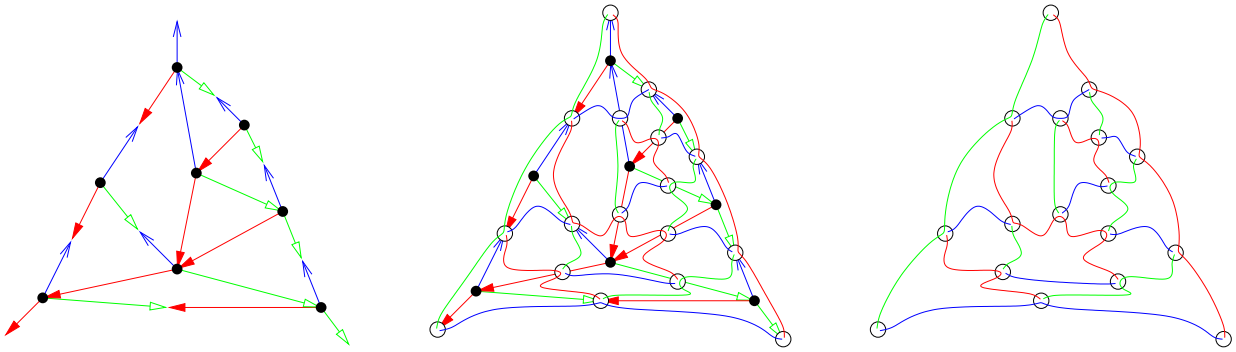

Figure 2.7 – (a) A Schnyder wood (b) The construction (c) The corresponding contact representation by strings

De Fraysseix et al. [57] proved that strict [5] contact representations by triangles of a planar triangulation are, up to homeomorphism and up to the three outer triangles, in one-to-one correspondence with its Schnyder woods. We showed that tiling primal-dual contact representations by triangles of a planar map are in one-to-one correspondence with its Schnyder woods.

Theorem 2.16. *The tiling primal-dual contact representations by triangles of a planar map are, up to homeomorphism, in one-to-one correspondence with its Schnyder woods.*

Particular types of triangles The construction given by de Fraysseix et al. [57] to obtain a strict contact representation by triangles of a planar triangulation can be slightly modified to give a strict tiling primal-dual contact representation by triangles (the three triangles corresponding to the outer face have to be modified to obtain the tiling property). In de Fraysseix et al.'s construction, all the triangles have a horizontal side at their bottom and moreover it is possible to require that all the triangles are right (with the right angle on the left extremity of the horizontal side). This leads us to conjecture the following.

Conjecture 2.17. *Every 3-connected planar map admits a strict tiling primal-dual contact representation by right triangles where all triangles have a horizontal and a vertical side and where the right angle is bottom-left for primal vertices and the outer face and top-right otherwise.*

One may wonder if it is possible to obtain primal-dual contact representations by homothetic triangles ? Such a representation is a representation where vertex-triangles and the outer-face-triangle are positively homothetic to a given triangle Δ and inner-face-triangles are negatively homothetic to Δ. The 4-connected planar triangulation on the left of Figure 2.2 has a unique contact representation by homothetic triangles (for a fixed size of the external triangles). The central face corresponds to an empty triangle and there are some extra contacts between non adjacent faces. So it is not possible to have a primal-dual contact representation by homothetic triangles for this graph.

4. A contact representation by strings is said *stretchable* if there exists a homeomorphism which transforms it into a contact representation by segments.

5. A contact representations by triangles is *strict* if we never have two triangle corners that intersect.

2.4 1-String Representations

This section is devoted to the proof of Theorem 2.8 [J9]. As already mentionned, every planar graph is the induced subgraph of some planar triangulation. It is thus sufficient to prove Theorem 2.8 for triangulations. The proof proceeds by induction on the number of separating triangles. In the following we provide some definitions, then Section 2.4.1 is devoted to 1-string representations of a family of near-triangulations that includes 4-connected triangulations. In this section we use a decomposition technique of 4-connected triangulations that is inspired on Whitney's work [99] and that we already used to partition the edges of planar graphs into two outerplanar graphs [C3]. Then in Section 2.4.2 we finally prove Theorem 2.8 for all triangulations. We will finally give in Section 2.4.3 a partial idea of the modifications performed in this proof to obtain the first proof of Theorem 2.9.

We need that in a 1-string representation of a near-triangulation T, each inner face of T corresponds to some topological region of the string representation.

Definition 2.18. Let $T = (V, E)$ be a near-triangulation with a 1-string representation $\mathcal{T}$. Given an inner face abc of T, an (a, b, c)-*region* is a pseudo-disk that only intersects the strings of a, b, or c as shown in Figure 2.8. This region does not contain intersection points between these strings, and going around its border (clockwisely or not) one successively meets a, a, b, b, c, a, and c. When the vertices a, b, and c are not mentionned, we call such a region a *face-region*.

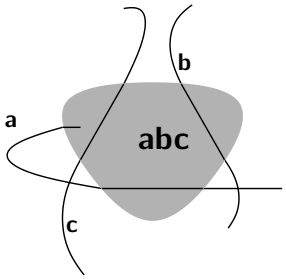

Figure 2.8 – An (a, b, c)-region abc.

As it should be clear from the context, from now on we use the same notation, to denote a vertex or a face and the corresponding string or face-region. Note that according to this definition the region abc intersects the string a twice and one end of a is in abc.

Definition 2.19. A *strong 1-string representation* (S1SR for short) of a near-triangulation T is a 1-string representation of T together with a set of disjoint face-regions, one for each inner face of T. A *partial S1SR* of a near-triangulation T is an S1SR where the crossings corresponding to some edges of T are missing (but no face-region is missing).

In [99], Whitney considered a special family of near-triangulations, it is why we call them W-triangulations.

Definition 2.20. A *W-triangulation* is a 2-connected near-triangulation containing no separating triangle, and which outer boundary is the union of three induced paths $(a_1, \ldots, a_p)$, $(b_1, \ldots, b_q)$, and $(c_1, \ldots, c_r)$, with $a_1 = c_r$, $b_1 = a_p$ and $c_1 = b_q$, and with $p \geq 2$, $q \geq 2$ and $r \geq 2$ (see Figure 2.9.(a)).

Note that by cutting its outer boundary into three paths of length one, every 4-connected triangulation is a W-triangulation.

2.4.1 Proof for 4-connected triangulations.

The following proposition describes the shape of a partial S1SR of a W-triangulation.

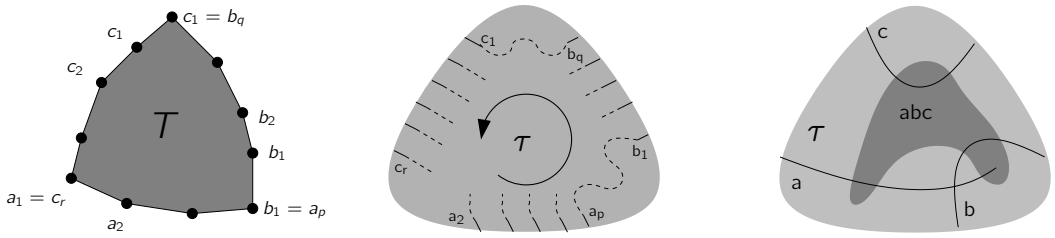

Figure 2.9 – (a) 3-boundary of T (b) Proposition 2.21 (c) Initial case of the induction

Proposition 2.21. *Every W-triangulation T, bounded by $(a_1, \ldots, a_p)$, $(b_1, \ldots, b_q)$, and $(c_1, \ldots, c_r)$ has a partial S1SR contained inside a pseudo-disk τ that satisfies the following properties (see Figure 2.9.(b)) :*

(a) The missing crossings are all the outer edges, except a_1a_2.

(b) On the boundary of τ we successively have the ends of $a_2, a_3, \ldots, a_p, b_1, \ldots, b_q, c_1, \ldots, c_r$.

Observe that since $a_p = b_1$, $b_q = c_1$, and $c_r = a_1$, both ends of strings b_1 and c_1 lie on the boundary of τ, but it is not the case for a_1 or any other string.

We prove Proposition 2.21 by induction on n, the number of vertices in T. The initial case $n = 3$ is easy to prove since there is only one W-triangulation having at most 3 vertices, K_3. See Figure 2.9.(c) for an illustration. For the induction, we successively consider the case where there is a chord a_1b_i, with $1 < i < q$, the case where there is a chord a_ib_j, with $1 < i < p$ and $1 < j \leq q$, and the case where there is a chord a_ic_j, with $1 < i \leq p$ and $1 < j < r$. We then finish with the case where there is no such chords. We do not sketch this latter case in this manuscript. The three first cases are similar in the sense that for each of them the considered chord cuts T into two smaller W-triangulations, on which we apply the induction, and we finish by combining the two obtained partial S1SR into a partial S1SR of T. Figures 2.10, 2.11, and 2.12 illustrate these three cases.

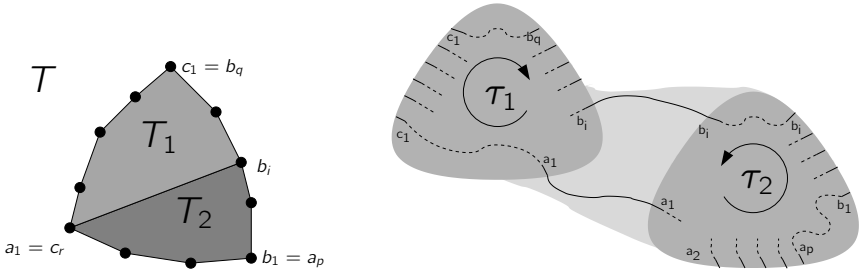

Figure 2.10 – Case where there is a chord a_1b_i, with $1 < i < q$.

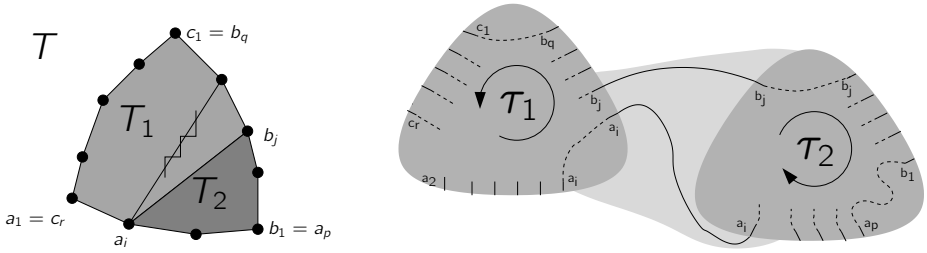

Figure 2.11 – Case where there is a chord a_ib_j, with $1 < i < p$ and $1 < j \leq q$. If there are several chords a_ib_j, we consider one which maximizes j (i.e. there is no chord a_ib_k with $j < k \leq q$).

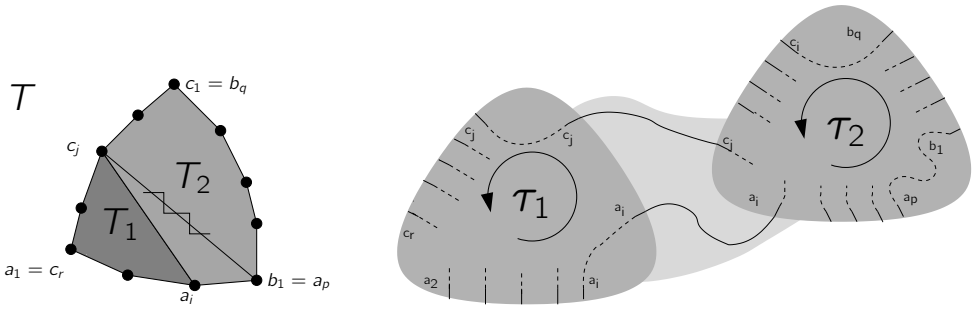

Figure 2.12 – Case where there is a chord $a_i c_j$, with $1 < i \leq p$ and $1 < j < r$. If there are several chords $a_i c_j$, we consider one which maximizes i (i.e. there is no chord $a_k c_j$ with $i < k < r$).

2.4.2 Proof in the general case

Theorem 2.22. *Every triangulation T admits an S1SR.*

Proof. We prove this result by induction on the number of separating triangles. Note that if T has no separating triangle, and has a, b, and c, as outer vertices then T is a W-triangulation bounded by the paths (a, b), (b, c), and (c, a). By Proposition 2.21, T admits a partial S1SR in a pseudo-disk τ which missing crossings are those corresponding to edges ac and bc. To obtain an S1SR of T it is sufficient to extend a, b, and c outside τ so that c crosses a and b, as depicted in Figure 2.13.

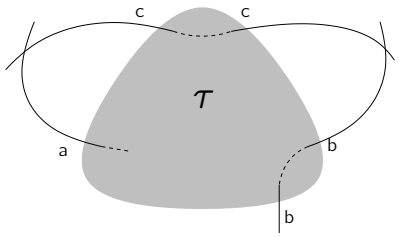

Figure 2.13 – S1SR of T obtained from the partial S1SR of Proposition 2.21.

Suppose now that T is a triangulation that contains at least one separating triangle. Consider a separating triangle (a, b, c) such that there is no other separating triangle lying inside. Let T_1 be the triangulation obtained by removing the vertices lying strictly inside (a, b, c). Let T_2 be the subgraph of T induced by the vertices lying strictly inside (a, b, c). In T_1, the cycle (a, b, c) is a face of the triangulation and is no more a separating triangle. Thus T_1 has one separating triangle less than T, and so we have by induction hypothesis that T_1 admits an S1SR. This S1SR contains a face-region for abc as depicted in the left of Figure 2.15. One can show that by the choice of abc, T_2 is either a single vertex, or a W-triangulation (where the bordering paths $(a_1, \ldots, a_p)$, $(b_1, \ldots, b_q)$, and $(c_1, \ldots, c_r)$, respectively correspond to the neighbors of a, b, and c).

If T_2 is a single vertex v we add a string v inside the face-region abc, as depicted in the right of Figure 2.15. As abc is not a face of T this region is available. We also add the face-regions for the three new faces of T.

If T_2 is a W-triangulation we add its partial S1SR, given by Proposition 2.21, inside the face-region abc, as depicted in Figure 2.16. As abc is not a face of T this region is available. We also have to add several face-regions for the faces of T that are not faces of T_1 nor of T_2.

This concludes the proof of Theorem 2.22. □

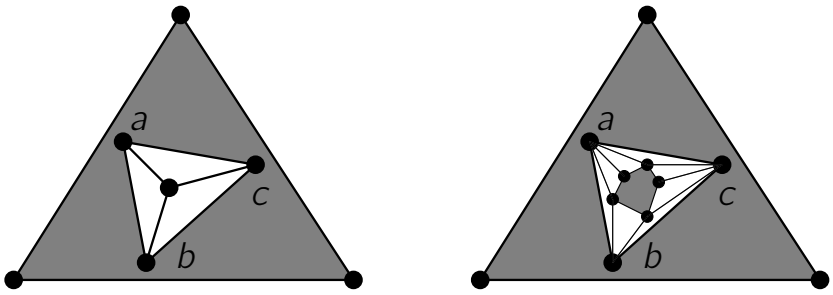

Figure 2.14 – T_2 is either a single vertex, or a W-triangulation.

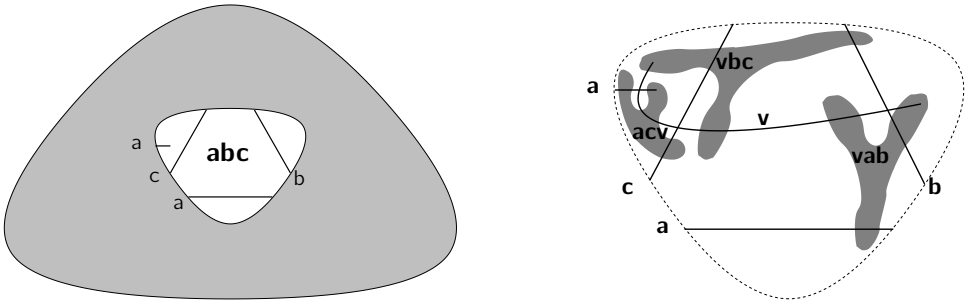

Figure 2.15 – The face-region *abc* and its modification to insert v.

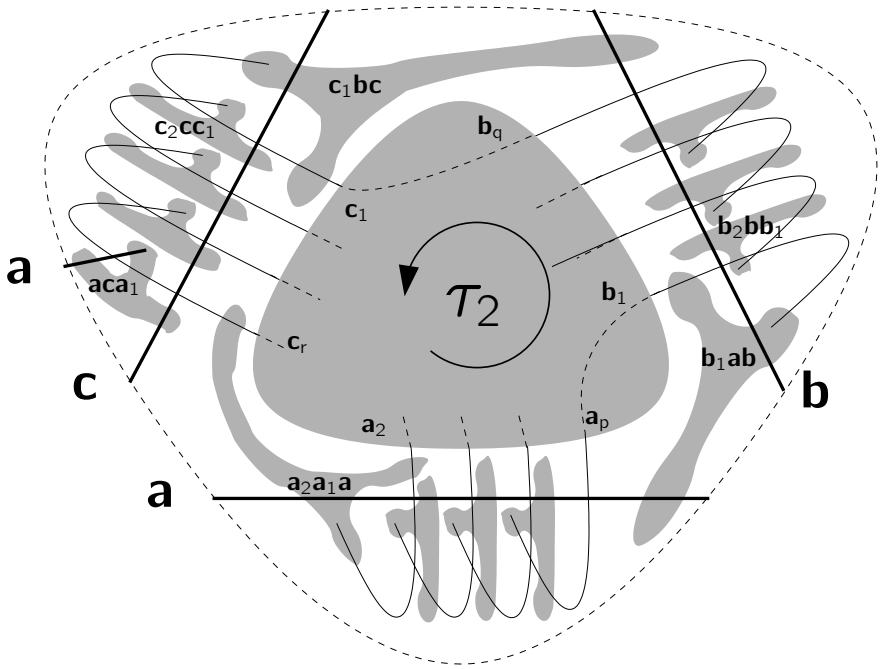

Figure 2.16 – Addition of a partial S1SR of T_2 inside the face-region *abc*.

2.4.3 Improvements for getting segment intersection representations

We here only provide a very partial idea of the modifications we did to obtain the first proof of Theorem 2.9 [C12]. The paper in full length was never submitted for publication, and thus never properly reviewed. It is however available in Jérémie Chalopin's homepage and in mine. Here face-regions are replaced by face-segments.

Definition 2.23. Let $T = (V, E)$ be a near-triangulation with a segment intersection representation. Given a face abc of T, an (a, b, c)-*segment* is a segment $[p, q]$ that only intersects segments a, b, and c, at points p, p, and q respectively. The points p and q are respectively called the *cross-end* and the *flat-end* of segment abc.

There are analogues of S1SR, and partial S1SR.

Definition 2.24. A *strong segment representation* (SSR for short) of a near-triangulation T is a segment intersection representation of T together with a set of (almost) disjoint [6] face-segments, one for each inner face of T. A *partial SSR* of a near-triangulation T is an SSR where the crossings corresponding to some edges of T are missing, as well as some face-segments.

As for 1-strings we prove the following proposition for W-triangulations using the same decomposition.

Proposition 2.25. *For any triplet (A, B, C) of non-aligned points, every W-triangulation T (bounded by $(a_1, \ldots, a_p)$, $(b_1, \ldots, b_q)$, and $(c_1, \ldots, c_r)$) has a partial SSR contained inside the quadrilateral $ABCD$, for some point D in the triangle ABC, and that satisfies the following properties (see Figure 2.17).*

(a) If $p = 2$ then $A = D$, otherwise it is in the interior of ABC.

(b) The segment a_1 is of the form $]C, p[$, and contains D.

(c) Each segment a_i, with $i \geq 2$, is of the form $]A, p[$, and a_2 contains D.

(d) Each segment b_i is of the form $]B, p[$.

(e) Each segment c_i is of the form $]C, p[$.

(f) The missing crossings are at the closure of several open segments, on the border of $ABCD$ (for example at points A, B, and C where several segments converge).

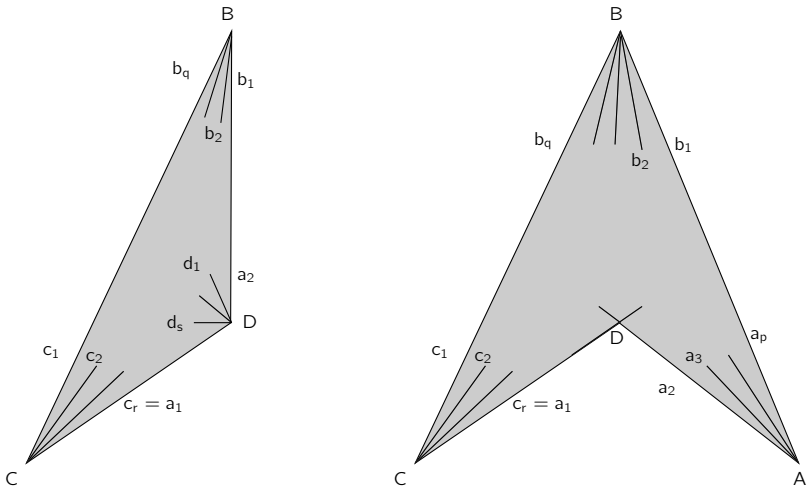

Figure 2.17 – Proposition 2.25 for one W-triangulation T with $p = 2$ and one with $p > 2$.

Then Theorem 2.9 is proved by induction on the number of separating triangles.

6. Two face-segments are only allowed to intersect at their cross-end.

2.5 L-Representations

This section is devoted to the proofs of Theorem 2.4, and Theorem 2.11 [C25]. The common ingredient of these proofs is what we call *2-sided near-triangulations*. In Section 2.5.1, we present the 2-sided near-triangulations, allowing us to provide a new decomposition of planar 4-connected triangulations (see [14] and [99] for other decompositions of 4-connected triangulations). This decomposition is simpler than the one provided by Whitney [99] that is used in [C12]. In Section 2.5.2, we show that every 2-sided near-triangulation admits a contact representation with thick L's (i.e. Theorem 2.4). A variant of this result (where some configurations are not allowed), and the observation that every triangle free planar graph is an induced subgraph of some 4-connected triangulation, imply Theorem 2.10 [C25]. Then in Section 2.5.3 we use 2-sided near-triangulations to prove Theorem 2.11.

2.5.1 2-sided near-triangulations

Definition 2.26. A *2-sided near-triangulation* is a 2-connected near-triangulation T without separating triangles, such that going clockwise on its outer face, the vertices are denoted $a_1, a_2, \dots, a_p, b_q, \dots, b_2, b_1$, with $p \geq 1$ and $q \geq 1$, and such that there is neither a chord $a_i a_j$ nor $b_i b_j$ (that is an edge $a_i a_j$ or $b_i b_j$ such that $|i-j| > 1$).

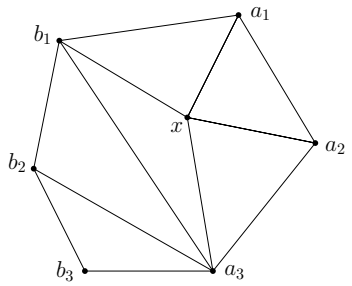

Figure 2.18 – Example of a 2-sided near-triangulation.

Remark that 4-connected triangulations being the triangulations without separating triangles, 4-connected triangulations are 2-sided near-triangulations. The structure of the 2-sided near-triangulations allows us to describe the following decomposition.

Lemma 2.27. *Given a 2-sided near-triangulation T with at least 4 vertices, one can always perform one of the following operations :*

- **(a_p-removal)** *This operation applies if $p > 1$, if a_p has no neighbor b_i with $i < q$, and if none of the inner neighbors (i.e. neighbors that do not lie on the outer face) of a_p has a neighbor b_i with $i < q$. This operation consists in removing a_p from T, and in denoting $b_{q+1}, \dots, b_{q+r}$ the new vertices on the outer face in anti-clockwise order, if any. This yields a 2-sided near-triangulation T' (see Figure 2.19a).*
- **(b_q-removal)** *This operation applies if $q > 1$, if b_q has no neighbor a_i with $i < p$, and if none of the inner neighbors of b_q has a neighbor a_i with $i < p$. This operation consists in removing b_q from T, and in denoting $a_{p+1}, \dots, a_{p+r}$ the new vertices on the outer face in clockwise order, if any. This yields a 2-sided near-triangulation T'. This operation is strictly symmetric to the previous one.*
- **(cutting)** *This operation applies if $p > 1$, $q > 1$ and if the unique common neighbor of a_p and b_q, denoted d, has a neighbor a_i with $i < p$, and a neighbor b_j with $j < q$. This operation consists in cutting T into three 2-sided near-triangulations T', T_a and T_b (see Figure 2.19b) :*
  - *T' is the 2-sided near-triangulation contained in the cycle formed by vertices $(a_1, \dots, a_i, d, b_j, \dots, b_1)$, and the vertex d is renamed a_{i+1}.*
  - *T_a (resp. T_b) is the 2-sided near-triangulation contained in the cycle $(a_i, \dots, a_p, d)$ (resp. $(d, b_q, \dots, b_j)$), where the vertex d is denoted b_1 (resp. a_1).*

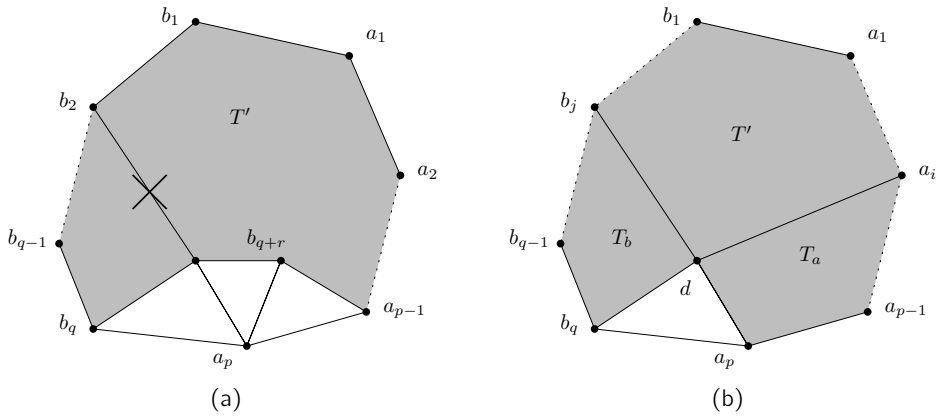

Figure 2.19 – Illustrations of (a) the a_p-removal operation and (b) the cutting operation.

2.5.2 Thick ⌞-contact representations

A *thick* ⌞ is an ⌞ shape where the two segments are turned into thick rectangles (see the left of Figure 2.20). Here we do not allow thick | or −, so going clockwise around a thick ⌞ from the bottom-right corner, we call its sides *bottom*, *left*, *top*, *vertical interior*, *horizontal interior*, and *right*. We draw them in the integer grid, that is such that their bend points have integer coordinates, and we ask the two rectangles to be of thickness one, and of length at least two.

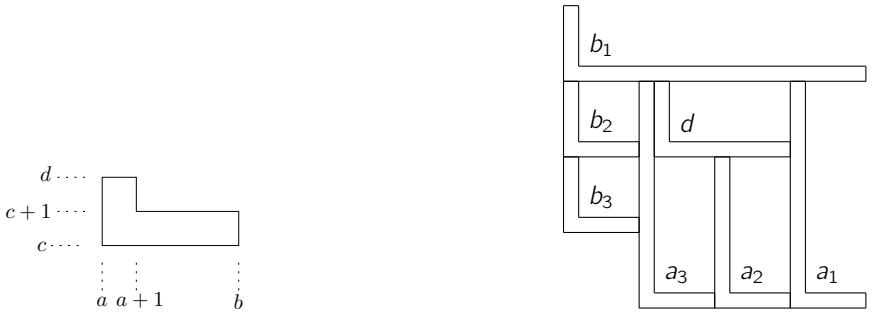

Figure 2.20 – A thick ⌞and a TLCR of the near-triangulation from Figure 2.18.

Definition 2.28. A *Thick ⌞-Contact Representation* (TLCR for short) is a contact representation by thick ⌞'s such that two touching thick ⌞'s touch on a segment [7].

We now show that every 2-sided near-triangulation has a TLCR (see the right part of Figure 2.20 for an illustration).

Theorem 2.29. *Every 2-sided near-triangulation T has a TLCR with the following properties :*
- *Every thick ⌞ is included in the positive quadrant $\{(x, y) : x \geq 0, y \geq 0\}$.*
- *The thick ⌞'s of vertices a_i have their bottom side on the $(y = 0)$-line and they appear in decreasing order from left to right. Furthermore their horizontal interior side does not intersect any other thick ⌞'s side.*
- *The thick ⌞'s of vertices b_i have their left side on the $(x = 0)$-line and they appear in decreasing order from bottom to top. Furthermore their vertical interior side does not intersect any other thick ⌞'s side.*

7. This deviate's a little from the original result in [C25] where L's can intersect on a single vertex

Proof. We proceed by induction on the number of vertices. The theorem clearly holds for the 2-sided near-triangulation with three vertices. Let T be a 2-sided near-triangulation ; it can thus be decomposed using one of the three operations described in Lemma 2.27. We go through the these operations successively (we skip the (b_q-removal) as it is purely symmetrical to the (a_p-removal)).

(a_p-removal) Let T' be the 2-sided near-triangulation resulting from an a_p-removal operation on T. By the induction hypothesis, T' has a TLCR with the required properties (see Figure 2.21a). We can now modify this TLCR slightly in order to obtain a TLCR of T (thus adding a thick $\llcorner$ corresponding to vertex a_p).

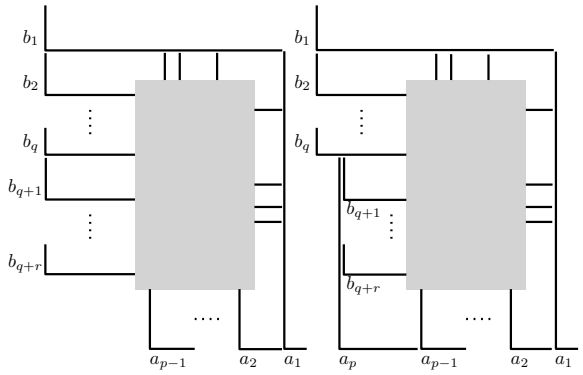

(a) TLCR of T' (b) TLCR of T

Figure 2.21 – The (a_p-removal) operation for a TLCR. Here, the grey region contains the corners of the inner vertices of T'.

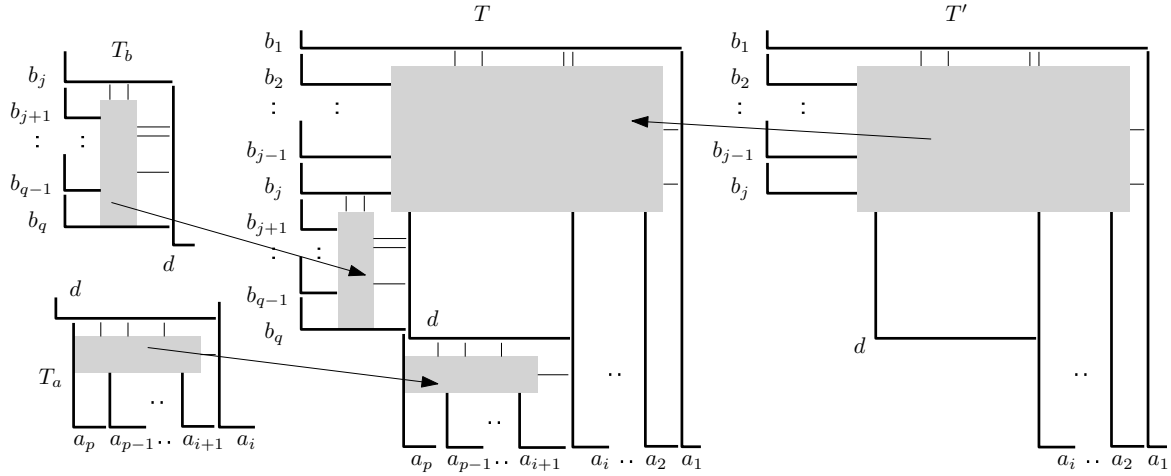

Figure 2.22 – The (cutting) operation for a TLCR.

(cutting) Let T', T_a and T_b be the three 2-sided near-triangulations resulting from the cutting operation described in Lemma 2.27. By induction hypothesis, each of them has a TLCR satisfying Theorem 2.29. We modify the TLCR of T' in order to include the ones of T_a and T_b, as they are given by the induction (see Figure 2.22). □

2.5.3 The ⌞-intersection representations

Using Theorem 2.29, one can prove that every 4-connected triangulation has an ⌞-intersection representation. To allow us to work on every triangulation (not only the 4-connected ones) we need to enrich the ⌞-intersection representations with the notion of *anchor*[8], an analogue of the face regions of Section 2.4.

Consider a near-triangulation T, and any inner face abc of T. Note that if the ⌞'s of a, b and c do not intersect at a common point or segment, then their horizontal (resp. vertical) subpaths lie on three different lines. They thus form a rectangle whose top side belongs to the ⌞ with the up-most corner, whose right side belongs to the ⌞ with the right-most corner, and whose other sides belong to the third ⌞.

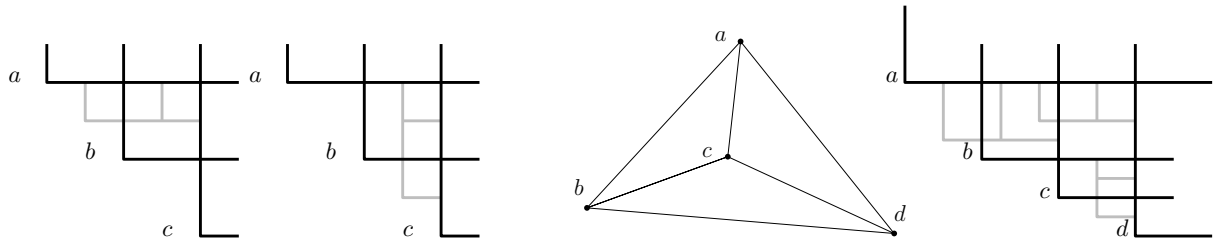

Figure 2.23 – The two possible anchors for the three ⌞ corresponding to a face abc. An example of a triangulation and a corresponding FLIR (the anchors are drawn in gray).

Definition 2.30. Given an ⌞-intersection representation of a near-triangulation T, and an inner face abc of T, an *anchor* for abc is a union of three segments intersecting the ⌞'s of a, b and c and no other ⌞, and such that the middle corner is in the rectangle described by a, b and c as depicted in Figure 2.23.

Definition 2.31. A *full ⌞-intersection representation* (FLIR) of a near-triangulation T is an ⌞-intersection representation of T together with a set of pairwise disjoint anchors, one for each inner face of T.

Let us now prove that every 2-sided near-triangulation admits a FLIR.

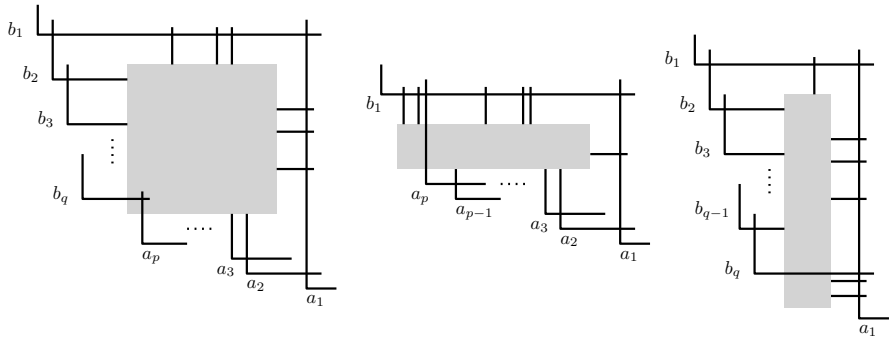

Figure 2.24 – Illustration of Proposition 2.32 when $p > 1$ and $q > 1$, when $p > 1$ and $q = 1$, and when $p = 1$ and $q > 1$.

Proposition 2.32. *Every 2-sided near-triangulation has a FLIR such that among the corners of the ⌞ paths and of the anchors :*

- *from left to right, the first corners are those of vertices $b_1, b_2, \dots b_q$ and the last one is the corner of vertex a_1, and*
- *from bottom to top, the first corners are those of vertices $a_1, a_2, \dots a_p$ and the last one is the corner of vertex b_1.*

8. The notion was introduced in [55] under the name of *private region*.

As the $\llcorner$ of a_i and a_{i+1} (resp. b_i and b_{i+1}) intersect, the FLIR is rather constrained. This is illustrated in Figure 2.24, where the grey region contains the inner part of the representation. Proposition 2.32 is proved by decomposing the 2-sided near-triangulation as indicated in Lemma 2.27. Figure 2.25 and Figure 2.26 respectively illustrate what is done for the (a_p-removal) operation and for the (cutting) operation.

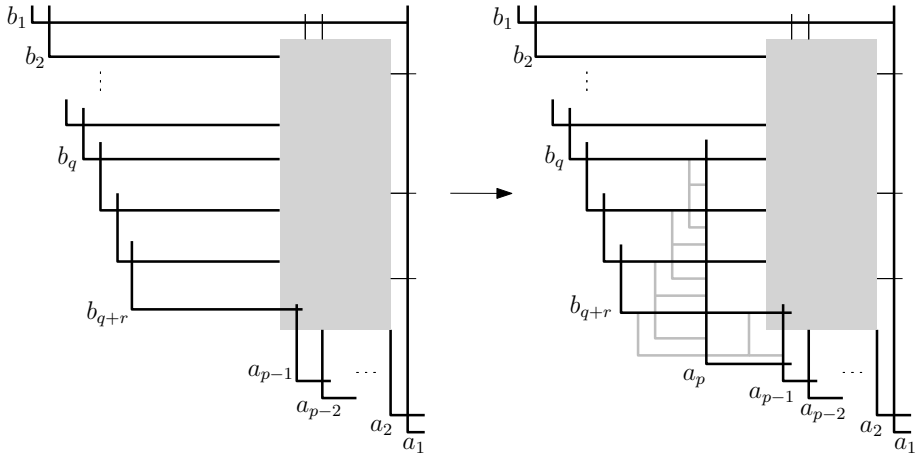

Figure 2.25 – The (a_p-removal) operation.

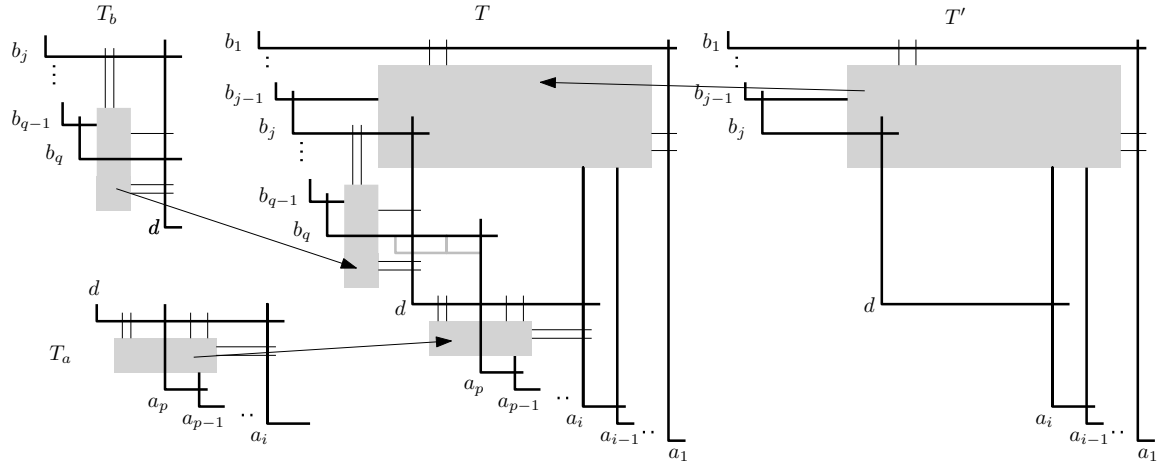

Figure 2.26 – The (cutting) operation.

We can now prove Theorem 2.11 by showing the following.

Proposition 2.33. *Every triangulation T with outer vertices x, y, z has a FLIR such that among the corners of the $\llcorner$ paths and of the anchors :*

— *the corner of x is the top-most and left-most,*
— *the corner of y is the second left-most, and*
— *the corner of z is the bottom-most and right-most.*

Note that in this proposition there is no constraint on x, y, z, so by renaming the outer vertices, other FLIRs can be obtained. As in Section 2.4.2 this proposition is proved by induction on the number of separating triangles in T. The initial case where T has no separating triangle follows from Proposition 2.32. For the induction case, consider a separating triangle (a, b, c) such that there is no other separating triangle lying inside. Let T_1 (resp.

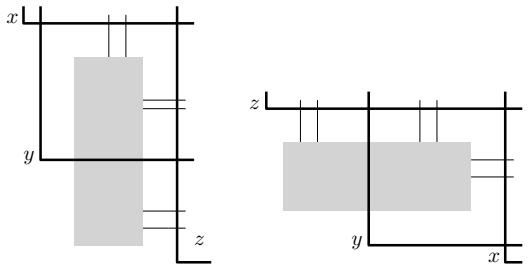

Figure 2.27 – Illustration of Proposition 2.33, and the FLIR obtained after reflection with respect to a line of slope 1.

T_2) be the triangulation obtained by removing the vertices lying strictly inside (a, b, c) (resp. strictly outside (a, b, c)). In T_1, the cycle (a, b, c) is an inner face of the triangulation and is no more a separating triangle, and T_2 has no separating triangle. Thus T_1 and T_2 have less separating triangles than T, and so by induction hypothesis they have a FLIR. The FLIR of T_{out} contains an anchor for the face *abc* as depicted in Figure 2.28a. Figure 2.28b illustrates the FLIR of T_{in} and Figure 2.28c shows how it can be included in the FLIR of T_{out} instead of *abc*'s anchor.

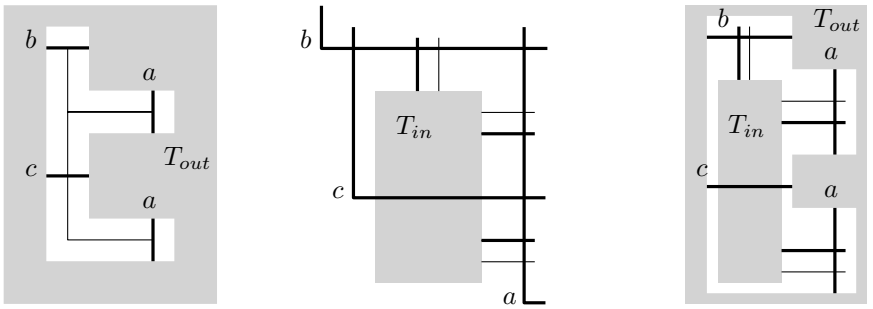

(a) The vertical anchor of *abc* in the FLIR of T_{out}

(b) The FLIR of T_{in}

(c) The inclusion of the FLIR of T_{in} in the FLIR of T_{out}

Figure 2.28 – Merging the FLIRs of T_{in} and T_{out}.

Chapitre 3

Research Project

This chapter gathers recent unpublished results (most of them not fully written yet), and several questions I am interested in. These will probably form a large part of my researches in the next five or ten years.

3.1 Schnyder woods in higher genus

We recently proved that every triangulation admits a 1-EDGE angle labeling. We have seen that this labeling is thus 1-FACE, but there may be vertices of type 0. The proof is not included here.

This result does not answer Conjecture 1.22, but notice that every vertex incident to a loop is of type k for some $k \geq 1$. So Conjecture 1.22 holds for the triangulations such that every vertex is incident to a loop, like triangulations with only one vertex.

We wonder whether one could build a 1-EDGE, $\mathbb{N}^*$-VERTEX, 1-FACE angle labeling for a triangulation (c.f. Conjecture 1.22) starting from a 1-EDGE, 1-FACE angle labeling. The difficulty here remains in getting ride of the sinks, by changing the orientations of some edges into another weak Schnyder orientation with less sinks. Looking at the difference, Δ, between the given weak Schnyder orientation and one given by Theorem 1.24 (with outdegrees at least three and divisible by three) indicates how to get rid of some sinks, but the problem is that maybe Δ has no subgraph that is null-homological (this would ensure us that after reverting the edges of this subgraph we still have a weak Schnyder orientation).

I am also very interested in Conjecture 1.21 and in its weakening, Conjecture 1.25. Actually we wonder for every essentially 3-connected map G, if the map $\hat{G}$ has three disjoint perfect matchings ? Orienting the edge of these matchings from primal- and dual-vertices towards edge-vertices, and orienting the other edges in the other direction would give an orientation fulfilling Conjecture 1.25 where primal- and dual-vertices have outdegree exactly three (while edge-vertices have indegree 0 or 3).

We have seen with K. Knauer that some other orientations of bipartite quadragulations [1] are easy to construct. Those are orientations where every vertex has a positve even outdegree. Similar orientations in the plane [66, 41, 34] and on the torus [81] are linked to contact representations by horizontal and vertical segments (in the plane and on the flat torus respectively). This is one of the motivations for the following topic.

1. $\hat{G}$ is a (bipartite) quadrangulation, that is a map where all faces have length four.

3.2 Intersection graphs on surfaces

Our work with K. Knauer leads to a contact representation of every quadrangulation embedded on a surface $\mathbb{S}$, by pseudo-segments and a few (at most $g_E - 2$, where g_E is the Euler genus of $\mathbb{S}$) polygons with an even number of sides, drawn on $\mathbb{S}$.

It would be interesting also to construct contact representations by (straight) triangles in the flat torus. Probably the easiest way towards such construction would be to adapt the study of stretchable contact representations by pseudo-segments done by Aerts et al. [1]. Indeed such contact representation (even a primal dual one) with pseudo-segments, is easy to construct from a toroidal Schnyder wood.

Another interesting question about contact representations on the flat torus is whether every essentially 4-connected toroidal triangulation [2] has a contact representation by rectangles with aligned sides. This would extend the planar case [97]. Recently Bonichon et al. showed that these triangulations admit "toroidal" transversal structures [3], but to achieve the contact representation one needs an extra property : there should be no bridge in each of the two colored graphs.

One could also wonder whether the toroidal counterpart of Scheinerman's conjecture holds on the flat torus.

Conjecture 3.1. Every toroidal graph has an intersection representation by segments drawn on the flat torus.

It is also open to know whether these graphs have a intersection representation by L's on the flat torus. In this case this may not lead to an answer of the previous question, as we do not know if intersection representation by L's can be turned into intersection representation by segments on the flat torus.

On the flat torus, one could also ask for intersection or contact representations by segments with constrained slopes. For exemple, does any k-chromatic toroidal graph admit a segment intersection representation where segments use at most k different slopes, and where parallel segments do not intersect (and thus induce an independent set in the graph). We will discuss more this type of questions in the next section.

It is well known that the graph obtained by subdividing each edge of a non-planar graph does not have a 1-string representation in the plane. Actually this holds for any surface $\mathbb{S}$: A subdivision of a graph G that cannot be embedded on $\mathbb{S}$, does not have a 1-string representation on $\mathbb{S}$. On the other hand, can Theorem 2.8 be extended to any surface ?

Conjecture 3.2. Every graph embedded on a surface $\mathbb{S}$ has a 1-string representation drawn on the surface $\mathbb{S}$.

For the torus, this would be a first step towards Conjecture 3.1. It is worth mentionning that one should probably slightly modify the definition of face-region (see Definition 2.18) as each face-regions contains a string end, but there are only $2n$ of them versus $2n - 4 + 4g$ faces, for an n-vertex triangulation of genus g. My suggestion would be to modify this definition so that going around the border of an (a, b, c)-region one successively meets string a, a, b, b, c, a, a, and c. An "old" face region always contains such face region, and these new face regions also allow the addition of a vertex or of a W-triangulation in a way that is similar to the ones depicted in Figure 2.15 and Figure 2.16.

2. As already observed such representation is not possible if there is a separating triangle.
3. A toroidal counterpart of the "planar" transversal structures which are in bijection with contact representations by rectangles with aligned sides in the plane.

3.3 Slope constraints for segment intersection graphs

In [66, 34, 41] (resp. [23]) it is shown that bipartite (resp. triangle-free) planar graphs admit a contact representation by segments where only 2 (resp. 3) slopes are allowed for the segments, and where parallel segments do not intersect. So these constructions induce a 2-coloring (resp. 3-coloring) of the vertices. Note that Castro *et al.* do not prove the 3-colorability of triangle-free planar graphs, they use such coloring of the graphs (by Grötzsch's theorem) in their construction. West [98] proposed a stronger version of Scheinerman's conjecture in which only 4 slopes are allowed, thus using the fact that these graphs are 4-colorable.

We proved (manuscript under progress) that 3-colorable planar graphs have an **intersection** representation with segments whose slopes are determined by the color of the corresponding vertices. This was done trough **contact** representations with three slopes, and generalizing this approach for West's conjecture asks for particular 4-colorings of planar graphs.

Conjecture 3.3. Every planar triangulation admits a four coloring with colors $\{1, 2, 3, 4\}$ in such a way that there is no induced 4-cycle colored 1, 2, 3 and 4 clockwisely.

3.4 Extensions to $\mathbb{R}^d$ through Simplicial Complexes

Abstract simplicial complexes generalize the notion of graphs. An *abstract simplicial complex* Δ with vertex set V is a set of subsets of V which is closed by inclusion (*i.e.* $\forall Y \in \Delta$, $X \subseteq Y \Rightarrow X \in \Delta$). An element of Δ is called a *face*. A maximal element of Δ according to the inclusion order is called a *facet*.

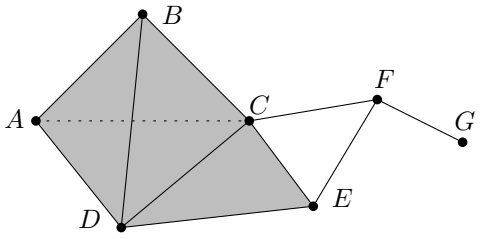

Figure 3.1 – An abstract simplicial complex whose facets are $\{A, B, C, D\}, \{C, D, E\}, \{C, F\}, \{E, F\}, \{F, G\}$

The notion of *Dushnik-Miller* dimension of a poset has been introduced by Dushnik and Miller [37]. It is also known as the *order dimension* of a poset. This notion of dimension can be applied to an abstract simplicial complex as follows.

Definition 3.4. Let Δ be an abstract simplicial complex. The inclusion poset of Δ is the poset $(\subset, \Delta)$. The Dushnik-Miller dimension $\dim_{DM}(\Delta)$ of Δ is the Dushnik-Miller dimension of the inclusion poset of Δ.

Low dimensions are well known :
— $\dim_{DM}(\Delta) = 1$ if and only if Δ is a vertex.
— $\dim_{DM}(\Delta) \leq 2$ if and only if Δ is a union of paths.
— $\dim_{DM}(\Delta) \leq 3$ if and only if Δ is planar (i.e. embeddable in $\mathbb{R}^2$).
There are complexes with arbitrarily high Dushnik-Miller dimension : for any integer n, $\dim_{DM}(K_n) = O(\log \log n)$ where K_n denotes the complete graph on n vertices [67]. Similarly $\dim_{DM}(K_n^*) = n$ where K_n^* denotes the complete simplex on n vertices. The following theorem shows that the Dushnik-Miller dimension in higher dimensions also captures some geometrical properties.

Theorem 3.5 (Bayer *et al.* [17], and Ossona de Mendez [84])**.** *Any simplicial complex* Δ *such that* $\dim_{DM}(\Delta) \leq d + 1$ *has a straight line embedding in* $\mathbb{R}^d$.

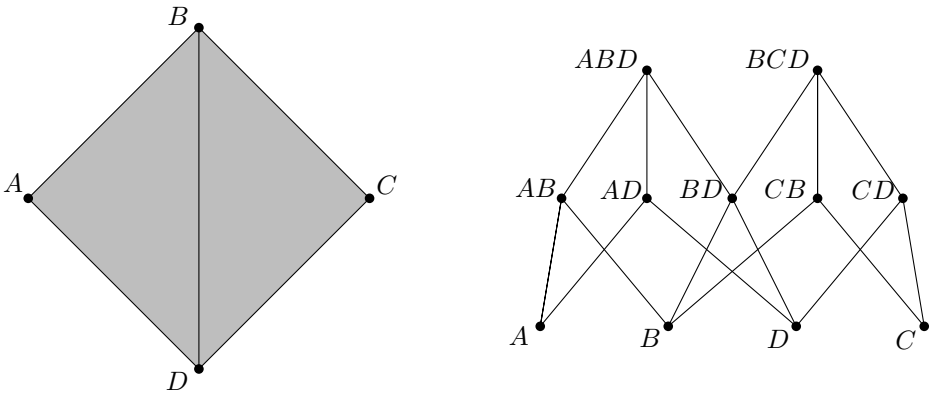

Figure 3.2 – An abstract simplicial complex with facets $\{A, B, D\}$ and $\{B, C, D\}$, and its inclusion poset.

For $d = 2$, this theorem states that if a simplicial complex has dimension at most 3 then it is planar. Brightwell and Trotter [20] proved that the converse also holds (for $d = 2$). For higher d, the converse is false : take for example K_n the complete graph which has a straight line embedding in $\mathbb{R}^3$ (and therefore in $\mathbb{R}^d$ for $d \geq 3$) and which has Dushnik-Miller dimension $O(\log \log n)$.

We would like to extend (as much as possible) properties of planar triangulations to simplicial complexes with fixed Dushnik-Miller dimension. One goal would be also to study (non-simplicial) cell complexes as the case of dimension three corresponds to internally 3-connected planar maps [20, 44, 79], and it is already well understood.

In [C23, S4] we study variants of Delaunay complexes in $\mathbb{R}^d$. TD-Delaunay graphs have been introduced by Chew et al. [31], and this notion generalizes naturally to higher dimensions. For a set $\mathcal{P}$ of points of $\mathbb{R}^d$ in "general position", there is a TD-Delaunay complex $\mathsf{TDD}(\mathcal{P})$. It is easy to see that for any point set $\mathcal{P}$ of $\mathbb{R}^d$ in general position, $\mathsf{TDD}(\mathcal{P})$ is an abstract simplicial complex with Dushnik-Miller dimension at most $d + 1$. The reciprocal statement holds for $d \leq 3$ in the sense that every simplicial complex Δ with Dushnik-Miller dimension $d \leq 3$ is contained in $\mathsf{TDD}(\mathcal{P})$ for some point set $\mathcal{P}$. This naturally raised the question to know if this extends to greater d [75, 39]. Actually, with Mary [75] we proved this when Δ already admits some particular embedding, but finally we recently showed [S4] that this statement fails already for $d = 4$.

Similar Delaunay type graphs, R-Delaunay graphs, were defined by Felsner [49]. He showed that those graphs can have a quadratic number of edges. Chen *et al.*s [30] showed that R-Delaunay graphs can have arbitrarily large chromatic number. We proved that the class of R-Delaunay graphs is strictly included in the class TD-Delaunay complexes of $\mathbb{R}^3$.

In another work (See [C24] for a preliminary version) we study contact representation by d-dimensional boxes in $\mathbb{R}^d$. We showed that the complexes admiting such representation have Dushnik-Miller dimension at most $d+1$. This extends the case $d = 2$ [97]. Formally we showed that tilings of $\mathbb{R}^d$ with d-dimensional boxes, such that there are $2d$ infinite boxes and such that at most $d + 1$ boxes intersect at any point, induce simplicial complexes with Dushnik-Miller dimension $d + 1$. This raises the question of an exact characterization of these complexes. It raises also the question of characterizing the complexes defined from a contact representation of axis aligned rectangles in $\mathbb{R}^3$ (extending [66, 41, 34]). We conjectured for a while that those are charcaterized by their Dushnik-Miller dimension equal to 4, by their 3-colorability (parallel rectangle are not allowed to intersect), and by their Helly property (tree pairwise intersecting rectangles intersect), but we recently found a counter-example. With L. Isenmann, we are currently studying additional properties to correct this.

Publication list

International journals

[J27] B. Albar, and D. Gonçalves. On triangles in K_r-minor free graphs. *Journal of Graph Theory* 88(1), 154-173, 2018.

[J26] M. Axenovich, D. Gonçalves, J. Rollin, and T. Ueckerdt. The k-strong induced arboricity of a graph. *Eur. J. of Combin.* 67, 1-20, 2018.

[J25] N. Cohen, D. Gonçalves, E.J. Kim, C. Paul, I. Sau, D.M. Thilikos, and M. Weller. A polynomial-time algorithm for Outerplanar Diameter Improvement. *J. of Comput. and Syst. Sci.* 89, 315-327, 2017.

[J24] V. Despré, D. Gonçalves, and B. Lévêque. Encoding Toroidal Triangulations. *Disc. & Comput. Geom.* 57(3), 507-544, 2017.

[J23] L. Esperet, D. Gonçalves, and A. Labourel. Coloring Non-Crossing Strings. *Elec. J. of Combin.* 23(4) : #4, 18 pp, 2016.

[J22] B. Albar, D. Gonçalves, and K. Knauer. Orienting triangulations. *Journal of Graph Theory* 83(4), 392-405, 2016.

[J21] B. Albar, D. Gonçalves, and J.L. Ramírez Alfonsín. Detecting minors in matroids through triangles. *European Journal of Combinatorics* 53, 50-58, 2016.

[J20] M.C. Francis, D. Gonçalves, and P. Ochem. The Maximum Clique Problem in Multiple Interval Graphs. *Algorithmica* 71 (4), 812-836, 2015.

[J19] S. Bessy, D. Gonçalves, and J.-S. Sereni. Two floor building needing eight colors. *Journal of Graph Algorithms and Applications*, 19(1), 1-9, 2015.

[J18] D. Gonçalves, and B. Lévêque. Toroidal Maps : Schnyder Woods, Orthogonal Surfaces and Straight-Line Representations. *Discrete and Computational Geometry* 51(1), 67-131, 2014.

[J17] N. Bousquet, D. Gonçalves, G.B. Mertzios, C. Paul, I. Sau, and S. Thomassé. Parameterized Domination in Circle Graphs. *Theory of Comp. Syst.* 54(1), 45-72, 2014.

[J16] D. Gonçalves, A. Parreau, and A. Pinlou. Locally identifying coloring in bounded expansion classes of graphs. *Discrete Applied Mathematics* 161(18), 2946-2951, 2013.

[J15] D. Gonçalves, and E.J. Kim. On Exact Algorithms for Permutation CSP. *Theo. Comp. Sci.* 511, 109-116, 2013.

[J14] J. Bang-Jensen, D. Gonçalves, and A. Yeo. Partitioning the arcs of a digraph into a star forests of the underlying graph with prescribed orientation properties *Theo. Comp. Sci.* 475, 13-20, 2013.

[J13] D. Gonçalves, B. Leveque, and A. Pinlou. Triangle Contact Representations and Duality. *Discrete and Computational Geometry* 48, 239-254, 2012.

[J12] D. Gonçalves, F. Havet, A. Pinlou, and S. Thomassé. On spanning galaxies in digraphs. *Discrete Applied Mathematics* 160 (6), 744-754, 2012.

[J11] D. Gonçalves, A. Pinlou, M. Rao, and S. Thomassé. The Domination Number of Grids. *SIAM J. Discrete Math.* 25 (3), 1443-1453, 2011.

[J10] D. Gonçalves. On Vertex Partitions and some Minor-Monotone Parameters. *Journal of Graph Theory* 66 (1), 49-56, 2011.

[J9] J. Chalopin, D. Gonçalves, and P. Ochem. Planar graphs are in 1-STRING. *Discrete and Computational Geometry* 43(3), 626-647, 2010.

[J8] J. Daligault, M. Rao, and D. Gonçalves. Diamond-free Circle Graphs are Helly Circle. *Discrete Math.* 310(4), 845-849, 2010.

[J7] D. Gonçalves. A Planar linear hypergraph whose edges cannot be represented as straight line segments. *Eur. J. Combin.* 30, 280-282, 2009.

[J6] D. Gonçalves. Covering planar graphs with forests, one having bounded maximum degree. *J. Combin. Theory Ser. B* 99, 314-322, 2009.

[J5] D. Gonçalves, and P. Ochem. On star and caterpillar arboricity. *Discrete Math.* 309, 3694-3702, 2009.

[J4] D. Gonçalves. On the L(p,1)-labelling of graphs. *Discrete Math.* 308 (8), 1405-1414, 2008.

[J3] J. Bang-Jensen, D. Gonçalves, and I.L. Gørtz. Finding well-balanced pairs of edge-disjoint trees in edge-weighted graphs. *Discrete Optimization* 4 (3-4), 334-348, 2007.

[J2] D. Gonçalves. Caterpillar arboricity of planar graphs. *Discrete Math.* 307 (16), 2112-2121, 2007.

[J1] D. Gonçalves, A. Raspaud, and M.A. Shalu. On Oriented Labelling Parameters. *Formal Models, Languages and Applications* (Eds. K.G. Subramanian, K. Rangarajan, M. Mukund), Series in Machine Perception and artificial Intelligence Vol. 66, World Scientific, Singapore. Chap. 3, 34-45, 2006.

International conferences

[C25] D. Gonçalves, L. Isenmann, and C. Pennarun. Planar Graphs as L-intersection or L-contact graphs. *29th Annual ACM-SIAM Symposium on Discrete Algorithms* (SODA 2018).

[C24] M. Francis, and D. Gonçalves. Dushnik-Miller dimension of contact systems of d-dimensional boxes. *9th European Conference on Combinatorics, Graph Theory, and Applications* (EUROCOMB 2017).

[C23] D. Gonçalves, and L. Isenmann. Dushnik-Miller dimension of TD-Delaunay complexes. *33rd European Workshop on Computational Geometry* (EuroCG 2017).

[C22] S. Bessy, M. Bougeret, D. Gonçalves, and C. Paul. Maximum Independent Set in EPG Graphs. *13th Workshop on Approximation and Online Algorithms* (WAOA 2015). *LNCS* 9499, 158-169.

[C21] N. Cohen, D. Gonçalves, E.J. Kim, C. Paul, I. Sau, D.M. Thilikos, and M. Weller. A Polynomial-time Algorithm for Outerplanar Diameter Improvement. *10th International Computer Science Symposium in Russia* (CSR 2015). *LNCS* 9139, 123-142.

[C20] B. Albar, D. Gonçalves, and K. Knauer. Orienting triangulations. *31st European Workshop on Computational Geometry* (EuroCG 2015).

[C19] D. Gonçalves, M. Montassier, and A. Pinlou. Entropy compression method applied to graph colorings. *9th International Colloquium on Graph Theory and combinatorics* (ICGT 2014).

[C18] B. Albar, D. Gonçalves, and J.L Ramírez Alfonsín. Detecting minors in matroids through triangles. *9th International Colloquium on Graph Theory and combinatorics* (ICGT 2014).

[C17] B. Albar, and D. Gonçalves. Too Many Triangles. *VII Latin-American Algorithms, Graphs and Optimization Symposium* (LAGOS 2013).

[C16] M.C. Francis, D. Gonçalves, and P. Ochem. The Maximum Clique Problem in Multiple Interval Graphs. *38th International Workshop on Graph-Theoretic Concepts in Computer Science* (WG 2012), *LNCS* 7551, 57-68, 2012.

[C15] N. Bousquet, D. Gonçalves, G. Mertzios, C. Paul, I. Sau, and S. Thomassé. Domination in Circle Graphs. *38st International Workshop on Graph-Theoretic Concepts in Computer Science* (WG 2012), *LNCS* 7551, 308-319, 2012.

[C14] D. Gonçalves, and E.J. Kim. On Exact Algorithms for Permutation CSP. *International Workshop on Approximation, Parameterized and EXact algorithms* (APEX 2012).

[C13] D. Gonçalves, B. Levêque, and A. Pinlou. Triangle contact representations and duality. *18th International Symposium on Graph Drawing* (GD 2010), *LNCS* 6502, 262-273, 2011.

[C12] J. Chalopin, and D. Gonçalves. Every planar graph is the intersection graph of segments in the plane. *41st Annual ACM Symposium on Theory of Computing* (STOC 2009).

[C11] D. Gonçalves, F. Havet, A. Pinlou, and S. Thomassé. Spanning galaxies in digraphs. *5th European Conference on Combinatorics, Graph Theory, and Applications* (EUROCOMB 2009).

[C10] L. Esperet, D. Gonçalves, and A. Labourel. Coloring a set of touching strings. *5th European Conference on Combinatorics, Graph Theory, and Applications* (EUROCOMB 2009).

[C9] D. Gonçalves. Covering planar graphs with forests, one having a bounded maximum degree. *1st Topological & Geometric Graph Theory International Conference* (TGGT 2008).

[C8] J. Chalopin, D. Gonçalves, and P. Ochem. Planar graphs are in 1-STRING. *18th Annual ACM-SIAM Symposium on Discrete Algorithms* (SODA 2007).

[C7] D. Gonçalves. On Vertex Partitions and the Colin de Verdière Parameter. *6th Czech-Slovak International Symposium on Combinatorics, Graph Theory, Algorithms and Applications* (CS 2006).

[C6] J. Chalopin, D. Gonçalves, and P. Ochem. On graph classes defined by overlap and intersection models. *6th Czech-Slovak International Symposium on Combinatorics, Graph Theory, Algorithms and Applications* (CS 2006).

[C5] D. Gonçalves, and P. Ochem. On some Arboricities in Planar Graphs. *7th International Colloquium on Graph Theory* (ICGT 2005).

[C4] D. Gonçalves. On the L(p,1)-labelling of graphs. *3rd European Conference on Combinatorics, Graph Theory, and Applications* (EUROCOMB 2005).

[C3] D. Gonçalves. Edge Partition of Planar Graphs into Two Outerplanar Graphs. *37th Annual ACM Symposium on Theory of Computing* (STOC 2005).

[C2] D. Gonçalves, and M. Montassier. Acyclic choosability of graphs with small maximum degree. *31st International Workshop on Graph-Theoretic Concepts in Computer Science* (WG 2005), *LNCS* 3787, p. 239-248.

[C1] D. Gonçalves. Caterpillar arboricity of planar graphs. *2nd European conference on Combinatorics, Graph Theory and Applications* (EUROCOMB 2003).

Submitted articles

[S4] D. Gonçalves, and L. Isenmann. Dushnik-Miller dimension of TD-Delaunay complexes. `http://arxiv.org/abs/1803.09576`

[S3] S. Bessy, M. Bougeret, D. Gonçalves, and C. Paul. On independent set on B_1-EPG graphs. `http://arxiv.org/abs/1510.00598`

[S2] D. Gonçalves, K. Knauer, and B. Lévêque. Structure of Schnyder labelings on orientable surfaces. `http://arxiv.org/abs/1501.05475`

[S1] D. Gonçalves, M. Montassier, and A. Pinlou. Entropy compression method applied to graph colorings. http://arxiv.org/abs/1406.4380

Bibliography

[1] N. Aerts, and S. Felsner, Straight-Line Triangle Representations via Schnyder Labelings, *Journal of Graph Algorithms and Applications*, 19(1) : 467–505, 2015.

[2] N. Aerts, and S. Felsner, Vertex Contact Representations of Paths on a Grid, *Journal of Graph Algorithms and Applications*, 19(3) : 817–849, 2015.

[3] A.R. Ahmed, F. De Luca, S. Devkota, A. Efrat, M.I. Hossain, S. Kobourov, J. Li, S. Abida Salma, and E. Welch, L-Graphs and Monotone L-Graphs, *ArXiv*, 1703.01544, 2017.

[4] M.J. Alam, T. Biedl, S. Felsner, M. Kaufmann, S.G. Kobourov, and T. Ueckerdt, Computing cartograms with optimal complexity, *Discrete & Computational Geometry*, 50(3) : 784–810, 2013.

[5] M. Albenque, D. Poulalhon, Generic method for bijections between blossoming trees and planar maps, *Electronic Journal of Combinatorics*, 22(2), #38, 2015.

[6] E. Andreev, On convex polyhedra in Lobachevsky spaces, *Mat. Sbornik, Nov. Ser.*, 81 : 445–478, 1970.

[7] A. Asinowski, E. Cohen, M.C. Golumbic, V. Limouzy, M. Lipshteyn, and M. Stern, Vertex Intersection Graphs of Paths on a Grid, *J. Graph Algorithms Appl.*, 16(2) : 129–150, 2012.

[8] M. Badent, C. Binucci, E. Di Giacomo, W. Didimo, S. Felsner, F. Giordano, J. Kratochvíl, P. Palladino, M. Patrignani, F. Trotta, Homothetic triangle contact representations of planar graphs, *In Proceedings of the 19th Canadian Conference on Computational Geometry CCCG '07*, 233–236, 2007.

[9] J. Barát, C. Thomassen, Claw-decompositions and Tutte-orientations, *Journal of Graph Theory*, 52 : 135–146, 2006.

[10] J. Barbay, L. Castelli Aleardi, M. He, J. I. Munro, Succinct representation of labeled graphs, *Algorithmica* 61 : 224–257, 2012.

[11] O. Bernardi, and G. Chapuy, A bijection for covered maps, or a shortcut between Harer-Zagier's and Jackson's formulas, *Journal of Combinatorial Theory A* 118 : 1718–1748, 2011.

[12] T. Biedl, and M. Derka, 1-String B_1-VPG Representations of Planar Partial 3-Trees and Some Subclasses, *ArXiv*, 1506.07246, 2015.

[13] T. Biedl, and M. Derka, 1-String B_2-VPG representation of planar graphs, *Journal of Computational Geometry*, 7(2), 2016.

[14] T. Biedl, and M. Derka, The (3,1)-ordering for 4-connected planar triangulations, *Journal of Graph Algorithms and Applications*, 20(2) : 347–362, 2016.

[15] T. Biedl, and M. Derka, Order-Preserving 1-String Representations of Planar Graphs, *Proc. of SOFSEM 2017*, 283–294, 2017.

[16] A. Bondy, and M.R. Murty, Graph Theory, *Graduate Texts in Mathematics*, Springer-Verlag London, 2008.

[17] D. Bayer, I. Peeva, and B. Sturmfels. Monomial Resolutions. *Math. Research Letters*, 5(1) : 31–46, 1998.

[18] N. Bonichon, C. Gavoille, N. Hanusse, and D. Ilcinkas. Connections between theta-graphs, Delaunay triangulations, and orthogonal surfaces, *Proc. of WG '10*, LNCS 6410, 266–278, 2010.

[19] N. Bonichon, A bijection between realizers of maximal plane graphs and pairs of non-crossing Dyck paths, *Discrete Mathematics* 298 : 104–114, 2005.

[20] G. Brightwell and W.T. Trotter. The order dimension of convex polytopes. *SIAM Journal on Discrete Mathematics* 6(2) : 230–245, 1993.

[21] L. Castelli Aleardi, E. Fusy, T. Lewiner, Schnyder woods for higher genus triangulated surfaces, with applications to encoding, *Discrete and Computational Geometry* 42 : 489–516, 2009.

[22] L. Castelli Aleardi, O. Devillers, and E. Fusy, Canonical Ordering for Triangulations on the Cylinder, with Applications to Periodic Straight-Line Drawings, *International Symposium on Graph Drawing GD 2012*, 376–387, 2012.

[23] N. de Castro, F. Cobos, J.C. Dana, A. Márquez, and M. Noy. Triangle-free planar graphs as segment intersection graphs. *J. Graph Algorithms Appl.*, 6(1) : 7–26, 2002.

[24] D. Catanzaro, S. Chaplick, S. Felsner, B.V. Halldórsson, M.M. Halldórsson, T. Hixon, and J. Stacho, Max point-tolerance graphs, *Discrete Applied Mathematics*, 216 : 84–97, 2017.

[25] E. Chambers, D. Eppstein, M. Goodrich, and M. Löffler, Drawing graphs in the plane with a prescribed outer face and polynomial area, *LNCS* 6502, 129–140, 2011.

[26] S. Chaplick, V. Jelínek, J. Kratochvíl, and T. Vyskočil, Bend-bounded path intersection graphs : Sausages, noodles, and waffles on a grill, *Proc. of Graph-Theoretic Concepts in Computer Science*, 274–285, 2012.

[27] S. Chaplick, S.G. Kobourov, and T. Ueckerdt, Equilateral L-contact graphs, *Proc. of the International Workshop on Graph-Theoretic Concepts in Computer Science*, 139–151, 2013.

[28] S. Chaplick, and T. Ueckerdt, Planar Graphs as VPG-Graphs, *J. Graph Algorithms Appl.*, 17(4) : 475–494, 2013.

[29] G. Chapuy, A new combinatorial identity for unicellular maps, via a direct bijective approach, *Advances in Applied Mathematics* 47 : 874–893, 2011.

[30] X. Chen, J. Pach, M. Szegedy, and G. Tardos. Delaunay graphs of point sets in the plane with respect to axis-parallel rectangles. *Random Structures and Algorithms* 34(1) : 11–23, 2009.

[31] P. Chew and R.L. Drysdale, Voronoi diagrams based on convex distance functions, *Proc. 1st Ann. Symp. on Computational Geometry*, 235–244, 1985.

[32] E. Cohen, M.C. Golumbic, W.T. Trotter, and R. Wang, Posets and VPG Graphs., *Order*, 33(1) : 39–49, 2016.

[33] Y. Colin de Verdière, Un principe variationnel pour les empilements de cercles, *Inventiones Mathematicae*, 104(1) : 655–669, 1991.

[34] J. Czyzowicz, E. Kranakis, and J. Urrutia. A simple proof of the representation of bipartite planar graphs as the contact graphs of orthogonal straight line segments. *Inform. Process. Lett.*, 66(3) : 125–126, 1998.

[35] G. Di Battista, R. Tamassia, and L. Vismara, Output-sensitive reporting of disjoint paths, *Algorithmica*, 23 : 302–340, 1999.

[36] C. Duncan, M. Goodrich, and S. Kobourov, Planar drawings of h igher-genus graphs, *Journal of Graph Algorithms and Applications*,15 : 13–32, 2011.

[37] B. Dushnik, and E.W. Miller. Partially ordered sets, *American Journal of Mathematics*, 63(3) : 600–610, 1941.

[38] G. Ehrlich, S. Even, and R.E. Tarjan. Intersection Graphs of Curves in the Plane. *J. Combin. Theory. Ser. B*, 21 : 8–20, 1976.

[39] W. Evans, S. Felsner, G. Kobourov, and T. Ueckerdt, Graphs admitting d-realizers : spanning-tree-decompositions and box-representations *Proc. of EuroCG '14*, 2014.

[40] M.C. Francis, and A. Lahiri, VPG and EPG bend-numbers of Halin graphs, *Discrete Applied Mathematics*, 215 : 95–105, 2016.

[41] H. de Fraysseix, and P. Ossona de Mendez, and J. Pach. Representation of planar graphs by segments. *Intuitive geometry (Szeged, 1991), Colloq. Math. Soc. János Bolyai*, 63 : 109–117, 1994.

[42] H. de Fraysseix, and P. Ossona de Mendez. Intersection Graphs of Jordan Arcs. *DIMACS Series in Discrete Mathematics and Theoretical Computer Science*, 49 : 11–28, 1999.

[43] H. de Fraysseix, and P. Ossona de Mendez. Representations by contact and intersection of segments. *Algorithmica*, 47(4) : 453–463, 2007.

[44] S. Felsner, Convex Drawings of Planar Graphs and the Order Dimension of 3-Polytopes, *Order*, 18 : 19–37, 2001.

[45] S. Felsner, Geodesic Embeddings and Planar Graphs, *Order*, 20 : 135–150, 2003.

[46] S. Felsner, Lattice structures from planar graphs, *Electron. J. Combin.*, 11, #15, 2004.

[47] S. Felsner, *Geometric graphs and arrangements : some chapters from combinatorial geometry*, Advanced Lectures in Mathematics, Vieweg, 2004.

[48] S. Felsner, and W. T. Trotter. Posets and planar graphs. *J. Graph Theory* 49, 262–272, 2005.

[49] S. Felsner, Empty Rectangles and Graph Dimension, *ArXiv* : 0601.767, 2006.

[50] S. Felsner, and F. Zickfeld, Schnyder Woods and Orthogonal Surfaces, *Discrete & Comput. Geom.*, 40 : 103–126, 2008.

[51] S. Felsner, Triangle Contact Representations, Prague Midsummer Combinatorial Workshop XV, July 2009.

[52] S. Felsner, K. Knauer, ULD-lattices and Δ-bonds, *Combin. Proba. Comput.* 18(5) : 707–724, 2009.

[53] S. Felsner, and M.C. Francis, Contact representations of planar graphs with cubes, *Proc. of SoCG '11*, 315–320, 2011.

[54] S. Felsner, Rectangle and Square Representations of Planar Graphs, *Thirty Essays in Geometric Graph Theory* edited by J. Pach, Springer, 213–248, 2012.

[55] S. Felsner, K. Knauer, G.B. Mertzios, and T. Ueckerdt, Intersection graphs of L-shapes and segments in the plane, *Discrete Applied Mathematics*, 206 : 48–55, 2016.

[56] S. Felsner, H. Schrezenmaier, and R. Steiner, Pentagon contact representations, *ENDM proc. of Eurocomb 2017*, 2017.

[57] H. de Fraysseix, and P. Ossona de Mendez, P. Rosenstiehl, On Triangle Contact Graphs, *Combinatorics, Probability and Computing*, 3 : 233–246, 1994.

[58] H. de Fraysseix, and P. Ossona de Mendez, On topological aspects of orientations, *Discrete Mathematics*, 229 : 57–72, 2001.

[59] H. de Fraysseix, and P.O. de Mendez, Barycentric systems and stretchability, *Discrete Applied Mathematics*, 155 : 1079–1095, 2007.

[60] H. de Fraysseix, J. Pach, and R. Pollack, Small sets supporting fary embeddings of planar graphs, *Proc. of the twentieth annual ACM symposium on Theory of computing, STOC '88*, 426–433, 1988.

[61] É. Fusy, Transversal structures on triangulations : A combinatorial study and straight-line drawings, *Disc. Math.* 309(7) : 1870–1894, 2009.

[62] É. Fusy, New bijective links on planar maps via orientations, *Eur. J. of Combin.*, 31(1) : 145–160, 2010.

[63] E.R. Gansner, Y. Hu, M. Kaufmann, and S.G. Kobourov, Optimal Polygonal Representation of Planar Graphs, *Algorithmica*, 63(3) : 672–691, 2012.

[64] E.R. Gansner, Y. Hu, and S.G. Kobourov, On Touching Triangle Graphs, *Proc. Graph Drawing '10* LNCS 6502, 250–261, 2010.

[65] P. Giblin, *Graphs, surfaces and homology*, Cambridge University Press, Cambridge, third edition, 2010.

[66] I.B.-A. Hartman, I. Newman, and R. Ziv. On grid intersection graphs. *Discrete Math.*, 87(1) :41–52, 1991.

[67] S. Hoşten, and W. D. Morris. The order dimension of the complete graph. *Discrete mathematics*, 201(1-3) : 133–139, 1999.

[68] B. Kappelle, Kontact- und Schnittdarstellungen planarer Graphen, *Master Thesis, TU Berlin*, 2015.

[69] M. Kaufmann, J. Kratochvíl, K. A. Lehmann, and A. R. Subramanian. Max-tolerance graphs as intersection graphs : Cliques, cycles and recognition. *In Proc. SODA '06*, 832–841, 2006.

[70] S. Kobourov, T. Ueckerdt, and K. Verbeek, Combinatorial and geometric properties of planar Laman graphs, *Proceedings of the twenty-fourth annual ACM-SIAM symposium on Discrete algorithms (SODA 2013)*, 1668–1678, 2013.

[71] P. Koebe, Kontaktprobleme der konformen Abbildung, *Berichte Äuber die Verhandlungen d. SÄachs. Akad. d. Wiss., Math.-Phys. Klasse*, 88 : 141–164, 1936.

[72] J. Kratochvíl, Geometric representations of Graphs, *Graduate Course, Barcelona, april 2005*, retrieved Jan. 2006 at `http://kam.mff.cuni.cz/~honza/ig.ps`.

[73] J. Kratochvíl, *Bertinoro Workshop on Graph Drawing*, 2007.

[74] L. Lovász, Geometric Representations of Graphs, *manuscript*, 2009. `http://www.cs.elte.hu/~lovasz/geomrep.pdf`.

[75] A. Mary, Dimension de poset et subdivisions simpliciales, *Master Thesis, Univ. of Montpellier*, 2010.

[76] W. S. Massey, *Algebraic Topology : An Introduction*, Harcourt, Brace and World, New York, 1967

[77] S. Mehrabi, Approximation Algorithms for Independence and Domination on B_1-VPG and B_1-EPG Graphs, *ArXiv*, 1702.05633, 2017.

[78] M. Middendorf, and F. Pfeiffer, The max clique problem in classes of string-graphs, *Discrete mathematics*, 108(1-3) : 365–372, 1992.

[79] E. Miller, Planar graphs as minimal resolutions of trivariate monomial ideals, *Documenta Mathematica* 7 : 43–90, 2002.

[80] B. Mohar, Straight-line representations of maps on the torus and other flat surfaces, *Discrete Mathematics* 155 : 173–181, 1996.

[81] B. Mohar, and P. Rosenstiehl, Tessellation and visibility representations of maps on the torus, *Discrete Comput. Geom.* 19 : 249–263, 1998.

[82] B. Mohar, and C. Thomassen, Graphs on surfaces, *Johns Hopkins Studies in the Mathematical Sciences*, Johns Hopkins University Press, Baltimore, MD, 2001.

[83] T. Müller, and E.J. van Leeuwen and J. van Leeuwen, Integer Representations of Convex Polygon Intersection Graphs, *SIAM J. Discrete Math.* 27(1), 205–231, 2013.

[84] P. Ossona de Mendez, Geometric Realization of Simplicial Complexes, *Proc. of Int. Symp. on Graph Drawing 1999 LNCS* 1731, 323–332, 1999.

[85] D. Poulalhon, and G. Schaeffer, Optimal coding and sampling of triangulations, *Algorithmica* 46 : 505–527, 2006.

[86] J. Propp, Lattice structure for orientations of graphs, manuscript, 1993, *ArXiv* :math/0209005.

[87] E.R. Scheinerman. Intersection classes and multiple intersection parameters of graphs. *PhD Thesis, Princeton University*, 1984.

[88] W. Schnyder, Planar graphs and poset dimension, *Order*, 5 : 323–343, 1989.

[89] W. Schnyder, Embedding planar graphs on the grid, *in Proc. of the First Annual ACM-SIAM Symposium on Discrete Algorithms, SODA '90*, 138–148, 1990.

[90] O. Schramm, Combinatorically Prescribed Packings and Applications to Conformal and Quasiconformal Maps, *Modified version of PhD thesis from 1990, ArXiv*, 0709.0710.

[91] O. Schramm, Square tilings with prescribed combinatorics, *Isr. J. Math.*, 84 : 97–118, 1993.

[92] H. Schrezenmaier, Homothetic triangle contact representations, *Proc. of WG '17*, LNCS 10520, 425–437, 2017.

[93] R. Škrekovski, List Improper Colourings of Planar Graphs, *Combinatorics, Probability and Computing*, 8(3) : 293–299, 1999.

[94] Y. Sun, and M. Sarrafzadeh, Floorplanning by Graph Dualization : L-shaped Modules, *Algorithmica* 10 : 429–456, 1993.

[95] W.T. Trotter. Combinatorics and partially ordered sets : Dimension theory. *Johns Hopkins Series in the Mathematical Sciences*, The Johns Hopkins University Press, 1992.

[96] M. van Kreveld, and B. Speckmann, On rectangular cartograms, *Computational Geometry*, 37(3) : 175–187, 2007.

[97] C. Thomassen, Plane representations of graphs, *Progress in graph theory (Bondy and Murty, eds.)*, 336–342, 1984.

[98] D. West. Open problems. *SIAM J. Discrete Math. Newslett.*, 2(1) : 10–12, 1991.

[99] H. Whitney. A theorem on graphs. *Ann. of Math. (2)*, 32(2) : 378–390, 1931.

Appendix : Papers

Discrete Comput Geom (2014) 51:67–131
DOI 10.1007/s00454-013-9552-7

Toroidal Maps: Schnyder Woods, Orthogonal Surfaces and Straight-Line Representations

Daniel Gonçalves · Benjamin Lévêque

Received: 6 July 2012 / Revised: 1 July 2013 / Accepted: 25 September 2013 /
Published online: 31 October 2013

Abstract A Schnyder wood is an orientation and coloring of the edges of a planar map satisfying a simple local property. We propose a generalization of Schnyder woods to graphs embedded on the torus with application to graph drawing. We prove several properties on this new object. Among all we prove that a graph embedded on the torus admits such a Schnyder wood if and only if it is an essentially 3-connected toroidal map. We show that these Schnyder woods can be used to embed the universal cover of an essentially 3-connected toroidal map on an infinite and periodic orthogonal surface. Finally we use this embedding to obtain a straight-line flat torus representation of any toroidal map in a polynomial size grid.

Keywords Schnyder woods · Toroidal graphs · Embedding

1 Introduction

A closed curve on a surface is *contractible* if it can be continuously transformed into a single point. Given a graph embedded on the torus, a *contractible loop* is an edge forming a contractible cycle. Two *homotopic multiple edges* are two edges with the same extremities such that their union forms a contractible cycle. In this paper, we will almost always consider graphs embedded on the torus with no contractible loop and no homotopic multiple edges. We call these graphs *toroidal graphs* for short and keep the distinction with *graph embedded on the torus* that may have contractible loops or homotopic multiple edges. A *map* on a surface is a graph embedded on this surface where every face is homeomorphic to an open disk. A *map embedded on the torus* is a graph embedded on the torus that is a map (it may contains contractible loops or homotopic multiple edges). A *toroidal map* is a toroidal graph that is a map

D. Gonçalves · B. Lévêque ( )
LIRMM, CNRS, Université Montpellier 2, 161 rue Ada, 34095 Montpellier Cedex 5, France
e-mail: benjamin.leveque@lirmm.fr

Fig. 1 Schnyder property

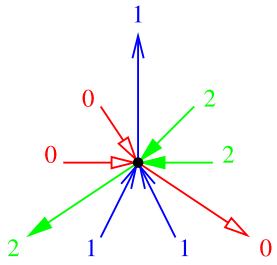

(it has no contractible loop and no homotopic multiple edges). A *toroidal triangulation* is a toroidal map where every face has size three. A general graph (i.e., not embedded on a surface) is *simple* if it contains no loop and no multiple edges. Since some loops and multiple edges are allowed in toroidal graphs, the class of toroidal graphs is larger than the class of simple toroidal graphs.

The torus is represented by a parallelogram in the plane whose opposite sides are pairwise identified. This representation is called the *flat torus*. The *universal cover* G^∞ of a graph G embedded on the torus is the infinite planar graph obtained by replicating a flat torus representation of G to tile the plane (the tiling is obtained by translating the flat torus along two vectors corresponding to the sides of the parallelogram). Note that a graph G embedded on the torus has no contractible loop and no homotopic multiple edges if and only if G^∞ is simple.

Given a general graph G, let n be the number of vertices and m the number of edges. Given a graph embedded on a surface, let f be the number of faces. Euler's formula says that any map on a surface of genus g satisfies $n - m + f = 2 - 2g$, where the plane is the surface of genus 0, and the torus the surface of genus 1.

Schnyder woods were originally defined for planar triangulations by Schnyder [26].

Definition 1 (Schnyder wood, Schnyder property) Given a planar triangulation G, a *Schnyder wood* is an orientation and coloring of the edges of G with the colors 0, 1, 2 where each inner vertex v satisfies the *Schnyder property* (see Fig. 1 where each color is represented by a different type of arrow):

- Vertex v has outdegree one in each color.
- The edges $e_0(v)$, $e_1(v)$, $e_2(v)$ leaving v in colors 0, 1, 2, respectively, occur in counterclockwise order.
- Each edge entering v in color i enters v in the counterclockwise sector from $e_{i+1}(v)$ to $e_{i-1}(v)$ (where $i+1$ and $i-1$ are understood modulo 3).

For higher genus triangulated surfaces, a generalization of Schnyder woods has been proposed by Castelli Aleardi et al. [3], with applications to encoding. Unfortunately, in this definition, the simplicity and the symmetry of the original Schnyder wood are lost. Here we propose an alternative generalization of Schnyder woods for toroidal graphs, with application to graph drawings.

By Euler's formula, a planar triangulation satisfies $m = 3n - 6$. Thus, there are not enough edges in the graph for all vertices to be of outdegree three. This explains

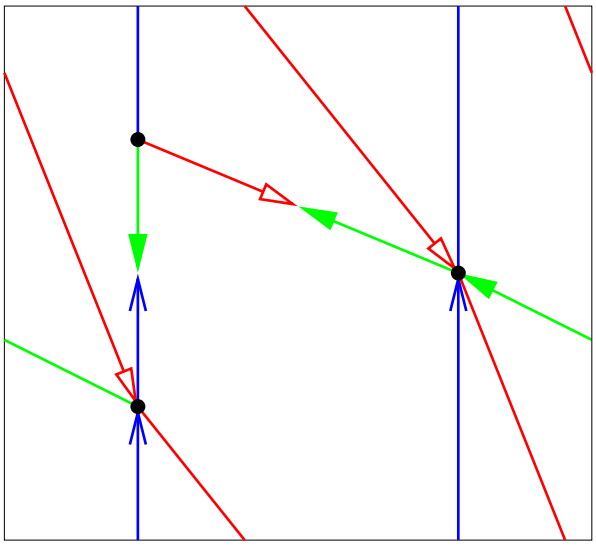

Fig. 2 Example of a Schnyder wood of a toroidal graph

why just some vertices (inner ones) are required to satisfy the Schnyder property. For a toroidal triangulation, Euler's formula gives exactly $m = 3n$, so there is hope for a nice object satisfying the Schnyder property for every vertex. This paper shows that such an object exists. Here we do not restrict ourselves to triangulations and we directly define Schnyder woods in a more general framework.

Felsner [7, 8] (see also [20]) has generalized Schnyder woods to 3-connected planar maps by allowing edges to be oriented in one direction or in two opposite directions. We also allow edges to be oriented in two directions in our definition.

Definition 2 (Toroidal Schnyder wood) Given a toroidal graph G, a *(toroidal) Schnyder wood* of G is an orientation and coloring of the edges of G with the colors 0, 1, 2, where every edge e is oriented in one direction or in two opposite directions (each direction having a distinct color), satisfying the following (see example of Fig. 2):

(T1) Every vertex v satisfies the Schnyder property (see Definition 1)
(T2) Every monochromatic cycle of color i intersects at least one monochromatic cycle of color $i - 1$ and at least one monochromatic cycle of color $i + 1$.

Note that in this definition each vertex has exactly one outgoing arc in each color. Thus, there are monochromatic cycles and the term "wood" has to be handled with care here. The graph induced by one color is not necessarily connected, but each connected component has exactly one directed cycle. We will prove that all the monochromatic cycles of one color have the same homotopy.

In the case of toroidal triangulations, $m = 3n$ implies that there are too many edges to have bi-oriented edges. Thus, we can use this general definition of Schnyder wood for toroidal graphs and keep in mind that when restricted to toroidal triangulations all edges are oriented in one direction only.

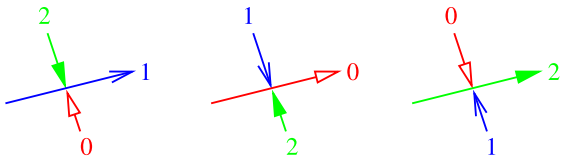

Fig. 3 Rules for the dual Schnyder wood

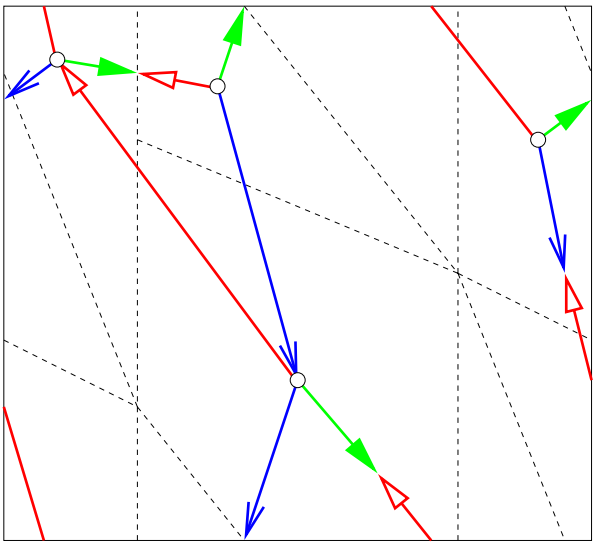

Fig. 4 Dual Schnyder wood of the Schnyder wood of Fig. 2

Extending the notion of essentially 2-connectedness [23], we say that a toroidal graph G is *essentially k-connected* if its universal cover is k-connected. Note that an essentially 1-connected toroidal graph is a toroidal map. We prove that essentially 3-connected toroidal maps are characterized by the existence of Schnyder woods.

Theorem 1 *A toroidal graph admits a Schnyder wood if and only if it is an essentially* 3*-connected toroidal map*.

The *dual* of a Schnyder wood is the orientation and coloring of the edges of G^* obtained by the rules represented on Fig. 3.

Our definition supports duality and we have the following results.

Theorem 2 *There is a bijection between Schnyder woods of a toroidal map and Schnyder woods of its dual*.

The dual Schnyder wood of the Schnyder wood of Fig. 2 is represented on Fig. 4.

In our definition of Schnyder woods, two properties are required: a local one (T1) and a global one (T2). This second property is important for using Schnyder woods

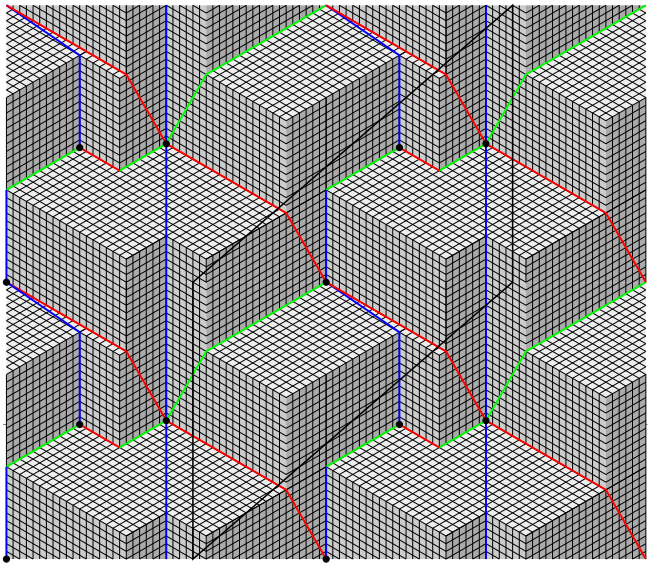

Fig. 5 Geodesic embedding of the toroidal map of Fig. 2

to embed toroidal graphs on orthogonal surfaces, as has been done in the plane by Miller [20] (see also [8]).

Theorem 3 *The universal cover of an essentially* 3*-connected toroidal map admits a geodesic embedding on an infinite and periodic orthogonal surface.*

A geodesic embedding of the toroidal map of Fig. 2 is represented on Fig. 5. The black parallelogram represents a copy of the graph of Fig. 2; this is the basic tile that is used to fill the plane.

A *straight-line flat torus representation* of a toroidal map G is the restriction to a flat torus of a periodic straight-line representation of G^∞. The problem of finding a straight-line flat torus representation of a toroidal map was previously solved on exponential size grids [21]. There are several works that represent a toroidal map inside a parallelogram in a polynomial size grid [5, 6], but in these representations the opposite sides of the parallelogram do not perfectly match. In the embeddings obtained by Theorem 3, vertices are not coplanar, but we prove that for toroidal triangulations one can project the vertices on a plane to obtain a periodic straight-line representation of G^∞. This gives the first straight-line flat torus representation of any toroidal map in a polynomial size grid.

Theorem 4 *A toroidal graph admits a straight-line flat torus representation in a polynomial size grid.*

In Sect. 2, we explain how our definition of Schnyder woods in the torus generalizes the planar case. In Sect. 3, we show that our Schnyder woods are of two fundamentally different types. In Sect. 4, we study the behavior of Schnyder woods

in the universal cover; we define the notion of regions and show that the existence of Schnyder woods for a toroidal graph implies that the graph is an essentially 3-connected toroidal map. In Sect. 5, we define the angle labeling and the dual of a Schnyder wood. In Sect. 6, we show how the definition of Schnyder woods can be relaxed for one of the two types of Schnyder wood. This relaxation is used in the next sections for proving the existence of a Schnyder wood. In Sect. 7, we use a result of Fijavz [13] on the existence of non-homotopic cycles in simple toroidal triangulations to obtain a short proof of existence of Schnyder woods for simple triangulations. In Sect. 8, we prove a technical lemma showing how a Schnyder wood of a graph G can be derived from a Schnyder wood of the graph G', where G' is obtained from G by contracting an edge. This lemma is then used in Sect. 9 to prove the existence of Schnyder woods for any essentially 3-connected toroidal maps. In Sect. 10, we use Schnyder woods to embed the universal cover of essentially 3-connected toroidal maps on periodic and infinite orthogonal surfaces by generalizing the region vector method defined in the plane. In Sect. 11, we show that the dual map can also be embedded on this orthogonal surface. In Sect. 12, we show that, in the case of toroidal triangulations, this orthogonal surface can be projected on a plane to obtain a straight-line flat torus representation.

2 Generalization of the Planar Case

Felsner [7, 8] has generalized planar Schnyder woods by allowing edges to be oriented in one direction or in two opposite directions. The formal definition is the following:

Definition 3 (Planar Schnyder wood) Given a planar map G, let x_0, x_1, x_2 be three distinct vertices occurring in counterclockwise order on the outer face of G. The *suspension* G^σ is obtained by attaching a half-edge that reaches into the outer face to each of these special vertices. A *(planar) Schnyder wood* rooted at x_0, x_1, x_2 is an orientation and coloring of the edges of G^σ with the colors 0, 1, 2, where every edge e is oriented in one direction or in two opposite directions (each direction having a distinct color), satisfying the following (see the example of Fig. 6):

(P1) Every vertex v satisfies the Schnyder property and the half-edge at x_i is directed outwards and colored i
(P2) There is no monochromatic cycle.

In the definition given by Felsner [8], property (P2) is in fact replaced by "There is no interior face the boundary of which is a monochromatic cycle", but the two are equivalent by results of [7, 8].

With our definition of Schnyder woods for toroidal graphs, the goal is to generalize the definition of Felsner. In the torus, property (P1) can be simplified as every vertex plays the same role: there are no special outer vertices with a half-edge reaching into the outer face. This explains property (T1) in our definition. Then if one asks that every vertex satisfies the Schnyder property, there are necessarily monochromatic

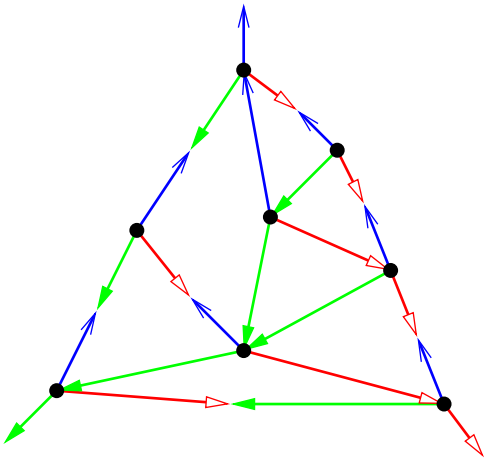

Fig. 6 Example of a Schnyder wood of a planar map

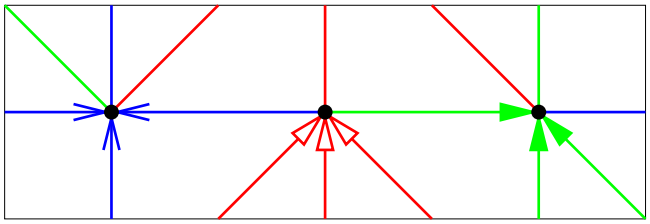

Fig. 7 An orientation and coloring of the edges of a toroidal triangulation satisfying (T1) but not (T2), as there is no pair of intersecting monochromatic cycles

cycles and (P2) is not satisfied. This explains why (P2) has been replaced by (T2) in our generalization to the torus.

It would have been possible to replace (P2) by "there is no contractible monochromatic cycles", but this is not enough to suit our needs. Our goal is to use Schnyder woods to embed universal covers of toroidal graphs on orthogonal surfaces, as has been done in the plane by Miller [20] (see also [8]). The difference is that our surface is infinite and periodic. In such a representation the three colors 0, 1, 2 correspond to the three directions of the space. Thus, the monochromatic cycles with different colors have to intersect each other in a particular way. This explains why property (T2) is required. Figure 7 gives an example of an orientation and coloring of the edges of a toroidal triangulation satisfying (T1) but not (T2), as there is no pair of intersecting monochromatic cycles.

Let G be a toroidal graph given with a Schnyder wood. Let G_i be the directed graph induced by the edges of color i. This definition includes edges that are half-colored i, and in this case, the edges get only the direction corresponding to color i. Each graph G_i has exactly n edges, so it does not induce a rooted tree (contrarily to planar Schnyder woods). Note also that G_i is not necessarily connected (for example, in the graph of Fig. 8, every Schnyder wood has one color whose corresponding

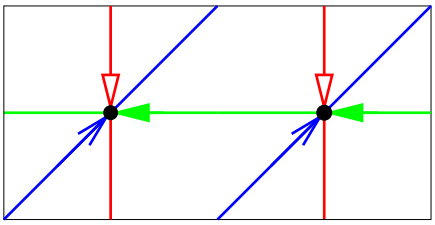

Fig. 8 A toroidal graph where every Schnyder wood has one color whose corresponding subgraph is not connected

subgraph is not connected). But each component of G_i has exactly one outgoing arc for each of its vertices. Thus, each connected component of G_i has exactly one directed cycle that is a *monochromatic cycle* of color i, or *i-cycle* for short. Note that monochromatic cycles can contain edges oriented in two directions with different colors, but the *orientation* of an i-cycle is the orientation given by the (half-)edges of color i. The graph G_i^{-1} is the graph obtained from G_i by reversing all its edges. The graph $G_i \cup G_{i-1}^{-1} \cup G_{i+1}^{-1}$ is obtained from the graph G by orienting edges in one or two directions depending on whether this orientation is present in G_i, G_{i-1}^{-1}, or G_{i+1}^{-1}. The following lemma shows that our property (T2) in fact implies that there are no contractible monochromatic cycles.

Lemma 1 *The graph $G_i \cup G_{i-1}^{-1} \cup G_{i+1}^{-1}$ contains no contractible directed cycle.*

Proof Suppose there is a contractible directed cycle in $G_i \cup G_{i-1}^{-1} \cup G_{i+1}^{-1}$. Let C be such a cycle containing the minimum number of faces in the closed disk D bounded by C. Suppose by symmetry that C turns clockwise around D. Then, by (T1), there is no edge of color $i-1$ leaving the closed disk D. So there is an $(i-1)$-cycle in D, and this cycle is C by minimality of C. Then, by (T1), there is no edge of color i leaving D. So, again by minimality of C, the cycle C is an i-cycle. Thus, all the edges of C are oriented clockwise in color i and counterclockwise in color $i-1$. Then, by (T1), all the edges of color $i+1$ incident to C have to leave D. Thus, there is no $(i+1)$-cycle intersecting C, a contradiction to property (T2). □

Let G be a planar map and let x_0, x_1, x_2 be three distinct vertices occurring in counterclockwise order on the outer face of G. One can transform G^σ into the following toroidal map G^+ (see Fig. 9): Add a vertex v in the outer face of G. Add three non-parallel and non-contractible loops on v. Connect the three half-edges leaving x_i to v such that there are no two such edges entering v consecutively. Then we have the following.

Theorem 5 *The Schnyder woods of a planar map G rooted at x_0, x_1, x_2 are in bijection with the Schnyder woods of the toroidal map G^+ (where the orientation of one of the loops is fixed).*

Proof ($\Longrightarrow$) We are given a Schnyder wood of the planar graph G, rooted at x_0, x_1, x_2. Orient and color the graph G^+ as in the example of Fig. 9, i.e., the edges of the original graph G have the same color and orientation as in G^σ, the edge from

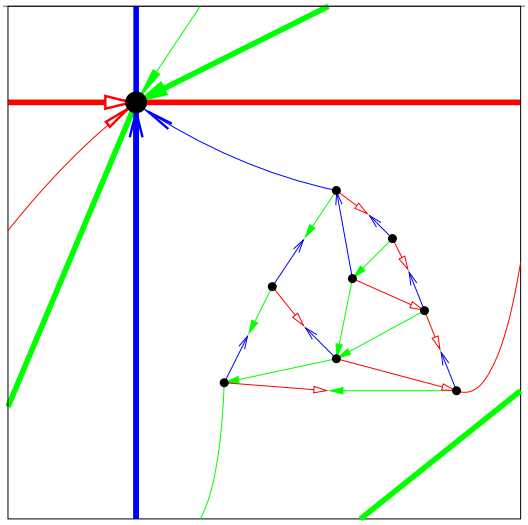

Fig. 9 The toroidal Schnyder wood corresponding to the planar Schnyder wood of Fig. 6

x_i to v is colored i and leaving x_i, and the three loops around v are colored and oriented appropriately so that v satisfies the Schnyder property. Then it is clear that all the vertices of G^+ satisfy (T1). By (P2), we know that G^σ has no monochromatic cycles. All the edges between G and v are leaving G, so there is no monochromatic cycle of G^+ involving vertices of G. Thus, the only monochromatic cycles of G^+ are the three loops around v and they satisfy (T2).

($\Longleftarrow$) Given a Schnyder wood of G^+, the restriction of the orientation and coloring to G and the three edges leaving v gives a Schnyder wood of G^σ. The three loops around v are three monochromatic cycles corresponding to three edges leaving v; thus, they have different colors by (T1). Thus, the three edges between G and v are entering v with three different colors. The three loops around v have to leave v in counterclockwise order $0, 1, 2$ and we can assume the colors such that the edge leaving x_i is colored i. Clearly, all the vertices of G^σ satisfy (P1). By Lemma 1, there are no contractible monochromatic cycles in G^+, so G^σ satisfies (P2). □

A planar map G is *internally 3-connected* if there exist three vertices on the outer face such that the graph obtained from G by adding a vertex adjacent to the three vertices is 3-connected. Miller [20] (see also [7]) proved that a planar map admits a Schnyder wood if and only if it is internally 3-connected. The following results show that the notion of essentially 3-connected is the natural generalization of internally 3-connected to the torus.

Theorem 6 *A planar map G is internally 3-connected if and only if there exist three vertices on the outer face of G such that G^+ is an essentially 3-connected toroidal map.*

Proof ($\Longrightarrow$) Let G be an internally 3-connected planar map. By definition, there exist three vertices x_0, x_1, x_2 on the outer face such that the graph G' obtained from G by adding a vertex adjacent to these three vertices is 3-connected. Let G'' be the graph obtained from G by adding three vertices y_0, y_1, y_2 that form a triangle and by adding the three edges $x_i y_i$. It is not difficult to check that G'' is 3-connected. Since G^∞ can be obtained from the (infinite) triangular grid, which is 3-connected, by gluing copies of G'' along triangles, G^∞ is clearly 3-connected. Thus, G^+ is an essentially 3-connected toroidal map.

($\Longleftarrow$) Suppose there exist three vertices on the outer face of G such that G^+ is an essentially 3-connected toroidal map, i.e., G^∞ is 3-connected. A copy of G is contained in a triangle $y_0y_1y_2$ of G^∞. Let G'' be the subgraph of G^∞ induced by this copy plus the triangle, and let x_i be the unique neighbor of y_i in the copy of G. Since G'' is connected to the rest of G^∞ by a triangle, G'' is also 3-connected. Let us now prove that this implies that G is internally 3-connected for x_0, x_1, and x_2. This is equivalent to saying that the graph G', obtained by adding a vertex z connected to x_0, x_1, and x_2, is 3-connected. If G' had a separator $\{a, b\}$ or $\{a, z\}$, with $a, b \in V(G') \setminus \{z\}$, then $\{a, b\}$ or $\{a, y_i\}$, for some $i \in [0, 2]$, would be a separator of G''. This would contradict the 3-connectedness of G''. So G is internally 3-connected. □

3 Two Different Types of Schnyder Woods

Two non-contractible closed curves are *homotopic* if one can be continuously transformed into the other. Homotopy is an equivalence relation, and as we are on the torus we have the following.

Lemma 2 *Let C_1, C_2 be two non-contractible closed curves on the torus. If C_1, C_2 are not homotopic, then their intersection is non-empty.*

Two non-contractible oriented closed curves on the torus are *fully homotopic* if one can be continuously transformed into the other by preserving the orientation. We say that two monochromatic directed cycles C_i, C_j of different colors are *reversal* if one is obtained from the other by reversing all the edges ($C_i = C_j^{-1}$). We say that two monochromatic cycles are *crossing* if they intersect but are not reversal. We define the *right side* of an i-cycle C_i, as the right side while "walking" along the directed cycle by following the orientation given by the edges colored i.

Let G be a toroidal graph given with a Schnyder wood.

Lemma 3 *All i-cycles are non-contractible, non-intersecting, and fully homotopic.*

Proof By Lemma 1, all i-cycles are non-contractible. If there exist two such distinct i-cycles that are intersecting, then there is a vertex that has two outgoing edges of color i, a contradiction to (T1). So the i-cycles are non-intersecting. Then, by Lemma 2, they are homotopic.

Suppose that there exist two i-cycles C_i, C_i' that are not fully homotopic. By the first part of the proof, cycles C_i, C_i' are non-contractible, non-intersecting, and homotopic. Let R be the region between C_i and C_i' situated on the right of C_i. Suppose

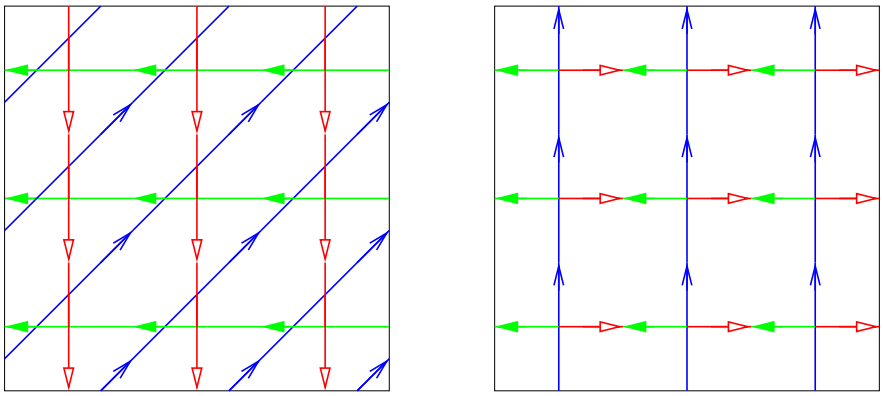

Fig. 10 The two types of Schnyder woods on toroidal graphs

by symmetry that C_i^{-1} is not an $(i+1)$-cycle. By (T2), there exists a cycle C_{i+1} intersecting C_i and thus C_{i+1} is crossing C_i. By property (T1), C_{i+1} is entering C_i from its right side and so it is leaving the region R when it crosses C_i. To enter the region R, the cycle C_{i+1} has to enter C_i or C_i' from their left side, a contradiction to property (T1). □

Lemma 4 *If two monochromatic cycles are crossing, then they are of different colors and they are not homotopic.*

Proof By Lemma 3, two crossing monochromatic cycles are not of the same color. Suppose that there exist two monochromatic cycles C_{i-1} and C_{i+1}, of color $i-1$ and $i+1$, that are crossing and homotopic. By Lemma 1, the cycles C_{i-1} and C_{i+1} are not contractible. Since $C_{i-1} \neq C_{i+1}^{-1}$ and $C_{i-1} \cap C_{i+1} \neq \emptyset$, the cycle C_{i+1} is leaving C_{i-1}. It is leaving C_{i-1} on its right side by (T1). Since C_{i-1} and C_{i+1} are homotopic, the cycle C_{i+1} is entering C_{i-1} at least once from its right side. This is in contradiction with (T1). □

Let $\mathcal{C}_i$ be the set of i-cycles of G. Let $(\mathcal{C}_i)^{-1}$ denote the set of cycles obtained by reversing all the cycles of $\mathcal{C}_i$. By Lemma 3, the cycles of $\mathcal{C}_i$ are non-contractible, non-intersecting, and fully homotopic. So we can order them as follows: $\mathcal{C}_i = \{C_i^0, \ldots, C_i^{k_i-1}\}$, $k_i \geq 1$, such that, for $0 \leq j \leq k_i - 1$, there is no i-cycle in the region $R(C_i^j, C_i^{j+1})$ between C_i^j and C_i^{j+1} containing the right side of C_i^j (superscript understood modulo k_i).

We show that Schnyder woods are of two different types (see Fig. 10):

Theorem 7 *Let G be a toroidal graph given with a Schnyder wood. Then all i-cycles are non-contractible, non-intersecting, and fully homotopic, and either*:

- *For every pair of two monochromatic cycles C_i, C_j of different colors i, j, the two cycles C_i and C_j are not homotopic and thus intersect* (*we say the Schnyder wood is of* Type 1);

or

- *There exists a color i such that $\mathcal{C}_{i-1} = (\mathcal{C}_{i+1})^{-1}$ and for any pair of monochromatic cycles C_i, C_j of colors i, j, with $j \neq i$, the two cycles C_i and C_j are not homotopic and thus intersect* (*we say the Schnyder wood is of* Type 2, *or* Type 2.i *if we want to specify the color i*).

Moreover, if G is a toroidal triangulation, then there are no edges oriented in two directions and the Schnyder wood is of Type 1.

Proof By Lemma 3, all i-cycles are non-contractible, non-intersecting, and fully homotopic. Suppose that there exist a $(i-1)$-cycle C_{i-1} and a $(i+1)$-cycle C_{i+1} that are homotopic. We prove that the Schnyder wood is of Type 2.i. We first prove that $\mathcal{C}_{i-1} = (\mathcal{C}_{i+1})^{-1}$. Let C'_{i-1} be any $(i-1)$-cycle. By (T2), C'_{i-1} intersects an $(i+1)$-cycle C'_{i+1}. By Lemma 3, C'_{i-1} (resp. C'_{i+1}) is homotopic to C_{i-1} (resp. C_{i+1}). So C'_{i-1} and C'_{i+1} are homotopic. By Lemma 4, C'_{i-1} and C'_{i+1} are reversal. Thus, $\mathcal{C}_{i-1} \subseteq (\mathcal{C}_{i+1})^{-1}$ and so by symmetry $\mathcal{C}_{i-1} = (\mathcal{C}_{i+1})^{-1}$. Now we prove that for any pair of monochromatic cycles C'_i, C'_j of colors i, j, with $j \neq i$, the two cycles C'_i and C'_j are not homotopic. By (T2), C'_j intersects an i-cycle C_i. Since $\mathcal{C}_{i-1} = (\mathcal{C}_{i+1})^{-1}$, cycle C'_j is bi-oriented in color $i-1$ and $i+1$, and thus we cannot have $C'_j = C_i^{-1}$. So C'_j and C_i are crossing and by Lemma 4, they are not homotopic. By Lemma 3, C'_i and C_i are homotopic. Thus, C'_j and C'_i are not homotopic. Thus, the Schnyder wood is of Type 2.i.

If there are no two monochromatic cycles of different colors that are homotopic, then the Schnyder wood is of Type 1.

For toroidal triangulation, $m = 3n$ by Euler's formula, so there are no edges oriented in two directions, and thus only Type 1 is possible. □

Note that in a Schnyder wood of Type 1, we may have edges that are in two monochromatic cycles of different colors (see Fig. 2).

We do not know if the set of Schnyder woods of a given toroidal graph has a kind of lattice structure as in the planar case [9]. De Fraysseix et al. [15] proved that Schnyder woods of a planar triangulation are in one-to-one correspondence with the orientation of the edges of the graph where each inner vertex has outdegree three. It is possible to retrieve the coloring of the edges of a Schnyder wood from the orientation. The situation is different for toroidal triangulations. There exist orientations of toroidal triangulations where each vertex has outdegree three but there is no corresponding Schnyder wood. For example, if one considers a toroidal triangulation with just one vertex, the orientations of edges that satisfy (T1) are the orientations where there are not three consecutive edges leaving the vertex (see Fig. 11).

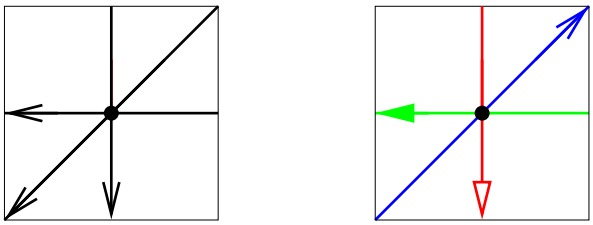

Fig. 11 Two different orientations of a toroidal triangulation. Only the second one corresponds to a Schnyder wood

4 Schnyder Woods in the Universal Cover

Let G be a toroidal graph given with a Schnyder wood. Consider the orientation and coloring of the edges of G^∞ that correspond to the Schnyder wood of G.

Lemma 5 *The orientation and coloring of the edges of G^∞ satisfy the following*:

(U1) *Every vertex of G^∞ satisfies the Schnyder property*
(U2) *There is no monochromatic cycle in G^∞.*

Proof Clearly, (U1) is satisfied. Now we prove (U2). Suppose by contradiction that there is a monochromatic cycle U of color i in G^∞. Let C be the closed curve of G corresponding to edges of U. If C self-intersects, then there is a vertex of G with two edges leaving v in color i, a contradiction to (T1). So C is a monochromatic cycle of G. Since C corresponds to a cycle of G^∞, it is a contractible cycle of G, a contradiction to Lemma 1. □

One can remark that properties (U1) and (U2) are the same as in the definition of Schnyder woods for 3-connected planar graphs (properties (P1) and (P2)). Note that if the orientation and coloring of the edges of G^∞, corresponding to an orientation and coloring of the edges of G, satisfy properties (U1) and (U2), we do not necessarily have a Schnyder wood of G. For example, the graph G^∞ obtained by replicating the graph G of Fig. 7 satisfies (U1) and (U2), whereas the orientation and coloring of G do not make a Schnyder wood as (T2) is not satisfied.

Recall that the notation $\mathcal{C}_i = \{C_i^0, \ldots, C_i^{k_i-1}\}$ denotes the set of i-cycles of G such that there is no i-cycle in the region $R(C_i^j, C_i^{j+1})$. As monochromatic cycles are not contractible by Lemma 1, a directed monochromatic cycle C_i^j corresponds to a family of infinite directed monochromatic paths of G^∞ (infinite in both directions of the path). This family is denoted $\mathcal{L}_i^j$. Each element of $\mathcal{L}_i^j$ is called a *monochromatic line* of color i, or i*-line* for short. By Lemma 3, all i-lines are non-intersecting and oriented in the same direction. Given any two i-lines L, L', the unbounded region between L and L' is noted $R(L, L')$. We say that two i-lines L, L' are *consecutive* if no i-lines are contained in $R(L, L')$.

Let v be a vertex of G^∞. For each color i, vertex v is the starting vertex of a unique infinite directed monochromatic path of color i, denoted $P_i(v)$. Indeed this is a path

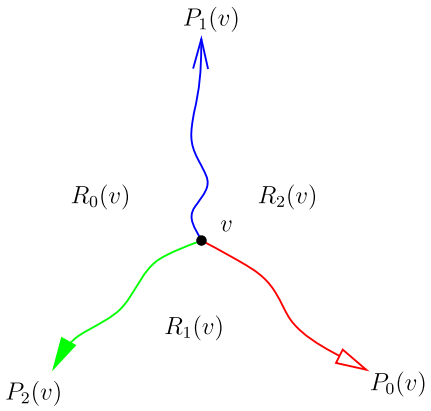

Fig. 12 Regions corresponding to a vertex

since there is no monochromatic cycle in G^∞ by property (U2), and it is infinite (in one direction of the path only) because every reached vertex of G^∞ has exactly one edge leaving in color i by property (U1). As $P_i(v)$ is infinite, it necessarily contains two vertices u, u' of G^∞ that are copies of the same vertex of G. The subpath of $P_i(v)$ between u and u' corresponds to an i-cycle of G and thus is part of an i-line of G^∞. Let $L_i(v)$ be the i-line intersecting $P_i(v)$.

Lemma 6 *The graph $G_i^\infty \cup (G_{i-1}^\infty)^{-1} \cup (G_{i+1}^\infty)^{-1}$ contains no directed cycle.*

Proof Suppose there is a contractible directed cycle C in $G_i^\infty \cup (G_{i-1}^\infty)^{-1} \cup (G_{i+1}^\infty)^{-1}$. Let D be the closed disk bounded by C. Suppose by symmetry that C turns around D clockwise. Then, by (U1), there is no edge of color $i-1$ leaving the closed disk D. So there is an $(i-1)$-cycle in D, a contradiction to (U2). □

Lemma 7 *For every vertex v and color i, the two paths $P_{i-1}(v)$ and $P_{i+1}(v)$ only intersect on v.*

Proof If $P_{i-1}(v)$ and $P_{i+1}(v)$ intersect on two vertices, then $G_{i-1}^\infty \cup (G_{i+1}^\infty)^{-1}$ contains a cycle, contradicting Lemma 6. □

By Lemma 7, for every vertex v, the three paths $P_0(v)$, $P_1(v)$, $P_2(v)$ divide G^∞ into three unbounded regions $R_0(v)$, $R_1(v)$, and $R_2(v)$, where $R_i(v)$ denotes the region delimited by the two paths $P_{i-1}(v)$ and $P_{i+1}(v)$. Let $R_i^\circ(v) = R_i(v) \setminus (P_{i-1}(v) \cup P_{i+1}(v))$ (see Fig. 12).

Lemma 8 *For all distinct vertices u, v, we have*:

(i) *If $u \in R_i(v)$, then $R_i(u) \subseteq R_i(v)$.*
(ii) *If $u \in R_i^\circ(v)$, then $R_i(u) \subsetneq R_i(v)$.*
(iii) *There exists i and j with $R_i(u) \subsetneq R_i(v)$ and $R_j(v) \subsetneq R_j(u)$.*

Proof (i) Suppose by symmetry that the Schnyder wood is not of Type 2.(i+1). Then in G, i-cycles are not homotopic to $(i-1)$-cycles. Thus in G^∞, every i-line crosses

every $(i-1)$-line. Moreover an i-line crosses an $(i-1)$-line exactly once and from its right side to its left side by (U1). Vertex v is between two consecutive monochromatic $(i-1)$-lines L_{i-1}, L'_{i-1}, with L'_{i-1} situated on the right of L_{i-1}. Let R be the region situated on the right of L_{i-1}, so $v \in R$.

Claim 1 *For any vertex w of R, the path $P_i(w)$ leaves the region R.*

Proof of Claim 1 The i-line $L_i(w)$ has to cross L_{i-1} exactly once and from right to left; thus, $P_i(w)$ leaves the region R. This proves Claim 1. □

The path $P_{i+1}(v)$ cannot leave the region R as this would contradict (U1). Thus, by Claim 1 for $w = v$, we have $R_i(v) \subseteq R$ and so $u \in R$. Moreover, the paths $P_{i-1}(u)$ and $P_{i+1}(u)$ cannot leave region $R_i(v)$ as this would contradict (U1). Thus by Claim 1 for $w = u$, the path $P_i(u)$ leaves the region $R_i(v)$ and so $R_i(u) \subseteq R_i(v)$.

(ii) By (i), $R_i(u) \subseteq R_i(v)$, so the paths $P_{i-1}(u)$ and $P_{i+1}(u)$ are contained in $R_i(v)$. Then none of them can contain v as this would contradict (U1). So all the faces of $R_i(v)$ incident to v are not in $R_i(u)$ (and there is at least one such face).

(iii) By symmetry, we prove that there exists i with $R_i(u) \subsetneq R_i(v)$. If $u \in R_i^\circ(v)$ for some color i, then $R_i(u) \subsetneq R_i(v)$ by (ii). Suppose now that $u \in P_i(v)$ for some i. By Lemma 7, at least one of the two paths $P_{i-1}(u)$ and $P_{i+1}(u)$ does not contain v. Suppose by symmetry that $P_{i-1}(u)$ does not contain v. As $u \in P_i(v) \subseteq R_{i+1}(v)$, we have $R_{i+1}(u) \subseteq R_{i+1}(v)$ by (i), and as none of $P_{i-1}(u)$ and $P_i(u)$ contains v, we have $R_{i+1}(u) \subsetneq R_{i+1}(v)$. □

Lemma 9 *If a toroidal graph G admits a Schnyder wood, then G is essentially 3-connected.*

Proof Let u, v, x, y be any four distinct vertices of G^∞. Let us prove that there exists a path between u and v in $G^\infty \setminus \{x, y\}$. Suppose by symmetry, that the Schnyder wood is of Type 1 or Type 2.1. Then the monochromatic lines of color 0 and 2 form a kind of grid; i.e., the 0-lines intersect all the 2-lines. Let L_0, L'_0 be 0-lines and L_2, L'_2 be 2-lines, such that u, v, x, y are all in the interior of the bounded region $R(L_0, L'_0) \cap R(L_2, L'_2)$.

By Lemma 7, the three paths $P_i(v)$, for $0 \le i \le 2$, are disjoint except on v. Thus, there exists i, such that $P_i(v) \cap \{x, y\} = \emptyset$. Similarly there exists j, such that $P_j(u) \cap \{x, y\} = \emptyset$. The two paths $P_i(v)$ and $P_j(u)$ are infinite, so they intersect the boundary of $R(L_0, L'_0) \cap R(L_2, L'_2)$. Thus, $P_i(v) \cup P_j(u) \cup L_0 \cup L'_0 \cup L_2 \cup L'_2$ contains a path from u to v in $G^\infty \setminus \{x, y\}$. □

By Lemma 9, if G admits a Schnyder wood, then it is essentially 3-connected, so it is a map and each face is a disk.

Note that if (T2) is not required in the definition of Schnyder woods, then Lemma 9 is false. Figure 13 gives an example of an orientation and a coloring of the edges of a toroidal graph satisfying (T1), such that there are no contractible monochromatic cycles, but where (T2) is not satisfied as there is a 0-cycle not intersecting any 2-cycle. This graph is not essentially 3-connected; indeed, G^∞ is not connected.

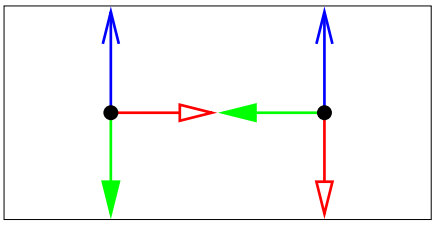

Fig. 13 An orientation and a coloring of the edges of a toroidal graph satisfying (T1) but not essentially 3-connected

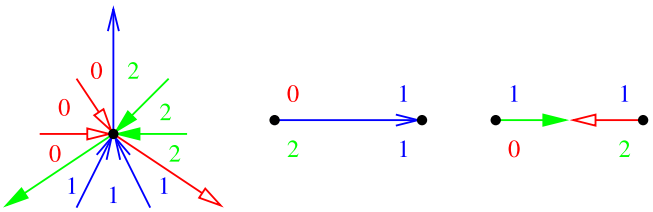

Fig. 14 Angle labeling around vertices and edges

5 Duality of Schnyder Woods

We are given a planar map G, and x_0, x_1, x_2, three distinct vertices occurring in counterclockwise order on the outer face of G. A *Schnyder angle labeling* [7] of G with respect to x_0, x_1, x_2 is a labeling of the angles of G^σ satisfying the following:

(L1) The label of the angles at each vertex form, in counterclockwise order, non-empty intervals of 0's, 1's, and 2's. The two angles at the half-edge at x_i have labels $i+1$ and $i-1$

(L2) The label of the angles at each inner face form, in counterclockwise order, non-empty intervals of 0's, 1's, and 2's. At the outer face the same is true in clockwise order.

Felsner [8] proved that, for planar maps, Schnyder woods are in bijection with Schnyder angle labellings. In the toroidal case, we do not see a simple definition of Schnyder angle labeling that would be equivalent to our definition of Schnyder woods. This is due to the fact that, unlike (P2) which is local and can be checked just by considering faces, (T2) is global. Nevertheless, we have one implication.

The *angle labeling corresponding to* a Schnyder wood of a toroidal map G is a labeling of the angles of G such that the angles at a vertex v in the counterclockwise sector between $e_{i+1}(v)$ and $e_{i-1}(v)$ are labeled i (see Fig. 14).

Lemma 10 *The angle labeling corresponding to a Schnyder wood of a toroidal map satisfies the following*: *the angles at each vertex and at each face form*, *in counterclockwise order*, *non-empty intervals of* 0*'s*, 1*'s*, *and* 2*'s*.

Proof Clearly, the property is true at each vertex by (T1). To prove that the property is true at each face, we count the number of color changes around vertices, faces, and edges. This number of changes is denoted d. For a vertex v there are exactly three changes, so $d(v) = 3$ (see Fig. 14). For an edge e, that can be either oriented in one or two directions, there are also exactly three changes, so $d(e) = 3$ (see Fig. 14). Now consider a face F. Suppose we cycle counterclockwise around F; then an angle colored i is always followed by an angle colored i or $i + 1$. Consequently, $d(F)$ must be a multiple of 3. Suppose that $d(F) = 0$; then all its angles are colored with one color i. In that case the cycle around face F would be completely oriented in counterclockwise order in color $i + 1$ (and in clockwise order in color $i - 1$). This cycle being contractible, this would contradict Lemma 1. So $d(F) \geq 3$.

The sum of the changes around edges must be equal to the sum of the changes around faces and vertices. Thus $3m = \sum_e d(e) = \sum_v d(v) + \sum_F d(F) = 3n + \sum_F d(F)$. Euler's formula gives $m = n + f$, so $\sum_F d(F) = 3f$ and this is possible only if $d(F) = 3$ for every face F. □

There is no converse to Lemma 10. Figure 7 gives an example of a coloring and orientation of the edges of a toroidal triangulation not satisfying (T2) but where the angles at each vertex and at each face form, in counterclockwise order, non-empty intervals of 0's, 1's, and 2's.

Let G be a toroidal graph given with a Schnyder wood. By Lemma 9, G is an essentially 3-connected toroidal map, and thus the dual G^* of G has no contractible loop and no homotopic multiple edges. Let $\widetilde{G}$ be a simultaneous drawing of G and G^* such that only dual edges intersect.

The *dual* of the Schnyder wood is the orientation and coloring of the edges of G^* obtained by the following method (see Figs. 3 and 4): Let e be an edge of G and e^* the dual edge of e. If e is oriented in one direction only and colored i, then e^* is oriented in two directions, entering e from the right side in color $i - 1$ and from the left side in color $i + 1$ (the right side of e is the right side while following the orientation of e). Symmetrically, if e is oriented in two directions in colors $i + 1$ and $i - 1$, then e^* is oriented in one direction only and colored i such that e is entering e^* from its right side in color $i - 1$.

Lemma 11 *Let G be a toroidal map. The dual of a Schnyder wood of a toroidal map G is a Schnyder wood of the dual G^*. Moreover we have*:

(i) *On the simultaneous drawing $\widetilde{G}$ of G and G^*, the i-cycles of the dual Schnyder wood are homotopic to the i-cycles of the primal Schnyder wood and oriented in opposite directions.*
(ii) *The dual of a Schnyder wood is of Type 2.i if and only if the primal Schnyder wood is of Type 2.i.*

Proof In every face of $\widetilde{G}$, there is exactly one angle of G and one angle of G^*. Thus a Schnyder angle labeling of G corresponds to an angle labeling of G^*. The dual of the Schnyder wood is defined such that an edge e is leaving F in color i if and only if the angle at F on the left of e is labeled $i - 1$ and the angle at F on the right of e is labeled $i + 1$, and such that an edge e is entering F in color i if and only if at

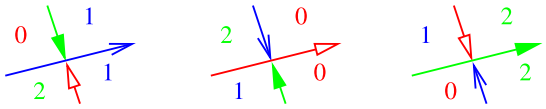

Fig. 15 Rules for the dual Schnyder wood and angle labeling

least one of the angles at F incident to e is labeled i (see Fig. 15). By Lemma 10, the angles at a face form, in counterclockwise order, non-empty intervals of 0's, 1's, and 2's. Thus, the edges around a vertex of G^* satisfy property (T1).

Consider $\widetilde{G}$ with the orientation and coloring of primal and dual edges.

Let C be a i-cycle of G^*. Suppose, by contradiction, that C is contractible. Let D be the disk delimited by C. Suppose by symmetry that C is going anticlockwise around D. Then all the edges of G that are dual to edges of C are entering D in color $i-1$. Thus, D contains an $(i-1)$-cycle of G, a contradiction to Lemma 1. Thus, every monochromatic cycle of G^* is non-contractible.

The dual of the Schnyder wood is defined in such a way that an edge of G and an edge of G^* of the same color never intersect in $\widetilde{G}$. Thus the i-cycles of G^* are homotopic to i-cycles of G. Consider a i-cycle C_i (resp. C_i^*) of G (resp. G^*). The two cycles C_i and C_i^* are homotopic. By symmetry, we assume that the primal Schnyder wood is not of Type 2.(i −1). Let C_{i+1} be an $(i+1)$-cycle of G. The two cycles C_i and C_{i+1} are not homotopic and C_i is entering C_{i+1} on its left side. Thus, the two cycles C_i^* and C_{i+1} are not homotopic, and by the dual rules C_i^* is entering C_{i+1} on its right side. So C_i and C_i^* are homotopic and going in opposite directions.

Suppose the Schnyder wood of G is of Type 1. Then two monochromatic cycles of G of different colors are not homotopic. Thus, the same is true for monochromatic cycles of the dual. So (T2) is satisfied and the dual of the Schnyder wood is a Schnyder wood of Type 1.

Suppose now that the Schnyder wood of G is of Type 2. Assume by symmetry that it is of Type 2.i. Then all monochromatic cycles of color i and j, with $j \in \{i-1, i+1\}$, intersect. Now suppose, by contradiction, that there is a j-cycle C^*, with $j \in \{i-1, i+1\}$, that is not equal to a monochromatic cycle of color in $\{i-1, i+1\} \setminus \{j\}$. By symmetry we can assume that C^* is of color $i-1$. Let C be the $(i-1)$-cycle of the primal that is the first on the right side of C^* in $\widetilde{G}$. By definition of Type 2.i, C^{-1} is an $(i+1)$-cycle of G. Let R be the region delimited by C^* and C situated on the right side of C^*. Cycle C^* is not an $(i+1)$-cycle, so there is at least one edge of color $i+1$ leaving a vertex of C^*. By (T1) in the dual, this edge is entering the interior of the region R. An edge of G^* of color $i+1$ cannot intersect C and cannot enter C^* from its right side. So in the interior of the region R there is at least one $(i+1)$-cycle C_{i+1}^* of G^*. Cycle C_{i+1}^* is homotopic to C^* and going in the opposite direction (i.e., C_{i+1}^* and C^* are not fully homotopic). If C_{i+1}^* is not an $(i-1)$-cycle, then we can define $R' \subsetneq R$ the region delimited by C_{i+1}^* and C situated on the left side of C_{i+1}^* and as before we can prove that there is an $(i-1)$-cycle of G^* in the interior of R'. So in any case, there is an $(i-1)$-cycle C_{i-1}^* of G^* in the interior of R and C_{i-1}^* is fully homotopic to C^*. Let $R'' \subsetneq R$ be the region delimited by C^* and C_{i-1}^* situated on the right side of C^*. Clearly, R'' does not contain C. Thus, by the

definition of C, the region R'' does not contain any $(i-1)$-cycle of G. But R'' is non-empty and contains at least one vertex v of G. The path $P_{i-1}(v)$ cannot leave R'', a contradiction. So (T2) is satisfied and the dual Schnyder wood is of Type 2.i. □

By Lemma 11, we have Theorem 2.

6 Relaxing the Definition

In the plane, the proof of existence of Schnyder woods can be done without too much difficulty, as the properties to be satisfied are only local. In the toroidal case, things are much more complicated, as property (T2) is global. The following lemma shows that property (T2) can be relaxed a bit in the case of Schnyder woods of Type 1.

Lemma 12 *Let G be a toroidal graph given with an orientation and coloring of the edges of G with the colors* 0, 1, 2, *where every edge e is oriented in one direction or in two opposite directions. The orientation and coloring is a Schnyder wood of Type* 1 *if and only if it satisfies the following*:

(T1') *Every vertex v satisfies the Schnyder property.*
(T2') *For each pair i, j of different colors, there exists an i-cycle intersecting a j-cycle.*
(T3') *There are no monochromatic cycles C_i, C_j of different colors i, j such that $C_i = C_j^{-1}$.*

Proof ($\Longrightarrow$) If we have a Schnyder wood of Type 1, then property (T1') is satisfied, as it is equal to property (T1). Property (T1) implies that there always exist monochromatic cycles of each color, and thus property (T2') is a relaxation of (T2). Property (T3') is implied by definition of Type 1 (see Theorem 7).

($\Longleftarrow$) Conversely, suppose we have an orientation and coloring satisfying (T1'), (T2'), (T3'). We prove several properties.

Claim 2 *All i-cycles are non-contractible, non-intersecting, and homotopic.*

Proof of Claim 2 Suppose there is a contractible monochromatic cycle. Let C be such a cycle containing the minimum number of faces in the closed disk D bounded by C. Suppose by symmetry that C turns around D clockwise. Let i be the color of C. Then, by (T1'), there is no edge of color $i-1$ leaving the closed disk D. So there is an $(i-1)$-cycle in D and this cycle is C by minimality of C, a contradiction to (T3').

If there exist two distinct i-cycles that are intersecting, then there is a vertex that has two outgoing edges of color i, a contradiction to (T1'). So the i-cycles are non-intersecting. Then, by Lemma 2, they are homotopic. This proves Claim 2. □

Claim 3 *If two monochromatic cycles are intersecting, then they are not homotopic.*

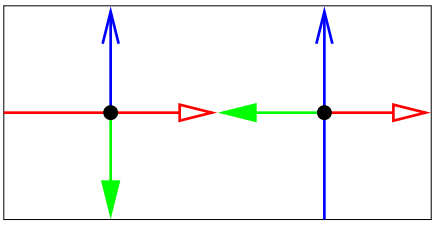

Fig. 16 An orientation and coloring of the edges of toroidal graph satisfying (T1') and (T2') but that is not a Schnyder wood

Proof of Claim Suppose by contradiction that there exist C, C', two distinct directed monochromatic cycles that are homotopic and intersecting. By Claim 2, they are not contractible and of different color. Suppose C is an $(i-1)$-cycle and C' an $(i+1)$-cycle. By (T1'), C' is leaving C on its right side. Since C, C' are homotopic, the cycle C' is entering C at least once from its right side, a contradiction with (T1'). This proves Claim 3. □

We are now able to prove that (T2) is satisfied. Let C_i be any i-cycle of color i. We have to prove that C_i intersects at least one $(i-1)$-cycle and at least one $(i+1)$-cycle. Let j be either $i-1$ or $i+1$. By (T2'), there exists an i-cycle C'_i intersecting a j-cycle C'_j of color j. The two cycles C'_i, C'_j are not reversal by (T3'); thus, they are crossing. By claim (3), C'_i and C'_j are not homotopic. By Claim 2, C_i and C'_i are homotopic. Thus, by Lemma 2, C_i and C'_j are not homotopic and intersecting.

Thus, (T1) and (T2) are satisfied, and the orientation and coloring are a Schnyder wood. By (T3') and Theorem 7 it is a Schnyder wood of Type 1. □

Note that for toroidal triangulations, there are no edges oriented in two directions in an orientation and coloring of the edges satisfying (T1'), by Euler's formula. So (T3') is automatically satisfied. Thus, in the case of toroidal triangulations it is sufficient to have properties (T1') and (T2') to have a Schnyder wood. This is not true in general, as shown by the example of Fig. 16 that satisfies (T1') and (T2') but that is not a Schnyder wood. There is a monochromatic cycle of color 1 that is not intersecting any monochromatic cycle of color 2, so (T2) is not satisfied.

7 Existence for Simple Triangulations

In this section we present a short proof of existence of Schnyder woods for simple triangulations. Sections 8 and 9 contain the full proof of existence for essentially 3-connected toroidal maps.

Fijavz [13] proved a useful result concerning the existence of particular non-homotopic cycles in toroidal triangulations with no loop and no multiple edges. (Recall that in this paper we are less restrictive, as we allow non-contractible loops and non-homotopic multiple edges.)

Theorem 8 ([13]) *A simple toroidal triangulation contains three non-contractible and non-homotopic cycles that all intersect on one vertex and that are pairwise disjoint otherwise.*

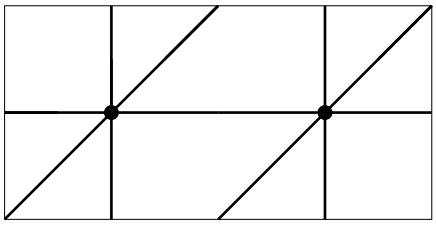

Fig. 17 A toroidal triangulation that does not contain three non-contractible and non-homotopic cycles that all intersect on one vertex and that are pairwise disjoint otherwise

Theorem 8 is not true for all toroidal triangulations, as shown by the example on Fig. 17.

Theorem 8 can be used to prove the existence of particular Schnyder woods for simple toroidal triangulations. We first need the following lemma.

Lemma 13 *If G is a connected near-triangulation (i.e., all inner faces are triangles) whose outer boundary is a cycle, and with three vertices x_0, x_1, x_2 on its outer face such that the three outer paths between the x_i are chordless, then G' is internally 3-connected for vertices x_i.*

Proof Let G' be the graph obtained from G by adding a vertex z adjacent to the three vertices x_i. We have to prove that G' is 3-connected. Let S be a separator of G' of minimum size and suppose by contradiction that $1 \leq |S| \leq 2$. Let $G'' = G' \setminus S$.

For $v \in S$, the vertices of $N_{G'}(v) \setminus S$ should appear in several connected components of G'', otherwise $S \setminus \{v\}$ is also a separator of G'. Since G is a near-triangulation, the neighbors of an inner vertex v of G form a cycle, and thus there are at least two vertex-disjoint paths between any two vertices of $N(v)$ in $G' \setminus \{v\}$. So S contains no inner vertex of G. Similarly, the three neighbors of z in G' belong to a cycle of $G' \setminus \{z\}$ (the outer boundary of G), so S does not contain z. Thus, S contains only vertices that are on the outer boundary of G.

Let $v \in S$. Vertex v is on the outer face of G, so its neighbors in G form a path P where the two extremities of P are the two neighbors of v on the outer face of G. So S contains an inner vertex u of P. Vertex u is also on the outer face of G, so uv is a chord of the outer cycle of G. As the three outer paths between the x_i are chordless, we have that u, v lie on two different outer paths between pairs of x_i. But then all the vertices of $P \setminus \{u\}$ are in the same components of G'' because of z, a contradiction. □

Theorem 9 *A simple toroidal triangulation admits a Schnyder wood with three monochromatic cycles of different colors all intersecting on one vertex and that are pairwise disjoint otherwise.*

Proof Let G be a simple toroidal triangulation. By Theorem 8, let C_0, C_1, C_2 be three non-contractible and non-homotopic cycles of G that all intersect on one vertex x and that are pairwise disjoint otherwise. By eventually shortening the cycles C_i, we can assume that the three cycles C_i are chordless. By symmetry, we can assume that the six edges e_i, e'_i of the cycles C_i incident to x appear around x in the counterclockwise order $e_0, e'_2, e_1, e'_0, e_2, e'_1$ (see Fig. 18). The cycles C_i divide G into two regions, denoted R_1, R_2 such that R_1 is the region situated in the counterclockwise sector

between e_0 and e'_2 of x and R_2 is the region situated in the counterclockwise sector between e'_2 and e_1 of x. Let G_i be the subgraph of G contained in the region R_i (including the three cycles C_i).

Let G'_1 (resp. G'_2) be the graph obtained from G_1 (resp. G_2) by replacing x by three vertices x_0, x_1, x_2, such that x_i is incident to the edges in the counterclockwise sector between e_{i+1} and e'_i (resp. e'_i and e_{i-1}) (see Fig. 19). The two graphs G'_1 and G'_2 are near-triangulation and the C_i are chordless, so by Lemma 13, they are internally 3-connected planar maps for vertices x_i. The vertices x_0, x_1, x_2 appear in counterclockwise order on the outer face of G'_1 and G'_2. By a result of Miller [20] (see also [7, 8]), the two graphs G'_i admit planar Schnyder woods rooted at x_0, x_1, x_2. Orient and color the edges of G that intersect the interior of R_i by giving them the same orientation and coloring as in a planar Schnyder wood of G'_i. Orient and color the cycle C_i in color i such that it is entering x by edge e'_i and leaving x by edge e_i. We claim that the orientation and the coloring that are obtained form a toroidal Schnyder wood of G (see Fig. 19).

Clearly, any interior vertex of the region R_i satisfies (T1). Let us show that (T1) is also satisfied for any vertex v of a cycle C_i distinct from x. In a Schnyder wood of G'_1, the cycle C_i is oriented in two directions, from x_{i-1} to x_i in color i and from x_i to x_{i-1} in color $i-1$. Thus the edge leaving v in color $i+1$ is an inner edge of G'_1 and vertex v has no edges entering in color $i+1$. Symmetrically, in G'_2 the edge leaving v in color $i-1$ is an inner edge of G'_2 and vertex v has no edges entering in color $i-1$. Then one can paste G'_1 and G'_2 along C_i, orient C_i in color i, and see that v satisfies (T1). The definition of the G'_i and the orientation of the cycles are done so that x satisfies (T1). The cycles C_i being pairwise intersecting, (T2') is satisfied, so by Lemma 12, the orientation and coloring form a Schnyder wood. □

Note that in the Schnyder wood obtained by Theorem 9, we do not know if there are several monochromatic cycles of one color or not. So given any three monochromatic cycles of different color, they might not all intersect on one vertex. But for any two monochromatic cycles of different color, we know that they intersect exactly once. We wonder whether Theorem 9 can be modified as follows: Does a simple

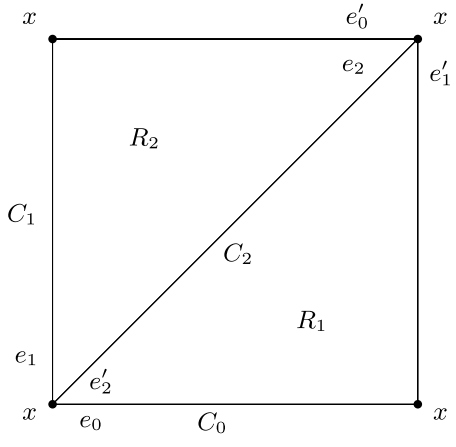

Fig. 18 Notation of the proof of Theorem 9

toroidal triangulation admit a Schnyder wood such that there is just one monochromatic cycle per color? Moreover, can one require that the monochromatic cycles of different colors pairwise intersect exactly once? Or, as in Theorem 9, that they all intersect on one vertex and that they are pairwise disjoint otherwise?

8 The Contraction Lemma

We prove the existence of Schnyder woods for essentially 3-connected toroidal maps by contracting edges until we obtain a graph with just a few vertices. Then the graph can be decontracted step by step to obtain a Schnyder wood of the original graph.

Given a toroidal map G, the *contraction* of a non-loop edge e of G is the operation consisting of continuously contracting e until its two ends are merged. We denote the obtained graph as G/e. On Fig. 20 the contraction of an edge e is represented. We consider three different cases corresponding to whether the faces adjacent to the edge e are triangles or not. Note that only one edge of each set of homotopic multiple edges that is possibly created is preserved.

The goal of this section is to prove the following lemma, which plays a key role in the proof of Sect. 9.

Lemma 14 *If G is a toroidal map given with a non-loop edge e whose extremities are of degree at least three and such that G/e admits a Schnyder wood of Type* 1, *then G admits a Schnyder wood of Type* 1.

The proof of Lemma 14 is long and technical. In the planar case, an analogous lemma can be proved without too much difficulty (see Sect. 2.6 of [12]), as there are special outer vertices where the contraction can be done to reduce the case analysis and as properties (P1) and (P2) are local and not too difficult to preserve during the decontraction process.

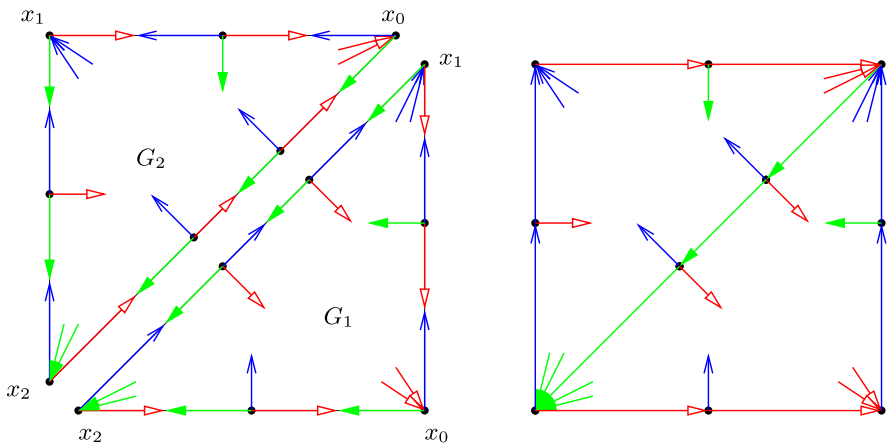

Fig. 19 Gluing two planar Schnyder woods into a toroidal one to prove Theorem 9

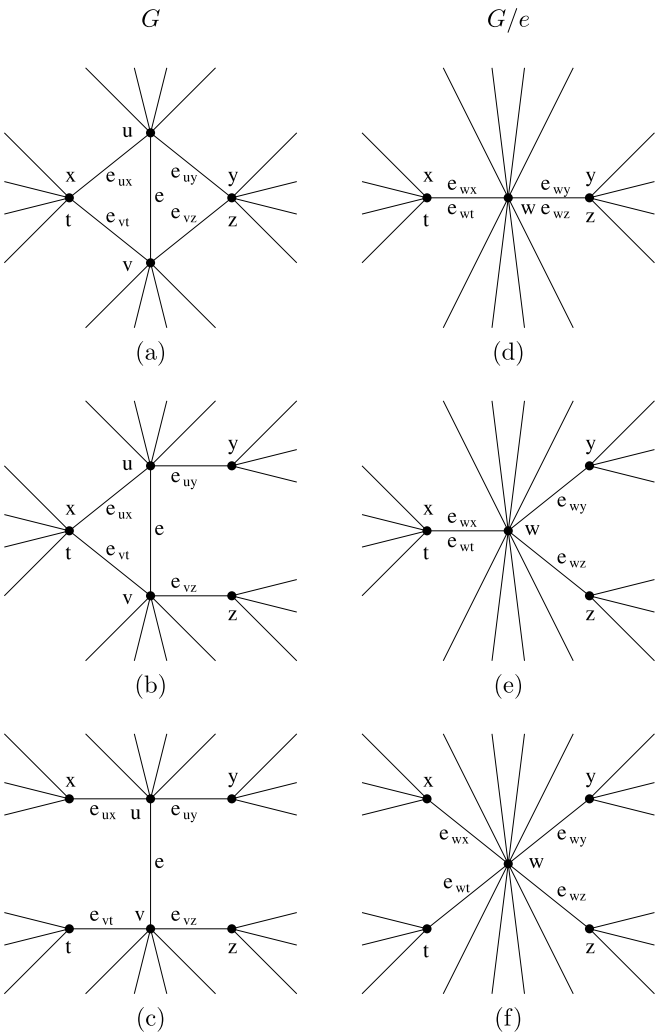

Fig. 20 The contraction operation

In the toroidal case there is a huge case analysis for the following reasons. One has to consider the three different kinds of contractions depicted on Fig. 20. For each of these cases, one must consider the different ways that the edges can be oriented and colored (around the contraction point) in G/e. For each of these cases, one must show that the Schnyder wood G/e can be extended to a Schnyder wood of G. This would be quite easy if one just has to satisfy (T1), which is a local property, but satisfying (T2) is much more complicated. Instead of proving (T2), that is considering intersections between every pair of monochromatic cycles, we prove (T2') and (T3'), which is equivalent for our purposes by Lemma 12. Property (T2') is simpler than (T2), as it considers just one intersection for each pair of colors instead of all the intersections. Even with this simplification, proving (T2') is the main difficulty of the proof. For

each considered case, one has to analyze the different ways in which the monochromatic cycles go through the contracted vertex or not and show that there always exist a coloring and orientation of G where (T2') is satisfied. Some cases are non-trivial and involve the use of lemmas like Lemmas 15 and 16.

Lemma 15 *Let G be a toroidal map given with a Schnyder wood and let y, w be two vertices of G such that $e_i(y)$ is entering w. Suppose that there is a directed path Q_{i-1} of color $i-1$ from y to w, and a directed path Q_{i+1} of color $i+1$ from y to w. Consider the two directed cycles $C_{i-1} = Q_{i-1} \cup \{e_i(y)\}^{-1}$ and $C_{i+1} = Q_{i+1} \cup \{e_i(y)\}^{-1}$. Then C_{i-1} and C_{i+1} are not homotopic.*

Proof By Lemma 1, the cycles C_{i-1} and C_{i+1} are not contractible. Suppose that C_{i-1} and C_{i+1} are homotopic. The path Q_{i+1} is leaving C_{i-1} at y on the right side of C_{i-1}. Since C_{i-1} and C_{i+1} are homotopic, the path Q_{i+1} is entering C_{i-1} at least once from its right side. This is in contradiction with (T1). □

The sector $[e_1, e_2]$ of a vertex w, for e_1 and e_2 two edges incident to w, is the counterclockwise sector of w between e_1 and e_2, including the edges e_1 and e_2. The sectors $]e_1, e_2]$, $[e_1, e_2[$, and $]e_1, e_2[$ are defined analogously by excluding the corresponding edges from the sectors.

Lemma 16 *Let G be a toroidal map given with a Schnyder wood and let w, x, y be three vertices such that $e_{i-1}(x)$ and $e_{i+1}(y)$ are entering w. Suppose that there is a directed path Q_{i-1} of color $i-1$ from y to w, entering w in the sector $[e_i(w), e_{i-1}(x)]$, and a directed path Q_{i+1} of color $i+1$ from x to w, entering w in the sector $[e_{i+1}(y), e_i(w)]$. Consider the two directed cycles $C_{i-1} = Q_{i-1} \cup \{e_{i+1}(y)\}^{-1}$ and $C_{i+1} = Q_{i+1} \cup \{e_{i-1}(x)\}^{-1}$. Then either C_{i-1} and C_{i+1} are not homotopic or $C_{i-1} = C_{i+1}^{-1}$.*

Proof By Lemma 1, the cycles C_{i-1} and C_{i+1} are not contractible. Suppose that C_{i-1} and C_{i+1} are homotopic and that $C_{i-1} \neq C_{i+1}^{-1}$. Since $C_{i-1} \neq C_{i+1}^{-1}$, the cycle C_{i+1} is leaving C_{i-1}. By (T1) and the assumption on the sectors, C_{i+1} is leaving C_{i-1} on its right side. Since C_{i-1} and C_{i+1} are homotopic, the path Q_{i+1} is entering C_{i-1} at least once from its right side. This is in contradiction with (T1). □

We are now able to prove Lemma 14.

Proof of Lemma 14 Let u, v be the two extremities of e. Vertices u and v are of degree at least three. Let x, y (resp. z, t) be the neighbors of u (resp. v) such that x, v, y (resp. z, u, t) appear consecutively and in counterclockwise order around u (resp. v) (see Fig. 20(c)). Note that u and v are distinct by the definition of edge contraction, but that x, y, z, t are not necessarily distinct, nor necessarily distinct from u and v. Depending on whether the faces incident to e are triangles or not, we are, by symmetry, in one of the three cases of Fig. 20(a, b, c). Let $G' = G/e$ and consider a Schnyder wood of Type 1 of G'. Let w be the vertex of G' resulting from the contraction of e.

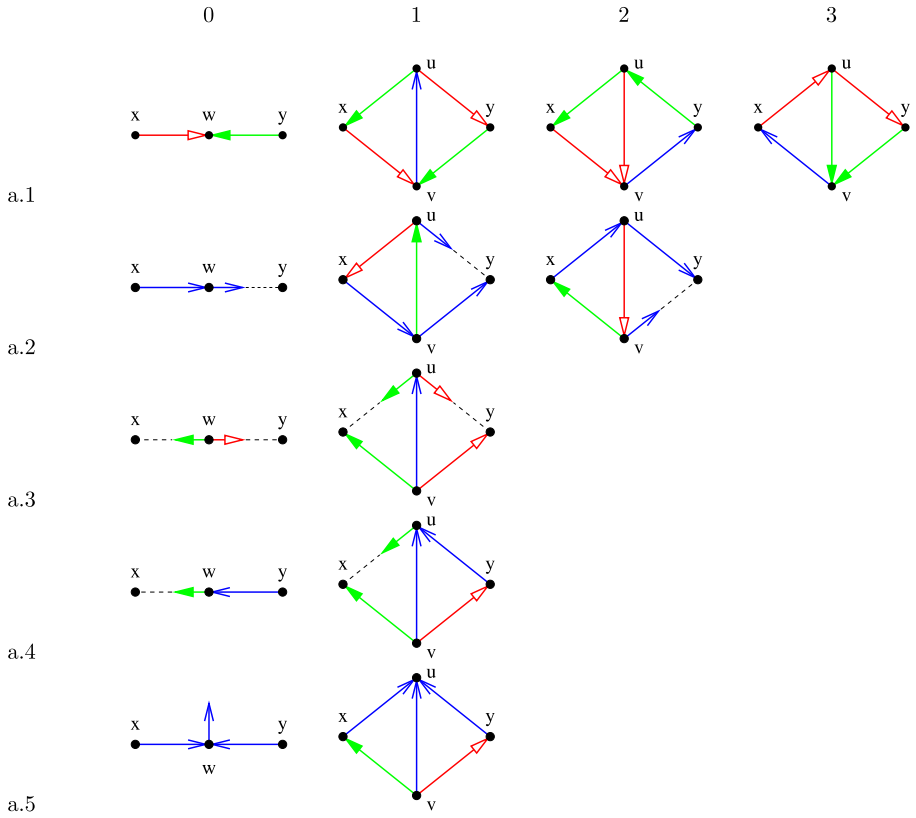

Fig. 21 Decontraction rules for case (**a**)

For each case (a), (b), (c), there are different cases corresponding to the different possibilities of orientation and coloring of the edges $e_{wx}, e_{wy}, e_{wz}, e_{wt}$ in G'. For example, for case (a), there should be 6 cases depending on if e_{wx} and e_{wy} are both entering w, both leaving w, or one entering w and one leaving w (3 cases), multiplied by the coloring, both of the same or not (2 cases). The case where w has two edges leaving in the same color is impossible by (T1). So, by symmetry, only 5 cases remain represented by figures $a.k.0$, for $k = 1, \ldots, 5$, on Fig. 21 (in the notation $\alpha.k.l$, $a.k$ indicates the line on the figures and ℓ the column). For cases (b) and (c), there are more cases to consider, but the analysis is similar. These cases are represented in the first columns of Figs. 22 and 23. On these figures, a dotted half-edge represents the possibility for an edge to be unidirected or bidirected. In the last case of each figure, we have indicated where the edge is leaving in color 1, as there are two possibilities (up or down).

In each case $\alpha.k$, $\alpha \in \{a, b, c\}$, we show how one can color and orient the edges of G to obtain a Schnyder wood of G from the Schnyder wood of G'. Only the edges e, e_{ux}, e_{uy}, e_{vt}, e_{vz} of G have to be specified; all the other edges of G keep the orientation and coloring of their corresponding edge in G'. In each case $\alpha.k$, there might be several possibilities for coloring and orienting these edges to satisfy (T1). Only

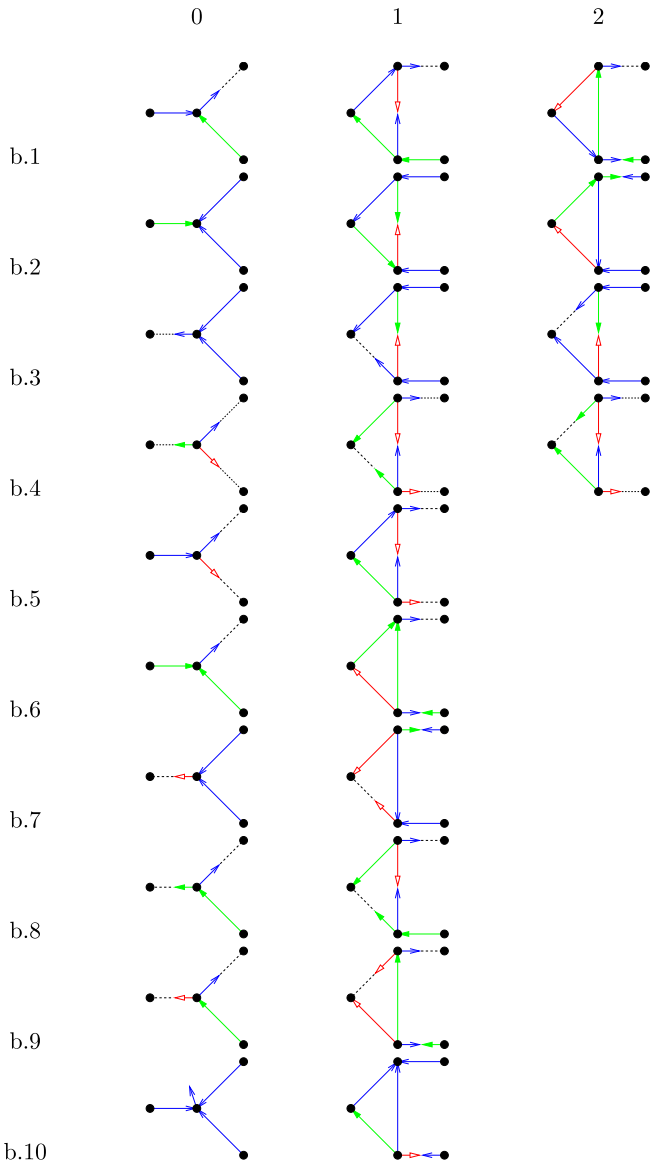

Fig. 22 Decontraction rules for case (**b**)

some of these possibilities, the ones that are useful for our purpose, are represented on figures $\alpha.k.\ell$, $\ell \geq 1$, of Figs. 21 through 23. A dotted half-edge represents the fact that the edge is unidirected or bidirected like the corresponding half-edge of G'.

In each case $\alpha.k$, $\alpha \in \{a, b, c\}$, we show that one of the colorings $\alpha.k.\ell$, $\ell \geq 1$, gives a Schnyder wood of Type 1 of G. By Lemma 12, we just have to prove that, in each case $\alpha.k$, there is one coloring satisfying (T1'), (T2'), and (T3'). Properties

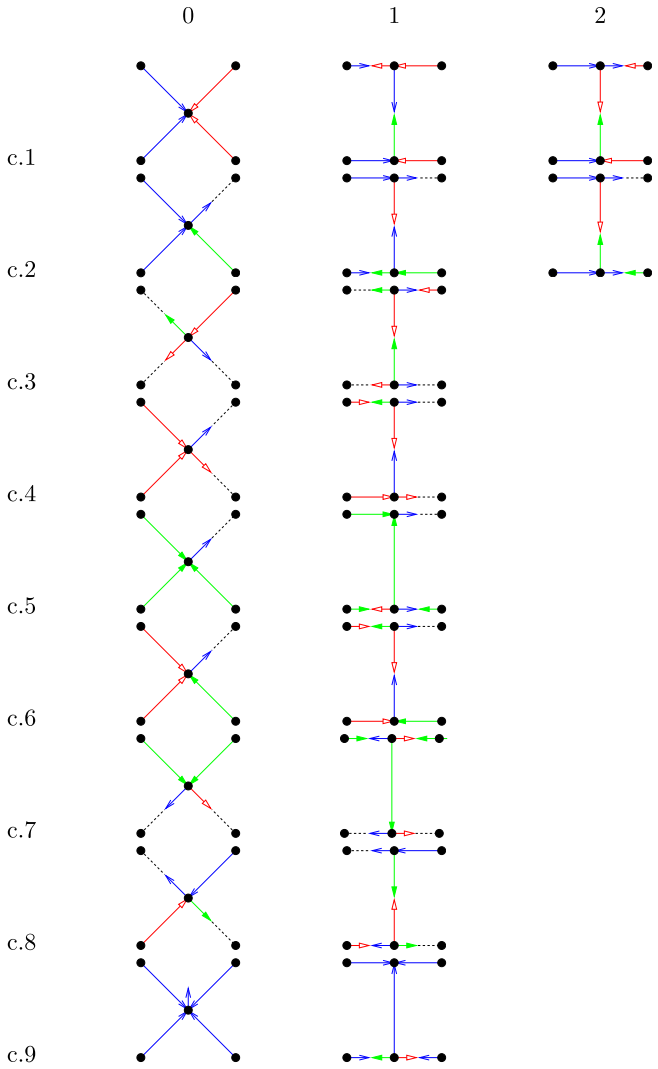

Fig. 23 Decontraction rules for case (**c**)

(T1') and (T3') are satisfied for any colorings $\alpha.k.\ell$, $\ell \geq 1$, but this is not the case for property (T2'). This explains why several possible colorings of G must be considered.

(T1') One can easily check that in all the cases $\alpha.k.\ell$, property (T1') is satisfied for every vertex of G. To do so one can consider the angle labeling around vertices w, x, y, (z), (t) of G' in the case $\alpha.k.0$. Then one can see that this angle labeling exports well around vertices $u, v, x, y, (z), (t)$ of G and thus the Schnyder property is satisfied for these vertices. On Fig. 24, an example is given on how the angle labeling is modified during the decontraction process. It corresponds to case $c.2.1$ where the dotted half-edge is unidirected. We do not discuss this part in more detail, as it is easy to check.

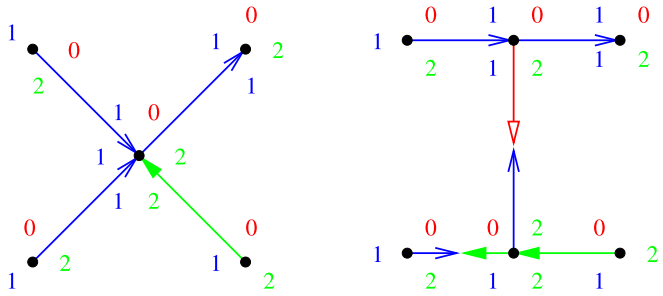

Fig. 24 Example of (T1') preservation during decontraction

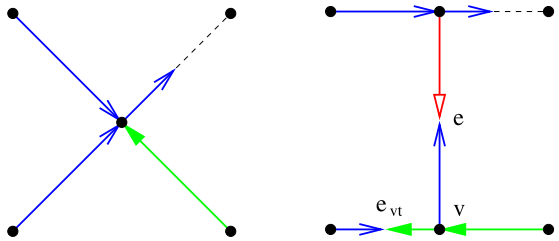

Fig. 25 Example of (T3') preservation during decontraction

(T3') One can easily check that in all the cases $\alpha.k.\ell$, property (T3') is satisfied for G. If (T3') is not satisfied in G after applying one of the colorings $\alpha.k.\ell$, then there exist two monochromatic cycles C, C' of different colors that are reversal. By property (T3') of Lemma 12, there are no reversal cycles in G'. Thus C, C' have to use a bidirected edge e' of the figures that is newly created and distinct from edge e and distinct from the half-dotted edges (otherwise the cycles are still reversal when e is contracted). Only some cases have such an edge, and one can note that, for all these cases, the cycle, after entering u or v by edge e', must use the edge e that is either unidirected or bidirected with different colors than e', a contradiction. For example, in case c.2.1 of Fig. 25, two reversal cycles of G that do not correspond to reversal cycles when e is contracted, have to use edge e_{vt}. Then one of the two cycles is entering v by e_{vt} in color 1 and thus has to continue by using the only edge leaving v in color 1, edge e. As e and e_{vt} are colored differently, this is not possible. We do not further detail this part, which is easy to check.

(T2') Proving property (T2') is the main difficulty of the proof. For each case $\alpha.k$, there is a case analysis considering the different ways in which the monochromatic cycles of G' go through w or not. We say that a monochromatic cycle C of G' is *safe* if C does not contain w. Depending on whether there are safe monochromatic cycles or not for each color, there may be a different case $\alpha.k.\ell$ and a different argument that is used to prove that property (T2') is preserved.

• *Case a.1: e_{wx} and e_{wy} are entering w in different colors.*

We can assume by symmetry that $e_{wx} = e_0(x)$ and $e_{wy} = e_2(y)$ (case a.1.0 of Fig. 21). We apply one of the colorings a.1.1, a.1.2, and a.1.3 of Fig. 21.

We have a case analysis corresponding to whether there are monochromatic cycles of G' that are safe.

⋆ *Subcase a*.1.{0, 1, 2}*: There are safe monochromatic cycles of colors* {0, 1, 2}.

Let C'_0, C'_1, C'_2 be safe monochromatic cycles of color 0, 1, 2 in G'. As the Schnyder wood of G' is of Type 1, they pairwise intersect in G'. Apply the coloring a.1.1 on G. As C'_0, C'_1, C'_2 do not contain vertex w, they are not modified in G. Thus, they still pairwise intersect in G. So (T2') is satisfied.

⋆ *Subcase a*.1.{0, 2}*: There are safe monochromatic cycles of colors exactly* {0, 2}.

Let C'_0, C'_2 be safe monochromatic cycles of color 0, 2 in G'. Let C'_1 be a 1-cycle in G'. As the Schnyder wood of G' is of Type 1, C'_0, C'_1, C'_2 pairwise intersect in G'. None of those intersections contains w as C'_0 and C'_2 do not contain w. By (T1), the cycle C'_1 enters w in the sector $]e_{wx}, e_{wy}[$ and leaves in the sector $]e_{wy}, e_{wx}[$. Apply the coloring a.1.1 on G. The cycle C'_1 is replaced by a new cycle $C_1 = C'_1 \setminus \{w\} \cup \{u, v\}$. The cycles C'_0, C'_1, C'_2 were intersecting outside w in G' so C'_0, C_1, C'_2 are intersecting in G. So (T2') is satisfied.

⋆ *Subcase a*.1.{1, 2}*: There are safe monochromatic cycles of colors exactly* {1, 2}.

Let C'_1, C'_2 be safe monochromatic cycles of color 1, 2 in G'. Let C'_0 be a 0-cycle in G'. The cycles C'_0, C'_1, C'_2 pairwise intersect outside w. The cycle C'_0 enters w in the sector $[e_1(w), e_{wx}[$, $[e_{wx}, e_{wx}]$, or $]e_{wx}, e_2(w)]$. Apply the coloring a.1.2 on G. Depending on which of the three sectors C'_0 enters, it is replaced by one of the three following cycles: $C_0 = C'_0 \setminus \{w\} \cup \{u, v\}$, $C_0 = C'_0 \setminus \{w\} \cup \{x, v\}$, $C_0 = C'_0 \setminus \{w\} \cup \{v\}$. In any of the three possibilities, C_0, C'_1, C'_2 are intersecting in G. So (T2') is satisfied.

⋆ *Subcase a*.1.{0, 1}*: There are safe monochromatic cycles of colors exactly* {0, 1}.

This case is completely symmetric to the case a.1.{1, 2}.

⋆ *Subcase a*.1.{2}*: There are safe monochromatic cycles of color* 2 *only.*

Let C'_2 be a safe 2-cycle in G'. Let C'_0, C'_1 be monochromatic cycles of color 0, 1 in G'.

Suppose that there exists a path Q'_0 of color 0 from y to w such that this path does not intersect C'_2. Suppose also that there exists a path Q'_1 of color 1 from y to w such that this path does not intersect C'_2. Let $C''_0 = Q'_0 \cup \{e_{wy}\}$ and $C''_1 = Q'_1 \cup \{e_{wy}\}$. By Lemma 1, C''_0, C''_1, C'_2 are not contractible. Both C''_0, C''_1 do not intersect C'_2, so by Lemma 2, they are both homotopic to C'_2. Thus, cycles C''_0, C''_1 are homotopic to each other, contradicting Lemma 15 (with $i = 2, w, y, Q'_0, Q'_1$). So we can assume that one of Q'_0 or Q'_1 as above does not exist.

Suppose that in G', there does not exist a path of color 0 from y to w such that this path does not intersect C'_2. Apply the coloring a.1.1 on G. Cycle C'_1 is replaced by $C_1 = C'_1 \setminus \{w\} \cup \{u, v\}$, and intersects C'_2. Let C_0 be a 0-cycle of G. Cycle C_0 has to contain u or v or both, otherwise it is a safe cycle of G' of color 0. In any case it intersects C_1. If C_0 contains v, then $C'_0 = C_0 \setminus \{v\} \cup \{w\}$, and so C_0 is intersecting C'_2 and (T2') is satisfied. Suppose now that C_0 does not contain v. Then C_0 contains u and y, the extremity of the edge leaving u in color 0. Let Q_0 be the part of C_0 consisting of the path from y to u. The path $Q'_0 = Q_0 \setminus \{u\} \cup \{w\}$ is from y to w. Thus, by assumption, Q'_0 intersects C'_2. So C_0 intersects C'_2 and (T2') is satisfied.

Suppose now that in G', there does not exist a path of color 1 from y to w such that this path does not intersect C'_2. Apply the coloring a.1.2 on G. Depending on which of the three sectors C'_0 enters, $[e_1(w), e_{wx}[$, $[e_{wx}, e_{wx}]$, or $]e_{wx}, e_2(w)]$, it is replaced

by one of the following three cycles: $C_0 = C'_0 \setminus \{w\} \cup \{u, v\}$, $C_0 = C'_0 \setminus \{w\} \cup \{x, v\}$, $C_0 = C'_0 \setminus \{w\} \cup \{v\}$. In any of the three possibilities, C_0 contains v and intersects C'_2. Let C_1 be a 1-cycle of G. Cycle C_1 has to contain u or v or both, otherwise it is a safe cycle of G' of color 1. Vertex u has no edge entering it in color 1, so C_1 does not contain u and thus it contains v and intersects C_0. Then C_1 contains y, the extremity of the edge leaving v in color 1. Let Q_1 be the part of C_1 consisting of the path from y to v. The path $Q'_1 = Q_1 \setminus \{v\} \cup \{w\}$ is from y to w. Thus, by assumption, Q'_1 intersects C'_2. So C_1 intersects C'_2 and (T2') is satisfied.

⋆ *Subcase a*.1.{0}*: There are safe monochromatic cycles of color* 0 *only.*

This case is completely symmetric to the case a.1.{2}.

⋆ *Subcase a*.1.{1}*: There are safe monochromatic cycles of color* 1 *only.*

Let C'_1 be a safe 1-cycle in G'. Let C'_0 and C'_2 be monochromatic cycles of color 0 and 2 in G'.

Suppose C'_0 is entering w in the sector $]e_{wx}, e_2(w)]$. Apply the coloring a.1.3 on G. The 0-cycle C'_0 is replaced by $C_0 = C'_0 \setminus \{w\} \cup \{v\}$ and thus contains v and still intersects C'_1. Depending on which of the three sectors C'_2 enters, $[e_0(w), e_{wy}[$, $[e_{wy}, e_{wy}]$, or $]e_{wy}, e_1(w)]$, it is replaced by one of the following three cycles: $C_2 = C'_2 \setminus \{w\} \cup \{v\}$, $C_2 = C'_2 \setminus \{w\} \cup \{y, v\}$, $C_2 = C'_2 \setminus \{w\} \cup \{u, v\}$. In any case, C_2 contains v and still intersects C'_1. Cycle C_0 and C_2 intersect on v. So (T2') is satisfied.

The case where C'_2 is entering w in the sector $[e_0(w), e_{wy}[$ is completely symmetric and we apply the coloring a.1.2 on G.

It remains to deal with the case where C'_0 is entering w in the sector $[e_1(w), e_{wx}]$ and C'_2 is entering w in the sector $[e_{wy}, e_1(w)]$. Suppose that there exists a path Q'_0 of color 0, from y to w, entering w in the sector $[e_1(w), e_{wx}]$, such that this path does not intersect C'_1. Suppose also that there exists a path Q'_2 of color 2, from x to w, entering w in the sector $[e_{wy}, e_1(w)]$, such that this path does not intersect C'_1. Let $C''_0 = Q'_0 \cup \{e_{wy}\}$ and $C''_2 = Q'_2 \cup \{e_{wx}\}$. By Lemma 1, C''_0, C'_1, C''_2 are not contractible. Cycles C''_0, C''_2 do not intersect C'_1, so by Lemma 2 they are homotopic to C'_1. Thus, cycles C''_0, C''_2 are homotopic to each other. Thus, by Lemma 16 (with $i = 1, w, x, y, Q'_0, Q'_2$), we have $C''_0 = (C''_2)^{-1}$, contradicting (T3') in G'. So we can assume that one of Q'_0 or Q'_2 as above does not exist. By symmetry, suppose that in G' there does not exist a path of color 0, from y to w, entering w in the sector $[e_1(w), e_{wx}]$, such that this path does not intersect C'_1. Apply the coloring a.1.3 on G. Depending on which of the two sectors C'_2 enters, $[e_{wy}, e_{wy}]$ or $]e_{wy}, e_1(w)]$, it is replaced by one of the following two cycles: $C_2 = C'_2 \setminus \{w\} \cup \{y, v\}$, $C_2 = C'_2 \setminus \{w\} \cup \{u, v\}$. In any case, C_2 still intersects C'_1. Let C_0 be a 0-cycle of G. Cycle C_0 has to contain u or v or both, otherwise it is a safe cycle of G' of color 0. Suppose C_0 does not contain u; then $C'_0 = C_0 \setminus \{v\} \cup \{w\}$ and C'_0 is not entering w in the sector $[e_1(w), e_{wx}]$, a contradiction. So C_0 contains u. Thus, C_0 contains y, the extremity of the edge leaving u in color 0, and it intersects C_2. Let Q_0 be the part of C_0 consisting of the path from y to u. The path $Q'_0 = Q_0 \setminus \{u\} \cup \{w\}$ is from y to w and entering w in the sector $[e_1(w), e_{wx}]$. Thus, by assumption, Q'_0 intersects C'_1. So C_0 intersects C'_1 and (T2') is satisfied.

⋆ *Subcase a*.1.{}*: There are no safe monochromatic cycles.*

Let C'_0, C'_1, C'_2 be monochromatic cycles of color 0, 1, 2 in G'. They all pairwise intersect on w.

Suppose first that C'_0 is entering w in the sector $]e_{wx}, e_2(w)]$. Apply the coloring a.1.3 on G. The 0-cycle C'_0 is replaced by $C_0 = C'_0 \setminus \{w\} \cup \{v\}$ and thus contains v. Depending on which of the three sectors C'_2 enters, $[e_0(w), e_{wy}[$, $[e_{wy}, e_{wy}]$, or $]e_{wy}, e_1(w)]$, it is replaced by one of the following three cycles: $C_2 = C'_2 \setminus \{w\} \cup \{v\}$, $C_2 = C'_2 \setminus \{w\} \cup \{y, v\}$, $C_2 = C'_2 \setminus \{w\} \cup \{u, v\}$. In any case, C_2 contains v. Let C_1 be a 1-cycle in G. Cycle C_1 has to contain u or v or both, otherwise it is a safe cycle of G' of color 1. Vertex u has no edge entering it in color 1, so C_1 does not contain u and thus it contains v. So C_0, C_1, C_2 all intersect on v and (T2') is satisfied.

The case where C'_2 is entering w in the sector $[e_0(w), e_{wy}[$ is completely symmetric and we apply the coloring a.1.2 on G.

It remains to deal with the case where C'_0 is entering w in the sector $[e_1(w), e_{wx}]$ and C'_2 is entering w in the sector $[e_{wy}, e_1(w)]$. Apply the coloring a.1.1 on G. Cycle C'_1 is replaced by $C_1 = C'_1 \setminus \{w\} \cup \{u, v\}$. Let C_0 be a 0-cycle in G. Cycle C_0 has to contain u or v or both, otherwise it is a safe cycle of G' of color 0. Suppose $C_0 \cap \{v, x\} = \{v\}$; then $C_0 \setminus \{v\} \cup \{w\}$ is a 0-cycle of G' entering w in the sector $]e_{wx}, e_2(w)]$, contradicting the assumption on C'_0. Suppose C_0 contains u; then C_0 contains y, the extremity of the edge leaving u in color 0. So C_0 contains $\{v, x\}$ or $\{u, y\}$. Similarly, C_2 contains $\{v, y\}$ or $\{u, x\}$. In any case, C_0, C_1, C_2 pairwise intersect. So (T2') is satisfied.

• *Case a.2: e_{wx} and e_{wy} have the same color; one is entering w, the other is leaving w.*

We can assume by symmetry that $e_{wx} = e_1(x)$ and $e_{wy} = e_1(w)$ (case a.2.0 of Fig. 21). We apply one of the colorings a.2.1 and a.2.2 of Fig. 21.

We have a case analysis corresponding to whether there are monochromatic cycles of G' that are safe.

⋆ *Subcase a.2.$\{0, 1, 2\}$: There are safe monochromatic cycles of colors* $\{0, 1, 2\}$.

Let C'_0, C'_1, C'_2 be safe monochromatic cycles of color $0, 1, 2$ in G'. They pairwise intersect in G'. Apply the coloring a.2.1 on G. C'_0, C'_1, C'_2 still pairwise intersect in G. So (T2') is satisfied.

⋆ *Subcase a.2.$\{0, 2\}$: There are safe monochromatic cycles of colors exactly* $\{0, 2\}$.

Let C'_0, C'_2 be safe monochromatic cycles of color $0, 2$ in G'. Let C'_1 be a 1-cycle in G'. Cycles C'_0, C'_2 still intersect in G. Apply the coloring a.2.1 on G. Depending on which of the three sectors C'_1 enters, $[e_2(w), e_{wx}[$, $[e_{wx}, e_{wx}]$, or $]e_{wx}, e_0(w)]$, it is replaced by one of the following three cycles: $C_1 = C'_1 \setminus \{w\} \cup \{u, y\}$, $C_1 = C'_1 \setminus \{w\} \cup \{x, v, y\}$, $C_1 = C'_1 \setminus \{w\} \cup \{v, y\}$. In any of the three possibilities, C_1 still intersects both C'_0, C'_2. So (T2') is satisfied.

⋆ *Subcase a.2.$\{1, 2\}$: There are safe monochromatic cycles of colors exactly* $\{1, 2\}$.

Let C'_1, C'_2 be safe monochromatic cycles of color $1, 2$ in G'. Let C'_0 be a 0-cycle in G'. Cycles C'_1, C'_2 still intersect in G. Apply the coloring a.2.2 on G. Depending on which of the two sectors C'_0 enters, $[e_{wy}, e_{wy}]$ or $]e_{wy}, e_2(w)]$, it is replaced by one of the following two cycles: $C_0 = C'_0 \setminus \{w\} \cup \{y, v\}$, $C_0 = C'_0 \setminus \{w\} \cup \{u, v\}$. In either of the two possibilities, C_0 still intersects both C'_1, C'_2. So (T2') is satisfied.

⋆ *Subcase a.2.$\{0, 1\}$: There are safe monochromatic cycles of colors exactly* $\{0, 1\}$.

This case is completely symmetric to the case $a.2.\{1, 2\}$.

⋆ *Subcase a.2.$\{2\}$: There are safe monochromatic cycles of color* 2 *only.*

Let C'_2 be a safe 2-cycle in G'. Let C'_0, C'_1 be monochromatic cycles of color $0, 1$ in G'.

Apply the coloring a.2.2 on G. Depending on which of the three sectors C'_1 enters, $[e_2(w), e_{wx}[$, $[e_{wx}, e_{wx}]$, or $]e_{wx}, e_0(w)]$, it is replaced by one of the following three cycles: $C_1 = C'_1 \setminus \{w\} \cup \{u, y\}$, $C_1 = C'_1 \setminus \{w\} \cup \{x, u, y\}$, $C_1 = C'_1 \setminus \{w\} \cup \{v, y\}$. Depending on which of the two sectors C'_0 enters, $[e_{wy}, e_{wy}]$ or $]e_{wy}, e_2(w)]$, it is replaced by one of the following two cycles: $C_0 = C'_0 \setminus \{w\} \cup \{y, v\}$, $C_0 = C'_0 \setminus \{w\} \cup \{u, v\}$. In any case, C_0 and C_1 intersect each other and intersect C'_2. So (T2') is satisfied.

⋆ *Subcase a.2.{0}: There are safe monochromatic cycles of color* 0 *only.*

This case is completely symmetric to the case $a.2.\{0\}$.

⋆ *Subcase a.2.{1}: There are safe monochromatic cycles of color* 1 *only.*

Let C'_1 be a safe 1-cycle in G'. Let C'_0, C'_2 be monochromatic cycles of color 0, 2 in G'. Suppose that there exists a path Q'_0 of color 0, from x to w, that does not intersect C'_1. Suppose also that there exists a path Q'_2 of color 2, from x to w, that does not intersect C'_1. Let $C''_0 = Q'_0 \cup \{e_{wx}\}$ and $C''_2 = Q'_2 \cup \{e_{wx}\}$. By Lemma 1, C''_0, C'_1, C''_2 are not contractible. Both of C''_0, C''_2 do not intersect C'_1, so by Lemma 2, they are both homotopic to C'_1. Thus, cycles C''_0, C''_2 are homotopic to each other, contradicting Lemma 15 (with $i = 1, w, x, Q'_0, Q'_2$). So we can assume that one of Q'_0 or Q'_2 as above does not exist.

By symmetry, suppose that in G' there does not exist a path of color 0, from x to w, that does not intersect C'_1. Apply the coloring a.2.1 on G. Depending on which of the two sectors C'_2 enters, $[e_1(w), e_{wy}[$, $[e_{wy}, e_{wy}]$, it is replaced by one of the following two cycles: $C_2 = C'_2 \setminus \{w\} \cup \{v, u\}$, $C_2 = C'_2 \setminus \{w\} \cup \{y, u\}$. In either of the two possibilities C_2 intersects C'_1. Let C_0 be a 0-cycle of G. Cycle C_0 has to contain u or v or both, otherwise it is a safe cycle of G' of color 0. Vertex v has no edge entering it in color 0, so C_0 does not contain v and so it contains u and x, the extremity of the edge leaving u in color 0. Thus, C_0 intersects C_2. Let Q_0 be the part of C_0 consisting of the path from x to u. The path $Q'_0 = Q_0 \setminus \{u\} \cup \{w\}$ of G' is from x to w, and thus by assumption Q'_0 intersects C'_1. So C_0 intersects C'_1 and (T2') is satisfied.

⋆ *Subcase a.2.{}: There are no safe monochromatic cycles.*

Let C'_0, C'_1, C'_2 be monochromatic cycles of color 0, 1, 2 in G'.

Suppose C'_1 is entering w in the sector $[e_2(w), e_{wx}]$. Apply the coloring a.2.1 on G. Cycle C'_1 is replaced by $C_1 = C'_1 \setminus \{w\} \cup \{u, y\}$ or $C_1 = C'_1 \setminus \{w\} \cup \{x, v, y\}$. Cycle C'_0 is replaced by $C_0 = C'_0 \setminus \{w\} \cup \{u, x\}$ or $C_0 = C'_0 \setminus \{w\} \cup \{y, u, x\}$. Cycle C'_2 is replaced by $C_2 = C'_2 \setminus \{w\} \cup \{v, u\}$ or $C_2 = C'_2 \setminus \{w\} \cup \{y, u\}$. So C_0, C_1, C_2 all intersect each other and (T2') is satisfied.

The case where C'_1 is entering w in the sector $[e_{wx}, e_0(w)]$ is completely symmetric, and we apply the coloring a.2.2 on G.

• *Cases a.3, a.4, a.5:*

The proof is simpler for the remaining cases (cases a.3.0, a.4.0, a.5.0 on Fig. 21). For each situation, there is only one way to extend the coloring to G in order to preserve (T1') and this coloring also preserves (T2'). Indeed, in each coloring of G, for cases a.3.1, a.4.1, a.5.1 on Fig. 21, one can check that every non-safe monochromatic cycle C' is replaced by a cycle C with $C' \setminus \{w\} \cup \{u\} \subseteq C$. Thus, all non-safe cycles intersect on u and a non-safe cycle of color i intersects all safe cycles of colors $i - 1$ and $i + 1$. So (T2') is always satisfied.

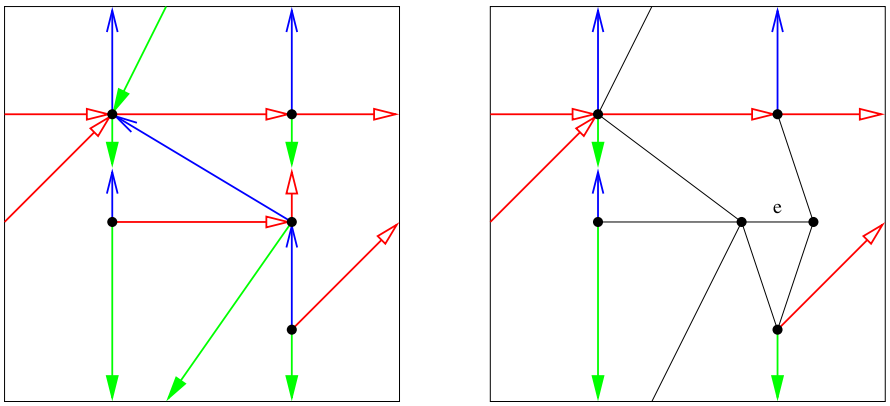

Fig. 26 (**a**) The graph obtained by contracting the edge e of the graph (**b**). It is not possible to color and orient the black edges of (**b**) to obtain a Schnyder wood

It remains to analyze the situation for the decontraction cases (b) and (c). The colorings that are needed are represented on Figs. 22 and 23. The proofs are similar to those for case (a) and we omit them. □

Note that we are not able to prove a lemma analogous to Lemma 14 for Type 2 Schnyder woods. In the example of Fig. 26, it is not possible to decontract the graph G' (Fig. 26(a)) and extend its Schnyder wood to G (Fig. 26(b)) without modifying the edges that are not incident to the contracted edge e. Indeed, if we keep the edges non-incident to e unchanged, there are only two possible ways to extend the coloring in order to preserve (T1), but none of them fulfills (T2).

9 Existence for Essentially 3-Connected Toroidal Maps

We are given a map G embedded on a surface. The *angle map* [22] of G is a map $A(G)$ on this surface whose vertices are the vertices of G plus the vertices of G^* (i.e., the faces of G), and whose edges are the angles of G, each angle being incident with the corresponding vertex and face of G. Note that if G contains no homotopic multiple edges, then every face of G has degree at least three in $A(G)$.

Mohar and Rosenstiehl [23] proved that a map G is essentially 2-connected if and only if the angle map A of G has no pair of (multiple) edges bounding a disk (i.e., no walk of length 2 bounding a disk). As every face in an angle map is a quadrangle, such a disk contains some vertices of G. The following claim naturally extends this characterization to essentially 3-connected toroidal maps.

Lemma 17 *A toroidal map G is essentially 3-connected if and only if the angle map $A(G)$ has no walk of length at most 4 bounding a disk which is not a face.*

Proof In G^∞ any minimal separator of size 1 or 2, $S = \{v_1\}$ or $S = \{v_1, v_2\}$, corresponds to a separating cycle of length 2 or 4 in $A(G^\infty)$, $C = (v_1, f_1)$ or $C = (v_1, f_1, v_2, f_2)$, i.e., a cycle of length at most 4 bounding a disk D which is not a face.

($\Longrightarrow$) Any walk in $A(G)$ of length at most 4 bounding a disk which is not a face lifts to a cycle of length at most 4 bounding a disk which is not a face in $A(G^\infty)$. Thus, such a walk implies the existence of a small separator in G^∞, contradicting its 3-connectedness.

($\Longleftarrow$) According to [23], if G is essentially 2-connected, $A(G)$ has no walk of length 2 bounding a disk. Let us now show that if G is essentially 2-connected but not essentially 3-connected, $A(G)$ has a walk of length 4 bounding a disk which is not a face.

If G is essentially 2-connected but not essentially 3-connected, then $A(G^\infty)$ has a cycle C of length 4 bounding a disk which is not a face, and this cycle corresponds to a contractible walk W of length 4 in $A(G)$. Since W is contractible, it contains a subwalk bounding a disk. $A(G)$ being bipartite, this subwalk has even length, and since $A(G)$ is essentially 2-connected, it has no such walk of length 2. Thus, W bounds a disk. Finally, this disk is not a single face, since otherwise C would bound a single face in $A(G^\infty)$. □

A non-loop edge e of an essentially 3-connected toroidal map is *contractible* if the contraction of e keeps the map essentially 3-connected. We have the following lemma.

Lemma 18 *An essentially* 3*-connected toroidal map that is not reduced to a single vertex has a contractible edge.*

Proof Let G be an essentially 3-connected toroidal map with at least 2 vertices. Note that for any non-loop e, the map $A(G/e)$ has no walk of length 2 bounding a disk which is not a face; otherwise, $A(G)$ contains a walk of length at most 4 bounding a disk which is not a face and thus, by Lemma 17, G is not essentially 3-connected.

Suppose by contradiction that contracting any non-loop edge e of G yields a non-essentially 3-connected map G/e. By Lemma 17, it means that the angle map $A(G)$ has no walk of length at most 4 bounding a disk which is not a face. For any non-loop e, let $W_4(e)$ be the 4-walk of $A(G/e)$ bounding a disk, which is maximal in terms of the faces it contains. Among all the non-loop edges, let e be the one such that the number of faces in $W_4(e)$ is minimum. Let $W_4(e) = (v_1, f_1, v_2, f_2)$ and assume that the endpoints of e, say a and b, are contracted into v_2 (see Fig. 27(a)). Note that, by maximality of $W_4(e)$, v_1 and v_2 do not have any common neighbor f out of $W_4(e)$, such that (v_1, f, v_2, f_1) bounds a disk.

Assume one of f_1 or f_2 has a neighbor inside $W_4(e)$. By symmetry, assume v_3 is a vertex inside $W_4(e)$ such that there is a face $F = (v_1, f_1, v_3, f_w)$ in $A(G/e)$, with eventually $f_w = f_2$. Consider now the contraction of the edge v_1v_3. Let $P(v_1, v_3) = (v_1, f_x, v_y, f_z, v_3)$ be the path from v_1 to v_3 corresponding to $W_4(v_1v_3)$ and $P(a, b) = (a, f_2, v_1, f_1, b)$ the path corresponding to $W_4(e)$. Suppose that $f_z = f_2$; then (v_1, f_2, v_3, f_w) bounds a face by Lemma 17 and f_w has degree two in $A(G)$, a contradiction. So $f_z \neq f_2$.

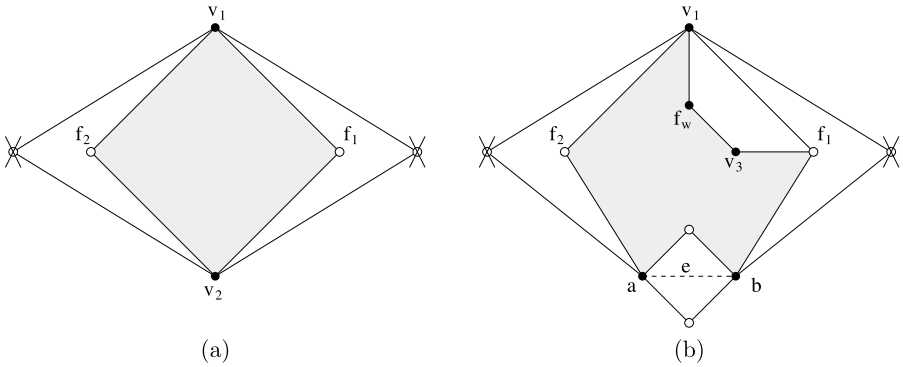

Fig. 27 Notation of the proof of Lemma 18

Fig. 28 Notation of the proof of Lemma 18

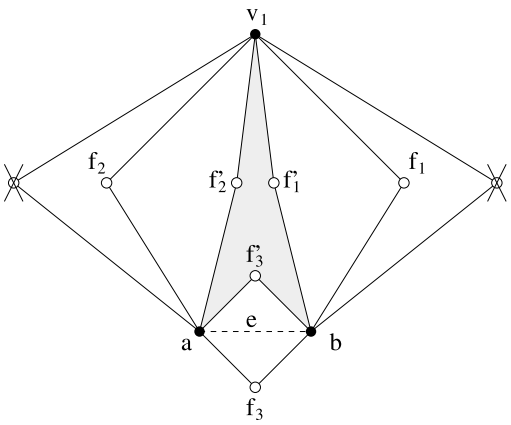

Suppose that all the faces of $W_4(v_1v_3)$ are in $W_4(e)$. Then with F, $W_4(e)$ contains more faces than $W_4(v_1v_3)$, a contradiction to the choice of e. So in $A(G)$, $P(v_1, v_3)$ must cross the path $P(a, b)$. Then v_y or f_z must intersect $P(a, b)$. Suppose $f_z \neq f_1$. Then $v_y = a$ or b. In this case, (v_1, f_x, v_2, f_1) bounds a disk, a contradiction. Thus, $f_z = f_1$ and the cycle (v_1, f_x, v_y, f_1) bounds a face by Lemma 17. This implies that $W_4(v_1v_3)$ bounds a face, a contradiction.

Assume now that neither f_1 nor f_2 has a neighbor inside $W_4(e)$. Let f_1', f_2', f_3, and f_3' be vertices of $A(G)$ such that (v_1, f_1, b, f_1'), (v_1, f_2, a, f_2'), and (a, f_3, b, f_3') are faces (see Fig. 28). Suppose $f_1' = f_2' = f_3'$. Then in $A(G/e)$, the face f_1' is deleted (of the two homotopic multiple edges between v_1, v_2 that are created, only one is kept in G/e). Then $W_4(e)$ bounds a face, a contradiction. Thus, there exists some i such that $f_i' \neq f_{i+1}'$. Assume that $i = 1$ (resp. $i = 2$ or 3), and let v_3 and f'' be such that there is a face (v_1, f_1', v_3, f'') in $A(G)$ (resp. (a, f_2', v_3, f'') or (b, f_3', v_3, f'')). As above, considering the contraction of the edge v_1v_3 (resp. av_3 or bv_3) yields a contradiction. □

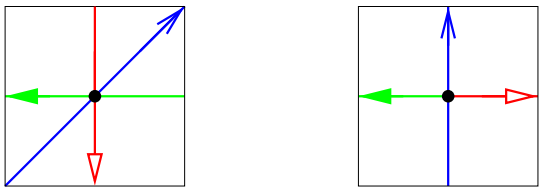

(a) The 3-loops (b) The 2-loops

Fig. 29 The two essentially 3-connected toroidal maps on one vertex

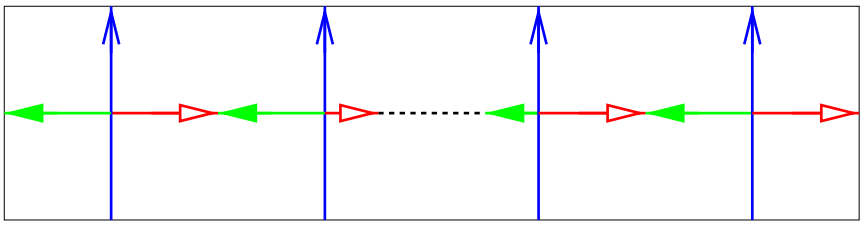

Fig. 30 The family of basic toroidal maps, having only Schnyder woods of Type 2

Fig. 31 The brick, an essentially 3-connected toroidal map with two vertices

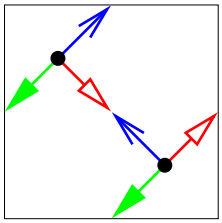

Lemma 18 shows that an essentially 3-connected toroidal map can be contracted step by step by keeping it essentially 3-connected until a map with just one vertex is obtained. The two essentially 3-connected toroidal maps on one vertex are represented on Fig. 29 with a Schnyder wood. The graph of Fig. 29(a), the *3-loops*, admits a Schnyder wood of Type 1, and the graph of Fig. 29(b), the *2-loops*, admits a Schnyder wood of Type 2.

It would be convenient if one could contract any essentially 3-connected toroidal map to obtain one of the two graphs of Fig. 29 and then decontract the graph to obtain a Schnyder wood of the original graph. Unfortunately, for Type 2 Schnyder woods we are not able to prove that property (T2) can be preserved during the decontraction process (see Sect. 8). Fortunately, most essentially 3-connected toroidal maps admit Schnyder woods of Type 1. A toroidal map is *basic* if it consists of a non-contractible cycle on n vertices, $n \geq 1$, plus n homotopic loops (see Fig. 30). We prove in this section that non-basic essentially 3-connected toroidal maps admit Schnyder woods of Type 1. For this purpose, instead of contracting these maps to one of the two graphs of Fig. 29, we contract them to the graph of Fig. 29(a) or to the graph of Fig. 31, *the brick*. (One can draw the universal cover of the brick to understand its name.)

Lemma 19 *A non-basic essentially* 3*-connected toroidal map can be contracted to the* 3*-loops* (*Fig.* 29(*a*)) *or to the brick* (*Fig.* 31).

Proof Let us prove the lemma by induction on the number of edges of the map. As the 3-loop and the brick are the only non-basic essentially 3-connected toroidal maps with at most 3 edges, the lemma holds for the maps with at most 3 edges. Consider now a non-basic essentially 3-connected toroidal map G with at least 4 edges. As G has at least 2 vertices, it has at least one contractible edge by Lemma 18. If G has a contractible edge e whose contraction yields a non-basic map G', then by the induction hypothesis on G' we are done. Let us prove that such an edge always exists. We assume, by contradiction, that the contraction of any contractible edge e yields a basic map G'. Let us denote v_i, with $1 \leq i \leq n$, the vertices of G' in such a way that $(v_1, v_2, \ldots, v_n)$ is a cycle of G'. We can assume that v_1 is the vertex resulting from the contraction of e. Let u and v be the endpoints of e in G.

Suppose first that u or v is incident to a loop in G. By symmetry, we can assume that v is incident to a loop and that u is in the cylinder between the loops around v and v_n (note that if $n = 1$ then $v_n = v$), and note that u is the only vertex here. Since G is non-basic and u has at least 3 incident edges, 2 of them go to the same vertex but are non-homotopic. Since after the contraction of e there is only one edge left in the cylinder, we can deduce that u has at least 2 edges in common with v. On the other side since G is essentially 3-connected u has an edge e' with v_n. This edge e' is contractible, since its contraction yields a graph containing the basic graph on n vertices. But since this graph has 2 non-homotopic edges linking (uv_n) and v, it is non-basic. So G has a contractible edge whose contraction produces a non-basic graph, contradicting our assumption.

Suppose now that u and v do not have an incident loop; we thus have that G contains a cycle C of length 2 containing e. Let e' be the other edge of C. Since G is essentially 3-connected, both u and v have at least degree three, and at least one of them has an incident edge on the left (resp. right) of C. If $n = 1$, since G has at least 4 edges, there are 2 (non-homotopic) edges, say f_1 and f_2 between u and v and distinct from e and e'. In this case, since the cycles (e, f_1) and (e, f_2) were not homotopic, the edges f_1 and f_2 remain non-homotopic in G'. So in this case G has one vertex and 3 edges, and it is thus non-basic. Assume now that $n \geq 2$. In this case, u and v are contained in a cylinder bordered by the loops at v_2 and at v_n (with eventually $n = 2$). In this case, we can assume that u has at least one incident edge f_1 on the left of C to v_n, and that v has at least one incident edge f_2 on the right of C to v_2. In this case, one can contract f_1 and note that the obtained graph, which contains at least 3 non-homotopic edges around v (e, e' and f_2), is essentially 3-connected and non-basic. So G has a contractible edge whose contraction produces a non-basic graph, contradicting our assumption. □

Lemma 20 *A basic toroidal map admits only Schnyder woods of Type* 2.

Proof A basic toroidal map admits Schnyder woods of Type 2, as shown by Fig. 30. Suppose that a basic toroidal map G on n vertices admits a Schnyder wood of Type 1. Consider one of the vertical loops e and suppose by symmetry that it is oriented

upward in color 1. In a Schnyder wood of Type 1, all the monochromatic cycles of different colors are not homotopic; thus, all the loops homotopic to e are also oriented upward in color 1 and they are not bi-oriented. There remains just a cycle on n vertices for edges of color 0 and 2. Thus, the Schnyder wood is the one of Fig. 30, a contradiction. □

We are now able to prove the following theorem.

Theorem 10 *A toroidal graph admits a Schnyder wood of Type* 1 *if and only if it is an essentially* 3*-connected non-basic toroidal map*.

Proof ($\Longrightarrow$) If G is a toroidal graph given with a Schnyder wood of Type 1, then, by Lemma 9, G is essentially 3-connected and by Lemma 20, G is not basic.

($\Longleftarrow$) Let G be a non-basic essentially 3-connected toroidal map. By Lemma 19, G can be contracted to the 3-loops or to the brick. Both of these graphs admit Schnyder woods of Type 1 (see Figs. 29(a) and 31). So by Lemma 14 applied successively, G admits a Schnyder wood of Type 1. □

Theorem 10 and Lemma 20 imply Theorem 1. One related open problem is to characterize which essentially 3-connected toroidal maps have Schnyder woods of Type 2.

Here is a remark about how to compute a Schnyder wood for an essentially 3-connected toroidal triangulation. Instead of looking carefully at the technical proof of Lemma 14 to determine which coloring of the decontracted graph must be chosen among the possible choices, one can try the possible cases $\alpha.k.\ell$, $\ell \geq 1$, and then check which obtained coloring is a Schnyder wood. To do so, one just has to check if (T2') is satisfied. Checking that (T2') is satisfied can be done by the following method: start from any vertex v, walk along $P_0(v)$, $P_1(v)$, $P_2(v)$, and mark the three monochromatic cycles C_0, C_1, C_2 reached by the three paths P_i. Property (T2') is then satisfied if the cycles C_0, C_1, C_2 pairwise intersect.

The existence of Schnyder woods for toroidal triangulations implies the following theorem.

Theorem 11 *A toroidal triangulation contains three non-contractible and non-homotopic cycles that are pairwise edge-disjoint*.

Proof One just has to apply Theorem 10 to obtain a Schnyder wood of Type 1 and then, for each color i, choose arbitrarily an i-cycle. These cycles are edge-disjoint as, by Euler's formula, there are no bi-oriented edges in Schnyder woods of toroidal triangulations. □

The conclusion of Theorem 11 is weaker than the one of Theorem 8, but it is not restricted to simple toroidal triangulations. Recall that Theorem 8 is not true for general toroidal triangulations, as shown by the graph of Fig. 17.

A non-empty family $\mathcal{R}$ of linear orders on the vertex set V of a simple graph G is called a *realizer* of G if for every edge e, and every vertex x not in e, there is some

order $<_i \in \mathcal{R}$ so that $y <_i x$ for every $y \in e$. The *dimension* [10] of G is defined as the least positive integer t for which G has a realizer of cardinality t. Realizers are usually used on finite graphs, but here we allow G to be an infinite simple graph.

Schnyder woods were originally defined by Schnyder [26] to prove that a finite planar graph G has dimension at most three. A consequence of Theorem 1 is an analogous result for the universal cover of a toroidal graph.

Theorem 12 *The universal cover of a toroidal graph has dimension at most three.*

Proof By eventually adding edges to G, we may assume that G is a toroidal triangulation. By Theorem 1, it admits a Schnyder wood. For $i \in \{0, 1, 2\}$, let $<_i$ be the order induced by the inclusion of the regions R_i in G^∞. That is, $u <_i v$ if and only if $R_i(u) \subsetneq R_i(v)$. Let $<'_i$ be any linear extension of $<_i$ and consider $\mathcal{R} = \{<'_0, <'_1, <'_2\}$. Let e be any edge of G^∞ and v be any vertex of G^∞ not in e. Edge e is in a region $R_i(v)$ for some i; thus, $R_i(u) \subseteq R_i(v)$ for every $u \in e$ by Lemma 8(i). As there are no edges oriented in two directions in a Schnyder wood of a toroidal triangulation, we have $R_i(u) \neq R_i(v)$ and so $u <_i v$. Thus $\mathcal{R}$ is a realizer of G^∞. □

10 Orthogonal Surfaces

Given two points $u = (u_0, u_1, u_2)$ and $v = (v_0, v_1, v_2)$ in $\mathbb{R}^3$, we note $u \vee v = (\max(u_i, v_i))_{i=0,1,2}$ and $u \wedge v = (\min(u_i, v_i))_{i=0,1,2}$. We define an order $\geq$ among the points in $\mathbb{R}^3$, in such a way that $u \geq v$ if $u_i \geq v_i$ for $i = 0, 1, 2$.

Given a set $\mathcal{V}$ of pairwise incomparable elements in $\mathbb{R}^3$, we define the set of vertices that dominates $\mathcal{V}$ as $\mathcal{D}_\mathcal{V} = \{u \in \mathbb{R}^3 \mid \exists v \in \mathcal{V}$ such that $u \geq v\}$. The *orthogonal surface* $\mathcal{S}_\mathcal{V}$ generated by $\mathcal{V}$ is the boundary of $\mathcal{D}_\mathcal{V}$. (Note that orthogonal surfaces are well defined even when $\mathcal{V}$ is an infinite set.) If $u, v \in \mathcal{V}$ and $u \vee v \in \mathcal{S}_\mathcal{V}$, then $\mathcal{S}_\mathcal{V}$ contains the union of the two line segments joining u and v to $u \vee v$. Such arcs are called *elbow geodesics*. The *orthogonal arc* of $v \in \mathcal{V}$ in the direction of the standard basis vector e_i is the intersection of the ray $v + \lambda e_i$ with $\mathcal{S}_\mathcal{V}$.

Let G be a planar map. A *geodesic embedding* of G on the orthogonal surface $\mathcal{S}_\mathcal{V}$ is a drawing of G on $\mathcal{S}_\mathcal{V}$ satisfying the following:

(D1) There is a bijection between the vertices of G and $\mathcal{V}$.
(D2) Every edge of G is an elbow geodesic.
(D3) Every orthogonal arc in $\mathcal{S}_\mathcal{V}$ is part of an edge of G.
(D4) There are no crossing edges in the embedding of G on $\mathcal{S}_\mathcal{V}$.

Miller [20] (see also [8, 11]) proved that a geodesic embedding of a planar map G on an orthogonal surface $\mathcal{S}_\mathcal{V}$ induces a Schnyder wood of G. The edges of G are colored with the direction of the orthogonal arc contained in the edge. An orthogonal arc intersecting the ray $v + \lambda e_i$ corresponds to the edge leaving v in color i. Edges represented by two orthogonal arcs correspond to edges oriented in two directions.

Conversely, it has been proved that a Schnyder wood of a planar map G can be used to obtain a geodesic embedding of G. Let G be a planar map given with a Schnyder wood. The method is the following (see [8] for more details): For every

vertex v, one can divide G into the three regions bounded by the three monochromatic paths going out from v. The *region vector* associated to v is the vector obtained by counting the number of faces in each of these three regions. The mapping of each vertex on its region vector gives the geodesic embedding. (Note that in this approach, the vertices are all mapped on the same plane, as the sum of the coordinates of each region vector is equal to the total number of inner faces of the map.)

Our goal is to generalize geodesic embedding to the torus. More precisely, we want to represent the universal cover of a toroidal map on an infinite and periodic orthogonal surface.

Let G be a toroidal map. Consider any flat torus representation of G in a parallelogram P. The graph G^∞ is obtained by replicating P to tile the plane. Given any of these parallelograms Q, let Q^{top} (resp. Q^{right}) be the copy of P just above (resp. on the right of) Q. Given a vertex v in Q, we denote v^{top} (resp. v^{right}) its copies in Q^{top} (resp. Q^{right}).

A mapping of the vertices of G^∞ in $\mathbb{R}^d$, $d \in \{2, 3\}$, is *periodic* with respect to vectors S and S' of $\mathbb{R}^d$, if there exists a flat torus representation P of G such that for any vertex v of G^∞, vertex v^{top} is mapped on $v + S$ and v^{right} is mapped on $v + S'$. A *geodesic embedding* of a toroidal map G is a geodesic embedding of G^∞ on $\mathcal{S}_{\mathcal{V}^\infty}$, where $\mathcal{V}^\infty$ is a periodic mapping of G^∞ with respect to two non-collinear vectors (see example of Fig. 5).

As in the plane, Schnyder woods can be used to obtain geodesic embeddings of toroidal maps. For that purpose, we need to generalize the region vector method. The idea is to use the regions $R_i(v)$ to compute the coordinates of the vertex v of G^∞. The problem is that, contrarily to the planar case, these regions are unbounded and contain an infinite number of faces. The method is thus generalized by the following.

Let G be a toroidal map, given with a Schnyder wood and a flat torus representation in a parallelogram P.

Recall that $\mathcal{C}_i = \{C_i^0, \ldots, C_i^{k_i-1}\}$ denotes the set of i-cycles of G such that there is no i-cycle in the region $R(C_i^j, C_i^{j+1})$. Recall that $\mathcal{L}_i^j$ denotes the set of i-lines of G^∞ corresponding to C_i^j. The *positive side* of an i-line is defined as the right side while "walking" along the directed path by following the orientation of the edges colored i.

Lemma 21 *For any vertex v, the two monochromatic lines $L_{i-1}(v)$ and $L_{i+1}(v)$ intersect. Moreover, if the Schnyder wood is of Type 2.i, then $L_{i+1}(v) = (L_{i-1}(v))^{-1}$ and v is situated on the right of $L_{i+1}(v)$.*

Proof Let j, j' be such that $L_{i-1}(v) \in \mathcal{L}_{i-1}^j$ and $L_{i+1}(v) \in \mathcal{L}_{i+1}^{j'}$. If the Schnyder wood is of Type 1 or Type 2.j with $j \neq i$, then the two cycles C_{i-1}^j and $C_{i+1}^{j'}$ are not homotopic, and so the two lines $L_{i-1}(v)$ and $L_{i+1}(v)$ intersect.

If the Schnyder wood is of Type 2.i, we consider the case where $v \in L_{i-1}(v)$, and the case where v does not belong to either $L_{i-1}(v)$ or $L_{i+1}(v)$. Then v lies between two consecutive $(i+1)$-lines (which are also $(i-1)$-lines). Let us denote those two lines L_{i+1} and L'_{i+1}, such that L'_{i+1} is situated on the right of L_{i+1} and $v \notin L'_{i+1}$. By property (T1), $P_{i+1}(v)$ and $P_{i-1}(v)$ cannot reach L'_{i+1}. Thus, $L_{i+1} = L_{i+1}(v) = (L_{i-1}(v))^{-1}$. □

The *size* of the region $R(C_i^j, C_i^{j+1})$ of G, denoted $f_i^j = |R(C_i^j, C_i^{j+1})|$, is equal to the number of faces in $R(C_i^j, C_i^{j+1})$. Remark that for each color, we have that $\sum_{j=0}^{k_i-1} f_i^j$ equals the total number of faces f of G. If L and L' are consecutive i-lines of G^∞ with $L \in \mathcal{L}_i^j$ and $L' \in \mathcal{L}_i^{j+1}$, then the *size* of the (unbounded) region $R(L, L')$, denoted $|R(L, L')|$, is equal to f_i^j. If L and L' are any i-lines, the *size* of the (unbounded) region $R(L, L')$, denoted $|R(L, L')|$, is equal to the sum of the size of all the regions delimited by consecutive i-lines inside $R(L, L')$. For each color i, choose arbitrarily an i-line L_i^* in $\mathcal{L}_i^0$ that is used as an origin for i-lines. Given an i-line L, we define the value $f_i(L)$ of L as follows: $f_i(L) = |R(L, L_i^*)|$ if L is on the positive side of L_i^* and $f_i(L) = -|R(L, L_i^*)|$ otherwise.

Consider two vertices u, v such that $L_{i-1}(u) = L_{i-1}(v)$ and $L_{i+1}(u) = L_{i+1}(v)$. Even if the two regions $R_i(u)$ and $R_i(v)$ are unbounded, their *difference* is bounded. Let $d_i(u, v)$ be the number of faces in $R_i(u) \setminus R_i(v)$ minus the number of faces in $R_i(v) \setminus R_i(u)$. For any vertex, by Lemma 21, there exists $z_i(v)$, a vertex on the intersection of the two lines $L_{i-1}(v)$ and $L_{i+1}(v)$. Let N be a constant $\geq n$ (in this section we can have $N = n$, but in Sect. 12 we need to choose N bigger). We are now able to define the region vector of a vertex of G^∞, that is, a mapping of this vertex in $\mathbb{R}^3$.

Definition 4 (Region vector) The i-th coordinate of the *region vector* of a vertex v of G^∞ is equal to $v_i = d_i(v, z_i(v)) + N \times (f_{i+1}(L_{i+1}(v)) - f_{i-1}(L_{i-1}(v)))$ (see Fig. 32).

For each color i, let c_i (resp. c'_i), be the algebraic number of times an i-cycle is traversing the vertical (resp. horizontal) side of the parallelogram P (which was the parallelogram containing the flat torus representation of G) from right to left (resp. from bottom to top). This number increases by one each time a monochromatic cycle traverses the side in the given direction and decreases by one when it traverses in the other direction. Let S and S' be the two vectors of $\mathbb{R}^3$ with coordinates $S_i = N(c_{i+1} - c_{i-1})f$ and $S'_i = N(c'_{i+1} - c'_{i-1})f$. Note that $S_0 + S_1 + S_2 = 0$ and $S'_0 + S'_1 + S'_2 = 0$

We use the example of the toroidal map G of Fig. 2 to illustrate the region vector method. This toroidal map has $n = 3$ vertices, $f = 4$ faces, and $e = 7$ edges. Let $N = n = 3$. There are two edges that are oriented in two directions. The Schnyder wood is of Type 1, with two 1-cycles. We choose as origin the three bold monochromatic lines of Fig. 33. We give them value 0 and compute the other values $f_i(L)$ as explained formally at the beginning of this section; i.e., we compute the "number" of faces between L and the origin L^* and put a minus if we are on the left of L^*. (This corresponds to values indicated on the border of Fig. 33, which are values $0, -4, -8, -12$ for lines of color 0, values $-4, -2, 0, 2, 4$ for lines of color 1, and values $0, 4$ for lines of color 2.) Then we compute the region vector of the points according to Definition 4. For example, the point v of Fig. 33 has the following values (the three points $z_i(v)$ are represented on the figure): $v_0 = d_0(v, z_0(v)) + N \times (f_1(L_1(v)) - f_2(L_2(v))) = 0 + 3(0 - 0) = 0$, $v_1 = d_1(v, z_1(v)) + N \times (f_2(L_2(v)) - f_0(L_0(v))) = 0 + 3(0 - (-4)) = 12$, $v_2 = d_2(v, z_2(v)) + N \times (f_0(L_0(v)) - f_1(L_1(v))) = 1 + 3(-4 - 0) = -11$. We compute

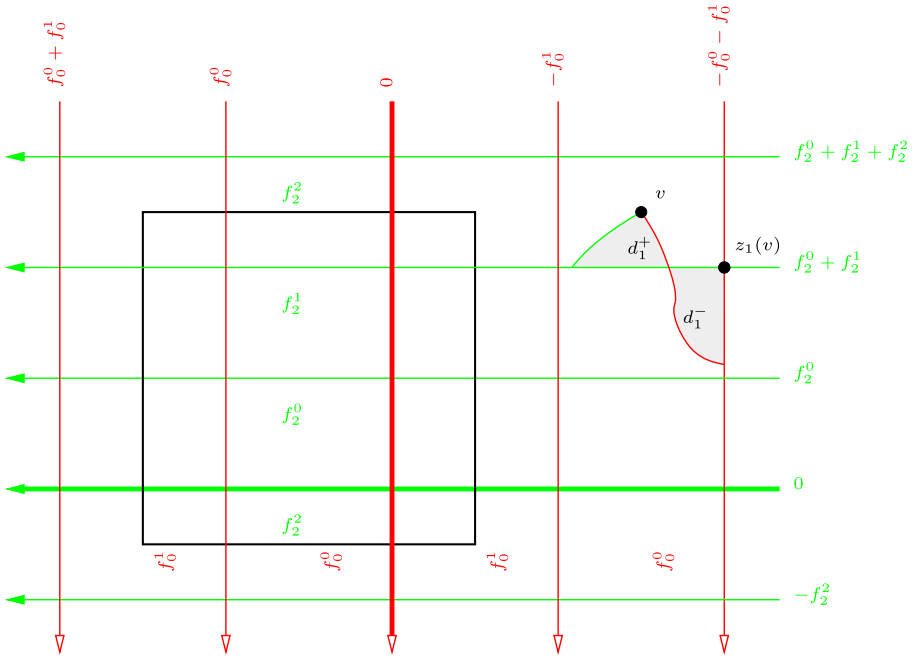

Fig. 32 Coordinate 1 of vertex v is equal to the number of faces in the region d_1^+, minus the number of faces in the region d_1^-, plus N times $(f_2^0 + f_2^1) - (-f_0^0 - f_0^1)$

similarly the region vectors of all the vertices that are in the black box representing one copy of the graph and let $\mathcal{V} = \{(0,0,0), (0,12,-11), (6,12,-18)\}$ be the set of these vectors. Then we compute the c_i's and c_i''s by algebraically counting the number of times the monochromatic cycles cross the sides of the black box. A monochromatic cycle of color 0 goes -1 time from right to left and 2 times from bottom to top. So $c_0 = -1$ and $c_0' = -2$. Similarly, $c_1 = 0$, $c_1' = 1$, $c_2 = 1$, $c_2' = 0$. Then we compute $S_i = N(c_{i+1} - c_{i-1})f$ and $S_i' = N(c_{i+1}' - c_{i-1}')f$ and obtain $S = (-12, 24, -12)$, $S' = (12, 24, -36)$. Then the region vectors of the vertices of G^∞ are $\{u \in \mathbb{R}^3 \mid \exists v \in \mathcal{V}, k_1, k_2 \in \mathbb{Z} \text{ such that } u = v + kS + k'S\}$. In this example, the points are not coplanar; they lie on the two different planes of equations $x + y + z = 0$ and $x + y + z = 1$. The geodesic embedding that is obtained by mapping each vertex to its region vector is the geodesic embedding of Fig. 5. The black parallelogram has as sides the vectors S, S' and represents a basic tile.

Lemma 22 *The sum of the coordinates of a vertex v equals the number of faces in the bounded region delimited by the lines $L_0(v)$, $L_1(v)$, and $L_2(v)$ if the Schnyder wood is of Type* 1, *and this sum equals zero if the Schnyder wood is of Type* 2.

Proof We have $v_0 + v_1 + v_2 = d_0(v, z_0(v)) + d_1(v, z_1(v)) + d_2(v, z_2(v)) = \sum_i (|R_i(v) \setminus R_i(z_i(v))| - |R_i(z_i(v)) \setminus R_i(v)|)$. We use the characteristic function $\mathbf{1}$ to deal with infinite regions. We note $\mathbf{1}(R)$, the function defined on the faces of G^∞ that has value 1 on each face of region R and 0 elsewhere. Given a function

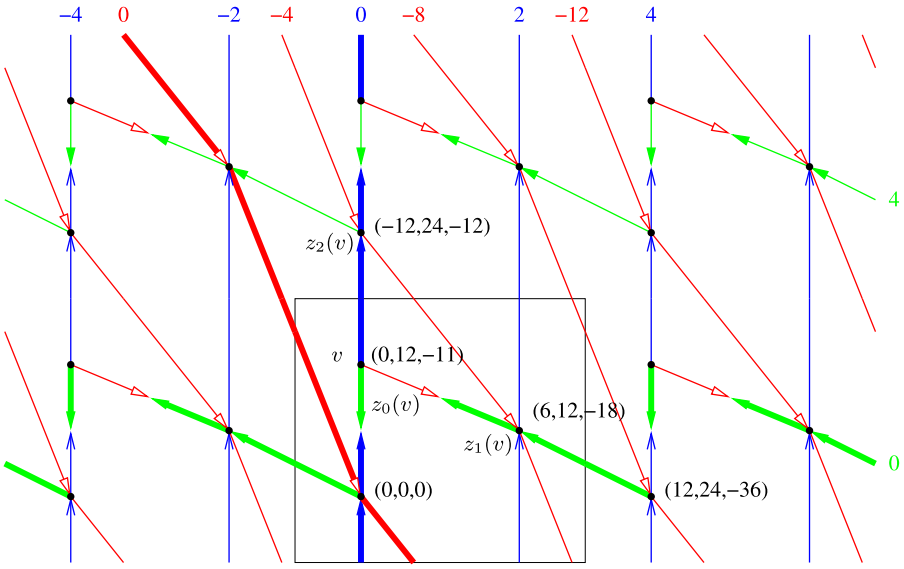

Fig. 33 Computation of the region vectors for the Schnyder wood of Fig. 2

$g : F(G^\infty) \longrightarrow \mathbb{Z}$, we note that $|g| = \sum_{F \in F(G^\infty)} g(F)$ (when the sum is finite). Thus, $\sum_i v_i = \sum_i (|\mathbf{1}(R_i(v) \setminus R_i(z_i(v)))| - |\mathbf{1}(R_i(z_i(v)) \setminus R_i(v))|) = |\sum_i (\mathbf{1}(R_i(v) \setminus R_i(z_i(v))) - \mathbf{1}(R_i(z_i(v)) \setminus R_i(v)))|$. Now we compute $g = \sum_i (\mathbf{1}(R_i(v) \setminus R_i(z_i(v))) - \mathbf{1}(R_i(z_i(v)) \setminus R_i(v)))$. We have:

$$g = \sum_i \big(\mathbf{1}\big(R_i(v) \setminus R_i\big(z_i(v)\big)\big) + \mathbf{1}\big(R_i(v) \cap R_i\big(z_i(v)\big)\big) - \mathbf{1}\big(R_i\big(z_i(v)\big) \setminus R_i(v)\big) - \mathbf{1}\big(R_i(v) \cap R_i\big(z_i(v)\big)\big)\big)$$

As $R_i(v) \setminus R_i(z_i(v))$ and $R_i(z_i(v)) \setminus R_i(v)$ are disjoint from $R_i(v) \cap R_i(z_i(v))$, we have:

$$g = \sum_i \big(\mathbf{1}\big(R_i(v)\big) - \mathbf{1}\big(R_i\big(z_i(v)\big)\big)\big) = \sum_i \mathbf{1}\big(R_i(v)\big) - \sum_i \mathbf{1}\big(R_i\big(z_i(v)\big)\big)$$

Because the interior of the three regions $R_i(v)$, for $i = 0, 1, 2$, is disjoint and spans the whole plane $\mathbb{P}$ (by definition), we have $\sum_i \mathbf{1}(R_i(v)) = \mathbf{1}(\cup_i (R_i(v))) = \mathbf{1}(\mathbb{P})$. Moreover, the regions $R_i(z_i(v))$, for $i = 0, 1, 2$, are also disjoint and $\sum_i \mathbf{1}(R_i(z_i(v))) = \mathbf{1}(\cup_i (R_i(z_i(v)))) = \mathbf{1}(\mathbb{P} \setminus T)$, where T is the bounded region delimited by the lines $L_0(v)$, $L_1(v)$, and $L_2(v)$. So $g = \mathbf{1}(\mathbb{P}) - \mathbf{1}(\mathbb{P} \setminus T) = \mathbf{1}(T)$. And thus $\sum_i v_i = |g| = |\mathbf{1}(T)|$. □

Lemma 22 shows that if the Schnyder wood is of Type 1, then the set of points are not necessarily coplanar as in the planar case [12], but all the copies of a vertex lie on the same plane (the bounded region delimited by the lines $L_0(v)$, $L_1(v)$ and $L_2(v)$ has the same number of faces for any copies of a vertex v). Surprisingly, for Schnyder woods of Type 2, all the points are coplanar.

Lemma 23 *The mapping is periodic with respect to S and S'.*

Proof Let v be any vertex of G^∞. Then $v_i^{\text{top}} - v_i = N(f_{i+1}(L_{i+1}(v^{\text{top}})) - f_{i+1}(L_{i+1}(v))) - N(f_{i-1}(L_{i-1}(v^{\text{top}})) - f_{i-1}(L_{i-1}(v))) = N(c_{i+1} - c_{i-1})f$. So $v^{\text{top}} = v + S$. Similarly, $v^{\text{right}} = v + S'$. □

For each color i, let γ_i be the integer such that two monochromatic cycles of G of respective colors $i-1$ and $i+1$ intersect exactly γ_i times, with the convention that $\gamma_i = 0$ if the Schnyder wood is of Type 2.i. By Lemma 3, γ_i is properly defined and does not depend on the choice of the monochromatic cycles. Note that if the Schnyder wood is of Type 2.i, then $\gamma_{i-1} = \gamma_{i+1}$ and if the Schnyder wood is not of Type 2.i, then $\gamma_i \neq 0$. Let $\gamma = \max(\gamma_0, \gamma_1, \gamma_2)$. Let $Z_0 = ((\gamma_1 + \gamma_2)Nf, -\gamma_1 Nf, -\gamma_2 Nf)$, $Z_1 = (-\gamma_0 Nf, (\gamma_0 + \gamma_2)Nf, -\gamma_2 Nf)$, and $Z_2 = (-\gamma_0 Nf, -\gamma_1 Nf, (\gamma_0 + \gamma_1)Nf)$.

Lemma 24 *For any vertex u, we have $\{u + k_0 Z_0 + k_1 Z_1 + k_2 Z_2 \mid k_0, k_1, k_2 \in \mathbb{Z}\} \subseteq \{u + kS + k'S' \mid k, k' \in \mathbb{Z}\}$.*

Proof Let u, v be two copies of the same vertex, such that v is the first copy of u in the direction of $L_0(u)$. (That is, $L_0(u) = L_0(v)$ and on the path $P_0(u) \setminus P_0(v)$ there are not two copies of the same vertex.) Then $v_i - u_i = N(f_{i+1}(L_{i+1}(v)) - f_{i+1}(L_{i+1}(u))) - N(f_{i-1}(L_{i-1}(v)) - f_{i-1}(L_{i-1}(u)))$. We have $|R(L_0(v), L_0(u))| = 0$, $|R(L_1(v), L_1(u))| = \gamma_2 f$, and $|R(L_2(v), L_2(u))| = \gamma_1 f$. So $v_0 - u_0 = N(\gamma_1 + \gamma_2)f$, $v_1 - u_1 = -N\gamma_1 f$, and $v_2 - u_2 = -N\gamma_2 f$. Thus, $v = u + Z_0$, and similarly for the other colors. So the first copy of u in the direction of $L_i(u)$ is equal to $u + Z_i$. By Lemma 23, all the copies of u are mapped on $\{u + kS + k'S' \mid k, k' \in \mathbb{Z}\}$, and so we have the result. □

Lemma 25 *We have $dim(Z_0, Z_1, Z_2) = 2$, and if the Schnyder wood is not of Type 2.i, then $dim(Z_{i-1}, Z_{i+1}) = 2$.*

Proof We have $\gamma_0 Z_0 + \gamma_1 Z_1 + \gamma_2 Z_2 = 0$ and so $dim(Z_0, Z_1, Z_2) \leq 2$. We can assume by symmetry that the Schnyder wood is not of Type 2.1 and so $\gamma_1 \neq 0$. Thus, $Z_0 \neq 0$ and $Z_2 \neq 0$. Suppose by contradiction that $dim(Z_0, Z_2) = 1$. Then there exist $\alpha \neq 0$, $\beta \neq 0$, such that $\alpha Z_0 + \beta Z_2 = 0$. The sum of this equation for the coordinates 0 and 2 gives $(\alpha + \beta)\gamma_1 = 0$ and thus $\alpha = -\beta$. Then the equation for coordinate 0 gives $\gamma_0 + \gamma_1 + \gamma_2 = 0$, contradicting the fact that $\gamma_1 > 1$ and $\gamma_0, \gamma_2 \geq 0$. □

Lemma 26 *The vectors S, S' are not collinear.*

Proof By Lemma 24, the set $\{u + k_0 Z_0 + k_1 Z_1 + k_2 Z_2 \mid k_0, k_1, k_2 \in \mathbb{Z}\}$ is a subset of $\{u + kS + k'S' \mid k, k' \in \mathbb{Z}\}$. By Lemma 25, we have $dim(Z_0, Z_1, Z_2) = 2$, thus $dim(S, S') = 2$. □

Lemma 27 *If u, v are two distinct vertices such that v is in $L_{i-1}(v)$, u is in $P_{i-1}(v)$, both u and v are in the region $R(L_{i+1}(u), L_{i+1}(v))$, and $L_{i+1}(u)$ and $L_{i+1}(v)$ are two consecutive $(i+1)$-lines with $L_{i+1}(u) \in \mathcal{L}_{i+1}^j$ (see Fig. 34), then $d_i(z_i(v), v) + d_i(u, z_i(u)) < (n-1) \times f_{i+1}^j$.*

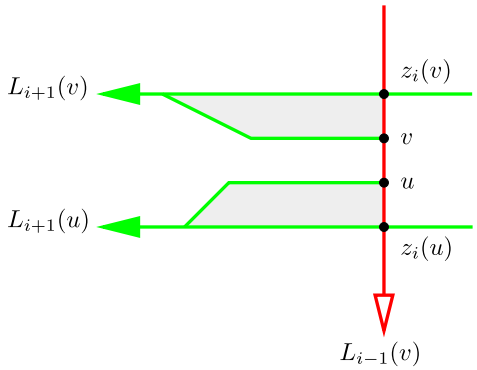

Fig. 34 The *gray area*, corresponding to the quantity $d_i(z_i(v), v) + d_i(u, z_i(u))$, has size bounded by $(n-1) \times f^j_{i+1}$

Proof Let $Q_{i+1}(v)$ the subpath of $P_{i+1}(v)$ between v and $L_{i+1}(v)$ (maybe $Q_{i+1}(v)$ has length 0 if $v = z_i(v)$). Let $Q_{i+1}(u)$ be the subpath of $P_{i+1}(u)$ between u and $L_{i+1}(u)$ (maybe $Q_{i+1}(u)$ has length 0 if $u = z_i(u)$). The path $Q_{i+1}(v)$ cannot contain two different copies of a vertex of G, otherwise $Q_{i+1}(v)$ will correspond to a non-contractible cycle of G and thus will contain an edge of $L_{i+1}(v)$. So the length of $Q_{i+1}(v)$ is $\leq n-1$.

The total number of times a copy of a given face of G can appear in the region $R = R_i(z_i(v)) \setminus R_i(v)$, corresponding to $d_i(z_i(v), v)$, can be bounded as follows. Region R is between two consecutive copies of $L_{i+1}(u)$. So in R, all the copies of a given face are separated by a copy of $L_{i-1}(v)$. Each copy of $L_{i-1}(v)$ intersecting R must intersect $Q_{i+1}(v)$ on a specific vertex. As $Q_{i+1}(v)$ has at most n vertices, a given face can appear at most $n-1$ times in R. Similarly, the total number of times that a copy of a given face of G can appear in the region $R_i(u) \setminus R_i(z_i(u))$, corresponding to $d_i(u, z_i(u))$, is $\leq (n-1)$.

A given face of G can appear in only one of the two gray regions of Fig. 34. So a face is counted $\leq n-1$ times in the quantity $d_i(z_i(v), v) + d_i(u, z_i(u))$. Only the faces of the region $R(C^j_{i+1}, C^{j+1}_{i+1})$ can be counted, and there is at least one face of $R(C^j_{i+1}, C^{j+1}_{i+1})$ (for example, one incident to v) that is not counted. So in total $d_i(z_i(v), v) + d_i(u, z_i(u)) \leq (n-1) \times (f^j_{i+1} - 1) < (n-1) \times f^j_{i+1}$. □

Clearly, the symmetric of Lemma 27, where the roles of $i+1$ and $i-1$ are exchanged, is also true.

The bound of Lemma 27 is somehow sharp. In the example of Fig. 35, the rectangle represents a toroidal map G and the universal cover is partially represented. If the map G has n vertices and f faces ($n = 5$ and $f = 5$ in the example), then the gray region, representing the quantity $d_1(z_1(v), v) + d_1(u, z_1(u))$, has size $\frac{n(n-1)}{2} = \Omega(n \times f)$.

Lemma 28 *Let u, v be vertices of G^∞ such that $R_i(u) \subseteq R_i(v)$, then $u_i \leq v_i$. Moreover, if $R_i(u) \subsetneq R_i(v)$, then $v_i - u_i > (N-n)(|R(L_{i-1}(u), L_{i-1}(v))| + |R(L_{i+1}(u), L_{i+1}(v))|) \geq 0$.*

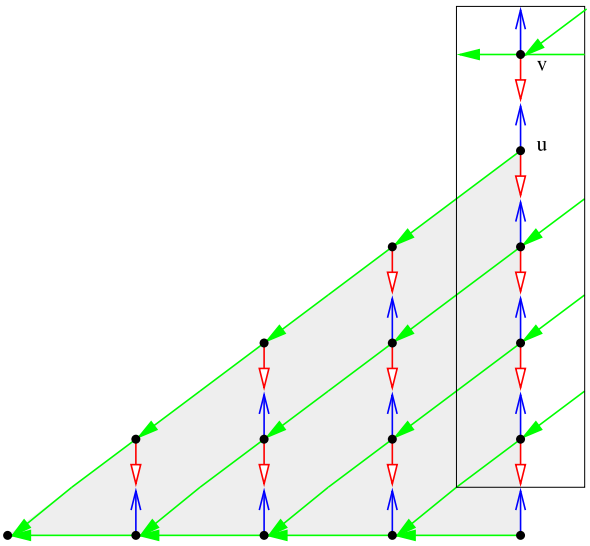

Fig. 35 Example of a toroidal map where $d_1(u, z_1(u))$ has size $\Omega(n \times f)$

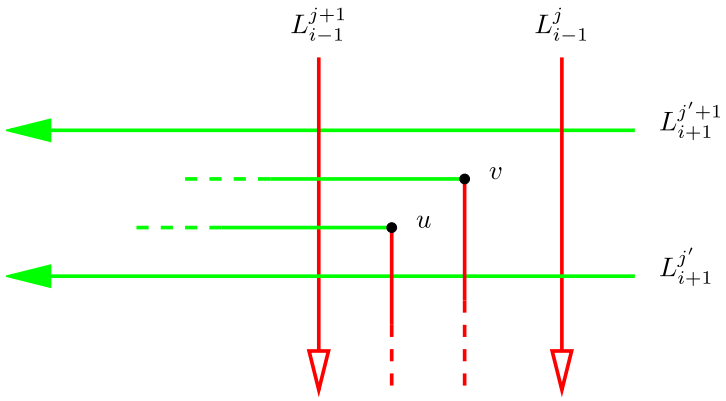

Fig. 36 Positions of u and v in the proof of Lemma 28

Proof We distinguish two cases depending on whether the Schnyder wood is of Type 2.i or not.

• *Case 1: The Schnyder wood is not of Type 2.i.*

Suppose first that u and v are both in a region delimited by two consecutive lines of color $i-1$ and two consecutive lines of color $i+1$. Let L_{i-1}^{j}, L_{i-1}^{j+1}, $L_{i+1}^{j'}$, $L_{i+1}^{j'+1}$ be these lines such that L_{i-1}^{j+1} is on the positive side of L_{i-1}^{j}, $L_{i+1}^{j'+1}$ is on the positive side of $L_{i+1}^{j'}$, and $L_k^{\ell} \in \mathcal{L}_k^{\ell}$ (see Fig. 36). We distinguish cases corresponding to equality or not between lines $L_{i-1}(u)$, $L_{i-1}(v)$ and $L_{i+1}(u)$, $L_{i+1}(v)$.

⋆ *Case 1.1:* $L_{i-1}(u) = L_{i-1}(v)$ *and* $L_{i+1}(u) = L_{i+1}(v)$. Then $v_i - u_i = d_i(v, z_i(v)) - d_i(u, z_i(u)) = d_i(v, u)$. Thus clearly, if $R_i(u) \subseteq R_i(v)$, then $u_i \leq v_i$ and if $R_i(u) \subsetneq R_i(v)$, $v_i - u_i > 0 = (N - n)(|R(L_{i-1}(u), L_{i-1}(v))| + |R(L_{i+1}(u), L_{i+1}(v))|)$.

⋆ *Case 1.2:* $L_{i-1}(u) = L_{i-1}(v)$ *and* $L_{i+1}(u) \neq L_{i+1}(v)$. As $u \in R_i(v)$, we have $L_{i+1}(u) = L_{i+1}^{j'}$ and $L_{i+1}(v) = L_{i+1}^{j'+1}$. Then $v_i - u_i = d_i(v, z_i(v)) - d_i(u, z_i(u)) + N(f_{i+1}(L_{i+1}(v)) - f_{i+1}(L_{i+1}(u))) = d_i(v, z_i(v)) - d_i(u, z_i(u)) + Nf_{i+1}^{j'}$. Let u' be the intersection of $P_{i+1}(u)$ with L_{i-1}^{j+1} (maybe $u = u'$). Let v' be the intersection of $P_{i+1}(v)$ with L_{i-1}^{j+1} (maybe $v = v'$). Since $L_{i+1}(u) \neq L_{i+1}(v)$, we have $u' \neq v'$. Since $u \in R_i(v)$, we have $u' \in R_i(v')$ and so $u' \in P_{i-1}(v')$. Then, by Lemma 27, $d_i(z_i(v'), v') + d_i(u', z_i(u')) < (n-1) f_{i+1}^{j'}$. If $L_{i-1}(u) = L_{i-1}^{j+1}$, then one can see that $d_i(v, z_i(v)) - d_i(u, z_i(u)) \geq d_i(v', z_i(v')) - d_i(u', z_i(u'))$. If $L_{i-1}(u) = L_{i-1}^{j}$, one can see that $d_i(v, z_i(v)) - d_i(u, z_i(u)) \geq d_i(v', z_i(v')) - d_i(u', z_i(u')) - f_{i+1}^{j'}$. So finally, $v_i - u_i = d_i(v, z_i(v)) - d_i(u, z_i(u)) + Nf_{i+1}^{j'} \geq d_i(v', z_i(v')) - d_i(u', z_i(u')) + (N - 1) f_{i+1}^{j'} > (N - n) f_{i+1}^{j'} = (N - n)(|R(L_{i-1}(u), L_{i-1}(v))| + |R(L_{i+1}(u), L_{i+1}(v))|) \geq 0$.

⋆ *Case 1.3:* $L_{i-1}(u) \neq L_{i-1}(v)$ *and* $L_{i+1}(u) = L_{i+1}(v)$. This case is completely symmetric to the previous case.

⋆ *Case 1.4:* $L_{i-1}(u) \neq L_{i-1}(v)$ *and* $L_{i+1}(u) \neq L_{i+1}(v)$. As $u \in R_i(v)$, we have $L_{i+1}(u) = L_{i+1}^{j'}$, $L_{i+1}(v) = L_{i+1}^{j'+1}$, $L_{i-1}(u) = L_{i-1}^{j+1}$, and $L_{i-1}(v) = L_{i-1}^{j}$. Then $v_i - u_i = d_i(v, z_i(v)) - d_i(u, z_i(u)) + N(f_{i+1}(L_{i+1}(v)) - f_{i+1}(L_{i+1}(u))) - N(f_{i-1}(L_{i-1}(v)) - f_{i-1}(L_{i-1}(u))) = d_i(v, z_i(v)) - d_i(u, z_i(u)) + Nf_{i+1}^{j'} + Nf_{i-1}^{j}$. Let u' be the intersection of $P_{i+1}(u)$ with L_{i-1}^{j+1} (maybe $u = u'$). Let u'' be the intersection of $P_{i-1}(u)$ with $L_{i+1}^{j'}$ (maybe $u = u''$). Let v' be the intersection of $P_{i+1}(v)$ with L_{i-1}^{j+1} (maybe $v = v'$). Let v'' be the intersection of $P_{i-1}(v)$ with $L_{i+1}^{j'}$ (maybe $v = v''$). Since $L_{i+1}(u) \neq L_{i+1}(v)$, we have $u' \neq v'$. Since $u \in R_i(v)$, we have $u' \in R_i(v')$ and so $u' \in P_{i-1}(v')$. Then, by Lemma 27, $d_i(z_i(v'), v') + d_i(u', z_i(u')) < (n-1) f_{i+1}^{j'}$. Symmetrically, $d_i(z_i(v''), v'') + d_i(u'', z_i(u'')) < (n-1) f_{i-1}^{j}$. Moreover, we have $d_i(v, z_i(v)) - d_i(u, z_i(u)) \geq d_i(v', z_i(v')) - d_i(u', z_i(u')) + d_i(v'', z_i(v'')) - d_i(u'', z_i(u'')) - f_{i+1}^{j'} - f_{i-1}^{j}$. So finally, $v_i - u_i = d_i(v, z_i(v)) - d_i(u, z_i(u)) + Nf_{i+1}^{j'} + Nf_{i-1}^{j} \geq d_i(v', z_i(v')) - d_i(u', z_i(u')) + d_i(v'', z_i(v'')) - d_i(u'', z_i(u'')) + (N-1) f_{i+1}^{j'} + (N-1) f_{i-1}^{j} > (N-n) f_{i+1}^{j'} + (N-n) f_{i-1}^{j} = (N-n)(|R(L_{i-1}(u), L_{i-1}(v))| + |R(L_{i+1}(u), L_{i+1}(v))|) \geq 0$.

Suppose now that u and v do not lie in a region delimited by two consecutive lines of color $i-1$ and/or in a region delimited by two consecutive lines of color $i+1$. One can easily find distinct vertices $w_0, \ldots, w_r$ (w_i, $1 \leq i < r$ chosen at intersections of monochromatic lines of colors $i-1$ and $i+1$) such that $w_0 = u$, $w_r = v$, and for $0 \leq \ell \leq r-1$, we have $R_i(w_\ell) \subsetneq R_i(w_{\ell+1})$ and $w_\ell, w_{\ell+1}$ are both in a region delimited by two consecutive lines of color $i-1$ and in a region delimited by two consecutive lines of color $i+1$. Thus, by the first part of the proof, $(w_\ell)_i - (w_{\ell+1})_i > (N-n)(|R(L_{i-1}(w_{\ell+1}), L_{i-1}(w_\ell))| + |R(L_{i+1}(w_{\ell+1}), L_{i+1}(w_\ell))|)$. Thus $v_i - u_i >$

$(N-n)\sum_\ell(|R(L_{i-1}(w_{\ell+1}),L_{i-1}(w_\ell))|+|R(L_{i+1}(w_{\ell+1}),L_{i+1}(w_\ell))|)$. For any a,b,c such that $R_i(a)\subseteq R_i(b)\subseteq R_i(c)$, we have $|R(L_j(a),L_j(b))|+|R(L_j(b),L_j(c))|=|R(L_j(a),L_j(c))|$. Thus, we obtain the result by summing the size of the regions.

• *Case 2: The Schnyder wood is of Type 2.i.*

Suppose first that u and v are both in a region delimited by two consecutive lines of color $i+1$.

Let L^j_{i+1},L^{j+1}_{i+1} be these lines such that L^{j+1}_{i+1} is on the positive side of L^j_{i+1}, and $L^\ell_{i+1}\in\mathcal{L}^\ell_{i+1}$. We can assume that we do not have both u and v in L^{j+1}_{i+1} (by eventually choosing other consecutive lines of color $i+1$). We consider two cases:

⋆ *Case 2.1:* $v\notin L^{j+1}_{i+1}$. Then by Lemma 21, $L^j_{i+1}=L_{i+1}(u)=(L_{i-1}(u))^{-1}=L_{i+1}(v)=(L_{i-1}(v))^{-1}$. Then $v_i-u_i=d_i(v,z_i(v))-d_i(u,z_i(u))=d_i(v,u)$. Thus clearly, if $R_i(u)\subseteq R_i(v)$, then $u_i\le v_i$ and if $R_i(u)\subsetneq R_i(v)$, then $v_i-u_i>0=(N-n)(|R(L_{i-1}(u),L_{i-1}(v))|+|R(L_{i+1}(u),L_{i+1}(v))|)$.

⋆ *Case 2.2:* $v\in L^{j+1}_{i+1}$. Then $L^{j+1}_{i+1}=L_{i+1}(v)=(L_{i-1}(v))^{-1}$ and $d_i(v,z_i(v))=0$. By assumption $u\notin L^{j+1}_{i+1}$ and by Lemma 21, $L^j_{i+1}=L_{i+1}(u)=(L_{i-1}(u))^{-1}$. Then $v_i-u_i=d_i(v,z_i(v))-d_i(u,z_i(u))+N(f_{i+1}(L_{i+1}(v))-f_{i+1}(L_{i+1}(u)))-N(f_{i-1}(L_{i-1}(v))-f_{i-1}(L_{i-1}(u)))=-d_i(u,z_i(u))+2Nf^j_{i+1}$. Let L_i and L'_i be two consecutive i-lines such that u lies in the region between them and L'_i is on the right of L_i. Let u' be the intersection of $P_{i+1}(u)$ with L_i (maybe $u=u'$). Let u'' be the intersection of $P_{i-1}(u)$ with L'_i (maybe $u=u''$). Then, by Lemma 27, $d_i(u',z_i(u'))<(n-1)f^j_{i+1}$ and $d_i(u'',z_i(u''))<(n-1)f^j_{i+1}$. Thus, we have $d_i(u,z_i(u))\le d_i(u',z_i(u'))+d_i(u'',z_i(u''))+f^j_{i+1}<(2(n-1)+1)f^j_{i+1}$. So finally, $v_i-u_i>-(2n-1)f^j_{i+1}+2Nf^j_{i+1}>2(N-n)f^j_{i+1}=(N-n)\times(|R(L_{i-1}(u),L_{i-1}(v))|+|R(L_{i+1}(u),L_{i+1}(v))|)\ge 0$.

If u and v do not lie in a region delimited by two consecutive lines of color $i+1$, then as in case 1, one can find intermediate vertices to obtain the result. □

Lemma 29 *If two vertices u,v are adjacent, then for each color i, we have $|v_i-u_i|\le 2Nf$.*

Proof Since u,v are adjacent, they are both in a region delimited by two consecutive lines of color $i-1$ and in a region delimited by two consecutive lines of color $i+1$. Let L^j_{i-1},L^{j+1}_{i-1} be these two consecutive lines of color $i-1$ and $L^{j'}_{i+1},L^{j'+1}_{i+1}$ these two consecutive lines of color $i+1$ where $L^\ell_k\in\mathcal{L}^\ell_k$, L^{j+1}_{i-1} is on the positive side of L^j_{i-1}, and $L^{j'+1}_{i+1}$ is on the positive side of $L^{j'}_{i+1}$ (see Fig. 36 when the Schnyder wood is not of Type 2.i). If the Schnyder wood is of Type 2.i, we assume that $L^{j+1}_{i-1}=(L^{j'}_{i+1})^{-1}$ and $L^j_{i-1}=(L^{j'+1}_{i+1})^{-1}$. Let z be a vertex on the intersection of L^{j+1}_{i-1} and $L^{j'}_{i+1}$. Let z' be a vertex on the intersection of L^j_{i-1} and $L^{j'+1}_{i+1}$. Thus, we have $R_i(z)\subseteq R_i(u)\subseteq R_i(z')$ and $R_i(z)\subseteq R_i(v)\subseteq R_i(z')$. So by Lemma 28, $z_i\le u_i\le z'_i$ and $z_i\le v_i\le z'_i$. So $|v_i-u_i|\le z'_i-z_i=N(f_{i+1}(L^{j'+1}_{i+1})-f_{i+1}(L^{j'}_{i+1}))-N(f_{i-1}(L^j_{i-1})-f_{i-1}(L^{j+1}_{i-1}))=Nf^{j'}_{i+1}+Nf^j_{i-1}\le 2Nf$. □

We are now able to prove the following theorem.

Theorem 13 *If G is a toroidal map given with a Schnyder wood, then the mapping of each vertex of G^∞ on its region vector gives a geodesic embedding of G.*

Proof By Lemmas 23 and 26, the mapping of G^∞ on its region vector is periodic with respect to S, S' that are not collinear. For any pair u, v of distinct vertices of G^∞, by Lemma 8(iii), there exists i, j with $R_i(u) \subsetneq R_i(v)$ and $R_j(v) \subsetneq R_j(u)$; thus, by Lemma 28, $u_i < v_i$ and $v_j < u_j$. So $\mathcal{V}^\infty$ is a set of pairwise incomparable elements of $\mathbb{R}^3$.

(D1) $\mathcal{V}^\infty$ is a set of pairwise incomparable elements, so the mapping between vertices of G^∞ and $\mathcal{V}^\infty$ is a bijection.

(D2) Let $e = uv$ be an edge of G^∞. We show that $w = u \vee v$ is on the surface $S_{\mathcal{V}^\infty}$. By definition, $u \vee v$ is in $\mathcal{D}_{\mathcal{V}^\infty}$. Suppose, by contradiction, that $w \notin S_{\mathcal{V}^\infty}$. Then there exists $x \in \mathcal{V}^\infty$ with $x < w$. Let x also denote the corresponding vertex of G^∞. Edge e is in a region $R_i(x)$ for some i. So $u, v \in R_i(x)$ and thus by Lemma 8(i), $R_i(u) \subseteq R_i(x)$ and $R_i(v) \subseteq R_i(x)$. Then by Lemma 28, $w_i = \max(u_i, v_i) \leq x_i$, a contradiction. Thus, the elbow geodesic between u and v is on the surface.

(D3) Consider a vertex $v \in \mathcal{V}$ and a color i. Let u be the extremity of the arc $e_i(v)$. We have $u \in R_{i-1}(v)$ and $u \in R_{i+1}(v)$, so by Lemma 8(i), $R_{i-1}(u) \subseteq R_{i-1}(v)$ and $R_{i+1}(u) \subseteq R_{i+1}(v)$. Thus, by Lemma 8(iii), $R_i(v) \subsetneq R_i(u)$. So, by Lemma 28, $v_i < u_i$, $u_{i-1} \leq v_{i-1}$, and $u_{i+1} \leq v_{i+1}$. So the orthogonal arc of vertex v in the direction of the basis vector e_i is part of the elbow geodesic of the edge $e_i(v)$.

(D4) Suppose there exists a pair of crossing edges $e = uv$ and $e' = u'v'$ on the surface $S_{\mathcal{V}^\infty}$. The two edges e, e' cannot intersect on orthogonal arcs, so they intersect on a plane orthogonal to one of the coordinate axes. Up to symmetry we may assume that we are in the situation of Fig. 37 with $u_1 = u'_1$, $u_2 > u'_2$, and $v_2 < v'_2$. Between u and u', there is a path consisting of orthogonal arcs only. With (D3), this implies that there is a bidirected path P^* colored 0 from u to u' and colored 2 from u' to u. We have $u \in R_2(v)$, so by Lemma 8(i), $R_2(u) \subseteq R_2(v)$. We have $u' \in R_2(u)$, so $u' \in R_2(v)$. If $P_0(v)$ contains u', then there is a contractible cycle containing v, u, u' in $G_1 \cup G_0^{-1} \cup G_2^{-1}$, contradicting Lemma 1, so $P_0(v)$ does not contain u'. If $P_1(v)$ contains u', then $u' \in P_1(u) \cap P_0(u)$, contradicting Lemma 7. So $u' \in R_2^\circ(v)$. Thus, the edge $u'v'$ implies that $v' \in R_2(v)$. So by Lemma 28, $v'_2 \leq v_2$, a contradiction. □

Theorems 1 and 13 imply Theorem 3.

One can ask: What is the "size" of the obtained geodesic embedding of Theorem 13? Of course, this mapping is infinite so there is no real size, but as the object is periodic, one can consider the smallest size of the vectors such that the mapping is periodic with respect to them. There are several such pairs of vectors, one is S, S'. Recall that $S_i = N(c_{i+1} - c_{i-1})f$ and $S'_i = N(c'_{i+1} - c'_{i-1})f$. Unfortunately, the size of S, S' can be arbitrarily large. Indeed, the values of $c_{i+1} - c_{i-1}$ and $c'_{i+1} - c'_{i-1}$ are unbounded, as a toroidal map can be artificially "very twisted" in the considered flat torus representation (independent of the number of vertices or faces). Nevertheless, we can prove the existence of bounded size vectors for which the mapping is periodic with respect to them.

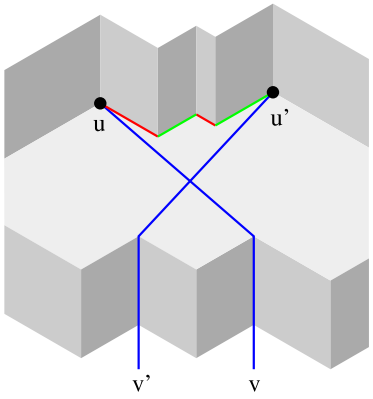

Fig. 37 A pair of crossing elbow geodesics

Lemma 30 *If G is a toroidal map given with a Schnyder wood, then the mapping of each vertex of G^∞ on its region vector gives a periodic mapping of G^∞ with respect to non-collinear vectors Y and Y', where the size of Y and Y' is in $\mathcal{O}(\gamma Nf)$. In general, we have $\gamma \leq n$, and in the case where G is a simple toroidal triangulation given with a Schnyder wood obtained by Theorem 9, we have $\gamma = 1$.*

Proof By Lemma 24, the vectors Z_{i-1}, Z_{i+1} (when the Schnyder wood is not of Type 2.i) span a subset of S, S' (it can happen that this subset is strict). Thus, in the parallelogram delimited by the vectors Z_{i-1}, Z_{i+1} (that is, a parallelogram by Lemma 25), there is a parallelogram with sides Y, Y' containing a copy of V. The size of the vectors Z_i is in $\mathcal{O}(\gamma Nf)$ and so the size of Y and Y' is also.

In general, we have $\gamma_i \leq n$, as each intersection between two monochromatic cycles of G of color $i-1$ and $i+1$ corresponds to a different vertex of G and thus $\gamma \leq n$. In the case of simple toroidal triangulation given with a Schnyder wood obtained by Theorem 9, we have, for each color i, $\gamma_i = 1$, and thus $\gamma = 1$. □

As in the plane, one can give weights to faces of G. Then all their copies in G^∞ have the same weight, and instead of counting the number of faces in each region one can compute the weighted sum.

Note that the geodesic embeddings of Theorem 13 are not necessarily rigid. A geodesic embedding is *rigid* [11, 20] if for every pair $u, v \in \mathcal{V}$ such that $u \vee v$ is in $\mathcal{S}_\mathcal{V}$, u and v are the only elements of $\mathcal{V}$ that are dominated by $u \vee v$. The geodesic embedding of Fig. 5 is not rigid, as the bend corresponding to the loop of color 1 is dominated by three vertices of G^∞. We do not know if it is possible to build a rigid geodesic embedding from the Schnyder wood of a toroidal map. Maybe a technique similar to the one presented in [11] can be generalized to the torus.

It has already been mentioned that in the geodesic embeddings of Theorem 13 the points corresponding to vertices are not coplanar. The problem of building a coplanar geodesic embedding from the Schnyder wood of a toroidal map is open. In the plane, there are some examples of maps G [11] for which it is not possible to require both rigidity and coplanarity. Thus, the same is true in the torus for the graph G^+.

Another question related to coplanarity is whether one can require that the points of the orthogonal surface corresponding to edges of the graph (i.e., bends) are copla-

nar. This property is related to contact representation by homotopic triangles [11]. It is known that in the plane, not all Schnyder woods are supported by such surfaces. Kratochvil's conjecture [19], recently proved [17], states that every 4-connected planar triangulation admits a contact representation by homothetic triangles. Can this be extended to the torus?

When considering not necessarily homothetic triangles, it has been proved [14] that there is a bijection between Schnyder woods of planar triangulations and contact representations by triangles. This result has been generalized to internally 3-connected planar maps [16] by exhibiting a bijection between Schnyder woods of internally 3-connected planar maps and primal-dual contact representations by triangles (i.e., representations where both the primal and the dual are represented). It would be interesting to generalize these results to the torus.

11 Duality of Orthogonal Surfaces

Given an orthogonal surface generated by $\mathcal{V}$, let $\mathcal{F}_\mathcal{V}$ be the maximal points of $\mathcal{S}_\mathcal{V}$, i.e., the points of $\mathcal{S}_\mathcal{V}$ that are not dominated by any vertex of $\mathcal{S}_\mathcal{V}$. If $A, B \in \mathcal{F}_\mathcal{V}$ and $A \wedge B \in \mathcal{S}_\mathcal{V}$, then $\mathcal{S}_\mathcal{V}$ contains the union of the two line segments joining A and B to $A \wedge B$. Such arcs are called *dual elbow geodesics*. The *dual orthogonal arc* of $A \in \mathcal{F}_\mathcal{V}$ in the direction of the standard basis vector e_i is the intersection of the ray $A + \lambda e_i$ with $\mathcal{S}_\mathcal{V}$.

Given a toroidal map G, let $G^{\infty *}$ be the dual of G^∞. A *dual geodesic embedding* of G is a drawing of $G^{\infty *}$ on the orthogonal surface $\mathcal{S}_{\mathcal{V}^\infty}$, where $\mathcal{V}^\infty$ is a periodic mapping of G^∞ with respect to two non-collinear vectors, satisfying the following (see the example of Fig. 38):

(D1*) There is a bijection between the vertices of $G^{\infty *}$ and $\mathcal{F}_{\mathcal{V}^\infty}$.
(D2*) Every edge of $G^{\infty *}$ is a dual elbow geodesic.
(D3*) Every dual orthogonal arc in $\mathcal{S}_{\mathcal{V}^\infty}$ is part of an edge of $G^{\infty *}$.
(D4*) There are no crossing edges in the embedding of $G^{\infty *}$ on $\mathcal{S}_{\mathcal{V}^\infty}$.

Let G be a toroidal map given with a Schnyder wood. Consider the mapping of each vertex on its region vector. We consider the dual of the Schnyder wood of G. By Lemma 11, it is a Schnyder wood of G^*. A face F of G^∞ is mapped on the point $\bigvee_{v \in F} v$. Let $\widetilde{G^\infty}$ be a simultaneous drawing of G^∞ and $G^{\infty *}$ such that only dual edges intersect. To avoid confusion, we denote R_i the regions of the primal Schnyder wood and R_i^* the regions of the dual Schnyder wood.

Lemma 31 *For any face F of G^∞, we have that $\bigvee_{v \in F} v$ is a maximal point of $\mathcal{S}_{\mathcal{V}^\infty}$.*

Proof Let F be a face of G^∞. For any vertex u of $\mathcal{V}^\infty$, there exists a color i, such that the face F is in the region $R_i(u)$. Thus for $v \in F$, we have $v \in R_i(u)$. By Lemma 28, we have $v_i \leq u_i$ and so $F_i \leq u_i$. So $F = \bigvee_{v \in F} v$ is a point of $\mathcal{S}_{\mathcal{V}^\infty}$.

Suppose, by contradiction, that F is not a maximal point of $\mathcal{S}_{\mathcal{V}^\infty}$. Then there is a point $\alpha \in \mathcal{S}_{\mathcal{V}^\infty}$ that dominates F and, for at least one coordinate j, we have $F_j < \alpha_j$. By Lemma 10, the angles at F form, in counterclockwise order, non-empty intervals

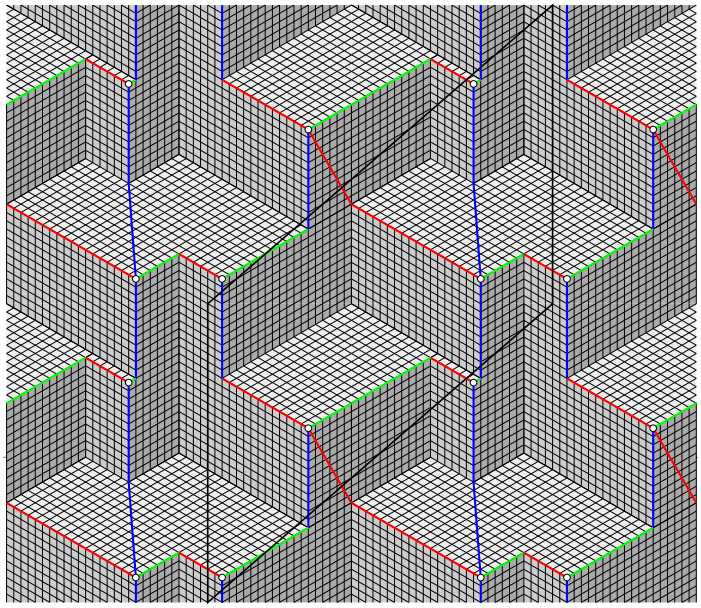

Fig. 38 Dual geodesic embedding of the toroidal map of Fig. 2

of 0's, 1's, and 2's. For each color, let z^i be a vertex of F with angle i. We have that F is in the region $R_i(z^i)$. So $z^{i-1} \in R_i(z^i)$ and by Lemma 8(i), we have $R_i(z^{i-1}) \subseteq R_i(z^i)$. Since F is in $R_{i-1}(z^{i-1})$, it is not in $R_i(z^{i-1})$ and thus $R_i(z^{i-1}) \subsetneq R_i(z^i)$. Then by Lemma 28, we have $(z^{i-1})_i < (z^i)_i$ and symmetrically $(z^{i+1})_i < (z^i)_i$. So $F_{j-1} = (z^{j-1})_{j-1} > (z^j)_{j-1}$ and $F_{j+1} > (z^j)_{j+1}$. Thus, α strictly dominates z^j, a contradiction to $\alpha \in \mathcal{S}_{\mathcal{V}^\infty}$. Thus, F is a maximal point of $\mathcal{S}_{\mathcal{V}^\infty}$. □

Lemma 32 *If two faces A, B are such that $R_i^*(B) \subseteq R_i^*(A)$, then $A_i \leq B_i$.*

Proof Let $v \in B$ be a vertex whose angle at B is labeled i. We have $v \in R_i^*(B)$ and so $v \in R_i^*(A)$. In $\widetilde{G^\infty}$, the path $P_i(v)$ cannot leave $R_i^*(A)$, the path $P_{i+1}(v)$ cannot intersect $P_{i+1}(A)$, and the path $P_{i-1}(v)$ cannot intersect $P_{i-1}(A)$. Thus, $P_{i+1}(v)$ intersects $P_{i-1}(A)$ and the path $P_{i-1}(v)$ cannot intersect $P_{i+1}(A)$. So $A \in R_i(v)$. Thus, for all $u \in A$, we have $u \in R_i(v)$, so $R_i(u) \subseteq R_i(v)$, and so $u_i \leq v_i$. Then $A_i = \max_{u \in A} u_i \leq v_i \leq \max_{w \in B} w_i = B_i$. □

Theorem 14 *If G is a toroidal map given with a Schnyder wood and each vertex of G^∞ is mapped on its region vector, then the mapping of each face of $G^{\infty *}$ on the point $\bigvee_{v \in F} v$ gives a dual geodesic embedding of G.*

Proof By Lemmas 23 and 26, the mapping is periodic with respect to non-collinear vectors.

(D1*) Consider a counting of elements on the orthogonal surface, where we count two copies of the same object just once (note that we are on an infinite and periodic

object). We have that the sum of primal orthogonal arcs plus dual ones is exactly $3m$. There are $3n$ primal orthogonal arcs and thus there are $3m - 3n = 3f$ dual orthogonal arcs. Each maximal point of $\mathcal{S}_{\mathcal{V}^\infty}$ is incident to 3 dual orthogonal arcs and there is no dual orthogonal arc incident to two distinct maximal points. So there are f maximal points. Thus by Lemma 31, we have a bijection between faces of G^∞ and maximal points of $\mathcal{S}_{\mathcal{V}^\infty}$.

Let $\mathcal{V}^{\infty *}$ be the maximal points of $\mathcal{S}_{\mathcal{V}^\infty}$. Let $\mathcal{D}^*_{\mathcal{V}^\infty} = \{A \in \mathbb{R}^3 \mid \exists B \in \mathcal{V}^{\infty *}$ such that $A \leq B\}$. Note that the boundary of $\mathcal{D}^*_{\mathcal{V}^\infty}$ is $\mathcal{S}_{\mathcal{V}^\infty}$.

(D2*) Let $e = AB$ be an edge of $G^{\infty *}$. We show that $w = A \wedge B$ is on the surface $S_{\mathcal{V}^\infty}$. By definition, w is in $\mathcal{D}^*_{\mathcal{V}^\infty}$. Suppose, by contradiction, that $w \notin S_{\mathcal{V}^\infty}$. Then there exists C, a maximal point of $S_{\mathcal{V}^\infty}$ with $w < C$. By the bijection (D1*) between maximal points and vertices of $G^{\infty *}$, the point C corresponds to a vertex of $G^{\infty *}$, also denoted C. Edge e is in a region $R^*_i(C)$ for some i. So $A, B \in R^*_i(C)$ and thus, by Lemma 8(i), $R^*_i(A) \subseteq R^*_i(C)$ and $R^*_i(B) \subseteq R^*_i(C)$. Then by Lemma 32, we have $C_i \leq \min(A_i, B_i) = w_i$, a contradiction. Thus, the dual elbow geodesic between A and B is also on the surface.

(D3*) Consider a vertex A of $G^{\infty *}$ and a color i. Let B be the extremity of the arc $e_i(A)$. We have $B \in R^*_{i-1}(A)$ and $B \in R^*_{i+1}(A)$, so by Lemma 8(i), $R^*_{i-1}(B) \subseteq R^*_{i-1}(A)$ and $R^*_{i+1}(B) \subseteq R^*_{i+1}(A)$. Thus by Lemma 32, $A_{i-1} \leq B_{i-1}$ and $A_{i+1} \leq B_{i+1}$. As A and B are distinct maximal points of $\mathcal{S}_{\mathcal{V}^\infty}$, they are incomparable, and thus $B_i < A_i$. So the dual orthogonal arc of vertex A in the direction of the basis vector e_i is part of edge $e_i(A)$.

(D4*) Suppose there exists a pair of crossing edges $e = AB$ and $e' = A'B'$ of $G^{\infty *}$ on the surface $S_{\mathcal{V}^\infty}$. The two edges e, e' cannot intersect on orthogonal arcs, so they intersect on a plane orthogonal to one of the coordinate axes. Up to symmetry we may assume that we are in the situation $A_1 = A'_1$, $A'_0 > A_0$, and $B'_0 < B_0$. Between A and A' there is a path consisting of orthogonal arcs only. With (D3*), this implies that there is a bidirected path P^* colored 2 from A to A' and colored 0 from A' to A. We have $A \in R_0(B)$, so by Lemma 8(i), $R_0(A) \subseteq R_0(B)$. We have $A' \in R_0(A)$, so $A' \in R_0(B)$. If $P_2(B)$ contains A', then there is a contractible cycle containing A, A', B in $G^*_1 \cup G_0^{*-1} \cup G_2^{*-1}$, contradicting Lemma 1, so $P_2(B)$ does not contain A'. If $P_1(B)$ contains A', then $A' \in P_1(A) \cap P_2(A)$, contradicting Lemma 7. So $A' \in R^\circ_0(B)$. Thus, the edge $A'B'$ implies that $B' \in R_0(B)$. So by Lemma 32, $B'_0 \geq B_0$, a contradiction. □

Theorems 13 and 14 can be combined to obtain a simultaneous representation of a Schnyder wood and its dual on an orthogonal surface. The projection of this 3-dimensional object on the plane of the equation $x + y + z = 0$ gives a representation of the primal and the dual where edges are allowed to have one bend and two dual edges have to cross on their bends (see the example of Fig. 39).

Theorem 15 *An essentially* 3*-connected toroidal map admits a simultaneous flat torus representation of the primal and the dual where edges are allowed to have one bend and two dual edges have to cross on their bends. Such a representation is contained in a (triangular) grid of size* $\mathcal{O}(n^2 f) \times \mathcal{O}(n^2 f)$ *in general and* $\mathcal{O}(nf) \times \mathcal{O}(nf)$ *if the map is a simple triangulation. Furthermore, the length of the edges are in* $\mathcal{O}(nf)$.

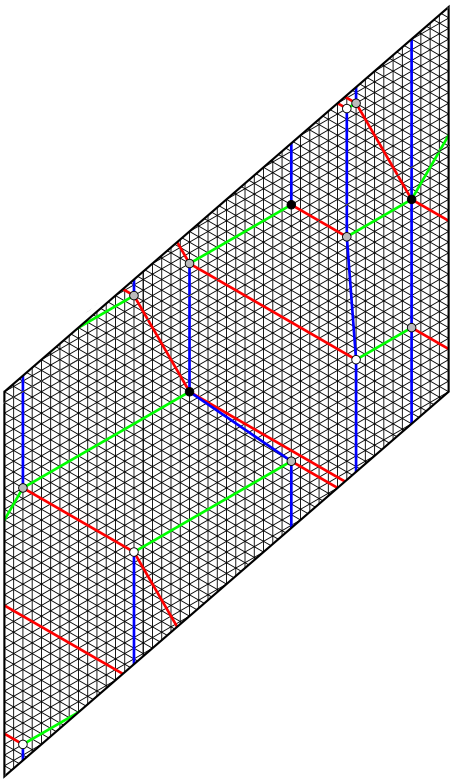

Fig. 39 Simultaneous representation of the primal and the dual of the toroidal map of Fig. 2 with edges having one bend (in *gray*)

Proof Let G be an essentially 3-connected toroidal map. By Theorem 1 (or Theorem 9 if G is a simple triangulation), G admits a Schnyder wood (where monochromatic cycles of different colors intersect just once if G is simple). By Theorems 13 and 14, the mapping of each vertex of G^∞ on its region vector gives a primal and dual geodesic embedding. Thus, the projection of this embedding on the plane of the equation $x + y + z = 0$ gives a representation of the primal and the dual of G^∞ where edges are allowed to have one bend and two dual edges have to cross on their bends.

By Lemma 30, the obtained mapping is a periodic mapping of G^∞ with respect to non-collinear vectors Y and Y' where the size of Y and Y' is in $\mathcal{O}(\gamma Nf)$, with $\gamma \leq n$ in general and $\gamma = 1$ in case of a simple triangulation. Let $N = n$. The embedding gives a representation in the flat torus of sides Y, Y' where the size of the vectors Y and Y' is in $\mathcal{O}(n^2 f)$ in general and in $\mathcal{O}(nf)$ if the graph is simple and the Schnyder wood is obtained by Theorem 9. By Lemma 29, the lengths of the edges in this representation are in $\mathcal{O}(nf)$. □

12 Straight-Line Representation of Toroidal Maps

The geodesic embedding obtained by the region vector method can be used to obtain a straight-line representation of a toroidal map (see Fig. 40). For this purpose, we

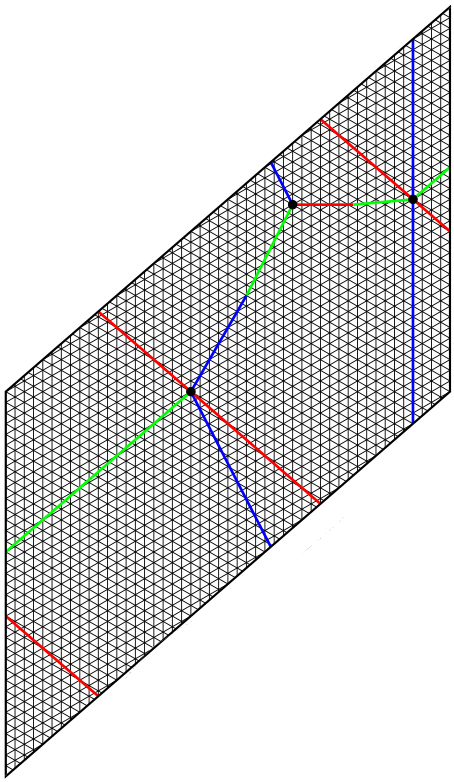

Fig. 40 Straight-line representation of the graph of Fig. 2 obtained by projecting the geodesic embedding of Fig. 5

have to choose N bigger than previously. Note that Fig. 40 is the projection of the geodesic embedding of Fig. 5 obtained with the value of $N = n$. In this particular case this gives a straight-line representation, but in this section we only prove that such a technique works for triangulations and for N sufficiently large. To obtain a straight-line representation of a general toroidal map, one first has to triangulate it.

Let G be a toroidal triangulation given with a Schnyder wood and V^∞ the set of region vectors of vertices of G^∞. The Schnyder wood is of Type 1 by Theorem 7. Recall that γ_i is the integer such that two monochromatic cycles of G of colors $i-1$ and $i+1$ intersect exactly γ_i times.

Lemma 33 *For any vertex v, the number of faces in the bounded region delimited by the three lines $L_i(v)$ is strictly less than* $(5\min(\gamma_i) + \max(\gamma_i))f$.

Proof Suppose by symmetry that $\min(\gamma_i) = \gamma_1$. Let $L_i = L_i(v)$ and $z_i = z_i(v)$. Let T be the bounded region delimited by the three monochromatic lines L_i. The boundary of T is a cycle C oriented clockwise or counterclockwise. Assume that C is oriented counterclockwise (the proof is similar if oriented clockwise). The region T is on the left sides of the lines L_i. We have $z_{i-1} \in P_i(z_{i+1})$.

We define, for $j, k \in \mathbb{N}$, monochromatic lines $L_2(j)$, $L_0(k)$ and vertices $z(j,k)$ as follows (see Fig. 41). Let $L_2(1)$ be the first 2-line intersecting $L_0 \setminus \{z_1\}$ while walking from z_1, along L_0 in the direction of L_0. Let $L_0(1)$ be the first 0-line of color 0

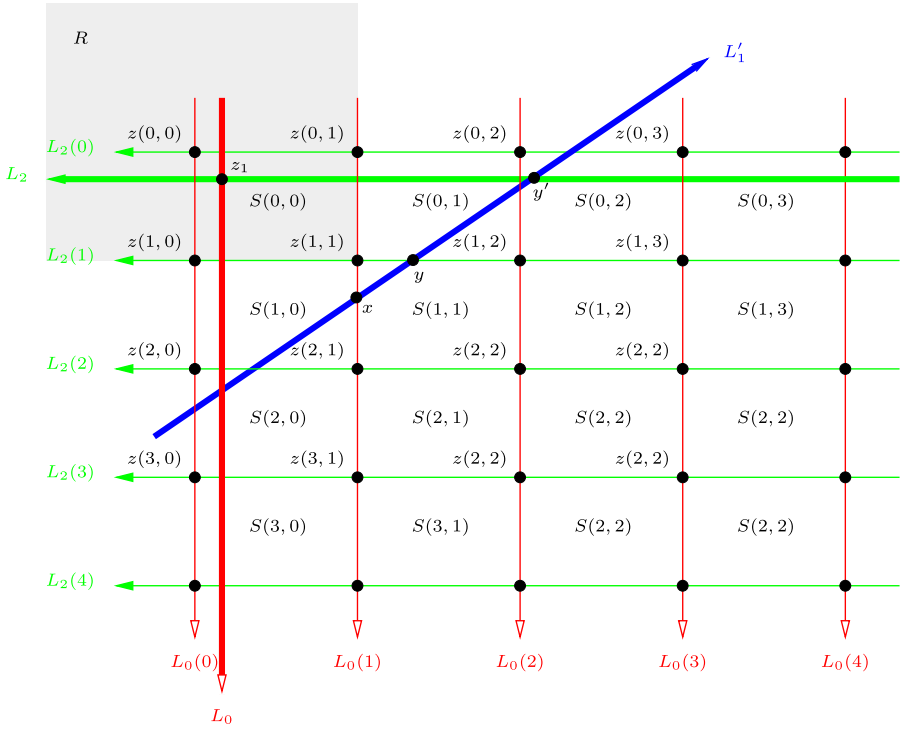

Fig. 41 Notation of the proof of Lemma 33

intersecting $L_2 \setminus \{z_1\}$ while walking from z_1, along L_2 in the reverse direction of L_2. Let $z(1,1)$ be the intersection between $L_2(1)$ and $L_0(1)$. Let $z(j,1)$, $j \geq 0$, be the consecutive copies of $z(1,1)$ along $L_0(1)$ such that $z(j+1,1)$ is after $z(j,1)$ in the direction of $L_0(1)$. Let $L_2(j)$, $j \geq 0$, be the 2-line of color 2 containing $z(j,1)$. Note that we may have $L_2 = L_2(0)$, but in any case L_2 is between $L_2(0)$ and $L_2(1)$. Let $z(j,k)$, $k \geq 0$, be the consecutive copies of $z(j,1)$ along $L_2(j)$ such that $z(j,k+1)$ is after $z(j,k)$ in the reverse direction of $L_2(j)$. Let $L_0(k)$, $k \geq 0$, be the 0-line containing $z(1,k)$. Note that we may have $L_0 = L_0(0)$, but in any case L_0 is between $L_0(0)$ and $L_0(1)$. Let $S(j,k)$ be the region delimited by $L_2(j)$, $L_2(j+1)$, $L_0(k)$, $L_0(k+1)$. All the regions $S(j,k)$ are copies of $S(0,0)$. The region $S(0,0)$ may contain several copies of a face of G, but the number of copies of a face in $S(0,0)$ is equal to γ_1. Let R be the unbounded region situated on the right of $L_0(1)$ and on the right of $L_2(1)$. As $P_0(v)$ cannot intersect $L_0(1)$ and $P_2(v)$ cannot intersect $L_2(1)$, vertex v is in R. Let $P(j,k)$ be the subpath of $L_0(k)$ between $z(j,k)$ and $z(j+1,k)$. All the lines $L_0(k)$ are composed only of copies of $P(0,0)$. The interior vertices of the path $P(0,0)$ cannot contains two copies of the same vertex, otherwise there will be a vertex $z(j,k)$ between $z(0,0)$ and $z(1,0)$. Thus, all interior vertices of a path $P(j,k)$ correspond to distinct vertices of G.

The Schnyder wood is of Type 1, thus 1-lines are crossing 0-lines. As a line $L_0(k)$ is composed only of copies of $P(0,0)$, any path $P(j,k)$ is crossed by a 1-line. Let

L'_1 be the first 1-line crossing $P(1,1)$ on a vertex x while walking from $z(1,1)$ along $L_0(1)$. By (T1), line L'_1 is not intersecting $R \setminus \{z(1,1)\}$. As $v \in R$, we have that L_1 is on the left of L'_1 (maybe $L_1 = L'_1$). Thus, the region T is included in the region T' delimited by L_0, L'_1, L_2.

Let y be the vertex where L'_1 is leaving $S(1,1)$. We claim that $y \in L_2(1)$. Note that by (T1), we have $y \in L_2(1) \cup P(1,2)$. Suppose, by contradiction, that y is an interior vertex of $P(1,2)$. Let d_x be the length of the subpath of $P(1,1)$ between $z(1,1)$ and x. Let d_y be the length of the subpath of $P(1,2)$ between $z(1,2)$ and y. Suppose $d_y < d_x$; then there should be a distinct copy of L'_1 intersecting $P(1,1)$ between $z(1,1)$ and x on a copy of y, a contradiction to the choice of L'_1. So $d_x \leq d_y$. Let A be the subpath of L'_1 between x and y. Let B be the subpath of $P(1,1)$ between x and the copy of y (if $d_x = d_y$, then B is just a single vertex). Consider all the copies of A and B between lines $L_2(1)$ and $L_2(2)$. They form an infinite line L situated on the right of $L_2(1)$ that prevents L'_1 from crossing $L_2(1)$, a contradiction.

By the positions of x and y, we have that L'_1 intersects $S(0,1)$ and $S(1,0)$. We claim that L'_1 cannot intersect both $S(0,3)$ and $S(3,0)$. Suppose by contradiction that L'_1 intersects both $S(0,3)$ and $S(3,0)$. Then L'_1 is crossing $S(0,2)$ without crossing $L_2(0)$ or $L_2(1)$. Similarly, L'_1 is crossing $S(2,0)$ without crossing $L_0(0)$ or $L_0(1)$. Thus, by superposing what happens in $S(0,2)$ and $S(2,0)$ in a square $S(j,k)$, we have that there are two crossing 1-lines, a contradiction. Thus, L'_1 intersects at most one of $S(0,3)$ and $S(3,0)$.

Suppose that L'_1 does not intersect $S(3,0)$. Then the part of T' situated right of $L_0(2)$ (the left part of Fig. 41) is strictly included in $(S(0,0) \cup S(1,0) \cup S(2,0) \cup S(0,1) \cup S(1,1))$. Thus, this part of T' contains at most $5\gamma_1 f$ faces. Now consider the part of T' situated on the left of $L_0(2)$ (the right part of Fig. 41). Let y' be the intersection of L'_1 with L_2. Let Q be the subpath of L'_1 between y and y'. By the definition of $L_2(1)$, there are no 2-lines between L_2 and $L_2(1)$. So Q cannot intersect a 2-line on one of its interior vertices. Thus, Q is crossing at most γ_2 consecutive 0-lines (that are not necessarily lines of type $L_0(k)$). Let L'_0 be the γ_2+1-th consecutive 0-line that is on the left of $L_0(2)$ (counting $L_0(2)$). Then the part of T' situated on the left of $L_0(2)$ is strictly included in the region delimited by $L_0(2), L'_0, L_2, L_2(1)$, and thus contains at most γ_2 copies of a face of G. Thus, T' contains at most $(\gamma_2 + 5\gamma_1) f$ faces.

Symmetrically, if L'_1 does not intersect $S(0,3)$ we have that T' contains at most $(\gamma_0 + 5\gamma_1) f$ faces. Then in any case, T' contains at most $(\max(\gamma_0, \gamma_2) + 5\gamma_1) f$ faces and the lemma is true. □

The bound of Lemma 33 is somehow sharp. In the example of Fig. 42, the rectangle represents a toroidal triangulation G and the universal cover is partially represented. For each value of $k \geq 0$, there is a toroidal triangulation G with $n = 4(k+1)$ vertices, where the gray region, representing the region delimited by the three monochromatic lines $L_i(v)$, contains $4\sum_{j=1}^{2k+1} + 3(2k+2) = \Omega(n \times f)$ faces. Figure 42 represents such a triangulation for $k = 2$.

For planar graphs the region vector method gives vertices that all lie on the same plane. This property is very helpful in proving that the positions of the points on P give straight-line representations. In the torus, things are more complicated, as

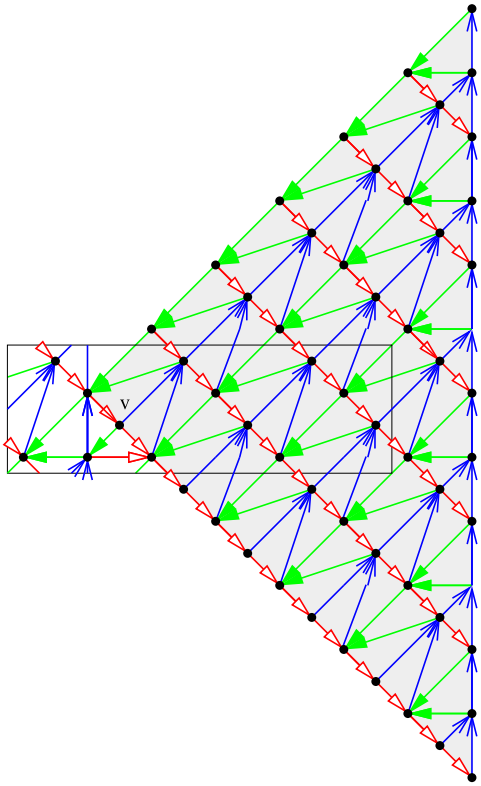

Fig. 42 Example of a toroidal triangulation where the number of faces in the region delimited by the three monochromatic lines $L_i(v)$ contains $\Omega(n \times f)$ faces

our generalization of the region vector method does not give coplanar points. But Lemmas 22 and 33 show that all the points lie in the region situated between the two planes of equations $x+y+z=0$ and $x+y+z=t$, with $t=(5\min(\gamma_i)+\max(\gamma_i))f$. Note that t is bounded by $6nf$ by Lemma 30 and this is independent from N. Thus, from "far away" it looks like the points are coplanar and by taking N sufficiently large, non-coplanar points are "far enough" from each other to enable the region vector method to give straight-line representations.

Let $N=t+n$.

Lemma 34 *Let u, v be two vertices such that $e_{i-1}(v)=uv$, $L_i=L_i(u)=L_i(v)$, and such that both u, v are in the region $R(L_i, L_i')$ for L_i' an i-line consecutive to L_i. Then $v_{i+1}-u_{i+1}<|R(L_i, L_i')|$ and $e_{i-1}(v)$ is going counterclockwise around the closed disk bounded by $\{e_{i-1}(v)\}\cup P_i(u)\cup P_i(v)$.*

Proof Let y be the first vertex of $P_i(v)$ that is also in $P_i(u)$. Let Q_u (resp. Q_v) be the part of $P_i(u)$ (resp. $P_i(v)$) between u (resp. v) and y.

Let D be the closed disk bounded by the cycle $C=(Q_v)^{-1}\cup\{e_{i-1}(v)\}\cup Q_u$. If C is going clockwise around D, then $P_{i+1}(v)$ is leaving v in D and thus has to intersect Q_u or Q_v. In both cases, there is a cycle in $G_{i+1}\cup(G_i)^{-1}\cup(G_{i-1})^{-1}$, a contradiction to Lemma 6. So C is going clockwise around D.

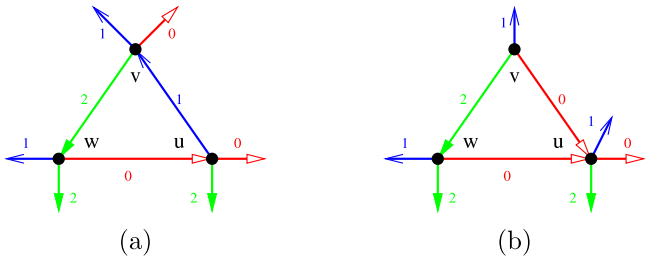

Fig. 43 (**a**) Case 1 and (**b**) case 2 of the proof of Lemma 35

As $L_i(u) = L_i(v)$ and $L_{i-1}(u) = L_{i-1}(v)$, we have $v_{i+1} - u_{i+1} = d_{i+1}(v, u)$, and this is equal to the number of faces in D. We have $D \subsetneq R(L_i, L'_i)$. Suppose D contains two copies of a given face. Then, these two copies are on different sides of a 1-line. By property (T1), it is not possible to have a 1-line entering D. So D contains at most one copy of each face of $R(L_i, L'_i)$. □

Lemma 35 *For any face F of G^∞, incident to vertices u, v, w (given in counterclockwise order around F), the cross product $\overrightarrow{vw} \wedge \overrightarrow{vu}$ has strictly positive coordinates.*

Proof Consider the angle labeling corresponding to the Schnyder wood. By Lemma 10, the angles at F are labeled in counterclockwise order $0, 1, 2$. As $\overrightarrow{uv} \wedge \overrightarrow{uw} = \overrightarrow{vw} \wedge \overrightarrow{vu} = \overrightarrow{wu} \wedge \overrightarrow{wv}$, we may assume that u, v, w are such that u is in the angle labeled 0, vertex v in the angle labeled 1, and vertex w in the angle labeled 2. The face F is either a cycle completely directed into one direction or it has two edges oriented in one direction and one edge oriented in the other. Let

$$\overrightarrow{X} = \overrightarrow{vw} \wedge \overrightarrow{vu} = \begin{pmatrix} (w_1 - v_1)(u_2 - v_2) - (w_2 - v_2)(u_1 - v_1) \\ -(w_0 - v_0)(u_2 - v_2) + (w_2 - v_2)(u_0 - v_0) \\ (w_0 - v_0)(u_1 - v_1) - (w_1 - v_1)(u_0 - v_0) \end{pmatrix}$$

By symmetry, we consider the following two cases:

• *Case 1: The edges of the face F are in counterclockwise order $e_1(u)$, $e_2(v)$, $e_0(w)$ (see Fig. 43(a)).*

We have $v \in P_1(u)$, so $v \in R_0(u) \cap R_2(u)$ and $u \in R_1^\circ(v)$ (as there are no edges oriented in two directions). By Lemma 8, we have $R_0(v) \subseteq R_0(u)$, $R_2(v) \subseteq R_2(u)$, and $R_1(u) \subsetneq R_1(v)$. In fact, the first two inclusions are strict as $u \notin R_0(v) \cup R_2(v)$. So by Lemma 28, we have $v_0 < u_0$, $v_2 < u_2$, $u_1 < v_1$. We can prove similar inequalities for the other pairs of vertices and we obtain $w_0 < v_0 < u_0$, $u_1 < w_1 < v_1$, $v_2 < u_2 < w_2$. By just studying the signs of the different terms occurring in the values of the coordinates of $\overrightarrow{X}$, it is clear that $\overrightarrow{X}$ has strictly positive coordinates. (For the first coordinates, it is easier if written in the following form: $X_0 = (u_1 - w_1)(v_2 - w_2) - (u_2 - w_2)(v_1 - w_1)$.)

• *Case 2: The edges of the face F are in counterclockwise order $e_0(v)$, $e_2(v)$, $e_0(w)$ (see Fig. 43(b)).*

As in the previous case, one can easily obtain the following inequalities: $w_0 < v_0 < u_0$, $u_1 < w_1 < v_1$, $u_2 < v_2 < w_2$ (the only difference with case 1 is between u_2

and v_2). Exactly as in the previous case, it is clear that X_0 and X_2 are strictly positive. But there is no way to reformulate X_1 to have a similar proof. Let $A = w_2 - v_2$, $B = u_0 - v_0$, $C = v_0 - w_0$, and $D = v_2 - u_2$, so $X_1 = AB - CD$ and A, B, C, D are all strictly positive.

Vertices u, v, w are in the region $R(L_1, L_1')$ for L_1' a 1-line consecutive to L_1. We consider two cases depending on equality or not between $L_1(u)$ and $L_1(v)$.

⋆ *Subcase 2.1:* $L_1(u) = L_1(v)$.

We have $X_1 = A(B - D) + D(A - C)$.

We have $B - D = (u_0 + u_2) - (v_0 + v_2) = (v_1 - u_1) + (\sum u_i - \sum v_i)$. Since $u \in P_0(v)$, we have $L_0(u) = L_0(v)$. Suppose that $L_2(u) = L_2(v)$; then by Lemma 22, we have $\sum u_i = \sum v_i$, and thus $B - D = v_1 - u_1 > 0$. Suppose now that $L_2(u) \neq L_2(v)$. By Lemmas 22 and 33, $\sum u_i - \sum v_i > -t$. By Lemma 28, $v_1 - u_1 > (N - n)|R(L_2(u), L_2(v))| \geq N - n$. So $B - D > N - n - t \geq 0$.

We have $A - C = (w_0 + w_2) - (v_0 + v_2) = (v_1 - w_1) + (\sum w_i - \sum v_i) > \sum w_i - \sum v_i$. Suppose that $L_1(v) = L_1(w)$; then by Lemma 22, we have $\sum v_i = \sum w_i$ and thus $A - C = v_1 - w_1 > 0$. Then $X_1 > 0$. Suppose now that $L_1(v) \neq L_1(w)$. By Lemma 34, $D = v_2 - u_2 < |R(L_1, L_1')|$. By Lemma 28, $A = w_2 - v_2 > (N - n) \times |R(L_1, L_1')|$. By Lemmas 22 and 33, $\sum w_i - \sum v_i > -t$, so $A - C > -t$. Then $X_1 > (N - n - t)|R(L_1, L_1')| > 0$.

⋆ *Subcase 2.2:* $L_1(u) \neq L_1(v)$.

We have $X_1 = B(A - C) + C(B - D)$.

Suppose that $L_1(w) \neq L_1(v)$. Then $L_1(w) = L_1(u)$. By Lemma 34 $e_0(w)$ is going counterclockwise around the closed disk D bounded by $\{e_0(w)\} \cup P_1(w) \cup P_1(u)$. Then v is inside D and $P_1(v)$ has to intersect $P_1(w) \cup P_1(u)$, so $L_1(v) = L_1(u)$, contradicting our assumption. So $L_1(v) = L_1(w)$.

By Lemma 28, $B = u_0 - v_0 > (N - n)|R(L_1, L_1')|$. We have $A - C = (w_0 + w_2) - (v_0 + v_2) = (v_1 - w_1) + (\sum w_i - \sum v_i)$. By Lemma 22, we have $\sum v_i = \sum w_i$ and thus $A - C = v_1 - w_1 > 0$. By (the symmetric of) Lemma 34, $C = v_0 - w_0 < |R(L_1, L_1')|$. By Lemmas 22 and 33, $B - D = (u_0 + u_2) - (v_0 + v_2) = (v_1 - u_1) + (\sum u_i - \sum v_i) > -t$. So $X_1 > (N - n - t)|R(L_1, L_1')| > 0$. □

Let G be an essentially 3-connected toroidal map. Consider a periodic mapping of G^∞, embedded graph H (finite or infinite), and a face F of H. Denote $(f_1, f_2, \ldots, f_t)$ the counterclockwise facial walk around F. Given a mapping of the vertices of H in $\mathbb{R}^2$, we say that F is *correctly oriented* if for any triplet $1 \leq i_1 < i_2 < i_3 \leq t$, the points f_{i_1}, f_{i_2}, and f_{i_3} form a counterclockwise triangle. Note that a correctly oriented face is drawn as a convex polygon.

Lemma 36 *Let G be an essentially 3-connected toroidal map given with a periodic mapping of G^∞ such that every face of G^∞ is correctly oriented. This mapping gives a straight-line representation of G^∞.*

Proof We proceed by induction on the number of vertices n of G. Note that the theorem holds for $n = 1$, so we assume that $n > 1$. Given any vertex v of G, let $(u_0, u_1, \ldots, u_{d-1})$ be the sequence of its neighbors in counterclockwise order (subscript understood modulo d). Every face being correctly oriented, for every

$i \in [0, d-1]$ the oriented angle (oriented counterclockwise) $(\overrightarrow{vu_i}, \overrightarrow{vu_{i+1}}) < \pi$. Let the winding number k_v of v be the integer such that $2k_v\pi = \sum_{i\in[0,d-1]}(\overrightarrow{vu_i}, \overrightarrow{vu_{i+1}})$. It is clear that $k_v \geq 1$. Let us prove that $k_v = 1$ for every vertex v.

Claim 4 *For any vertex v, its winding number $k_v = 1$.*

Proof of Claim 4 In a flat torus representation of G, we can sum up all the angles by grouping them around the vertices or around the faces.

$$\sum_{v\in V(G)} \sum_{u_i\in N(v)} (\overrightarrow{vu_i}, \overrightarrow{vu_{i+1}}) = \sum_{F\in F(G)} \sum_{f_i\in F} (\overrightarrow{f_i f_{i-1}}, \overrightarrow{f_i f_{i+1}})$$

The faces being correctly oriented, they form convex polygons. Thus, the angles of a face F sum at $(|F|-2)\pi$.

$$\sum_{v\in V(G)} 2k_v\pi = \sum_{F\in F(G)} (|F|-2)\pi$$

$$\sum_{v\in V(G)} k_v = \frac{1}{2} \sum_{F\in F(G)} |F| - f$$

$$\sum_{v\in V(G)} k_v = m - f$$

So by Euler's formula $\sum_{v\in V(G)} k_v = n$, and thus $k_v = 1$ for every vertex v. This proves Claim 4. □

Let v be a vertex of G that minimizes the number of loops whose ends are on v. Thus, either v has no incident loop, or every vertex is incident to at least one loop.

Assume that v has no incident loop. Let v' be any copy of v in G^∞ and denote its neighbors $(u_0, u_1, \ldots, u_{d-1})$ in counterclockwise order. As $k_v = 1$, the points $u_0, u_1, \ldots, u_{d-1}$ form a polygon P containing the point v' and the segments $[v', u_i]$ for any $i \in [0, d-1]$. It is well known that any polygon admits a partition into triangles by adding some of the chords. Let us call O the outerplanar graph with outer boundary $(u_0, u_1, \ldots, u_{d-1})$, obtained by this "triangulation" of P. Let us now consider the toroidal map $G' = (G \setminus \{v\}) \cup O$ and its periodic embedding obtained from the mapping of G^∞ by removing the copies of v. It is easy to see that in this embedding every face of G' is correctly oriented (including the inner faces of O, or the faces of G that have been shortened by an edge u_iu_{i+1}). Thus by the induction hypothesis, the mapping gives a straight-line representation of G'^∞. It is also a straight-line representation of G^∞ minus the copies of v where the interiors of each copy of the polygons P are pairwise disjoint and do not intersect any vertex or edge. Thus, one can add the copies of v on their initial positions and add the edges with their neighbors without intersecting any edge. The obtained drawing is thus a straight-line representation of G^∞.

Assume now that every vertex is incident to at least one loop. Since these loops are non-contractible and do not cross each other, they form homothetic cycles. Thus, G is as depicted in Fig. 44, where the dotted segments stand for edges that may be in G but not necessarily. Since the mapping is periodic, the edges corresponding to

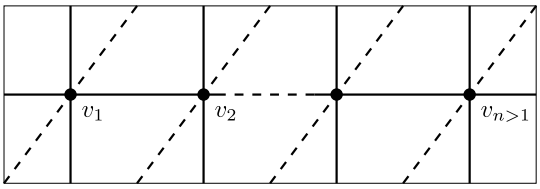

Fig. 44 The graph G if every vertex is incident to a loop

loops of G form several parallel lines, cutting the plane into infinite strips. Since for any $1 \leq i \leq n$, $k_{v_i} = 1$, a line of copies of v_i divides the plane, in such a way that their neighbors which are copies of v_{i-1} and their neighbors which are copies of v_{i+1} are in distinct half-planes. Thus, adjacent copies of v_i and v_{i+1} are on two lines bounding a strip. Then one can see that the edges between copies of v_i and v_{i+1} are contained in this strip without intersecting each other. Thus, the obtained mapping of G^∞ is a straight-line representation. □

A plane is *positive* if it has equation $\alpha x + \beta y + \gamma z = 0$ with $\alpha, \beta, \gamma \geq 0$.

Theorem 16 *If G is a toroidal triangulation given with a Schnyder wood, and V^∞ the set of region vectors of vertices of G^∞, then the projection of V^∞ on a positive plane gives a straight-line representation of G^∞.*

Proof Let $\alpha, \beta, \gamma \geq 0$ and consider the projection of V^∞ on the plane P of the equation $\alpha x + \beta y + \gamma z = 0$. A normal vector of the plane is given by the vector $\overrightarrow{n} = (\alpha, \beta, \gamma)$. Consider a face F of G^∞. Suppose that F is incident to vertices u, v, w (given in counterclockwise order around F). By Lemma 35, $(\overrightarrow{uv} \wedge \overrightarrow{uw}).\overrightarrow{n}$ is positive. Thus, the projection of the face F on P is correctly oriented. So by Lemma 36, the projection of V^∞ on P gives a straight-line representation of G^∞. □

Theorems 1 and 16 imply Theorem 4. Indeed, any toroidal graph G can be transformed into a toroidal triangulation G' by adding a linear number of vertices and edges and such that G' is simple if and only if G is simple (see for example the proof of Lemma 2.3 of [21]). Then by Theorem 1, G' admits a Schnyder wood. By Theorem 16, the projection of the set of region vectors of vertices of G'^∞ on a positive plane gives a straight-line representation of G'^∞. The grid where the representation is obtained can be the triangular grid, if the projection is done on the plane of equation $x + y + z = 0$, or the square grid, if the projection is done on one of the planes of equations $x = 0$, $y = 0$, or $z = 0$. By Lemma 30, and the choice of N, the obtained mapping is a periodic mapping of G^∞ with respect to non-collinear vectors Y and Y' where the size of these vectors is in $\mathcal{O}(\gamma^2 n^2)$ with $\gamma \leq n$ in general and $\gamma = 1$ if the graph is simple and the Schnyder wood obtained by Theorem 9. By Lemma 29, the lengths of the edges in this representation are in $\mathcal{O}(n^3)$ in general and in $\mathcal{O}(n^2)$ if the graph is simple. When the graph is not simple, there is a non-contractible cycle of length 1 or 2 and thus the size of one of the two vectors Y, Y' is in $\mathcal{O}(n^3)$. Thus, the grid obtained in Theorem 4 has size in $\mathcal{O}(n^3) \times \mathcal{O}(n^4)$ in general and $\mathcal{O}(n^2) \times \mathcal{O}(n^2)$ if the graph is simple.

The method presented here gives a polynomial algorithm to obtain flat torus straight-line representations of any toroidal maps in polynomial size grids. Indeed, all the proofs lead to polynomial algorithms, even the proof of Theorem 8 [13], which uses results from Robertson and Seymour [25] on disjoint paths problems.

It would be nice to extend Theorem 16 to obtain convex straight-line representations for essentially 3-connected toroidal maps.

13 Conclusion

We have proposed a generalization of Schnyder woods to toroidal maps with application to graph drawing. Along these lines, several questions were raised. We recall some briefly:

- Does the set of Schnyder woods of a given toroidal map have a kind of lattice structure?
- Does any simple toroidal triangulation admit a Schnyder wood where the set of edges of each color induces a connected subgraph?
- Is it possible to use Schnyder woods to embed the universal cover of a toroidal map on rigid or coplanar orthogonal surfaces?
- Which toroidal maps admit (primal-dual) contact representation by (homothetic) triangles in a flat torus?
- Can geodesic embeddings be used to obtain convex straight-line representations for essentially 3-connected toroidal maps?

The guideline of Castelli Aleardi et al. [3] to generalize Schnyder woods to higher genus was to preserve the tree structure of planar Schnyder woods and to use this structure for efficient encoding. For that purpose they introduce several special rules (even in the case of genus 1). Our main guideline while working on this paper was that the surface of genus 1, the torus, seems to be the perfect surface to define Schnyder woods. Euler's formula gives exactly $m = 3n$ for toroidal triangulations. Thus, a simple and symmetric object can be defined by relaxing the tree constraint. For genus 0, the plane, there are not enough edges in planar triangulations to have out-degree three for every vertex. For higher genus (the double torus, ...) there are too many edges in triangulations. An open problem is to find what would be the natural generalization of our definition of toroidal Schnyder woods to higher genus.

The results presented here motivated Castelli Aleardi and Fusy [4] to develop direct methods to obtain straight-line representations for toroidal maps. They manage to generalize planar canonical ordering to the cylinder to obtain straight-line representations of simple toroidal triangulations in grids of size $\mathcal{O}(n) \times \mathcal{O}(n^2)$, thus improving the size of our grid, which is $\mathcal{O}(n^2) \times \mathcal{O}(n^2)$ in the case of a simple toroidal map. It should be interesting to investigate further the links between the two methods, as canonical orderings are strongly related to Schnyder woods.

Planar Schnyder woods appear to have many applications in various areas like enumeration [1], compact coding [24], representation by geometric objects [14, 16], graph spanners [2], graph drawing [7, 18], etc. In this paper we use a new definition of Schnyder wood for graph drawing purposes, and it would also be interesting to see if it can be used in other computer science domains.

Acknowledgements The authors thank Nicolas Bonichon, Luca Castelli Aleardi, and Eric Fusy for fruitful discussions about this work. They also thank student Chloé Desdouits for developing a software to visualize orthogonal surfaces.

References

1. Bonichon, N.: A bijection between realizers of maximal plane graphs and pairs of non-crossing Dyck paths. Discrete Math. **298**, 104–114 (2005)
2. Bonichon, N., Gavoille, C., Hanusse, N., Ilcinkas, D.: Connections between Theta-graphs, Delaunay triangulations, and orthogonal surfaces. In: Proceeding WG'10 Proceedings of the 36th International Conference on Graph-Theoretic Concepts in Computer Science, pp. 266–278. Springer, Berlin (2010)
3. Castelli Aleardi, L., Fusy, E., Lewiner, T.: Schnyder woods for higher genus triangulated surfaces, with applications to encoding. Discrete Comput. Geom. **42**, 489–516 (2009)
4. Castelli Aleardi, L., Fusy, E.: Canonical ordering for triangulations on the cylinder, with applications to periodic straight-line drawings. In: Proceeding GD'12 Proceedings of the 20th International Conference on Graph Drawing, pp. 376–387. Springer, Berlin (2012)
5. Chambers, E., Eppstein, D., Goodrich, M., Löffler, M.: Drawing graphs in the plane with a prescribed outer face and polynomial area. Lect. Notes Comput. Sci. **6502**, 129–140 (2011)
6. Duncan, C., Goodrich, M., Kobourov, S.: Planar drawings of higher-genus graphs. J. Graph Algorithms Appl. **15**, 13–32 (2011)
7. Felsner, S.: Convex drawings of planar graphs and the order dimension of 3-polytopes. Order **18**, 19–37 (2001)
8. Felsner, S.: Geodesic embeddings and planar graphs. Order **20**, 135–150 (2003)
9. Felsner, S.: Lattice structures from planar graphs. Electron. J. Comb. **11**(1), R15 (2004)
10. Felsner, S., Trotter, W.T.: Posets and planar graphs. J. Graph Theory **49**, 273–284 (2005)
11. Felsner, S., Zickfeld, F.: Schnyder woods and orthogonal surfaces. Discrete Comput. Geom. **40**, 103–126 (2008)
12. Felsner, S.: Geometric Graphs and Arrangements. Vieweg, Wiesbaden (2004)
13. Fijavz, G.: Personal communication (2011)
14. de Fraysseix, H., Ossona de Mendez, P., Rosenstiehl, P.: On triangle contact graphs. Comb. Probab. Comput. **3**, 233–246 (1994)
15. de Fraysseix, H., Ossona de Mendez, P.: On topological aspects of orientations. Discrete Math. **229**, 57–72 (2001)
16. Gonçalves, D., Lévêque, B., Pinlou, A.: Triangle contact representations and duality. Discrete Comput. Geom. **48**, 239–254 (2012)
17. Gonçalves, D., Lévêque, B., Pinlou, A.: Triangle contact representations and duality (GD'10). Lect. Notes Comput. Sci. **6502**, 262–273 (2011)
18. Kant, G.: Drawing planar graphs using the canonical ordering. Algorithmica **16**, 4–32 (1996)
19. Kratochvíl, J.: In: Bertinoro Workshop on Graph Drawing (2007)
20. Miller, E.: Planar graphs as minimal resolutions of trivariate monomial ideals. Doc. Math. **7**, 43–90 (2002)
21. Mohar, B.: Straight-line representations of maps on the torus and other flat surfaces. Discrete Math. **155**, 173–181 (1996)
22. Rosenstiehl, P.: Embedding in the plane with orientation constraints: The angle graph. Annals New York Academy of Sciences (1989)
23. Mohar, B., Rosenstiehl, P.: Tessellation and visibility representations of maps on the torus. Discrete Comput. Geom. **19**, 249–263 (1998)
24. Poulalhon, D., Schaeffer, G.: Optimal coding and sampling of triangulations. Algorithmica **46**, 505–527 (2006)
25. Robertson, N., Seymour, P.D.: Graph minors. VI. Disjoint paths across a disc. J. Comb. Theory, Ser. B **41**, 115–138 (1986)
26. Schnyder, W.: Planar graphs and poset dimension. Order **5**, 323–343 (1989)

Discrete Comput Geom (2017) 57:507–544
DOI 10.1007/s00454-016-9832-0

Encoding Toroidal Triangulations

Vincent Despré[1] · **Daniel Gonçalves**[2] · **Benjamin Lévêque**[3]

Received: 12 November 2015 / Revised: 16 September 2016 / Accepted: 27 September 2016 /
Published online: 26 October 2016

Abstract Poulalhon and Schaeffer introduced an elegant method to linearly encode a planar triangulation optimally. The method is based on performing a special depth-first search algorithm on a particular orientation of the triangulation: the minimal Schnyder wood. Recent progress toward generalizing Schnyder woods to higher genus enables us to generalize this method to the toroidal case. In the plane, the method leads to a bijection between planar triangulations and some particular trees. For the torus we obtain a similar bijection but with particular unicellular maps (maps with only one face).

Keywords Toroidal triangulations · Schnyder woods · Alpha-orientations · Distributive lattices · Poulalhon and Schaeffer's method · Unicellular maps · Bijective encoding

Mathematics Subject Classification 05C10 · 05C30 · 05A19 · 68R10 · 06D99

Editor in Charge: János Pach

Vincent Despré
vincent.despre@gipsa-lab.fr

Daniel Gonçalves
daniel.goncalves@lirmm.fr

Benjamin Lévêque
benjamin.leveque@cnrs.fr

1 GIPSA-Lab, University Grenoble Alpes, Grenoble, France

2 CNRS, LIRMM, University Montpellier, Montpellier, France

3 CNRS, G-SCOP, University Grenoble Alpes, Grenoble, France

1 Introduction

A graph embedded on a surface is called a *map* on this surface if all its faces are homeomorphic to open disks. A map is a triangulation if all its faces have length three. A closed curve on a surface is *contractible* if it can be continuously transformed into a single point. Given a graph embedded on a surface, a *contractible loop* is an edge forming a contractible curve. Two edges of an embedded graph are called *homotopic multiple edges* if they have the same extremities and their union encloses a region homeomorphic to an open disk. In this paper, we restrict ourself to graphs embedded on surfaces that do not have contractible loops nor homotopic multiple edges. Note that this is a weaker assumption, than the graph being *simple*, i.e. not having loops nor multiple edges. In this paper we distinguish cycles from closed walk as cycles have no repeated vertices. A *triangle* of a map is a closed walk of length three enclosing a region that is homeomorphic to an open disk. This region is called the *interior* of the triangle. Note that a triangle is not necessarily a face of the map as its interior may be not empty. Note also that a triangle is not necessarily a cycle since non-contractible loops are allowed. We denote by n the number of vertices, m the number of edges and f the number of faces of a given map.

Poulalhon and Schaeffer introduced in [20] a method (called here PS method for short) to linearly encode a planar triangulation with a binary word of length $\log_2 \binom{4n}{n} \sim n \log_2 \left(\frac{256}{27}\right) \approx 3.2451\, n$ bits. This is asymptotically optimal since it matches the information theory lower bound. The method is the following. Given a planar triangulation G, it considers the minimal *Schnyder wood* of G (that is the orientation where all inner vertices have outdegree 3 and that contains no cycle oriented clockwise). Then a special depth-first search algorithm is applied by "following" ingoing edges and "cutting" outgoing ones. The algorithm outputs a rooted spanning tree with exactly two leaves (also called stems) on each vertex from which the original triangulation can be recovered in a straightforward way. This tree can be encoded very efficiently. A nice aspect of this work, besides its interesting encoding properties, is that the method gives a bijection between planar triangulations and a particular type of plane trees.

Aleardi et al. [3] adapt PS method to encode planar triangulations with boundaries. A consequence is that a triangulation of any oriented surface can be encoded by cutting the surface along non-contractible cycles and see the surface as a planar map with boundaries. This method is a first attempt to generalize PS algorithm to higher genus. The obtained algorithm is asymptotically optimal (in terms of number of bits) but it is not linear, nor bijective.

The goal of this paper is to present a new generalization of PS algorithm to higher genus based on some strong structural properties. Applied on a well chosen orientation of a toroidal triangulation, what remains after the execution of the algorithm is a *unicellular map*, i.e. a map with only one face (which corresponds to the natural generalization of trees when going to higher genus, see [7,8]), that can be encoded optimally using $3.2451\, n$ bits. Moreover, the algorithm can be performed in linear time and leads to a new bijection between toroidal triangulations and a particular type of unicellular maps.

The two main ingredients that make PS algorithm work in an orientation of a planar map are minimality and accessibility of the orientation. *Minimality* means that there is no clockwise cycle. *Accessibility* means that there exists a root vertex such that all the vertices have an oriented path directed toward the root vertex. Given $\alpha : V \to \mathbb{N}$, an orientation of G is an α-orientation if for every vertex $v \in V$ its outdegree $d^+(v)$ equals $\alpha(v)$. The existence and uniqueness of minimal orientations in the plane is given by the following result of Felsner [12] (related to older results of Propp [21] and de Mendez [10]): the set of α-orientations of a given planar map carries a structure of distributive lattice. This gives the existence and uniqueness of a minimal α-orientation as soon as an α-orientation exists. Felsner's result enables several analogues of PS method to other kind of planar maps, see [2,4,11]. In all these cases the accessibility of the considered α-orientations is a consequence of the natural choice of α, like in Poulalhon and Schaeffer's original work [20] where any orientation of the inner edges of a planar triangulation with inner vertices having outdegree 3 is accessible for any choice of root vertex on the outer face. (Note that the conventions may differs in the literature: the role of outgoing and incoming edges are sometimes exchanged and/or the role of clockwise and counterclockwise.)

For higher genus, the minimality can be obtained by the following generalization of Felsner's result. The second author, Knauer and the third author [16] showed that on any oriented surface the set of orientations of a given map having the same homology carries a structure of distributive lattice. Note that α has been removed here since it is captured by the homology (see Sect. 2 for a brief introduction to homology). Note also that this result is equivalent to an older result of Propp [21] where the lattice structure is described in the dual setting. Since this result is very general, there is hope to be able to further generalize PS method to other oriented surfaces. Note that a given map on an oriented surface can have several α-orientations (for the same given α) that are not homologous. So the set of α-orientations of a given map is now partitioned into distributive lattices contrarily to the planar case where there is only one lattice (and thus only one minimal element). In the case of toroidal triangulations we manage to face this problem and maintain a bijection by recent results on the structure of 3-*orientations* of toroidal triangulations (i.e. α-orientation such that $\alpha(v) = 3$ for all vertices v). We identify a special lattice (and thus a special minimal orientation) using the notion of Schnyder woods generalized to the torus by the second and third author in [15] (further generalized in [16], see also [18] for a unified presentation).

The main issue while trying to extend PS algorithm to higher genus is the accessibility. Accessibility toward the outer face is given almost for free in the planar case because of Euler's formula that sums to a strictly positive value. For an oriented surface of genus $g \geq 1$ new difficulties occur. Already in genus 1 (the torus), even if the orientation is minimal and accessible PS algorithm can visit all the vertices but not all the angles of the map because of the existence of non-contractible cycles. We can show that the special minimal orientation that we choose has the nice property that this problem never occurs. In genus $g \geq 2$ things get even more difficult with separating non-contractible cycles that make having accessibility of the vertices already difficult to obtain.

Another problem is to recover the original map after the execution of the algorithm. If what remains after the execution of PS method is a spanning unicellular map then the map can be recovered with the same simple rules as in the plane. Unfortunately for

many minimal orientations the algorithm leads to a spanning unicellular embedded graph that is not a map (the only face is not a disk) and it is not possible to directly recover the original map. Here again, the choice of our special orientation ensures that this never happens.

Finally the method presented here can be implemented in linear time. Clearly the execution of PS algorithm is linear but the difficulty lies in providing the algorithm with the appropriate orientation in input. Computing the minimal Schnyder wood of a planar triangulation can be done in linear time quite easily by using a so-called shelling order (or canonical order, see [17]). Other similar ad-hoc linear algorithms can sometimes be found for other kinds of α-orientations of planar maps (see for example [13, Chap. 3]). Such methods are not known in higher genus. We solve this problems by first computing an orientation in our special lattice and then go down in the lattice to find the minimal orientation. All this can be performed in linear time.

A brief introduction to homology and to the corresponding terminology used in the paper is given in Sect. 2. In Sect. 3, we present the definitions and results we need concerning the generalization of Schnyder woods to the toroidal case. In Sect. 4, we introduce a reformulation of Poulalhon and Schaeffer's original algorithm that is applicable to any orientation of any map on an oriented surface. The main theorem of this paper is proved in Sect. 5, that is, for a toroidal triangulation given with an appropriate root and orientation, the output of the algorithm is a toroidal spanning unicellular map. In Sect. 6, we show how one can recover the original triangulation from the output. This output is then used in Sect. 7 to optimally encode a toroidal triangulation. The linear time complexity of the method is discussed in Sect. 8. In Sect. 9 (resp. Sect. 11), we exhibit a bijection between appropriately rooted toroidal triangulations and rooted (resp. non-rooted) toroidal unicellular maps. To obtain the non-rooted bijection, further structural results concerning the particular Schnyder woods considered in this paper are given in Sect. 10. Finally, a possible generalization to higher genus is discussed in Sect. 12.

2 A Bit of Homology

We need a bit of surface homology of general maps, which we discuss now. The presentation is not standard but it is short and sufficient to fit our needs. For a deeper introduction to homology we refer to [14].

Consider a map G with edge set E, on an orientable surface of genus g, given with an arbitrary orientation of its edges. This fixed arbitrary orientation is implicit and is used to manipulate flows. A *flow* ϕ on G is a vector in $\mathbb{Z}^E$. For any $e \in E$, we denote by ϕ_e the coordinate e of ϕ.

A *walk* W of G is a sequence of edges with a direction of traversal such that the ending point of an edge is the starting point of the next edge. A walk is *closed* if the start and end vertices coincide. A walk has a *characteristic flow* $\phi(W)$ defined by

$$\phi(W)_e := \text{times } W \text{ traverses } e \text{ forward} - \text{times } W \text{ traverses } e \text{ backward.}$$

This definition naturally extends to sets of walks. From now on we consider that a set of walks and its characteristic flow are the same object. We do similarly for oriented subgraphs as they can be seen as sets of walks.

A *facial walk* is a closed walk bounding a face. Let $\mathcal{F}$ be the set of counterclockwise facial walks and let $\mathbb{F} = \langle \phi(\mathcal{F}) \rangle$ the subgroup of $\mathbb{Z}^E$ generated by $\mathcal{F}$. Two flows ϕ, ϕ' are said to be *homologous* if $\phi - \phi' \in \mathbb{F}$. A flow ϕ is 0-homologous if it is homologous to the zero flow, i.e. $\phi \in \mathbb{F}$.

Let $\mathcal{W}$ be the set of *closed* walks and let $\mathbb{W} = \langle \phi(\mathcal{W}) \rangle$ the subgroup of $\mathbb{Z}^E$ generated by $\mathcal{W}$. The group $H(G) = \mathbb{W}/\mathbb{F}$ is the *first homology group* of G. Since $\dim(\mathbb{W}) = m - n + 1$ and $\dim(\mathbb{F}) = f - 1$, Euler's Formula gives $\dim(H(G)) = 2g$. So $H(G) \cong \mathbb{Z}^{2g}$ only depends on the genus of the map. A set $(B_1, \ldots, B_{2g})$ of (closed) walks of G is said to be a *basis for the homology* if $(\phi(B_1), \ldots, \phi(B_{2g}))$ is a basis of $H(G)$.

3 Toroidal Schnyder Woods

Schnyder [22] introduced Schnyder woods for planar triangulations using the following local property:

Given a map G, a vertex v and an orientation and coloring of the edges incident to v with the colors 0, 1, 2, we say that a vertex v satisfies the *Schnyder property* if (see Fig. 1):

- Vertex v has out-degree one in each color.
- The edges $e_0(v)$, $e_1(v)$, $e_2(v)$ leaving v in colors 0, 1, 2, respectively, occur in counterclockwise order.
- Each edge entering v in color i enters v in the counterclockwise sector from $e_{i+1}(v)$ to $e_{i-1}(v)$ (where $i + 1$ and $i - 1$ are understood modulo 3).

Given a planar triangulation G, a (*planar*) *Schnyder wood* of G is an orientation and coloring of the inner edges of G with the colors 0, 1, 2, where each inner vertex v satisfies the *Schnyder property*. In [15,16] (see also the HDR thesis of the third author [18]) a generalization of Schnyder woods for higher genus has been proposed. Since this paper deals with triangulations of the torus only, we use a simplified version of the definitions and results from [15,16,18]).

The definition of Schnyder woods for toroidal triangulations is the following. Given a toroidal triangulation G, a (*toroidal*) *Schnyder wood* of G is an orientation and coloring of the edges of G with the colors 0, 1, 2, where each vertex satisfies the Schnyder property (see Fig. 2 for an example). The three colors 0, 1, 2 are completely symmetric in the definition, thus we consider that two Schnyder woods that are obtained one

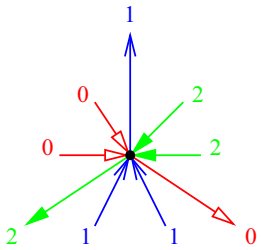

Fig. 1 The Schnyder property. The correspondence between *red*, *blue*, *green* and 0, 1, 2 and the *arrow shapes* used here serves as a convention for all figures in the paper

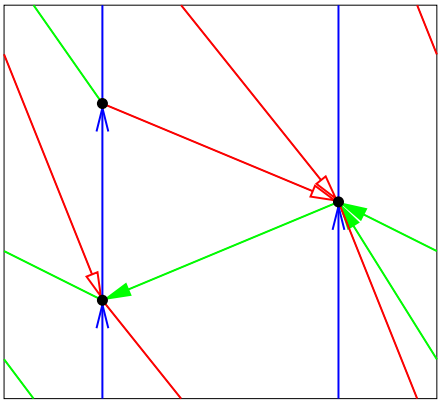

Fig. 2 A Schnyder wood of a toroidal triangulation (opposite sides are identified in order to form a torus)

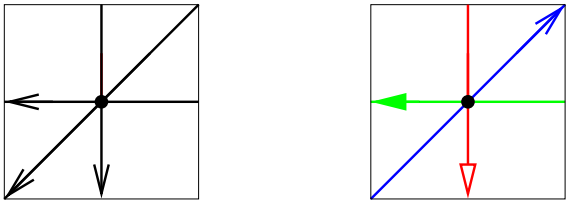

Fig. 3 Two different orientations of a toroidal triangulation. Only the one on the *right* corresponds to a Schnyder wood

from the other by a (cyclic) permutation of the colors are in fact the same object. We consider that a Schnyder wood and its underlying orientation are the same object since one can easily recover a coloring of the edges in a greedy way (by choosing the color of an edge arbitrarily and then satisfying the Schnyder property at every vertex).

Note that the situation is quite different from the planar case. In a Schnyder wood of a toroidal triangulation, each vertex has exactly one outgoing arc in each color, so there are monochromatic cycles contrarily to the planar case (one can show that these monochromatic cycles are non-contractible). Moreover the graph induced by one color is not necessarily connected. Also, by a result of de Fraysseix and de Mendez [9], there is a bijection between orientations of the internal edges of a planar triangulation where every inner vertex has outdegree 3 and Schnyder woods. Thus, in the planar case, any orientation with the proper outdegrees corresponds to a Schnyder wood. This is not true for toroidal triangulations since there exists 3-orientations that do not correspond to a Schnyder wood (see Fig. 3).

A Schnyder wood of a toroidal triangulation is said to be *crossing*, if for each pair i, j of different colors, there exists a monochromatic cycle of color i intersecting a monochromatic cycle of color j. The existence of crossing Schnyder woods is proved in [15, Thm. 1] (note that in [15] the crossing property is included in the definition of Schnyder woods, see [18] for a unified presentation):

Theorem 1 [15] *A toroidal triangulation admits a crossing Schnyder wood.*

Figure 4 depicts two different Schnyder woods of the same graph where just the one on the left is crossing (on the right case the red and green monochromatic cycles do not intersect, we say that the Schnyder wood is "half-crossing" since blue crosses

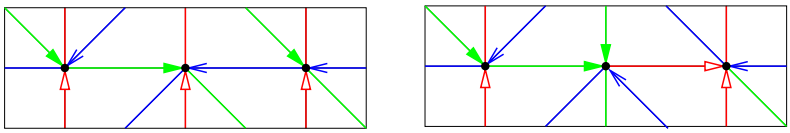

Fig. 4 A crossing and an half-crossing Schnyder wood

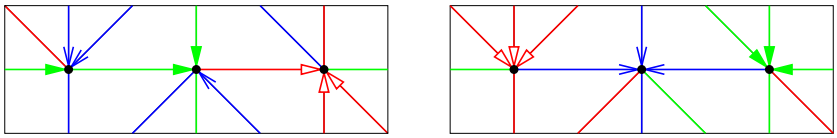

Fig. 5 Non-crossing Schnyder woods

both green and red, see [16,18] for a formal definition). Note that the Schnyder wood on the right is obtained from the one on the left by flipping a clockwise triangle into a counterclockwise triangle.

Consider a toroidal triangulation G given with a crossing Schnyder wood. Let D_0 be the corresponding 3-orientation of G. Let $O(G)$ be the set of all the orientations of G that are homologous to D_0. A consequence of [16] is that all the crossing Schnyder woods of G are homologous to each other. So $O(G)$ contains all the crossing Schnyder woods of G. Thus the definition of $O(G)$ does not depend on the particular choice of D_0 and thus it is uniquely defined. Another consequence of [16] is that every orientation of $O(G)$ corresponds to a Schnyder wood. Thus we call the elements of $O(G)$ the *homologous-to-crossing Schnyder woods* (or *HTC Schnyder woods* for short). Note that all the crossing Schnyder woods are HTC.

Figure 5 gives an example of an HTC Schnyder wood that is not crossing and a Schnyder woods that is not HTC. The example on the left is obtained from the crossing Schnyder wood of Fig. 4 by flipping two triangles (one to obtain the half-crossing Schnyder wood of Fig. 4 and then another one flipped from counterclockwise to clockwise). Thus it is HTC since the difference with a crossing Schnyder wood is a 0-homologous oriented subgraph. The example on the right of Fig. 5 is obtained from the crossing Schnyder wood of Fig. 4 by reversing the three vertical red monochromatic cycles. The union of these three cycles is not a 0-homologous oriented subgraph, thus the resulting orientation is not HTC.

Let us now define briefly what a lattice is. Consider a partial order $\leq$ on a set S. Given two elements x, y of S, let $m(x, y)$ (resp. $M(x, y)$) be the set of elements z of S such that $z \leq x$ and $z \leq y$ (resp. $z \geq x$ and $z \geq y$). If $m(x, y)$ (resp. $M(x, y)$) is not empty and admits a unique maximal (resp. minimal) element, we say that x and y admit a *meet* (resp. a *join*), noted $x \vee y$ (resp. $x \wedge y$). Then $(S, \leq)$ is a *lattice* if any pair of elements of S admits a meet and a join. Thus in particular a lattice has a unique minimal (resp. maximal) element. A lattice is *distributive* if the two operators $\vee$ and $\wedge$ are distributive on each other.

It is proved in [16] that on any oriented surface the set of orientations of a given map having the same homology carries a structure of distributive lattice for a particular order defined below. Thus in particular the set of HTC Schnyder woods carries a structure of distributive lattice.

Let us define an order on the orientations of G. For that purpose, choose an arbitrary face f_0 of G and let F_0 be its counterclockwise facial walk (this choice of a particular face corresponds to the choice of the outer face in the planar case). Let $\mathcal{F}$ be the set of counterclockwise facial walks of G and $\mathcal{F}' = \mathcal{F} \setminus F_0$. We say that a 0-homologous oriented subgraph T of G is *counterclockwise* (resp. *clockwise*) w.r.t. f_0, if its characteristic flow can be written as a combination with positive (resp. negative) coefficients of characteristic flows of $\mathcal{F}'$, i.e. $\phi(T) = \sum_{F\in\mathcal{F}'} \lambda_F \phi(F)$, with $\lambda \in \mathbb{N}^{|\mathcal{F}'|}$ (resp. $-\lambda \in \mathbb{N}^{|\mathcal{F}'|}$). Given two orientations D and D' of G, let $D \setminus D'$ denote the subgraph of D induced by the edges that are not oriented as in D'. We set $D \leq_{f_0} D'$ if and only if $D \setminus D'$ is counterclockwise. In [16, Thm. 7] the following is proved:

Theorem 2 [16] *$(O(G), \leq_{f_0})$ is a distributive lattice.*

Since $(O(G), \leq_{f_0})$ is a distributive lattice, it has a unique minimal element. The following lemma gives a property of this minimum that is essential to apply Poulalhon and Schaeffer's method.

Lemma 1 *The minimal element of $(O(G), \leq_{f_0})$ is the only HTC Schnyder wood that contains no clockwise (non-empty) 0-homologous oriented subgraph w.r.t. f_0.*

Proof Let $D_{\min}$ be the minimal element of $(O(G), \leq_{f_0})$. Suppose by contradiction that $D_{\min}$ contains a clockwise non-empty 0-homologous oriented subgraph T w.r.t. f_0. The orientation of G obtained from $D_{\min}$ by reversing all the edges of T gives an orientation $D \in O(G)$ such that $T = D_{\min} \setminus D$. Furthermore, by definition of $\leq_{f_0}$, we have $D \leq_{f_0} D_{\min}$, a contradiction to the minimality of $D_{\min}$. So $D_{\min}$ contains no clockwise non-empty 0-homologous oriented subgraph w.r.t. f_0.

We now show that this characterizes $D_{\min}$. For any $D \in O(G)$, distinct from $D_{\min}$, we have $D_{\min} \leq_{f_0} D$. Thus $T = D \setminus D_{\min}$ is a non-empty clockwise 0-homologous oriented subgraph of D. □

The crossing Schnyder wood of Fig. 6 is the minimal HTC Schnyder wood for the choice of f_0 corresponding to the shaded face. This example is used in the next sections to illustrate Poulalhon and Schaeffer's method.

The two HTC Schnyder woods of Fig. 4 are not minimal (for any choice of special face f_0) since they contain several triangles that are oriented clockwise. On the contrary, the HTC Schnyder wood of Fig. 5 is minimal w.r.t to its only face oriented clockwise. These examples shows that the minimal HTC Schnyder wood is not always crossing.

We define the dual orientation D^* of an orientation D of G as an orientation of the edges of the dual map G^* of G satisfying the following rule: the dual e^* of an edge e goes from the face on the left of e to the face on the right of e. The following lemma gives the key property of HTC Schnyder woods that we need in this paper:

Lemma 2 *If D is an orientation corresponding to an HTC Schnyder wood, then the dual orientation D^* contains no oriented non-contractible cycle.*

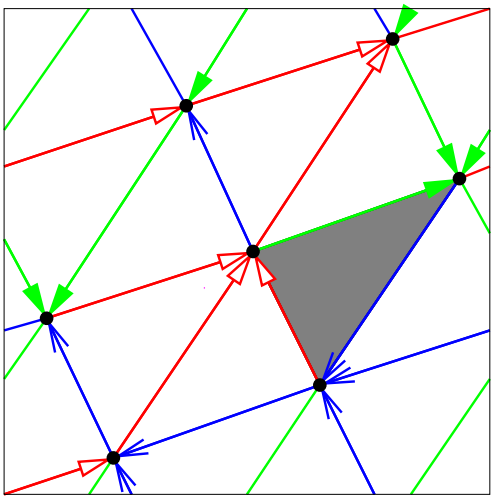

Fig. 6 The minimal HTC Schnyder wood of K_7 w.r.t. the shaded face

Proof We first prove the property for a crossing Schnyder wood and then show that it is stable by reversing a 0-homologous oriented subgraph. Thus it is true for all HTC Schnyder woods.

Consider a crossing Schnyder wood of G by Theorem 1 and let D_0 be the corresponding orientation. For $i \in \{0, 1, 2\}$, let C_i be a monochromatic cycle of color i. In a crossing Schnyder wood, the monochromatic cycles are not contractible and any two monochromatic cycles of different colors are not homologous and intersecting [15]. Thus for any $i \in \{0, 1, 2\}$, the two cycles C_{i-1} and C_{i+1} generate the homology of the torus with respect to $\mathbb{Q}$. That is, for any curve C and $i \in \{0, 1, 2\}$, there exists $(k, k_{i-1}, k_{i+1}) \in \mathbb{Z}^3$, $k \neq 0$, such that kC is homologous to $k_{i-1}B_{i-1} + k_{i+1}B_{i+1}$. By the Schnyder property, the cycle C_{i-1} is crossing C_i (maybe several time) from left to right so there exists $\alpha_1, \alpha_2, \alpha_3 \in \mathbb{N}$, such that $\sum \alpha_i C_i$ is 0-homologous. Thus for any curve C there exists $i \in \{0, 1, 2\}$, $(k, k_{i-1}, k_{i+1}) \in \mathbb{N}^3$, $k \neq 0$, $k_{i-1} \neq 0$, such that kC is homologous to $k_{i-1}B_{i-1} + k_{i+1}B_{i+1}$.

Suppose now by contradiction that D_0^* contains an oriented non-contractible cycle C^*. Let $i \in \{0, 1, 2\}$, $(k, k_{i-1}, k_{i+1}) \in \mathbb{N}^3$, $k \neq 0$, $k_{i-1} \neq 0$, such that kC^* is homologous to $k_{i-1}C_{i-1} + k_{i+1}C_{i+1}$. Then C_{i+1} is crossing C^* at least once from left to right, contradicting the fact that C^* is an oriented cycle of D_0^*. So D_0^* contains no oriented non-contractible cycle.

Consider now a HTC Schnyder wood of G and let D be the corresponding orientation. Since D and D_0 are both element of $O(G)$ they are homologous to each other. Let T be the 0-homologous oriented subgraph of D such that $T = D \setminus D_0$. Thus D_0 is obtained from D by reversing the edges of T.

Suppose by contradiction that D^* contains an oriented non-contractible cycle C^*. The oriented subgraph T is 0-homologous thus it intersects C^* exactly the same number of time from right to left than from left to right. Since C^* is oriented foward, T cannot intersect it from left to right. So T does not intersect C^* at all. Thus reversing T to go from D to D_0 does not affect C^*. Thus C^* is an oriented non-contractible cycle of D_0^*, a contradiction. □

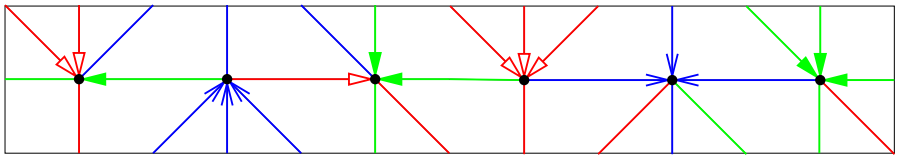

Fig. 7 A Schnyder wood that is not HTC but contains no oriented non-contractible cycle in the dual

For the non-HTC Schnyder wood of Fig. 5, one can see that there is an horizontal oriented non-contractible cycle in the dual, so it does not satisfy the conclusion of Lemma 2. Note that this property is not a characterization of being HTC. Figure 7 is a Schnyder wood that is not HTC but satisfies the conclusion of Lemma 2 (we leave the reader check that this Schnyder wood is not HTC, it will be easier after Sect. 9 and the definition of γ).

4 Poulalhon and Schaeffer's Algorithm on Oriented Surfaces

In this section we introduce a reformulation of Poulalhon and Schaeffer's original algorithm. This version is more general in order to be applicable to any orientation of any map on an oriented surface. The execution slightly differs from the original formulation, even on planar triangulations. In [20], the authors first delete some outer edges of the triangulation before executing the algorithm. We do not consider some edges to be special here since we want to apply the algorithm on any surface but the core of the algorithm is the same. We show general properties of the algorithm in this section before considering toroidal triangulations in the forthcoming sections.

ALGORITHM PS

INPUT : An oriented map G on an oriented surface S, a root vertex v_0 and a root edge e_0 incident to v_0.

OUTPUT : A graph U with stems, embedded on the oriented surface S.

The algorithm explores some of the edges of the map, marking one edge on each iteration.

1. Let $v := v_0$, $e := e_0$, $U := \emptyset$, none of the edges is marked.
2. Let v' be the extremity of e different from v.

Case 1 e is non-marked and entering v. Add e to U and let $v := v'$.
Case 2 e is non-marked and leaving v. Add a stem to U incident to v and corresponding to e.
Case 3 e is already marked and entering v. Do nothing.
Case 4 e is already marked and leaving v. Let $v := v'$.

3. Mark e.
4. Let e be the next edge around v in counterclockwise order after the current e.
5. While $(v, e) \neq (v_0, e_0)$ go back to 2.
6. Return U.

We insist on the fact that the output of ALGORITHM PS is a graph embedded on the same surface as the input map but that this embedded graph is not necessarily a map

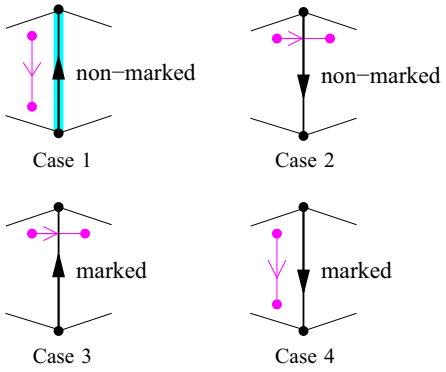

Fig. 8 The four cases of ALGORITHM PS

(i.e some faces may not be homeomorphic to open disks). In the following section we show that in our specific case the output U is a unicellular map on the contrary to some examples presented later on (see Fig. 14).

Consider any oriented map G on an oriented surface given with a root vertex v_0 and a root edge e_0 incident to v_0. When ALGORITHM PS is considering a couple (v, e) we see this like it is considering the angle at v that is just before e in counterclockwise order. The particular choice of v_0 and e_0 is thus in fact a particular choice of a root angle a_0 that automatically defines a root vertex v_0, a root edge e_0, as well as a root face f_0. From now on we consider that the input of ALGORITHM PS is an oriented map plus a root angle (without specifying the root vertex, face and edge).

The *angle graph* of G, is the graph defined on the angles of G and where two angles are adjacent if and only if they are consecutive around a vertex or around a face. An execution of ALGORITHM PS can be seen as a walk in the angle graph. Figure 8 illustrates the behavior of the algorithm corresponding to Case 1–4. In each case, the algorithm is considering the angle in top left position and depending on the marking of the edge and its orientation the next angle that is considered is the one that is the end of the magenta arc of the angle graph. The cyan edge of Case 1 represents the edge that is added to U by the algorithm. The stems of U added in Case 2 are not represented in cyan, in fact we will represent them later by an edge in the dual. Indeed seeing the execution of ALGORITHM PS as a walk in the angle graph enables us to show that ALGORITHM PS behaves exactly the same in the primal or in the dual map (as explained later).

In Fig. 9, we give an example of an execution of ALGORITHM PS on the orientation corresponding to the minimal HTC Schnyder wood of K_7 of Fig. 6.

Let a be a particular angle of the map G. It is adjacent to four other angles in the *angle graph* (see Fig. 10). Let v, f be such that a is an angle of vertex v and face f. The *next-vertex* (resp. *previous-vertex*) angle of a is the angle appearing just after (resp. before) a in counterclockwise order around v. Similarly, the *next-face* (resp. *previous-face*) angle of a is the angle appearing just after (resp. before) a in clockwise order around f. These definitions enable one to orient consistently the edges of the angle graph like in Fig. 10 so that for every oriented edge (a, a'), a' is a next-vertex or next-face angle of a.

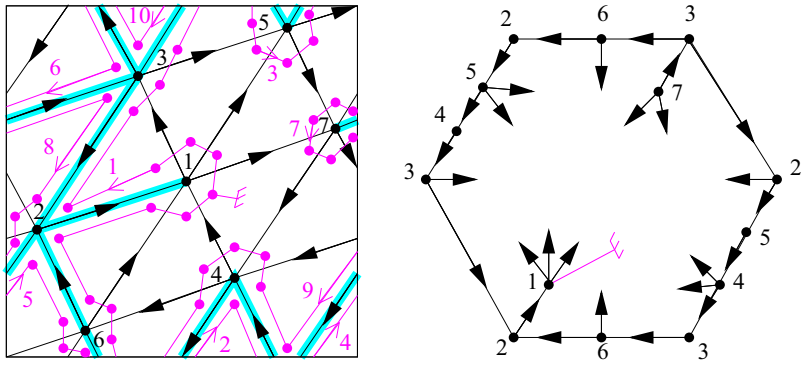

Fig. 9 An execution of ALGORITHM PS on K_7 given with the orientation corresponding to the minimal HTC Schnyder wood of Fig. 6. Vertices are numbered in *black*. The root angle is identified by a root symbol and chosen in the face for which the orientation is minimal (i.e. the *shaded face* of Fig. 6). The *magenta arrows* and numbers are here to help the reader to follow the cycle in the angle graph. The output U is a toroidal unicellular map, represented here as an hexagon where the opposite sides are identified.

Fig. 10 Orientation of the edges of the angle graph

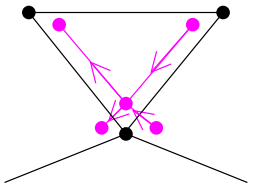

The different cases depicted in Fig. 8 show that an execution of ALGORITHM PS is just an oriented walk in the angle graph (i.e. a walk that is following the orientation of the edges described in Fig. 10). The condition in the while loop ensures that when the algorithm terminates, this walk is back to the root angle. The following proposition shows that the algorithm actually terminates:

Proposition 1 *Consider an oriented map G on an oriented surface and a root angle a_0. The execution of* ALGORITHM PS *on (G, a_0) terminates and corresponds to a cycle in the angle graph.*

Proof We consider the oriented walk W in the angle graph corresponding to the execution of ALGORITHM PS . Note that W may be infinite. The walk W starts with a_0, and if it is finite it ends with a_0 and contains no other occurrence of a_0 (otherwise the algorithm should have stopped earlier). Toward a contradiction, suppose that W is not simple (i.e. some angles different from the root angle a_0 are repeated). Let $a \neq a_0$ be the first angle along W that is met for the second time. Let a_1, a_2 be the angles appearing before the first and second occurrence of a in W, respectively. Note that $a_1 \neq a_2$ by the choice of a.

If a_1 is the previous-vertex angle of a, then a_2 is the previous-face angle of a. When the algorithm considers a_1, none of a and a_2 are already visited, thus edge e is not marked. Since the execution then goes to a after a_1, we are in Case 2 and the edge e

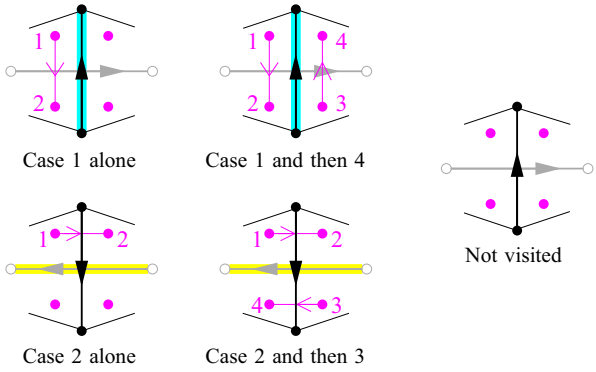

Fig. 11 The different cases of ALGORITHM PS seen in a dual way. The number of the angles gives the order in which the algorithm visits them (unvisited angles are not numbered). The edges of P and Q are respectively *cyan* and *yellow*

between a and a_1 is oriented from v, where v is the vertex incident to a. Afterward, when the algorithm reaches a_2, Case 3 applies and the algorithm cannot go to a, a contradiction. The case where a_1 is the previous-face angle of a is similar.

So W is simple. Since the angle graph is finite, W is finite. So the algorithm terminates, thus W ends on the root angle and W is a cycle. □

In the next section we see that in some particular cases the cycle in the angle graph corresponding to the execution of PS algorithm (Proposition 1) can be shown to be Hamiltonian like in Fig. 9.

By Proposition 1, an angle is considered at most once by ALGORITHM PS. This implies that the angles around an edge can be visited in different ways depicted in Fig. 11. Consider an execution of ALGORITHM PS on G. Let C be the cycle formed in the angle graph by Proposition 1. Let P be the set of edges of the output U (without the stems) and Q be the set of dual edges of edges of G corresponding to stems of U. These edges are represented in Fig. 11 in cyan for P and in yellow for Q. They are considered with their orientation (recall that the dual edge e^* of an edge e goes from the face on the left of e to the face on the right of e). Note that C does not cross an edge of P or Q, and moreover P and Q do not intersect (i.e. an edge can be in P or its dual in Q but both cases cannot happen).

One can remark that the cases of Fig. 11 are dual of each other. One can see that ALGORITHM PS behaves exactly the same if applied on the primal map or on the dual map. The only modifications to make is to start the algorithm with the face f_0 as the root vertex, the dual of edge e_0 as the root edge and to replace counterclockwise by clockwise at Line 4. Then the cycle C formed in the angle graph is exactly the same and the output is Q with stems corresponding to P (instead of P with stems corresponding to Q). Note that this duality is also illustrated by the fact that the minimality of the orientation of G w.r.t. the root face is nothing else than the accessibility of the dual orientation toward the root face. Indeed, a clockwise 0-homologous oriented subgraph of G w.r.t f_0 corresponds to a directed cut of the dual where all the edges are oriented from the part containing f_0. The following lemma shows the connectivity of P and Q:

Lemma 3 *At each step of the algorithm, for every vertex v appearing in an edge of P (resp. Q), there is an oriented path from v to v_0 (resp. f_0) consisting only of edges of P (resp. Q). In particular P and Q are connected.*

Proof If at a step a new vertex is reached then it correspond to Case 1 and the corresponding edge is added in P and oriented from the new vertex, so the property is satisfied by induction. As observed earlier the algorithm behaves similarly in the dual map. □

Let $\overline{C}$ be the set of angles of G that are not in C. Any edge of G is bounded by exactly 4 angles. Since C is a cycle, the 4 angles around an edge are either all in C, all in $\overline{C}$ or 2 in each set (see Fig. 11). Moreover, if they are 2 in each set, these sets are separated by an edge of P or an edge of Q. Hence the frontier between C and $\overline{C}$ is a set of edges of P and Q. Moreover this frontier is a union of oriented closed walks of P and of oriented closed walks of Q. In the next section we study this frontier in more details to show that $\overline{C}$ is empty in the case considered there.

5 From Toroidal Triangulations to Unicellular Maps

Let G be a toroidal triangulation. In order to choose appropriately the root angle a_0, we have to consider separating triangles. A *separating triangle* is a triangle that is different from a face of G, that is a triangle whose interior in non empty. We say that an angle is *in the strict interior of a separating triangle* T if it is in the interior of T and not incident to a vertex of T. We choose as root angle a_0 any angle that is not in the strict interior of a separating triangle. One can easily see that such an angle a_0 always exists. Indeed the interiors of two triangles are either disjoint or one is included in the other. So, the angles that are incident to a triangle whose interior is maximal by inclusion satisfy the property.

A subgraph of a graph is *spanning* if it is covering all the vertices. The main result of this section is the following theorem (see Fig. 9 for an example):

Theorem 3 *Consider a toroidal triangulation G, a root angle a_0 that is not in the strict interior of a separating triangle and the orientation of the edges of G corresponding to the minimal HTC Schnyder wood w.r.t. the root face f_0 containing a_0. Then the output U of* ALGORITHM PS *applied on (G, a_0) is a toroidal spanning unicellular map.*

The choice of a root angle that is not in the interior of a separating triangle is necessary to be able to use Poulalhon and Schaeffer method. Indeed, in a 3-orientation of a toroidal triangulation, by Euler's formula, all the edges that are incident to a separating triangle and in its interior are oriented towards the triangle. Thus if one applies ALGORITHM PS from an angle in the strict interior of a triangle, the algorithm will remain stuck in the interior of the triangle and will not visit all the vertices.

Consider a toroidal triangulation G, a root angle a_0 that is not in the strict interior of a separating triangle and the orientation of the edges of G corresponding to the minimal HTC Schnyder wood w.r.t. the root face f_0 containing a_0. Let U be the output of ALGORITHM PS applied on (G, a_0). We use the same notation as in the previous section: the cycle in the angle graph is C, the set of angles that are not in C is $\overline{C}$, the set of edges of U is P, the dual edges of stems of U is Q.

Lemma 4 *The frontier between C and $\overline{C}$ contains no oriented closed walk of Q.*

Proof Suppose by contradiction that there exists such a walk W. Then along this walk, all the dual edges of W are edges of G oriented from the region containing C toward $\overline{C}$ as one can see in Fig. 11. By Lemma 2, the walk W does not contain any oriented non-contractible cycle. So W contains an oriented contractible cycle W', and then either C is in the contractible region delimited by W', or not. The two case are considered below:

- *C lies in the non-contractible region of W'*

  Then consider the plane map G' obtained from G by keeping only the vertices and edges that lie (strictly) in the contractible region delimited by W'. Let n' be the number of vertices of G'. All the edges incident to G' that are not in G' are entering G'. So in G' all the vertices have outdegree 3 as we are considering 3-orientations of G. Thus the number of edges of G' is exactly $3n'$, contradicting the fact that the maximal number of edges of planar map on n vertices is $3n - 6$ by Euler's formula.

- *C lies in the contractible region of W'*

  All the dual edges of W' are edges of G oriented from its contractible region toward its exterior. Consider the graph G_{out} obtained from G by removing all the edges that are cut by W' and all the vertices and edges that lie in the contractible region of W'. As G is a map, the face of G_{out} containing W' is homeomorphic to an open disk. Let F be its facial walk (in G_{out}) and let k be the length of F. We consider the map obtained from the facial walk F by putting back the vertices and edges that lied inside. We transform this map into a plane map G' by duplicating the vertices and edges appearing several times in F, in order to obtain a triangulation of a cycle of length k. Let n', m', f' be the number of vertices, edges and faces of G'. Every inner vertex of G' has outdegree 3, there are no other inner edges, so the total number of edges of G' is $m' = 3(n' - k) + k$. All the inner faces have length 3 and the outer face has length k, so $2m' = 3(f' - 1) + k$. By Euler's formula $n' - m' + f' = 2$. Combining the three equalities gives $k = 3$ and F is hence a separating triangle of G. This contradicts the choice of the root angle, as it should not lie in the strict interior of a separating triangle.

□

A *Hamiltonian cycle* of a graph is a cycle visiting every vertex once.

Lemma 5 *The cycle C is a Hamiltonian cycle of the angle graph, all the edges of G are marked exactly twice, the subgraph Q of G^* is spanning, and, if $n \geq 2$, the subgraph P of G is spanning.*

Proof Suppose for a contradiction that $\overline{C}$ is non empty. By Lemma 4 and Sect. 4, the frontier T between C and $\overline{C}$ is a union of oriented closed walks of P. Hence a face of G has either all its angles in C or all its angles in $\overline{C}$. Moreover T is a non-empty union of oriented closed walk of P that are oriented clockwise according to the set of faces containing $\overline{C}$ (see the first case of Fig. 11). This set does not contain f_0 since a_0 is in f_0 and C. As in Sect. 3, let $\mathcal{F}$ be the set of counterclockwise facial

walks of G and F_0 be the counterclockwise facial walk of f_0. Let $\mathcal{F}' = \mathcal{F} \setminus F_0$, and $\mathcal{F}_{\overline{C}} \subseteq \mathcal{F}'$ be the set of counterclockwise facial walks of the faces containing $\overline{C}$. We have $\phi(T) = -\sum_{F \in \mathcal{F}_{\overline{C}}} \phi(F)$. So T is a clockwise non-empty 0-homologous oriented subgraph w.r.t. f_0. This contradicts Lemma 1 and the minimality of the orientation w.r.t. f_0. So $\overline{C}$ is empty, thus C is Hamiltonian and all the edges of G are marked twice.

Suppose for a contradiction that $n \geq 2$ and P is not spanning. Since the algorithm starts at v_0, P is not covering a vertex v of G different from v_0. Then the angles around v cannot be visited since by Fig. 11 the only way to move from an angle of one vertex to an angle of another vertex is through an edge of P incident to them. So P is spanning. The proof is similar for Q (note that in this case we have $f \geq 2$). □

Lemma 6 *The first cycle created in P (resp. in Q) by the algorithm is oriented.*

Proof Let e be the first edge creating a cycle in P while executing ALGORITHM PS and consider the steps of ALGORITHM PS before e is added to P. So P is a tree during all these steps. For every vertex of P we define $P(v)$ the unique path from v to v_0 in P (while P is empty at the beginning of the execution, we define $P(v_0) = \{v_0\}$). By Lemma 3, this path $P(v)$ is an oriented path. We prove the following

Claim 1 *Consider a step of the algorithm before e is added to P and where the algorithm is considering a vertex v. Then all the angles around the vertices of P different from the vertices of $P(v)$ are already visited.*

Proof Suppose by contradiction that there is such a step of the algorithm where some angles around the vertices of P different from the vertices of $P(v)$ have not been visited. Consider the first such step. Then clearly we are not at the beginning of the algorithm since $P = P(v) = \{v_0\}$. So at the step just before, the conclusion holds and now it does not hold anymore. Clearly at the step before we were considering a vertex v' distinct from v, otherwise $P(v)$ and P have not changed and we have the conclusion. So from v' to v we are either in Case 1 or Case 4 of ALGORITHM PS (see Fig. 12). If v has been considered by Case 1, then $P(v)$ contains $P(v')$ and the conclusion holds. If v has been considered by Case 4, then since P is a tree, all the angles around v' have been considered and v' is the only element of $P \setminus P(v)$ that is not in $P \setminus P(v')$. Thus the conclusion also holds. □

Consider the iteration of ALGORITHM PS where e is added to P. The edge e is added to P by Case 1, so e is oriented from a vertex u to a vertex v such that v is already in P or v is the root vertex v_0. Consider the step of the algorithm just before u is added to P. By Claim 1, vertex u is not in $P \setminus P(v)$ (otherwise e would have been considered before and it would be a stem). So $u \in P(v)$ and $P(v) \cup \{e\}$ induces an oriented cycle of G. The proof is similar for Q. □

Lemma 7 *P is a spanning unicellular map of G and Q is a spanning tree of G^*. Moreover one is the dual of the complement of the other.*

Proof Suppose that Q contains a cycle, then by Lemma 6 it contains an oriented cycle of G^*. This cycle is contractible by Lemma 2. Recall that by Lemma 5, C is a

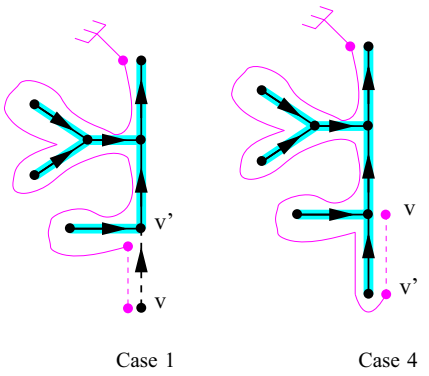

Fig. 12 The two cases of the proof of Claim 1

Hamiltonian cycle, moreover it does not cross Q, a contradiction. So Q contains no cycle and is a tree.

By Lemma 5, all the edges of G are marked at the end. So every edge of G is either in P or its dual in Q (and not both). Thus P and Q are the dual of the complement of each other. So P is the dual of the complement of a spanning tree of G^*. Thus P is a spanning unicellular map of G. □

Theorem 3 is then a direct reformulation of Lemma 7 by the definition of P and Q.

A toroidal unicellular map on n vertices has exactly $n + 1$ edges: $n - 1$ edges of a tree plus 2 edges corresponding to the size of a basis of the homology (i.e. plus $2g$ in general for an oriented surface of genus g). Thus a consequence of Theorem 3 is that the obtained unicellular map U has exactly n vertices, $n + 1$ edges and $2n - 1$ stems since the total number of edges is $3n$. The orientation of G induces an orientation of U such that the stems are all outgoing, and such that while walking clockwise around the unique face of U from a_0, the first time an edge is met, it is oriented counterclockwise according to this face, see Fig. 13 where all the tree-like parts and stems are not represented. There are two types of toroidal unicellular maps depicted in Fig. 13. Two cycles of U may intersect either on a single vertex (square case) or on a path (hexagonal case). The square can be seen as a particular case of the hexagon where one side has length zero and thus the two corners of the hexagon are identified.

In Fig. 14, we give several examples of executions of ALGORITHM PS on minimal 3-orientations. These examples show how important is the choice of the minimal HTC Schnyder wood in order to obtain Theorem 3. In particular, the third example shows that ALGORITHM PS can visit all the angles of the triangulation (i.e. the cycle in the angle graph is Hamiltonian) without outputting a unicellular map.

Note that the orientations of Fig. 14 are not Schnyder woods. One may wonder if the fact of being a Schnyder wood is of any help for our method. This is not the case since there are examples of minimal Schnyder woods that are not HTC and where ALGORITHM PS does not visit all the vertices. One can obtain such an example by replicating 3 times horizontally and then 3 times vertically the second example of Fig. 14 to form a 3×3 tiling and starts ALGORITHM PS from the same root angle. Conversely, there are minimal Schnyder woods that are not HTC where ALGORITHM

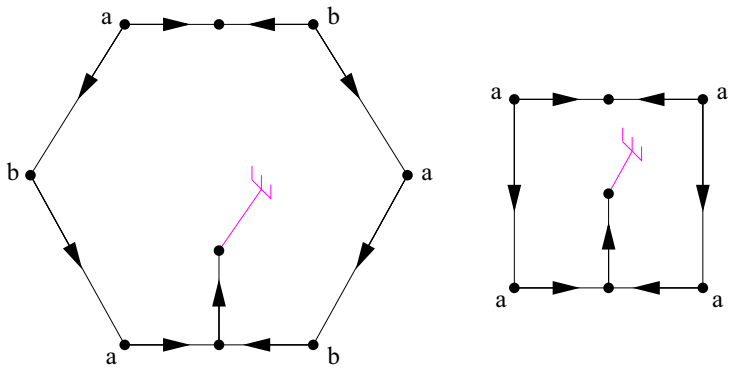

Fig. 13 The two types of rooted toroidal unicellular maps

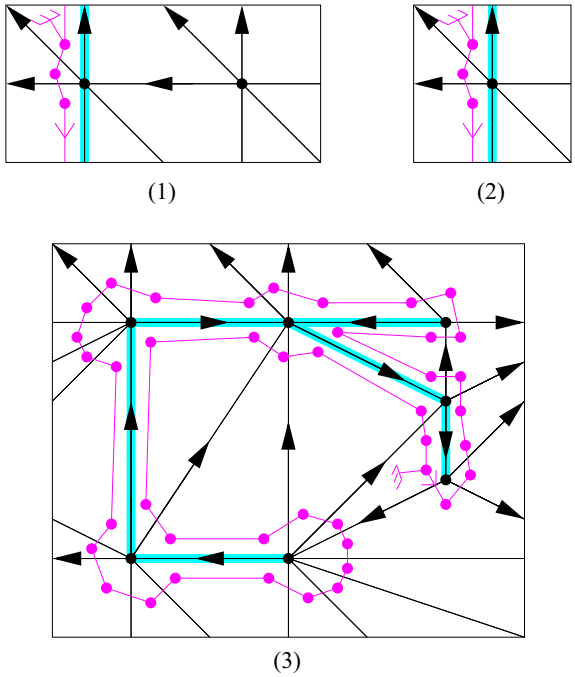

Fig. 14 Examples of minimal 3-orientations that are not HTC Schnyder woods and where ALGORITHM PS respectively: **1** does not visit all the vertices, **2** visits all the vertices but not all the angles, and **3** visits all the angles but does not output an unicellular map

PS does output a toroidal spanning unicellular map (the Schnyder wood of Fig. 7 can serve as an example while starting from an angle of the only face oriented clockwise).

6 Recovering the Original Triangulation

This section is dedicated to show how to recover the original triangulation from the output of ALGORITHM PS. The method is very similar to [20] since like in the plane

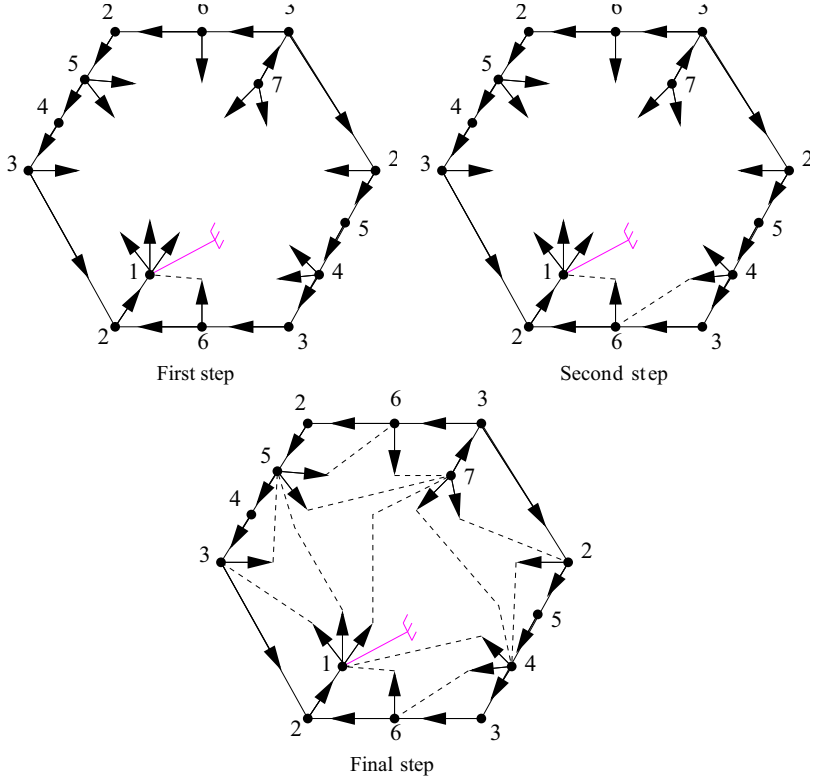

Fig. 15 Example of how to recover the original toroidal triangulation K_7 from the output of ALGORITHM PS

the output has only one face that is homeomorphic to an open disk (i.e. a tree in the plane and a unicellular map in general).

Theorem 4 *Consider a toroidal triangulation G, a root angle a_0 that is not in the strict interior of a separating triangle and the orientation of the edges of G corresponding to the minimal HTC Schnyder wood w.r.t. the root face f_0 containing a_0. From the output U of* ALGORITHM PS *applied on (G, a_0) one can reattach all the stems to obtain G by starting from the root angle a_0 and walking along the face of U in counterclockwise order (according to this face): each time a stem is met, it is reattached in order to create a triangular face on its left side.*

Theorem 4 is illustrated in Fig. 15 where one can check that the obtained toroidal triangulation is K_7 (like on the input of Fig. 9).

In fact in this section we define a method, more general than the one described in Theorem 4, that will be useful in next sections.

Let $\mathcal{U}_r(n)$ denote the set of toroidal unicellular maps U rooted on a particular angle, with exactly n vertices, $n+1$ edges and $2n-1$ stems satisfying the following property. A vertex that is not the root, has exactly 2 stems if it is not a corner, 1 stem if it is the corner of an hexagon and 0 stem if it is the corner of a square. The root vertex

has 1 additional stem, i.e. it has 3 stems if it is not a corner, 2 stems if it is the corner of an hexagon and 1 stem if it is the corner of a square. Note that the output U of ALGORITHM PS given by Theorem 3 is an element of $\mathcal{U}_r(n)$.

Similarly to the planar case [20], we define a general way to reattach step by step all the stems of an element U of $\mathcal{U}_r(n)$. Let $U_0 = U$, and, for $1 \leq k \leq 2n-1$, let U_k be the map obtained from U_{k-1} by reattaching one of its stem (we explicit below which stem is reattached and how). The *special face of* U_0 is its only face. For $1 \leq k \leq 2n-1$, the *special face of* U_k is the face on the right of the stem of U_{k-1} that is reattached to obtain U_k. For $0 \leq k \leq 2n-1$, the border of the special face of U_k consists of a sequence of edges and stems. We define an *admissible triple* as a sequence (e_1, e_2, s), appearing in counterclockwise order along the border of the special face of U_k, such that $e_1 = (u, v)$ and $e_2 = (v, w)$ are edges of U_k and s is a stem attached to w. The *closure* of the admissible triple consists in attaching s to u, so that it creates an edge (w, u) oriented from w to u and so that it creates a triangular face (u, v, w) on its left side. The *complete closure* of U consists in closing a sequence of admissible triple, i.e. for $1 \leq k \leq 2n-1$, the map U_k is obtained from U_{k-1} by closing any admissible triple.

Note that, for $0 \leq k \leq 2n-1$, the special face of U_k contains all the stems of U_k. The closure of a stem reduces the number of edges on the border of the special face and the number of stems by 1. At the beginning, the unicellular map U_0 has $n+1$ edges and $2n-1$ stems. So along the border of its special face, there are $2n+2$ edges and $2n-1$ stems. Thus there is exactly three more edges than stems on the border of the special face of U_0 and this is preserved while closing stems. So at each step there is necessarily at least one admissible triple and the sequence U_k is well defined. Since the difference of three is preserved, the special face of U_{2n-2} is a quadrangle with exactly one stem. So the reattachment of the last stem creates two faces that have length three and at the end U_{2n-1} is a toroidal triangulation. Note that at a given step there might be several admissible triples but their closure are independent and the order in which they are performed does not modify the obtained triangulation U_{2n-1}.

We now apply the closure method to our particular case. Consider a toroidal triangulation G, a root angle a_0 that is not in the strict interior of a separating triangle and the orientation of the edges of G corresponding to the minimal HTC Schnyder wood w.r.t. the root face f_0. Let U be the output of ALGORITHM PS applied on (G, a_0).

Lemma 8 *When a stem of U is reattached to form the corresponding edge of G, it splits the (only) face of U into two faces. The root angle of U is in the face that is on the right side of the stem.*

Proof By Lemma 5, the execution of ALGORITHM PS corresponds to a Hamiltonian cycle $C = (a_0, \ldots, a_{2m}, a_0)$ in the angle graph of G. Thus C defines a total order $<$ on the angles of G where $a_i < a_j$ if and only if $i < j$. Let us consider now the angles on the face of U. Note that such an angle corresponds to several angles of G, that are consecutive in C and that are separated by a set of incoming edges of G (those incoming edges corresponding to stems of U). Thus the order on the angles of G defines automatically an order on the angles of U. The angles of U considered in clockwise order along the border of its face, starting from the root angle, correspond to a sequence of strictly increasing angles for $<$.

Consider a stem s of U that is reattached to form an edge e of G. Let a_s be the angle of U that is situated just before s (in clockwise order along the border of the face of U) and a'_s be the angle of U where s should be reattached. If $a'_s < a_s$, then when ALGORITHM PS consider the angle a_s, the edge corresponding to s is already marked and we are not in Case 2 of ALGORITHM PS . So $a_s < a'_s$ and a_0 is on the right side of s. □

Recall that U is an element of $\mathcal{U}_r(n)$ so we can apply on U the complete closure procedure described above. We use the same notation as before, i.e. let $U_0 = U$ and for $1 \leq k \leq 2n-1$, the map U_k is obtained from U_{k-1} by closing any admissible triple. The following lemma shows that the triangulation obtained by this method is G:

Lemma 9 *The complete closure of U is G, i.e. $U_{2n-1} = G$.*

Proof We prove by induction on k that every face of U_k is a face of G, except for the special face. This is true for $k = 0$ since $U_0 = U$ has only one face, the special face. Let $0 \leq k \leq 2n-2$, and suppose by induction that every non-special face of U_k is a face of G. Let (e_1, e_2, s) be the admissible triple of U_k such that its closure leads to U_{k+1}, with $e_1 = (u, v)$ and $e_2 = (v, w)$. The closure of this triple leads to a triangular face (u, v, w) of U_{k+1}. This face is the only "new" non-special face while going from U_k to U_{k+1}.

Suppose, by contradiction, that this face (u, v, w) is not a face of G. Let a_v (resp. a_w) be the angle of U_k at the special face, between e_1 and e_2 (resp. e_2 and s). Since G is a triangulation, and (u, v, w) is not a face of G, there exists at least one stem of U_k that should be attached to a_v or a_w to form a proper edge of G. Let s' be such a stem that is the nearest from s. In G the edges corresponding so s and s' should be incident to the same triangular face. Let x be the origin of the stem s'. Let $z \in \{v, w\}$ such that s' should be reattached to z. If $z = v$, then s should be reattached to x to form a triangular face of G. If $z = w$, then s should be reattached to a common neighbor of w and x located on the border of the special face of U_k in counterclockwise order between w and x. So in both cases s should be reattached to a vertex y located on the border of the special face of U_k in counterclockwise order between w and x (with possibly $y = x$). To summarize s goes from w to y and s' from x to z, and z, x, y, w appear in clockwise order along the special face of U_k. By Lemma 8, the root angle is on the right side of both s and s', this is not possible since their right sides are disjoint, a contradiction.

So for $0 \leq k \leq 2n-2$, all the non-special faces of U_k are faces of G. In particular every face of U_{2n-1} except one is a face of G. Then clearly the (triangular) special face of U_{2n-1} is also a face of G, hence $U_{2n-1} = G$. □

Lemma 9 shows that one can recover the original triangulation from U with any sequence of admissible triples that are closed successively. This does not explain how to find the admissible triples efficiently. In fact the root angle can be used to find a particular admissible triple of U_k:

Lemma 10 *For $0 \leq k \leq 2n-2$, let s be the first stem met while walking counterclockwise from a_0 in the special face of U_k. Then before s, at least two edges are met and the last two of these edges form an admissible triple with s.*

Proof Since s is the first stem met, there are only edges that are met before s. Suppose by contradiction that there is only zero or one edge met before s. Then the reattachment of s to form the corresponding edge of G is necessarily such that the root angle is on the left side of s, a contradiction to Lemma 8. So at least two edges are met before s and the last two of these edges form an admissible triple with s. □

Lemma 10 shows that one can reattach all the stems by walking once along the face of U in counterclockwise order. Thus we obtain Theorem 4.

Note that U is such that the complete closure procedure described here never *wraps over the root angle*, i.e. when a stem is reattached, the root angle is always on its right side (see Lemma 8). The property of never wrapping over the root angle is called *balanced* in [2]. Let $\mathcal{U}_{r,b}(n)$ denote the set of elements of $\mathcal{U}_r(n)$ that are balanced. So the output U of ALGORITHM PS given by Theorem 3 is an element of $\mathcal{U}_{r,b}(n)$. We exhibit in Sect. 9 a bijection between appropriately rooted toroidal triangulations and a particular subset of $\mathcal{U}_{r,b}(n)$.

The possibility to close admissible triples in any order to recover the original triangulation is interesting compared to the simpler method of Theorem 4 since it enables to recover the triangulation even if the root angle is not given. This property is used in Sect. 11 to obtain a bijection between toroidal triangulations and some unrooted unicellular maps.

Moreover if the root angle is not given, then one can simply start from any angle of U, walk twice around the face of U in counterclockwise order and reattach all the admissible triples that are encountered along this walk. Walking twice ensures that at least one complete round is done from the root angle. Since only admissible triples are considered, we are sure that no unwanted reattachment is done during the process and that the final map is G. This enables to reconstruct G in linear time even if the root angle is not known. This property is used in Sect. 7.

7 Optimal Encoding

The results presented in the previous sections allow us to generalize the encoding of planar triangulations, defined by Poulalhon and Schaeffer [20], to triangulations of the torus. The construction is direct and it is hence really different from the one of [3] where triangulations of surfaces are cut in order to deal with planar triangulations with boundaries. Here we encode the unicellular map outputted by ALGORITHM PS by a plane rooted tree with n vertices and with exactly two stems attached to each vertex, plus $O(\log(n))$ bits. As in [3], this encoding is asymptotically optimal and uses approximately $3.2451n$ bits. The advantage of our method is that it can be implemented in linear time. Moreover we believe that our encoding gives a better understanding of the structure of triangulations of the torus. It is illustrated with new bijections that are obtained in Sects. 9 and 11 .

Consider a toroidal triangulation G, a root angle a_0 that is not in the strict interior of a separating triangle and the orientation of the edges of G corresponding to the minimal HTC Schnyder wood w.r.t. the root face f_0. Let U be the output of ALGORITHM PS applied on (G, a_0). As already mentioned at the end of Sect. 6, to retrieve the triangulation G one just needs to know U without the information of its root angle

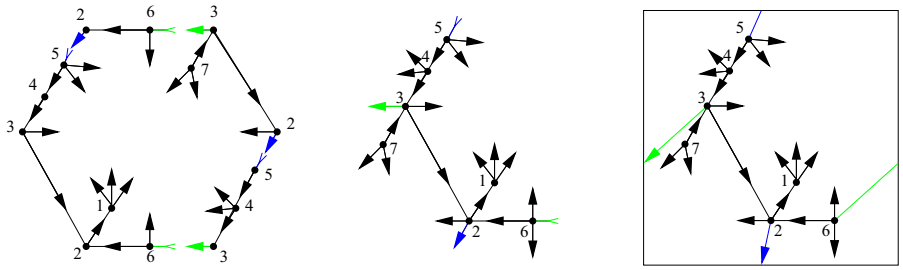

Fig. 16 From unicellular maps to trees with special stems and back

(by walking twice around the face of U in counterclockwise order and reattaching all the admissible triples that are encountered along this walk, one can recover G). Hence to encode G, one just has to encode U without the position of the root angle around the root vertex (see Fig. 16a).

By Lemma 3, the unicellular map U contains a spanning tree T which is oriented from the leaves to the root vertex. The tree T contains exactly $n-1$ edges, so there is exactly 2 edges of U that are not in T. We call these edges the *special edges* of U. We cut these two special edges to transform them into stems of T (see Fig. 16a, b). We keep the information of where are the special stems in T and on which angle of T they should be reattached. This information can be stored with $O(\log(n))$ bits. One can recover U from T by reattaching the special stems in order to form non-contractible cycles with T (see Fig. 16c).

So T is a plane tree on n vertices, each vertex having 2 stems except the root vertex v_0 having three stems. Choose any stem s_0 of the root vertex, remove it and consider that T is rooted at the angle where s_0 should be attached. The information of the root enables to put back s_0 at its place. So now we are left with a rooted plane tree T on n vertices where each vertex has exactly 2 stems (see Fig. 17a).

This tree T can easily be encoded by a binary word on $6n-2$ bits: that is, walking in counterclockwise order around T from the root angle, writing a "1" when going down along T (our convention for *down* is with the root vertex at the top), and a "0" when going up along T (see Fig. 17a). As in [20], one can encode T more compactly by using the fact that each vertex has exactly two stems. Thus T is encoded by a binary word on $4n-2$ bits: that is, walking in counterclockwise order around T from the root angle, writing a "1" when going down along an edge of T, and a "0" when going up along an edge or along a stem of T (see Fig. 17b where the "red 1's" of Fig. 17a have been removed). Indeed there is no need to encode when going down along stems, as this information can be retrieved afterward. While reading the binary word to recover T, when a "0" is met, we should go up in the tree, except if the vertex that we are considering does not have already its two stems, then in that case we should create a stem (i.e. add a "red 1" before the "0"). So we are left with a binary word on $4n-2$ bits with exactly $n-1$ bits "1" and $3n-1$ bits "0".

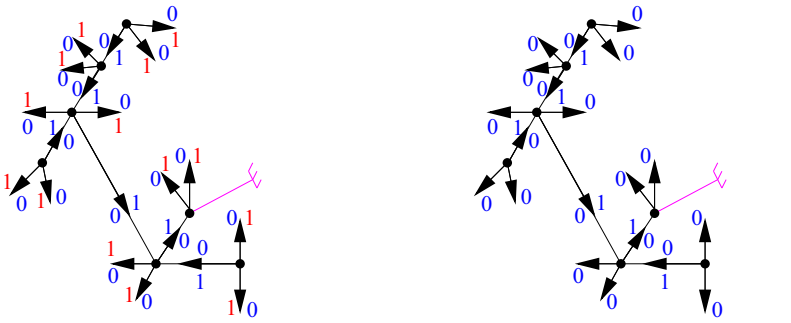

Fig. 17 Encoding a rooted tree with two stems at each vertex

Similarly to [20], using [6, Lem. 7], this word can then be encoded with a binary word of length $\log_2 \binom{4n-2}{n-1} + o(n) \sim n \log_2 \left(\frac{256}{27}\right) \approx 3.2451\, n$ bits. Thus we have the following theorem whose linearity is discussed in Sect. 8:

Theorem 5 *Any toroidal triangulation on n vertices, can be encoded with a binary word of length* $3.2451n + o(n)$ *bits, the encoding and decoding being linear in n.*

8 Linear Complexity

In this section we show that the encoding method described in this paper, that is encoding a toroidal triangulation via a unicellular map and recovering the original triangulation, can be performed in linear time. The only difficulty lies in providing ALGORITHM PS with the appropriate input it needs in order to apply Theorem 3. Then clearly the execution of ALGORITHM PS, the encoding phase and the recovering of the triangulation are linear. Thus we have to show how one can find in linear time a root angle a_0 that is not in the strict interior of a separating triangle, as well as the minimal HTC Schnyder wood w.r.t. the root face f_0.

Consider a toroidal triangulation G. Let us see how one can build a Schnyder wood of G in linear time. The *contraction* of a non-loop-edge e of G is the operation consisting of continuously contracting e until merging its two ends, as shown in Fig. 18. Note that only one edge of each pair of homotopic multiple edges is preserved (edges e_{wx} and e_{wy} in the figure). Note that the contraction operation is also defined when some vertices are identified: $x = u$ and $y = v$, or, $x = v$ and $y = u$.

An edge e is said to be *contractible* if it is not a loop and if after contracting e and identifying the borders of the two newly created length two faces, one obtains a triangulation that is still without contractible loop or homotopic multiple edges. In [15] the existence of crossing Schnyder wood is proved by contraction. Unfortunately this proof cannot easily be transformed into a linear algorithm because of the crossing property that has to be maintained during the contraction process. Nevertheless we use contractions to obtain non-necessarily crossing Schnyder woods. If the triangulation

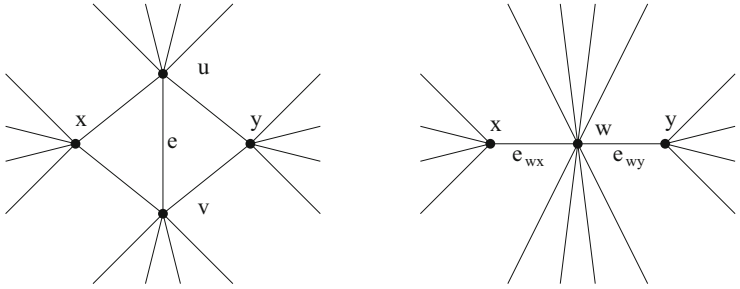

Fig. 18 The contraction operation

obtained after contracting a contractible edge admits a Schnyder wood it is then easy to obtain a Schnyder wood of G. The rules for decontracting an edge in the case of toroidal triangulations are depicted in [15, Fig. 21] where for each case one can choose any of the proposed colorings. For any toroidal triangulation, one can find contractible edges until the toroidal map has only one vertex (see [19]). A Schnyder wood of the toroidal map on one vertex is depicted on the right of Fig. 3. Thus one can obtain a Schnyder wood of any toroidal triangulation by this process. Nevertheless, to maintain linearity we have to be more precise since it is not trivial to find contractible edges.

Consider an edge e of G with distinct ends u, v, and with incident faces uvx and vuy, such that these vertices appear in clockwise order around the corresponding face (so we are in the situation of Figure 18). The edge e is contractible if and only if, every walk enclosing an open disk containing a face other than uvx and vuy, goes through an edge distinct from e at least three times. Equivalently e is non-contractible if and only if it belongs to a separating triangle or u, v are both incident to a loop-edge ℓ_u, ℓ_v, respectively, such that the walk of length four (ℓ_u, e, ℓ_v, e) encloses an open disk with at least three faces (i.e. with at least one face distinct from uvx and vuy). To avoid the latter case, if vertex u is incident to a loop-edge ℓ_u, we consider e to be an edge that is consecutive to that loop, so that we have $x = u$. In such a case, if there is a loop ℓ_v incident to v and a walk of length four of the form (ℓ_u, e, ℓ_v, e) enclosing a disk with at least three faces, then there is also a separating triangle containing e. In the following we show how to find such separating triangle, if there is one. If u and v have more common neighbors, than simply x and y, consider their second common neighbor going clockwise around u from e (the first one being x, and the last being y) and call it x'. Call y' their second common neighbor going counterclockwise around u from e. Now, either uvx' or uvy' is a separating triangle or the edge e is contractible. We consider these two cases below:

- If e is contractible, then it is contracted and we apply the procedure recursively to obtain a Schnyder wood of the contracted graph. Then we update the Schnyder wood as described above. Note that this update is done in constant time.
- If uvx' (resp. uvy') is a separating triangle, one can remove its interior, recursively obtain a toroidal Schnyder wood of the remaining toroidal triangulation, build a planar Schnyder wood of the planar triangulation inside uvx' (resp. uvy'), and then superimpose the two (by eventually permuting the colors) to obtain a Schnyder

wood of the whole graph. Note that computing a planar Schnyder wood can be done in linear time using a canonical ordering (see [17]).

The difficulty here is to test whether uvx' or uvy' are triangles. For that purpose, one first needs to compute a basis (B_1, B_2) for the homology. Consider a spanning tree of the dual map G^*. The map obtained from G by removing those edges is unicellular, and removing its treelike parts one obtains two cycles (B_1, B_2) (intersecting on a path with at least one vertex) that form a basis for the homology. This can be computed in linear time for G and then updated when some edge is contracted or when the interior of some separating triangle is removed. The updating takes constant time when some edge is contracted, and it takes $O(n')$ time when removing n' vertices in the interior of some separating triangle. The overall cost of constructing and maintaining the basis is thus linear in the size of G. Then a closed walk of length three W, given with an arbitrary orientation, encloses a region homeomorphic to an open disk if and only if W crosses B_i from right to left as many times as W crosses B_i from left to right, for every $i \in \{1, 2\}$. This test can be done in constant time for uvx' and uvy' once the half edges on the right and left sides of the cycles B_i are marked. Marking the half edges of G and maintaining this marking while contracting edges or while removing the interior of separating triangles can clearly be done in linear time. We thus have that the total running time to compute a Schnyder wood of G is linear.

From this Schnyder wood, one can compute in linear time a root angle a_0 not in the strict interior of a separating triangle. First note that in a 3-orientation of a toroidal triangulation, the edges that are inside a separating triangle and that are incident to the three vertices on the border are all oriented toward these three vertices by Euler's formula. Thus an oriented non-contractible cycle cannot enter in the interior of a separating triangle. Now follow any oriented monochromatic path of the Schnyder wood and stop the first time this path is back to a previously met vertex v_0. The end of this path forms an oriented monochromatic cycle C containing v_0. If C is a contractible cycle then Euler's formula is violated in the contractible region. Thus C is an oriented non-contractible cycle and cannot contain some vertices that are in the interior of a separating triangle. So v_0 is not in the interior of a separating triangle and we can choose as root angle a_0 any angle incident to v_0.

In [16] (see also [18]) it is proved how one can transform any 3-orientation (hence a Schnyder wood) of a toroidal triangulation into a HTC Schnyder wood. The method consists in computing a so called "middle-path" (a directed path where the next edge chosen is the one leaving in the "middle") and reversing some non-contractible "middle-cycles". Clearly the method is linear even if not explicitly mentioned in [16]. Let D_0 be the corresponding obtained orientation of G.

It remains to compute the minimal HTC Schnyder wood w.r.t. the root face f_0. There is a generic known method Meunier, F.: Personal communication (2015) (see also [23, p. 23]) to compute in linear time a minimal α-orientation of a planar map as soon as an α-orientation is given. This method also works on oriented surfaces and can be applied to obtain the minimal HTC Schnyder wood in linear time. We explain the method briefly below.

It is much simpler to compute the minimal orientation $D_{\min}$ homologous to D_0 in a dual setting. The first observation to make is that two orientations D_1, D_2 of G

are homologous if and only if there dual orientations D_1^*, D_2^* of G^* are equivalent up to reversing some directed cuts. Furthermore $D_1 \leq_{f_0} D_2$ if and only if D_1^* can be obtained from D_2^* by reversing directed cuts oriented from the part containing f_0. Let us compute $D^*_{\min}$ which is the only orientation of G^*, obtained from D_0^* by reversing directed cuts, and without any directed cut oriented from the part containing f_0. For this, consider the orientation D_0^* of $G^* = (F, E^*)$ and compute the set $X \subseteq F$ of vertices of G^* that have an oriented path toward f_0. Then $(X, F \setminus X)$ is a directed cut oriented from the part containing f_0 that one can reverse. Then update the set of vertices that can reach f_0 and go on until $X = F$. It is not difficult to see that this can be done in linear time. Thus we obtain the minimal HTC Schnyder wood w.r.t. f_0 in linear time.

9 Bijection with Rooted Unicellular Maps

Given a toroidal triangulation G with a root angle a_0, we have defined a unique associated orientation: the minimal HTC Schnyder wood w.r.t. the root face f_0. Suppose that G is oriented according to the minimal HTC Schnyder wood. If a_0 is not in the strict interior of a separating triangle then Theorems 3 and 4 show that the execution of ALGORITHM PS on (G, a_0) gives a toroidal unicellular map with stems from which one can recover the original triangulation. Thus there is a bijection between toroidal triangulations rooted from an appropriate angle and their image by ALGORITHM PS. The goal of this section is to describe this image.

Recall from Sect. 6 that the output of ALGORITHM PS on (G, a_0) is an element of $\mathcal{U}_{r,b}(n)$. One may hope that there is a bijection between toroidal triangulations rooted from an appropriate angle and $\mathcal{U}_{r,b}(n)$ since this is how it works in the planar case. Indeed, given a planar triangulation G, there is a unique orientation of G (the minimal Schnyder wood) on which ALGORITHM PS, performed from an outer angle, outputs a spanning tree. In the toroidal case, things are more complicated since the behavior of ALGORITHM PS on minimal HTC Schnyder woods does not characterize such orientations.

Figure 19 gives an example of two (non-homologous) orientations of the same triangulation that are both minimal w.r.t. the same root face. For these two orientations, the execution of ALGORITHM PS from the same root angle gives two different elements of $\mathcal{U}_{r,b}(2)$ (from which the original triangulation can be recovered by the method of Theorem 4). Thus we have to exhibit a particular property of HTC Schnyder woods that can be used to characterize which particular subset of $\mathcal{U}_{r,b}(n)$ is in bijection with appropriately rooted toroidal triangulations.

For that purpose we now introduce a function γ which is reminiscent to the one in [16]. Consider a particular orientation of G. Let C be a cycle that is given with an arbitrary direction (C is not necessarily a directed cycle). Then $\gamma(C)$ is defined by,

$$\gamma(C) = \#\text{ edges leaving } C \text{ on its right } - \#\text{ edges leaving } C \text{ on its left}.$$

By the Schnyder property, it is clear that in a toroidal Schnyder wood, a monochromatic cycle C always satisfies $\gamma(C) = 0$. Consider a crossing Schnyder wood

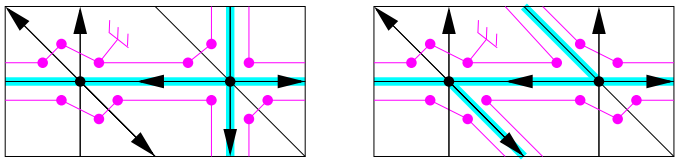

Fig. 19 A graph that can be represented by two different unicellular maps

of G and C_1, C_2 two monochromatic cycles of different colors. Thus we have $\gamma(C_1) = \gamma(C_2) = 0$. By [15, Thm. 7], the two cycles C_1, C_2 are non-contractible and non-homologous, thus they form a basis for the homology. While returning a 0-homologous oriented subgraph, the value of γ on a given cycle does not change. Thus any HTC Schnyder wood also satisfies $\gamma(C_1) = \gamma(C_2) = 0$. Moreover it is proved in [16] (see also [18]) that if a 3-orientation of a toroidal triangulation satisfies γ equals 0 for two cycles forming a basis for the homology, then γ equals 0 for any non-contractible cycle. Thus any HTC Schnyder wood satisfies γ equals 0 for any non-contractible cycle. We call this property the γ_0 *property*. Note that, for a 3-orientation, it is sufficient to satisfy γ equals 0 on any two cycles forming a basis for the homology to have the γ_0 property.

Actually the γ_0 property characterizes the 3-orientations that are HTC Schnyder woods. Indeed a consequence of [16, Thm. 5 and Lem. 18] is that if two 3-orientations both satisfy the γ_0 property, then they are homologous to each other and thus HTC. Note that for the 3-orientation on the right of Fig. 19, we have γ equals ± 2 for the horizontal cycle and this explain why this orientation is not HTC (one can find similar arguments for previous examples of non-HTC Schnyder woods presented in this paper, see Figs. 5, 7).

Let us translate this γ_0 property on $\mathcal{U}_r(n)$. Consider an element U of $\mathcal{U}_r(n)$ whose edges and stems are oriented w.r.t. the root angle as follows: the stems are all outgoing, and while walking clockwise around the unique face of U from a_0, the first time an edge is met, it is oriented counterclockwise w.r.t. the face of U. Then one can compute γ on the cycles of U (edges and stems count). We say that a unicellular map of $\mathcal{U}_r(n)$ satisfies the γ_0 property if γ equals zero on its (non-contractible) cycles. Let us call $\mathcal{U}_{r,b,\gamma_0}(n)$ the set of elements of $\mathcal{U}_{r,b}(n)$ satisfying the γ_0 property. So the output of ALGORITHM PS given by Theorem 3 is an element of $\mathcal{U}_{r,b,\gamma_0}(n)$.

Let $\mathcal{T}_r(n)$ be the set of toroidal triangulations on n vertices rooted at an angle that is not in the strict interior of a separating triangle. Then we have the following bijection:

Theorem 6 *There is a bijection between* $\mathcal{T}_r(n)$ *and* $\mathcal{U}_{r,b,\gamma_0}(n)$.

Proof Consider the mapping g that associates to an element of $\mathcal{T}_r(n)$, the output of ALGORITHM PS executed on the minimal HTC Schnyder wood w.r.t. the root face. By the above discussion the image of g is in $\mathcal{U}_{r,b,\gamma_0}(n)$ and g is injective since one can recover the original triangulation from its image by Theorem 4.

Conversely, given an element U of $\mathcal{U}_{r,b,\gamma_0}(n)$ with root angle a_0, one can build a toroidal map G by the complete closure procedure described in Sect. 6. The number of stems and edges of U implies that G is a triangulation. Recall that a_0 defines an

orientation on the edges and stems of U. Consider the orientation D of G induced by this orientation. Since U is balanced, the execution of ALGORITHM PS on (G, a_0) corresponds to the cycle in the angle graph of U obtained by starting from the root angle and walking clockwise in the face of U. Thus the output of ALGORITHM PS executed on (G, a_0) is U. It remains to show that G is appropriately rooted and that D corresponds to the minimal HTC Schnyder wood w.r.t. this root.

First note that by definition of $\mathcal{U}_r(n)$, the orientation D is a 3-orientation.

Suppose by contradiction that a_0 is in the strict interior of a separating triangle. Then, since we are considering a 3-orientation, by Euler's formula, the edges in the interior of this triangle and incident to its border are all entering the border. So ALGORITHM PS started from the strict interior cannot visit the vertices on the border of the triangle and outside. Thus the output of ALGORITHM PS is not a toroidal unicellular map, a contradiction. So a_0 is not in the strict interior of a separating triangle.

The γ_0 property of U implies that γ equals zero on two cycles of U. Hence these two cycles considered in G also satisfy γ equals 0 and form a basis for the homology. So D is an HTC Schnyder wood.

Suppose by contradiction that D is not minimal. Then, by Lemma 1, it contains a clockwise (non-empty) 0-homologous oriented subgraph w.r.t. f_0. With the notations of Sect. 3, let T be such a subgraph with $\phi(T) = -\sum_{F\in\mathcal{F}'} \lambda_F \phi(F)$, with $\lambda \in \mathbb{N}^{|\mathcal{F}'|}$. Let $\lambda_{F_0} = 0$, and $\lambda_{\max} = \max_{F\in\mathcal{F}} \lambda_F$. For $0 \leq i \leq \lambda_{\max}$, let $X_i = \{F \in \mathcal{F} \mid \lambda_F \geq i\}$. For $1 \leq i \leq \lambda_{\max}$, let T_i be the oriented subgraph such that $\phi(T_i) = -\sum_{F\in X_i} \phi(F)$. Then we have $\phi(T) = \sum_{1\leq i\leq\lambda_{\max}} \phi(T_i)$. Since T is an oriented subgraph, we have $\phi(T) \in \{-1, 0, 1\}^{|E(G)|}$. Thus for any edge of G, incident to faces F_1 and F_2, we have $(\lambda_{F_1} - \lambda_{F_2}) \in \{-1, 0, 1\}$. So, for $1 \leq i \leq \lambda_{\max}$, the oriented graph T_i is the frontier between the faces with λ value equal to i and $i - 1$. So all the T_i are edge disjoint and are oriented subgraphs of D. Since T is non-empty, we have $\lambda_{\max} \geq 1$, and T_1 is non-empty. All the edges of T_1 have a face of X_1 on their right and a face of X_0 on their left. Since U is an unicellular map, and T_1 is a (non-empty) 0-homologous oriented subgraph, at least one edge of T_1 corresponds to a stem of U. Let s be the last stem of U corresponding to a edge of T_1 that is reattached by the complete closure procedure. Consider the step where s is reattached. As the root angle (and thus f_0) is in the special face (see the terminology of Sect. 6), the special face is in the region defined by X_0. Thus it is on the left of s when it is reattached. This contradicts the fact that U is balanced. Thus D is the minimal HTC Schnyder wood w.r.t. f_0. □

10 The Lattice of HTC Schnyder Woods

In this section, we push further the study of HTC Schnyder woods in order to remove the root and the balanced property of the unicellular maps considered in Theorem 6 and obtain a simplified bijection in Theorem 7 of Sect. 11.

Consider a toroidal triangulation G given with a crossing Schnyder wood. Let D_0 be the corresponding 3-orientation of G. Let f_0 be any face of G. Recall from Sect. 3 that $O(G)$ denotes the set of all the orientations of G that are homologous to D_0. The elements of $O(G)$ are the HTC Schnyder woods of G and $(O(G), \leq_{f_0})$ is a distributive

lattice. We first recall some general results and terminology from [16] before studying the consequences of considering HTC Schnyder woods.

We need to reduce the graph G. We call an edge of G *rigid* w.r.t. $O(G)$ if it has the same orientation in all the elements of $O(G)$. Rigid edges do not play a role for the structure of $O(G)$. We delete them from G and call the obtained embedded graph $\widetilde{G}$. Note that this graph is embedded but it is not necessarily a map, as some faces may not be homeomorphic to open disks. Note also that $\widetilde{G}$ might be empty if all the edges are rigid, i.e. $|O(G)| = 1$ and $\widetilde{G}$ has no edge but a unique face that is all the surface.

Lemma 11 [16] *Given an edge e of G, the following are equivalent*:

1. *e is non-rigid*,
2. *e is contained in a 0-homologous oriented subgraph of D_0,*
3. *e is contained in a 0-homologous oriented subgraph of any element of $O(G)$.*

By Lemma 11, one can build $\widetilde{G}$ by keeping only the edges that are contained in a 0-homologous oriented subgraph of D_0. Note that this implies that all the edges of $\widetilde{G}$ are incident to two distinct faces of $\widetilde{G}$. Denote by $\widetilde{\mathcal{F}}$ the set of oriented subgraphs of $\widetilde{G}$ corresponding to the boundaries of faces of $\widetilde{G}$ considered counterclockwise. Let $\widetilde{f_0}$ be the face of $\widetilde{G}$ containing f_0 and $\widetilde{F_0}$ be the element of $\widetilde{\mathcal{F}}$ corresponding to the boundary of $\widetilde{f_0}$. Let $\widetilde{\mathcal{F}}' = \widetilde{\mathcal{F}} \setminus \widetilde{F_0}$. The elements of $\widetilde{\mathcal{F}}'$ are sufficient to generate the entire lattice $(O(G), \leq_{f_0})$ (see [16]), i.e. two elements D, D' of $O(G)$ are linked in the Hasse diagram of the lattice, with $D \leq_{f_0} D'$, if and only if $D \setminus D' \in \widetilde{\mathcal{F}}'$.

Lemma 12 [16] *For every element $\widetilde{F} \in \widetilde{\mathcal{F}}$ there exists D in $O(G)$ such that $\widetilde{F}$ is an oriented subgraph of D.*

By Lemma 12, for every element $\widetilde{F} \in \widetilde{\mathcal{F}}'$ there exists D in $O(G)$ such that $\widetilde{F}$ is an oriented subgraph of D. Thus there exists D' such that $\widetilde{F} = D \setminus D'$ and D, D' are linked in the Hasse diagram of the lattice. Thus the elements of $\widetilde{\mathcal{F}}'$ form a minimal set that generates the lattice.

Let $D_{\max}$ (resp. $D_{\min}$) be the maximal (resp. minimal) element of $(O(G), \leq_{f_0})$.

Lemma 13 [16] $\widetilde{F_0}$ (resp. $-\widetilde{F_0}$) is an oriented subgraph of $D_{\max}$ (resp. $D_{\min}$).

From now on we use some specific properties of the object considered in this paper, i.e. HTC Schnyder woods.

Lemma 14 *Consider an orientation D in $O(G)$ and a closed walk W of $\widetilde{G}$. If on the left side of W, there is no incident outgoing edges of D, then W is a triangle with its interior on its left side.*

Proof Consider a closed walk W of $\widetilde{G}$ such that on its left side there is no incident outgoing edges of D. Let W_{left} be the edges of D that are incident to the left side of W. By assumption they are all entering W. Note that W cannot cross itself otherwise it has at least one incident outgoing edges of D on its left side. However it may have repeated vertices but in that case it intersects itself tangentially on the right side.

Suppose first that W is a non-contractible cycle. Then consider the closed walk W^* of the dual orientation D^* that is obtained by considering all the dual edges of

W_{left} with their corresponding orientation. Since all the edges of W_{left} are entering W we have that W^* is an oriented closed walk. Moreover it is non-contractible and thus contains an oriented non-contractible cycle, a contradiction to Lemma 2. So W is not a non-contractible cycle.

Suppose by contradiction that there is an oriented subwalk W' of W, that forms a cycle C enclosing a region R on its right side that is homeomorphic to an open disk. Let v be the starting and ending vertex of W'. Note that we do not consider that W' is a strict subwalk of W, so we might have $W' = W$. Consider the graph G' obtained from G by keeping all the vertices and edges that lie in the region R, including W'. Since W can intersect itself only tangentially on the right side, we have that G' is a plane map whose outer face boundary is W' and whose interior is triangulated. Let k be the length of W'. Let n', m', f' be the number of vertices, edges and faces of G'. By Euler's formula, $n' - m' + f' = 2$. All the inner faces have length 3 and the outer face has length k, so $2m' = 3(f' - 1) + k$. Since there is no outgoing incident edges of D on the left side of W, all the vertices of G', except v, have their outgoing edges in G'. Since W' is oriented, v has at least one outgoing edge in G'. Thus, as we are considering a 3-orientation, we have $m' \geq 3(n' - 1) + 1$. Combining these three equalities gives $k \leq -1$, a contradiction. So there is no oriented subwalk of W, that forms a cycle enclosing an open disk on its right side.

Recall that since there is no incident outgoing edges of G on the left side of W, the walk W can only intersect itself tangentially and on its right side. Thus following W on its left, one draws a curve that does not intersect itself. This curve is thus either enclosing a region homeomorphic to an open disk or forming a non-contractible non-self intersecting curve. Suppose, by contradiction, that we are in the second case. Since there is no subwalk of W, that forms a cycle enclosing an open disk on its right side, we have that W is a non-contractible cycle, a contradiction. So the left side of W encloses a region R homeomorphic to an open disk.

Consider the graph G' obtained from G by keeping only the vertices and edges that lie in the region R, including W. The vertices of W appearing several times are duplicated so that G' is a plane triangulation of a cycle. Let k be the length of W. Let n', m', f' be the number of vertices, edges and faces of G'. By Euler's formula, $n' - m' + f' = 2$. All the inner faces have length 3 and the outer face has length k, so $2m' = 3(f' - 1) + k$. All the inner vertices have outdegree 3 as we are considering a 3-orientation of G. All the edges of W_{left} are oriented toward W, and there are k outer edges, so $m' = 3(n' - k) + k$. Combining these three equalities gives $k = 3$, i.e. W has length three and the lemma holds. □

The boundary of a face of $\widetilde{G}$ may be composed of several closed walks. Let us call *quasi-contractible* the faces of $\widetilde{G}$ that are homeomorphic to a disk or to a disk with punctures. Note that such a face may have several boundaries (if there is some punctures) but exactly one of these boundaries enclose the face. Let us call *outer facial walk* this special boundary. Then we have the following:

Lemma 15 *All the faces of $\widetilde{G}$ are quasi-contractible and their outer facial walk is a triangle.*

Proof Suppose by contradiction that there is a face $\widetilde{f}$ of $\widetilde{G}$ that is not quasi-contractible or whose outer facial walk is not a triangle. Let $\widetilde{F}$ be the element of $\widetilde{\mathcal{F}}$ corresponding to the boundary of $\widetilde{f}$. By Lemma 12, there exists an orientation D in $O(G)$ such that $\widetilde{F}$ is an oriented subgraph of D.

All the faces of G have length three. Thus $\widetilde{f}$ is not a face of G and contains in its interior at least one edge of G. Start from any such edge e and consider the *left-walk* $W = (e_i)_{i\geq 0}$ of D obtained by the following: if the edge e_i is entering a vertex v, then e_{i+1} is choosen among the three edges leaving v as the edge that is on the left coming from e_i (i.e. the first one while going clockwise around v). Suppose that for $i \geq 0$, edge e_i is entering a vertex v that is on the border of $\widetilde{f}$. Recall that by definition $\widetilde{F}$ is oriented counterclockwise according to its interior, so either e_{i+1} is in the interior of $\widetilde{f}$ or e_{i+1} is on the border of $\widetilde{f}$. Thus W cannot leave $\widetilde{f}$.

Since G has a finite number of edges, some edges are used several times in W. Consider a minimal subsequence $W' = e_k, \ldots, e_\ell$ such that no edge appears twice and $e_k = e_{\ell+1}$. Thus W ends periodically on the sequence of edges $e_k, \ldots, e_\ell$. By Lemma 14, all the closed walks that are part of $\widetilde{F}$ have some outgoing incident edges of D on their left side. Thus we have that W' contains at least one edge that is not an edge of $\widetilde{F}$, thus it contains at least one rigid edge.

By construction, on the left side of W', there is no incident outgoing edges of D. So, by Lemma 14, W' is a triangle with its interior on its left side. So W' is a 0-homologous oriented subgraph of D, thus all its edges are non-rigid by Lemma 11, a contradiction. □

By Lemma 15, every face of $\widetilde{G}$ is quasi-contractible and its outer facial walk is a triangle. So $\widetilde{G}$ contains all the triangles of G whose interiors are maximal by inclusion, i.e. it contains all the edges that are not in the interior of a separating triangle. In particular, $\widetilde{G}$ is non-empty and $|O(G)| \geq 2$. The status (rigid or not) of an edge lying inside a separating triangle is determined as in the planar case: such an edge is rigid if and only if it is in the interior of a separating triangle and incident to this triangle. Thus an edge of G is rigid if and only if it is in the interior of a separating triangle and incident to this triangle.

Since $(O(G), \leq_{f_0})$ is a distributive lattice, any element D of $O(G)$ that is distinct from $D_{\max}$ and $D_{\min}$ contains at least one neighbor above and at least one neighbor below in the Hasse diagram of the lattice. Thus it has at least one face of $\widetilde{G}$ oriented counterclockwise and at least one face of $\widetilde{G}$ oriented clockwise. Thus by Lemma 15, it contains at least one triangle oriented counterclockwise and at least one triangle oriented clockwise. Next lemma shows that this property is also true for $D_{\max}$ and $D_{\min}$.

Lemma 16 *In $D_{\max}$ (resp. $D_{\min}$) there is a counterclockwise (resp. clockwise) triangle containing f_0, and a clockwise (resp. counterclockwise) triangle not containing f_0.*

Proof By Lemma 15, $\widetilde{f_0}$ is quasi-contractible and its outer facial walk is a triangle T. By lemma 13, $\widetilde{F_0}$ is an oriented subgraph of $D_{\max}$. Thus T is oriented counterclockwise and contains f_0. The second part of the lemma is clear since $|O(G)| \geq 2$ so $D_{\max}$ has at least one neighbor below in the Hasse diagram of the lattice. Similarly for $D_{\min}$. □

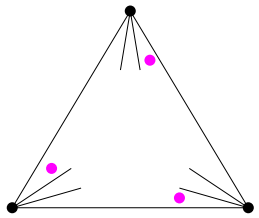

Fig. 20 Angles that are in a separating triangle but not in its clockwise interior

Thus by above remarks and Lemma 16, all the HTC Schnyder woods have at least one triangle oriented counterclockwise and at least one triangle oriented clockwise. Note that this property does not characterize HTC Schnyder woods. Figure 7 gives an example of a Schnyder wood that is not HTC but satisfies the property. Note also that not all Schnyder woods satisfy the property. The right of Fig. 5 is an example of a Schnyder wood that is no HTC and has no oriented triangle.

Lemma 16 is used in the next section to obtained a bijection with unrooted unicellular maps.

11 Bijection with Unrooted Unicellular Maps

To remove the root and the balanced property of the unicellular maps considered in Theorem 6, we have to root the toroidal triangulation more precisely than before. We say that an angle is not *in the clockwise interior of a separating triangle* if it is not in its interior, or if it is incident to a vertex v of the triangle and situated just before an edge of the triangle in counterclockwise order around v (see Fig. 20).

Consider a toroidal triangulation G. Consider a root angle a_0 that is not in the clockwise interior of a separating triangle. Note that the choice of a_0 is equivalent to the choice of a root vertex v_0 and a root edge e_0 incident to v_0 such that none is in the interior of a separating triangle. Consider the orientation of the edges of G corresponding to the minimal HTC Schnyder wood w.r.t. the root face f_0. By Lemma 16, there is a clockwise triangle containing f_0. Thus by the choice of a_0, the edge e_0 is leaving the root vertex v_0. This is the essential property used in this section. Consider the output U of ALGORITHM PS on (G, a_0). Since e_0 is leaving v_0 and a_0 is just before e_0 in counterclockwise order around v_0, the execution of ALGORITHM PS starts by Case 2 and e_0 corresponds in U to a stem s_0 attached to v_0. We call this stem s_0 the *root stem*.

The recovering method defined in Theorem 4 says that s_0 is the last stem reattached by the procedure. So there exists a sequence of admissible triples of U (see the terminology and notations of Sect. 6) such that s_0 belongs to the last admissible triple. Let $U_0 = U$ and for $1 \leq k \leq 2n-2$, the map U_k is obtained from U_{k-1} by closing any admissible triple that does no contain s_0. As noted in Sect. 6, the special face of U_{2n-2} is a quadrangle with exactly one stem. This stem being s_0, we are in the situation of Fig. 21.

Consequently, if one removes the root stem s_0 from U to obtain a unicellular map U' with n vertices, $n+1$ edges and $2n-2$ stems, one can recover the graph U_{2n-2} by applying a complete closure procedure on U' (see example of Fig. 22). Note that then,

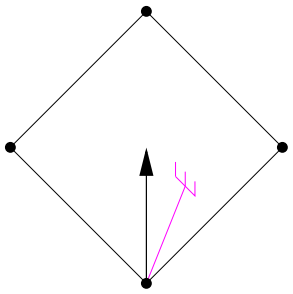

Fig. 21 The situation just before the last stem (i.e. the root stem) is reattached

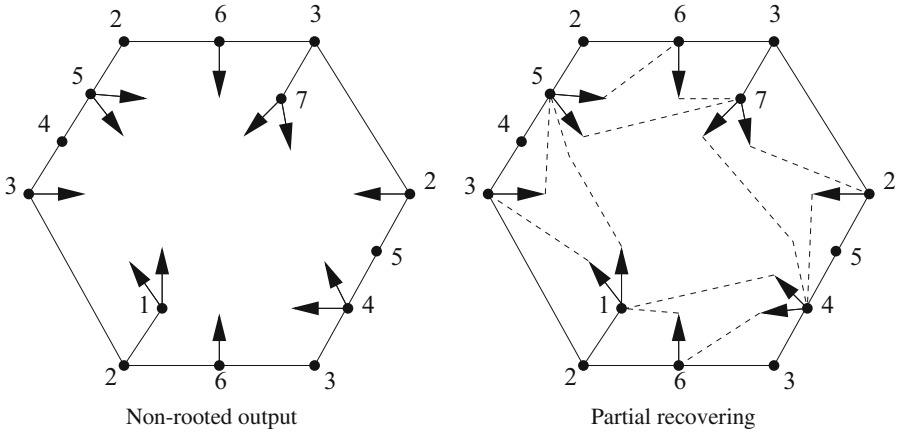

Fig. 22 Example of K_7 where the root angle, the root stem and the orientation w.r.t. the root angle have been removed from the output of Fig. 9. The complete closure procedure leads to a quadrangular face

there are four different ways to finish the closure of U_{2n-2} to obtain an oriented toroidal triangulation. This four cases correspond to the four ways to place the (removed) root stem in a quadrangle, they are obtained by pivoting Fig. 21 by 0°, 90°, 180° and 270°. Note that only one of this four cases leads to the original rooted triangulation G, except if there are some symmetries (like in the example of Fig. 22).

Let $\mathcal{U}(n)$ denote the set of (non-rooted) toroidal unicellular maps, with exactly n vertices, $n+1$ edges and $2n-2$ stems satisfying the following: a vertex has exactly 2 stems if it is not a corner, 1 stem if it is the corner of an hexagon and 0 stem if it is the corner of a square. Note that the output of Theorem 3 on an appropriately rooted toroidal triangulation is an element of $\mathcal{U}(n)$ when the root stem is removed.

Note that an element U' of $\mathcal{U}(n)$ is non-rooted so we cannot orient automatically its edges w.r.t. the root angle like in Sect. 9. Nevertheless one can still orient all the stems as outgoing and compute γ on the cycles of U' by considering only its stems in the counting (and not the edges nor the root stem anymore). We say that a unicellular map of $\mathcal{U}(n)$ satisfies the γ_0 property if γ equals zero on its (non-contractible) cycles. Let us call $\mathcal{U}_{\gamma_0}(n)$ the set of elements of $\mathcal{U}(n)$ satisfying the γ_0 property.

A surprising property is that an element U' of $\mathcal{U}(n)$ satisfies the γ_0 property if and only if any element U of $\mathcal{U}_r(n)$ obtained from U' by adding a root stem anywhere in U'

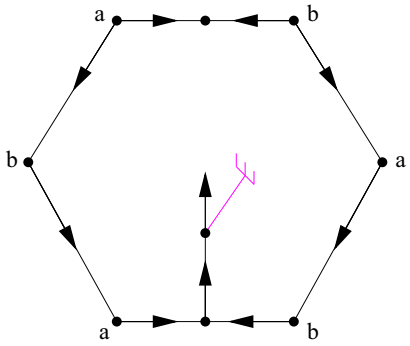

Fig. 23 The parts of the unicellular map showing the correspondence while computing γ with or without the orientation w.r.t. the root plus the root stem

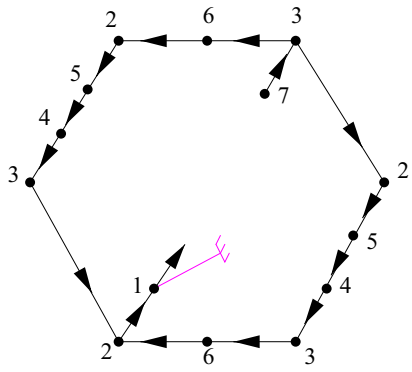

Fig. 24 The difference between the rooted output of Fig. 9 and the non-rooted output of Fig. 22

satisfies the γ_0 property (note that in U we count the edges and the root stem to compute γ). One can see this by considering the unicellular map of Fig. 23. It represents the general case of the underlying rooted hexagon of U. The edges represent in fact paths (some of which can be of length zero). One can check that it satisfies γ equals zero on its (non-contractible) cycles. It corresponds exactly to the set of edges that are taken into consideration when computing γ on U but not when computing γ on U'. Thus it does not affect the counting (the tree-like parts are not represented since they do not affect the value γ). So the output of Theorem 3 on an appropriately rooted toroidal triangulation is an element of $\mathcal{U}_{\gamma_0}(n)$ when the root stem is removed.

For the particular case of K_7, the difference between the rooted output of Fig. 9 and the non-rooted output of Fig. 22 is represented in Fig. 24 (one can superimpose the last two to obtain the first). One can check that these three unicellular maps (rooted, non-rooted and the difference) all satisfy γ equals zero on their cycles.

There is an "almost" four-to-one correspondence between toroidal triangulations on n vertices, given with a root angle that is not in the clockwise interior of a separating triangle, and elements of $\mathcal{U}_{\gamma_0}(n)$. The "almost" means that if the automorphism group of an element U of $\mathcal{U}_{\gamma_0}(n)$ is not trivial, some of the four ways to add a root stem in U are isomorphic and lead to the same rooted triangulation. In the example of Fig. 22, one can root in four ways the quadrangle but this gives only two different rooted

triangulations (because of the symmetries of K_7). We face this problem by defining another class for which we can formulate a bijection.

Let $\mathcal{T}(n)$ be the set of toroidal maps on n vertices, where all the faces have length three, except one that has length four and which is not in a separating triangle. Then we have the following bijection:

Theorem 7 *There is a bijection between $\mathcal{T}(n)$ and $\mathcal{U}_{\gamma_0}(n)$.*

Proof Let a (for "add") be an arbitrarily chosen mapping defined on the maps G' of $\mathcal{T}(n)$ that adds a diagonal e_0 in the quadrangle of G' and roots the obtained toroidal triangulation G at a vertex v_0 incident to e_0 (this defines the root angle a_0 situated just before e_0 in counterclockwise order around v_0). Note that the added edge cannot create homotopic multiple edges, since otherwise the quadrangle would be in a separating triangle. Moreover the root angle of G is not in the clockwise interior of a separating triangle. Thus the image of a is in $\mathcal{T}'_r(n)$, the subset of $\mathcal{T}_r(n)$ corresponding to toroidal triangulations rooted at an angle that is not in the clockwise interior of a separating triangle.

Let $\mathcal{U}'_{r,b,\gamma_0}(n)$ be the elements of $\mathcal{U}_{r,b,\gamma_0}(n)$ that have their root angle just before a stem in counterclockwise order around the root vertex. Consider the mapping g, defined in the proof of Theorem 9. By above remarks and Theorem 9, the image of g restricted to $\mathcal{T}'_r(n)$ is in $\mathcal{U}'_{r,b,\gamma_0}(n)$. Let r (for "remove") be the mapping that associates to an element of $\mathcal{U}'_{r,b,\gamma_0}(n)$ an element of $\mathcal{U}_{\gamma_0}(n)$ obtained by removing the root angle and its corresponding stem. Finally, let $h = r \circ g \circ a$ which associates to an element of $\mathcal{T}(n)$ an element of $\mathcal{U}_{\gamma_0}(n)$. Let us show that h is a bijection.

Consider an element G' of $\mathcal{T}(n)$ and its image U' by h. The complete closure procedure on U' gives G' thus the mapping h is injective.

Conversely, consider an element U' of $\mathcal{U}_{\gamma_0}(n)$. Apply the complete closure procedure on U'. At the end of this procedure, the special face is a quadrangle whose angles are denoted $\alpha^1, \ldots, \alpha^4$. We denote also by $\alpha^1, \ldots, \alpha^4$ the corresponding angles of U'. For $i \in \{1, \ldots, 4\}$, let U^i be the element of $\mathcal{U}_r(n)$ obtained by adding a root stem and a root angle in the angle α^i of U', with the root angle just before the stem in counterclockwise order around the root vertex. Note that by the choice of α^i, the U^i are all balanced. By above remarks they also satisfy the γ_0 property and thus they are in $\mathcal{U}'_{r,b,\gamma_0}(n)$.

By the proof of Theorem 6, the complete closure procedure on U^i gives a triangulation G^i of $\mathcal{T}_r(n)$ that is rooted from an angle a_0^i not in the strict interior of a separating triangle and oriented according to the minimal HTC Schnyder wood w.r.t. the root face. Moreover the output of ALGORITHM PS applied on (G^i, a_0^i) is U^i. Since in U^i, the root stem is present just after the root angle, the first edge seen by the execution of ALGORITHM PS on (G^i, a_0^i) is outgoing. So a_0 is not in the clockwise interior of a separating triangle (in a 3-orientation, all the edges that are in the interior of a separating triangle and incident to the triangle are entering the triangle). Thus the G^i are appropriately rooted and are elements of $\mathcal{T}'_r(n)$. Removing the root edge of any G_i, gives the same map G' of $\mathcal{T}(n)$. Exactly one of the G_i is the image of G' by the mapping a. Thus the image of G' by h is U' and the mapping h is surjective. □

A nice aspect of Theorem 7 comparing to Theorem 6 is that the unicellular maps that are considered are much simpler. They have no root nor balanced property anymore. It would be great to use Theorem 7 to count and sample toroidal triangulations. The main issue comparing to the planar case seems to be the γ_0 property.

12 Conclusion

Note that the work presented here is related to a work of Bernardi and Chapuy [5] (their convention for the orientation of the edges is the reverse of ours). Consider a map G (not necessarily a triangulation) on an oriented surface of genus g, rooted at a particular angle a_0. An orientation of G is *right* if for each edge e, the *right-walk* starting from e (when entering a vertex, the next chosen edge is the one leaving on the right) reaches the root edge e_0 via the root vertex v_0. A consequence of [5] is that ALGORITHM PS applied on an orientation of (G, a_0) outputs a spanning unicellular submap U if and only if the considered orientation is right. Note that in this characterization, the submap U is not necessarily a map of genus g, its genus can be any value in $\{0, \ldots, g\}$. In the particular case of toroidal triangulations we show that by considering minimal HTC Schnyder woods the output U is a toroidal spanning unicellular map. Hence by the above characterization, minimal HTC Schnyder woods are right. But here, the fact that U and G have the same genus is of particular interest as it yields a simple bijection.

The key property that makes U and G have same genus is the conclusion of Lemma 2 (no oriented non-contractible cycle in the dual orientation). Recently, Albar, the second author and Knauer [1] proved the following:

Theorem 8 ([1]) *A simple triangulation on a genus $g \geq 1$ orientable surface admits an orientation of its edges such that every vertex has outdegree at least* 3*, and divisible by* 3*.*

Theorem 8 is proved for simple triangulation but we believe it to be true for all triangulations. Moreover we hope for a possible generalization satisfying the conclusion of Lemma 2:

Conjecture 1 *A triangulation on a genus $g \geq 1$ orientable surface admits an orientation of its edges such that every vertex has outdegree at least* 3*, divisible by* 3*, and such that there is no oriented non-contractible cycle in the dual orientation.*

If Conjecture 1 is true, one can consider a minimal orientation satisfying its conclusion and apply ALGORITHM PS to obtain a unicellular map of the same genus as G. Note that more efforts should be made to obtain a bijection since there might be several minimal elements satisfying the conjecture and a particular one has to be identified (as the minimal HTC Schnyder wood in our case).

Acknowledgements We thank Luca Castelli Aleardi, Nicolas Bonichon, Eric Fusy and Frédéric Meunier for fruitful discussions about this work. This work was supported by the Grant EGOS ANR-12-JS02-002-01 and the project-team GALOIS supported by LabEx PERSYVAL-Lab ANR-11-LABX-0025.

References

1. Albar, B., Gonçalves, D., Knauer, K.: Orienting triangulations. J. Graph Theory **83**(4), 392–405 (2016)
2. Albenque, M., Poulalhon, D.: Generic method for bijections between blossoming trees and planar maps. Electron. J. Comb. **22**(2), paper P2.38 (2015)
3. Aleardi, L.C., Fusy, E., Lewiner, T.: Optimal encoding of triangular and quadrangular meshes with fixed topology. In: Proceedings of the 22nd Canadian Conference on Computational Geometry (CCCG 2010)
4. Bernardi, O.: Bijective counting of tree-rooted maps and shuffles of parenthesis systems. Electron. J. Comb. **14**, R9 (2007)
5. Bernardi, O., Chapuy, G.: A bijection for covered maps, or a shortcut between Harer-Zagier's and Jackson's formulas. J Comb Theory A **118**, 1718–1748 (2011)
6. Bonichon, N., Gavoille, C., Hanusse, N.: An information-theoretic upper bound of planar graphs using triangulation. Proceedings of the 20th Annual Symposium on Theoretical Aspects of Computer Science (STACS 2003). Lecture Notes in Computer Science, vol. 2607, pp. 499–510. Springer, Berlin (2003)
7. Chapuy, G.: A new combinatorial identity for unicellular maps, via a direct bijective approach. Adv. Appl. Math. **47**, 874–893 (2011)
8. Chapuy, G., Marcus, M., Schaeffer, G.: A bijection for rooted maps on orientable surfaces. SIAM J. Discrete Math. **23**, 1587–1611 (2009)
9. de Fraysseix, H., de Mendez, O.P.: On topological aspects of orientations. Discrete Math. **229**, 57–72 (2001)
10. de Mendez, P.O.: Orientations bipolaires. PhD Thesis (1994)
11. Duchi, E., Poulalhon, D., Schaeffer, G.: Uniform random sampling of simple branched coverings of the sphere by itself. In: Proceedings of the Twenty-Fifth Annual ACM-SIAM Symposium on Discrete Algorithms. pp. 294–304. Society for Industrial and Applied Mathematics, New York (2013)
12. Felsner, S.: Lattice structures from planar graphs. Electron. J. Comb. **11**, R15 (2004)
13. Fusy, E.: Combinatoire des cartes planaires et applications algorithmiques. PhD Thesis (2007). http://www.lix.polytechnique.fr/Labo/Eric.Fusy/Theses/these_eric_fusy.pdf
14. Giblin, P.: Graphs. Surfaces and Homology. Cambridge University Press, Cambridge (2010)
15. Gonçalves, D., Lévêque, B.: Toroidal maps: Schnyder woods, orthogonal surfaces and straight-line representations. Discrete Comput. Geom. **51**, 67–131 (2014)
16. Gonçalves, D., Knauer, K., Lévêque, B.: Structure of Schnyder labelings on orientable surfaces (2015). arXiv:1501.05475
17. Kant, G.: Drawing planar graphs using the canonical ordering. Algorithmica **16**, 4–32 (1996)
18. Lévêque, B.: Generalization of Schnyder woods to orientable surfaces and applications. HDR Thesis (2016). http://pagesperso.g-scop.grenoble-inp.fr/~levequeb/Publications/HDR.pdf
19. Mohar, B.: Straight-line representations of maps on the torus and other flat surfaces. Discrete Math. **155**, 173–181 (1996)
20. Poulalhon, D., Schaeffer, G.: Optimal coding and sampling of triangulations. Algorithmica **46**, 505–527 (2006)
21. Propp, J.: Lattice structure for orientations of graphs (1993). arXiv:math/0209005
22. Schnyder, W.: Planar graphs and poset dimension. Order **5**, 323–343 (1989)
23. Ueckerdt, T.: Geometric representations of graphs with low polygonal complexity. PhD Thesis (2011). http://www.math.kit.edu/iag6/~ueckerdt/media/thesis-ueckerdt.pdf

On the structure of Schnyder woods on orientable surfaces*

Daniel Gonçalves†, Kolja Knauer‡, Benjamin Lévêque§

January 8, 2018

Abstract

We propose a simple generalization of Schnyder woods from the plane to maps on orientable surfaces of higher genus. This is done in the language of angle labelings. Generalizing results of De Fraysseix and Ossona de Mendez, and Felsner, we establish a correspondence between these labelings and orientations and characterize the set of orientations of a map that correspond to such a Schnyder labeling. Furthermore, we study the set of these orientations of a given map and provide a natural partition into distributive lattices depending on the surface homology. This generalizes earlier results of Felsner and Ossona de Mendez. In the toroidal case, a new proof for the existence of Schnyder woods is derived from this approach.

1 Introduction

Schnyder [25] introduced Schnyder woods for planar triangulations with the following local property:

Definition 1.1 (Schnyder property) *Given a map G, a vertex v and an orientation and coloring[1] of the edges incident to v with the colors 0, 1, 2, we say that v satisfies the* Schnyder property*, (see Figure 1) if v satisfies the following local property:*

- *Vertex v has out-degree one in each color.*
- *The edges $e_0(v)$, $e_1(v)$, $e_2(v)$ leaving v in colors 0, 1, 2, respectively, occur in counterclockwise order.*

*This work was supported by the grant EGOS ANR-12-JS02-002-01

†CNRS, Université de Montpellier, LIRMM UMR 5506, CC477, 161 rue Ada, 34095 Montpellier Cedex 5, France. daniel.goncalves@lirmm.fr

‡Aix Marseille Université, LIF UMR 7279, Parc Scientifique et Technologique de Luminy, 163 avenue de Luminy - Case 901, 13288 Marseille Cedex 9, France. kolja.knauer@lif.univ-mrs.fr

§CNRS, Laboratoire G-SCOP UMR 5272, 46 Avenue Félix Viallet, 38031 Grenoble Cedex 1, France benjamin.leveque@cnrs.fr

[1]Throughout the paper colors and some of the indices are given modulo 3.

- *Each edge entering v in color i enters v in the counterclockwise sector from $e_{i+1}(v)$ to $e_{i-1}(v)$.*

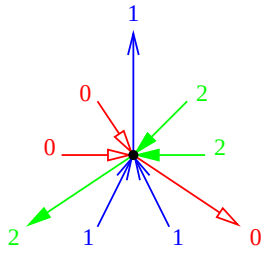

Figure 1: The Schnyder property. The depicted correspondence between red, blue, green, 0, 1, 2, and the arrow shapes will be used through the paper.

Definition 1.2 (Schnyder wood) *Given a planar triangulation G, a* Schnyder wood *is an orientation and coloring of the inner edges of G with the colors* 0, 1, 2 *(edges are oriented in one direction only), where each inner vertex v satisfies the* Schnyder property.

See Figure 2 for an example of a Schnyder wood.

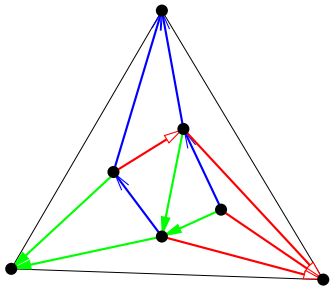

Figure 2: Example of a Schnyder wood of a planar triangulation.

Schnyder woods are today one of the main tools in the area of planar graph representations. Among their most prominent applications are the following: They provide a machinery to construct space-efficient straight-line drawings [26, 18, 8], yield a characterization of planar graphs via the dimension of their vertex-edge incidence poset [25, 8], and are used to encode triangulations [23, 3]. Further applications lie in enumeration [4], representation by geometric objects [13, 16], graph spanners [5], etc. The richness of

these applications has stimulated research towards generalizing Schnyder woods to non planar graphs.

For higher genus triangulated surfaces, a generalization of Schnyder woods has been proposed by Castelli Aleardi, Fusy and Lewiner [6], with applications to encoding. In this definition, the simplicity and the symmetry of the original definition of Schnyder woods are lost. Here we propose an alternative generalization of Schnyder woods for higher genus that generalizes the one proposed in [17] for the toroidal case.

A closed curve on a surface is *contractible* if it can be continuously transformed into a single point. Except if stated otherwise, we consider graphs embedded on orientable surfaces such that they do not have contractible cycles of size 1 or 2 (i.e. no contractible loops and no contractible double edges). Note that this is a weaker assumption, than the graph being *simple*, i.e. not having *any* cycles of size 1 or 2 (i.e. no loops and no multiple edges). A graph embedded on a surface is called a *map* on this surface if all its faces are homeomorphic to open disks. A map is a triangulation if all its faces are triangles.

In this paper we consider finite maps. We denote by n be the number of vertices and m the number of edges of a graph. Given a graph embedded on a surface, we use f for the number of faces. Euler's formula says that any map on an orientable surface of genus g satisfies $n-m+f = 2-2g$. In particular, the plane is the surface of genus 0, the torus the surface of genus 1, the double torus the surface of genus 2, etc. By Euler's formula, a triangulation of genus g has exactly $3n + 6(g-1)$ edges. So having a generalization of Schnyder woods in mind, for all $g \geq 2$ there are too many edges to force all vertices to have outdegree exactly three. This problem can be overcome by allowing vertices to fulfill the Schnyder property "several times", i.e. such vertices have outdegree 6, 9, etc. with the color property of Figure 1 repeated several times (see Figure 3).

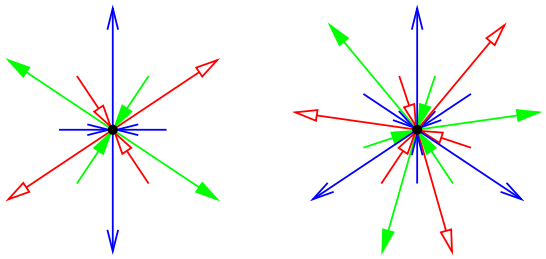

Outdegree six Outdegree nine

Figure 3: The Schnyder property repeated several times around a vertex.

Figure 4 is an example of such a Schnyder wood on a triangulation of the double torus. The double torus is represented by a fundamental polygon – an octagon. The sides of the octagon are identified according to their labels. All the vertices of the triangulation have outdegree three except two vertices, the circled ones, that have outdegree six. Each

of the latter appear twice in the representation.

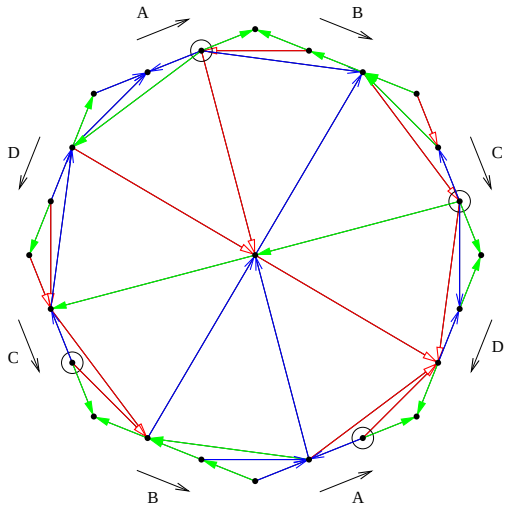

Figure 4: A Schnyder wood of a triangulation of the double torus.

In this paper we formalize this idea to obtain a concept of Schnyder woods applicable to general maps (not only triangulations) on arbitrary orientable surfaces. This is based on the definition of Schnyder woods via angle labelings in Section 2. We prove several basic properties of these objects. While every map admits a "trivial" Schnyder wood, the existence of a non-trivial one remains open but leads to interesting conjectures.

By a result of De Fraysseix and Ossona de Mendez [14], for any planar triangulation there is a bijection between its Schnyder woods and the orientations of its inner edges where every inner vertex has outdegree three. Thus, any orientation with the proper outdegree corresponds to a Schnyder wood and there is a unique way, up to symmetry of the colors, to assign colors to the oriented edges in order to fulfill the Schnyder property at every inner vertex. This is not true in higher genus as already in the torus, there exist orientations that do not correspond to any Schnyder wood (see Figure 5). In Section 3, we characterize orientations that correspond to our generalization of Schnyder woods.

In Section 4, we study the transformations between Schnyder orientations. We obtain a partition of the set of Schnyder woods into homology classes of orientations, each of these classes being a distributive lattice. This generalizes corresponding results obtained for the plane by Ossona de Mendez [22] and Felsner [10]. The particular properties of the minimal element of such a lattice recently led to an optimal linear encoding method for toroidal triangulations by Despré, the first author, and the third author [7]. This generalizes previous results of Poulalhon and Schaeffer for the plane [23].

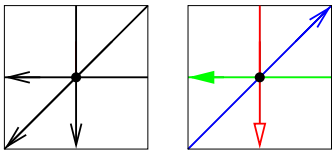

Figure 5: Two different orientations of a toroidal triangulation. Only the one on the right corresponds to a Schnyder wood.

In Section 5, we focus on toroidal triangulations. We use the characterization theorem of Section 3 to give a new proof of the existence of Schnyder woods in this case. We show that the so-called "crossing" property allows to define a canonical lattice. Note that this special lattice is the one used in [7] to obtain a bijection. Finally the results of the paper are illustrated by an example.

2 Generalization of Schnyder woods

2.1 Angle labelings

Consider a map G on an orientable surface. An *angle labeling* of G is a labeling of the angles of G (i.e. face corners of G) in colors 0, 1, 2. More formally, we denote an angle labeling by a function $\ell : \mathcal{A} \to \mathbb{Z}_3$, where $\mathcal{A}$ is the set of angles of G. Given an angle labeling, we define several properties of vertices, faces and edges that generalize the notion of Schnyder angle labeling in the planar case [12].

Consider an angle labeling ℓ of G. A vertex or a face v is of *type* k, for $k \geq 1$, if the labels of the angles around v form, in counterclockwise order, $3k$ nonempty intervals such that in the j-th interval all the angles have color $(j \mod 3)$. A vertex or a face v is of *type* 0, if the labels of the angles around v are all of color i for some i in $\{0, 1, 2\}$.

An edge e is of *type* 1 *or* 2 if the labels of the four angles incident to edge e are, in clockwise order, $i-1$, i, i, $i+1$ for some i in $\{0, 1, 2\}$. The edge e is of *type* 1 if the two angles with the same color are incident to the same extremity of e and of *type* 2 if the two angles are incident to the same side of e. An edge e is of *type* 0 if the labels of the four angles incident to edge e are all i for some i in $\{0, 1, 2\}$ (See Figure 6).

If there exists a function $f : V \to \mathbb{N}$ such that every vertex v of G is of type $f(v)$, we say that ℓ is f-VERTEX. If we do not want to specify the function f, we simply say that ℓ is VERTEX. We sometimes use the notation K-VERTEX if the labeling is f-VERTEX for a function f with $f(V) \subseteq K$. When $K = \{k\}$, i.e. f is a constant function, then we use the notation k-VERTEX instead of f-VERTEX. Similarly we define FACE, K-FACE, k-FACE, EDGE, K-EDGE, k-EDGE.

The following lemma expresses that property EDGE is the central notion here. Properties K-VERTEX and K-FACE are used later on to express additional requirements on

the angle labelings that are considered.

Lemma 2.1 *An* EDGE *angle labeling is* VERTEX *and* FACE.

Proof. Let ℓ be an EDGE angle labeling. Consider two counterclockwise consecutive angles a, a' around a vertex (or a face). Property EDGE implies that $\ell(a') = \ell(a)$ or $\ell(a') = \ell(a) + 1$ (see Figure 6). Thus by considering all the angles around a vertex or a face, it is clear that ℓ is also VERTEX and FACE. □

Thus we define a Schnyder labeling as follows:

Definition 2.2 (Schnyder labeling) *Given a map G on an orientable surface, a* Schnyder labeling *of G is an* EDGE *angle labeling of G.*

Figure 6 shows how an EDGE angle labeling defines an orientation and coloring of the edges of the graph with edges oriented in one direction or in two opposite directions.

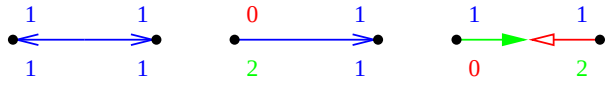

Figure 6: Correspondence between EDGE angle labelings and some bi-orientations and colorings of the edges.

In the next two sections, the correspondence from Figure 6 is used to show that Schnyder labelings correspond to or generalize previously defined Schnyder woods in the plane and in the torus. Hence, they are a natural generalization of Schnyder woods for higher genus.

2.2 Planar Schnyder woods

Originally, Schnyder woods were defined only for planar triangulations [25]. Felsner [8, 9] extended this definition to planar maps. To do so he allowed edges to be oriented in one direction or in two opposite directions (originally only one direction was possible). The formal definition is the following:

Definition 2.3 (Planar Schnyder wood) *Given a planar map G. Let x_0, x_1, x_2 be three vertices occurring in counterclockwise order on the outer face of G. The* suspension *G^σ is obtained by attaching a half-edge that reaches into the outer face to each of these special vertices. A* planar Schnyder wood *rooted at x_0, x_1, x_2 is an orientation and coloring of the edges of G^σ with the colors 0, 1, 2, where every edge e is oriented in one direction or in two opposite directions (each direction having a distinct color and being outgoing), satisfying the following conditions:*

- *Every vertex satisfies the Schnyder property and the half-edge at x_i is directed outward and colored i.*
- *There is no interior face whose boundary is a monochromatic cycle.*

See Figure 7 for two examples of planar Schnyder woods.

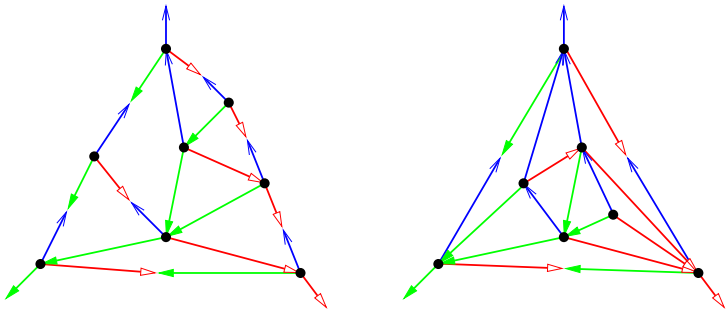

Figure 7: A planar Schnyder wood of a planar map and of a planar triangulation.

The correspondence of Figure 6 gives the following bijection, as proved by Felsner [9]:

Proposition 2.4 ([9]) *If G is a planar map and x_0, x_1, x_2 are three vertices occurring in counterclockwise order on the outer face of G, then the planar Schnyder woods of G^σ are in bijection with the $\{1,2\}$-EDGE, 1-VERTEX, 1-FACE angle labelings of G^σ (with the outer face being 1-FACE but in clockwise order).*

Felsner [8] and Miller [20] characterized the planar maps that admit a planar Schnyder wood. Namely, they are the internally 3-connected maps (i.e. those with three vertices on the outer face such that the graph obtained from G by adding a vertex adjacent to the three vertices is 3-connected).

2.3 Generalized Schnyder woods

Any map (on any orientable surface) admits a trivial EDGE angle labeling: the one with all angles labeled i (and thus all edges, vertices, and faces are of type 0). A natural non-trivial case, that is also symmetric for the duality, is to consider EDGE, $\mathbb{N}^*$-VERTEX, $\mathbb{N}^*$-FACE angle labelings of general maps (where $\mathbb{N}^* = \mathbb{N}\backslash\{0\}$). In planar Schnyder woods only type 1 and type 2 edges are used. Here we allow type 0 edges because they seem unavoidable for some maps (see discussion below). This suggests the following definition of Schnyder woods in higher genus.

First, the generalization of the Schnyder property is the following:

Definition 2.5 (Generalized Schnyder property) *Given a map G on a genus $g \geq 1$ orientable surface, a vertex v and an orientation and coloring of the edges incident to v with the colors 0, 1, 2, we say that v satisfies the* generalized Schnyder property *(see Figure 3), if v satisfies the following local property for $k \geq 1$:*

- *Vertex v has out-degree $3k$.*
- *The edges $e_0(v), \ldots, e_{3k-1}(v)$ leaving v in counterclockwise order are such that $e_j(v)$ has color j mod 3.*
- *Each edge entering v in color i enters v in a counterclockwise sector from $e_j(v)$ to $e_{j+1}(v)$ with $i \not\equiv j \pmod 3$ and $i \not\equiv j+1 \pmod 3$.*

Then, the generalization of Schnyder woods is the following (where the three types of edges depicted on Figure 6 are allowed):

Definition 2.6 (Generalized Schnyder wood) *Given a map G on a genus $g \geq 1$ orientable surface, a* generalized Schnyder wood *of G is an orientation and coloring of the edges of G with the colors 0, 1, 2, where every edge is oriented in one direction or in two opposite directions (each direction having a distinct color and being outgoing, or each direction having the same color and being incoming), satisfying the following conditions:*

- *Every vertex satisfies the generalized Schnyder property.*
- *There is no face whose boundary is a monochromatic cycle.*

When there is no ambiguity we call "generalized Schnyder woods" just "Schnyder woods". See Figure 8 for two examples of Schnyder woods in the torus.

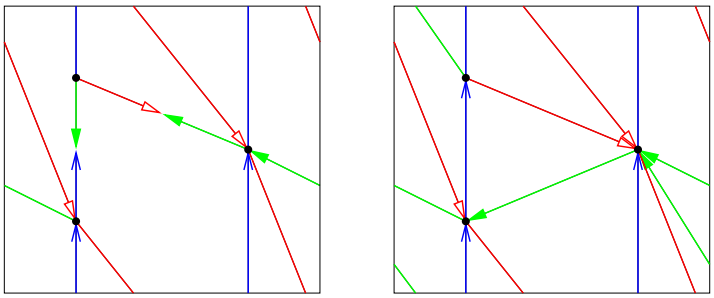

Figure 8: A Schnyder wood of a toroidal map and of a toroidal triangulation.

The first and third author already defined Schnyder woods for toroidal maps in [17]. Our definition is broader as in [17], there is also a (global) condition on the way monochromatic cycles intersect. See Section 5.2 for a discussion on this property.

Figure 4 is an example of a Schnyder wood on a triangulation of the double torus. The correspondence from Figure 6 immediately gives the following bijection whose proof is omitted.

Proposition 2.7 *If G is a map on a genus $g \geq 1$ orientable surface, then the generalized Schnyder woods of G are in bijection with the* EDGE, $\mathbb{N}^*$-VERTEX, $\mathbb{N}^*$-FACE *angle labelings of G.*

The examples in Figures 8 and 4 do not have type 0 edges. However, for all $g \geq 2$, there are genus g maps, with vertex degrees and face degrees at most five. Figure 9 depicts how to construct such maps, for all $g \geq 2$. For these maps, type 0 edges are unavoidable. Indeed, take such a map with an angle labeling that has only type 1 and type 2 edges. Around a type 1 or type 2 edge there are exactly three changes of labels, so in total there are exactly $3m$ such changes. As vertices and faces have degree at most five, they are either of type 0 or 1, hence the number of label changes should be at most $3n+3f$. Thus, $3m \leq 3n+3f$, which contradicts Euler's formula for $g \geq 2$. Furthermore, note that the maps described in Figure 9, as well as their dual maps, are 3-connected. Actually they can be modified to be 4-connected and of arbitrary large face-width.

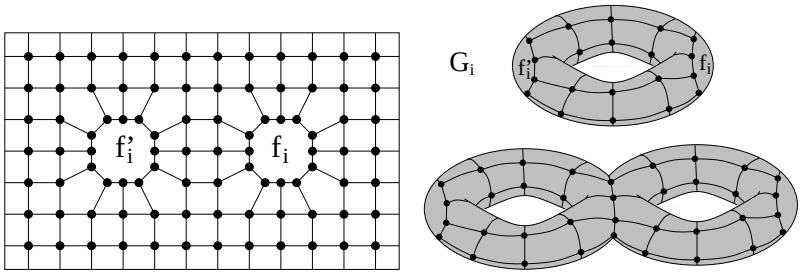

Figure 9: A toroidal map G_i with two distinguished faces, f_i and f'_i. Take g copies G_i with $1 \leq i \leq g$ and glue them by identifying f_i and f'_{i+1} for all $1 \leq i < g$. Faces f_1 and f'_g are filled to have only vertices and faces of degree at most five.

An orientation and coloring of the edges corresponding to an EDGE, $\mathbb{N}^*$-VERTEX, $\mathbb{N}^*$-FACE angle labelings is given for the double-toroidal map of Figure 10. It contains two edges of type 0 and it is 1-VERTEX and 1-FACE. Similarly, one can obtain EDGE, $\mathbb{N}^*$-VERTEX, $\mathbb{N}^*$-FACE angle labelings for any map in Figure 9.

2.4 Schnyder woods in the universal cover

In this section we prove some properties of Schnyder woods in the universal cover. We refer to [19] for the general theory of universal covers. The *universal cover* of the torus (resp. an orientable surface of genus $g \geq 2$) is a surjective mapping p from the plane

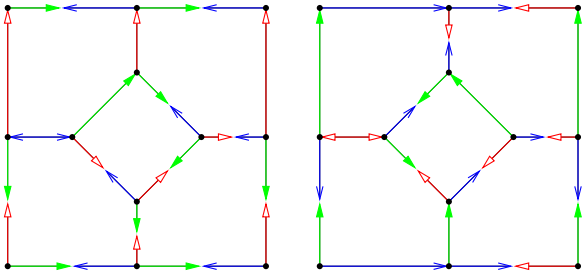

Figure 10: An orientation and coloring of the edges of a double-toroidal map that correspond to an EDGE, $\mathbb{N}^*$-VERTEX, $\mathbb{N}^*$-FACE angle labeling. Here, the two parts are toroidal and the two central faces are identified (by preserving the colors) to obtain a double-toroidal map.

(resp. the open unit disk) to the surface that is locally a homeomorphism. The universal cover of the torus is obtained by replicating a flat representation of the torus to tile the plane. Figure 11 shows how to obtain the universal cover of the double torus. The key property is that a closed curve on the surface corresponds to a closed curve in the universal cover if and only if it is contractible.

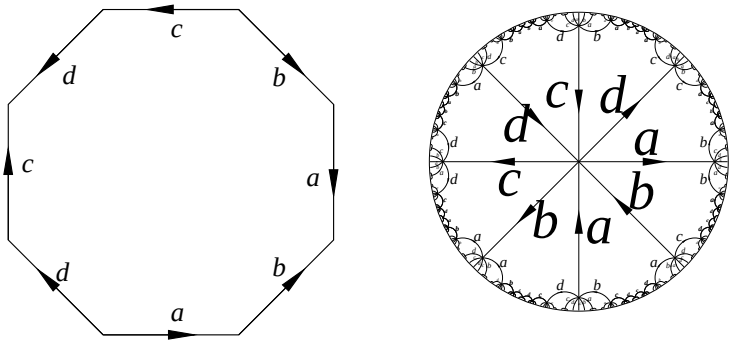

Figure 11: Canonical representation and universal cover of the double torus (source : Yann Ollivier `http://www.yann-ollivier.org/maths/primer.php`).

Universal covers can be used to represent a map on an orientable surface as an infinite planar map. Any property of the map can be lifted to its universal cover, as long as it is defined locally. Thus universal covers are an interesting tool for the study of Schnyder labelings since all the definitions we have given so far are purely local.

Consider a map G on a genus $g \geq 1$ orientable surface. Let G^∞ be the infinite planar map drawn on the universal cover and defined by $p^{-1}(G)$.

We need the following general lemma concerning universal covers:

Lemma 2.8 *Suppose that for a finite set of vertices X of G^∞, the graph $G^\infty \setminus X$ is not connected. Then $G^\infty \setminus X$ has a finite connected component.*

Proof. Suppose the lemma is false and $G^\infty \setminus X$ is not connected and has no finite component. Then it has a face bounded by an infinite number of vertices. As G is finite, the vertices of G^∞ have bounded degree. Putting back the vertices of X, a face bounded by an infinite number of vertices would remain. The border of this face does not correspond to a contractible cycle of G, a contradiction with G being a map. □

Recall that a graph is *k-connected* if it has at least $k+1$ vertices and if it remains connected after removing any $k-1$ vertices. Extending the notion of essentially 2-connectedness defined in [21] for the toroidal case, we say that G is *essentially k-connected* if G^∞ is k-connected. Note that the notion of being essentially k-connected is different from G being k-connected. There is no implications in any direction. But note that since G is a map, it is essentially 1-connected.

Suppose now that G is given with a Schnyder wood (i.e. an EDGE, $\mathbb{N}^*$-VERTEX, $\mathbb{N}^*$-FACE angle labeling by Proposition 2.7). Consider the orientation and coloring of the edges of G^∞ corresponding to the Schnyder wood of G.

Let G_i^∞ be the directed graph induced by the edges of color i of G^∞. This definition includes edges that are half-colored i, and in this case, the edges get only the direction corresponding to color i. The graph $(G_i^\infty)^{-1}$ is the graph obtained from G_i^∞ by reversing all its edges. The graph $G_i^\infty \cup (G_{i-1}^\infty)^{-1} \cup (G_{i+1}^\infty)^{-1}$ is obtained from the graph G by orienting edges in one or two directions depending on whether this orientation is present in G_i^∞, $(G_{i-1}^\infty)^{-1}$ or $(G_{i+1}^\infty)^{-1}$. Similarly to what happens for planar Schnyder woods, we have the following:

Lemma 2.9 *The graph $G_i^\infty \cup (G_{i-1}^\infty)^{-1} \cup (G_{i+1}^\infty)^{-1}$ does not contain directed cycle.*

Proof. Suppose there is a directed cycle in $G_i^\infty \cup (G_{i-1}^\infty)^{-1} \cup (G_{i+1}^\infty)^{-1}$. Let C be such a cycle containing the minimum number of faces in the map D with border C. Suppose by symmetry that C turns around D counterclockwisely. Every vertex of D has at least one outgoing edge of color $i+1$ in D. So there is a cycle of color $(i+1)$ in D and this cycle is C by minimality of C. Every vertex of D has at least one outgoing edge of color i in D. So, again by minimality of C, the cycle C is a cycle of color i. Thus all the edges of C are oriented in color i counterclockwisely and in color $i+1$ clockwisely.

By the definition of Schnyder woods, there is no face the boundary of which is a monochromatic cycle, so D is not a face. Let vx be an edge in the interior of D that is outgoing for v. The vertex v can be either in the interior of D or in C (if v has more

than three outgoing arcs). In both cases, v has necessarily an edge e_i of color i and an edge e_{i+1} of color $i+1$, leaving v and in the interior of D. Consider $W_i(v)$ (resp. $W_{i+1}(v)$) a monochromatic walk starting from e_i (resp. e_{i+1}), obtained by following outgoing edges of color i (resp. $i+1$). By minimality of C those walks are not contained in D. We hence have that $W_i(v) \setminus v$ and $W_{i+1}(v) \setminus v$ intersect C. Thus each of these walks contains a non-empty subpath from v to C. The union of these two paths, plus a part of C contradicts the minimality of C. □

Let v be a vertex of G^∞. For each color i, vertex v is the starting vertex of some walks of color i, we denote the union of these walks by $P_i(v)$. Every vertex has at least one outgoing edge of color i and the set $P_i(v)$ is obtained by following all these edges of color i starting from v. Note that for some vertices v, $P_i(v)$ may consist of a single walk. It is the case when v cannot reach a vertex of outdegree six or more.

Lemma 2.10 *For every vertex v and color i, the two graphs $P_{i-1}(v)$ and $P_{i+1}(v)$ intersect only on v.*

Proof. If $P_{i-1}(v)$ and $P_{i+1}(v)$ intersect on two vertices, then $G^\infty_{i-1} \cup (G^\infty_{i+1})^{-1}$ contains a cycle, contradicting Lemma 2.9. □

Now we can prove the following:

Theorem 2.11 *If a map G on a genus $g \geq 1$ orientable surface admits an* EDGE, $\mathbb{N}^*$-VERTEX, $\mathbb{N}^*$-FACE *angle labeling, then G is essentially 3-connected.*

Proof. Towards a contradiction, suppose that there exist two vertices x, y of G^∞ such that $G' = G^\infty \setminus \{x, y\}$ is not connected. Then, by Lemma 2.8, the graph G' has a finite connected component R. Let v be a vertex of R. By Lemma 2.9, for $0 \leq i \leq 2$, the graph $P_i(v)$ does not lie in R so it intersects either x or y. So for two distinct colors i, j, the two graphs $P_i(v)$ and $P_j(v)$ intersect in a vertex distinct from v, a contradiction to Lemma 2.10. □

2.5 Conjectures on the existence of Schnyder woods

Proving that every triangulation on a genus $g \geq 1$ orientable surface admits a 1-EDGE angle labeling would imply the following theorem of Barát and Thomassen [2]:

Theorem 2.12 ([2]) *A simple triangulation on a genus $g \geq 1$ orientable surface admits an orientation of its edges such that every vertex has outdegree divisible by three.*

Recently, Theorem 2.12 has been improved by Albar, the first author, and the second author [1]:

Theorem 2.13 ([1]) *A simple triangulation on a genus $g \geq 1$ orientable surface admits an orientation of its edges such that every vertex has outdegree at least three, and divisible by three.*

Note that Theorems 2.12 and 2.13 are proved only in the case of simple triangulations (i.e. no loops and no multiple edges). We believe them to be true also for non-simple triangulations without contractible loops nor contractible double edges.

Theorem 2.13 suggests the existence of 1-EDGE angle labelings with no sinks, i.e. 1-EDGE, $\mathbb{N}^*$-VERTEX angle labelings. One can easily check that in a triangulation, a 1-EDGE angle labeling is also 1-FACE. Thus we can hope that a triangulation on a genus $g \geq 1$ orientable surface admits a 1-EDGE, $\mathbb{N}^*$-VERTEX, 1-FACE angle labeling. Note that a 1-EDGE, 1-FACE angle labeling of a map implies that faces are triangles. So we propose the following conjecture, whose "only if" part follows from the previous sentence:

Conjecture 2.14 *A map on a genus $g \geq 1$ orientable surface admits a 1-*EDGE*, $\mathbb{N}^*$-*VERTEX*, 1-*FACE *angle labeling if and only if it is a triangulation.*

If true, Conjecture 2.14 would strengthen Theorem 2.13 in two ways. First, it considers more triangulations (not only simple ones). Second, it requires the coloring property around vertices.

How about general maps? We propose the following conjecture, whose "only if" part is Theorem 2.11:

Conjecture 2.15 *A map on a genus $g \geq 1$ orientable surface admits an* EDGE*, $\mathbb{N}^*$-*VERTEX*, $\mathbb{N}^*$-*FACE *angle labeling if and only if it is essentially 3-connected.*

Conjecture 2.15 implies Conjecture 2.14 since for a triangulation every face would be of type 1, and thus every edge would be of type 1. Conjecture 2.15 is proved in [17] for $g = 1$ whereas both conjectures are open for $g \geq 2$. Section 5 gives a new proof of Conjecture 2.14 for $g = 1$ based on the results in Section 3.

3 Characterization of Schnyder orientations

3.1 A bit of homology

In the next sections, we need a bit of surface homology of general maps, which we will discuss now. For a deeper introduction to homology we refer to [15].

For the sake of generality, in this subsection we consider that maps may have contractible cycles of size 1 or 2. Consider a map $G = (V, E)$, on an orientable surface of genus g, given with an arbitrary orientation of its edges. This fixed arbitrary orientation is implicit in all the paper and is used to handle flows. A *flow* ϕ on G is a vector in $\mathbb{Z}^E$. For any $e \in E$, we denote by ϕ_e the coordinate e of ϕ.

A *walk* W of G is a sequence of edges with a direction of traversal such that the ending point of an edge walk is the starting point of the next edge. A walk is *closed* if the start and end vertices coincide. A walk has a *characteristic flow* $\phi(W)$ defined by:

$$\phi(W)_e := \#\text{times } W \text{ traverses } e \text{ forward} - \#\text{times } W \text{ traverses } e \text{ backward}$$

This definition naturally extends to sets of walks. From now on we consider that a set of walks and its characteristic flow are the same object and by abuse of notation we can write W instead of $\phi(W)$. We do the same for *oriented subgraphs*, i.e., subgraphs that can be seen as a set of walks of unit length.

A *facial walk* is a closed walk bounding a face. Let $\mathcal{F}$ be the set of counterclockwise facial walks and let $\mathbb{F} =< \phi(\mathcal{F}) >$ be the subgroup of $\mathbb{Z}^E$ generated by $\mathcal{F}$. Two flows ϕ, ϕ' are *homologous* if $\phi - \phi' \in \mathbb{F}$. They are *weakly homologous* if $\phi - \phi' \in \mathbb{F}$ or $\phi + \phi' \in \mathbb{F}$. We say that a flow ϕ is 0-homologous if it is homologous to the zero flow, i.e. $\phi \in \mathbb{F}$.

Let $\mathcal{W}$ be the set of *closed* walks and let $\mathbb{W} =< \phi(\mathcal{W}) >$ be the subgroup of $\mathbb{Z}^E$ generated by $\mathcal{W}$. The group $H(G) = \mathbb{W}/\mathbb{F}$ is the *first homology group* of G. It is well-known that $H(G)$ only depends on the genus of the map, and actually it is isomorphic to $\mathbb{Z}^{2g}$.

A set $\{B_1, \ldots, B_{2g}\}$ of (closed) walks of G is said to be a *basis for the homology* if the equivalence classes of their characteristic vectors $([\phi(B_1)], \ldots, [\phi(B_{2g})])$ generate $H(G)$. Then for any closed walk W of G, we have $W = \sum_{F \in \mathcal{F}} \lambda_F F + \sum_{1 \leq i \leq 2g} \mu_i B_i$ for some $\lambda \in \mathbb{Z}^{\mathcal{F}}, \mu \in \mathbb{Z}^{2g}$. Moreover one of the λ_F can be set to zero (and then all the other coefficients are unique). Indeed, for any map, there exists a set of cycles that forms a basis for the homology and it is computationally easy to build. A possible way is by considering a spanning tree T of G, and a spanning tree T^* of G^* that contains no edges dual to T. By Euler's formula, there are exactly $2g$ edges in G that are not in T nor dual to edges of T^*. Each of these $2g$ edges forms a unique cycle with T. It is not hard to see that this set of cycles forms a basis for the homology.

The edges of the dual G^* of G are oriented such that the dual e^* of an edge e of G goes from the face on the right of e to the face on the left of e. Let $\mathcal{F}^*$ be the set of counterclockwise facial walks of G^*. Consider $\{B_1^*, \ldots, B_{2g}^*\}$ a set of closed walks of G^* that form a basis for the homology. Let p and d be flows of G and G^*, respectively. We define the following:

$$\beta(p, d) = \sum_{e \in G} p_e d_{e^*}$$

Note that β is a bilinear function.

Lemma 3.1 *Given two flows ϕ, ϕ' of G, the following properties are equivalent to each other:*

1. *The two flows ϕ, ϕ' are homologous.*

2. *For any closed walk W of G^* we have $\beta(\phi, W) = \beta(\phi', W)$.*

3. *For any $F \in \mathcal{F}^*$, we have $\beta(\phi, F) = \beta(\phi', F)$, and, for any $1 \leq i \leq 2g$, we have $\beta(\phi, B_i^*) = \beta(\phi', B_i^*)$.*

Proof. (1. $\implies$ 3.) Suppose that ϕ, ϕ' are homologous. Then we have $\phi - \phi' = \sum_{F \in \mathcal{F}} \lambda_F F$ for some $\lambda \in \mathbb{Z}^{\mathcal{F}}$. It is easy to see that, for any closed walk W of G^*, a facial walk $F \in \mathcal{F}$ satisfies $\beta(F, W) = 0$, so $\beta(\phi, W) = \beta(\phi', W)$ by linearity of β.

(3. $\implies$ 2.) Suppose that for any $F \in \mathcal{F}^*$, we have $\beta(\phi, F) = \beta(\phi', F)$, and, for any $1 \leq i \leq 2g$, we have $\beta(\phi, B_i^*) = \beta(\phi', B_i^*)$. Let W be any closed walk of G^*. We have $W = \sum_{F \in \mathcal{F}^*} \lambda_F F + \sum_{1 \leq i \leq 2g} \mu_i B_i^*$ for some $\lambda \in \mathbb{Z}^{\mathcal{F}}, \mu \in \mathbb{Z}^{2g}$. Then by linearity of β we have $\beta(\phi, W) = \beta(\phi', W)$.

(2. $\implies$ 1.) Suppose $\beta(\phi, W) = \beta(\phi', W)$ for any closed walk W of G^*. Let $z = \phi - \phi'$. Thus $\beta(z, W) = 0$ for any closed walk W of G^*. We label the faces of G with elements of $\mathbb{Z}$ as follows. Choose an arbitrary face F_0 and label it 0. Then, consider any face F of G and a path P_F of G^* from F_0 to F. Label F with $\ell_F = \beta(z, P_F)$. Note that the label of F is independent from the choice of P_F. Indeed, for any two paths P_1, P_2 from F_0 to F, we have $P_1 - P_2$ is a closed walk, so $\beta(z, P_1 - P_2) = 0$ and thus $\beta(z, P_1) = \beta(z, P_2)$. Let us show that $z = \sum_{F \in \mathcal{F}} \ell_F \phi(F)$.

$$
\begin{aligned}
\sum_{F \in \mathcal{F}} \ell_F \phi(F) &= \sum_{e \in G} \left(\ell_{F_2} - \ell_{F_1}\right) \phi(e) && \text{(face } F_2 \text{ is on the left of } e \text{ and } F_1 \text{ on the right)} \\
&= \sum_{e \in G} \left(\beta(z, P_{F_2}) - \beta(z, P_{F_1})\right) \phi(e) && \text{(definition of } \ell_F) \\
&= \sum_{e \in G} \beta(z, P_{F_2} - P_{F_1}) \phi(e) && \text{(linearity of } \beta) \\
&= \sum_{e \in G} \beta(z, e^*) \phi(e) && (P_{F_1} + e^* - P_{F_2} \text{ is a closed walk}) \\
&= \sum_{e \in G} \left(\sum_{e' \in G} z_{e'} \phi(e^*)_{e'^*} \right) \phi(e) && \text{(definition of } \beta) \\
&= \sum_{e \in G} z_e \phi(e) \\
&= z
\end{aligned}
$$

So $z \in \mathbb{F}$ and thus ϕ, ϕ' are homologous. □

3.2 General characterization

Consider a map G on an orientable surface of genus g. The mapping of Figure 6 shows how an EDGE angle labeling of G can be mapped to an orientation of the edges with

edges oriented in one direction or in two opposite directions. These edges can be defined more naturally in the primal-dual-completion of G.

The *primal-dual-completion* $\hat{G}$ is the map obtained from simultaneously embedding G and G^* such that vertices of G^* are embedded inside faces of G and vice-versa. Moreover, each edge crosses its dual edge in exactly one point in its interior, which also becomes a vertex of $\hat{G}$. Hence, $\hat{G}$ is a bipartite graph with one part consisting of *primal-vertices* and *dual-vertices* and the other part consisting of *edge-vertices* (of degree four). Each face of $\hat{G}$ is a quadrangle incident to one primal-vertex, one dual-vertex and two edge-vertices. Actually, the faces of $\hat{G}$ are in correspondance with the angles of G. This means that angle labelings of G correspond to face labelings of $\hat{G}$.

Given $\alpha : V \to \mathbb{N}$, an orientation of G is an *α-orientation* [10] if for every vertex $v \in V$ its outdegree $d^+(v)$ equals $\alpha(v)$. We call an orientation of $\hat{G}$ a *mod_3-orientation* if it is an α-orientation for a function α satisfying :

$$\alpha(v) \equiv \begin{cases} 0 \ (\mathrm{mod}3) & \text{if } v \text{ is a primal- or dual-vertex,} \\ 1 \ (\mathrm{mod}3) & \text{if } v \text{ is an edge-vertex.} \end{cases}$$

Note that an EDGE angle labeling of G corresponds to a mod_3-orientation of $\hat{G}$, by the mapping of Figure 12, where the three types of edges are represented. Type 0 corresponds to an edge-vertex of outdegree four. Type 1 and type 2 both correspond to an edge-vertex of outdegree 1; in type 1 (resp. type 2) the outgoing edge goes to a primal-vertex (resp. dual-vertex). In all cases we have $d^+(v) \equiv 1 \ (\mathrm{mod}\, 3)$ if v is an edge-vertex. By Lemma 2.1, the labeling is also VERTEX and FACE. Thus, $d^+(v) \equiv 0 \ (\mathrm{mod}3)$ if v is a primal- or dual-vertex.

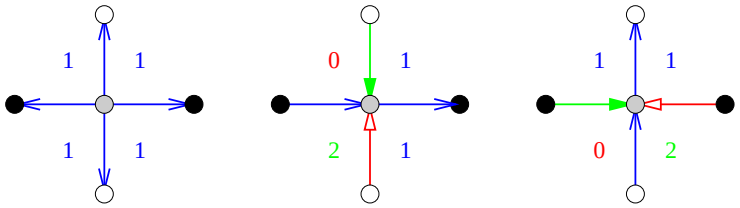

Figure 12: How to map an EDGE angle labeling to a mod_3-orientation of the primal-dual completion. Primal-vertices are black, dual-vertices are white and edge-vertices are gray. This serves as a convention for the other figures.

As mentioned earlier, De Fraysseix and Ossona de Mendez [14] give a bijection between internal 3-orientations and Schnyder woods of planar triangulations. Felsner [10] generalizes this result for planar Schnyder woods and orientations of the primal-dual completion having prescribed out-degrees. The situation is more complicated in higher genus (see Figure 5). It is not enough to prescribe outdegrees in order to characterize orientations corresponding to EDGE angle labelings.

We call an orientation of $\hat{G}$ corresponding to an EDGE angle labeling of G a *Schnyder orientation*. In this section we characterize which orientations of $\hat{G}$ are Schnyder orientations.

Consider an orientation of the primal-dual completion $\hat{G}$. Let $Out = \{(u,v) \in E(\hat{G}) \mid v \text{ is an edge-vertex}\}$, i.e. the set of edges of $\hat{G}$ which are going from a primal- or dual-vertex to an edge-vertex. We call these edges *out-edges*. For ϕ a flow of the dual of the primal-dual completion $\hat{G}^*$, we define $\delta(\phi) = \beta(Out, \phi)$. More intuitively, if W is a walk of $\hat{G}^*$, then:

$$\begin{aligned}\delta(W) = \quad & \#\text{out-edges crossing } W \text{ from left to right} \\ & -\#\text{out-edges crossing } W \text{ from right to left.}\end{aligned}$$

The bilinearity of β implies the linearity of δ. The following lemma gives a necessary and sufficient condition for an orientation to be a Schnyder orientation.

Lemma 3.2 *An orientation of $\hat{G}$ is a Schnyder orientation if and only if any closed walk W of $\hat{G}^*$ satisfies $\delta(W) \equiv 0 \pmod 3$.*

Proof. ($\Longrightarrow$) Consider an EDGE angle labeling ℓ of G and the corresponding Schnyder orientation (see Figure 12). Figure 13 illustrates how δ counts the variation of the label when going from one face of $\hat{G}$ to another face of $\hat{G}$. The represented cases correspond to a walk W of $\hat{G}^*$ consisting of just one edge. If the edge of $\hat{G}$ crossed by W is not an out-edge, then the two labels in the face are the same and $\delta(W) = 0$. If the edge crossed by W is an out-edge, then the labels differ by one. If W is going counterclockwise around a primal- or dual-vertex, then the label increases by 1 (mod3) and $\delta(W) = 1$. If W is going clockwise around a primal- or dual-vertex then the label decreases by 1 (mod3) and $\delta(W) = -1$. One can check that this is consistent with all the edges depicted in Figure 12. Thus for any walk W of $\hat{G}^*$ from a face F to a face F', the value of $\delta(W) \pmod 3$ is equal to $\ell(F') - \ell(F) \pmod 3$. Thus if W is a closed walk then $\delta(W) \equiv 0 \pmod 3$.

($\Longleftarrow$) Consider an orientation of $\hat{G}$ such that any closed walk W of $\hat{G}^*$ satisfies $\delta(W) \equiv 0 \pmod 3$. Pick any face F_0 of $\hat{G}$ and label it 0. Consider any face F of $\hat{G}$ and a path P of $\hat{G}^*$ from F_0 to F. Label F with the value $\delta(P) \bmod 3$. Note that the label of F is independent from the choice of P as for any two paths P_1, P_2 going from F_0 to F, we have $\delta(P_1) \equiv \delta(P_2) \pmod 3$ since $\delta(P_1 - P_2) \equiv 0 \pmod 3$ as $P_1 - P_2$ is a closed walk.

Consider an edge-vertex v of $\hat{G}$ and a walk W of $\hat{G}^*$ going clockwise around v. By assumption $\delta(W) \equiv 0 \pmod 3$ and $d(v) = 4$ so $d^+(v) \equiv 1 \pmod 3$. One can check (see Figure 12) that around an edge-vertex v of outdegree four, all the labels are the same and thus v corresponds to an edge of G of type 0. One can also check that around an edge-vertex v of outdegree 1, the labels are in clockwise order, $i-1$, i, i, $i+1$ for some i in $\{0,1,2\}$ where the two faces with the same label are incident to the outgoing edge of v. Thus, v corresponds to an edge of G of type 1 or 2 depending on the outgoing

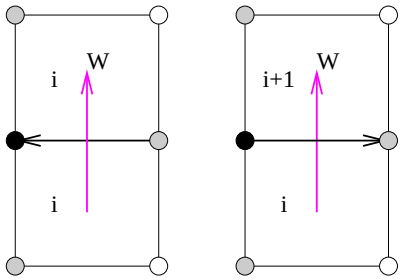

Figure 13: How δ counts the variation of the labels.

edge reaching a primal- or a dual-vertex. So the obtained labeling of the faces of $\hat{G}$ corresponds to an EDGE angle labeling of G and the considered orientation is a Schnyder orientation. □

We now study properties of δ w.r.t homology in order to simplify the condition of Lemma 3.2. Let $\hat{\mathcal{F}}^*$ be the set of counterclockwise facial walks of $\hat{G}^*$.

Lemma 3.3 *In a* mod_3*-orientation of* $\hat{G}$*, any* $F \in \hat{\mathcal{F}}^*$ *satisfies* $\delta(F) \equiv 0 \pmod 3$.

Proof. If F corresponds to an edge-vertex v of $\hat{G}$, then v has degree exactly four and outdegree one or four by definition of mod_3-orientations. So there are exactly zero or three out-edges crossing F from right to left, and $\delta(F) \equiv 0 \pmod 3$.

If F corresponds to a primal- or dual-vertex v, then v has outdegree 0 (mod3) by definition of mod_3-orientations. So there are exactly 0 (mod3) out-edges crossing F from left to right, and $\delta(F) \equiv 0 \pmod 3$. □

Lemma 3.4 *In a* mod_3*-orientation of* $\hat{G}$*, if* $\{B_1, \ldots, B_{2g}\}$ *is a set of cycles of* $\hat{G}^*$ *that forms a basis for the homology, then for any closed walk* W *of* $\hat{G}^*$ *homologous to* $\mu_1 B_1 + \cdots + \mu_{2g} B_{2g}$*, we have* $\delta(W) \equiv \mu_1 \delta(B_1) + \cdots + \mu_{2g} \delta(B_{2g}) \pmod 3$.

Proof. We have $W = \sum_{F \in \hat{\mathcal{F}}^*} \lambda_F F + \sum_{1 \leq i \leq 2g} \mu_i B_i$ for some $\lambda \in \mathbb{Z}^{\mathcal{F}}$. Then by linearity of δ and Lemma 3.3, the claim follows. □

Lemma 3.4 can be used to simplify the condition of Lemma 3.2 and show that if $\{B_1, \ldots, B_{2g}\}$ is a set of cycles of $\hat{G}^*$ that forms a basis for the homology, then an orientation of $\hat{G}$ is a Schnyder orientation if and only if it is a mod_3-orientation such that $\delta(B_i) \equiv 0 \pmod 3$, for all $1 \leq i \leq 2g$. Now, we define a new function γ that is used to formulate a similar characterization theorem (see Theorem 3.7).

Consider a (not necessarily directed) cycle C of G together with a direction of traversal. We associate to C its corresponding cycle in $\hat{G}$ denoted by $\hat{C}$. We define $\gamma(C)$ by:

$$\gamma(C) = \#\text{ edges of } \hat{G} \text{ leaving } \hat{C} \text{ on its right} - \#\text{ edges of } \hat{G} \text{ leaving } \hat{C} \text{ on its left}$$

Since it considers cycles of $\hat{G}$ instead of walks of $\hat{G}^*$, it is easier to deal with parameter γ rather than parameter δ. However γ does not enjoy the same property w.r.t. homology as δ. For homology we have to consider walks as flows, but two walks going several time through a given vertex may have the same characteristic flow but different γ. This explains why δ is defined first. Now we adapt the results for γ.

The value of γ is related to δ by the next lemmas. Let C be a cycle of G with a direction of traversal. Let $W_L(C)$ be the closed walk of $\hat{G}^*$ just on the left of C and going in the same direction as C (i.e. $W_L(C)$ is composed of the dual edges of the edges of $\hat{G}$ incident to the left of $\hat{C}$). Note that since the faces of $\hat{G}^*$ have exactly one incident vertex that is a primal-vertex, walk $W_L(C)$ is in fact a cycle of $\hat{G}^*$. Similarly, let $W_R(C)$ be the cycle of $\hat{G}^*$ just on the right of C.

Lemma 3.5 *Consider an orientation of $\hat{G}$ and a cycle C of G, then $\gamma(C) = \delta(W_L(C)) + \delta(W_R(C))$.*

Proof. We consider the different cases that can occur. An edge that is entering a primal-vertex of $\hat{C}$, is not counting in either $\gamma(C), \delta(W_L(C)), \delta(W_R(C))$. An edge that is leaving a primal-vertex of $\hat{C}$ from its right side (resp. left side) is counting $+1$ (resp. -1) for $\gamma(C)$ and $\delta(W_R(C))$ (resp. $\delta(W_L(C))$).

For edges incident to edge-vertices of $\hat{C}$ both sides have to be considered at the same time. Let v be an edge-vertex of $\hat{C}$. Vertex v is of degree four so it has exactly two edges incident to $\hat{C}$ and not on C. One of these edges, e_L, is on the left side of $\hat{C}$ and dual to an edge of $W_L(C)$. The other edge, e_R, is on the right side of $\hat{C}$ and dual to an edge of $W_R(C)$. If e_L and e_R are both incoming edges for v, then e_R (resp. e_L) is counting -1 (resp. $+1$) for $\delta(W_R(C))$ (resp. $\delta(W_L(C))$) and not counting for $\gamma(C)$. If e_L and e_R are both outgoing edges for v, then e_R and e_L are not counting for both $\delta(W_R(C))$, $\delta(W_L(C))$ and sums to zero for $\gamma(C)$. If e_L is incoming and e_R is outgoing for v, then e_R (resp. e_L) is counting 0 (resp. $+1$) for $\delta(W_R(C))$ (resp. $\delta(W_L(C))$), and counting $+1$ (resp. 0) for $\gamma(C)$. The last case, e_L is outgoing and e_R is incoming, is symmetric and one can see that in the four cases we have that e_L and e_R count the same for $\gamma(C)$ and $\delta(W_L(C)) + \delta(W_R(C))$. We conclude $\gamma(C) = \delta(W_L(C)) + \delta(W_R(C))$. □

Lemma 3.6 *In a mod_3-orientation of G, a cycle C of G satisfies*

$$\delta(W_L(C)) \equiv 0 \pmod 3 \quad \textit{and} \quad \delta(W_R(C)) \equiv 0 \pmod 3 \iff \gamma(C) \equiv 0 \pmod 3$$

Proof. ($\Longrightarrow$) Clear by Lemma 3.5.

($\Longleftarrow$) Suppose that $\gamma(C) \equiv 0 \pmod 3$. Let x_L (resp. y_L) be the number of edges of $\hat{G}$ that are dual to edges of $W_L(C)$, that are outgoing for a primal-vertex of $\hat{C}$ (resp. incoming for an edge-vertex of $\hat{C}$). Similarly, let x_R (resp. y_R) be the number of edges of $\hat{G}$ that are dual to edges of $W_R(C)$, that are outgoing for a primal-vertex of $\hat{C}$ (resp. incoming for an edge-vertex of $\hat{C}$). So $\delta(W_L(C)) = y_L - x_L$ and $\delta(W_R(C)) = x_R - y_R$. So by Lemma 3.5, $\gamma(C) = \delta(W_L(C)) + \delta(W_R(C)) = (y_L + x_R) - (x_L + y_R) \equiv 0 \pmod 3$.

Let k be the number of vertices of C. So $\hat{C}$ has k primal-vertices, k edge-vertices and $2k$ edges. Edge-vertices have outdegree 1 (mod 3) so their total number of outgoing edges on $\hat{C}$ is $k + (y_L + y_R) \pmod 3$. Primal-vertices have outdegree 0 (mod3) so their total number of outgoing edges on $\hat{C}$ is $-(x_L + x_R) \pmod 3$. So in total $2k \equiv k + (y_L + y_R) - (x_L + x_R) \pmod 3$. So $(y_L + y_R) - (x_L + x_R) \equiv 0 \pmod 3$. By combining this with plus (resp. minus) $(y_L + x_R) - (x_L + y_R) \equiv 0 \pmod 3$, one obtains that $2\delta(W_L(C)) = 2(y_L - x_L) \equiv 0 \pmod 3$ (resp. $2\delta(W_R(C)) = 2(x_R - y_R) \equiv 0 \pmod 3$). Since $\delta(W_L(C))$ and $\delta(W_R(C))$ are integer we obtain $\delta(W_L(C)) \equiv 0 \pmod 3$ and $\delta(W_R(C)) \equiv 0 \pmod 3$. □

Finally we have the following characterization theorem concerning Schnyder orientations:

Theorem 3.7 *Consider a map G on an orientable surface of genus g. Let $\{B_1, \ldots, B_{2g}\}$ be a set of cycles of G that forms a basis for the homology. An orientation of $\hat{G}$ is a Schnyder orientation if and only if it is a* mod_3*-orientation such that $\gamma(B_i) \equiv 0 \pmod 3$, for all $1 \leq i \leq 2g$.*

Proof. ($\Longrightarrow$) Consider an EDGE angle labeling ℓ of G and the corresponding Schnyder orientation (see Figure 12). Type 0 edges correspond to edge-vertices of outdegree four, while type 1 and 2 edges correspond to edge-vertices of outdegree 1. Thus $d^+(v) \equiv 1 \pmod 3$ if v is an edge-vertex. By Lemma 2.1, the labeling is VERTEX and FACE. Thus $d^+(v) \equiv 0 \pmod 3$ if v is a primal- or dual-vertex. So the orientation is a mod_3-orientation. By Lemma 3.2, we have $\delta(W) \equiv 0 \pmod 3$ for any closed walk W of $\hat{G}^*$. So we have that $\delta(W_L(B_1)), \ldots, \delta(W_L(B_{2g}))$, $\delta(W_R(B_1)), \ldots, \delta(W_R(B_{2g}))$ are all congruent to 0 (mod3). Thus, by Lemma 3.6, we have $\gamma(B_i) \equiv 0 \pmod 3$, for all $1 \leq i \leq 2g$.

($\Longleftarrow$) Consider a mod_3-orientation of G such that $\gamma(B_i) \equiv 0 \pmod 3$, for all $1 \leq i \leq 2g$. By Lemma 3.6, we have $\delta(W_L(B_i)) \equiv 0 \pmod 3$ for all $1 \leq i \leq 2g$. Moreover $\{W_L(B_1), \ldots, W_L(B_{2g})\}$ forms a basis for the homology. So by Lemma 3.4, $\delta(W) \equiv 0 \pmod 3$ for any closed walk W of $\hat{G}^*$. So the orientation is a Schnyder orientation by Lemma 3.2. □

The condition of Theorem 3.7 is easy to check: choose $2g$ cycles that form a basis for the homology and check whether γ is congruent to 0 mod 3 for each of them.

When restricted to triangulations and to edges of type 1 only, the defintion of γ can be simplified. Consider a triangulation G on an orientable surface of genus g and an orientation of the edges of G. Figure 14 shows how to transform the orientation of

G into an orientation of $\hat{G}$. Note that all the edge-vertices have outdegree exactly 1. Furthermore, all the dual-vertices only have outgoing edges and since we are considering triangulations they have outdegree exactly three.

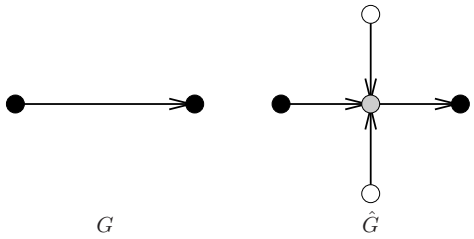

Figure 14: How to transform an orientation of a triangulation G into an orientation of $\hat{G}$.

Then the definition of γ can be simplified by the following:

$\gamma(C) = \#$ edges of G leaving C on its right $- \#$ edges of G leaving C on its left

Note that comparing to the general definition of γ, only the symbols $\hat{}$ have been removed.

The orientation of the toroidal triangulation on the left of Figure 5 is an example of a 3-orientation of a toroidal triangulation where some non contractible cycles have value γ not congruent to 0 mod 3. The value of γ for the three loops is $2, 0$ and -2. This explains why this orientation does not correspond to a Schnyder wood. On the contrary, on the right of the figure, the three loops have γ equal to 0 and we have a Schnyder wood.

4 Structure of Schnyder orientations

4.1 Transformations between Schnyder orientations

We investigate the structure of the set of Schnyder orientations of a given graph. For that purpose we need some definitions that are given on a general map G and then applied to $\hat{G}$.

Consider a map G on an orientable surface of genus g. Given two orientations D and D' of G, let $D \setminus D'$ denote the subgraph of D induced by the edges that are not oriented as in D'.

An oriented subgraph T of G is *partitionable* if its edge set can be partitioned into three sets T_0, T_1, T_2 such that all the T_i are pairwise homologous, i.e. $T_i - T_j \in \mathbb{F}$ for $i, j \in \{0, 1, 2\}$. An oriented subgraph T of G is called a *topological Tutte-orientation* if $\beta(T, W) \equiv 0 \pmod 3$ for every closed walk W in G^* (more intuitively, the number of

edges crossing W from left to right minus the number of those crossing W from right to left is divisible by three).

The name "topological Tutte-orientation" comes from the fact that an oriented graph T is called a *Tutte-orientation* if the difference of outdegree and indegree is divisible by three, i.e. $d^+(v) - d^-(v) \equiv 0 \pmod 3$, for every vertex v. So a topological Tutte-orientation is a Tutte orientation, since the latter requires the condition of the topological Tutte orientation only for the walks W of G^* going around a vertex v of G.

The notions of partitionable and topological Tutte-orientation are equivalent:

Lemma 4.1 *An oriented subgraph of G is partitionable if and only if it is a topological Tutte-orientation.*

Proof. ($\Longrightarrow$) If T is partitionable, then by definition it is the disjoint union of three homologous edge sets T_0, T_1, and T_2. Hence by Lemma 3.1, $\beta(T_0, W) = \beta(T_1, W) = \beta(T_2, W)$ for any closed walk W of G^*. By linearity of β this implies that $\beta(T, W) \equiv 0 \pmod 3$ for any closed walk W of G^*. So T is a topological Tutte-orientation.

($\Longleftarrow$) Let T be a topological Tutte-orientation of G, i.e. $\beta(T, W) \equiv 0 \pmod 3$ for any closed walk W of G^*. In the following, *T-faces* are the faces of T considered as an embedded graph. Note that T-faces are not necessarily disks. Let us introduce a $\{0, 1, 2\}$-labeling of the T-faces. Label an arbitrary T-face F_0 by 0. For any T-face F, find a path P of G^* from F_0 to F. Label F with $\beta(T, P) \pmod 3$. Note that the label of F is independent from the choice of P by our assumption on closed walks. For $0 \leq i \leq 2$, let T_i be the set of edges of T with two incident T-faces labeled $i - 1$ and $i + 1$. Note that an edge of T_i has label $i - 1$ on its left and label $i + 1$ on its right. The sets T_i form a partition of the edges of T. Let $\mathcal{F}_i$ be the counterclockwise facial walks of G that are in a T-face labeled i. We have $\phi(T_{i+1}) - \phi(T_{i-1}) = \sum_{F \in \mathcal{F}_i} \phi(F)$, so the T_i are homologous. □

Let us refine the notion of partitionable. Denote by $\mathcal{E}$ the set of *oriented Eulerian subgraphs* of G (i.e. the oriented subgraphs of G where each vertex has the same in- and out-degree). Consider a partitionable oriented subgraph T of G, with edge set partition T_0, T_1, T_2 having the same homology. We say that T is *Eulerian-partitionable* if $T_i \in \mathcal{E}$ for all $0 \leq i \leq 2$. Note that if T is Eulerian-partitionable then it is Eulerian. Note that an oriented subgraph T of G that is 0-homologous is also Eulerian and thus Eulerian-partitionable (with the partition $T, \emptyset, \emptyset$).

We now investigate the structure of Schnyder orientations. For that purpose, consider a map G on an orientable surface of genus g and apply the above definitions and results to orientations of $\hat{G}$.

Let D, D' be two orientations of $\hat{G}$ such that D is a Schnyder orientation and $T = D \setminus D'$. Let $Out = \{(u, v) \in E(D) \mid v \text{ is an edge-vertex}\}$. Similarly, let $Out' = \{(u, v) \in E(D') \mid v \text{ is an edge-vertex}\}$. Note that an edge of T is either in Out or in Out', so $\phi(T) = \phi(Out) - \phi(Out')$. By Lemma 3.2, for any closed walk W of $\hat{G}^*$, $\beta(Out, W) \equiv$

$0 \pmod 3$. The three following lemmas give necessary and sufficient conditions on T for D' being a Schnyder orientation.

Lemma 4.2 *D' is a Schnyder orientation if and only if T is partitionable.*

Proof. Let D' is a Schnyder orientation. By Lemma 3.2, this is equivalent to the fact that for any closed walk W of $\hat{G}^*$, we have $\beta(Out', W) \equiv 0 \pmod 3$. Since $\beta(Out, W) \equiv 0 \pmod 3$, this is equivalent to the fact that for any closed walk W of $\hat{G}^*$, we have $\beta(T, W) \equiv 0 \pmod 3$. Finally, by Lemma 4.1 this is equivalent to T being partitionable. □

Lemma 4.3 *D' is a Schnyder orientation having the same outdegrees as D if and only if T is Eulerian-partitionable.*

Proof. ($\Longrightarrow$) Suppose D' is a Schnyder orientation having the same outdegrees as D. Lemma 4.2 implies that T is partitionable into T_0, T_1, T_2 having the same homology. By Lemma 3.1, for each closed walk W of $\hat{G}^*$, we have $\beta(T_0, W) = \beta(T_1, W) = \beta(T_2, W)$. Since D, D' have the same outdegrees, we have that T is Eulerian. Consider a vertex v of $\hat{G}$ and a walk W_v of $\hat{G}^*$ going counterclockwise around v. For any oriented subgraph H of $\hat{G}^*$, we have $d^+_H(v) - d^-_H(v) = \beta(H, W_v)$, where $d^+_H(v)$ and $d^-_H(v)$ denote the outdegree and indegree of v restricted to H, respectively. Since T is Eulerian, we have $\beta(T, W_v) = 0$. Since $\beta(T_0, W_v) = \beta(T_1, W_v) = \beta(T_2, W_v)$ and $\sum \beta(T_i, W_v) = \beta(T, W_v) = 0$, we obtain that $\beta(T_0, W_v) = \beta(T_1, W_v) = \beta(T_2, W_v) = 0$. So each T_i is Eulerian.

($\Longleftarrow$) Suppose T is Eulerian-partitionable. Then Lemma 4.2 implies that D' is a Schnyder orientation. Since T is Eulerian, the two orientations D, D' have the same outdegrees. □

Consider $\{B_1, \ldots, B_{2g}\}$ a set of cycles of G that forms a basis for the homology. For $\Gamma \in \mathbb{Z}^{2g}$, an orientation of $\hat{G}$ is of *type* Γ if $\gamma(B_i) = \Gamma_i$ for all $1 \leq i \leq 2g$.

Lemma 4.4 *D' is a Schnyder orientation having the same outdegrees and the same type as D (for the considered basis) if and only if T is 0-homologous (i.e. D, D' are homologous).*

Proof. ($\Longrightarrow$) Suppose D' is a Schnyder orientation having the same outdegrees and the same type as D. Then, Lemma 4.3 implies that T is Eulerian-partitionable and thus Eulerian. So for any $F \in \hat{\mathcal{F}}^*$, we have $\beta(T, F) = 0$. Moreover, for $1 \leq i \leq 2g$, consider the region R_i between $W_L(B_i)$ and $W_R(B_i)$ containing B_i. Since T is Eulerian, it is going in and out of R_i the same number of times. So $\beta(T, W_L(B_i) - W_R(B_i)) = 0$. Since D, D' have the same type, we have $\gamma_D(B_i) = \gamma_{D'}(B_i)$. So by Lemma 3.5, $\delta_D(W_L(B_i)) + \delta_D(W_R(B_i)) = \delta_{D'}(W_L(B_i)) + \delta_{D'}(W_R(B_i))$. Thus $\beta(T, W_L(B_i) + W_R(B_i)) = \beta(Out - Out', W_L(B_i) + W_R(B_i)) = \delta_D(W_L(B_i)) + \delta_D(W_R(B_i)) - \delta_{D'}(W_L(B_i)) - \delta_{D'}(W_R(B_i)) = 0$.

By combining this with the previous equality, we obtain $\beta(T, W_L(B_i)) = \beta(T, W_R(B_i)) = 0$ for all $1 \leq i \leq 2g$. Thus by Lemma 3.1, we have that T is 0-homologous.

($\Longleftarrow$) Suppose that T is 0-homologous. Then T is in particular Eulerian-partitionable (with the partition $T, \emptyset, \emptyset$). So Lemma 4.3 implies that D' is a Schnyder orientation with the same outdegrees as D. Since T is 0-homologous, by Lemma 3.1, for all $1 \leq i \leq 2g$, we have $\beta(T, W_L(B_i)) = \beta(T, W_R(B_i)) = 0$. Thus $\delta_D(W_L(B_i)) = \beta(Out, W_L(B_i)) = \beta(Out', W_L(B_i)) = \delta_{D'}(W_L(B_i))$ and $\delta_D(W_R(B_i)) = \beta(Out, W_R(B_i)) = \beta(Out', W_R(B_i)) = \delta_{D'}(W_R(B_i))$. So by Lemma 3.5, $\gamma_D(B_i) = \delta_D(W_L(B_i)) + \delta_D(W_R(B_i)) = \delta_{D'}(W_L(B_i)) + \delta_{D'}(W_R(B_i)) = \gamma_{D'}(B_i)$. So D, D' have the same type. □

Lemma 4.4 implies that when you consider Schnyder orientations having the same outdegrees the property that they have the same type does not depend on the choice of the basis since being homologous does not depend on the basis. So we have the following:

Lemma 4.5 *If two Schnyder orientations have the same outdegrees and the same type (for the considered basis), then they have the same type for any basis.*

Lemma 4.2, 4.3 and 4.4 are summarized in the following theorem (where by Lemma 4.5 we do not have to assume a particular choice of a basis for the third item):

Theorem 4.6 *Let G be a map on an orientable surface and D, D' orientations of $\hat{G}$ such that D is a Schnyder orientation and $T = D \setminus D'$. We have the following:*

- *D' is a Schnyder orientation if and only if T is partitionable.*
- *D' is a Schnyder orientation having the same outdegrees as D if and only if T is Eulerian-partitionable.*
- *D' is a Schnyder orientation having the same outdegrees and the same type as D if and only if T is 0-homologous (i.e. D, D' are homologous).*

We show in the next section that the set of Schnyder orientations that are homologous (see third item of Theorem 4.6) carries a structure of distributive lattice.

4.2 The distributive lattice of homologous orientations

For the sake of generality, in this subsection we consider that maps may have contractible cycles of size 1 or 2. Consider a map G on an orientable surface and a given orientation D_0 of G. Let $O(G, D_0)$ be the set of all the orientations of G that are homologous to D_0. In this section we prove that $O(G, D_0)$ forms a distributive lattice. We show some additional interesting properties that are used in a recent paper by Despré, the first author, and the third author [7]. This generalizes results for the plane obtained by Ossona de Mendez [22] and Felsner [10]. The distributive lattice structure also can also

be derived from a result of Propp [24] interpreted on the dual map, see the discussion below Theorem 4.7.

In order to define an order on $O(G, D_0)$, fix an arbitrary face f_0 of G and let F_0 be its counterclockwise facial walk. Let $\mathcal{F}' = \mathcal{F} \setminus \{F_0\}$ (where $\mathcal{F}$ is the set of counterclockwise facial walks of G as defined earlier). Note that $\phi(F_0) = -\sum_{F \in \mathcal{F}'} \phi(F)$. Since the characteristic flows of $\mathcal{F}'$ are linearly independent, any oriented subgraph of G has at most one representation as a combination of characteristic flows of $\mathcal{F}'$. Moreover the 0-homologous oriented subgraphs of G are precisely the oriented subgraph that have such a representation. We say that a 0-homologous oriented subgraph T of G is *counterclockwise* (resp. *clockwise*) if its characteristic flow can be written as a combination with positive (resp. negative) coefficients of characteristic flows of $\mathcal{F}'$, i.e. $\phi(T) = \sum_{F \in \mathcal{F}'} \lambda_F \phi(F)$, with $\lambda \in \mathbb{N}^{|\mathcal{F}'|}$ (resp. $-\lambda \in \mathbb{N}^{|\mathcal{F}'|}$). Given two orientations D, D', of G we set $D \leq_{f_0} D'$ if and only if $D \setminus D'$ is counterclockwise. Then we have the following theorem.

Theorem 4.7 ([24]) *Let G be a map on an orientable surface given with a particular orientation D_0 and a particular face f_0. Let $O(G, D_0)$ the set of all the orientations of G that are homologous to D_0. We have $(O(G, D_0), \leq_{f_0})$ is a distributive lattice.*

We attribute Theorem 4.7 to Propp even if it is not presented in this form in [24]. Here we do not introduce Propp's formalism, but provide a new proof of Theorem 4.7 (as a consequence of the forthcoming Proposition 4.7). This allows us to introduce notions used later in the study of this lattice. It is notable that the study of this lattice found applications in [7], where the authors found a bijection between toroidal triangulations and unicellular toroidal maps.

To prove Theorem 4.7, we need to define the elementary flips that generates the lattice. We start by reducing the graph G. We call an edge of G *rigid with respect to* $O(G, D_0)$ if it has the same orientation in all elements of $O(G, D_0)$. Rigid edges do not play a role for the structure of $O(G, D_0)$. We delete them from G and call the obtained embedded graph $\widetilde{G}$. This graph is embedded but it is not necessarily a map, as some faces may not be homeomorphic to open disks. Note that if all the edges are rigid, i.e. $|O(G, D_0)| = 1$, then $\widetilde{G}$ has no edges.

Lemma 4.8 *Given an edge e of G, the following are equivalent:*

1. *e is non-rigid*
2. *e is contained in a 0-homologous oriented subgraph of D_0*
3. *e is contained in a 0-homologous oriented subgraph of any element of $O(G, D_0)$*

Proof. $(1 \Longrightarrow 3)$ Let $D \in O(G, D_0)$. If e is non-rigid, then it has a different orientation in two elements D', D'' of $O(G, D_0)$. Then we can assume by symmetry that e has a different orientation in D and D' (otherwise in D and D'' by symmetry). Since D, D'

are homologous to D_0, they are also homologous to each other. So $T = D \setminus D'$ is a 0-homologous oriented subgraph of D that contains e.

($3 \Longrightarrow 2$) Trivial since $D_0 \in O(G, D_0)$

($2 \Longrightarrow 1$) If an edge e is contained in a 0-homologous oriented subgraph T of D_0. Then let D be the element of $O(G, D_0)$ such that $T = D_0 \setminus D$. Clearly e is oriented differently in D and D_0, thus it is non-rigid. □

By Lemma 4.8, one can build $\widetilde{G}$ by keeping only the edges that are contained in a 0-homologous oriented subgraph of D_0. Note that this implies that all the edges of $\widetilde{G}$ are incident to two distinct faces of $\widetilde{G}$. Denote by $\widetilde{\mathcal{F}}$ the set of oriented subgraphs of $\widetilde{G}$ corresponding to the boundaries of faces of $\widetilde{G}$ considered counterclockwise. Note that any $\widetilde{F} \in \widetilde{\mathcal{F}}$ is 0-homologous and so its characteristic flows has a unique way to be written as a combination of characteristic flows of $\mathcal{F}'$. Moreover this combination can be written $\phi(\widetilde{F}) = \sum_{F \in X_{\widetilde{F}}} \phi(F)$, for $X_{\widetilde{F}} \subseteq \mathcal{F}'$. Let $\widetilde{f_0}$ be the face of $\widetilde{G}$ containing f_0 and $\widetilde{F_0}$ be the element of $\widetilde{\mathcal{F}}$ corresponding to the boundary of $\widetilde{f_0}$. Let $\widetilde{\mathcal{F}'} = \widetilde{\mathcal{F}} \setminus \{\widetilde{F_0}\}$. The elements of $\widetilde{\mathcal{F}'}$ are precisely the elementary flips which suffice to generate the entire distributive lattice $(O(G, D_0), \leq_{f_0})$.

We prove two technical lemmas concerning $\widetilde{\mathcal{F}'}$:

Lemma 4.9 *Let $D \in O(G, D_0)$ and T be a non-empty 0-homologous oriented subgraph of D. Then there exist edge-disjoint oriented subgraphs $T_1, \ldots, T_k$ of D such that $\phi(T) = \sum_{1 \leq i \leq k} \phi(T_i)$, and, for $1 \leq i \leq k$, there exists $\widetilde{X_i} \subseteq \widetilde{\mathcal{F}'}$ and $\epsilon_i \in \{-1, 1\}$ such that $\phi(T_i) = \epsilon_i \sum_{\widetilde{F} \in \widetilde{X_i}} \phi(\widetilde{F})$.*

Proof. Since T is 0-homologous, we have $\phi(T) = \sum_{F \in \mathcal{F}'} \lambda_F \phi(F)$, for $\lambda \in \mathbb{Z}^{|\mathcal{F}'|}$. Let $\lambda_{f_0} = 0$. Thus we have $\phi(T) = \sum_{F \in \mathcal{F}} \lambda_F \phi(F)$. Let $\lambda_{\min} = \min_{F \in \mathcal{F}} \lambda_F$ and $\lambda_{\max} = \max_{F \in \mathcal{F}} \lambda_F$. We may have $\lambda_{\min} = 0$ or $\lambda_{\max} = 0$ but not both since T is non-empty. For $1 \leq i \leq \lambda_{\max}$, let $X_i = \{F \in \mathcal{F}' \,|\, \lambda_F \geq i\}$ and $\epsilon_i = 1$. Let $X_0 = \emptyset$ and $\epsilon_0 = 1$. For $\lambda_{\min} \leq i \leq -1$, let $X_i = \{F \in \mathcal{F}' \,|\, \lambda_F \leq i\}$ and $\epsilon_i = -1$. For $\lambda_{\min} \leq i \leq \lambda_{\max}$, let T_i be the oriented subgraph such that $\phi(T_i) = \epsilon_i \sum_{F \in X_i} \phi(F)$. Then we have $\phi(T) = \sum_{\lambda_{\min} \leq i \leq \lambda_{\max}} \phi(T_i)$.

Since T is an oriented subgraph, we have $\phi(T) \in \{-1, 0, 1\}^{|E(G)|}$. Thus for any edge of G, incident to faces F_1 and F_2, we have $(\lambda_{F_1} - \lambda_{F_2}) \in \{-1, 0, 1\}$. So, for $1 \leq i \leq \lambda_{\max}$, the oriented graph T_i is the border between the faces with λ value equal to i and $i - 1$. Symmetrically, for $\lambda_{\min} \leq i \leq -1$, the oriented graph T_i is the border between the faces with λ value equal to i and $i + 1$. So all the T_i are edge disjoint and are oriented subgraphs of D.

Let $\widetilde{X_i} = \{\widetilde{F} \in \widetilde{\mathcal{F}'} \,|\, \phi(\widetilde{F}) = \sum_{F \in X'} \phi(F) \text{ for some } X' \subseteq X_i\}$. Since T_i is 0-homologous, the edges of T_i can be reversed in D to obtain another element of $O(G, D_0)$. Thus there is no rigid edge in T_i. Thus $\phi(T_i) = \epsilon_i \sum_{F \in X_i} \phi(F) = \epsilon_i \sum_{\widetilde{F} \in \widetilde{X_i}} \phi(\widetilde{F})$. □

Lemma 4.10 *Let $D \in O(G, D_0)$ and T be a non-empty 0-homologous oriented subgraph of D such that there exists $\widetilde{X} \subseteq \widetilde{\mathcal{F}'}$ and $\epsilon \in \{-1, 1\}$ satisfying $\phi(T) = \epsilon \sum_{\widetilde{F} \in \widetilde{X}} \phi(\widetilde{F})$. Then there exists $\widetilde{F} \in \widetilde{X}$ such that $\epsilon\, \phi(\widetilde{F})$ corresponds to an oriented subgraph of D.*

Proof. The proof is done by induction on $|\widetilde{X}|$. Assume that $\epsilon = 1$ (the case $\epsilon = -1$ is proved similarly).

If $|\widetilde{X}| = 1$, then the conclusion is clear since $\phi(T) = \sum_{\widetilde{F} \in \widetilde{X}} \phi(\widetilde{F})$. We now assume that $|\widetilde{X}| > 1$. Towards a contradiction, suppose that for any $\widetilde{F} \in \widetilde{X}$ we do not have the conclusion, i.e $\phi(\widetilde{F})_e \neq \phi(T)_e$ for some $e \in \widetilde{F}$. Let $\widetilde{F_1} \in \widetilde{X}$ and $e \in \widetilde{F_1}$ such that $\phi(\widetilde{F_1})_e \neq \phi(T)_e$. Since $\widetilde{F_1}$ is counterclockwise, we have $\widetilde{F_1}$ on the left of e. Let $\widetilde{F_2} \in \widetilde{\mathcal{F}}$ that is on the right of e. Note that $\phi(\widetilde{F_1})_e = -\phi(\widetilde{F_2})_e$ and for any other face $\widetilde{F} \in \widetilde{\mathcal{F}}$, we have $\phi(\widetilde{F})_e = 0$. Since $\phi(T) = \sum_{\widetilde{F} \in \widetilde{X}} \phi(\widetilde{F})$, we have $\widetilde{F_2} \in \widetilde{X}$ and $\phi(T)_e = 0$. By possibly swapping the role of $\widetilde{F_1}$ and $\widetilde{F_2}$, we can assume that $\phi(D)_e = \phi(\widetilde{F_1})_e$, i.e., e is oriented the same way in $\widetilde{F_1}$ and D. Since e is not rigid, there exists an orientation D' in $O(G, D_0)$ such that $\phi(D)_e = -\phi(D')_e$.

Let T' be the non-empty 0-homologous oriented subgraph of D such that $T' = D \setminus D'$. Lemma 4.9 implies that there exists edge-disjoint oriented subgraphs $T_1, \ldots, T_k$ of D such that $\phi(T) = \sum_{1 \leq i \leq k} \phi(T_i)$, and, for $1 \leq i \leq k$, there exists $\widetilde{X_i} \subseteq \widetilde{\mathcal{F}'}$ and $\epsilon_i \in \{-1, 1\}$ such that $\phi(T_i) = \epsilon_i \sum_{\widetilde{F} \in \widetilde{X_i}} \phi(\widetilde{F})$. Since T' is the disjoint union of $T_1, \ldots, T_k$, there exists $1 \leq i \leq k$, such that e is an edge of T_i. Assume by symmetry that e is an edge of T_1. Since $\phi(T_1)_e = \phi(D)_e = \phi(\widetilde{F_1})_e$, we have $\epsilon_1 = 1$, $\widetilde{F_1} \in \widetilde{X_1}$ and $\widetilde{F_2} \notin \widetilde{X_1}$.

Let $\widetilde{Y} = \widetilde{X} \cap \widetilde{X_1}$. Thus $\widetilde{F_1} \in \widetilde{Y}$ and $\widetilde{F_2} \notin \widetilde{Y}$. So $|\widetilde{Y}| < |\widetilde{X}|$. Let $T_{\widetilde{Y}}$ be the oriented subgraph of G such that $T_{\widetilde{Y}} = \sum_{\widetilde{F} \in \widetilde{Y}} \phi(\widetilde{F})$. Note that the edges of T (resp. T_1) are those incident to exactly one face of $\widetilde{X}$ (resp. $\widetilde{X_1}$). Similarly every edge of $T_{\widetilde{Y}}$ is incident to exactly one face of $\widetilde{Y} = \widetilde{X} \cap \widetilde{X_1}$, i.e. it has one incident face in $\widetilde{Y} = \widetilde{X} \cap \widetilde{X_1}$ and the other incident face not in $\widetilde{X}$ or not in $\widetilde{X_1}$. In the first case this edge is in T, otherwise it is in T_1. So every edge of $T_{\widetilde{Y}}$ is an edge of $T \cup T_1$. Hence $T_{\widetilde{Y}}$ is an oriented subgraph of D. So we can apply the induction hypothesis on $T_{\widetilde{Y}}$. This implies that there exists $\widetilde{F} \in \widetilde{Y}$ such that $\widetilde{F}$ is an oriented subgraph of D. Since $\widetilde{Y} \subseteq \widetilde{X}$, this is a contradiction to our assumption. □

We need the following characterization of distributive lattice from [11]:

Theorem 4.11 ([11]) *An oriented graph $\mathcal{H} = (V, E)$ is the Hasse diagram of a distributive lattice if and only if it is connected, acyclic, and admits an edge-labeling c of the edges such that:*

- *if $(u, v), (u, w) \in E$ then*

  (U1) $c(u, v) \neq c(u, w)$ and

  (U2) there is $z \in V$ such that $(v, z), (w, z) \in E$, $c(u, v) = c(w, z)$, and $c(u, w) = c(v, z)$.

- *if* $(v,z),(w,z) \in E$ *then*

  (L1) $c(v,z) \neq c(w,z)$ *and*

  (L2) there is $u \in V$ *such that* $(u,v),(u,w) \in E$, $c(u,v) = c(w,z)$, *and* $c(u,w) = c(v,z)$.

We define the directed graph $\mathcal{H}$ with vertex set $O(G, D_0)$. There is an oriented edge from D_1 to D_2 in $\mathcal{H}$ (with $D_1 \leq_{f_0} D_2$) if and only if $D_1 \setminus D_2 \in \widetilde{\mathcal{F}'}$. We define the label of that edge as $c(D_1, D_2) = D_1 \setminus D_2$. We show that $\mathcal{H}$ fulfills all the conditions of Theorem 4.11, and thus obtain the following:

Proposition 4.12 *$\mathcal{H}$ is the Hasse diagram of a distributive lattice.*

Proof. The characteristic flows of elements of $\widetilde{\mathcal{F}'}$ form an independent set, hence the digraph $\mathcal{H}$ is acyclic. By definition all outgoing and all incoming edges of a vertex of $\mathcal{H}$ have different labels, i.e. the labeling c satisfies (U1) and (L1). If (D_u, D_v) and (D_u, D_w) belong to $\mathcal{H}$, then $T_v = D_u \setminus D_v$ and $T_w = D_u \setminus D_w$ are both elements of $\widetilde{\mathcal{F}'}$, so they must be edge disjoint. Thus, the orientation D_z obtained from reversing the edges of T_w in D_v or equivalently T_v in D_w is in $O(G, D_0)$. This gives (U2). The same reasoning gives (L2). It remains to show that $\mathcal{H}$ is connected.

Given a 0-homologous oriented subgraph T of G, such that $T = \sum_{F \in \mathcal{F}'} \lambda_F \phi(F)$, we define $s(T) = \sum_{F \in \mathcal{F}'} |\lambda_F|$.

Let D, D' be two orientations in $O(G, D_0)$, and $T = D \setminus D'$. We prove by induction on $s(T)$ that D, D' are connected in $\mathcal{H}$. This is clear if $s(T) = 0$ as then $D = D'$. So we now assume that $s(T) \neq 0$ and so that D, D' are distinct. Lemma 4.9 implies that there exists edge-disjoint oriented subgraphs $T_1, \ldots, T_k$ of D such that $\phi(T) = \sum_{1 \leq i \leq k} \phi(T_i)$, and, for $1 \leq i \leq k$, there exists $\widetilde{X_i} \subseteq \widetilde{\mathcal{F}'}$ and $\epsilon_i \in \{-1, 1\}$ such that $\phi(T_i) = \epsilon_i \sum_{\widetilde{F} \in \widetilde{X_i}} \phi(\widetilde{F})$. Lemma 4.10 applied to T_1 implies that there exists $\widetilde{F_1} \in \widetilde{X_1}$ such that $\epsilon_1 \phi(\widetilde{F_1})$ corresponds to an oriented subgraph of D. Let T' be the oriented subgraph such that $\phi(T) = \epsilon_1 \phi(\widetilde{F_1}) + \phi(T')$. Thus:

$$\begin{aligned}
\phi(T') &= \phi(T) - \epsilon_1 \phi(\widetilde{F_1}) \\
&= \sum_{1 \leq i \leq k} \phi(T_i) - \epsilon_1 \phi(\widetilde{F_1}) \\
&= \sum_{\widetilde{F} \in (\widetilde{X_1} \setminus \{\widetilde{F_1}\})} \epsilon_1 \phi(\widetilde{F}) + \sum_{2 \leq i \leq k} \sum_{\widetilde{F} \in \widetilde{X_i}} \epsilon_i \phi(\widetilde{F}) \\
&= \sum_{\widetilde{F} \in (\widetilde{X_1} \setminus \{\widetilde{F_1}\})} \sum_{F \in X_{\widetilde{F}}} \epsilon_1 \phi(F) + \sum_{2 \leq i \leq k} \sum_{\widetilde{F} \in \widetilde{X_i}} \sum_{F \in X_{\widetilde{F}}} \epsilon_i \phi(F)
\end{aligned}$$

So T' is 0-homologous. Let D'' be such that $\epsilon_1 \widetilde{F_1} = D \setminus D''$. So we have $D'' \in O(G, D_0)$ and there is an edge between D and D'' in $\mathcal{H}$. Moreover $T' = D'' \setminus D'$ and $s(T') =$

$s(T) - |X_{\widetilde{F}_1}| < s(T)$. So the induction hypothesis on D'', D' implies that they are connected in $\mathcal{H}$. So D, D' are also connected in $\mathcal{H}$. □

Note that Proposition 4.12 gives a proof of Theorem 4.7 independent from Propp [24].

We continue to further investigate the set $O(G, D_0)$.

Proposition 4.13 *For every element $\widetilde{F} \in \widetilde{\mathcal{F}}$, there exists D in $O(G, D_0)$ such that $\widetilde{F}$ is an oriented subgraph of D.*

Proof. Let $\widetilde{F} \in \widetilde{\mathcal{F}}$. Let D be an element of $O(G, D_0)$ that maximizes the number of edges of $\widetilde{F}$ that have the same orientation in $\widetilde{F}$ and D, i.e. D maximizes the number of edges oriented counterclockwise on the boundary of the face of $\widetilde{G}$ corresponding to $\widetilde{F}$. Towards a contradiction, suppose that there is an edge e of $\widetilde{F}$ that does not have the same orientation in $\widetilde{F}$ and D. The edge e is in $\widetilde{G}$ so it is non-rigid. Let $D' \in O(G, D_0)$ such that e is oriented differently in D and D'. Let $T = D \setminus D'$. By Lemma 4.9, there exist edge-disjoint oriented subgraphs $T_1, \ldots, T_k$ of D such that $\phi(T) = \sum_{1 \leq i \leq k} \phi(T_i)$, and, for $1 \leq i \leq k$, there exists $\widetilde{X}_i \subseteq \widetilde{\mathcal{F}}'$ and $\epsilon_i \in \{-1, 1\}$ such that $\phi(T_i) = \epsilon_i \sum_{\widetilde{F}' \in \widetilde{X}_i} \phi(\widetilde{F}')$. W.l.o.g., we can assume that e is an edge of T_1. Let D'' be the element of $O(G, D_0)$ such that $T_1 = D \setminus D''$. The oriented subgraph T_1 intersects $\widetilde{F}$ only on edges of D oriented clockwise on the border of $\widetilde{F}$. So D'' contains strictly more edges oriented counterclockwise on the border of the face $\widetilde{F}$ than D, a contradiction. So all the edges of $\widetilde{F}$ have the same orientation in D. So $\widetilde{F}$ is a 0-homologous oriented subgraph of D. □

By Proposition 4.13, for every element $\widetilde{F} \in \widetilde{\mathcal{F}}'$ there exists D in $O(G, D_0)$ such that $\widetilde{F}$ is an oriented subgraph of D. Thus there exists D' such that $\widetilde{F} = D \setminus D'$ and D, D' are linked in $\mathcal{H}$. Thus, $\widetilde{\mathcal{F}}'$ is a minimal set that generates the lattice.

A distributive lattice has a unique maximal (resp. minimal) element. Let $D_{\max}$ (resp. $D_{\min}$) be the maximal (resp. minimal) element of $(O(G, D_0), \leq_{f_0})$.

Proposition 4.14 *$\widetilde{F}_0$ (resp. $-\widetilde{F}_0$) is an oriented subgraph of $D_{\max}$ (resp. $D_{\min}$).*

Proof. By Proposition 4.13, there exists D in $O(G, D_0)$ such that $\widetilde{F_0}$ is an oriented subgraph of D. Let $T = D \setminus D_{\max}$. Since $D \leq_{f_0} D_{\max}$, the characteristic flow of T can be written as a combination with positive coefficients of characteristic flows of $\widetilde{\mathcal{F}}'$, i.e. $\phi(T) = \sum_{\widetilde{F} \in \widetilde{\mathcal{F}}'} \lambda_F \phi(\widetilde{F})$ with $\lambda \in \mathbb{N}^{|\mathcal{F}'|}$. So T is disjoint from $\widetilde{F}_0$. Thus $\widetilde{F}_0$ is an oriented subgraph of $D_{\max}$. The proof is analogous for $D_{\min}$. □

Proposition 4.15 *$D_{\max}$ (resp. $D_{\min}$) contains no counterclockwise (resp. clockwise) non-empty 0-homologous oriented subgraph.*

Proof. Towards a contradiction, suppose that $D_{\max}$ contains a counterclockwise non-empty 0-homologous oriented subgraph T. Then there exists $D \in O(G, D_0)$ distinct from $D_{\max}$ such that $T = D_{\max} \setminus D$. We have $D_{\max} \leq_{f_0} D$ by definition of $\leq_{f_0}$, a contradiction to the maximality of $D_{\max}$. □

In the definition of counterclockwise (resp. clockwise) non-empty 0-homologous oriented subgraph, used in Proposition 4.15, the sum is taken over elements of $\mathcal{F}'$ and thus does not use F_0. In particular, $D_{\max}$ (resp. $D_{\min}$) may contain regions whose boundary is oriented counterclockwise (resp. clockwise) according to the region but then such a region contains F_0.

We conclude this section by applying Theorem 4.7 to Schnyder orientations:

Theorem 4.16 *Let G be a map on an orientable surface given with a particular Schnyder orientation D_0 of $\hat{G}$ and a particular face f_0 of $\hat{G}$. Let $S(\hat{G}, D_0)$ be the set of all the Schnyder orientations of $\hat{G}$ that have the same outdegrees and same type as D_0. We have that $(S(\hat{G}, D_0), \leq_{f_0})$ is a distributive lattice.*

Proof. By the third item of Theorem 4.6, we have $S(\hat{G}, D_0) = O(\hat{G}, D_0)$. Then the conclusion holds by Theorem 4.7. □

Theorem 4.16 is illustrated in Section 5.3 on an example. Note that the minimal element of the lattice and its properties (Proposition 4.12 to 4.15) are used in [7] to obtain a new bijection concerning toroidal triangulations.

5 Toroidal triangulations

5.1 New proof of the existence of Schnyder woods

In this section we look specifically at the case of toroidal triangulations. We study the structure of 3-orientations of toroidal triangulations and show how one can use it to prove the existence of Schnyder woods in toroidal triangulations. This corresponds to the case $g = 1$ of Conjecture 2.14. Given a toroidal triangulation G, a *3-orientation* of G is an orientation of the edges of G such that every vertex has outdegree exactly three. By Theorem 2.12, a simple toroidal triangulation admits a 3-orientation. This can be shown to be true also for non-simple triangulations, for example using edge-contraction.

Consider a toroidal triangulation G and a 3-orientation of G. Let G^∞ be the universal cover of G.

Lemma 5.1 *A cycle C of G^∞ of length k has exactly $k-3$ edges leaving C and directed towards the interior of C.*

Proof. Let x be the number of edges leaving C and directed towards the interior of C. Consider the cycle C and its interior as a planar graph C^o. Euler's formula gives

$n - m + f = 2$ where n, m, f are respectively the number of vertices, edges and faces of C^o. Every inner vertex has exactly outdegree three, so $m = 3(n-k) + k + x$. Every inner face is a triangle so $2m = 3(f-1) + k$. The last two equalities can be used to replace f and m in Euler's formula, and obtain $x = k - 3$. □

For an edge e of G, we define the *middle walk from* e as the sequence of edges $(e_i)_{i \geq 0}$ obtained by the following method. Let $e_0 = e$. If the edge e_i is entering a vertex v, then the edge e_{i+1} is chosen in the three edges leaving v as the edge in the "middle" coming from e_i (i.e. v should have exactly one edge leaving on the left of the path consisting of the two edges e_i, e_{i+1} and thus exactly one edge leaving on the right).

A directed cycle M of G is said to be a *middle cycle* if every vertex v of M has exactly one edge leaving v on the left of M (and thus exactly one edge leaving v on the right of M). Note that if M is a middle cycle, and e is an edge of M, then the middle walk from e consists of the sequence of edges of M repeated periodically. Note that a middle cycle is not contractible, otherwise in G^∞ it forms a contradiction to Lemma 5.1. Similar arguments lead to:

Lemma 5.2 *Two middle cycles that are weakly homologous are either vertex-disjoint or equal.*

We have the following useful lemma concerning middle walks and middle cycles:

Lemma 5.3 *A middle walk always ends on a middle cycle.*

Proof. Start from any edge e_0 of G and consider the middle walk $W = (e_i)_{i \geq 0}$ from e_0. The graph G has a finite number of edges, so some edges will be used several times in W. Consider a minimal subsequence $e_k, \ldots, e_\ell$ such that no edge appears twice and $e_k = e_{\ell+1}$. Thus W ends periodically on the sequence of edges $e_k, \ldots, e_\ell$. We prove that $e_k, \ldots, e_\ell$ is a middle cycle.

Assume that $k = 0$ for simplicity. Thus $e_0, \ldots, e_\ell$ is an Eulerian subgraph E. If E is a cycle then it is a middle cycle and we are done. So we can consider that it visits some vertices several times. Let e_i, e_j, with $0 \leq i < j \leq \ell$, such that e_i, e_j are both leaving the same vertex v. By definition of ℓ, we have $e_i \neq e_j$. Let A and B be the two closed walks $e_i, \ldots, e_{j-1}$ and $e_j, \ldots, e_{i-1}$, respectively, where indices are modulo $\ell + 1$.

Consider a copy v_0 of v in the universal cover G^∞. Define the walk P obtained by starting at v_0 following the edges of G^∞ corresponding to the edges of A, and then to the edges of B. Similarly, define the walk Q obtained by starting at v_0 following the edges of B, and then the edges of A. The two walks P and Q both start at v_0 and both end at the same vertex v_1 that is a copy of v. Note that v_1 and v_0 may coincide. All the vertices that are visited on the interior of P and Q have exactly one edge leaving on the left and exactly one edge leaving on the right. The two walks P and Q may intersect before they end at v_1 thus we define P' and Q' has the subwalks of P and Q starting at v_0, ending on the same vertex u (possibly distinct from v_1 or not) and such that P' and

Q' are not intersecting on their interior vertices. Then the union of P' and Q' forms a cycle C of G^∞. All the vertices of C except possibly v_0 and u, have exactly one edge leaving C and directed towards the interior of C, a contradiction to Lemma 5.1. □

A consequence of Lemma 5.3 is that any 3-orientation of a toroidal triangulation has a middle cycle. The 3-orientation of the toroidal triangulation on the left of Figure 5 is an example where there is a unique middle cycle (the diagonal). We show in Lemma 5.5 that for any toroidal triangulation there exists a 3-orientation with several middle cycles.

Note that a middle cycle C satisfies $\gamma(C) = 0$ (when C is considered in any direction). So, by Lemma 5.3, there is always a cycle with value γ equal to 0 in a 3-orientation of a toroidal triangulation.

The orientation of the toroidal triangulation on the left of Figure 5 is an example of a 3-orientation of a toroidal triangulation where some cycles have value γ not equal to 0. The value of γ for the three loops is $2, 0$ and -2.

Two non-contractible not weakly homologous cycles generate the homology of the torus with respect to $\mathbb{Q}$. That is if B_1, B_2 are non contractible cycles that are not weakly homologous, then for any cycle C there exists $k, k_1, k_2 \in \mathbb{Z}$, $k \neq 0$, such that kC is homologous to $k_1B_1 + kB_2$.

Lemma 5.4 *In a 3-orientation, consider B_1, B_2, C are non contractible cycles, such that B_1, B_2 are not weakly homologous. Let $k, k_1, k_2 \in \mathbb{Z}$, $k \neq 0$ such that kC is homologous to $k_1B_1 + k_2B_2$. Then $k\gamma(C) = k_1\,\gamma(B_1) + k_2\,\gamma(B_2)$.*

Proof. Let v be a vertex in the intersection of B_1 and B_2. Consider a drawing of G^∞ obtained by replicating a flat representation of G to tile the plane. Let v_0 be a copy of v. Consider the path B starting at v_0 and following k_1 times the edges corresponding to B_1 and then k_2 times the edges corresponding to B_2 (we are going backwards if k_i is negative). This path ends at a copy v_1 of v. Since C is non-contractible we have k_1 or k_2 not equal to 0 and thus v_1 is distinct from v_0. Let B^∞ be the infinite path obtained by replicating B (forwards and backwards) from v_0. Since kC is homologous to $k_1B_1 + k_2B_2$ we can find an infinite path C^∞, that corresponds to copies of C replicated, that does not intersect B^∞ and situated on the right side of B. Now we can find a copy B'^∞ of B^∞, such that C^∞ lies between B^∞ and B'^∞ without intersecting them. Choose a copy v'_0 of v on B'^∞. Let B' be the copy of B starting at v'_0 and ending at a vertex v'_1. Let R be the region bounded by B, B' and the segments $[v_0, v'_0], [v_1, v'_1]$.

Consider the toroidal triangulation H whose representation is R (obtained by identifying B, B' and $[v_0, v'_0], [v_1, v'_1]$). Note that H is just made of several copies of G. Let C' be the subpath of C^∞ intersecting the region R corresponding to exactly one copy of kC. Let R_1 be the subregion of R bounded by B and C' and R_2 the subregion of R bounded by B' and C'. By some counting arguments (Euler's formula + triangulation + 3-orientation) in the region R_1 and R_2, we obtain that $\gamma(C') = \gamma(B)$ and thus $k\gamma(C) = k_1\gamma(B_1) + k_2\gamma(B_2)$. □

By Lemma 5.3, a middle walk W always ends on a middle cycle. Let us denote by M_W this middle cycle and P_W the part of W before M_W. Note that P_W may be empty. We say that a middle walk is leaving a cycle C if its starting edge is incident to C and leaving C.

Let us now prove the main lemma of this section.

Lemma 5.5 *G admits a 3-orientation with two middle cycles that are not weakly homologous.*

Proof. Towards a contradiction, suppose that there is no 3-orientation of G with two middle cycles that are not weakly homologous. We first prove the following claim:

Claim 5.6 *There exists a 3-orientation of G with a middle cycle M, a middle walk W leaving M and $M_W = M$.*

Proof. Towards a contradiction, suppose that there is no 3-orientation of G with a middle cycle M, a middle walk W leaving M and $M_W = M$. We first prove the following:

(1) Any 3-orientation of G, middle cycle M and middle walk W leaving M are such that M does not intersect the interior of W.

Towards a contradiction, suppose that M intersects the interior of W. By assumption, cycles M_W and M are weakly homologous and $M_W \neq M$. Thus by Lemma 5.2, they are vertex-disjoint. So M intersects the interior of P_W. Assume by symmetry that P_W is leaving M on its left side. If P_W is entering M from its left side, in G^∞, the edges of P_W plus M form a cycle contradicting Lemma 5.1. So P_W is entering M from its right side. Hence M_W intersects the interior of P_W on a vertex v. Let e be the edge of P_W leaving v. Then the middle cycle M_W and the middle walk W' started on e satisfies $M_{W'} = M_W$, contradicting the hypothesis. So M does not intersect the interior of W. This proves (1).

Consider a 3-orientation, a middle cycle M and a middle walk W leaving M such that the length of P_W is maximized. By assumption M_W is weakly homologous to M. Assume by symmetry that P_W is leaving M on its left side. By assumption $M_W \neq M$. (1) implies that M does not intersect the interior of W. Let v (resp. e_0) be the starting vertex (resp. edge) of W. Consider now the 3-orientation obtained by reversing M_W. Consider the middle walk W' started at e_0. Walk W' follows P_W, then arrives on M_W and crosses it (since M_W has been reversed). (1) implies that M does not intersect the interior of W'. Similarly, (1) applied to M_W and $W' \setminus P_W$ (the walk obtained from W' by removing the first edges corresponding to P_W), implies that M_W does not intersect the interior of $W' \setminus P_W$. Thus, $M_{W'}$ is weakly homologous to M_W and $M_{W'}$ is in the interior of the region between M and M_W on the right of M. Thus $P_{W'}$ strictly contains P_W and is thus longer, a contradiction. ◇

By Claim 5.6, consider a 3-orientation of G with a middle cycle M and a middle walk W leaving M such that $M_W = M$. Note that W is leaving M from one side and

entering it in the other side, otherwise W and M contradicts Lemma 5.1. Let e_0 be the starting edge of W. Let v, u be the starting and ending point of P_W, respectively, where $u = v$ may occur. Consider the 3-orientation obtained by reversing M. Let Q be the directed path from u to v along M (Q is empty if $u = v$). Let C be the directed cycle $P_W \cup Q$. We compute the value γ of C. If $u \neq v$, then C is almost everywhere a middle cycle, except at u and v. At u, it has two edges leaving on its right side, and at v it has two edges leaving on its left side. So we have $\gamma(C) = 0$. If $u = v$, then C is a middle cycle and $\gamma(C) = 0$. Thus, in any case $\gamma(C) = 0$. Note that furthermore $\gamma(M) = 0$ holds. The two cycles M, C are non contractible and not weakly homologous so any non-contractible cycle of G has γ equal to zero by Lemma 5.4.

Consider the middle walk W' from e_0. By assumption $M_{W'}$ is weakly homologous to M. The beginning $P_{W'}$ is the same as for P_W. As we have reversed the edges of M, when arriving on u, path $P_{W'}$ crosses M and continues until reaching $M_{W'}$. Thus $M_{W'}$ intersects the interior of $P_{W'}$ at a vertex v'. Let u' be the ending point of $P_{W'}$ (note that we may have $u' = v'$). Let P' be the non-empty subpath of $P_{W'}$ from v' to u'. Let Q' be the directed path from u' to v' along $M_{W'}$ (Q' is empty if $u' = v'$). Let C' be the non-contractible directed cycle $P' \cup Q'$. We compute $\gamma(C')$. The cycle C' is almost everywhere a middle cycle, except at v'. At v', it has two edges leaving on its left or right side, depending on $M_{W'}$ crossing $P_{W'}$ from its left or right side. Thus, we have $\gamma(C') = \pm 2$, a contradiction. □

By Lemma 5.5, for any toroidal triangulation, there exists a 3-orientation with two middle cycles that are not weakly homologous. By Lemma 5.4, any non-contractible cycle of G has value γ equal to zero. Note that $\gamma(C) = 0$ for any non-contractible cycle C does not necessarily imply the existence of two middle cycle that are not weakly homologous. The 3-orientation of the toroidal triangulation of Figure 15 is an example where $\gamma(C) = 0$ for any non-contractible cycle C but all the middle cycle are weakly homologous. The colors should help the reader to compute all the middle cycles by starting from any edge and following the colors. One can see that all the middle cycles are vertical (up or down) and that the horizontal (non-directed) cycle has value γ equal to 0 so we have γ equal to 0 everywhere. Of course, the colors also show the underlying Schnyder wood.

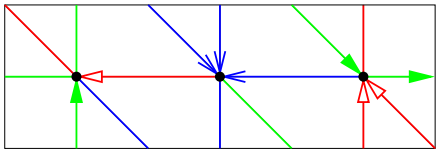

Figure 15: A 3-orientation of a toroidal triangulation with $\gamma(C) = 0$ for any non-contractible cycle C. All the middle cycle are weakly homologous.

By combining Lemma 5.5 and Theorem 3.7, we obtain the following:

Theorem 5.7 *A toroidal triangulation admits a 1-*EDGE*, 1-*VERTEX*, 1-*FACE *angle labeling and thus a Schnyder wood.*

Proof. By Lemma 5.5, there exists a 3-orientation with two middle cycles that are not weakly homologous. By Lemma 5.4, any non-contractible cycle of G has value γ equal to zero. Thus by Theorem 3.7, this implies that the orientation corresponds to an EDGE angle labeling. Then by Lemma 2.1, the labeling is also VERTEX and FACE. As all the edges are oriented in one direction only, it is 1-EDGE. As all the vertices have outdegree three, it is 1-VERTEX. Finally as all the faces are triangles it is 1-FACE (in the corresponding orientation of $\hat{G}$, all the edges incident to dual-vertices are outgoing). By Proposition 2.7, this 1-EDGE, 1-VERTEX, 1-FACE angle labeling corresponds to a Schnyder wood. □

Theorem 5.7 corresponds to the case $g = 1$ of Conjecture 2.14. By [17], we already knew that Schnyder woods exist for toroidal triangulations, but this section provides an alternative proof based on the structure of 3-orientations and the characterization theorem of Section 3.

5.2 The crossing property

A Schnyder wood of a toroidal triangulation is *crossing*, if for each pair i, j of different colors, there exist a monochromatic cycle of color i intersecting a monochromatic cycle of color j. In [17] a strengthening of Theorem 5.7 is proved :

Theorem 5.8 ([17]) *An essentially 3-connected toroidal map admits a crossing Schnyder wood.*

Theorem 5.8 is stronger than Theorem 5.7 for two reasons. First, it considers essentially 3-connected toroidal maps and not only triangulations, thus it proves Conjecture 2.15 for $g = 1$. Second, it shows the existence of crossing Schnyder woods.

However, what we have done in Section 5.1 for triangulation can be generalized to essentially 3-connected toroidal maps. For that purpose one has to work in the primal-dual completion. Proofs get more technical and instead of walks in the primal now walks in the dual of the primal-dual completion have to be considered. This is why we restrict ourselves to triangulations.

Even if we did not prove the existence of crossing Schnyder woods, Lemma 5.5 gives a bit of crossing in the following sense. A 3-orientation obtained by Lemma 5.5 has two middle cycles that are not weakly homologous. Thus in the corresponding Schnyder wood, these two cycles correspond to two monochromatic cycles that intersect. We say that the Schnyder wood obtained by Theorem 5.7 is *half-crossing*, i.e., there exists a pair i, j of different colors, such that there exist a monochromatic cycle of color i intersecting a monochromatic cycle of color j.

A half-crossing Schnyder wood is not necessarily crossing. The 3-orientation of the toroidal triangulation of Figure 16 is an example where two middle cycles are not weakly homologous, so it corresponds to a half-crossing Schnyder wood. However, It is not crossing because the green and the blue cycle do not intersect.

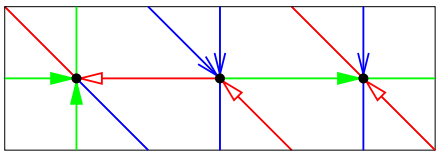

Figure 16: A not crossing but half-crossing Schnyder wood of a toroidal triangulation.

Consider a toroidal triangulation G and a pair $\{B_1, B_2\}$ of cycles that form a basis for the homology. Figure 14 shows how to transform an orientation of G into an orientation of $\hat{G}$. With this transformation a Schnyder wood of G naturally corresponds to a Schnyder orientation of $\hat{G}$. This allows us to not distinguish between a Schnyder wood or the corresponding Schnyder orientation of $\hat{G}$. Recall from Section 4.1, that the type of a Schnyder orientation of $\hat{G}$ in the basis $\{B_1, B_2\}$ is the pair $(\gamma(B_1), \gamma(B_2))$.

Lemma 5.9 *A half-crossing Schnyder wood is of type* $(0, 0)$ *(for the considered basis).*

Proof. Consider a half-crossing Schnyder wood of G and C_1, C_2 two crossing monochromatic cycles. We have $\gamma(C_1) = \gamma(C_2) = 0$. The cycles C_1, C_2 are not contractible and not weakly-homologous. So by Lemma 5.4, any non-contractible cycle C of G satisfies $\gamma(C) = 0$. Thus $\gamma(B_1) = \gamma(B_2) = 0$. □

A consequence of Lemma 5.9 is the following:

Theorem 5.10 *Let G be a toroidal triangulation, given with a particular half-crossing Schnyder wood D_0, then the set $T(G, D_0)$ of all Schnyder woods of G that have the same type as D_0 contains all the half-crossing Schnyder woods of G.*

Recall from Section 4.2, that the set $T(G, D_0)$ carries the structure of a distributive lattice. This lattice contains all the half-crossing Schnyder woods. It shows the existence of a canonical lattice useful for bijection purpose, see [7].

Note that $T(G, D_0)$ may contain Schnyder woods that are not half-crossing. The Schnyder wood of Figure 15 is an example where $\gamma(C) = 0$ for any non-contractible cycle C. So it is of the same type as any half-crossing Schnyder wood but it is not half-crossing.

Note also that in general there exist Schnyder woods not in $T(G, D_0)$. The Schnyder wood of Figure 17 is an example where the horizontal cycle has γ equal to ± 6. Thus it cannot be of the same type as a half-crossing Schnyder wood.

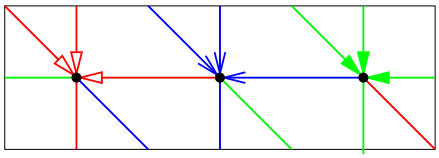

Figure 17: A Schnyder wood of a toroidal triangulation where $\gamma(C) \neq 0$ for a non-contractible cycle C.

5.3 A lattice example

Figure 18 illustrates the Hasse diagram of the set $T(G, D_0)$ for the toroidal triangulation G of Figure 16. Bold black edges are the edges of the Hasse diagram $\mathcal{H}$. Each node of the diagram is a Schnyder wood of G. Since we are considering a triangulation $\hat{G}$ is not represented in the figure. Indeed, all the edges of $\hat{G}$ incident to dual-vertices are outgoing in any Schnyder orientation of G, thus these edges are rigid and do not play a role for the structure of the lattice. In every Schnyder wood, a face is dotted if its boundary is directed. In the case of the special face f_0 the dot is black. Otherwise, the dot is magenta if the boundary cycle is oriented counterclockwise and cyan otherwise. An edge in the Hasse diagram from D to D' (with $D \leq D'$) corresponds to a face oriented counterclockwise in D whose edges are reversed to form a face oriented clockwise in D', i.e., a magenta dot is replaced by a cyan dot. The outdegree of a node is its number of magenta dots and its indegree is its number of cyan dots. By Proposition 4.13, all the faces have a dot at least once. The special face is not allowed to be flipped, it is oriented counterclockwise in the maximal Schnyder wood and clockwise in the minimal Schnyder wood by Proposition 4.14. By Proposition 4.15, the maximal (resp. minimal) Schnyder wood contains no other faces oriented counterclockwise (resp. clockwise), indeed in contains only cyan (resp. magenta) dots. The words "no", "half", "full" correspond to Schnyder woods that are not half-crossing, half-crossing (but not crossing), and crossing, respectively. By Theorem 5.10, the figure contains all the half-crossing Schnyder woods of G. The minimal element is the Schnyder wood of Figure 15, and its neighbor is the Schnyder wood of Figure 16.

The graph is very symmetric so the lattice does not depend on the choice of special face. In the example the two crossing Schnyder woods lie in the "middle" of the lattice. These Schnyder woods are of particular interests for graph drawing (see [17]) whereas the minimal Schnyder wood (not crossing in this example) is important for bijective encoding (see [7]).

The underlying toroidal triangulation of Figure 18 has only two Schnyder woods not depicted in Figure 18. One of them two Schnyder wood is shown in Figure 17 and the other one is a 180°rotation of Figure 17. Each of these Schnyder wood is alone in its lattice of homologous orientations. All their edges are rigid. They have no 0-homologous oriented subgraph.

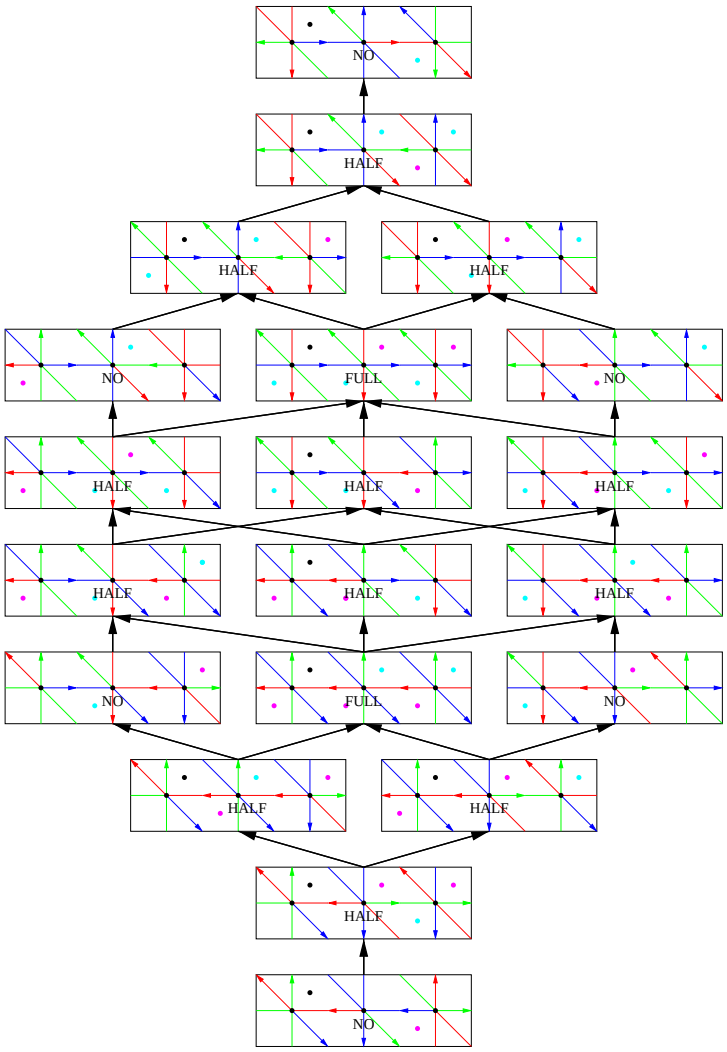

Figure 18: Example of the Hasse diagram of the distributive lattice of homologous orientations of a toroidal triangulation.

Theorem 4.6 says that one can take the Schnyder wood of Figure 17, reverse three or six vertical cycle (such cycles form an Eulerian-partitionable oriented subgraph) to obtain another Schnyder wood. Indeed, reversing any three of these cycles leads to one of the Schnyder wood of Figure 18 (for example reversing the three loops leads to the crossing Schnyder wood of the bottom part). Note that $\binom{3}{6} = 20$ and there are exactly twenty Schnyder woods on Figure 18. Reversing six cycles leads to the same picture pivoted by 180°.

6 Conclusions

In this paper we propose a generalization of Schnyder woods to higher genus via angle labelings. We show that these objects behave nicely with simple characterization theorems and strong structural properties. Unfortunately, we are not able to prove that every essentially 3-connected map admits a generalized Schnyder wood.

As mentioned earlier, planar Schnyder woods have applications in various areas. In the toroidal case, they already lead to some results concerning graph drawing [17] and optimal encoding [7]. It would be interesting to see which other applications can be generalized to higher genus.

Note also that the distributive lattice structure of homologous orientations of a given map (see Theorem 4.7) is a very general result that may be useful to study other objects (transversal structures, $\frac{d}{d-2}$-orientations, etc.) associated to other kinds of maps (4-connected triangulations, d-angulations, etc.).

References

[1] B. Albar, D. Gonçalves, K. Knauer, Orienting triangulations, manuscript, 2014, arXiv:1412.4979.

[2] J. Barát, C. Thomassen, Claw-decompositions and Tutte-orientations, Journal of Graph Theory 52 (2006) 135-146.

[3] J. Barbay, L. Castelli Aleardi, M. He, J. I. Munro, Succinct representation of labeled graphs, Algorithmica 61 (2012) 224-257.

[4] N. Bonichon, A bijection between realizers of maximal plane graphs and pairs of non-crossing Dyck paths, *Discrete Mathematics* 298 (2005) 104-114.

[5] N. Bonichon, C. Gavoille, N. Hanusse, D. Ilcinkas, Connections between Theta-Graphs, Delaunay Triangulations, and Orthogonal Surfaces. WG10 (2010).

[6] L. Castelli Aleardi, E. Fusy, T. Lewiner, Schnyder woods for higher genus triangulated surfaces, with applications to encoding, *Discrete and Computational Geometry* 42 (2009) 489-516.

[7] V. Despré, D. Gonçalves, B. Lévêque, Encoding toroidal triangulations, manuscript, 2015, arXiv:1507.05461.

[8] S. Felsner, Convex Drawings of Planar Graphs and the Order Dimension of 3-Polytopes, *Order* 18 (2001) 19-37.

[9] S. Felsner, Geodesic Embeddings and Planar Graphs, *Order* 20 (2003) 135-150.

[10] S. Felsner, Lattice structures from planar graphs, *Electron. J. Combin.* 11 (2004).

[11] S. Felsner, K. Knauer, ULD-lattices and Δ-bonds, *Comb. Probab. Comput.* 18 5 (2009) 707-724.

[12] S. Felsner, *Geometric Graphs and Arrangements*, Vieweg, 2004.

[13] H. de Fraysseix, P. Ossona de Mendez, P. Rosenstiehl, On Triangle Contact Graphs, *Combinatorics, Probability and Computing* 3 (1994) 233-246.

[14] H. de Fraysseix, P. Ossona de Mendez, On topological aspects of orientations, *Discrete Mathematics* 229 (2001) 57-72.

[15] P. Giblin, *Graphs, surfaces and homology*, Cambridge University Press, Cambridge, third edition, 2010.

[16] D. Gonçalves, B. Lévêque, A. Pinlou, Triangle contact representations and duality, *Discrete and Computational Geometry* 48 (2012) 239-254.

[17] D. Gonçalves, B. Lévêque, Toroidal maps : Schnyder woods, orthogonal surfaces and straight-line representations, *Discrete and Computational Geometry* 51 (2014) 67-131.

[18] G. Kant, Drawing planar graphs using the canonical ordering, *Algorithmica* 16 (1996) 4-32.

[19] W. S. Massey, *Algebraic Topology: An Introduction*, Harcourt, Brace and World, New York, 1967

[20] E. Miller, Planar graphs as minimal resolutions of trivariate monomial ideals, *Documenta Mathematica* 7 (2002) 43-90.

[21] B. Mohar, P. Rosenstiehl, Tessellation and visibility representations of maps on the torus, Discrete Comput. Geom. 19 (1998) 249-263.

[22] P. Ossona de Mendez, Orientations bipolaires, PhD Thesis, Paris, (1994).

[23] D. Poulalhon, G. Schaeffer, Optimal coding and sampling of triangulations, *Algorithmica* 46 (2006) 505-527.

[24] J. Propp, Lattice structure for orientations of graphs, manuscript, 1993, arXiv:math/0209005.

[25] W. Schnyder, Planar graphs and poset dimension, *Order* 5 (1989) 323-343.

[26] W. Schnyder, Embedding planar graphs on the grid, in Proceedings of the First Annual ACM-SIAM Symposium on Discrete Algorithms, *SODA '90* (1990) 138-148.

Orienting Triangulations*

Boris Albar,[1] Daniel Gonçalves,[2] and Kolja Knauer[1]

[1] *LIF, UMR 7279, CNRS & AIX-MARSEILLE UNIVERSITÉ*
MARSEILLE, FRANCE
E-mail: boris.albar@lif.univ-mrs.fr; kolja.knauer@lif.univ-mrs.fr

[2] *LIRMM, UMR 5506, CNRS & UNIVERSITÉ DE MONTPELLIER*
MONTPELLIER, FRANCE
E-mail: daniel.goncalves@lirmm.fr

Received September 17, 2014; Revised October 1, 2015

Published online 2 December 2015 in Wiley Online Library (wileyonlinelibrary.com).
DOI 10.1002/jgt.22005

Abstract: We prove that any triangulation of a surface different from the sphere and the projective plane admits an orientation without sinks such that every vertex has outdegree divisible by three. This confirms a conjecture of Barát and Thomassen and is a step toward a generalization of Schnyder woods to higher genus surfaces. © 2015 Wiley Periodicals, Inc. J. Graph Theory 83: 392–405, 2016

Keywords: *triangulations; surfaces; orientations*

1. INTRODUCTION

The notation and results we use for graphs and surfaces can be found in [10]. We start with some basic definitions:

A *map* (or 2-*cell embedding*) of a multigraph into a surface, is an embedding such that deleting the graph from the surface leaves a collection of open disks, called the *faces* of the map. A *triangulation* is a map of a simple graph (i.e. without loops or multiple edges) where every face is triangular (i.e. incident to three edges). A fundamental result in the topology of surfaces is that every surface admits a map. The *(orientable) genus* of a map

*Contract grant sponsors: EGOS, ANR-12-JS02-002-01; contract grant sponsor: PEPS grant EROS.

on an orientable surface is $\frac{1}{2}(2-n+m-f)$ and the *(nonorientable) genus* of a map on a nonorientable surface is $2-n+m-f$, where n, m, f denote the number of vertices, edges, and faces of the map, respectively. The *Euler genus* of a map is $2-n+m-f$, that is the nonorientable genus or twice the orientable genus. All the maps on a fixed surface have the same genus, which justifies to define the *(Euler) genus of a surface* as the (Euler) genus of any of the maps it admits. In [1] Barát and Thomassen conjectured the following:

Conjecture 1. *Let T be a triangulation of a surface of Euler genus $k \geq 2$. Then T has an orientation such that each outdegree is at least* 3*, and divisible by* 3.

One easily computes that the number of edges m of a triangulation T of a surface of Euler genus k is $3n-6+3k$. So while triangulations of Euler genus less than 2 simply have too few edges to satisfy the conjecture, in [1] the conjecture is proved for the case $k=2$, that is the torus and the Klein bottle. Moreover, they show that any triangulation T of a surface has an orientation such that each outdegree is divisible by 3, that is in order to prove the full conjecture they miss the property that there are no sinks.

Barát and Thomassen's conjecture was originally motivated in the context of claw-decompositions of graphs, since given an orientation with the claimed properties the outgoing edges of each vertex can be divided into claws, such that every vertex is the center of at least one claw.

Another motivation for this conjecture is, that it can be seen as a step toward the generalization of planar Schnyder woods to higher genus surfaces. A *Schnyder wood* [11] of a planar triangulation is an orientation and a $\{0,1,2\}$-coloring of the *inner* edges satisfying the following *local rule* on every *inner* vertex v: going counterclockwise around v one successively crosses an outgoing 0-arc, possibly some incoming 2-arcs, an outgoing 1-arc, possibly some incoming 0-arcs, an outgoing 2-arc, and possibly some incoming 1-arcs until coming back to the outgoing 0-arc.

Schnyder woods are one of the main tools in the area of planar graph representations and Graph Drawing. They provide a machinery to construct space-efficient straight-line drawings [6, 12], representations by touching T shapes [5], they yield a characterization of planar graphs via the dimension of their vertex-edge incidence poset [6, 11], and are used to encode triangulations efficiently [3]. In particular, the local rule implies that every Schnyder wood gives an orientation of the inner edges such that every inner vertex has outdegree 3 and the outer vertices are sinks with respect to inner edges. Indeed, this is a one-to-one correspondence between Schnyder woods and orientations of this kind. As a consequence, the set of Schnyder woods of a planar triangulation inherits a natural distributive lattice structure, which in particular provides any triangulation with a unique *minimal* Schnyder wood [7]. These unique representatives are an important tool in proofs and lie at the heart of many enumerative results, see for instance [2].

When generalizing Schnyder woods to higher genus one has to choose which of the properties of planar Schnyder woods are desired to be carried over to the more general situation. Examples are: the efficient encoding of triangulations on arbitrary surfaces [4] and the relation to orthogonal surfaces and small grid drawings for toroidal triangulations [9], which lead to different definitions of generalized Schnyder woods. In [9], the generalized Schnyder woods indeed satisfy the local rule with respect to *all* edges and vertices of a toroidal triangulation and henceforth lead to orientations having outdegree 3 at every vertex. An interesting open problem is to generalize the local rule to triangulations with higher Euler genus in such a way that for some vertices the sequence

mentioned in the local rule occurs several times around the vertex. Here, the mere existence of such objects is an open question. Clearly, such a generalized Schnyder wood would yield an orientation as claimed by the conjecture. Thus, proving the conjecture of Barát and Thomassen is a first step into that direction.

2. PRELIMINARIES

A map M on a surface $\mathbb{S}$ is characterized by a triple $(V(M), E(M), F(M))$, formed by the vertex, edge, and face sets of M. In the following we will restrict to triangulations $T = (V(T), E(T), F(T))$, that is the pair $(V(T), E(T))$ is a simple embedded graph such that every face is incident to exactly three edges.

A *submap* M' of T, is a triplet (V', E', F') where $V' \subseteq V(T), E' \subseteq E(T), F' \subseteq F(T)$, and such that:

- $uv \in E'$ implies $\{u, v\} \subseteq V'$, and
- $f \in F'$ implies $e' \in E'$ for any edge e incident to f.

The *boundary* $\partial M'$ of a submap $M' = (V', E', F')$ is the set of edges in E' that are incident to at most one face in M'.

For any vertex v of T its *surrounding* is the circular sequence of edges and faces successively met while going around v. This sequence as no particular direction as T can be nonorientable. In a submap M' of T a *(boundary) angle* at vertex v is a subsequence $(e_0, f_1, e_1, \ldots, f_t, e_t)$ of its surrounding such that the edges e_0 and e_t are the only elements of this sequence belonging to M'. Those edges are the *sides* of this angle. This angle can be denoted by $\widehat{e_0 v e_t}$ or simply by $\widehat{v}$. It can occur that $e_0 = e_t$. Consider for example a submap consisting of a single edge. Let us mention, that this definition could be modified in order to include the angle around a vertex with respect to a submap without edges. Since we will not consider this situation we prefer avoiding further technicalities.

Note that an edge is in $\partial M'$ if and only if it is a side of (at least) one angle of M'. Actually, the notion of angles endows the boundary $\partial M'$ of M' with some further structure. As each angle has two sides (possibly two occurrences of the same edge) and as each occurrence of an edge of $\partial M'$ is a side for two angles, one can define the *boundary sequence* of M', that is a collection of circular sequences, alternating between angles and edges, $(\widehat{a_0}, e_0, \widehat{a_1}, e_1, \ldots, \widehat{a_t}, e_t)$ (sometimes simply denoted by $(\widehat{a_0}, \widehat{a_1}, \ldots, \widehat{a_t})$ or $(e_0, e_1, \ldots, e_t)$), where e_i is the common edge of $\widehat{a_i}$ and $\widehat{a_{i+1}}$. Note that an edge e may appear twice in the boundary sequence, for example if e is a bridge of M'. Thus, if necessary we will refer to a specific *occurrence* of e in $\partial M'$. For simplicity, we denote the boundary sequence of M' by $\partial M'$. This naturally leads to the notion of *consecutive angles*. Note that two angles $(e_0, f_1, e_1, \ldots, f_t, e_t)$ and $(e'_0, f'_1, e'_1, \ldots, f'_t, e'_t)$ are *consecutive* on the boundary sequence if $e_t = e'_0$ and $f_t = f'_1$.

In the following, a *disk* is a submap M' of T if it is homeomorphic to a (closed) topological disk. Furthermore, a disk is a *k-disk* if its boundary is a cycle with k edges. A 3-disk is called *trivial* if it contains only one face. A disk is called *chordless* if its outer vertices (i.e. on its boundary) induce a graph that is a (chordless) cycle. A cycle is *contractible* if it is the boundary of a disk otherwise it is called *noncontractible*.

Given a triangulation T and a set of vertices $X \subseteq V(T)$, the *induced submap* $T[X]$ is the maximal submap with vertex set X. In other words this submap has edge set $\{uv \in E(T) \mid u \in X \text{ and } v \in X\}$, and face set $\{uvw \in F(T) \mid u \in X, v \in X, \text{ and } w \in X\}$.

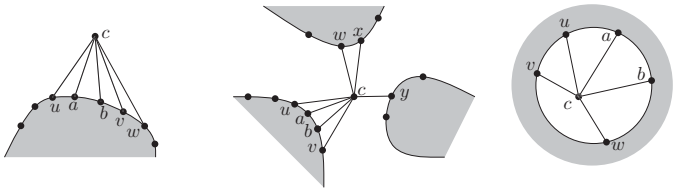

FIGURE 1. Different scenarios of stacking c on M'. Left: one neighboring path $P_1 = (u, a, b, v, w)$. Middle: three neighboring paths $P_1 = (u, a, b, v)$, $P_2 = (w, x)$, $P_3 = (y)$. Right: A boundary cycle $C = (u, v, w, b, a)$.

Given an induced submap $M' = T[X]$ of a triangulation T, and any occurrence of an edge ab in $\partial M'$ (corresponding to angles $\widehat{a}$ and $\widehat{b}$) there exists a unique vertex c such that there is a face abc in $F(T)\backslash F(M')$ that belongs to both angles $\widehat{a}$ and $\widehat{b}$. For any such vertex c (and $ab \in \partial M'$) we define the operation of *stackingc* on M', as adding c to X, that is going from $M' = T[X]$ to $M'' = T[X + c]$. In such stacking the *neighborhood* of c in M' is the graph with vertices x such that $cx \in E(M'')$ and edges xy such that $cxy \in F(M'')$. As T is simple, note that this neighborhood is either a cycle or a union of paths, one of which with at least one edge (the edge allowing the stacking), and let us call them the *neighboring cycle* and the *neighboring paths* of c in M', respectively. See Figure 1 for an illustration.

3. PROOF OF CONJECTURE 1

Let us consider for contradiction a minimal counterexample T. Note that T does not contain any nontrivial 3-disk D. Otherwise we would remove the interior of D and would replace it by a face. By minimality of T, this new triangulation would admit an orientation such that every vertex has non-zero outdegree divisible by 3. As D is a planar triangulation, there exists an orientation of its interior edges so that inner and outer vertices have outdegree 3 and 0, respectively. This is the case for orientations induced by a Schnyder wood on these triangulations [11]. Then the union of these two orientations would give us an orientation of T with nonzero outdegrees divisible by three. Let us now proceed by providing an outline of the proof.

3.1. Outline

We first prove that one can partition the edges of the triangulation T into the following graphs:

- The *initial graph* I, which is an induced submap containing a non-contractible cycle. Furthermore, I contains an edge uv such that the map $I\backslash uv$ is a disk $\widetilde{D}$ whose underlying graph is a maximal outerplanar graph with only two degree two vertices, u and v. See Figure 2 for an illustration.
- The *correction graph* B (with blue edges in the figures), which is oriented acyclically in such a way that each vertex of $V(T)\backslash V(I)$ has outdegree 2, while the other vertices have outdegree 0,
- The *last correction path* G (with green edges in the figures), which is a $\{u, v\}$-path.

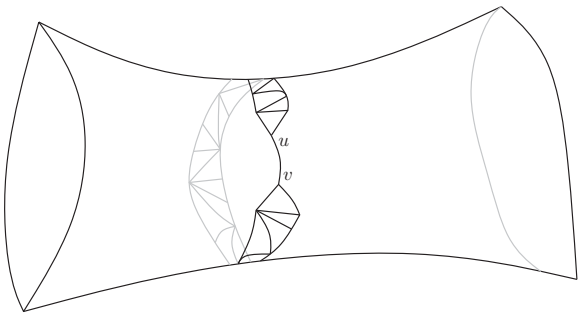

FIGURE 2. Example of a submap I.

- The *nonzero graph* R (with red edges in the figures), which is oriented in such a way that all vertices in $(V(T)\backslash V(G)) \cup \{u, v\}$ have outdegree at least 1.

The existence of such graph I is proven in Section 3.2, then in Section 3.3 we prove the existence of graphs B, G, and R (with the mentioned orientations). To do the latter we start from I and we incrementally conquer the whole triangulation T by stacking the vertices one by one (this procedure is inspired by [4]).

Finally, the edges of I, B, and G are (re)oriented, to obtain the desired orientation. The orientation of edges in R does not change, as they ensure that many vertices (all vertices of T except the interior vertices of the path G) have nonzero outdegree. The $\{u, v\}$-path G is either oriented from u to v or from v to u, but this will be decided later. However in both cases its interior vertices are ensured to have nonzero outdegree. Hence all vertices are ensured to have nonzero outdegree and it remains to prove that they have outdegree divisible by 3.

We start in Section 3.4 by reorienting the B-arcs in order to ensure that vertices of $V(T)\backslash V(I)$ have outdegree divisible by 3 (this part is inspired by the proof of Theorem 4.5 in [1]). In the last step, in Section 3.5, we choose the orientation of the $\{u, v\}$-path G, and we orient I in order to achieve the desired orientation.

3.2. Existence of *I*

To prove the existence of I, we first need the following lemma.

Lemma 1. *Any triangulation T with Euler genus at least 2, has an induced submap I obtained from a disk D by stacking a vertex v, such that for any two neighbors a, b of v belonging to distinct neighboring paths (of v w.r.t. D), every cycle C in I going through edges av and vb is noncontractible.*

Proof. Any face of T is an induced disk. Consider a maximal induced disk D of T. For any edge xy of ∂D, stack a vertex v on xy. Let us denote by I the map obtained by stacking v on D. As T has Euler genus at least two the neighborhood of v is not a cycle. Also, as D is maximal, v has at least two neighboring paths. Assume for contradiction, that there is a contractible cycle C of I going through av, vb (where a and b belong to distinct neighboring paths of v w.r.t. D) and through some $\{a, b\}$-path P of ∂D. Denote by D' the disk bounded by C and note that (as I is induced) D' contains vertices not in

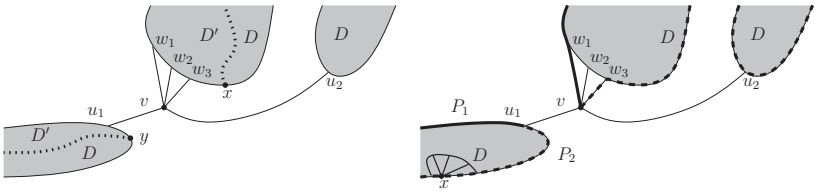

FIGURE 3. The situation in Claim 1 (left) and Claim 2 (right) in the proof of Lemma 2.

I. As $\partial D'$ intersects D on a path it is clear that $V(D) \cup V(D')$ induces disk with v on its boundary. Furthermore, as only two neighbors of v in this disk are on the border, we have that $(V(D) \cup V(D'))\backslash\{v\}$ also induces a disk. This disk is larger than D, contradicting its maximality. □

Lemma 2. *Any triangulation T' with Euler genus at least 2, has an induced submap I containing a noncontractible cycle, and an edge uv such that $I\backslash uv$ is a disk $\widetilde{D}$, and for each of the two $\{u, v\}$-paths of $\partial\widetilde{D}$, all its interior vertices have a neighbor in the interior of the other $\{u, v\}$-path.*

Proof. Among the induced subgraphs of T' that satisfy Lemma 1 let I be a minimal one. Let v and D be the vertex of I and the disk $I\backslash\{v\}$ described in Lemma 1, respectively. As v is stacked on D let us denote by $(w_1, \ldots, w_s)$, with $s \geq 2$, some neighboring path of v, and let us denote by $u_1, \ldots, u_t$, with $t \geq 1$, the other neighbors of v in D. Finally, let us denote by $\widetilde{D}$ the disk obtained from D by adding vertex v, edges vw_i for $1 \leq i \leq s$, and faces vw_iw_{i+1} for $1 \leq i < s$. The minimality of I implies all the needed properties:

Claim 1. *∂D induces no chord xy inside D such that some $\{x, y\}$-path of ∂D contains both an edge w_iw_{i+1}, for some $1 \leq i < s$, and a vertex u_j, for some $1 \leq j \leq t$.*

Proof. If such chord xy exists, let $D' \subsetneq D$ be the disk with boundary in $\partial D + xy$ which contains both w_iw_{i+1} and u_j. Then the graph induced by $V(D') \cup \{v\}$ contradicts the minimality of I. See the left of Figure 3. □

This implies that $\partial\widetilde{D}$ has no chord at u_j, for all $1 \leq j \leq t$.

Claim 2. *For all $1 \leq j \leq t$, every interior vertex x of a $\{v, u_j\}$-path of $\partial\widetilde{D}$ is adjacent to an interior vertex of the other $\{v, u_j\}$-path.*

Proof. Let P_1 and P_2 be the $\{v, u_j\}$-path of $\partial\widetilde{D}$ containing w_1 and w_s, respectively. Assume for contradiction, there exists an inner vertex x in P_1 having no neighbor in the interior of P_2. By Claim 1 this implies that D (the disk induced by $V(I)\backslash\{v\}$) has no chord at x. Thus the map induced by $V(D)\backslash\{x\}$ is a disk containing P_2 on its border, hence containing the vertex u_j and the edge $w_{s-1}w_s$. Hence the map induced by $V(I)\backslash\{x\}$ contradicts the minimality of I. See the right of Figure 3. □

As $\partial\widetilde{D}$ has no chord at u_j, for all $1 \leq j \leq t$, this implies that $t = 1$. This concludes the proof of the lemma. □

Consider now our counterexample T, and let I, uv and $\widetilde{D}$ $(= I\backslash uv)$ be an induced submap, an edge and a disk, verifying Lemma 2. In the beginning of the section we have seen that by minimality, T does not contain nontrivial 3-disks. Hence by the properties

of I, if $\widetilde{D}$ would contain an inner vertex, this vertex would be in a chordless 4-disk of $\widetilde{D}$. By the following lemma this is not possible, hence $\widetilde{D}$ is a maximal outerplanar graph. Finally, the adjacency property between vertices of $\partial\widetilde{D}\backslash\{u, v\}$ imply that u and v are the only degree two vertices of $\widetilde{D}$.

Lemma 3. *The submap $\widetilde{D}$ does not contain chordless 4-disks.*

Proof. If $\widetilde{D}$ would contain such a disk D_4, with boundary (v_1, v_2, v_3, v_4), we would remove the interior of D_4 and we would add one of the two possible diagonals, say v_2v_4 (if v_2v_4 are not uv's ends), and the corresponding two triangular faces, $v_1v_2v_4$ and $v_2v_3v_4$. The obtained map T' is defined on the same surface as T and is smaller. Furthermore as I is an induced submap without nontrivial 3-disk and as $v_2v_4 \neq uv$, there is no edge v_2v_4 in T. Hence T' is simple and it is a triangulation. Now by minimality of T, this new triangulation T' has an orientation such that every vertex has nonzero outdegree divisible by 3. Let us suppose without loss of generality that in this orientation the edge v_2v_4 is oriented from v_2 to v_4.

Using the fact that for any planar triangulation, there exists an orientation of the interior edges such that inner and outer vertices have outdegree 3 and 0 [11], respectively, one can orient the inner edges of D_4 in such a way that inner vertices, vertex v_2, and vertices v_1, v_3, and v_4 have outdegree 3, 1 and 0, respectively. For this consider the orientation given by a Schnyder wood of the triangulation $D_4 + v_1v_3$ (with outer face $v_1v_3v_4$) and notice that the edges v_2v_1 and v_2v_3 are necessarily oriented from v_2 to v_1 and v_3, respectively (as v_1, v_3, and v_4 have outdegree 0).

Then the union of these orientations, of $T'\backslash v_2v_4$ and of D_4's inner edges, would give us an orientation of T with nonzero outdegrees divisible by three. □

3.3. Existence of *B*, *G*, and *R*

As mentioned in the outline, we will start from I and we incrementally explore the whole triangulation T by stacking the vertices one by one. At each step, we will assign the newly explored edges to B, G, or R, and we will orient those assigned to B or R. At each step the *explored region* is a submap of T induced by some vertex set X. Such explored region is denoted by $T[X]$ and its boundary $\partial T[X]$. The connected pieces of the surface obtained after removing $T[X]$ are called the *unexplored regions*, and if one of them is homeomorphic to an open disk it is called an *unexplored disk*. Given an unexplored disk D (by abuse of notation) we denote by ∂D the cycle of $\partial T[X]$ bordering D. During the exploration we maintain the following invariants:

(I) The graphs I, B, G, and R partition the edges of $T[X]$.

(II) All interior vertices of $T[X]$ (i.e. in $X\backslash V(\partial T[X])$) have at least one outgoing R-arc, or two incident G-edges. Furthermore G either is an $\{u, v\}$-path, or is the union of two vertex disjoint paths G_u and G_v, going from u to u_*, and from v to v_*, respectively, for some vertices u_* and v_* on $\partial T[X]$.

Here the vertices u_* and v_* may coincide with vertices u and v, respectively, if G_u or G_v is a trivial path with only one vertex.

(III) The graph B is acyclically oriented in such a way that the vertices of I have outdegree 0, while the other vertices of $T[X]$ have outdegree 2.

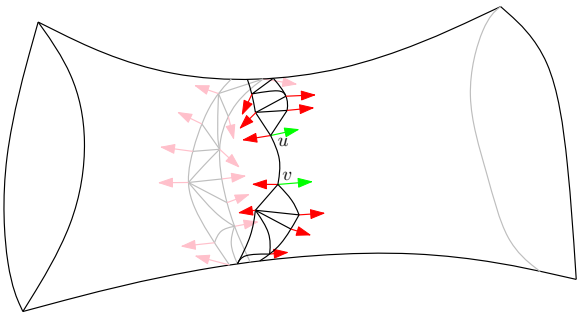

FIGURE 4. Assigning requests to I in order to satisfy the invariants.

Furthermore, to help us in properly finishing the construction of the graphs B, G, and R in the further steps, we introduce the notion of *requests* on the angles of $\partial T[X]$. There are two types of requests, G-requests and R-request. An angle is allowed to have at most one request, and an angle having no request is called *free*. Informally, a G-request (resp. an R-request) for an angle $\widehat{a}$ means that in a further step an edge inside this angle will be added in G (resp. in R and oriented from a to the other end). In the figures, a G-request (resp. an R-request) is depicted by a green (resp. red) arrow.

(IV) Every vertex of $(\partial T[X]\backslash\{u_*, v_*\}) \cup \{u, v\}$ having (still) no outgoing R-arc, has an incident angle with an R-request.
(V) If G is not a $\{u, v\}$-path (yet), the vertices u_* and v_* (at the end of G_u and G_v, respectively), have one incident angle each, say $\widehat{u_*}$ and $\widehat{v_*}$, that are consecutive on $\partial T[X]$, and that have a G-request. Furthermore, there are no other G-requests.
(VI) If there is an unexplored disk D', then there are at least three free angles (of $\partial T[X]$) around D'.

Before starting this exploration, let us observe that if these invariants are maintained until the end of the exploration, we obtain the desired partition of the edges. Note that at the end of the exploration $T[X]$ has no border, hence no requests, and by (V) G is thus an $\{u, v\}$-path. As u and v have degree 1 in G, by (II) every vertex in $(V(T)\backslash V(G)) \cup \{u, v\}$ has out-degree at least 1 in R. Finally, by (III) B is oriented acyclically in such a way that each vertex of $V(T)\backslash V(I)$ has outdegree 2, while the other vertices have outdegree 0. We can now proceed to the exploration itself.

This exploration starts with $T[X] = I$. In this case as all the edges of $T[X]$ are in I and as there are no interior vertices yet, (I), (II), and (III) are trivially satisfied. Since I contains a noncontractible cycle and since the Euler genus of T is at least two there is no unexplored disk, hence (VI) is satisfied. Since uv appears twice in $\partial T[X]$, the vertices u, v appear twice consecutively in $\partial T[X]$. To achieve (V), choose the angles of one consecutive appearance of u, v as G-requests. To achieve (IV), all the other angles are assigned R-requests. See Figure 4 for an illustration.

For the rest of the construction in each step we enlarge the explored submap $T[X]$ by stacking a vertex x on $T[X]$. The vertex x is chosen according to the following rules:

(i) If there is only one edge in the neighborhood of x in $T[X]$, this edge is not $\{u_*, v_*\}$.

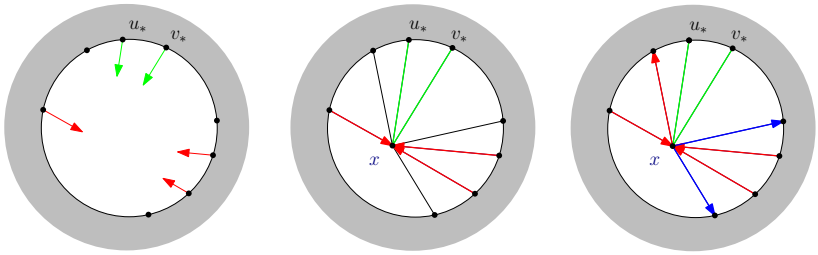

FIGURE 5. Case where x is in an unexplored disk D and has a neighboring cycle.

(ii) If x belongs to an unexplored disk D, either x is adjacent to all the vertices of ∂D or x has exactly one neighboring path P on ∂D such that P does not contain all the free angles of ∂D.

(iii) In the case x does not belong to an unexplored disk, if possible we choose x such that no unexplored disk is created. Furthermore, if unexplored disks are created we choose x in order to minimize the total surface of these unexplored disks (measured by the number of faces in these regions).

Let us explain why choosing such a vertex x is always possible. If there is an unexplored disk D, let us choose x inside D. If there is a vertex adjacent to all the vertices of ∂D we are fine ((i) follows). Otherwise, one can show that there are at least two vertices inside D, say x_1 and x_2, having exactly one neighboring path $P \neq (u_*, v_*)$ on ∂D, say P_1 and P_2, respectively. These two paths intersect on at most two vertices, so one of them, say P_1, avoids one of the (at least) three free angles around D. In that case choosing x_1 as the next vertex to stack fulfills (i) and (ii). Now if there is no unexplored disk, as there are at least three edges on $\partial T[X]$ there are candidates fulfilling (i). As (iii) is not constraining we are done.

In the following we show how to extend B, G, R on the newly introduced edges and how to deal with the newly created angles to maintain all invariants valid. We will describe the construction and we will check the validity of invariants only for the nontrivial ones. We distinguish cases according to the topology of the unexplored region containing x.

(1) The vertex x is contained in an unexplored disk D and has a neighboring cycle. By (VI) the unexplored disk containing x has at least three free angles. We orient the corresponding edges from x to its neighbors, put two into B and the rest into R. All non-free angles satisfy their request with the edge incident to x. See Figure 5 for an illustration.

We have assigned all the newly explored edges, hence (I) remains valid. As (IV) and (V) were valid in $T[X]$, all the neighbors of x (i.e. the vertices around D) have now (in $T[X + x]$) an outgoing R-arc or two incident G-edges. The vertex x also does, hence (II) is valid. In the acyclic graph B, adding the vertex x with only outgoing B-arcs cannot create any circuit, hence (III) remains valid. As in this case, as $\partial T[X + x]$ is included in $\partial T[X]$, (IV) remains valid. If u_* and v_* were around D in $T[X]$, the two parts of G are now connected by the adjunction of xu_* and xv_* in G. Otherwise, G was already an $\{u, v\}$-path, or u_* and v_* were elsewhere in $\partial T[X]$ fulfilling (V). Hence in any case (V) holds. Finally, as no unexplored disk has been created and as the requests around existing unexplored disks have not changed, (VI) remains valid.

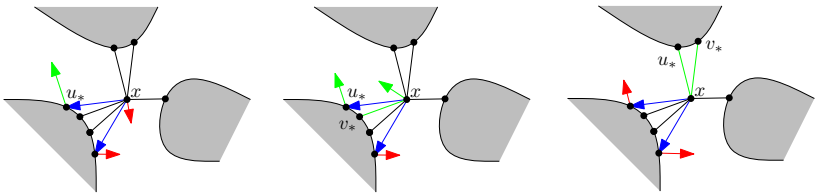

FIGURE 6. Case where x is not in an unexplored disk. (left) One G-request is on a neighboring path of x. (center) One G-request is on an outer angle and one is on an inner angle. (right) Both of the G-requests are on outer angles.

For the remaining cases we introduce some further notation. Given a neighboring path $P = (p_1, \ldots, p_s)$ of x, with corresponding angles $\widehat{p_1}, \ldots, \widehat{p_s}$, the *inner angles* are the angles $\widehat{p_i}$ with $1 < i < s$. The other ones are the *outer angles*. An inner angle with an R- or G-requests, has to satisfy its constraint (this cannot be further delayed). Hence for any inner angle $\widehat{p_i}$ with a G-request (resp. an R-request) we add the edge xp_i to G (resp. to R oriented toward x). This is a preprocessing step valid for both the remaining two cases.

(2) The unexplored region containing x is not a disk. For simplicity assume, that there are no free angles. Otherwise we assign an R-request to all these angles. Here after the preprocessing step described above, there is an intermediate step 2.1) and a final step 2.2). See Figure 6 for an illustration of how this case is handled.

(2.1) The intermediate step. This step depends on the position of the G-requests, if any.

If there is no G-request on the neighboring paths of x, then we assign an R-request to some angle $\widehat{x}$ incident to x.

If only one G -request, say on $\widehat{u_*}$, is on a neighboring path of x, then by (V) $\widehat{v_*}$ is next to it, hence $\widehat{u_*}$ is an end of this neighboring path. Here the new angle at u_* (inside the former angle $\widehat{u_*}$) that is created by stacking x inherits $\widehat{u_*}$'s G-request. If two angles are created inside the former angle $\widehat{u_*}$, that is if u_* is alone in its neighboring path, we choose the angle next to v_* in order to fulfill (V). Then we assign an R-request to some angle $\widehat{x}$ incident to x.

If one G -request, say $\widehat{u_*}$, is on an outer angle and the other one, $\widehat{v_*}$, is on an inner one, we have added the edge v_*x to G in the preprocessing. Here the new angle at u_* inherits $\widehat{u_*}$'s G-request and the next angle on $\partial T[X + x]$, that is incident to x gets a G-request too.

If both G -requests are on inner angles, the edges v_*x and u_*x have been added to G in the preprocessing. Hence x has already two incident G-edges and does not need any request around. We thus leave all angles incident to x free.

If both of the G -requests are on outer angles, then by (i) x has one neighboring path of length one, (u_*, v_*), and at least one other neighboring path of length at least one. In that case, we add edges v_*x and u_*x to G and we leave the new angles at u_* and v_*, as well as all angles incident to x, free.

(2.2) The final step. We now assign two outgoing B-arcs to x, depending on the G-requests. If there is an outer angle $\widehat{u_*}$ (in $T[X + x]$) with a G-request add the arc xu_* directed toward u_* to B. The remaining one or two needed B-arcs are chosen arbitrarily among the edges from x to outer vertices. All other edges, between x and outer vertices will be put into R and directed toward x, and the corresponding angles will be left free.

Note that among the newly created outer angles and the angles associated to x there are at most 3 requests: two at the angles receiving a B-arc from x and one at an angle incident to x.

If adding x creates an unexplored disk D', we still have to argue, that (VI) is satisfied with respect to D'. We make use of the following:

Claim 3. *For any unexplored disk D' created by stacking a vertex x on $T[X]$, the vertex x appears several times on the boundary of D'.*

Proof. Suppose we create an unexplored disk D' such that x appears only once on its boundary. Assume x is chosen such that the number of faces in D' is minimized. Since there are no nontrivial 3-disks, the boundary of D' is of length at least four. Therefore D' contains an unexplored vertex x' that could have been stacked on a subpath of $\partial D' \backslash x$. Furthermore, x' can be chosen such that the path does not only contain the G-requests. Hence, stacking x' would either not create any unexplored disk, or would create some included in D', hence smaller. Both cases contradict the choice of x with respect to (iii).□

This claim and the fact that T is simple imply that there are at least six angles on the boundary of D' incident to outer vertices of the neighborings paths of x (4 of them) or incident to x (2 of them). As argued above at most 3 of these angles have a request. Thus, there are at least 3 free angles on the boundary of D' and (VI) is satisfied.

(3) The unexplored region containing x is a disk, but x 's neighborhood is not a cycle. By (ii) the vertex x has only one neighboring path. Let us denote this path by $P = (p_1, \ldots, p_s)$ for some $s \geq 2$ and $\widehat{p_1}, \ldots, \widehat{p_s}$ the corresponding angles. Denote by t the number of free angles on P.

We start with the preprocessing described above, that deals with nonfree interior angles (by fulfilling the requests). To fulfill (VI) we have to maintain the number of free angles in this unexplored disk above three. Since by (ii) there is at least one free angle not on P, to achieve this we need to have at least $\min\{t, 2\}$ free angles among the new angles $\widehat{p_1}, \widehat{x}$, and $\widehat{p_s}$.

To achieve that we need to exploit free angles as follows. For any free angle $\widehat{p_i}$ (inner or not), the edge xp_i is added either to B or to R, in both cases oriented toward p_i. Among these t angles, $\min\{t, 2\}$ lead to a B-arc, and $\max\{0, t-2\}$ lead to an R-arc. It remains to deal with the (at least $2-t$) angles that are neither inner nor free. We proceed by distinguishing cases according to the position of G-requests.

If there is no G -request on P, we proceed as follows. Let us first deal with the new angle $\widehat{x}$. If $t \leq 2$, the vertex x has no outgoing R-arc and we hence assign an R-request to the angle $\widehat{x}$. Otherwise (i.e. if $t \geq 3$) the vertex x has an outgoing R-arc, we hence leave $\widehat{x}$ free. Then we use $\max\{0, 2-t\}$ of the nonfree outer angles to add B-arcs leaving x. We satisfy the possibly remaining non-free outer angles (that are $\min\{2, t\}$), by adding R-arcs toward x, and leave their new incident angle free. If $t \leq 2$ (resp. $t \geq 3$), there are hence $\min\{2, t\} = t$ (resp. $1 + \min\{2, t\} = 3$) free angles among the new angles $\widehat{p_1}$, $\widehat{x}$, and $\widehat{p_s}$. We hence have the expected (at least) $\min\{t, 2\}$ free angles.

If only one G -request (say on $\widehat{u_*}$) is on P, then $\widehat{u_*}$ is an end of P, say $p_1 = u_*$ (see Fig. 7). Here the new angle at u_* inherits $\widehat{u_*}$'s G-request, and we add the edge xp_1 in B if $t \leq 1$, or in R otherwise (if $t \geq 2$). In both cases xp_1 is oriented toward p_1. Hence, if $t \leq 1$ we assign an R-request to angle $\widehat{x}$ and otherwise we leave $\widehat{x}$ free. If $t = 0$ then $\widehat{p_s}$ is not free, then as it cannot have a G-request, $\widehat{p_s}$ has an R-request. In that case we add xp_s in B oriented from x to p_s and the new angle $\widehat{p_s}$ inherits the R-request. If $t \geq 1$, we satisfy

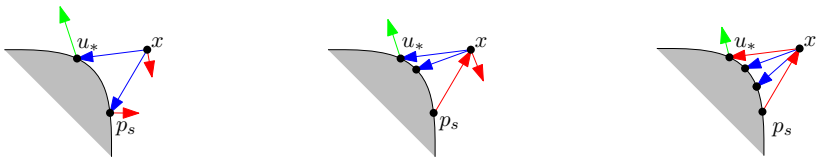

FIGURE 7. Case where there is only one G-request (on $\widehat{u_*}$) and where $\widehat{p_s}$ has an R-request. The 3 subcases from left to right correspond to $t = 0$, $t = 1$, and $t = 2$.

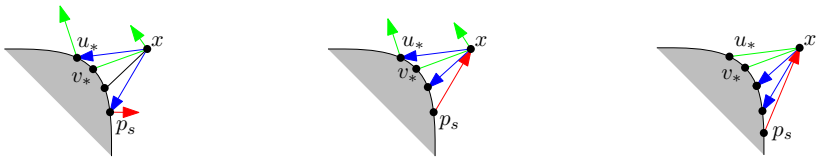

FIGURE 8. Case where there is one G-request on an outer angle, and one in an inner angle, and where $\widehat{p_s}$ has an R-request. The three subcases from left to right correspond to $t = 0$, $t = 1$, and $t = 2$.

the R-request of $\widehat{p_s}$ (if it has one) with edge xp_s. In any case, $\widehat{p_s}$ having a request or not in $T[X]$, the new angle $\widehat{p_s}$ is left free. Hence if $t \geq 2$ the angle $\widehat{x}$ is free , and if $t \geq 1$ the angle $\widehat{p_s}$ is free. We hence have the expected (at least) $\min\{t, 2\}$ free angles.

If one G -request say $\widehat{u_*}$ is on an outer angle and the other one $\widehat{v_*}$ on an inner one, say $u_* = p_1$ and $v_* = p_2$ with $s > 2$, we have added the edge p_2x to G (see Fig. 8). Around p_1, if $t \leq 1$ we assign the new angles $\widehat{p_1}$ and $\widehat{x}$ a G-request, and we add the edge xp_1 in B oriented from x to p_1. Otherwise (i.e. $t \geq 2$) we add the edge p_1x to G, and we leave both new angles $\widehat{p_1}$ and $\widehat{x}$ as free. Around p_s, if $t = 0$ (hence $\widehat{p_s}$ has an R-request) we add xp_s in B oriented from x to p_s, and the new angle $\widehat{p_s}$ keeps its R-request. Otherwise (i.e. $t \geq 1$), if $\widehat{p_s}$ has an R-request we add xp_s in R and orient it from p_s to x, and in any case ($\widehat{p_s}$ having an R-request or not) we leave the new angle $\widehat{p_s}$ as free. Hence if $t \geq 1$ the angle $\widehat{p_s}$ is free, and if $t \geq 2$ both $\widehat{p_1}$ and $\widehat{x}$ are free. We hence have the expected (at least) $\min\{t, 2\}$ free angles.

If both G -requests are on inner angles, edges v_*x and u_*x have been added to G. Now x is an inner vertex of G, and we thus leave $\widehat{x}$ free. Then we use $\max\{0, 2 - t\}$ of the outer angles for B-arcs from x, and the remaining non-free outer angles have their R-requests satisfied, and are left free. In any case, $\min\{2, t\}$ of the outer angles are free (as is the angle $\widehat{x}$).

Finally by definition of stacking P, x's unique neighboring path is distinct from (u_*, v_*) and hence all cases have been addressed.

3.4. Reorienting B

Given a partial orientation O of T we define the *demand* of a vertex v as $\mathrm{dem}_O(v) := -\delta^+_{|O}(v) \bmod 3$, where $\delta^+_{|O}(v)$ denotes the outdegree of v with respect to O. We want to find an orientation of T with all demands 0.

Recall we will not modify the orientation on R, which guarantees that all vertices in $(V(T)\backslash V(G)) \cup \{u, v\}$ have nonzero outdegrees. Furthermore, as G will be oriented

either entirely forward or backwards (this will be chosen later), all its interior vertices will have nonzero outdegrees. Hence every vertex of $T[X]$ has nonzero outdegree. Suppose that G is entirely oriented forward.

Now we linearly order vertices in $V(T)\backslash V(I) = (v_1, \ldots, v_\ell)$ such that with respect to B every vertex has its two outgoing B-neighbors among its predecessors and I. Denote by B_i the subgraph of B induced by the arcs leaving $v_i, \ldots, v_\ell$ (before the reorienting). We process $V(T)\backslash V(I)$ from the last to the first element. At a given vertex v_i we look at $\mathrm{dem}_{G\cup R\cup B_i}(v_i)$ and reorient the two originally outgoing B-arcs of v_i in such a way that afterwards $\mathrm{dem}_{G\cup R\cup B_i}(v_i) = 0$ (i.e. $\delta^+_{|G\cup R\cup B_i}(v_i) \equiv 0 \bmod 3$). As these B-arcs were heading at I or at a predecessor, the demand on the vertices v_j, with $j > i$, is not modified and hence remains 0.

3.5. Orienting *G* and *I*

Denote by O the partial orientation of T obtained after 3.4. Pick an orientation of G (either all forward or all backward) and of uv such that for the resulting partial orientation O' we have $\mathrm{dem}_{O'}(v) \equiv 1 \bmod 3$.

Now, take the triangle Δ of I containing v. Since $\widetilde{D} = I\backslash uv$ is a maximal outerplanar graph with only two degree two vertices, $\widetilde{D}$ can be peeled by removing degree two vertices until reaching Δ. When a vertex x is removed orient its two incident edges so that $\mathrm{dem}_{O'}(x) = 0$ (as for B-arcs). We obtain a partial orientation O'', such that all vertices except the ones of Δ have nonzero outdegree divisible by 3.

Since the number of edges of T, and the number of edges of Δ are divisible by 3, the number of edges of $T\backslash\Delta$ is divisible by 3. As this number equals the sum of the outdegrees in O'', and as every vertex out of Δ has outdegree divisible by 3, then the outdegree of Δ's vertices sum up to a multiple of 3. Hence their demands sum up to 0, 3 or 6. As $\mathrm{dem}_{O''}(v) = \mathrm{dem}_{O'}(v) = 1$, the demands of the other two vertices of Δ are either both 1, or 0 and 2. It is easy to see that in either case Δ can be oriented to satisfy all three demands.

4. TOWARD SCHNYDER WOODS

We see our proof of Conjecture 1 as a step toward generalizing Schnyder woods to triangulations of arbitrary orientable surfaces (the notion does not have much sense for nonorientable ones). By results of [8] another step toward generalizing Schnyder woods to maps of arbitrary orientable surfaces can be formulated after introducing a couple of definitions:

A map G is said essentially k-connected, if its universal cover is k-connected. Given a map G, its *primal-dual-completion* $\hat{G}$ is the map obtained from simultaneously embedding G and its dual, G^*, such that vertices of G^* are embedded inside faces of G and vice versa. Moreover, each edge crosses its dual edge in exactly one point in the interior, which also becomes a vertex of $\hat{G}$. Hence, $\hat{G}$ is a bipartite graph with one bipartition consisting of *primal-vertices* and *dual-vertices* and the other partition consisting of *edge-vertices* (of degree 4).

Conjecture 2. *Given an essentially 3-connected map G, the map $\hat{G}$ has an orientation where primal- and dual-vertices have nonzero outdegrees divisible by three, and where*

edge-vertices have indegrees divisible by three, that is indegree 0 or 3 (i.e. outdegree 4 or 1).

REFERENCES

[1] J. Barát and C. Thomassen, Claw-decompositions and Tutte-orientations, J Graph Theory 52 (2006), 135–146.

[2] O. Bernardi, Bijective counting of tree-rooted maps and shuffles of parenthesis systems, Electron J Combin 14 (2007), 36.

[3] O. Bernardi and N. Bonichon, Intervals in Catalan lattices and realizers of triangulations, J Combin Theory Ser A 116 (2009), 55–75.

[4] L. Castelli-Aleardi, E. Fusy, and T. Lewiner, Schnyder woods for higher genus triangulated surfaces, with applications to encoding, Disc Comput Geometry 42 (2009), 489–516.

[5] H. de Fraysseix, P. O. de Mendez, and P. Rosenstiehl, On triangle contact graphs, Combin Probab Comput 3 (1994), 233–246.

[6] S. Felsner, Convex drawings of planar graphs and the order dimension of 3-polytopes, Order 18 (2001), 19–37.

[7] S. Felsner, Lattice structures from planar graphs, Electron J Combin 11 (2004), 24.

[8] D. Gonçalves, K. Knauer, and B. Lévêque, Structure of Schnyder labelings on orientable surfaces, CoRR, abs/1501.05475 (2015).

[9] D. Gonçalves and B. Lévêque, Toroidal maps: Schnyder woods, orthogonal surfaces and straight-line representations, Disc Comput Geometry 51 (2014), 67–131.

[10] B. Mohar and C. Thomassen, Graphs on surfaces, Johns Hopkins Studies in the Mathematical Sciences, Johns Hopkins University Press, Baltimore, MD, 2001.

[11] W. Schnyder, Planar graphs and poset dimension, Order 5 (1989), 323–343.

[12] W. Schnyder, Embedding planar graphs on the grid, in Proceedings of the First Annual ACM-SIAM Symposium on Discrete Algorithms, SODA 90, Philadelphia, PA, USA, 1990, pp. 138–148.

Discrete Comput Geom (2012) 48:239–254
DOI 10.1007/s00454-012-9400-1

Triangle Contact Representations and Duality

Daniel Gonçalves · Benjamin Lévêque · Alexandre Pinlou

Received: 4 February 2011 / Revised: 3 November 2011 / Accepted: 27 January 2012 /
Published online: 16 February 2012

Abstract A contact representation by triangles of a graph is a set of triangles in the plane such that two triangles intersect on at most one point, each triangle represents a vertex of the graph and two triangles intersects if and only if their corresponding vertices are adjacent. De Fraysseix, Ossona de Mendez and Rosenstiehl proved that every planar graph admits a contact representation by triangles. We strengthen this in terms of a simultaneous contact representation by triangles of a planar map and of its dual.

A primal–dual contact representation by triangles of a planar map is a contact representation by triangles of the primal and a contact representation by triangles of the dual such that for every edge uv, bordering faces f and g, the intersection between the triangles corresponding to u and v is the same point as the intersection between the triangles corresponding to f and g. We prove that every 3-connected planar map admits a primal–dual contact representation by triangles. Moreover, the interiors of the triangles form a tiling of the triangle corresponding to the outer face and each contact point is a corner of exactly three triangles. Then we show that these representations are in one-to-one correspondence with generalized Schnyder woods defined by Felsner for 3-connected planar maps.

Keywords Triangle contact representation · 3-Connected planar maps · Schnyder wood · Duality

1 Introduction

A *contact system* is a set of curves (closed or not) in the plane such that two curves cannot cross but may intersect tangentially. A *contact point* of a contact system is a point that is in the intersection of at least two curves. A *contact representation* of

D. Gonçalves · B. Lévêque (✉) · A. Pinlou
LIRMM, CNRS, Université Montpellier 2, 161 rue Ada, 34095 Montpellier Cedex 5, France
e-mail: benjamin.leveque@lirmm.fr

a graph $G = (V, E)$ is a contact system $\mathcal{C} = \{c(v) : v \in V\}$, such that two curves intersect if and only if their corresponding vertices are adjacent.

The Circle Packing Theorem of Koebe [14] states that every planar graph admits a contact representation by circles.

Theorem 1 (Koebe [14]) *Every planar graph admits a contact representation by circles.*

Theorem 1 implies that every planar graph has a contact representation by convex polygons, and de Fraysseix et al. [3] strengthened this by showing that every planar graph admits a contact representation by triangles. A contact representation by triangles is *strict* if each contact point is a corner of exactly one triangle. De Fraysseix et al. [3] proved the following:

Theorem 2 (De Fraysseix et al. [3]) *Every planar graph admits a strict contact representation by triangles.*

Moreover, de Fraysseix et al. [3] proved that strict contact representations by triangles of a planar triangulation are in one-to-one correspondence with its Schnyder woods defined by Schnyder [16]. (Schnyder wood will be defined in Sect. 2.2.)

Andreev [1] strengthen Theorem 1 in terms of a simultaneous contact representation of a planar map and of its dual. The *dual* of a planar map $G = (V, E)$ is noted $G^* = (V^*, E^*)$. A *primal–dual contact representation* $(\mathcal{V}, \mathcal{F})$ of a planar map G is two contact systems $\mathcal{V} = \{c(v) : v \in V\}$ and $\mathcal{F} = \{c(f) : f \in V^*\}$, such that $\mathcal{V}$ is a contact representation of G, and $\mathcal{F}$ is a contact representation of G^*, and for every edge uv, bordering faces f and g, the intersection between $c(u)$ and $c(v)$ is the same point as the intersection between $c(f)$ and $c(g)$. A *contact point* of a primal–dual contact representation is a contact point of V or a contact point of F. Andreev [1] proved the following:

Theorem 3 (Andreev [1]) *Every* 3*-connected planar map admits a primal–dual contact representation by circles.*

Our main result is an analogous strengthening of Theorem 2. We say that a primal–dual contact representation by triangles is *tiling* if the triangles corresponding to vertices and those corresponding to bounded faces form a tiling of the triangle corresponding to the outer face (see Fig. 1). We say that a primal–dual contact representation by triangles is *strict* if each contact point is a corner of exactly three triangles corresponding to vertices or faces (see Fig. 1). We prove the following:

Theorem 4 *Every* 3*-connected planar map admits a strict tiling primal–dual contact representation by triangles.*

Gansner et al. [11] study representation of graphs by triangles where two vertices are adjacent if and only if their corresponding triangles are intersecting on a side (touching representation by triangles). Theorem 4 shows that for 3-connected planar

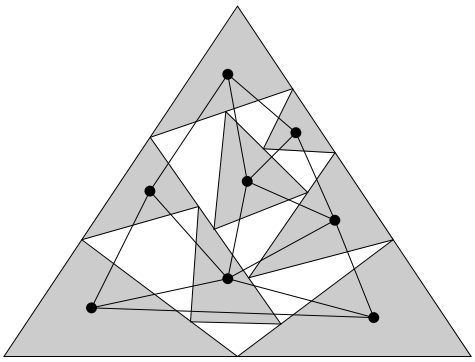

Fig. 1 A strict tiling primal–dual contact representation by triangles

graphs, the incidence graph between vertices and faces admits a touching representation by triangles.

The tools needed to prove Theorem 4 are introduced in Sect. 2. In Sect. 2.1, we present a result of de Fraysseix et al. [5] concerning the stretchability of a contact system of arcs. In Sect. 2.2, we define (generalized) Schnyder woods and present related results obtained by Felsner [7]. In Sect. 3, we define a contact system of arcs, based on a Schnyder wood, and show that this system of arcs is stretchable. When stretched, this system gives the strict tiling primal–dual contact representation by triangles. In Sect. 4, we show that strict tiling primal–dual contact representations by triangles of a planar map are in one-to-one correspondence with its Schnyder woods. In Sect. 5, we define the class of planar maps admitting a Schnyder wood and thus a strict tiling primal–dual contact representation by triangles. In Sect. 6, we discuss possible improvements of Theorem 4.

2 Tools

2.1 Stretchability

An *arc* is a non-closed curve. An *internal point* of an arc is a point of the arc distinct from its extremities. A contact system of arcs is *strict* if each contact points is internal to at most one arc. A contact system of arcs is *stretchable* if there exists a homeomorphism which transforms it into a contact system whose arcs are straight line segments. An *extremal point* of a contact system of arcs is a point on the outer-boundary of the system and which is internal to no arc.

We define in Sect. 3 a contact system of arcs such that when stretched it gives a strict tiling primal–dual contact representation by triangles. To prove that our contact system of arcs is stretchable, we need the following theorem of de Fraysseix et al. [5].

Theorem 5 (de Fraysseix et al. [5]) *A strict contact system of arcs is stretchable if and only if each subsystem of cardinality at least two has at least three extremal points*.

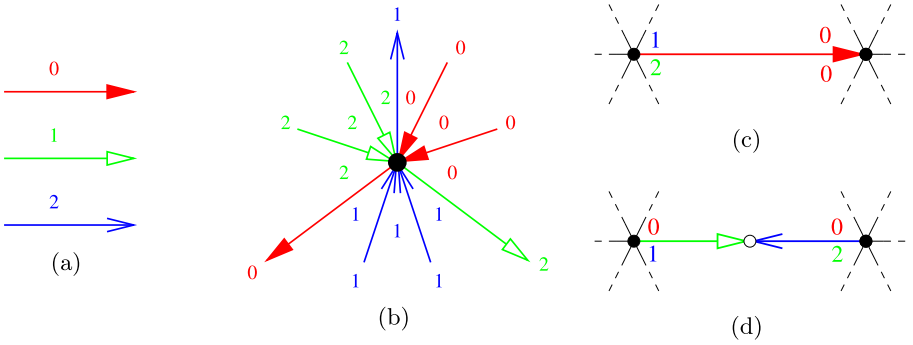

Fig. 2 (**a**) Edge colored, respectively, with color 0, 1, and 2. We use distinct arrow types to distinguish those colors. (**b**) Rules for Schnyder woods and angle labelings. (**c**) Example of angle labeling around an uni-directed edge colored 0. (**d**) Example of angle labeling around a bi-directed edge colored 2 and 1

2.2 Schnyder Woods

The contact system of arcs defined in Sect. 3 is constructed from a Schnyder wood.

Schnyder woods where introduced by Schnyder [16] and then generalized by Felsner [7]. Here we use the definition from [7] except if explicitly mentioned. We refer to *classic Schnyder woods* defined by Schnyder [16] or *generalized Schnyder woods* defined by Felsner [7] when there is a discussion comparing both.

Given a planar map G. Let x_0, x_1, x_2 be three distinct vertices occurring in clockwise order on the outer face of G. The *suspension* G^σ is obtained by attaching a half-edge that reaches into the outer face to each of these special vertices. A *Schnyder wood* rooted at x_0, x_1, x_2 is an orientation and coloring of the edges of G^σ with the colors 0, 1, 2 satisfying the following rules (see Fig. 2):

- Every edge e is oriented in one direction or in two opposite directions. We will, respectively, say that e is uni- or bi-directed. The directions of edges are colored such that if e is bi-directed the two directions have distinct colors.
- The half-edge at x_i is directed outwards and colored i.
- Every vertex v has out-degree one in each color. The edges $e_0(v)$, $e_1(v)$, $e_2(v)$ leaving v in colors 0, 1, 2, respectively, occur in clockwise order. Each edge entering v in color i enters v in the clockwise sector from $e_{i+1}(v)$ to $e_{i-1}(v)$ (where $i+1$ and $i-1$ are understood modulo 3).
- There is no interior face the boundary of which is a directed monochromatic cycle.

The difference with the original definition of Schnyder [16] it that edges can be oriented in two opposite directions.

A Schnyder wood of G^σ defines a labeling of the angles of G^σ where every angle in the clockwise sector from $e_{i+1}(v)$ to $e_{i-1}(v)$ is labeled i.

A *Schnyder angle labelings* of G^σ is a labeling of the angles of G^σ with the labels 0, 1, 2 satisfying the following rules (see Fig. 2):

- The two angles at the half-edge of the special vertex x_i have labels $i+1$ and $i-1$ in clockwise order.

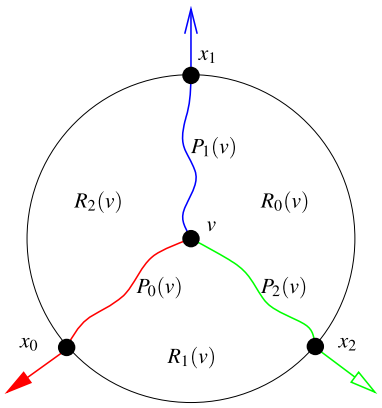

Fig. 3 Directed paths and regions corresponding to a vertex

- Rule of vertices: The labels of the angles at each vertex form, in clockwise order, a nonempty interval of 0's, a nonempty interval of 1's and a nonempty interval of 2's.
- Rule of faces: The labels of the angles at each interior face form, in clockwise order, a nonempty interval of 0's, a nonempty interval of 1's and a nonempty interval of 2's. At the outer face the same is true in counterclockwise order.

Felsner [8] proved the following correspondence:

Theorem 6 (Felsner [8]) *Schnyder woods of G^σ are in one-to-one correspondence with Schnyder angle labelings.*

Several properties of Schnyder woods will be used. Given a Schnyder wood, let T_i be the set of edges colored i with the direction they have in this color. Felsner [7] proved the following:

Lemma 1 (Felsner [7]) *For $i \in \{0, 1, 2\}$, the digraph T_i is a tree rooted at x_i.*

By Lemma 1, every vertex v is the starting vertex of a unique directed path $P_i(v)$ from v to x_i, composed of arcs colored i (see Fig. 3). Felsner [7] proved the following:

Lemma 2 (Felsner [7]) *For every vertex v and $i, j \in \{0, 1, 2\}$, $i \neq j$, the two paths $P_i(v)$ and $P_j(v)$ have v as only common vertex.*

By Lemma 2, for every vertex v, the three paths $P_0(v)$, $P_1(v)$, $P_2(v)$ divide G into three regions $R_0(v)$, $R_1(v)$ and $R_2(v)$, where $R_i(v)$ denotes the region bounded by and including the two paths $P_{i-1}(v)$ and $P_{i+1}(v)$ (see Fig. 3). In fact $R_i(v)$ will also be used to denote the set of vertices in this region. Let $r_i(v)$ be the number of faces in the region $R_i(v)$.

Felsner [7] proved the following:

Lemma 3 (Felsner [7]) *For all distinct vertices u, v, we have*

(i) *$R_i(u) \subseteq R_i(v)$ if and only if $u \in R_i(v)$.*

(ii) *$R_i(u) = R_i(v)$ if and only if there is a path between u and v, with all edges oriented in two opposite directions, colored $i-1$ in one direction and $i+1$ in the other direction.*
(iii) *There exist i and j with $R_i(u) \subsetneq R_i(v)$ and $R_j(v) \subsetneq R_j(u)$.*

From Lemma 3 we can deduce some lemmas that will be use several time in the proof of Lemma 7.

Lemma 4 *For all distinct vertices u, v such that $u \in P_i(v)$, we have $v \in R_i(v) \subsetneq R_i(u)$.*

Proof We can assume without loss of generality that $i = 1$. By induction it suffices to show that for all u, v such that $e_1(v) = uv$, we have $R_1(v) \subsetneq R_1(u)$. We have $u \in P_1(v)$, so $u \in R_0(v)$ and $u \in R_2(v)$ (see Fig. 3). By Lemma 3(i), we have $R_0(u) \subseteq R_0(v)$ and $R_2(u) \subseteq R_2(v)$. So by Lemma 3(iii), $R_1(v) \subsetneq R_1(u)$. □

Lemma 5 *Let vertices u, v be such that $u \in P_{i-1}(v)$ and $v \in P_{i+1}(u)$, then $R_i(u) = R_i(v)$ and there is a bi-directed path between u and v colored $i-1$ from v to u and colored $i+1$ from u and v.*

Proof We can assume without loss of generality that $i = 1$. As $u \in P_0(v) \subseteq R_1(v)$, Lemma 3(i) implies that $R_1(u) \subseteq R_1(v)$. As $v \in P_2(u) \subseteq R_2(u)$, Lemma 3(i) also implies that $R_0(v) \subseteq R_0(u)$. So $R_0(w) = R_0(v)$ and by Lemma 3(ii), there is a bi-directed path Q in color 0 and 2 between v and w. As $u \in P_0(v)$, by Lemma 2, we have $u \notin P_2(v)$, so Q is colored 0 from v to u and colored 2 from u to v. □

Lemma 6 *Let u, v, w be such that uv is uni-directed from u to v in color $i+1$, $w \in P_i(v)$ and $v \notin P_{i-1}(w)$, then $R_i(u) \subsetneq R_i(w)$.*

Proof We can assume without loss of generality that $i = 1$.

Suppose $R_1(u) \not\subseteq R_1(w)$. Then by Lemma 3(i) $u \notin R_1(w)$. Since $w \in P_1(v)$, Lemma 4 implies that $v \in R_1(w)$. Since u and v are adjacent, vertex v is on the "border" of $R_1(w)$, that is, we have either $v \in P_0(w)$ or $v \in P_2(w)$ (see Fig. 3). So by the assumption that $v \notin P_0(w)$, we have $v \in P_2(w)$. We also have $w \in P_1(v)$, so Lemma 5 implies that $R_0(v) = R_0(w)$. Now since $u \notin R_1(w)$ and u is adjacent to v in $P_2(w)$, we have $u \in R_0(w)$. So $u \in R_0(v)$, a contradiction to the fact that the edge uv is uni-directed from u to v in color 2 by definition of Schnyder woods (see Fig. 2).

Suppose we have equality $R_1(u) = R_1(w)$, then by Lemma 3(ii) there is a bi-directed path Q in colors 0, 2 between u and w. The edge $e_2(u)$ (leaving u in color 2) is equal to uv and is uni-directed so it is not an edge of Q. So the path Q is colored 0 from u to w and colored 2 from w to u. The path $P_2(w)$ goes from w to u by path Q and then to v by edge uv, so $v \in P_2(w)$. We also have $w \in P_1(v)$, so Lemma 5 implies that $R_0(w) = R_0(v)$ and that there is a bi-directed path Q' in colored 1 from v to w and colored 2 from w to v. There is a unique path from w to v colored 0, so the neighbor of v along Q' is u, contradicting the fact that uv is uni-directed.

So $R_1(u) \subsetneq R_1(w)$. □

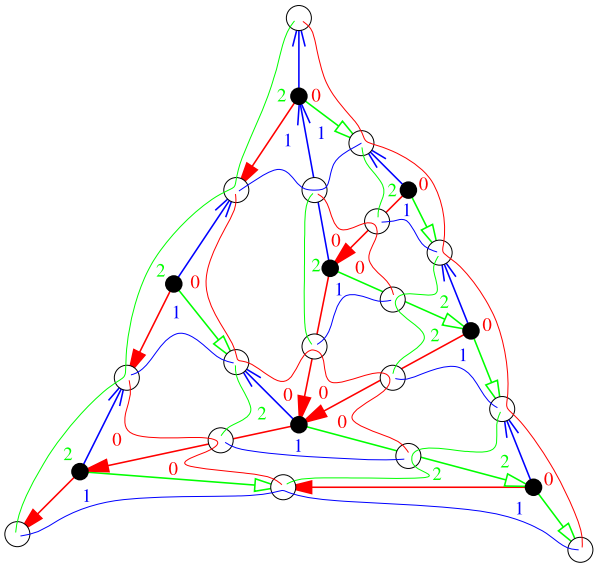

Fig. 4 A Schnyder wood with its corresponding angle labeling and contact system of arcs

3 Mixing Tools

Given a planar map G and a Schnyder wood of G rooted at x_0, x_1, x_2 we construct a contact system of arcs $\mathcal{A}$ *corresponding* to the Schnyder wood by the following method (see Fig. 4).

Each vertex v is represented by three arcs $a_0(v), a_1(v), a_2(v)$, where the arc $a_i(v)$ is colored i and represent the interval of angles labeled i of v. It may be the case that $a_i(u) = a_i(v)$ for some values of i, u and v. For every edge e of G, we choose a point $p(e)$ on its interior. There is also such a point on the half-edge leaving x_i, for $i \in \{0, 1, 2\}$. The points $p(e)$ are the contact points of the contact system of arcs.

Actually the arcs of $\mathcal{A}$ are completely defined by the following subarcs: For each angle labeled i at a vertex v in-between the edges e and e', there is a subarc of $a_i(v)$ going from $p(e)$ to $p(e')$ along e and e'. Each contact point $p(e)$ is the end of 4 such subarcs. The Schnyder labeling implies that the three colors are represented at $p(e)$ and so the two subarcs with the same color are merged and form a longer arc.

One can easily see that this defines a contact system of arcs whose contact points are the points $p(e)$. By construction, there are no crossing arcs. Moreover, there is no closed curve as a closed curve in color i would imply the existence of a cycle of G with edges bi-oriented in color $i - 1$ and $i + 1$, which is forbidden by Lemma 1.

It is also clear that the arcs satisfy the following rules:

- For every edge $e = vw$ uni-directed from v to w in color i: The arcs $a_{i+1}(v)$ and $a_{i-1}(v)$ end at $p(e)$ and the arc $a_i(w)$ goes through $p(e)$.
- For every edge $e = vw$ bi-directed, leaving v in color i and leaving w in color j: Let k be such that $\{i, j, k\} = \{0, 1, 2\}$. The arcs $a_j(v)$ and $a_i(w)$ ends at $p(e)$, and the arcs $a_k(v)$ and $a_k(w)$ are equal and go through $p(e)$.

Remark Felsner [8] has shown that generalized Schnyder woods can be embedded on orthogonal drawings where the position of a vertex in the 3-dimensional space is given by the coordinates $(r_1(v), r_2(v), r_3(v))$. The contact system of arcs corresponding to a Schnyder wood can also be drawn on this surface in such a way that the contact points are precisely the edge-vertices of the drawing (see [9] for definition of edge-vertices). A possible generalization of shelling orders [6] to generalized Schnyder wood is to consider the orders given by the three coordinates in the orthogonal drawing. The proof of Lemma 7 is not using orthogonal drawings but relies on considering the orders on $r_i(v)$ and thus can be understood as considering the corresponding shelling orders in orthogonal drawings. Here we do not use orthogonal drawings in the proof as the only properties that are useful concerning the regions $R_i(v)$ are given by Lemma 3.

The following lemma will be used to transform the contact system of arcs into a strict tiling primal–dual contact representation by triangles.

Lemma 7 *The contact system of arcs corresponding to a Schnyder wood is stretchable.*

Proof Let G be a planar map, given with a Schnyder wood rooted at x_0, x_1, x_2. Let $\mathcal{A}$ be the contact system of arcs corresponding to the Schnyder wood as defined before. By definition of $\mathcal{A}$, every point $p(e)$, corresponding to an edge e uni- or bi-directed, is interior to one arc and is the end of two other arcs, so the contact system of arcs $\mathcal{A}$ is strict. By Theorem 5, we have to prove that each subsystem of $\mathcal{A}$, of cardinality at least two, has at least three extremal points. Let $\mathcal{B}$ be a subsystem of arcs of cardinality at least two. Let $S_{\mathcal{B}}$ be the set of vertices v such that there exists $i \in \{0, 1, 2\}$ with $a_i(v) \in \mathcal{B}$. The set $S_{\mathcal{B}}$ has cardinality at least one. We have to prove that $\mathcal{B}$ has at least three extremal points.

Let s_i be a vertex v of $S_{\mathcal{B}}$, such that $(r_i(v), r_{i+1}(v))$ is lexicographically minimum.

Claim 1 $P_{i-1}(s_i) \cap S_{\mathcal{B}} = \{s_i\}$.

Proof Suppose there exists $v \in P_{i-1}(s_i) \cap S_{\mathcal{B}}$ distinct from $\{s_i\}$. Vertex v is in $R_i(s_i)$ and in $R_{i+1}(s_i)$, so by Lemma 3(i) it satisfies $R_i(v) \subseteq R_i(s_i)$ and $R_{i+1}(v) \subseteq R_{i+1}(s_i)$. By the choice of s_i we have in fact $R_i(v) = R_i(s_i)$ and $R_{i+1}(v) = R_{i+1}(s_i)$. This contradicts Lemma 3(iii). This proves Claim 1. □

Let s'_i be the last vertex of $P_{i+1}(s_i)$ (i.e. the farthest from s_i) that is in $S_{\mathcal{B}}$ (maybe $s_i = s'_i$). By Lemma 3(i), we have $R_i(s'_i) \subseteq R_i(s_i)$. Thus, by definition of s_i, we have $R_i(s'_i) = R_i(s_i)$. By Lemma 3(ii), there is a bi-directed path Q_i in color $i-1$ and $i+1$ between s_i and s'_i. By Claim 1 we have $s'_i \notin P_{i-1}(s_i) \setminus \{s_i\}$ so Q is colored $i+1$ from s_i to s'_i and colored $i-1$ from s'_i to s_i. By definition of s'_i, we have the analog of Claim 1, that is, $P_{i+1}(s'_i) \cap S_{\mathcal{B}} = \{s'_i\}$.

Claim 1 can be restated by

Claim 2 $(R_i(s_i) \cap S_{\mathcal{B}}) = (R_i(s'_i) \cap S_{\mathcal{B}}) \subseteq Q_i$.

We now try to find some extremal points of $\mathcal{B}$ on the edges leaving s_i, s'_i.

Claim 3 *If $p(e_{i-1}(s_i))$ belongs to some arc in $\mathcal{B}$, then it is an extremal point of $\mathcal{B}$. Similarly, if $p(e_{i+1}(s'_i))$ belongs to some arc in $\mathcal{B}$, then it is an extremal point of $\mathcal{B}$.*

Proof Suppose $p(e_{i-1}(s_i))$ belongs to some arc in $\mathcal{B}$. Let v such that $e_{i-1}(s_i) = s_i v$. Since $s_i v$ is not uni-directed from v to s_i, the only arc going through $p(e_{i-1}(s_i))$ is an arc $a_j(v)$ for some $j \in \{1, 2, 3\}$. Then, since $v \notin S_{\mathcal{B}}$, this arc does not belong to $\mathcal{B}$ and $p(e_{i-1}(s_i))$ is not an internal point of an arc of $\mathcal{B}$. By Claim 1, we have $P_{i-1}(s_i) \cap S_{\mathcal{B}} = \{s_i\}$, so $p(e_{i-1}(s_i))$ is the only contact point on $P_{i-1}(s_i)$ that is a point of $\mathcal{B}$. Thus we can go along $P_{i-1}(s_i)$ from $p(e_{i-1}(s_i))$ to the outer-region without crossing any arc of B. This means that the point $p(e_{i-1}(s_i))$ is on $\mathcal{B}$'s outer boundary, and thus this point is an extremal point of $\mathcal{B}$. Similarly for $p(e_{i+1}(s'_i))$. This proves Claim 3. □

By Claim 3, we have many candidates for extremal points of B, but the points $p(e_{i-1}(s_i))$ and $p(e_{i+1}(s'_i))$, for $i \in \{0, 1, 2\}$, do not necessarily belongs to some arc in $\mathcal{B}$ and also they are not necessarily disjoint.

Claim 4 *At least one of $p(e_{i-1}(s_i))$, $p(e_{i+1}(s_i))$ and at least one of $p(e_{i-1}(s'_i))$, $p(e_{i+1}(s'_i))$ is an extremal point of B.*

Proof Since $s_i \in S_{\mathcal{B}}$, at least one of the arcs $a_{i-1}(s_i), a_i(s_i), a_{i+1}(s_i)$ is in $\mathcal{B}$. If $a_i(s_i)$ or $a_{i+1}(s_i)$ is in $\mathcal{B}$, then $p(e_{i-1}(s_i))$ belongs to some arc in $\mathcal{B}$ and so it is an extremal point by Claim 3. So we can assume that $a_{i-1}(s_i)$ is in $\mathcal{B}$ and that $a_i(s_i)$ and $a_{i+1}(s_i)$ are not. If $s_i = s'_i$, then the point $p(e_{i+1}(s_i)) = p(e_{i+1}(s'_i))$ belongs to some arc in $\mathcal{B}$ and so it is extremal by Claim 3. So we can assume that $s_i \neq s'_i$. The edge $e_{i+1}(s_i)$ is in Q_i and bi-directed in colors $i + 1$ and $i - 1$. By definition the arc $a_{i-1}(s_i)$ ends at $p(e_{i+1}(s_i))$, and since $a_i(s_i)$ is not in $\mathcal{B}$, $p(e_{i+1}(s_i))$ is not an internal point of an arc of $\mathcal{B}$. By Claim 1, we have $P_{i-1}(s_i) \cap S_{\mathcal{B}} = \{s_i\}$ so there is no contact point on $P_{i-1}(s_i)$ that is a point of $\mathcal{B}$. Thus we can go along $e_{i-1}(s_i)$ and then along $P_{i+1}(s_i)$ from $p(e_{i-1}(s_i))$ to the outer-region without crossing any arc. This means that the point $p(e_{i-1}(s_i))$ is on $\mathcal{B}$'s outer boundary, and thus this point is an extremal point of $\mathcal{B}$. Similarly for s'_i. This proves Claim 4. □

For $i \in \{0, 1, 2\}$, let consider the three arcs $a_i(s_i)$, that, respectively, go from $p(e_{i-1}(s_i))$ to $p(e_{i+1}(s'_i))$. If the three of them are in $\mathcal{B}$, by Claim 3 the ends of these three arcs are extremal; and since no three of them coincide, we have the three required extremal points. If exactly two of them are in $\mathcal{B}$, for example $a_0(s_0)$ and $a_1(s_1)$, then we may have $s'_1 = s_0$ but the points $p(e_0(s_1))$, $p(e_2(s'_1))$ and $p(e_1(s'_0))$ are distinct (by Claim 1) and form our three extremal points (by Claim 3). If none of the $a_i(s_i)$ are in $\mathcal{B}$, then by Claim 4, for each $i \in \{0, 1, 2\}$, one of $p(e_{i-1}(s_i))$ and $p(e_{i+1}(s_i))$ is an extremal point for s_i. We choose one of these extremal point for each i and claim that they are distinct. Suppose not, then either (a) there exists i such that $s_i = s_{i+1}$ and the point $p(e_{i-1}(s_i)) = p(e_{i-1}(s_{i+1}))$ is extremal, or (b) there exist i, $j \neq i$ and $k \neq i + 1$ such that s_i and s_{i+1} are adjacent and the point $p(e_j(s_i)) = p(e_k(s_{i+1})) = p(s_i s_{i+1})$ is extremal.

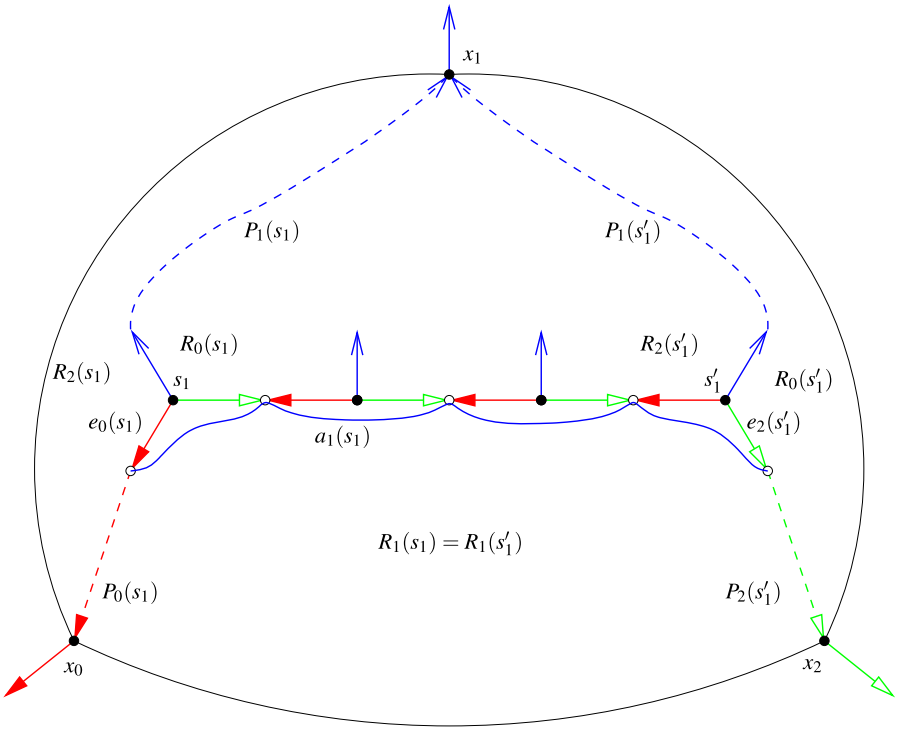

Fig. 5 Case where $a_1(s_1)$ is an arc of $\mathcal{B}$

(a) The point $p(e_{i-1}(s_i))$ is extremal and neither $a_i(s_i)$ nor $a_{i+1}(s_{i+1})$ belong to $\mathcal{B}$, so the arc $a_{i-1}(v) \in \mathcal{B}$, where $s_i v = e_{i-1}(s_i)$. Thus $v \in S_{\mathcal{B}}$ contradicting Claim 1.

(b) Note that by definition of a Schnyder wood we also have $j \neq k$. If $j = i-1$ or $k = i$ we have $s_{i+1} \in P_{i-1}(s_i)$ or $s_i \in P_i(s_{i+1})$ contradicting Claim 1. So $j = i+1$ and $k = i-1$. The edge $s_i s_{i+1}$ is bi-directed with colors $i-1$, $i+1$, so by Lemma 3(ii) we have $R_i(s_i) = R_i(s_{i+1})$. Vertex s_i is in $P_{i-1}(s_{i+1})$, so by Lemma 3(i) we have $R_{i+1}(s_i) \subseteq R_{i+1}(s_{i+1})$. Moreover, by definition of s_{i+1}, we have $R_{i+1}(s_i) = R_{i+1}(s_{i+1})$, contradicting Lemma 3(iii).

It remains to study the case where exactly one of the $a_i(s_i)$ is in $\mathcal{B}$. We can assume by symmetry that $a_1(s_1) \in \mathcal{B}$ and $a_0(s_0), a_2(s_2)$ are not in $\mathcal{B}$ (see Fig. 5). By Claim 3 the two distinct points $p(e_0(s_1))$ and $p(e_2(s'_1))$ are extremal points of $\mathcal{B}$. It remains to find a third extremal point, distinct from these two. By Claim 4, one of $p(e_1(s_2))$ and $p(e_0(s_2))$ is an extremal point. Suppose $p(e_1(s_2))$ is extremal. By Claim 1, there is no vertex of $P_0(s_1) \setminus \{s_1\}$ in $S_{\mathcal{B}}$, so $e_0(s_1)$ is distinct from $e_1(s_2)$. Similarly $e_2(s'_1)$ is distinct from $e_1(s_2)$ and so $p(e_1(s_2))$ is a third extremal point. So we can assume that $p(e_1(s_2))$ is not extremal and that $p(e_0(s_2))$ is. Edge $e_2(s'_1)$ has an extremity not in $S_{\mathcal{B}}$, so it is distinct to $e_0(s_2)$. If $p(e_0(s_2)) \neq p(e_0(s_1))$, we are done. So we can assume that $p(e_0(s_2)) = p(e_0(s_1))$, and so $s_2 = s_1$. Note that $s'_2 = s_1$ by definition of s'_2 and Claim 1. Similarly, we can assume that $s'_0 = s_0 = s'_1$.

The rest of the proof is dedicated to find a third extremal point.

Claim 5 *We have* $S_{\mathcal{B}} \subseteq R_0(s_1) \cap R_2(s'_1)$.

Proof As $s_1 = s'_2 = s_2$ and $s'_1 = s_0 = s'_0$, by Claim 2 for $i = \{0, 1, 2\}$, we have $R_1(s_1) \cap S_{\mathcal{B}} \subseteq Q_1$ and $R_2(s_1) \cap S_{\mathcal{B}} \subseteq Q_2 = \{s_1\}$ and $R_0(s'_1) \cap S_{\mathcal{B}} \subseteq Q_2 = \{s'_1\}$. So $S_{\mathcal{B}} \subseteq R_0(s_1) \cap R_2(s'_1)$ (see Fig. 5). This proves Claim 5. □

For an edge $e = uv$ we define $r_i(e) = \max(r_i(u), r_i(v))$, for $i \in \{0, 1, 2\}$. For the three half-edges of the outer boundary $e_j(x_j)$ (added to G to obtain G^σ, see Sect. 2.2), we define $r_i(e_j(x_j))$ equal to $+\infty$ if $i = j$ and 0 otherwise. Let e^* be an edge e (maybe half-edge) such that $p(e)$ belongs to some arc in $\mathcal{B}$ and $(r_1(e), r_2(e))$ is lexicographically maximum. We prove that $p(e^*)$ is a third extremal point. If $p(e_1(x_1))$ is a point of $\mathcal{B}$, it is extremal and distinct from $e_0(s_1)$ and $e_2(s'_1)$. So we may assume that e^* is distinct from the half-edge $e_1(x_1)$.

Claim 6 *The edge* e^* *is distinct from* $e_0(s_1)$ *and* $e_2(s'_1)$.

Proof We have $r_1(e_0(s_1)) = r_1(s_1) = r_1(s'_1) = r_1(e_2(s'_1))$. So we can prove the claim by showing that $r_1(e^*) > r_1(s_1)$.

Suppose there exists $v \in S_{\mathcal{B}} \setminus Q_1$. Vertex v has an incident edge $e_i(v)$ such that $p(e_i(v))$ belongs to some arc in $\mathcal{B}$ and such that $r_1(e^*) \geq r_1(e_i(v)) \geq r_1(v)$. So it suffices to show that $r_1(v) > r_1(s_1)$. By Claim 5, we have $v \in R_0(s_1)$, so Lemma 3(i) implies that $R_0(v) \subseteq R_0(s_1)$. So Lemma 3(iii) implies that $R_2(s_1) \subsetneq R_2(v)$ or $R_1(s_1) \subsetneq R_1(v)$. If $R_1(s_1) \subsetneq R_1(v)$ we are done as $r_1(v) > r_1(s_1)$. So we may assume that $R_2(s_1) \subsetneq R_2(v)$. Similarly we may assume that $R_0(s'_1) \subsetneq R_0(v)$. So $P_0(v)$ intersects $P_2(s_1)$ and $P_2(v)$ intersects $P_0(s'_1)$. By Lemma 2, the two paths $P_0(v)$ and $P_2(v)$ have only v has a common point, so they both intersects Q_1 and then continue, one on $P_0(s'_1)$ and the other on $P_2(s_1)$. So $R_1(s_1) \subseteq R_1(v)$. As $v \notin R_1(s_1)$, by Lemma 3(i) we have $R_1(v) \nsubseteq R_1(s_1)$, so $R_1(s_1) \subsetneq R_1(v)$ and we are done.

We can now assume that $S_{\mathcal{B}} \subseteq Q_1$. Consider an arc a in $\mathcal{B} \setminus \{a_1(s_1)\}$ (it exists since $|\mathcal{B}| \geq 2$). Let $v \in S_{\mathcal{B}}$ and $i \in \{0, 2\}$ such that $a = a_i(v)$. This implies that $p(e_1(v))$ belongs to some arc in $\mathcal{B}$. If $e_1(v)$ is a half-edge, then clearly $r_1(e^*) = r_1(e_1(v)) > r_1(s_1)$. So we may assume that $e_1(v)$ is not a half-edge. Let $e_1(v) = uv$. By Lemma 4, $R_1(v) \subsetneq R_2(u)$. Thus $r_1(e^*) \geq r_1(e_1(v)) = r_1(u) > r_1(v) = r_1(s_1)$. This proves Claim 6. □

Claim 7 *The point* $p(e^*)$ *is extremal.*

Proof Suppose $p(e^*)$ is not extremal. By definition of an extremal point, it is either not on $\mathcal{B}$'s outer boundary or internal to an arc a of $\mathcal{B}$.

Let $e^* = xy$ in such a way that $r_1(x) \geq r_1(y)$. By Lemma 4, for any vertex v on $P_1(x)$ we have $r_1(v) > r_1(x)$. So none of the contact points on $P_1(x)$'s edges is a point of $\mathcal{B}$. Since $P_1(x)$ does not intersect any arc of $\mathcal{B}$, $p(e^*)$ lies on $\mathcal{B}$'s outer boundary.

Now suppose there exists an arc a of $\mathcal{B}$ such that $p(e^*)$ is internal to a. We consider three cases corresponding to the color of a.

Case 1: a is an arc of color 2. By definition of the arcs, either e^* is uni-directed in color 2 or e^* is bi-directed in colors 0, 1. Let $e^* = uv$ such that e^* is directed

from u to v in color 1 or 2. Then $a = a_2(v)$ by definition of the arcs. Let z be the vertex of $P_1(v)$ such that there is a bi-directed path Q in colors 0, 1 between v and z which length is maximum (maybe $v = z$ if $e_1(v)$ is not bi-directed). When $v \neq z$, since $z \in P_1(v)$, Lemma 2 implies that $z \notin P_0(v)$. So Q is colored 1 from v to z and colored 0 from z to v. By definition of the arcs, the arc $a = a_2(v) = a_2(z)$ ends at $p(e_1(z))$. Thus $p(e_1(z))$ belongs to some arc in $\mathcal{B}$. If $z = x_1$, then $r_1(e_1(z)) = +\infty$, contradicting the choice of e^*. So we may assume that $z \neq x_1$. Let w be such that $e_1(z) = zw$. By Lemma 4, $R_1(v) \subsetneq R_1(w)$. If uv is bi-directed, that is, uv is directed from u to v in color 1, then Lemma 4 implies that $R_1(u) \subsetneq R_1(w)$. If uv is uni-directed in color 2 from u to v, then Lemma 6 implies that $R_1(u) \subsetneq R_1(w)$. In both cases we have $r_1(e^*) = \max\{r_1(u), r_1(v)\} < r_1(w) \leq r_1(e_1(z))$, a contradiction to the choice of e^*.

Case 2: a is an arc of color 0. This case is completely symmetric to Case 1 as in the proof of case 1 we just use the fact that e^* was chosen in order to maximize r_1. (In case 3, the proof is similar to case 1 but this time the order on r_2 will also useful.)

Case 3: a is an arc of color 1. By definition of the arcs, either e^* is uni-directed in color 1 or e^* is bi-directed in colors 0, 2. Let $e^* = uv$ such that e^* is directed from u to v in color 1 or 2. Then $a = a_1(v)$ by definition of the arcs. Let z be the vertex of $P_2(v)$ such that there is a bi-directed path Q in colors 0, 2 between v and z which length is maximum (maybe $v = z$ if $e_2(v)$ is not bi-directed). When $v \neq z$, since $z \in P_2(v)$, Lemma 2 implies that $z \notin P_0(v)$. So Q is colored 2 from v to z and colored 0 from z to v. By definition of the arcs, the arc $a = a_1(v) = a_1(z)$ ends at $p(e_2(z))$. Thus $p(e_2(z))$ belongs to some arc in $\mathcal{B}$. Vertex v is in $P_0(z)$, so by Lemma 3(i), $R_1(v) \subseteq R_1(z)$. If e^* is bi-directed, then it is directed from v to u in color 0 and by Lemma 3(i), $R_1(u) \subseteq R_1(v)$. If e^* is directed from u to v in color 1, then by Lemma 4 $R_1(u) \subsetneq R_1(v)$. In both cases $R_1(u) \subseteq R_1(v) \subseteq R_1(z)$, so $r_1(e^*) = \max\{r_1(u), r_1(v)\} \leq r_1(z) \leq r_1(e_2(z))$, and by the choice of e^* we have $r_1(e^*) = r_1(e_2(z))$. If $z = x_2$, then $r_2(e_2(z)) = +\infty$, contradicting the choice of e^*. So we may assume that $z \neq x_2$. Let w be such that $e_2(z) = zw$. By Lemma 4, $R_2(v) \subsetneq R_2(w)$. If uv is bi-directed, that is, directed from u to v in color 2, then Lemma 4 implies, $R_2(u) \subsetneq R_2(w)$. If uv is uni-directed in color 1 from u to v, then Lemma 6 implies that $R_2(u) \subsetneq R_2(w)$. In both cases $R_2(u) \subsetneq R_2(w)$, so $r_2(e^*) = \max\{r_2(u), r_2(v)\} < r_2(w) \leq r_2(e_2(z))$, a contradiction to the choice of e^*. This proves Claim 7. □

By Claims 6 and 7, we have a third extremal point of $\mathcal{B}$. Thus the contact system of arcs is stretchable. □

4 One-to-One Correspondence

De Fraysseix et al. [3] already proved that strict contact representations by triangles of a planar triangulation are in one-to-one correspondence with its Schnyder woods defined by Schnyder [16]. In this section, we are going to prove a similar result for primal–dual contact representations.

De Fraysseix et al. [4] proved that classic Schnyder woods of a planar triangulation are in one-to-one correspondence with orientation of the edges of the graph where

each interior vertex has out-degree 3. This shows that it is possible to retrieve the coloring of the edges of a classic Schnyder wood from the orientation of all the edges of this Schnyder wood.

For generalized Schnyder woods (with some edges bi-directed) such a property is not true: it is not always possible to retrieve the coloring of the edges of a generalized Schnyder wood from the orientation of the edges (see for example the graph of Fig. 8 in [9]). But Felsner proved that a Schnyder wood of a planar map uniquely defines a Schnyder wood of the dual and when both the orientation of the edges of the primal and the dual are given, then the coloring of the Schnyder wood can be retrieved. We will use this to obtain the one-to-one correspondence with strict tiling primal–dual contact representations by triangles. To this purpose, we need to introduce some formalism from [9].

The *suspension dual* $G^{\sigma *}$ is obtained from the dual G^* by the following: The dual-vertex corresponding to the unbounded face is replaced by a triangle with vertices y_0, y_1, y_2. More precisely, let X_i be the set of edges on the boundary of the outer face of G between vertices x_j and x_k, with $\{i, j, k\} = \{0, 1, 2\}$. Let Y_i be the set of dual edges to the edges in X_i, i.e. $Y_0 \cup Y_1 \cup Y_2$ is the set of edges containing the vertex f_∞ of G^* which corresponds to the unbounded face of G. Exchange f_∞ by y_i at all the edges of Y_i, add three edges y_0y_1, y_1y_2, y_2y_0, and finally add a half-edge at each y_i inside the face $y_0y_1y_2$. The resulting graph is the suspension dual $G^{\sigma *}$. Felsner [8, 9] proved that Schnyder woods of G^σ are in one-to-one correspondence with Schnyder woods of $G^{\sigma *}$.

The *completion* of a plane suspension G^σ and its dual $G^{\sigma *}$ is obtain by the following: Superimpose G^σ and $G^{\sigma *}$ so that exactly the primal–dual pairs of edges cross (the half-edge at x_i cross the dual edge y_jy_k, for $\{i, j, k\} = \{0, 1, 2\}$). The common subdivision of each crossing pair of edges is a new edge-vertex. Add a new vertex v_∞ which is the second endpoint of the six half-edges reaching into the unbounded face. The resulting graph is the completion $\widetilde{G^\sigma}$.

An *s-orientation* of $\widetilde{G^\sigma}$ is an orientation of the edges of $\widetilde{G^\sigma}$ satisfying the following out-degrees:

- $d^+(v) = 3$ for all primal- and dual-vertices v.
- $d^+(e) = 1$ for all edge-vertices e.
- $d^+(v_\infty) = 0$ for the special vertex v_∞.

Felsner [9] proved the following:

Theorem 7 (Felsner [9]) *Schnyder woods of G^σ are in one-to-one correspondence with s-orientations of $\widetilde{G^\sigma}$.*

We are now able to prove the following correspondence:

Theorem 8 *The non-isomorphic strict tiling primal–dual contact representations by triangles of a planar map are in one-to-one correspondence with its Schnyder woods.*

Proof Given a strict tiling primal–dual contact representation by triangles $(\mathcal{V}, \mathcal{F})$ of a graph G, one can associate a corresponding suspension G^σ, its suspension dual

$G^{\sigma *}$, the completion $\widetilde{G^{\sigma}}$ and a s-orientation of the completion. The three vertices x_0, x_1, x_2 that define the suspension G^{σ} are, in clockwise order, the three triangles of $\mathcal{V}$ that share a corner with the triangle corresponding to the outer face. We modify our contact system by exchanging the triangle $c(f_\infty)$, representing the outer face f_∞, by three triangles $c(y_0), c(y_1), c(y_2)$ each one representing y_0, y_1, y_2 of the suspension dual. Each $c(y_i)$ share a side with $c(f_\infty)$ and two $c(y_i)$ have parallel and intersecting sides. The interiors of the triangles of this new system still form a tiling of a triangle $c(v_\infty)$ representing the vertex v_∞ of the completion. The edge-vertices of the completion corresponds to the corners of the triangles of the new system.

The s-orientation of $\widetilde{G^{\sigma}}$ is obtained by the following. For a primal- or dual-vertex v, represented by a triangle $c(v)$, all edges ve of $\widetilde{G^{\sigma}}$ are directed from v to e if e corresponds to a corner of $c(v)$ and from e to v otherwise. For the special vertex v_∞, all its incident edges are directed toward itself. Clearly, for every primal- or dual-vertex v, we have $d^+(v) = 3$ as $c(v)$ is a triangle and for v_∞ we have $d^+(v_\infty) = 0$. As the primal–dual contact representation $(\mathcal{V}, \mathcal{F})$ is strict, i.e. each contact point is a corner of exactly three triangles, we have $d^+(e) = 1$ for every edge-vertex that is a contact point of $(\mathcal{V}, \mathcal{F})$. For edge-vertices between special vertices x_i, y_j and v_∞ one can check that the out-degree constraint is also satisfied.

One can remark that two non-isomorphic triangle contact systems representing the same planar map G define two distinct orientations of $\widetilde{G^{\sigma}}$ and thus two different Schnyder woods of G^{σ} by Theorem 7.

Conversely, let G be a planar map, given with a Schnyder wood rooted at x_0, x_1, x_2 and the corresponding s-orientation of $\widetilde{G^{\sigma}}$. Let $\mathcal{A}$ be the contact system of arcs corresponding to the Schnyder wood as defined in Sect. 3. For each vertex $v \in V$, we note $c(v)$ the closed curve that is the union, for $i \in \{0, 1, 2\}$, of the part of the arc $a_i(v)$ between the contact point with $a_{i-1}(v)$ and $a_{i+1}(v)$. The set of curves $\mathcal{V} = (c(v))_{v \in V}$ is a contact representation of G by closed curves. For each interior face F, the labels of its angles form a nonempty interval of 0's, a nonempty interval of 1's and a nonempty interval of 2's by Theorem 6. By definition of the arcs, each interval of i's corresponds to only one arc, noted $a_i(f)$. We note $c(f)$ the closed curve that is the union, for $i \in \{0, 1, 2\}$, of the part of the arc $a_i(f)$ between the contact point with $a_{i-1}(f)$ and $a_{i+1}(f)$. For the outer face f_∞, the curve $c(f_\infty)$ is the union, for $i \in \{0, 1, 2\}$, of $a_{i+1}(x_i)$. The set of curves $\mathcal{F} = (c(f))_{f \in V^*}$ is a contact representation of G^* by closed curves.

By Lemma 7, the contact system of arcs $\mathcal{A}$ is stretchable. For each $v \in V \cup V^*$, the closed curves $c(v)$ is the union of three part of arcs of $\mathcal{A}$, so when stretched it becomes a triangle. Thus, we obtain a primal–dual contact representation by triangles $(\mathcal{V}, \mathcal{F})$ of G. By definition of $(\mathcal{V}, \mathcal{F})$ the interiors of the triangles form a tiling of the triangle corresponding to the outer face. Thus, the primal–dual contact representation by triangles $(\mathcal{V}, \mathcal{F})$ is tiling. By definition of $\mathcal{A}$, every contact point, corresponding to an uni- or bi-directed edge, is interior to one arc and is the extremity of two arcs. So each contact point of $(\mathcal{V}, \mathcal{F})$ is a corner of exactly three triangles. Thus, the primal–dual contact representation by triangles $(\mathcal{V}, \mathcal{F})$ is strict. The strict tiling primal–dual contact representation by triangles $(\mathcal{V}, \mathcal{F})$ corresponds to the s-orientation of $\widetilde{G^{\sigma}}$ and thus to the Schnyder wood by Theorem 7. □

5 Internally 3-Connected Planar Maps

A planar map G is *internally 3-connected* if there exist three vertices on the outer face such that the graph obtain from G by adding a vertex adjacent to the three vertices is 3-connected. Miller [15] proved the following (see also [7] for existence of Schnyder woods for 3-connected planar maps and [2] were the following result is stated in this form):

Theorem 9 (Miller [15]) *A planar map admits a Schnyder wood if and only if it is internally* 3*-connected.*

As a corollary of Theorems 8 and 9, we obtain the following:

Corollary 1 *A planar map admits a strict tiling primal–dual contact representation by triangles if and only if it is internally* 3*-connected.*

A 3-connected planar map is obviously internally 3-connected, so we obtain Theorem 4 as a consequence of Corollary 1.

Note that the representation of Theorem 4 is efficiently computable. Finding a Schnyder wood of an internally 3-connected planar map can be done linearly by contracting edges in a particular way (see [10]). Then the proof relies on the fact that the system of arcs defined in Sect. 3 is stretchable. Stretching a system of arc can be done by solving a system of linear equation (see [5]) and the number of equation and variable is linear in the size of the graph.

6 Particular Types of Triangle

The construction given by de Fraysseix et al. [3] to obtain a strict contact representation by triangles of a planar triangulation can be slightly modified to give a strict tiling primal–dual contact representation by triangles (the three triangles corresponding to the outer face have to be modified to obtain the tiling property). In de Fraysseix et al.'s construction, all the triangles have a horizontal side at their bottom and moreover it is possible to require that all the triangles are right (with the right angle on the left extremity of the horizontal side). This leads us to propose the following conjecture.

Conjecture 1 *Every* 3*-connected planar map admits a strict tiling primal–dual contact representation by right triangles where all triangles have a horizontal and a vertical side and where the right angle is bottom-left for primal vertices and the outer face and top-right otherwise.*

One may wonder if further requirements can be asked. Is it possible to obtain primal–dual contact representation by homothetic triangles? Such a representation is a representation where vertex-triangles and the outer-face-triangle are positively homothetic to a given triangle $\mathcal{T}$ and inner-face-triangles are negatively homothetic to $\mathcal{T}$. The 4-connected planar triangulation of Fig. 6 has a unique contact representation by homothetic triangles (for a fixed size of the external triangles). The central

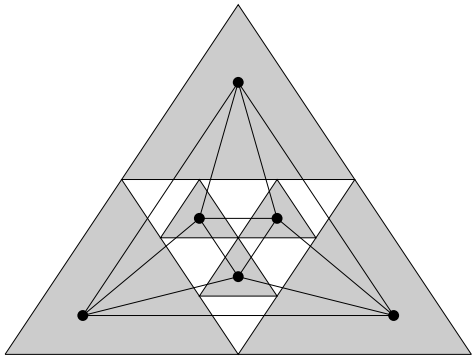

Fig. 6 A 4-connected planar triangulation and its contact representation by homothetic triangles

face corresponds to an empty triangle and there are some extra contacts between non adjacent faces. So it is not possible to have an "exact" primal–dual contact representation by homothetic triangles for this graph. The extended abstract version of this paper [12] contains results concerning representation by homothetic triangles that are now presented in a more general paper on the subject [13].

Acknowledgements This work was partially supported by the grant ANR-09-JCJC-0041.

References

1. Andreev, E.: On convex polyhedra in Lobachevskii spaces. Mat. Sb. **81**, 445–478 (1970)
2. Bonichon, N., Felsner, S., Mosbah, M.: Convex drawings of 3-connected plane graphs. Algorithmica **47**, 399–420 (2007)
3. de Fraysseix, H., Ossona de Mendez, P., Rosenstiehl, P.: On triangle contact graphs. Comb. Probab. Comput. **3**, 233–246 (1994)
4. de Fraysseix, H., Ossona de Mendez, P.: On topological aspects of orientations. Discrete Math. **229**, 57–72 (2001)
5. de Fraysseix, H., Ossona de Mendez, P.: Barycentric systems and stretchability. Discrete Appl. Math. **155**, 1079–1095 (2007)
6. de Fraysseix, H., Pach, J., Pollack, R.: Small sets supporting Fáry embeddings of planar graphs. In: Proceedings of the Twentieth Annual ACM Symposium on Theory of Computing, STOC '88, pp. 426–433 (1988)
7. Felsner, S.: Convex drawings of planar graphs and the order dimension of 3-polytopes. Order **18**, 19–37 (2001)
8. Felsner, S.: Geodesic embeddings and planar graphs. Order **20**, 135–150 (2003)
9. Felsner, S.: Lattice structures from planar graphs. Electron. J. Combin. **11** (2004)
10. Felsner, S.: Geometric Graphs and Arrangements. Vieweg, Wiesbaden (2004)
11. Gansner, E.R., Hu, Y., Kobourov, S.G.: On touching triangle graphs. In: Proc. Graph Drawing '10. Lecture Notes in Computer Science, vol. 6502, pp. 250–261. Springer, Berlin (2011)
12. Gonçalves, D., Lévêque, B., Pinlou, A.: Triangle contact representations and duality. In: Proc. Graph Drawing '10. Lecture Notes in Computer Science, vol. 6502, pp. 262–273. Springer, Berlin (2011)
13. Gonçalves, D., Lévêque, B., Pinlou, A.: Homothetic triangle representations of planar graphs. Manuscript (2011)
14. Koebe, P.: Kontaktprobleme der konformen Abbildung. Ber. Verh. Sachs. Akad. Wiss. Leipzig, Math.-Phys. Kl. **88**, 141–164 (1936)
15. Miller, E.: Planar graphs as minimal resolutions of trivariate monomial ideals. Doc. Math. **7**, 43–90 (2002)
16. Schnyder, W.: Planar graphs and poset dimension. Order **5**, 323–343 (1989)

Discrete Comput Geom (2010) 43: 626–647
DOI 10.1007/s00454-009-9196-9

Planar Graphs Have 1-string Representations

Jérémie Chalopin · Daniel Gonçalves · Pascal Ochem

Received: 9 August 2008 / Revised: 15 May 2009 / Accepted: 18 May 2009 /
Published online: 29 July 2009

Abstract We prove that every planar graph is an intersection graph of strings in the plane such that any two strings intersect at most once.

Keywords Planar graphs · Strings

1 Introduction

A *string* $\mathbf{s}$ is a curve of the plane homeomorphic to a segment. A string $\mathbf{s}$ has two ends, the points of $\mathbf{s}$ that are not ends of $\mathbf{s}$ are *internal points* of $\mathbf{s}$. Two strings $\mathbf{s_1}$ and $\mathbf{s_2}$ *cross* if they have a common point $\mathbf{p} \in \mathbf{s_1} \cap \mathbf{s_2}$ and if going around $\mathbf{p}$, we successively meet $\mathbf{s_1}$, $\mathbf{s_2}$, $\mathbf{s_1}$, and $\mathbf{s_2}$. This means that a tangent point is not a "crossing." In the following we consider string sets without tangent points.

In this paper, we consider intersection models for simple planar graphs (i.e., planar graphs without loops or multiple edges). A *string representation* of a graph $G = (V, E)$ is a set Σ of strings in the plane such that every vertex $v \in V$ maps to a string $\mathbf{v} \in \Sigma$ and such that $uv \in E$ if and only if the strings $\mathbf{u}$ and $\mathbf{v}$ cross (at least once). Similarly, a *segment representation* of a graph G is a string representation of G in which the strings are segments.

An abstract of this paper appeared in the Proceedings of the eighteenth annual ACM–SIAM Symposium on Discrete algorithms (SODA 2007).

J. Chalopin
LIF, CNRS et Aix-Marseille Université, CMI, 39 rue Joliot-Curie, 13453 Marseille Cedex 13, France

D. Gonçalves (✉)
LIRMM, CNRS et Université Montpellier 2, 161 rue Ada, 34392 Montpellier Cedex 05, France
e-mail: daniel.goncalves@lirmm.fr

P. Ochem
LRI, CNRS et Université Paris-Sud, Bât 490, 91405 Orsay Cedex, France

These notions were introduced by Ehrlich et al. [3], who proved the following:

Theorem 1 [3] *Planar graphs have a string representation.*

In [9], Koebe proved that planar graphs are the contact graphs of disks in the plane. Note that in this model the curves bounding two adjacent disks are tangent. However by inflating these circles we obtain string representations for planar graphs. In his PhD thesis, Scheinerman [10] conjectures a stronger result:

Conjecture 1 [10] *Planar graphs have a segment representation.*

Hartman et al. [8] and de Fraysseix et al. [4] proved Conjecture 1 for bipartite planar graphs. Castro et al. [1] proved Conjecture 1 for triangle-free planar graphs. Recently de Fraysseix and Ossona de Mendez [6] extended this to planar graphs that have a 4-coloring in which every induced cycle of length 4 uses at most three colors. Observe that, since parallel segments never cross, a set of parallel segments in a segment representation of a graph induces a stable set of vertices. The construction in [4, 8] (resp. [1]) has the nice property that there are only two (resp. three) possible slopes for the segments. So the construction induces a 2-coloring (resp. 3-coloring) of G. Note that Castro et al. do not prove the 3-colorability of triangle-free planar graphs, they use such coloring of the graphs (by Grötzsch's Theorem) in their construction. West [11] proposed a stronger version of Conjecture 1 in which only four slopes are allowed, thus using the fact that these graphs are 4-colorable.

Notice that two segments cross at most one point, whereas in the construction of Theorem 1, strings may cross twice. Let us define a *1-string representation* as a string representation in which any two strings cross at most once. Thus the following theorem is a step towards Conjecture 1.

Theorem 2 *Planar graphs have a* 1*-string representation.*

Note that if we would allow and consider tangent points, this theorem would directly follow from Koebe's theorem. Theorem 2 answers an open problem of de Fraysseix and Ossona de Mendez [5]. In the same article they noticed that Theorem 2 implies that any planar multigraph has a string representation such that the number of crossings between two strings equals the number of edges between the two corresponding vertices.

In the next section we provide some definitions and prove that it is sufficient to prove this theorem for triangulations. Section 3 is devoted to the study of string representations of 4-connected triangulations. In this section we use a decomposition technique of 4-connected triangulations that is inspired on Whitney's work [12] and that was recently used by the second author [7]. Then in Sect. 4 we finally prove Theorem 2 for all triangulations.

2 Preliminaries

2.1 Restriction to Triangulations

Lemma 1 *Every planar graph is an induced subgraph of some planar triangulation.*

Proof Let G be a planar graph embedded in the plane (i.e., a plane graph). The graph $h(G)$ is obtained from G by adding in every face f of G a new vertex v_f adjacent to every vertex incident to f in G. Notice that $h(G)$ is also a plane graph and that G is an induced subgraph of $h(G)$. Moreover, $h(G)$ is connected, $h(h(G))$ is 2-connected, and $h(h(h(G)))$ is a triangulation.

Note that we have to apply the h operator several times: if a facial walk goes through the same vertex several times, since multiples edges are not allowed, we obtain a nontriangular face. □

It is clear that a 1-string representation of a triangulation T induces a 1-string representation for any of its induced subgraphs. It is thus sufficient to prove Theorem 2 for triangulations.

2.2 String Representations

In a plane graph G, the unbounded face of G is called the *outer-face* and every other face of G is an *inner-face* of G. An *outer-vertex* (resp. *outer-edge*) of G is a vertex (resp. edge) of G incident to the outer-face. The other vertices (resp. edges) of G are *inner-vertices* (resp. *inner-edges*). The set of outer-vertices (resp. outer-edges, inner-vertices, and inner-edges) of G is denoted by $V_o(G)$ (resp. $E_o(G)$, $V_i(G)$, and $E_i(G)$). A *near-triangulation* is a plane graph in which all the inner-faces are triangles. An edge uv is a *chord* of some near-triangulation T if uv is an inner-edge linking two outer-vertices. From now on, we use the following notation: the strings corresponding to vertices of a graph G are denoted by bold letters, i.e., for any $v \in V(G)$, we denote its corresponding string by $\mathbf{v}$. We need that in a 1-string representation of a plane graph G, each face of G corresponds to some topological region of the string representation.

Definition 1 Let $G = (V, E)$ be a plane graph with a 1-string representation Σ. Given a face abc of G, consider a triplet (a, b, c) of its incident vertices. An (a, b, c)-*region* **abc** is a region of the plane homeomorphic to a disk such that (see Fig. 1):

- For any vertex $v \neq a$, b, and c, we have $\mathbf{abc} \cap \mathbf{v} = \emptyset$ (i.e., **abc** intersects only with **a**, **b**, **c**).
- $\mathbf{abc} \cap \mathbf{a} \cap \mathbf{b} = \emptyset$, $\mathbf{abc} \cap \mathbf{b} \cap \mathbf{c} = \emptyset$, and $\mathbf{abc} \cap \mathbf{c} \cap \mathbf{a} = \emptyset$ (i.e., **a**, **b**, **c** intersect outside **abc**).
- Both $\mathbf{abc} \cap \mathbf{b}$ and $\mathbf{abc} \cap \mathbf{c}$ are connected.
- The boundary of **abc** successively crosses (clockwise or anticlockwise) **a**, **a**, **b**, **b**, **c**, **a**, **c**.

Fig. 1 An (a, b, c)-region **abc**

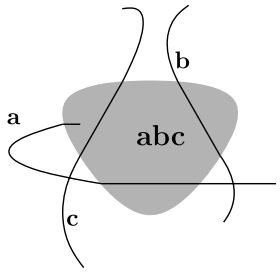

Note that according to this definition, **abc** $\cap$ **a** has two components, and one end of **a** is in **abc**. Note that the order in the triplet (a, b, c) matters: a region τ of the plane cannot be an (a, b, c)-region and a (c, b, a)-region for example. A region **abc** of the plane is an $\{a, b, c\}$-*region* if it is either an (a, b, c)-region, an (a, c, b)-region, a (b, a, c)-region, a (b, c, a)-region, a (c, a, b)-region, or a (c, b, a)-region. When the vertices a, b, and c are not mentioned, we call such a region a *face-region*.

Definition 2 A *strong 1-string representation* (S-representation, for short) of a near-triangulation T is a pair (Σ, R) such that:

(1) Σ is a 1-string representation of T.
(2) R is a set of disjoint face-regions such that for every inner-face abc of T, R contains an $\{a, b, c\}$-region.

A *partial strong 1-string representation* (PS-representation, for short) of a near-triangulation T is a triplet (Σ, R, F) in which $F \subseteq E(T)$ and such that (Σ, R) is a strong 1-string representation of T without the crossings corresponding to the edges of F.

In a PS-representation (Σ, R, F) of T, note that Σ is a 1-string representation of $T \setminus F$ and that each inner-face of T has a corresponding face-region in R.

2.3 Special Triangulations

In a near-triangulation T, a *separating 3-cycle* C is a cycle of length 3 such that some vertices of T lie inside C, whereas other vertices lie outside. It is well known that a triangulation is 4-connected if and only if it contains no separating 3-cycle. In [12], Whitney considered a special family of near-triangulations, it is why we call them W-triangulations.

Definition 3 A *W-triangulation* is a 2-connected near-triangulation containing no separating 3-cycle.

In particular, any 4-connected triangulation is a W-triangulation. Note that since a W-triangulation has no cut vertex, its outer-edges induce a cycle. The following lemma gives a sufficient condition for a subgraph of a W-triangulation T to be a W-triangulation.

Fig. 2 3-boundary of T

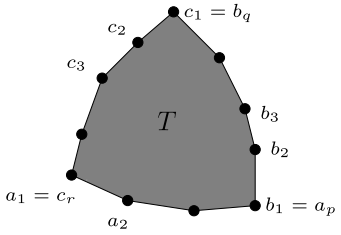

Lemma 2 *Let T be a W-triangulation and consider a cycle C of T. The subgraph induced by the vertices lying on and inside C is a W-triangulation.*

Proof Consider the near-triangulation T' inside some cycle C of T. By definition, T has no separating 3-cycle, and consequently T' does not have any separating 3-cycle. Since T' is clearly connected and has more than two vertices, we prove that it is 2-connected by showing that it does not contain any cut vertex.

Since the cycle C delimits the outer-face of T', any vertex $v \in V(T')$ appears at most once on the outer face. Since the outerface appears at most once around v and since all its other incident faces are triangles, T' contains a path linking all the neighbors of v. This implies that $T' \setminus v$ is connected, and thus T' has no cut vertex. □

Definition 4 A W-triangulation T is *3-bounded* if the outer-boundary of T is the union of three paths $(a_1, \ldots, a_p)$, $(b_1, \ldots, b_q)$, and $(c_1, \ldots, c_r)$ that satisfy the following conditions (see Fig. 2):

- $a_1 = c_r$, $b_1 = a_p$, and $c_1 = b_q$.
- the paths are nontrivial, i.e., $p \geq 2$, $q \geq 2$, and $r \geq 2$.
- there exists no chord $a_i a_j$, $b_i b_j$, or $c_i c_j$.

Such a *3-boundary* of T will be denoted by $(a_1, \ldots, a_p)$–$(b_1, \ldots, b_q)$–$(c_1, \ldots, c_r)$.

In the following, we will use the order on the three paths and their directions, i.e., $(a_1, \ldots, a_p)$–$(b_1, \ldots, b_q)$–$(c_1, \ldots, c_r)$ will be different from $(b_1, \ldots, b_q)$–$(c_1, \ldots, c_r)$–$(a_1, \ldots, a_p)$ and $(a_p, \ldots, a_1)$–$(c_r, \ldots, c_1)$–$(b_q, \ldots, b_1)$.

3 Proof for 4-connected Triangulations

The following property describes the shape of a PS-representation of a 3-bounded W-triangulation.

Property 1 *Consider a 3-bounded W-triangulation T with a 3-boundary $(a_1, \ldots, a_p)$–$(b_1, \ldots, b_q)$–$(c_1, \ldots, c_r)$. The W-triangulation T has Property 1 if T has a PS-representation (Σ, R, F) contained inside a region τ of the plane homeomorphic to the disk that satisfies the following properties (see Fig. 3):*

Fig. 3 Property 1

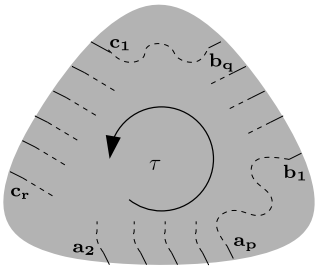

(a) $F = E_o(T) \setminus \{a_1a_2\}$ (*i.e., the missing crossings correspond to the outer edges, except* a_1a_2).
(b) *On the boundary of* τ, *we successively have the ends of* $\mathbf{a_2}, \mathbf{a_3}, \ldots, \mathbf{a_p}, \mathbf{b_1}, \ldots, \mathbf{b_q}, \mathbf{c_1}, \ldots, \mathbf{c_r}$.

If going clockwise (resp. anticlockwise) around the boundary of τ, we cross the strings in the order described in (b), we say that the PS-representation is *clockwise* (resp. *anticlockwise*). Note that by an axial symmetry, one can obtain a clockwise PS-representation from an anticlockwise PS-representation, and vice versa. Observe that since $a_p = b_1$, $b_q = c_1$, and $c_r = a_1$, both ends of $\mathbf{b_1}$ and $\mathbf{c_1}$ lie on the boundary of τ, but it is not the case for $\mathbf{a_1}$ or any other string (i.e., all the strings appearing on the boundary of τ have an end inside τ except $\mathbf{b_1}$ and $\mathbf{c_1}$).

Before proving that each 3-bounded W-triangulation has Property 1, we give some definitions and we present Property 2. Consider a 3-bounded W-triangulation $T \neq K_3$ whose boundary is $(a_1, \ldots, a_p)$–$(b_1, \ldots, b_q)$–$(c_1, \ldots, c_r)$ and such that T does not contain any chord a_ib_j or a_ic_j. Let $D \subseteq V_i(T)$ be the set of inner-vertices of T that are adjacent to some vertex a_i with $i > 1$ (the black vertices on the left of Fig. 4). Since T has at least 4 vertices, no separating 3-cycle, and no chord a_ia_j, a_ib_j, or a_ic_j, it follows that a_1 and a_2 (resp. b_1 and b_2) have exactly one common neighbor in $V_i(T)$ that will be denoted a (resp. d_1).

Since there is no chord a_ia_j, a_ib_j, or a_ic_j, for each vertex a_i with $i \in [2, p-1]$, all the neighbors of a_i (resp. a_p) except a_{i-1} and a_{i+1} (resp. a_{p-1} and b_2) are in D. Since for each $i \in [2, p]$, there is a path linking the neighbors of a_i in D and since the vertices a_i and a_{i+1} have a common neighbor in D, the set D induces a connected graph. Since a is in D, the set $D \cup \{a_1\}$ also induces a connected graph.

Definition 5 The *adjacent path* of T with respect to the 3-boundary $(a_1, \ldots, a_p)$–$(b_1, \ldots, b_q)$–$(c_1, \ldots, c_r)$ is the shortest path linking d_1 and a_1 in $T[D \cup \{a_1\}]$ (the graph induced by $D \cup \{a_1\}$). This path will be denoted $(d_1, d_2, \ldots, d_s, a_1)$.

Observation 1 *There exists neither an edge* d_id_j *with* $2 \leq i+1 < j \leq s$ *nor an edge* a_1d_i *with* $1 \leq i < s$. *Otherwise,* $(d_1, d_2, \ldots d_s, a_1)$ *would not be the shortest path between* d_1 *and* a_1.

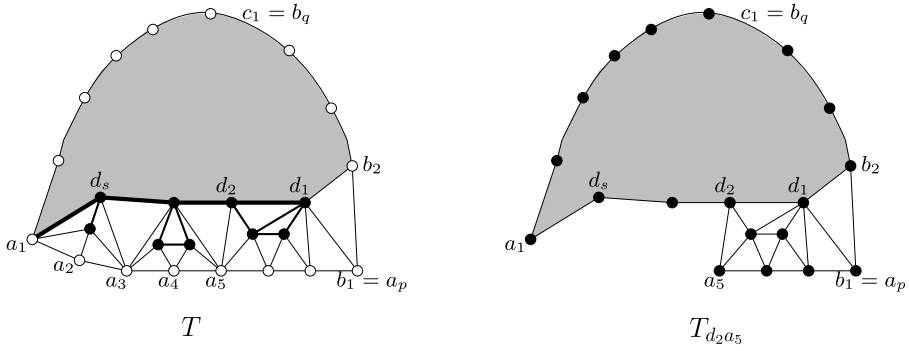

Fig. 4 The adjacent path of T and the graph $T_{d_2a_5}$

Definition 6 For each edge $d_xa_y \in E(T)$ with $x \in [1, s]$ and $y \in [2, p]$, the graph $T_{d_xa_y}$ is the graph lying inside the cycle $C = (a_1, d_s, \ldots, d_x, a_y, \ldots, a_p, b_2, \ldots, b_q, c_2, \ldots, c_r)$ (see Fig. 4).

Note that since $D \subseteq V_i(T)$, C is a cycle, and by Lemma 2, $T_{d_xa_y}$ is a W-triangulation. The following property describes the shape of a PS-representation of $T_{d_xa_y}$.

Property 2 *Consider a* 3*-bounded W-triangulation* T *with a* 3*-boundary* $(a_1, \ldots, a_p)$–$(b_1, \ldots, b_q)$–$(c_1, \ldots, c_r)$ *that does not have any chord* a_ib_j *or* a_ic_j*, and let* $(d_1, d_2, \ldots, d_s, a_1)$ *be its adjacent path. Consider an edge* $d_xa_y \in E(T)$ *with* $y > 1$.

The W-triangulation $T_{d_xa_y}$ has Property 2 if $T_{d_xa_y}$ has a PS-representation (Σ, R, F) satisfying the following properties (see Fig. 5):

(a) $F = E_o(G) \setminus \{d_xa_y\}$.
(b) Every string $\mathbf{v} \in \Sigma \setminus \{\mathbf{d_x}, \mathbf{a_y}\}$ is contained in a region τ of the plane homeomorphic to the disk. Furthermore, $\mathbf{d_x}$ and $\mathbf{a_y}$ have their ends in τ (or on the boundary of τ), but they cross each other outside τ.
(c) Each face-region of R is contained inside τ.
(d) On the boundary of τ, we successively have the ends of $\mathbf{a_y}, \ldots, \mathbf{a_p}, \mathbf{b_1}, \ldots, \mathbf{b_q}$, $\mathbf{c_1}, \ldots, \mathbf{c_r}$,
$\mathbf{a_1}, \mathbf{d_s}, \ldots, \mathbf{d_{x+1}}$, and then we successively have internal points of $\mathbf{d_x}, \mathbf{a_y}, \mathbf{d_x}$, and $\mathbf{a_y}$.

Here again, if going clockwise (resp. anticlockwise) around the boundary of τ, we cross the strings in the order described in (d), we say that the PS-representation is *clockwise* (resp. *anticlockwise*). In the proof of Theorem 2, we only use Property 1. However, in order to prove Property 1, we use Property 2. We prove these two properties by doing a "crossed" induction.

Proof of Properties 1 and 2

We prove, by induction on $m \geq 3$, that the following two statements hold:

Fig. 5 Property 2

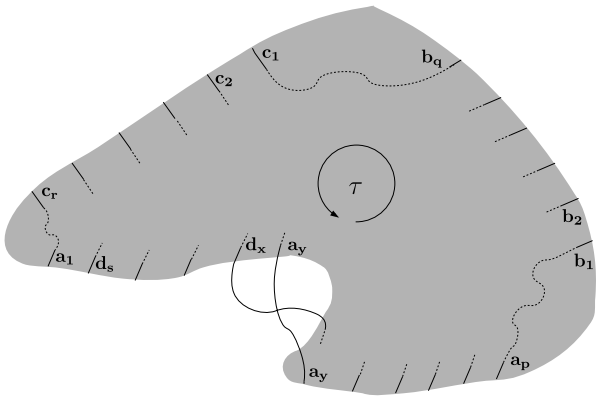

Fig. 6 Initial case for Property 1

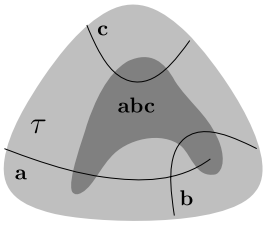

– Property 1 holds if T has at most m edges.
– Property 2 holds if $T_{d_x a_y}$ has at most m edges.

The initial case, $m = 3$, is easy to prove since there is only one W-triangulation having at most 3 edges, K_3. For Property 1, we have to consider all the possible 3-boundaries of K_3. All these 3-boundaries are equivalent, so let $V(K_3) = \{a, b, c\}$ and consider the 3-boundary (a, b)–(b, c)–(c, a). In Fig. 6 there is a PS-representation (Σ, R, F) of K_3 with $F = \{bc, ac\}$ that fulfills Property 1. For Property 2, since a W-triangulation $T_{d_x a_y}$ has at least 4 vertices, a_1, b_1, c_1, and d_1, we have $T_{d_x a_y} \neq K_3$, and there is no W-triangulation $T_{d_x a_y}$ with at most 3 edges. So by vacuity, Property 2 holds for $T_{d_x a_y}$ with at most 3 edges.

The induction step applies to both Property 1 and Property 2. This means that we prove Property 1 (resp. Property 2) for the W-triangulations T (resp. $T_{d_x a_y}$) with m edges using both Property 1 and Property 2 on W-triangulations with less than m edges. We first prove the induction for Property 1.

Case 1: Proof of Property 1 for a W-triangulation T with m edges Let $(a_1, \ldots, a_p)$–$(b_1, \ldots, b_q)$–$(c_1, \ldots, c_r)$ be the 3-boundary of T considered. We distinguish different cases according to the existence of a chord $a_i b_j$ or $a_i c_j$ in T. We successively consider the case where there is a chord $a_1 b_i$ with $1 < i < q$, the case where there is a chord $a_i b_j$ with $1 < i < p$ and $1 < j \leq q$, and the case where there is a chord $a_i c_j$ with $1 < i \leq p$ and $1 < j < r$. We then finish with the case where there is no chord $a_i b_j$ with $1 \leq i \leq p$ and $1 \leq j \leq q$ (by the definition of 3-boundary, T has no chord $a_1 b_q$, $a_i b_1$, or $a_p b_j$) and no chord $a_i c_j$ with $1 \leq i \leq p$ and $1 \leq j \leq r$ (by the definition of 3-boundary, T has no chord $a_p c_1$, $a_i c_r$, or $a_1 c_j$).

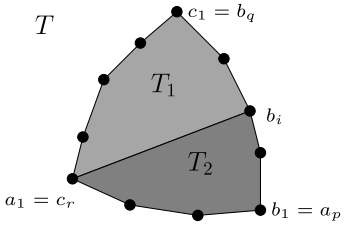

Fig. 7 Case 1.1: Chord a_1b_i

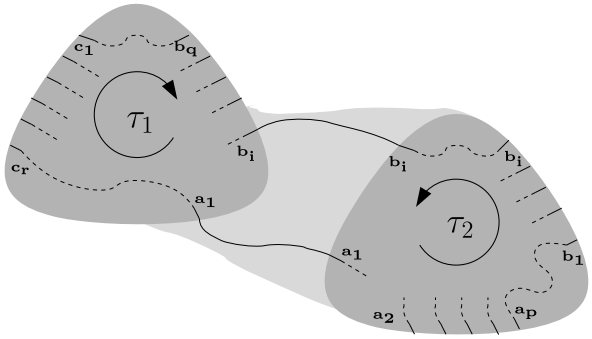

Fig. 8 Case 1.1: (Σ, R, F)

Case 1.1: There is a chord a_1b_i with $1 < i < q$ (see Fig. 7) Let T_1 (resp. T_2) be the subgraph of T that lies inside the cycle $(a_1, b_i, \ldots, b_q, c_2, \ldots, c_r)$ (resp. $(a_1, a_2, \ldots, a_p, b_2, \ldots, b_i, a_1)$). By Lemma 2, T_1 and T_2 are W-triangulations. Since T has no chord a_xa_y, b_xb_y, or c_xc_y, (b_i, a_1)–$(c_r, \ldots, c_1)$–$(b_q, \ldots, b_i)$ (resp. $(a_1, \ldots, a_p)$–$(b_1, \ldots, b_i)$–(b_ia_1)) is a 3-boundary of T_1 (resp. T_2). Furthermore, since $a_1a_2 \notin E(T_1)$ and $c_1c_2 \notin E(T_2)$, T_1 and T_2 have less edges than T, and Property 1 holds for T_1 and T_2 with the mentioned 3-boundaries. Let (Σ_1, R_1, F_1) (resp. (Σ_2, R_2, F_2)) be a clockwise (resp. anticlockwise) PS-representation contained in the region τ_1 (resp. τ_2) obtained for T_1 (resp. T_2) with $F_1 = E_o(T_1) \setminus \{a_1b_i\}$ (resp. $F_2 = E_o(T_2) \setminus \{a_1a_2\}$). In Fig. 8 we show how to associate these two representations to obtain (Σ, R, F), an anticlockwise PS-representation of T contained in τ. Note that the two strings $\mathbf{a_1}$ (resp. $\mathbf{b_i}$) from Σ_1 and Σ_2 have been linked.

We easily verify that (Σ, R, F) satisfies Property 1:

- Σ is a string representation of $T \setminus F$ with $F = E_o(T) \setminus \{a_1a_2\}$. Indeed, since $V(T_1) \cup V(T_2) = V(T)$ and $V(T_1) \cap V(T_2) = \{a_1, b_i\}$, every vertex $v \in V(T)$ has exactly one string in Σ. Furthermore, since $(E(T_1) \setminus F_1) \cup (E(T_2) \setminus F_2) = E(T) \setminus F$, Σ is a string representation of $T \setminus F$.
- Σ is a 1-string representation. The only edge that belongs to both T_1 and T_2 is a_1b_i. Since $\mathbf{a_1}$ and $\mathbf{b_i}$ cross each other in Σ_1 ($a_1b_i \notin F_1$) but not in Σ_2 ($a_1b_i \in F_2$), $\mathbf{a_1}$ and $\mathbf{b_i}$ cross exactly once in Σ.
- (Σ, R) is "strong": Each inner-face of T is an inner-face in T_1 or T_2, and the regions τ_1 and τ_2 are disjoint (so the face-regions in τ_1 are disjoint from the face-regions in τ_2).

Finally we see in Fig. 8 that point (b) of Property 1 is satisfied.

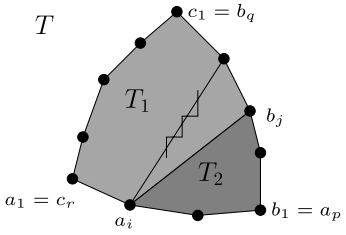

Fig. 9 Case 1.2: Chord $a_i b_j$

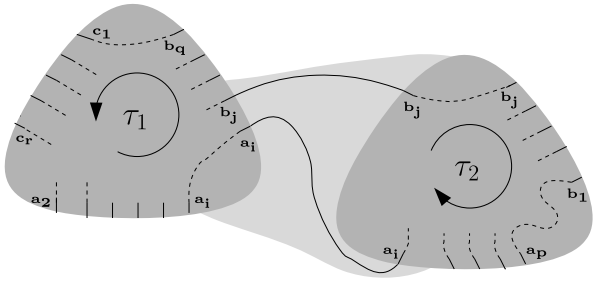

Fig. 10 Case 1.2: (Σ, R, F)

Case 1.2: There is a chord $a_i b_j$ with $1 < i < p$ and $1 < j \leq q$ (see Fig. 9) If there are several chords $a_i b_j$, we consider one that maximizes j, i.e., there is no chord $a_i b_k$ with $j < k \leq q$. Let T_1 (resp. T_2) be the subgraph of T that lies inside the cycle $(a_1, a_2, \ldots, a_i, b_j, \ldots, b_q, c_2, \ldots, c_r)$ (resp. $(a_i, \ldots, a_p, b_2, \ldots, b_j, a_i)$). By Lemma 2, T_1 and T_2 are W-triangulations. Since T has no chord $a_x a_y$, $b_x b_y$, $c_x c_y$, or $a_i b_k$ with $k > j$, $(a_1, \ldots, a_i)$–$(a_i, b_j, \ldots, b_q)$–$(c_1, \ldots, c_r)$ (resp. (a_i, b_j)–$(b_j, \ldots, b_1)$–$(a_p, \ldots, a_i)$) is a 3-boundary of T_1 (resp. T_2). Furthermore, since $b_1 b_2 \notin E(T_1)$ and $a_1 a_2 \notin E(T_2)$, T_1 and T_2 have less edges than T, and Property 1 holds for T_1 and T_2 with the mentioned 3-boundaries. Let (Σ_1, R_1, F_1) (resp. (Σ_2, R_2, F_2)) be an anticlockwise (resp. clockwise) PS-representation contained in the region τ_1 (resp. τ_2) obtained for T_1 (resp. T_2) with $F_1 = E_o(T_1) \setminus \{a_1 a_2\}$ (resp. $F_2 = E_o(T_2) \setminus \{a_i b_j\}$). In Fig. 10 we show how to associate these two representations to obtain (Σ, R, F), an anticlockwise PS-representation of T contained in τ. Note that in this construction the two strings $\mathbf{a_i}$ (resp. $\mathbf{b_j}$) from Σ_1 and Σ_2 have been linked.

As in Case 1.1, we easily verify that (Σ, R, F) satisfies Property 1.

Case 1.3: There is a chord $a_i c_j$ with $1 < i \leq p$ and $1 < j < r$ (see Fig. 11) If there are several chords $a_i c_j$, we consider one which maximizes i, i.e., there is no chord $a_k c_j$ with $i < k \leq p$. Let T_1 (resp. T_2) be the subgraph of T that lies inside the cycle $(a_1, a_2, \ldots, a_i, c_j, \ldots, c_r)$ (resp. $(c_j, a_i, \ldots, a_p, b_2, \ldots, b_q, c_2, \ldots, c_j)$). By Lemma 2, T_1 and T_2 are W-triangulations. Since T has no chord $a_x a_y$, $b_x b_y$, $c_x c_y$, or $a_k c_j$ with $k > i$, $(a_1, \ldots, a_i)$–(a_i, c_j)–$(c_j, \ldots, c_r)$ (resp. $(c_j, a_i, \ldots, a_p)$–$(b_1, \ldots, b_q)$–$(c_1, \ldots, c_j)$) is a 3-boundary of T_1 (resp. T_2). Furthermore, since $b_1 b_2 \notin E(T_1)$ and $a_1 a_2 \notin E(T_2)$, T_1 and T_2 have less edges than T, and Property 1 holds for T_1 and T_2 with the mentioned 3-boundaries. Let (Σ_1, R_1, F_1) (resp. (Σ_2, R_2, F_2)) be an anticlockwise PS-representation contained in the region τ_1 (resp. τ_2) obtained for T_1 (resp. T_2) with $F_1 = E_o(T_1) \setminus \{a_1 a_2\}$ (resp. $F_2 = E_o(T_2) \setminus \{c_j a_i\}$). In Fig. 12 we

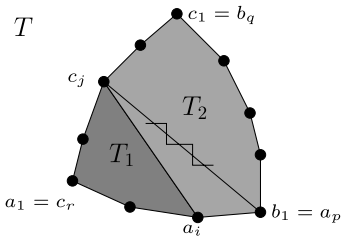

Fig. 11 Case 1.3: Chord $a_i c_j$

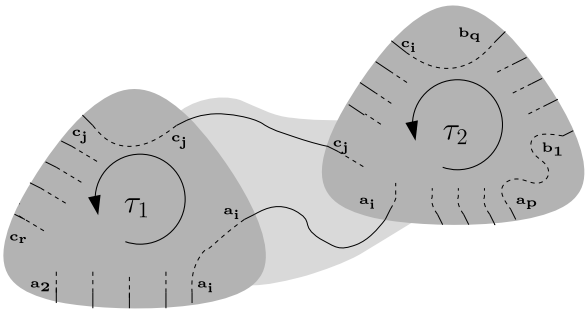

Fig. 12 Case 1.3: (Σ, R, F)

show how to associate these two representations to obtain (Σ, R, F), an anticlockwise PS-representation of T contained in τ. Note that in this construction the two strings $\mathbf{a_i}$ (resp. $\mathbf{c_j}$) from Σ_1 and Σ_2 have been linked.

As in Case 1.1, we easily verify that (Σ, R, F) satisfies Property 1.

Case 1.4: There is no chord $a_i b_j$ with $1 \le i \le p$ and $1 \le j \le q$, and no chord $a_i c_j$ with $1 \le i \le p$ and $1 \le j \le r$ (see Fig. 13) In this case we consider the adjacent path $(d_1, \ldots, d_s, a_1)$ (see Fig. 4) of T with respect to its 3-boundary, $(a_1, \ldots, a_p)$–$(b_1, \ldots, b_q)$–$(c_1, \ldots, c_r)$. Consider the edge $d_s a_y$ with $1 < y \le p$ and which minimizes y. This edge exists since, by the definition of the adjacent path, d_s is adjacent to some vertex a_y with $y > 1$. The W-triangulation $T_{d_s a_y}$ having less edges than T ($a_1 a_2 \notin E(T_{d_s a_y})$), Property 2 holds for $T_{d_s a_y}$. Let (Σ', R', F') be an anticlockwise PS-representation almost contained in the region τ' obtained for $T_{d_s a_y}$, with $F' = E_o(T_{d_s a_y}) \setminus \{d_s a_y\}$.

Now we distinguish two cases according to the position of a_y: either $y = 2$ (Case 1.4.1), or $y > 2$ (Case 1.4.2).

Case 1.4.1: $y = 2$ In Fig. 14, starting from (Σ', R', F'), we show how to extend the string $\mathbf{a_1} \in \Sigma'$ (in order to cross $\mathbf{d_s}$ and $\mathbf{a_2}$) and how to draw the (a_1, a_2, d_s)-region $\mathbf{a_1 a_2 d_s}$ to obtain (Σ, R, F), an anticlockwise PS-representation of T contained in a region τ.

One can verify on Fig. 14 that (Σ, R, F) satisfies Property 1.

Case 1.4.2: $y > 2$ Let us denote by $e_1, e_2, \ldots, e_t$ the neighbors of d_s strictly inside the cycle $(d_s, a_1, a_2, \ldots, a_y, d_s)$, going "from right to left" (see Fig. 13). By minimality of y we have $e_i \ne a_j$ for all $1 \le i \le t$ and $1 \le j \le y$.

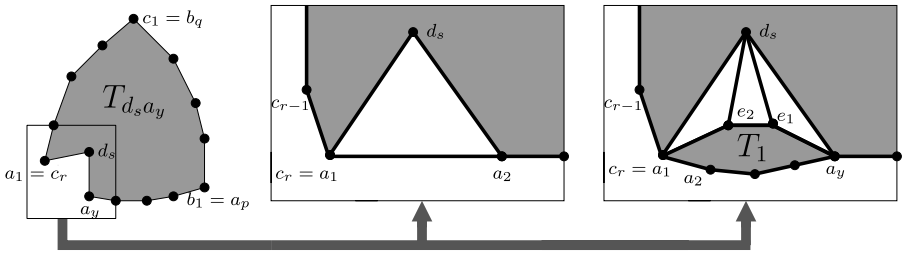

Fig. 13 Case 1.4: No chord $a_i b_j$ or $a_i c_j$

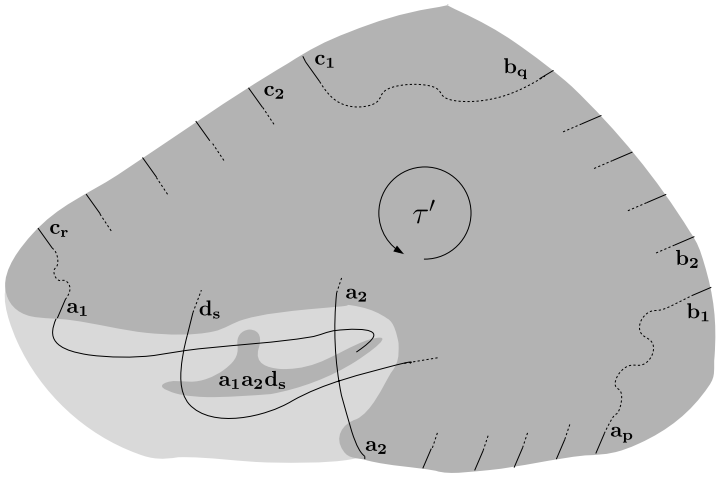

Fig. 14 Case 1.4.1

Let T_1 be the subgraph of T that lies inside the cycle $(a_1, \ldots, a_y, e_1, \ldots, e_t, a_1)$. By Lemma 2, T_1 is a W-triangulation. Since the W-triangulation T has no separating 3-cycle (d_s, a_1, e_i), (d_s, a_y, e_i), or (d_s, e_i, e_j), there exists no chord $a_1 e_i$, $a_y e_i$, or $e_i e_j$ in T_1. So (a_2, a_1)–$(a_1, e_t, \ldots, e_1, a_y)$–$(a_y, \ldots, a_2)$ is a 3-boundary of T_1. Finally, since T_1 has less edges than T ($a_1 d_s \notin E(T_1)$), Property 1 holds for T_1 with respect to the mentioned 3-boundary. Let (Σ_1, R_1, F_1) be a clockwise PS-representation contained in the region τ_1 obtained for T_1 with $F_1 = E_0(T_1) \setminus \{a_2 a_1\}$.

In Fig. 15, starting from (Σ', R', F') and (Σ_1, R_1, F_1), we show how to join the strings $\mathbf{a_1}$ (resp. $\mathbf{a_y}$) of Σ' and Σ_1, how to extend the strings $\mathbf{e_i}$ for $1 \le i \le t$, and how to draw the face-regions $\mathbf{a_y e_1 d_s}$, $\mathbf{e_t a_1 d_s}$, and $\mathbf{e_i e_{i-1} d_s}$ for $2 \le i \le t$, in order to obtain (Σ, R, F), an anticlockwise PS-representation of T contained in a region τ.

We verify that (Σ, R, F) satisfies Property 1:

- Σ is a string representation of $T \setminus F$ with $F = E_o(T) \setminus \{a_1 a_2\}$. Indeed, since $V(T_{d_s a_y}) \cup V(T_1) = V(T)$ and $V(T_{d_s a_y}) \cap V(T_1) = \{a_1, a_y\}$, every vertex $v \in V(T)$ has exactly one string in Σ. Furthermore, since $E(T) \setminus F = (E(T_{d_s a_y}) \setminus F') \cup (E(T_1) \setminus F_1) \cup \{a_y e_1, e_t a_1, d_s a_1\} \cup \{e_i e_{i-1} \mid i \in [2, t]\} \cup \{d_s e_i \mid i \in [1, t]\}$, Σ is a string representation of $T \setminus F$.

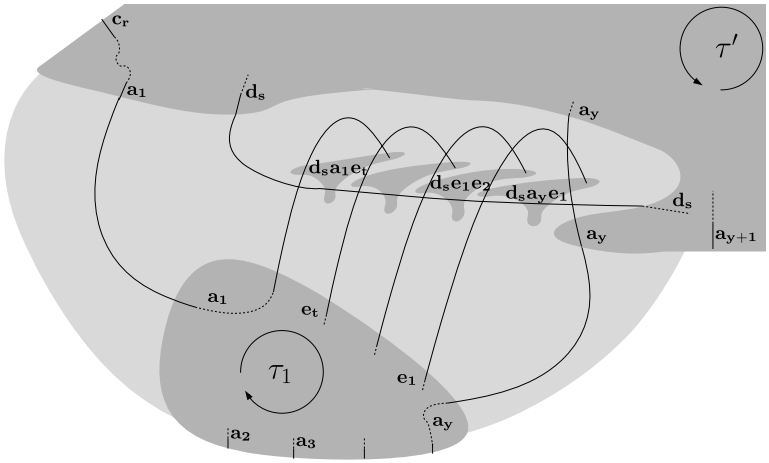

Fig. 15 Case 1.4.2

- Σ is a 1-string representation. Indeed $T_{d_s a_y}$ and T_1 do not have common edges, and the new crossings added correspond to edges missing in both $E(T_{d_s a_y}) \setminus F'$ and $E(T_1) \setminus F_1$.
- (Σ, R) is "strong": The only inner-faces of T not in $T_{d_s a_y}$ nor in T_1 are the faces $d_s a_y e_1$, $d_s a_1 e_t$, and $d_s e_i e_{i+1}$ with $1 \leq i < t$. These faces correspond to the new face-regions.

Finally we see in Fig. 15 that point (b) of Property 1 is satisfied.

So Property 1 holds for any W-triangulation T with m edges, and this concludes the proof of Case 1.

Case 2: Proof of Property 2 for a W-triangulation $T_{d_x a_y}$ with m edges Recall that the W-triangulation $T_{d_x a_y}$ is a subgraph of a W-triangulation T with 3-boundary $(a_1, \ldots, a_p)$–$(b_1, \ldots, b_q)$–$(c_1, \ldots, c_r)$. Moreover, T has no chord $a_i b_j$ or $a_i c_j$, and its adjacent path is $(d_1, \ldots, d_s, a_1)$, with $s \geq 1$. We distinguish the case where $d_x a_y = d_1 a_p$ and the case where $d_x a_y \neq d_1 a_p$.

Case 2.1: $d_x a_y = d_1 a_p$ (see Fig. 16) Let T_1 be the subgraph of $T_{d_1 a_p}$ that lies inside the cycle $(a_1, d_s, \ldots, d_1, b_2, \ldots, b_q, c_2, \ldots, c_r)$. By Lemma 2, T_1 is a W-triangulation. This W-triangulation has no chord $b_i b_j$, $c_i c_j$, $d_i d_j$, or $a_1 d_j$. We consider two cases according to the existence of an edge $d_1 b_i$ with $2 < i \leq q$.

- If T_1 has no chord $d_1 b_i$, then $(d_1, b_2, \ldots, b_q)$–$(c_1, \ldots, c_r)$–$(a_1, d_s, \ldots, d_1)$ is a 3-boundary of T_1.
- If T_1 has a chord $d_1 b_i$ with $2 < i \leq q$, note that $q > 2$ and that there cannot be a chord $b_2 a_1$ or $b_2 d_j$ with $1 < j \leq s$ (this would violate the planarity of $T_{d_x a_y}$, see Fig. 16). So in this case, $(b_2, d_1, \ldots, d_s, a_1)$–$(c_r, \ldots, c_1)$–$(b_q, \ldots, b_2)$ is a 3-boundary of T_1.

Finally, since T_1 is a W-triangulation with less edges than $T_{d_1 a_p}$ ($b_1 b_2 \notin E(T_1)$), Property 1 holds for T_1 with respect to at least one of the two mentioned 3-boundaries.

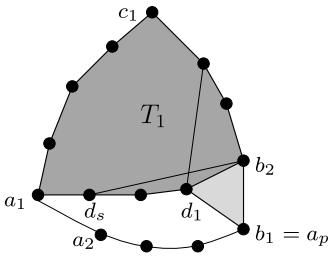

Fig. 16 Case 2.1: $T_{d_x a_y} = T_{d_1 a_p}$

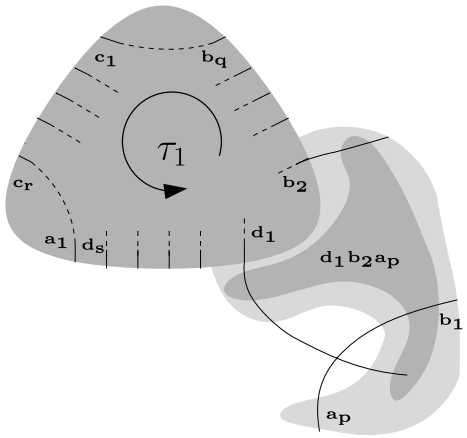

Fig. 17 Case 2.1: (Σ, R, F)

Whichever 3-boundary we consider, we obtain a PS-representation (Σ_1, R_1, F_1) of T_1 contained in a region τ_1, with the same following characteristics:

- $F_1 = E_o(T) \setminus \{d_1 b_2\}$,
- in the boundary of τ_1, we successively meet the ends of $\mathbf{d_1}, \ldots, \mathbf{d_s}, \mathbf{a_1}, \mathbf{c_r}, \ldots, \mathbf{c_1}$, $\mathbf{b_q}, \ldots, \mathbf{b_2}$ (clockwise or anticlockwise).

In Fig. 17 we modify (Σ_1, R_1, F_1), by extending the strings $\mathbf{d_1}$ and $\mathbf{b_2}$ and by adding a new string $\mathbf{a_p}$ and a new face-region $\mathbf{d_1 b_2 a_p}$. This leads to (Σ, R, F), a PS-representation of $T_{d_1 a_p}$ contained in a region τ.

We verify that (Σ, R, F) satisfies Property 2:

- Σ is a 1-string representation of $T_{d_1 a_p} \setminus F$: Indeed, $E(T_{d_1 a_p}) \setminus F$ is the disjoint union of $E(T_1) \setminus F_1$ and $\{a_p d_1\}$.
- (Σ, R) is "strong": The only inner-face of $T_{d_1 a_p}$ that is not an inner-face of T_1 is $d_1 a_p b_2$, which corresponds to the new face-region $\mathbf{d_1 a_p b_2}$.

Finally we see in Fig. 17 that the other points of Property 2 are satisfied.

Case 2.2: $T_{d_x a_y} \neq T_{d_1 a_p}$ In this case we consider an edge $d_z a_w \in E(T_{d_x a_y})$ such that $d_z a_w \neq d_x a_y$. Among all the possible edges $d_z a_w$, we choose the one that first maximizes z and then minimizes w. Such an edge necessarily exists, and actually one can see that $d_z = d_x$ or $d_z = d_{x-1}$. Indeed, if $d_x = d_1$, there is at least one edge $d_1 a_w$ with $w > y$, the edge $d_1 a_p$. If $x > 1$, it is clear by the definition of the adjacent path that the vertex d_{x-1} is adjacent to at least one vertex a_w with $w \geq y$.

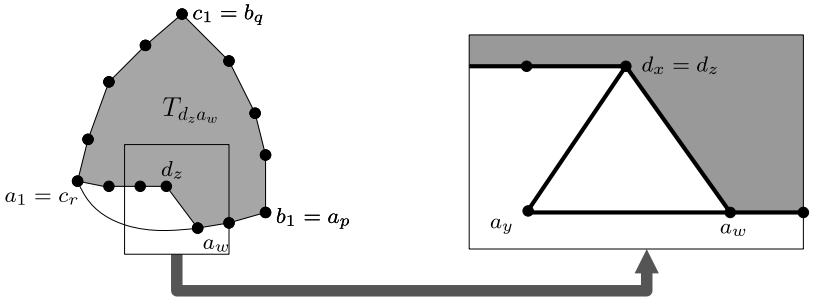

Fig. 18 Case 2.2.1: $z = x$ and $w = y + 1$

Fig. 19 Case 2.2.1: (Σ, R, F)

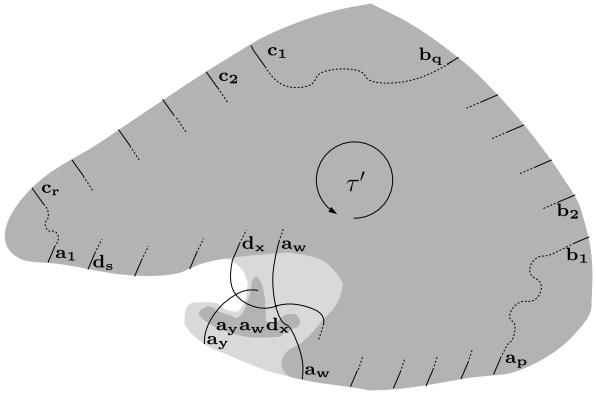

By Lemma 2, $T_{d_z a_w}$ is a W-triangulation. Since $d_x a_y \notin E(T_{d_z a_w})$, the W-triangulation $T_{d_z a_w}$ has less edges than $T_{d_x a_y}$, and so Property 2 holds for $T_{d_z a_w}$. Let (Σ', R', F') be an anticlockwise PS-representation almost contained in the region τ' obtained for $T_{d_z a_w}$ with $F' = E_o(T_{d_z a_w}) \setminus \{d_z a_w\}$.

We distinguish four cases according to the edge $d_z a_w$. When $z = x$, we consider the case where $w = y+1$ and the case where $w > y+1$. When $z = x-1$, we consider the case where $w = y$ and the case where $w > y$.

Case 2.2.1: $T_{d_x a_y} \neq T_{d_1 a_p}$, $z = x$, and $w = y + 1$ (see Fig. 18) In Fig. 19 we modify (Σ', R', F') by adding a new string $\mathbf{a_y}$ and a new face-region $\mathbf{a_y a_w d_x}$. This leads to (Σ, R, F), an anticlockwise PS-representation of $T_{d_x a_y}$ almost contained in a region τ.

We verify that (Σ, R, F) satisfies Property 2:

- Σ is a 1-string representation of $T_{d_x a_y} \setminus F$: Indeed, $E(T_{d_x a_y}) \setminus F$ is the disjoint union of $E(T_{d_z a_w}) \setminus F'$ and $\{d_x a_y\}$.
- (Σ, R) is "strong": The only inner-face of $T_{d_x a_y}$ that is not an inner-face of $T_{d_z a_w}$ is $d_x a_y a_w$, which corresponds to the new face-region $\mathbf{d_x a_y a_w}$.

Finally we see in Fig. 19 that the other points of Property 2 are satisfied.

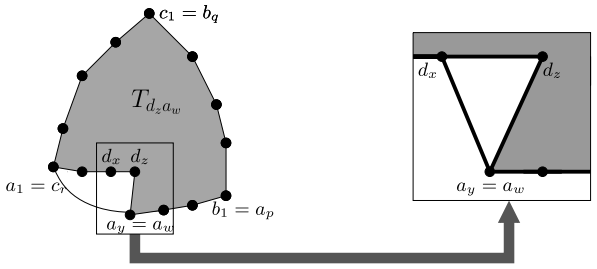

Fig. 20 Case 2.2.2: $T_{d_x a_y} \neq T_{d_1 a_p}$, $z = x - 1$, and $w = y$

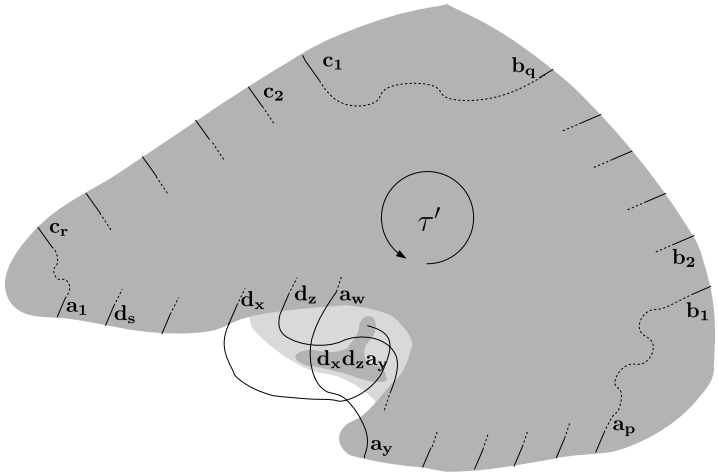

Fig. 21 Case 2.2.2: (Σ, R, F)

Case 2.2.2: $z = x - 1$ and $w = y$ (see Fig. 20) In Fig. 21, we modify (Σ', R', F') by extending the string $\mathbf{d_x}$ and by adding a new face-region $\mathbf{d_x d_z a_y}$. This leads to (Σ, R, F), an anticlockwise PS-representation of $T_{d_x a_y}$ almost contained in a region τ.

We verify that (Σ, R, F) satisfies Property 2:

- Σ is a 1-string representation of $T_{d_x a_y} \setminus F$: Indeed, $E(T_{d_x a_y}) \setminus F$ is the disjoint union of $E(T_{d_z a_w}) \setminus F'$ and $\{d_x d_z, d_x a_y\}$.
- (Σ, R) is "strong": The only inner-face of $T_{d_x a_y}$ that is not an inner-face of $T_{d_z a_w}$ is $d_x d_z a_y$, which corresponds to the new face-region $\mathbf{d_x d_z a_y}$.

Finally we see in Fig. 21 that the other points of Property 2 are satisfied.

Case 2.2.3: $z = x$ and $w > y + 1$ (see Fig. 22) Let us denote by $e_1, e_2, \ldots, e_t$ the neighbors of d_x strictly inside the cycle $(d_x, a_y, \ldots, a_w, d_x)$, going "from right to left" (see Fig. 22). Since there is no chord $a_i a_j$, we have $t \geq 1$. Furthermore by minimality of w we have $e_i \neq a_j$ for all $1 \leq i \leq t$ and $y \leq j \leq w$. Let T_1 be the subgraph of $T_{d_x a_y}$ that lies inside the cycle $(a_y, \ldots, a_w, e_1, \ldots, e_t, a_y)$. By Lemma 2, T_1 is a W-triangulation. Since the W-triangulation $T_{d_x a_y}$ has no separating 3-cycle (d_x, a_w, e_i) or (d_x, e_i, e_j), there exists no chord $a_w e_i$ or $e_i e_j$ in T_1. With the fact that

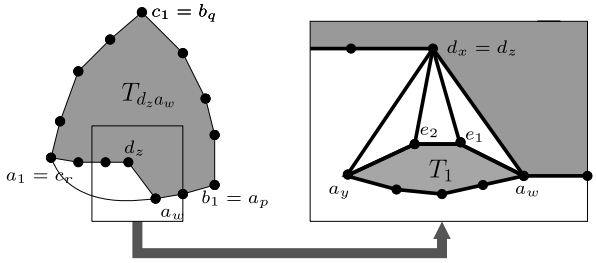

Fig. 22 Case 2.2.3: $T_{d_x a_y} \neq T_{d_1 a_p}$, $z = x$, and $w > y + 1$

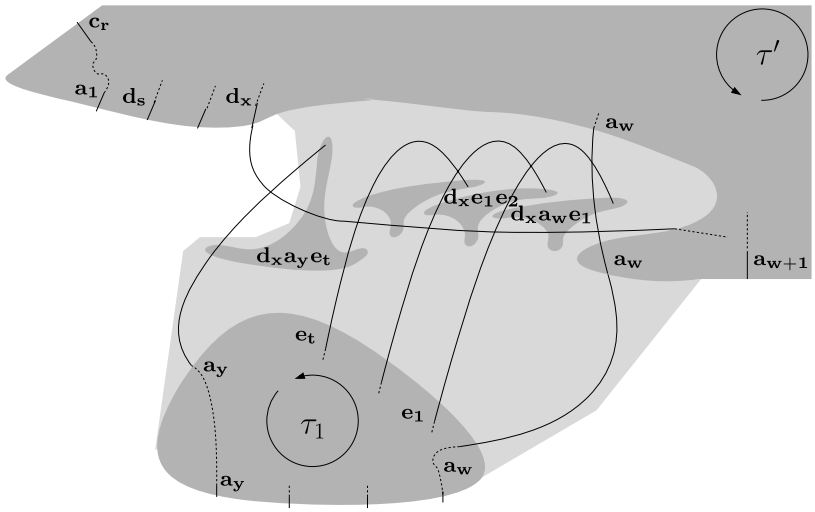

Fig. 23 Case 2.2.3: (Σ, R, F)

$t \geq 1$, we know that (e_t, a_y)–$(a_y, \ldots, a_w)$–$(a_w, e_1, \ldots, e_t)$ is a 3-boundary of T_1. Finally, since T_1 has less edges than $T_{d_x a_y}$ ($d_x a_y \notin E(T_1)$), Property 1 holds for T_1 with respect to the mentioned 3-boundary. Let (Σ_1, R_1, F_1) be an anticlockwise PS-representation contained in the region τ_1 obtained for T_1 with $F_1 = E_0(T_1) \setminus \{e_t a_y\}$.

In Fig. 23, starting from (Σ', R', F') and (Σ_1, R_1, F_1), we show how to join the strings $\mathbf{a_w}$ of Σ' and Σ_1, how to extend the string $\mathbf{a_y}$ and the strings $\mathbf{e_i}$ for $1 \leq i \leq t$, and how to draw the face-regions $\mathbf{a_y e_t d_x}$, $\mathbf{e_1 a_w d_x}$, and $\mathbf{e_i e_{i-1} d_x}$ for $1 < i \leq t$, in order to obtain (Σ, R, F), an anticlockwise PS-representation of $T_{d_x a_y}$ contained in a region τ.

We verify that (Σ, R, F) satisfies Property 2:

- Σ is a 1-string representation of $T_{d_x a_y} \setminus F$ with $F = E_o(T_{d_x a_y}) \setminus \{d_x a_y\}$: Indeed, $E(T_{d_x a_y}) \setminus F$ is the disjoint union of $E(T_{d_z a_w}) \setminus F'$, $E(T_1) \setminus F_1$, and $\{a_w e_1, d_x a_y\} \cup \{e_i e_{i-1} \mid i \in [2, t]\} \cup \{d_x e_i \mid i \in [1, t]\}$.
- (Σ, R) is "strong": The only inner-faces of $T_{d_x a_y}$ that are not inner-faces in $T_{d_z a_w}$ or T_1 are $d_x a_y e_t$, $d_x a_w e_1$, and the faces $d_x e_i e_{i-1}$ for $2 \leq i \leq t$, which correspond to the new face-regions.

Finally we see in Fig. 23 that the other points of Property 2 are satisfied.

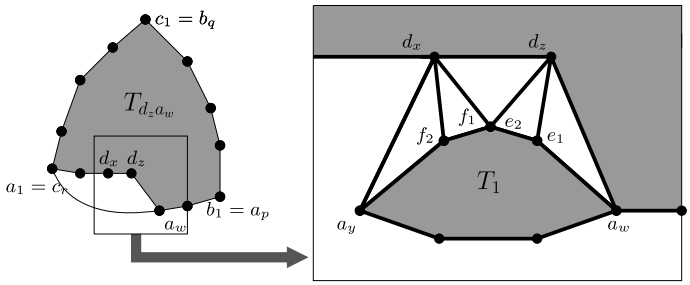

Fig. 24 Case 2.2.4: $T_{d_x a_y} \neq T_{d_1 a_p}$, $z = x - 1$, and $w > y$

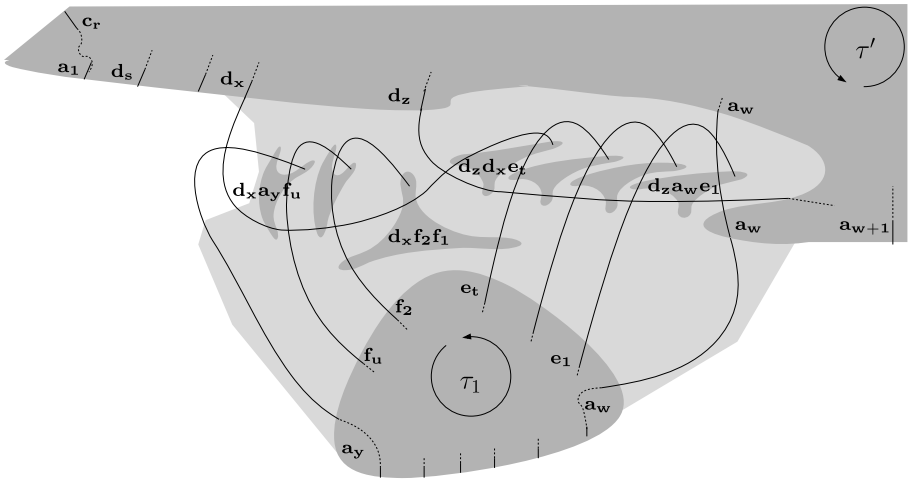

Fig. 25 Case 2.2.4: (Σ, R, F)

Case 2.2.4: $z = x - 1$ and $w > y$ (see Fig. 24) Let us denote by $e_1, e_2, \ldots, e_t$ the neighbors of d_z strictly inside the cycle $(d_z, d_x, a_y, \ldots, a_w, d_z)$, going "from right to left" (see Fig. 24). By maximality of z, there is no edge $d_x a_w$, so $t \geq 1$. Let us denote by $f_1, \ldots, f_u$ the neighbors of d_x strictly inside the cycle $(d_x, a_y, \ldots, a_w, d_z, d_x)$, going "from right to left" (see Fig. 24). Note that $f_1 = e_t$ and that by minimality of w, there is no edge $d_z a_y$, so $u \geq 1$.

By minimality of w (resp. maximality of z) we have $e_i \neq a_j$ (resp. $f_i \neq a_j$) for all $1 \leq i \leq t$ (resp. $1 \leq i \leq u$) and $y \leq j \leq w$. Let T_1 be the subgraph of $T_{d_x a_y}$ that lies inside the cycle $(a_y, \ldots, a_w, e_1, \ldots, e_t, f_2, \ldots, f_u, a_y)$. By Lemma 2, T_1 is a W-triangulation. Since the W-triangulation $T_{d_x a_y}$ has no separating 3-cycle (d_z, a_w, e_i), (d_z, e_i, e_j), (d_x, f_i, f_j), or (d_x, f_i, a_y), there exists no chord $a_w e_i$, $e_i e_j$, $f_i f_j$, or $f_i a_y$ in T_1. With the fact that $t \geq 1$ and $u \geq 1$, we know that $(f_1, f_2, \ldots, f_u, a_y)$–$(a_y, \ldots, a_w)$–$(a_w, e_1, \ldots, e_t)$ is a 3-boundary of T_1. Finally, since T_1 has less edges than $T_{d_x a_y}$ ($d_x a_y \notin E(T_1)$), Property 1 holds for T_1 with respect to the mentioned 3-boundary. Let (Σ_1, R_1, F_1) be an anticlockwise PS-representation contained in the region τ_1 obtained for T_1 with $F_1 = E_0(T_1) \setminus \{f_1 f_2\}$.

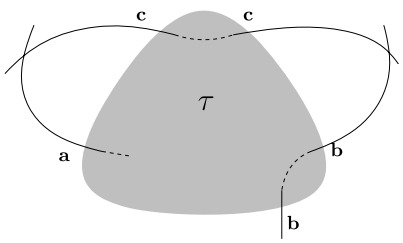

Fig. 26 S-representation of T from (Σ, R, F)

In Fig. 25, starting from (Σ', R', F') and (Σ_1, R_1, F_1), we show how to join the strings $\mathbf{a_w}$ of Σ' and Σ_1, how to extend the string $\mathbf{d_x}$, $\mathbf{a_y}$, the strings $\mathbf{e_i}$ for $1 \leq i \leq t$, and the strings $\mathbf{f_i}$ for $2 \leq i \leq u$, and how to draw the face-regions $\mathbf{d_z a_w e_1}$, $\mathbf{d_z e_i e_{i-1}}$ for $2 \leq i \leq t$, $\mathbf{d_z d_x e_t}$, $\mathbf{d_x f_i f_{i-1}}$ for $2 \leq i \leq u$, and $\mathbf{d_x a_y f_u}$ in order to obtain (Σ, R, F), an anticlockwise PS-representation of $T_{d_x a_y}$ almost contained in a region τ.

We verify that (Σ, R, F) satisfies Property 2:

- Σ is a 1-string representation of $T_{d_x a_y} \setminus F$ with $F = E_o(T_{d_x a_y}) \setminus \{d_x a_y\}$: Indeed, $E(T_{d_x a_y}) \setminus F$ is the disjoint union of $E(T_{d_z a_w}) \setminus F'$, $E(T_1) \setminus F_1$, and $\{d_x a_y, d_x d_z, a_w e_1, a_y f_u\} \cup \{d_z e_i \mid i \in [1,t]\} \cup \{d_x f_i \mid i \in [1,u]\} \cup \{e_i e_{i-1} \mid i \in [2,t]\} \cup \{f_i f_{i-1} \mid i \in [2,u]\}$.
- (Σ, R) is "strong": The only inner-faces of $T_{d_x a_y}$ that are not inner-faces in $T_{d_z a_w}$ or T_1 are $d_z a_w e_1$, $d_z e_i e_{i-1}$ for $2 \leq i \leq t$, $d_z d_x e_t$, $d_x f_i f_{i-1}$ for $2 \leq i \leq u$, and $d_x a_y f_u$, which correspond to the new face-regions.

Finally we see in Fig. 25 that the other points of Property 2 are satisfied. So, Property 2 holds for any W-triangulation $T_{d_x a_y}$ with m edges, and this completes the proofs of Properties 1 and 2.

4 Proof in the General Case

Theorem 3 *Every triangulation T admits an S-representation (Σ, R).*

Proof We prove this result by induction on the number of separating 3-cycles. Note that any triangulation T is 3-connected and that if T has no separating 3-cycle, then T is 4-connected and is a W-triangulation. Consequently, if T is a 4-connected triangulation whose outer-vertices are a, b, and c, then T is a W-triangulation 3-bounded by (a,b)–(b,c)–(c,a). By Property 1, T admits a PS-representation (Σ, R, F), with $F = \{bc, ca\}$, that is contained in a region τ. Furthermore, in the boundary of τ, we successively meet the ends of $\mathbf{b}, \mathbf{b}, \mathbf{c}, \mathbf{c}, \mathbf{a}$. To obtain an S-representation of T, it is sufficient to extend $\mathbf{a}$, $\mathbf{b}$, and $\mathbf{c}$ outside of τ so that $\mathbf{c}$ crosses $\mathbf{a}$ and $\mathbf{b}$, as depicted in Fig. 26.

Suppose now that T is a triangulation that contains at least one separating 3-cycle. Consider a separating 3-cycle (a,b,c) such that there is no other separating 3-cycle lying inside. This implies that the triangulation T' induced by the vertices on and inside (a,b,c) is 4-connected.

Let T_1 be the triangulation obtained by removing the vertices lying strictly inside (a,b,c). Let T_2 be the subgraph of T induced by the vertices lying strictly inside

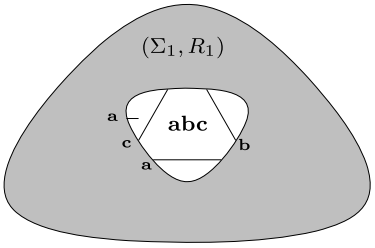

Fig. 27 In the S-representation (Σ_1, R_1) of T_1, the (a, b, c)-region **abc**

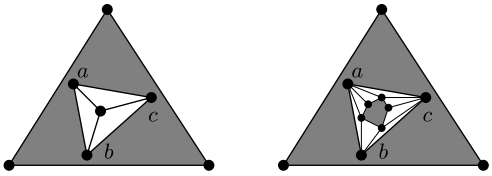

Fig. 28 The cases (A) and (B)

(a, b, c) (i.e., $T_2 = T' \setminus \{a, b, c\}$). In T_1, the cycle (a, b, c) is a face of the triangulation and is no more a separating 3-cycle. Thus, T_1 has one separating cycle less than T, and so we have by induction hypothesis that T_1 admits an S-representation (Σ_1, R_1). This S-representation contains a face-region **abc** corresponding to the face abc. Without loss of generality, say that **abc** is an (a, b, c)-region, as depicted in Fig. 27.

Since T' is a triangulation with at least four vertices, the neighbors of any vertex $v \in V(T')$ induce a cycle. Suppose that the vertex a (resp. b and c) has exactly one neighbor v that lies inside (a, b, c). Then there exists a cycle (b, v, c) (resp. (a, v, c) and (a, v, b)) in T', and consequently v is a neighbor of a, b, and c in T'. Suppose that there exists another vertex w in T', then w lies either inside the cycle (a, v, b), inside (a, v, c), or inside (b, v, c), and then one of these cycles is a separating 3-cycle. This is impossible by definition of (a, b, c). So we can distinguish two cases (see Fig. 28), (A) the case where T_2 is a single vertex, and (B) the case where each of the vertices a, b, and c has at least two neighbors inside (a, b, c).

Case (A): T_2 is a single vertex v To obtain an S-representation (Σ, R) of T (see Fig. 29), we add a string **v** in (Σ_1, R_1). Since $E(T) \setminus E(T_1) = \{va, vb, vc\}$, this string **v** crosses **a**, **b**, **c**. Moreover, we also define three disjoint face-regions **acv**, **vbc**, **vab** that correspond respectively to the faces acv, vbc, vab.

Since (Σ_1, R_1) is an S-representation of T_1 and since **v**, **acv**, **vbc**, **vab** are drawn inside **abc**, it is clear that $(\Sigma \cup \{\mathbf{v}\}, (R \setminus \{\mathbf{abc}\}) \cup \{\mathbf{acv}, \mathbf{vbc}, \mathbf{vab}\})$ is an S-representation of T.

Case (B): Each of the vertices a, b, and c has at least two neighbors inside (a, b, c) There exists a cycle $(c, a_1, \ldots, a_p, b)$ (resp. $(a, b_1, \ldots, b_q, c)$ and $(b, c_1, \ldots, c_r, a)$) in T' whose vertices are exactly the neighbors of a (resp. b and c). We already know that $p > 1, q > 1$, and $r > 1$ and that $a_p = b_1$, $b_q = c_1$, and $c_r = a_1$. Moreover, since b_1 and c (resp. c_1 and a, and a_1 and b) are the only two common neighbors of a and b (resp. b and c, and a and c) in T' (otherwise there would be a separating 3-cycle),

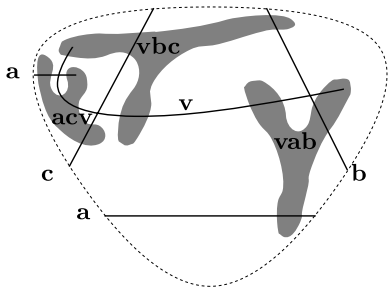

Fig. 29 Case (A): Modifications inside **abc**

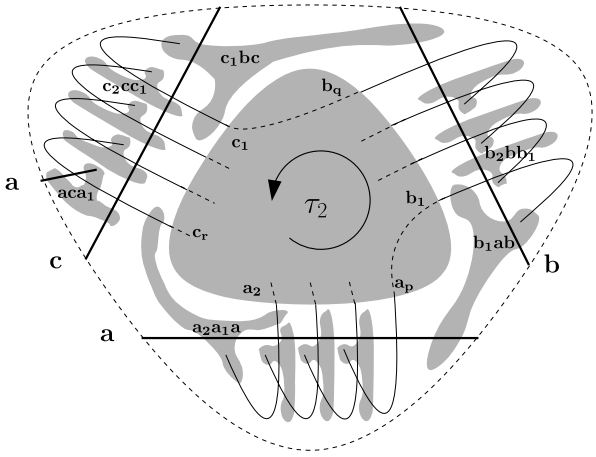

Fig. 30 Case (B): Modifications inside **abc**

we have that $(a_1, \ldots, a_p = b_1, \ldots, b_q = c_1, \ldots, c_r = a_1)$ is a cycle. This implies by Lemma 2 that T_2 is a W-triangulation.

Suppose that there exists an edge $a_i a_j$ (resp. $b_i b_j$, $c_i c_j$) with $1 < i + 1 < j \leq p$ (resp. $1 < i + 1 < j \leq q$, $1 < i + 1 < j \leq r$). Then, the cycle (a, a_i, a_j) (resp. (b, b_i, b_j), (c, c_i, c_j)) would be a separating 3-cycle of T'. Consequently, T_2 is 3-bounded by $(a_1, \ldots, a_p)$–$(b_1, \ldots, b_q)$–$(c_1, \ldots, c_r)$. With respect to this 3-boundary, T_2 has an anticlockwise PS-representation (Σ_2, R_2, F_2) with $F_2 = E_o \setminus \{a_1 a_2\}$ (cf. Property 1). Let τ_2 be a region of **abc** containing this representation.

Since **abc** is an (a, b, c)-region, on its boundary we successively cross **a**, **a**, **b**, **b**, **c**, **a**, and **c** when going anticlockwise (by doing an axial symmetry if necessary).

In Fig. 30, starting from (Σ_1, R_1) and (Σ_2, R_2), we obtain (Σ, R). We extend the strings $\mathbf{a_2}, \ldots, \mathbf{a_p}, \mathbf{b_1}, \ldots, \mathbf{b_q}, \mathbf{c_1}, \ldots, \mathbf{c_r}$ to obtain the crossings that correspond to the edges in the set $E(T) \setminus (E(T_1) \cup (E(T_2) \setminus F_2)) = \{aa_i \mid i \in [1, p]\} \cup \{bb_i \mid i \in [1, q]\} \cup \{cc_i \mid i \in [1, r]\} \cup \{a_i a_{i+1} \mid i \in [2, p-1]\} \cup \{b_i b_{i+1} \mid i \in [1, q-1]\} \cup \{c_i c_{i+1} \mid i \in [1, r-1]\}$. We also define face-regions for the faces in the set $\{abb_1, aca_1, bcc_1\} \cup \{aa_i a_{i+1} \mid i \in [1, p-1]\} \cup \{bb_i b_{i+1} \mid i \in [1, q-1]\} \cup \{cc_i c_{i+1} \mid i \in [1, r-1]\}$.

Since (Σ_1, R_1) is an S-representation of T_1 and (Σ_2, R_2, F_2) is a PS-representation of T_2, (Σ, R, F) is an S-representation of T.

- Σ is a 1-string representation of T: Indeed, we added all the crossings corresponding to the edges in $E(T) \setminus (E(T_1) \cup (E(T_2) \setminus F_2))$.

- (Σ, R) is "strong": Indeed, we added all the face-regions corresponding to the inner-faces of T that are neither in T_1 nor in T_2.

Consequently, every triangulation admits an S-representation, which proves Theorem 3 and then Theorem 2. □

5 Conclusion

The first and the second author recently improved the result presented in this article by proving Conjecture 1 [2]. For this, they use the same decomposition of triangulation, but their notion of face-region is quite different. One should also mention that their construction does not correspond to a stretching of the 1-string representation presented here.

Finally, an interesting question is whether the result presented here holds for other surfaces. For example, does any graph embedded on a surface $\mathbb{S}$ have a 1-string representation on $\mathbb{S}$?

References

1. de Castro, N., Cobos, F., Dana, J.C., Márquez, A., Noy, M.: Triangle-free planar graphs as segment intersection graphs. J. Graph Algorithms Appl. **6**(1), 7–26 (2002)
2. Chalopin, J., Gonçalves, D.: Every planar graph is the intersection graph of segments in the plane. In: Proceedings of the 41st Annual ACM Symposium on Theory of Computing (2009)
3. Ehrlich, G., Even, S., Tarjan, R.E.: Intersection graphs of curves in the plane. J. Combin. Theory., Ser. B **21**, 8–20 (1976)
4. de Fraysseix, H., Ossona de Mendez, P., Pach, J.: Representation of planar graphs by segments. Intuit. Geom. (Szeged, 1991), Colloq. Math. Soc. János Bolyai **63**, 109–117 (1994)
5. de Fraysseix, H., Ossona de Mendez, P.: Intersection graphs of Jordan arcs. DIMACS Ser. Discrete Math. Theor. Comput. Sci. **49**, 11–28 (1999)
6. de Fraysseix, H., Ossona de Mendez, P.: Representations by contact and intersection of segments. Algorithmica **47**(4), 453–463 (2007)
7. Gonçalves, D.: Edge-partition of planar graphs into two outerplanar graphs. In: Proceedings of the 37th Annual ACM Symposium on Theory of Computing, pp. 504–512 (2005)
8. Hartman, I.B.-A., Newman, I., Ziv, R.: On grid intersection graphs. Discrete Math. **87**(1), 41–52 (1991)
9. Koebe, P.: Kontaktprobleme der Konformen Abbildung. Ber. Sächs. Akad. Wiss. Leipzig, Math.—Phys. Kl. **88**, 141–164 (1936)
10. Scheinerman, E.R.: Intersection classes and multiple intersection parameters of graphs. PhD Thesis, Princeton University (1984)
11. West, D.: Open problems. SIAM J. Discrete Math. Newslett. **2**(1), 10–12 (1991)
12. Whitney, H.: A theorem on graphs. Ann. Math. (2) **32**(2), 378–390 (1931)

Planar Graphs as L-intersection or L-contact graphs*

Daniel Gonçalves[a], Lucas Isenmann[a], and Claire Pennarun[a]

[a] *LIRMM, CNRS & Univ. de Montpellier, France.*

Abstract

The $\llcorner$-*intersection graphs* are the graphs that have a representation as intersection graphs of axis-parallel $\llcorner$ shapes in the plane. A subfamily of these graphs are $\{\llcorner, |, -\}$-*contact graphs* which are the contact graphs of axis parallel $\llcorner$, $|$, and $-$ shapes in the plane. We prove here two results that were conjectured by Chaplick and Ueckerdt in 2013. We show that planar graphs are $\llcorner$-intersection graphs, and that triangle-free planar graphs are $\{\llcorner, |, -\}$-contact graphs. These results are obtained by a new and simple decomposition technique for 4-connected triangulations. Our results also provide a much simpler proof of the known fact that planar graphs are segment intersection graphs.

1 Introduction

The representation of graphs by contact or intersection of predefined shapes in the plane is a broad subject of research since the work of Koebe on the representation of planar graphs by contacts of circles [28]. In particular, the class of planar graphs has been widely studied in this context.

Given a shape[1] X, an X-*intersection representation* is a collection of X-shaped geometrical objects in the plane. The X-*intersection graph* described by such a representation has one vertex per geometrical object, and two vertices are adjacent if and only if the corresponding objects intersect. In the case where the shape X defines objects that are homeomorphic to a segment (resp. to a disc), an X-*contact representation* is an X-intersection representation such that if an intersection occurs between two objects, then it occurs at a single point that is the endpoint of one of them (resp. it occurs on their boundary). We say that a graph G is an X-*contact graph* if it is the X-intersection graph of an X-contact representation.

The case of shapes homeomorphic to discs has been widely studied; see for example the literature for triangles [19, 23], homothetic triangles [25, 35], axis parallel rectangles [36], squares [26, 33], hexagons [22], convex bodies [34], or axis aligned polygons [2]. Here, we focus on intersection and contact representations of planar graphs with objects that are homeomorphic to a segment. The more general representations of this type are the intersection or contact representation with curves. those are called *string* representations. It is known that every planar graph has a string-intersection representation [28]. However, if one forbids tangent curves, this representation may contain pairs of curves that cross several times. One may thus take an additional parameter into account, namely the maximal number of crossings of any two of the curves: a *1-string* representation of a graph is a string representation where every two curves intersect at most once. The question of finding a 1-string representation of planar graphs has been solved by Chalopin et al. in the positive [11], and additional parameters are now studied, like order-preserving representations [8].

Segment intersection graphs are in turn a specialization of the class of 1-string graphs. It is known that bipartite planar graphs are $\{|, -\}$-contact graphs [4, 18] (i.e., segment contact graphs with vertical or horizontal segments). De Castro et al. [16] showed that triangle-free planar graphs are segment contact graphs with only three different slopes. De Fraysseix and Ossona de Mendez [17] then proved that a larger class of planar graphs are segment intersection graphs. Finally, Chalopin and the first author extended this result to general planar graphs [10], which was conjectured by Scheinerman in his PhD thesis [32].

A graph is said to be a *VPG-graph* (Vertex-Path-Grid) if it has a contact or intersection representation in which each vertex is assigned to a path of vertical and horizontal segments (see [1, 15]). Asinowski et al. [3] showed that the class of VPG-graphs is equivalent to the class of graphs admitting a string-representation. They also defined the class B_k-*VPG*, which contains all VPG-graphs for which each vertex is represented by a path with at most k bends (see [20] for the determination of

*This research is partially supported by the ANR GATO, under contract ANR-16-CE40-0009.

[1] We do not provide a formal definition of *shape*, but a shape characterizes a family of connected geometric objects in the plane.

the value of k for some classes of graphs). It is known that B_k-VPG $\subsetneq B_{k+1}$-VPG, and that the recognition of graphs of B_k-VPG is an NP-complete problem [12]. These classes have interesting algorithmic properties (see [29] for approximation algorithms for independence and domination problems in B_1-VPG graphs), but most of the literature studies their combinatorial properties.

Chaplick and Ueckerdt [14] proved that planar graphs are B_2-VPG graphs. This result was recently improved by Biedl and Derka [6], as they showed that planar graphs have a 1-string B_2-VPG representation.

Various classes of graphs have been shown to have 1-string B_1-VPG representations, such as planar partial 3-trees [5] and Halin graphs [21]. In these representations, each vertex is assigned to a path formed by at most one horizontal and one vertical segment. There are different types of such paths. For example, the $\llcorner$ shape defines paths where the vertical segment is above and to the left of the horizontal one. Interestingly, it has been shown that the class of segment contact graphs is equivalent to the one of B_1-VPG contact graphs [27]. This implies in particular that triangle-free planar graphs are B_1-VPG contact graphs. This has been improved by Chaplick et al. [14] as they showed that triangle-free planar graphs are in fact $\{\llcorner, \ulcorner, |, -\}$-contact graphs (that is without using the shapes $\lrcorner$ and $\urcorner$). In the following, we will always precise when $|$ or $-$ shapes are allowed. This is specially important as for example some $\{\llcorner, |, -\}$-contact graphs like the octaedron are not $\llcorner$-contact graphs.

The restriction of B_1-VPG to $\llcorner$-intersection or $\llcorner$-contact graphs has been much studied (see for example [20]) and it has been shown that they are in relation with other structures such as Schnyder realizers, canonical orders or edge labelings [13]. The same authors also proved that the recognition of $\llcorner$-contact graphs can be done in quadratic time, and that this class is equivalent to the one restricted to equilateral $\llcorner$ shapes. The $\llcorner$-contact graphs where the corners lie on a straight line are called *monotone* or *linear* $\llcorner$-contact graphs. Those graphs have been recently studied further, in particular in relation with MPT (Max-Point Tolerance) graphs [9, 31].

Our contributions The two main results of this paper are the following:

THEOREM 1.1. *Every triangle-free planar graph is an $\{\llcorner, |, -\}$-contact graph.*

THEOREM 1.2. *Every planar graph is an $\llcorner$-intersection graph.*

Both results were conjectured in [14][2]. In both cases, one cannot restrict the representation to $|$ and $-$ shaped paths. Indeed, any $\{|, -\}$-intersection representation of a triangle-free planar graph can be turned into a $\{|, -\}$-contact representation, and any such representation defines a vertex partition of the graph into two forests of paths (one induced by the vertical paths and the other induced by the horizontal ones), but such partition is not always possible [37].

As a string contact graph (and thus a $\{\llcorner, |, -\}$-contact graph) with n vertices has at most $2n$ edges and as a triangle-free planar graph may have up to $2n-4$ edges, Theorem 1.1 cannot be extended to much denser graphs. However, for planar Laman graphs (a large family of planar graphs with at most $2n-3$ edges and which are B_1-VPG graphs [20]), the question of whether these graphs have a $\{\llcorner, |, -\}$-contact representation is open, up to our knowledge. The question whether triangle-free planar graphs are $\{\llcorner, |\}$-contact graphs is also open. Theorem 1.2 implies that planar graphs are in (1-string) B_1-VPG, improving the results of Biedl and Derka [6] stating that planar graphs are in (1-string) B_2-VPG. Since an $\{\llcorner, \ulcorner, |, -\}$-intersection representation can be turned into a segment intersection representation [30], this also directly provides a rather simple proof of the fact that planar graphs are segment intersection graphs [10].

The common ingredient of our results is what we call *2-sided near-triangulations*. In Section 2, we present the 2-sided near-triangulations, allowing us to provide a new decomposition of planar 4-connected triangulations (see [7] and [38] for other decompositions of 4-connected triangulations). This decomposition is simpler than the one provided by Whitney [38] that is used in [10]. In Section 3, we define thick $\llcorner$-contact representations (i.e., $\llcorner$-contact representations in which the $\llcorner$ are thick) with specific properties. We then show that every 2-sided near-triangulation admits such a representation. This result is used in Section 4 to prove Theorem 1.1. Then in Section 5 we use 2-sided near-triangulations to prove Theorem 1.2.

2 2-sided near-triangulations

In this paper we consider plane graphs with neither loops nor multiple edges. The infinite face is called the *outer face*, while the other faces are called *inner faces*. A *near-triangulation* is a plane graph such that every inner face is triangular. In a plane graph G, a *chord* is an edge not bounding the outer face but

[2] In fact, Theorem 1.1 has been proven in the master thesis (written in German) of B. Kappelle in 2015 [24] but never published.

that links two vertices of the outer face. A *separating triangle* of G is a cycle of length three such that both regions delimited by this cycle (the inner and the outer region) contain some vertices. It is well known that a triangulation is 4-connected if and only if it contains no separating triangle. Given a vertex v on the outer face, the *inner neighbors* of v are the neighbors of v that are not on the outer face. We define here 2-sided near-triangulations (see Figure 1) whose structure will be useful in the inductions of the proofs of Theorem 1.2 and Theorem 3.1.

DEFINITION 2.1. *A* 2-sided near-triangulation *is a 2-connected near-triangulation T without separating triangles, such that going clockwise on its outer face, the vertices are denoted $a_1, a_2, \ldots, a_p, b_q, \ldots, b_2, b_1$, with $p \geq 1$ and $q \geq 1$, and such that there is neither a chord $a_i a_j$ nor $b_i b_j$ (that is an edge $a_i a_j$ or $b_i b_j$ such that $|i-j| > 1$).*

Remark that 4-connected triangulations being the triangulations without separating triangles, 4-connected triangulations are 2-sided near-triangulations.

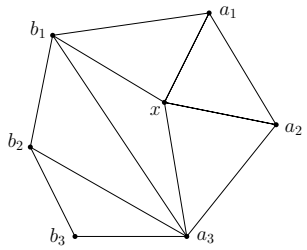

Figure 1: Example of a 2-sided near-triangulation.

The structure of the 2-sided near-triangulations allows us to describe the following decomposition:

LEMMA 2.1. *Given a 2-sided near-triangulation T with at least 4 vertices, one can always perform one of the following operations:*

- ***(a_p-removal)** This operation applies if $p > 1$, a_p has no neighbor b_i with $i < q$, and none of the inner neighbors of a_p has a neighbor b_i with $i < q$. This operation consists in removing a_p from T, and in denoting $b_{q+1}, \ldots, b_{q+r}$ the new vertices on the outer face in anti-clockwise order, if any. This yields a 2-sided near-triangulation T' (see Figure 2a).*
- ***(b_q-removal)** This operation applies if $q > 1$, b_q has no neighbor a_i with $i < p$, and none of the inner neighbors of b_q has a neighbor a_i with $i < p$. This operation consists in removing b_q from T, and in denoting $a_{p+1}, \ldots, a_{p+r}$ the new vertices on the outer face in clockwise order, if any. This yields a 2-sided near-triangulation T'. This operation is strictly symmetric to the previous one.*
- ***(cutting)** This operation applies if $p > 1$, $q > 1$ and the unique common neighbor of a_p and b_q, denoted d, has a neighbor a_i with $i < p$, and a neighbor b_j with $j < q$. This operation consists in cutting T into three 2-sided near-triangulations T', T_a and T_b (see Figure 2b):*
  - *T' is the 2-sided near-triangulation contained in the cycle formed by vertices $(a_1, \ldots, a_i, d, b_j, \ldots, b_1)$, and the vertex d is renamed a_{i+1}.*
  - *T_a (resp. T_b) is the 2-sided near-triangulation contained in the cycle $(a_i, \ldots, a_p, d)$ (resp. $(d, b_q, \ldots, b_j)$), where the vertex d is denoted b_1 (resp. a_1).*

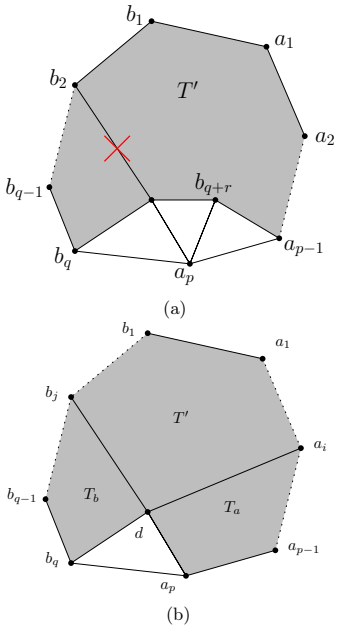

Figure 2: Illustrations of (a) the a_p-removal operation and (b) the cutting operation.

Proof. Suppose that a_p has no neighbor b_i with $i < q$ and none of the inner neighbors of a_p has a neighbor b_i with $i < q$. We denote $b_{q+1}, \ldots, b_{q+r}$ the inner neighbors of a_p in anti-clockwise order such that b_j is connected to b_{j+1} for every $q \leq j \leq r$. Let T' be the graph obtained by removing a_p and its incident edges from T. It is clear that T' is a near-triangulation, and that it has no separating triangle (otherwise T would have one too). Furthermore, as there is no chord incident to a_p, and as T' has at least three vertices its outer face is bounded by a cycle, and T' is thus 2-connected. As T is a 2-sided near-triangulation, T' has no chord a_ia_j, with $i, j < p$, or b_ib_j with $i, j \leq q$. From our assumption, the inner neighbors of a_p have no neighbors b_k with $k < q$, thus there is no chord b_ib_j with $i \leq q$ and $q < j$. Finally, we claim that there is no chord b_ib_j in T' with $q \leq i < j$. Supposing otherwise would mean that the vertices a_p, b_i, and b_j would form a triangle with at least one vertex inside, b_{i+1}, and at least one vertex outside, a_{p-1}: it would be a separating triangle, a contradiction. Therefore T' is a 2-sided near-triangulation.

The proof for the b_q-removal operation is analogous to the previous case.

Suppose that we are not in the first case nor in the second one. Let us first show that $p > 1$ and $q > 1$. Assume by contradiction that $p = 1$. Then as T is 2-connected, it has at least three vertices on the outer face and $q \geq 2$. In such a case one can always perform the b_q-removal operation, a contradiction.

Let us now show that a_p is not adjacent to a vertex b_i with $i < q$. Assume by contradiction that a_p is adjacent to a vertex b_i with $i < q$. Then by planarity, b_q (with $q > 1$) has no neighbor a_i with $i < p$, and has no inner neighbor adjacent to a vertex a_i with $i < p$. In such a case one can always perform the b_q-removal operation, a contradiction. Symmetrically, we deduce that b_q is not adjacent to a vertex a_i with $i < p$.

Vertices a_p and b_q have one common neighbor d such that da_pb_q is an inner face. Note that as there is no chord incident to a_p or b_q, then d is not on the outer face. Since the outer face is not triangular, they have no other common neighbor y, otherwise there would be a separating triangle ya_pb_q (separating d from both vertices a_1 and b_1).

As we are not in the first case nor in the second case, we have that a_p (resp. b_q) has (at least) one inner neighbor adjacent to a vertex b_i with $i < q$ (resp. a_i with $i < p$). By planarity, d is the only inner neighbor of a_p (resp. b_q) adjacent to a vertex b_i with $i < q$ (resp. a_i with $i < p$). We can thus apply the cutting operation.

We now show that T', T_a and T_b are 2-sided near-triangulations. Consider first T'. It is clear that it is a near-triangulation without separating triangles. It remains to show that there are no chords a_ia_j or b_ib_j. By definition of T', the only chord possible would have $d = a_{i+1}$ as an endpoint, but the existence of an edge da_k with $k < i$ would contradict the minimality of i. Thus T' is a 2-sided near-triangulation.

By definition, T_a is also a near-triangulation containing no separating triangles. Moreover, there is no chord a_ka_l with $i \leq k \leq l-2$ as there are no such chords in T. Therefore T_a is a 2-sided near-triangulation. Similarly, T_b is also a 2-sided near-triangulation. □

3 Thick ⌞-contact representation

A *thick* ⌞ is an ⌞ shape where the two segments are turned into thick rectangles (see Figure 3). Here we do not allow thick | or −, so going clockwise around a thick ⌞ from the bottom-right corner, we call its sides *bottom*, *left*, *top*, *vertical interior*, *horizontal interior*, and *right*. We draw them in the integer grid, that is such that their bend points have integer coordinates, and we ask the two rectangles to be of thickness one, and of length at least two. A thick ⌞ is described by four coordinates a, b, c, d such that $a+1 < b$ and $c+1 < d$. It is thus the union of two boxes: $([a, a+1]\times[c, d])\cup([a, b]\times[c, c+1])$. If not specified, the *corner* of a thick ⌞ denotes its bottom-left corner (with coordinates (a, c)).

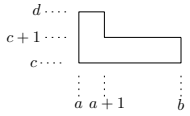

Figure 3: A thick ⌞.

Definition 3.1. *A* convenient thick ⌞-contact representation *(CTLCR) is a contact representation of thick* ⌞ *(which implies that the thick* ⌞ *interiors are disjoint) with the following properties:*

- *Two thick* ⌞ *intersect either on exactly one segment or on a point (Figure 5 lists the allowed ways two thick* ⌞ *can intersect). If the intersection is a segment, then it must be exactly one side of a thick* ⌞*. If the intersection is a point, then it is the bottom right corner of one thick* ⌞ *and the top left corner of the other one.*

- *If the bottom (resp. left) side of a thick* ⌞ *x is contained in the horizontal (resp. vertical) interior side of a thick* ⌞ *y, then the bottom (resp. left) side of y is not contained in the horizontal (resp. vertical) interior side of a thick* ⌞ *z (see Figure 4).*

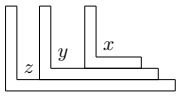

Figure 4: Forbidden configuration in a CTLCR.

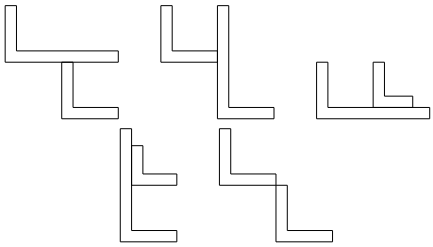

Figure 5: Allowed intersections in a CTLCR. From left to right and top to bottom: the intersection is the top, right, bottom, left side of a thick ⌞, and the intersection is a point at the bottom right corner of a thick ⌞ and at the top left corner of a thick ⌞.

Remark that in a CTLCR the removal of any thick ⌞ still leads to a CTLCR. We now show that every 2-sided near-triangulation has a CTLCR (see Figure 7 for an illustration).

THEOREM 3.1. *Every 2-sided near-triangulation T has a CTLCR with the following properties, for some integers X and Y :*

- *Every corner of a thick ⌞ is included in the non-positive quadrant $\{(x, y) : x \leq 0, y \leq 0\}$.*
- *The thick ⌞ of a_1 has the bottom-most corner and has coordinates $(0, -Y)$. Every vertex a_i is represented by a thick ⌞ whose corner has coordinates $(x, -Y)$ with $2 - X \leq x < 0$. Furthermore their horizontal interior side does not contain any other side.*
- *The thick ⌞ of b_1 has the left-most corner and has coordinates $(-X, 0)$. Every vertex b_i is represented by a thick ⌞ whose corner has coordinates $(-X, y)$ with $2 - Y \leq y < 0$. Furthermore their vertical interior side does not contain any other side.*
- *$Y + X \leq 3n - 3$, where n is the number of vertices in T*

Proof. We proceed by induction on the number of vertices. The theorem clearly holds for the 2-sided near-triangulation with three vertices. Let T be a 2-sided near-triangulation; it can thus be decomposed using one of the three operations described in Lemma 2.1. We go through the three operations successively.

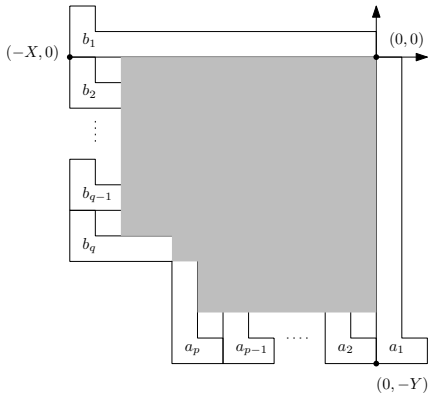

Figure 6: Typical CTLCR obtained from Theorem 3.1.

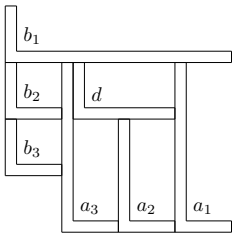

Figure 7: One of the CTLCR of the near-triangulation from Figure 1.

(a_p-removal) Let T' be the 2-sided near-triangulation resulting from an a_p-removal operation on T. By the induction hypothesis, T' has a CTLCR with the required properties for parameters X' and Y' (see Figure 9a). We can now modify this CTLCR slightly in order to obtain a CTLCR of T (thus adding a thick ⌞ corresponding to vertex a_p). Move the corners of the thick ⌞ corresponding to vertices $b_1, \ldots, b_q$ three units to the left. Since their vertical interior side do not contain any other side, one can do this without modifying the rest of the representation. Then one can add the thick ⌞ of a_p such that it touches the thick ⌞ of vertices b_q and a_{p-1} (as depicted in Figure 9b). One can easily check that the obtained representation is a CTLCR of T and satisfies all the requirements. Note in particular that in this case the vertical interior side of a_p can contain some sides, the left sides of $b_{q+1}, \ldots, b_{q+r}$, but in

the induction these thick $\llcorner$ are such that their vertical interior side do not contain any other side, so we avoid the configuration depicted in Figure 4.

(b_q-removal) This case is symmetric to the previous one.

(cutting) Let T', T_a and T_b be the three 2-sided near-triangulations resulting from the cutting operation described in Lemma 2.1. By induction hypothesis, each of them has a CTLCR satisfying the requirements of Theorem 3.1, with parameters X', Y', X_a, Y_a, X_b, and Y_b respectively. We are going to modify the CTLCR of T' in order to include the ones of T_a and T_b, as they are given by the induction (see Figure 8).

Given the CTLCR of T', move the corners of the thick $\llcorner$ corresponding to vertices $b_1, \ldots, b_j$ by at most $(X_b - 2)$ units to the left, so that the x-coordinates of the corners of b_j and $d = a_{i+1}$ differ by exactly X_b. Move the corner of $d = a_{i+1}$ downward by at most $Y_b - 2$ units, so that the y-coordinates of the corners of b_i and $d = a_{i+1}$ differ by exactly Y_b. As these y-coordinate originally already differ by at least 2, this move is of at most $(Y_b - 2)$ units. Move the corners of $a_1, \ldots, a_i$ by at most $(Y_b - 2) + Y_a$ units downward, so that the y-coordinates of the corners of $d = a_{i+1}$ and a_i differ by exactly Y_a. Again, since these thick $\llcorner$ have their vertical or horizontal interior sides that do not contain any other side, one can do this without modifying the rest of the representation. Now one has to modify the representation in order to prolong the horizontal part of the thick $\llcorner$ of $d = a_{i+1}$ so that its bottom side reaches length X_a. This can be done by cutting the CTLCR along a vertical line ℓ that crosses the thick $\llcorner$ of $d = a_{i+1}$, by moving the left part at most $(X_a - 2)$ units to the left (as this side has already length at least 2), and for any thick $\llcorner$ of the left side touching ℓ by prolonging its horizontal part to the right, until reaching the right part of the CTLCR. Now the corners of the thick $\llcorner$'s of b_j, $d = a_{i+1}$ and a_i are well placed so that one can add the CTLCR of T_a below the thick $\llcorner$ of d and the one of T_b on its left (see Figure 8). One can easily check that the obtained representation satisfies all the requirements.

Let us now check that these operations preserve the fact that $Y + X \leq 3n - 3$. Indeed, for the a_p-removal $Y = Y'$ and $X = X' + 3$ while T has one more vertex than T'. The case of b_q-removal is identical. For the cutting operation, we have that $X \leq X_a + X_b + X' - 4$ and that $Y \leq Y_a + Y_b + Y' - 2$. Thus $Y + X \leq (Y_a + X_a) + (Y_b + X_b) + (Y' + X') - 6 \leq 3n - 3 \times 3 + 4 \times 3 - 6 \leq 3n - 3$ because d is counted twice too much and b_j and a_i are counted both one time too much. □

Note that the last item of the theorem implies that such a CTLCR fits into a grid of width W and height H with $W + H \leq 3n + 1$. Actually, allowing two thick $\llcorner$ shapes to intersect on two segments (that is, allowing the corner of any thick $\llcorner$ x to be at the intersection of the vertical and horizontal interior sides of another thick $\llcorner$ y), one can reach $W + H \leq 2n + 3$. It is not clear whether allowing thick $|$ or $-$ would decrease this bound much further.

Similar representations with axis aligned polygons have been studied in the literature. For example, the problem of representing a planar graph G with such contact representations where the area of each polygon is prescribed by some weight function $w(v)$, defined on $V(G)$, has various applications. It has been shown [2] that finding such a representation is always possible for Hamiltonian triangulations even if restricting to thick $[$, $\llcorner$, $\ulcorner$, or $|$ shaped polygons, where the thickness of each part is not necessarily one. In the same paper the authors also consider this problem for 4-connected triangulations when restricting to thick $\llcorner$, $\ulcorner$, or $|$ shaped polygons (in relation with the so-called one-legged Hamiltonian cycles), but this remains open. We wonder whether our approach (through 2-sided near-triangulations) could lead to a positive answer, but the $\{\llcorner, |, -\}$-contact representations described in the following section lead to a representation with thick $\llcorner$, $|$, and $-$ shaped polygons for triangle-free planar graphs (leaving some holes in the representation).

4 $\{\llcorner, |, -\}$-contact representations for triangle-free planar graphs

We can now use the CTLCR to prove Theorem 1.1. Recall that a *$\{\llcorner, |, -\}$-contact representation* is a contact representation with some $\llcorner$, some vertical segments $|$, and some horizontal segments $-$, such that if an intersection occurs between two of these objects, then the intersection is an endpoint of one of the two objects. We need the following lemma as a tool (it is proved in appendix).

LEMMA 4.1. *For any plane triangle-free graph G, there exists a 4-connected triangulation T containing G as an induced subgraph.*

We can now prove Theorem 1.1, which asserts that every triangle-free planar graph has an $\{\llcorner, |, -\}$-contact representation.

Proof. [Proof of Theorem 1.1] Consider a triangle-free planar graph G. According to Lemma 4.1, there exists a 4-connected triangulation T containing G as an induced subgraph. Denoting a_1, b_2, b_1 the three exterior vertices of T in clockwise order, one sees that T is a 2-sided near-triangulation. By Theorem 3.1, T has a CTLCR

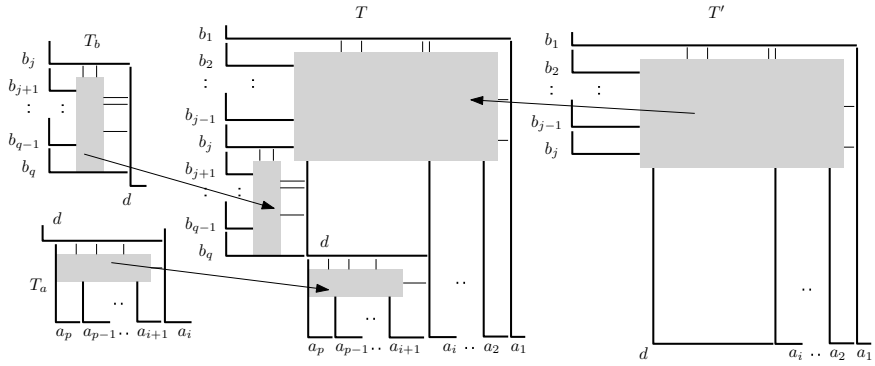

Figure 8: The (cutting) operation for a CTLCR.

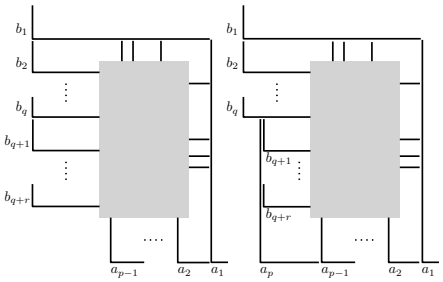

(a) CTLCR of T' (b) CTLCR of T

Figure 9: The (a_p-removal) operation for a CTLCR. Here, the grey region contains the corners of the inner vertices.

and removing every thick $\llcorner$ corresponding to a vertex of $T \setminus G$ leads to a CTLCR of G.

If a thick $\llcorner$ x has its bottom side included in the horizontal interior side of another thick $\llcorner$ y, then x does not contain any other side on its horizontal interior side. Furthermore, x does not intersect anyone on its right side nor on its bottom right corner. Indeed, if there was such an intersection with a thick $\llcorner$ z, then y and z would also intersect, contradicting the fact that G is triangle-free (see Figure 10). One can thus replace the thick $\llcorner$ of x by a thick $|$.

Similarly, if a thick $\llcorner$ x has its left side included in the vertical interior side of a thick $\llcorner$ y, we can replace the thick $\llcorner$ of x by a thick $-$.

Note that now the intersections are on segments of length 1, or on a point, between the bottom right corner

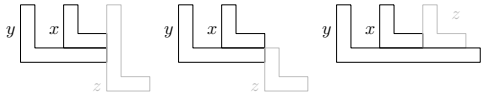

Figure 10: If a thick $\llcorner$ x has its bottom side included in the horizontal interior of a thick $\llcorner$ y, then x has no intersection with a thick $\llcorner$ z on its right side and on its bottom right corner.

of a thick $\llcorner$ or $-$, and the top left corner of a thick $\llcorner$ or $|$. Then, we replace each thick $\llcorner$, $|$, and $-$ by thin ones as depicted in Figure 11. It is clear that we obtain a $\{\llcorner, |, -\}$-contact representation whose contact graph is G. This concludes the proof. □

An example of the process is shown in Figure 12. Note that any $\{\llcorner, |, -\}$-contact representation with n paths fits into a grid of width and height at most n. Indeed, any horizontal (resp. vertical) line of the grid that does not contain any of the n_h horizontal (resp. n_v vertical) subpaths, nor contain any contact point between two vertical (resp. horizontal) subpaths can be deleted. As the number of contact points between two vertical (resp. horizontal) subpaths where the path on top (resp. on the right) is $|$ shaped (resp. $-$ shaped) is at most $n - n_h$ (resp. $n - n_v$), we end up with at most n horizontal (resp. vertical) lines. It is open to know whether this bound can be improved. Let G_t be the (bipartite) planar graph obtained by taking t cubes $C_1, \ldots, C_t$ and gluing C_i and C_{i+1} on a square, for all $1 \leq i < t$, such that C_i and C_{i+2} remain vertex disjoint, for all $1 \leq i < t - 1$. We believe that for this graph, with $n = 4t + 4$ vertices, any $\{\llcorner, |, -\}$-contact representation requires a grid of width and height at least $n/2$.

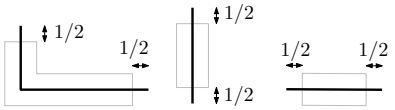

Figure 11: Replacing thick ⌞, |, and − by thin ones.

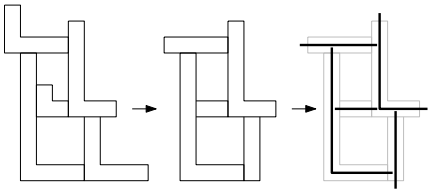

Figure 12: Given a CTLCR of a triangle-free graph G, we first replace some thick ⌞ by thick | and thick −, and then replace every thick shape by a thin one according to Figure 11.

5 The ⌞-intersection representations

An ⌞*-intersection representation* of a graph G is a representation of G such that vertices are represented by ⌞-shaped paths in a grid, that intersect if and only if the vertices are adjacent in G. Using Theorem 3.1, one can prove that every 4-connected triangulation has such a representation. To allow us to work on every triangulation (not only the 4-connected ones) we need to enrich our ⌞-intersection representations with the notion of *anchor*[3].

There are two types of anchors (see Figure 13). A *horizontal anchor* is a set $([x_1, x_3] \times y_1) \cup (x_1 \times [y_1, y_2]) \cup (x_2 \times [y_1, y_2])$ where $x_1 < x_2 < x_3$ and $y_1 < y_2$. The *middle corner* of such a horizontal anchor is the point (x_2, y_1). A *vertical anchor* is a set $(x_1 \times [y_1, y_3]) \cup ([x_1, x_2] \times y_1) \cup ([x_1, x_2] \times y_2)$ where $x_1 < x_2$ and $y_1 < y_2 < y_3$. The *middle corner* of such a vertical anchor is the point (x_1, y_2). In addition to middle corners, every anchor has a *main corner* which is the point of coordinate (x_1, y_1) for both types of anchors. An anchor can thus be seen as a union of three segments, or as the union of two ⌞ paths.

Consider a near-triangulation T, and any inner face abc of T. Note that if the ⌞ paths of a, b and c do not intersect at a common point or segment, then their horizontal (resp. vertical) subpaths lie on three different lines. They thus form a rectangle whose top side belongs to the ⌞ path with the up-most corner, whose right side belongs to the ⌞ path with the right-most corner, and

[3]The notion was introduced in [20] under the name of *private region*.

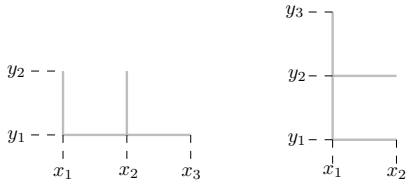

(a) An horizontal anchor. (b) A vertical anchor.

Figure 13: The two types of anchors (horizontal and vertical).

whose other sides belong to the third ⌞ path. Given an ⌞-intersection representation of T, an *anchor for abc* is an anchor intersecting the ⌞ paths of a, b and c and no other path, and such that the middle corner is in the rectangle described by a, b and c as depicted in Figure 14.

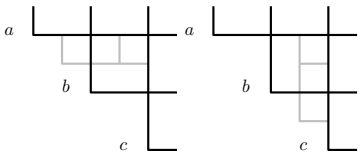

Figure 14: The two possible anchors for the ⌞ paths corresponding to a triangle *abc*.

Definition 5.1. *A* full ⌞-intersection representation *(FLIR) of a near-triangulation T is an ⌞-intersection representation of T together with a set of pairwise disjoint anchors, one for each inner face of T.*

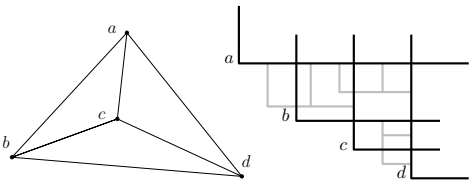

Figure 15: Example of a triangulation and a corresponding FLIR (the anchors are drawn in gray).

Let us now prove that every 2-sided near-triangulation admits an FLIR.

Proposition 5.1. *Every 2-sided near-triangulation has an FLIR such that among the corners of the ⌞ paths and of the anchors:*

- *from left to right, the first corners are those of vertices $b_1, b_2, \dots b_q$ and the last one is the corner of vertex a_1, and*
- *from bottom to top, the first corners are those of vertices $a_1, a_2, \dots a_p$ and the last one is the corner of vertex b_1.*

As the $\llcorner$ of a_i and a_{i+1} (resp. b_i and b_{i+1}) intersect, the FLIR is rather constrained. This is illustrated in Figure 16, where the grey region contains the corners of the inner vertices, and the corners of the anchors.

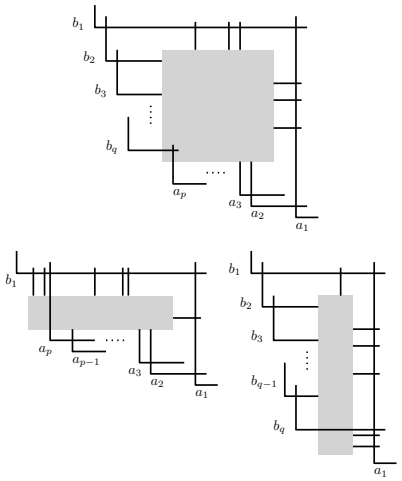

Figure 16: Illustration of Proposition 5.1 when $p > 1$ and $q > 1$, when $p > 1$ and $q = 1$, and when $p = 1$ and $q > 1$.

Proof. We proceed by induction on the number of vertices.

The result clearly holds for the 2-sided near-triangulation with three vertices, no matter if $p = 1$ and $q = 2$, or $p = 2$ and $q = 1$. Let T be a 2-sided near-triangulation with at least four vertices. By Lemma 2.1 we consider one of the following operations on T:

(a_p-removal) Consider the FLIR of T' obtained by induction and see in Figure 17 how one can add an $\llcorner$ for a_p and an anchor for each inner face $a_p b_j b_{j+1}$ with $q \leq j < q+r$ and for the inner face $a_p a_{p-1} b_{q+r}$. One can easily check that the obtained representation verifies all the requirements of Proposition 5.1.

(b_q-removal) This case is symmetric to the previous one.

(cutting) Consider the FLIRs of T', T_a and T_b. Figure 18 depicts how to combine them, and how to add an anchor for $da_p b_q$, in order to get the FLIR of T. One can easily check that the obtained representation verifies all the requirements of Proposition 5.1. □

We now prove Theorem 1.2 which asserts that every planar graph is a $\llcorner$-intersection graph. It is well known that every planar graph is an induced subgraph of some triangulation (see [11] for a proof similar to the one of Lemma 4.1). Thus, given a planar graph G, one can build a triangulation T for which G is an induced subgraph. If one can create an FLIR of T, then it remains to remove the $\llcorner$ paths corresponding to vertices of $T \backslash G$ along with the anchors in order to get an $\llcorner$-intersection representation of G. In order to prove Theorem 1.2, we thus only need to show that every triangulation admits an FLIR. Namely, proving the following proposition completes the proof of Theorem 1.2.

PROPOSITION 5.2. *Every triangulation T with outer-vertices x, y, z has an FLIR such that among the corners of the $\llcorner$ paths and of the anchors:*

- *the corner of x is the top-most and left-most,*
- *the corner of y is the second left-most, and*
- *the corner of z is the bottom-most and right-most.*

Note that in this proposition there is no constraint on x, y, z, so by renaming the outer vertices, other FLIRs can be obtained.

Another way to obtain more FLIRs is by applying a reflection with respect to a line of slope 1. In such an FLIR (see Figure 19) among the corners of the $\llcorner$ paths and of the anchors:

- the corner of x is the bottom-most and right-most,
- the corner of y is the second bottom-most, and
- the corner of z is the top-most and left-most.

This reflection operation is used later in the proof of Proposition 5.2.

Proof. We proceed by induction on the number of vertices in T. Let T be a triangulation with outer vertices x, y, z.

If T is 4-connected, then it is also a 2-sided near-triangulation. By Proposition 5.1 and by renaming the outer-vertices x to b_1, y to b_2 and z to a_1, T has an FLIR with the required properties.

If T is not 4-connected, then it has a separating triangle formed by vertices a, b and c. We call T_{in} and

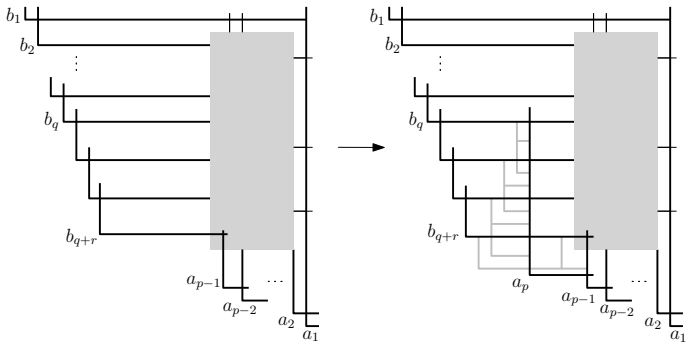

Figure 17: The (a_p-removal) operation.

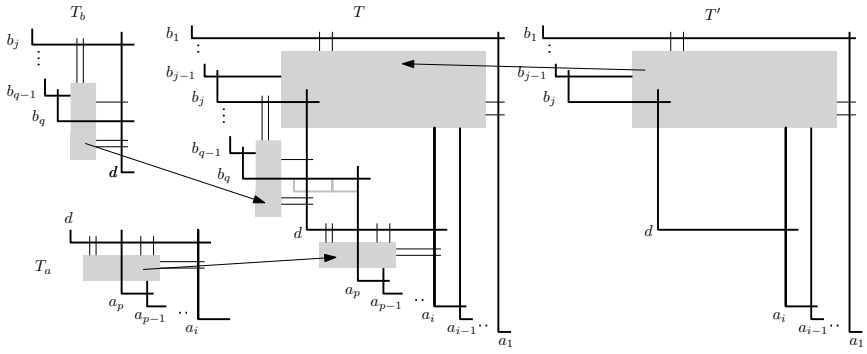

Figure 18: The (cutting) operation.

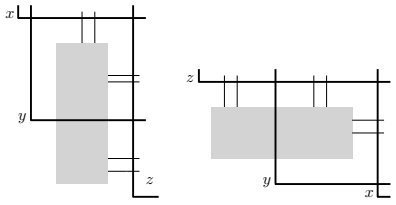

Figure 19: Illustration of Proposition 5.2, and the FLIR obtained after reflection with respect to a line of slope 1.

T_{out} the triangulations obtained from T by removing the vertices outside and inside abc respectively.

By the induction hypothesis, T_{out} has an FLIR verifying Proposition 5.2 (considering the outer vertices to be x, y, z in the same order as in T). Without loss of generality we can suppose that the $\llcorner$ paths of a, b and c appear in the following order: the top-most and left-most is b, the second left-most is c and the bottom-most is a. There are two cases according to the type of the anchor of the inner face abc.

If the anchor of abc in the FLIR of T_{out} is vertical (see Figure 20a), then applying the induction hypothesis on T_{in} with b, c, a as outer vertices considered in that order, T_{in} has an FLIR as depicted on the Figure 20b. Figure 20c depicts how to include the FLIR of $T_{in} \setminus \{a, b, c\}$ in the close neighborhood of the anchor of abc. As abc is not a face of T, the close neighborhood of its anchor is indeed available for this operation.

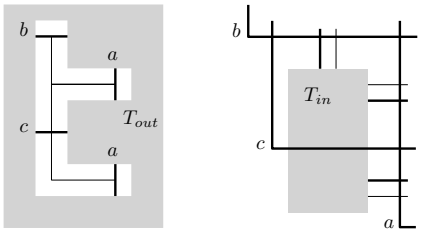

(a) The vertical anchor of abc in the FLIR of T_{out}

(b) The FLIR of T_{in}

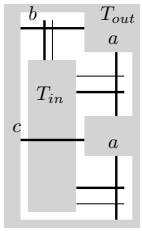

(c) The inclusion of the FLIR of T_{in} in the FLIR of T_{out}

Figure 20: FLIR inclusion in the case of a vertical anchor

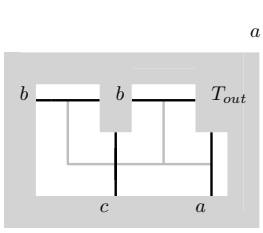

(a) The horizontal anchor of abc in the FLIR of T_{out}

(b) The FLIR of T_{in}

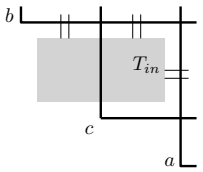

(c) The reflected FLIR of T_{in}

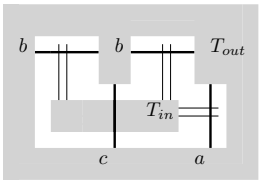

(d) The inclusion of the FLIR of T_{in} in the FLIR of T_{out}

Figure 21: FLIR inclusion in the case of a horizontal anchor

Now suppose that the anchor of abc in the FLIR of T_{out} is horizontal (see Figure 21a). By application of the induction hypothesis on T_{in} with a, c, b as outer vertices considered in that order, then T_{in} has an FLIR as depicted on the Figure 21b. By a reflection of slope 1, T_{in} has an FLIR such that b is the top-most and left-most, c is the second left-most and a is bottom-most (see Figure 21c). Similarly to the previous case, we include this last FLIR of $T_{in} \setminus \{a, b, c\}$ in the one from T_{out} (see Figure 21d).

As T_{in} and T_{out} cover T, and intersect only on the triangle abc, and as every inner face of T is an inner face in T_{in} or in T_{out}, these constructions clearly verify Proposition 5.2. This concludes the proof of the proposition. □

Note that as for $\{\llcorner, |, -\}$-contact representations any $\llcorner$-intersection representation with n paths fits into a grid of width and height at most n. Here also, it is open to know whether this bound can be improved. We believe that for the graph G_t described in the previous section any $\llcorner$-intersection representation requires a grid of width and height at least $n/2$.

References

[1] N. Aerts and S. Felsner. Vertex Contact Representations of Paths on a Grid. *Journal of Graph Algorithms and Applications*, 19(3):817 – 849, 2015.

[2] Md J. Alam, T. Biedl, S. Felsner, M. Kaufmann, S.G. Kobourov, and T. Ueckerdt. Computing cartograms with optimal complexity. *Discrete & Computational Geometry*, 50(3):784–810, 2013.

[3] A. Asinowski, E. Cohen, M.C. Golumbic, V. Limouzy, M. Lipshteyn, and M. Stern. Vertex intersection graphs of paths on a grid. *J. Graph Algorithms Appl.*, 16(2):129–150, 2012.

[4] I. Ben-Arroyo Hartman, I. Newman, and R. Ziv. On grid intersection graphs. *Discret. Math.*, 87:41–52, 1991.

[5] T. Biedl and M. Derka. 1-String B_1-VPG Representations of Planar Partial 3-Trees and Some Subclasses. *ArXiv e-prints*, 2015.

[6] T. Biedl and M. Derka. 1-String B_2-VPG representation of planar graphs. *Journal of Computational Geometry*, 7(2), 2016.

[7] T. Biedl and M. Derka. The (3,1)-ordering for 4-connected planar triangulations. *Journal of Graph Algorithms and Applications*, 20(2):347–362, 2016.

[8] T. Biedl and M. Derka. Order-preserving 1-string representations of planar graphs. In *Proceedings of SOFSEM 2017*, pages 283–294, 2017.

[9] D. Catanzaro, S. Chaplick, S. Felsner, B.V. Halldórs-

son, M.M. Halldórsson, T. Hixon, and J. Stacho. Max point-tolerance graphs. *Discrete Applied Mathematics*, 216:84–97, 2017.

[10] J. Chalopin and D. Gonçalves. Every planar graph is the intersection graph of segments in the plane. In *Proceedings of the forty-first annual ACM symposium on Theory of computing*, pages 631–638, 2009.

[11] J. Chalopin, D. Gonçalves, and P. Ochem. Planar graphs have 1-string representations. *Discrete & Computational Geometry*, 43(3):626–647, 2010.

[12] S. Chaplick, V. Jelínek, J. Kratochvíl, and T. Vyskočil. Bend-bounded path intersection graphs: Sausages, noodles, and waffles on a grill. In *Graph-Theoretic Concepts in Computer Science*, pages 274–285. Springer, 2012.

[13] S. Chaplick, S.G. Kobourov, and T. Ueckerdt. Equilateral L-contact graphs. In *International Workshop on Graph-Theoretic Concepts in Computer Science*, pages 139–151. Springer Berlin Heidelberg, 2013.

[14] S. Chaplick and T. Ueckerdt. Planar Graphs as VPG-Graphs. *J. Graph Algorithms Appl.*, 17(4):475–494, 2013.

[15] E. Cohen, M.C. Golumbic, W.T. Trotter, and R. Wang. Posets and VPG Graphs. *Order*, 33(1):39–49, 2016.

[16] N. de Castro, F. Cobos, J.C. Dana, A. Márquez, and M. Noy. Triangle-free planar graphs as segment intersection graphs. *J. Graph Algorithms Appl.*, 6(1):7–26, 2002.

[17] H. de Fraysseix and P. Ossona de Mendez. Representations by contact and intersection of segments. *Algorithmica*, 47(4):453–463, 2007.

[18] H. de Fraysseix, P. Ossona de Mendez, and J. Pach. Representation of planar graphs by segments. *Intuit. Geom. (Szeged, 1991), Colloq. Math. Soc. János Bolyai*, 63:109–117, 1994.

[19] H. de Fraysseix, P. Ossona de Mendez, and P. Rosenstiehl. On Triangle Contact Graphs. *Combinatorics, Probability and Computing*, 3:233–246, 1994.

[20] S. Felsner, K. Knauer, G.B. Mertzios, and T. Ueckerdt. Intersection graphs of L-shapes and segments in the plane. *Discrete Applied Mathematics*, 206:48–55, 2016.

[21] M.C. Francis and A. Lahiri. VPG and EPG bend-numbers of Halin graphs. *Discrete Applied Mathematics*, 215:95–105, 2016.

[22] E.R. Gansner, Y. Hu, M. Kaufmann, and S.G. Kobourov. Optimal Polygonal Representation of Planar Graphs. *Algorithmica*, 63(3):672–691, 2012.

[23] D. Gonçalves, B. Lévêque, and A. Pinlou. Triangle contact representations and duality. *Discrete and Computational Geometry*, 48:239–254, 2012.

[24] B. Kappelle. Kontact- und Schnittdarstellungen planarer Graphen. *Master Thesis, TU Berlin*, 2015.

[25] M. Kaufmann, J. Kratochvíl, K.A. Lehmann, and A.R. Subramanian. Max-tolerance graphs as intersection graphs: Cliques, cycles and recognition. *In Proc. SODA '06*, pages 832–841, 2006.

[26] R.W. Kenyon and S. Sheffield. Dimers, tilings and trees. *J. Comb. Theor. Ser. B*, 92:295–317, 2004.

[27] S. Kobourov, T. Ueckerdt, and K. Verbeek. Combinatorial and geometric properties of planar Laman graphs. In *Proceedings of the twenty-fourth annual ACM-SIAM symposium on Discrete algorithms (SODA 2013)*, pages 1668–1678. Society for Industrial and Applied Mathematics, 2013.

[28] P. Koebe. Kontaktprobleme der konformen Abbildung. *Ber. Sächs. Akad. Wiss. Leipzig, Math. Phys. Kl.*, 88:141–164, 1936.

[29] S. Mehrabi. Approximation Algorithms for Independence and Domination on B_1-VPG and B_1-EPG Graphs. *ArXiv e-prints*, 2017.

[30] M. Middendorf and F. Pfeiffer. The max clique problem in classes of string-graphs. *Discrete mathematics*, 108(1-3):365–372, 1992.

[31] A. Reyan Ahmed, F. De Luca, S. Devkota, A. Efrat, M. I. Hossain, S. Kobourov, J. Li, S. Abida Salma, and E. Welch. L-Graphs and Monotone L-Graphs. *ArXiv e-prints*, 2017.

[32] E.R. Scheinerman. Intersection Classes and Multiple Intersection Parameters of Graphs, 1984.

[33] O. Schramm. Square tilings with prescribed combinatorics. *Isr. J. Math.*, 84:97–118, 1993.

[34] O. Schramm. Combinatorically Prescribed Packings and Applications to Conformal and Quasiconformal Maps. *ArXiv e-prints*, 0709.0710, 2007.

[35] H. Schrezenmaier. Homothetic triangle contact representations. *Proceedings of WG '17*, 2017.

[36] C. Thomassen. Plane representations of graphs. *Progress in graph theory (Bondy and Murty, eds.)*, pages 336–342, 1984.

[37] R. Škrekovski. List improper colourings of planar graphs. *Combinatorics, Probability and Computing*, 8(3):293–299, 1999.

[38] H. Whitney. A theorem on graphs. *Ann. Math.*, 32(2):378–390, 1931.

A From triangle-free planar graphs to 4-connected triangulations

We here prove Lemma 4.1.

Proof. The main idea of the construction of T is to insert vertices and edges in every face of G (even for the exterior face).

For the sake of clarity, vertices of G are called *black* and vertices of $T \setminus G$ are called *red*. The new graph T contains G as an induced subgraph, along with other vertices and edges. More precisely, for every face of G, let $P = \{v_0, e_0, v_1, e_1, \ldots\}$ be the list of vertices and edges along the face boundary (see Figure 22), where e_i is the edge between vertices v_i and v_{i+1}; there can be repetitions of vertices or edges. For each face of G, given the list P, the graph T contains a vertex v'_i for each vertex v_i, a vertex e'_i for each edge e_i, and an additionnal vertex t. Each vertex v'_i is connected to e'_i and e'_{i+1} (with subscripts addition done modulo the size

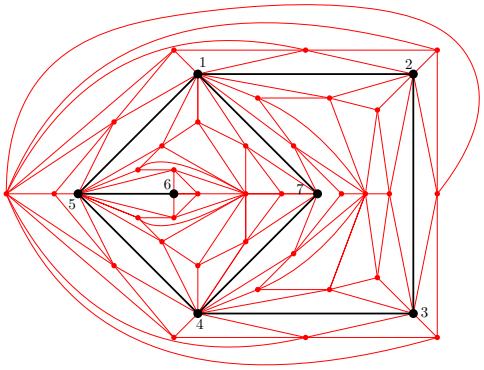

Figure 22: A planar triangle-free graph G (in black) and a 4-connected near-triangulation containing it as an induced subgraph (adding red vertices and edges). The boundary lists of the two inner faces of G are respectively $\{1,(1,2),2,(2,3),3,(3,4),4,(4,7),7,(7,1)\}$, $\{1,(1,7),7,(7,4),4,(4,5),5,(5,6),6,(6,5),5,(5,1)\}$ The outer face is $\{1,(1,2),2,(2,3),3,(3,4),4,(4,5),5,(5,1)\}$.

of the face), each vertex v_i is connected to v'_i, e'_{i-1} and e'_i, and the vertex t is connected to all vertices v'_i and e'_i (see Figures 22 and 23 for examples).

The new graph T is a triangulation, and we now show that it is 4-connected, i.e., has no separating triangle. Suppose that there is a separating triangle in the new graph. There are four cases depending on the colors of the edges of this triangle:

- The separating triangle contains three black edges. It is impossible since G is triangle-free.
- The separating triangle contains exactly one red edge. One of its endpoints must be a red vertex. But a red vertex is incident to only red edges, a contradiction.
- The separating triangle contains exactly two red edges. Then their common endpoint is a red vertex, and the triangle is made of two vertices v_i and v_{i+1}, together with the vertex e'_i. All these triangles are faces, a contradiction.
- The separating triangle contains three red edges. Since for each face, the red vertices (vertices v'_i, e'_i and t) induce a wheel graph centered on t, with at least 8 peripheral vertices (vertices v'_i and e'_i), this separating triangle has at least one black vertex. As two adjacent black vertices are linked by a black edge, this separating triangle has exactly one black vertex. As the two red vertices are two adjacent v'_i or e'_j vertices, we have that those are v'_i and e'_j, for some i and for $j = i$ or for $j = i+1$. Such a triangle is not separating, a contradiction.

This concludes the proof of the lemma. □

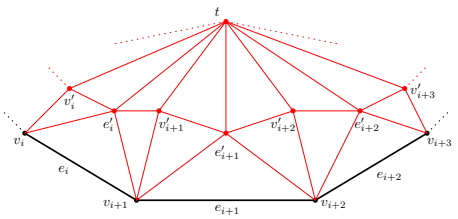

Figure 23: Zoom on the new connections.